

International conference

# MARID VI

## Marine and River Dune Dynamics 2019

1 - 3 April 2019 • Bremen, Germany

### Books of Abstracts

Editors:

Alice Lefebvre, Thierry Garlan and Christian Winter



Kiel University  
Christian-Albrechts-Universität zu Kiel



French Hydrographic &  
Oceanographic Office



# MARID VI

## Marine and River Dune Dynamics

Bremen, Germany  
1 - 3 April, 2019

### **Organising Committee:**

Dr Alice Lefebvre, MARUM, University of Bremen, Germany  
Prof Dr Christian Winter, Kiel University, Germany  
Dr Thierry Garlan, French Hydrographic Office, France  
Prof Dr Burghard Flemming, Senckenberg am Meer, Germany  
Dr Knut Krämer, MARUM, University of Bremen, Germany  
Dr Marius Becker, Kiel University, Germany

### **Scientific Committee:**

Dr Jaco Baas, Bangor University, United Kingdom  
Dr Marius Becker, Kiel University, Germany  
Prof Dr Jim Best, University of Illinois, United States of America  
Prof Dr Burghard Flemming, Senckenberg am Meer, Germany  
Dr Thierry Garlan, French Hydrographic Office, France  
Prof Dr Suzanne Hulscher, Twente University, Netherlands  
Prof Dr Maarten Kleinhans, Utrecht University, Netherlands  
Dr Sophie Le Bot, Université de Rouen, France  
Dr Alice Lefebvre, MARUM, University of Bremen, Germany  
Prof Dr Dan Parsons, University of Hull, United Kingdom  
Dr Marc Roche, Federal Public Service Economy, Self-employed, SME's and Energy, Belgium  
Prof Dr Alain Trentesaux, Université de Lille, France  
Prof Dr Vera Van Lancker, Royal Belgian Institute of Natural Sciences, Belgium  
Dr Katrien Van Landeghem, Bangor University, United Kingdom  
Prof Dr Christian Winter, Kiel University, Germany

### ***This publication should be cited as follows:***

Lefebvre, A., Garlan, T. and Winter, C. (Eds), 2019. MARID VI. Sixth International Conference on Marine and River Dune Dynamics. Bremen, Germany, 1-3 April 2019. MARUM – Center for Marine Environmental Sciences, University Bremen and SHOM. 267 pp. ISBN: 978-2-11-139488-9  
Reproduction is authorised, provided that appropriate mention is made of the source.

# **MARID VI is organised and sponsored by**

**MARUM Center for Marine Environmental Sciences,**  
University of Bremen,  
Leobener Str. 8,  
28359 Bremen, Germany



**SHOM, French Naval Hydrographic and Oceanographic Office**  
Oceanographic Center / Sedimentology,  
13 rue du Chatellier,  
29228 Brest Cedex 2, France



## **It is also supported by**

**Kiel Marine Science**  
Christian-Albrechts-Universität zu Kiel  
Ludewig-Meyn-Str. 10  
24118 Kiel, Germany



## **And sponsored by**

**MacArtney Germany GmbH**  
Wischhofstrasse 1-3  
D-24148 Kiel  
Germany  
Phone: +49 431 53550070  
Email: [mac\\_de@macartney.com](mailto:mac_de@macartney.com)  
Web: www.macartney.de



**J. Bornhöft Industriegeräte GmbH**  
Wellseedamm 3  
D-24145 Kiel  
Phone: +49 431 2370950  
Email: [info@bornhoeft.de](mailto:info@bornhoeft.de)  
Web: www.bornhoeft.de



## Preface & Welcome

Welcome to MARID VI, the sixth edition of the Marine and River Dune Dynamics conference series.

In 2000, a workshop on marine sand wave dynamics was organised by the French Naval Hydrographic and Oceanographic Office (SHOM) and the University of Lille 1 (France) under the aegis of the North Sea Hydrographic Commission. After the success of this first workshop, conferences covering marine and river dune dynamics were organised in 2004 (University of Twente, Enschede, the Netherlands), in 2008 (University of Leeds, United Kingdom), in 2013 (Royal Belgian Institute of Natural Sciences, Bruges Belgium) and in 2016 (Caernarfon, University of Bangor, North Wales, UK). Now known by the acronym MARID, these conferences provide state-of-the-art overviews and discussions on fundamental and applied knowledge of marine and river bedforms.

Bedforms are ubiquitous and dynamic features on a movable bed, which have been observed in many subaqueous environments, such as rivers, beaches, estuaries, tidal inlets, shallow seas, and deep waters. They are active morphodynamic elements which both reflect and influence hydrodynamic and sediment dynamics processes at various spatiotemporal scales. The study of their presence, size and movement is directly relevant for a wide range of applied and fundamental research. The processes governing bedform formation, dynamics and preservation have still not been unravelled adequately and the MARID VI delegates will outline progress derived from field observations, modelling studies and laboratory experiments across a wide number of disciplines, including earth sciences, oceanography, engineering, hydrography and biology.

MARID VI is held in Bremen, Germany, organised by MARUM - Center for Marine Environmental Sciences, University of Bremen, the University of Kiel and the French Naval Hydrographic and Oceanographic Office (SHOM). In keeping with the previous MARID conferences, we maintain the concept of a small, focused event with only plenary sessions to stimulate discussion among disciplines and methodologies. Scientific sessions are taking place in Haus der Wissenschaft on 1 and 2 April 2019 including talks from keynote speakers and oral and poster presentations by delegates. On 3 April a field trip is organised to the German North Sea coast and the Weser estuary to allow a convivial exchange between participants.

We hope that MARID VI will lead to fruitful and productive discussions, which in turn should help guide future collaborations to further investigate marine and river bedforms. The smaller, focussed format of the MARID conferences has proven to be ideally suited for such networking activities.

We wish you an enjoyable conference!

Alice Lefebvre, Thierry Garlan & Christian Winter.

## Table of Contents

Invited keynotes		
Authors	Title	Pages
<b>Heqin Cheng</b>	Dune dynamics in coarse silt, sand and gravel along the main channel from the estuarine front of the Yangtze River to the Three Gorges Dam.	45 - 50
<b>Daniel R. Parsons</b>	Enigmatic Bedforms in the Deep Sea	261 - 267
<b>Pieter C. Roos</b>	On the crest of sandwave modelling. Achievements from the past, directions for the future	197 - 202

Authors	Title	Pages
<b>M. Becker</b>	Flow over dunes and its influence on fluid mud entrainment: A concept of the dune-mud transition in tide-controlled, coastal plain estuaries	1 - 6
<b>V. Bellec, R. Bøe, L.R. Bjarnadóttir</b>	Sandwaves and megaripples on Spitsbergenbanken, Barents Sea	7 - 10
<b>E. Bouvet, A. Jarno, O. Blanpain, T. Garlan, F. Marin</b>	Experimental study of ripple dimensions under steady current	11 - 16
<b>L. Brakenhoff, M. van der Vegt, G. Ruessink</b>	Spatio-temporal bedform patterns on an ebb-tidal delta	17 - 22
<b>T. Branß, F. Núñez-González, J. Aberle</b>	Estimation of bedload by tracking supply-limited bedforms	23 - 28
<b>N.R. Bristow, G. Blois, J. Best, K.T. Christensen</b>	PIV measurements of flow around interacting barchan dunes in a refractive index matched flume	29 - 32
<b>G. Campmans, P.C. Roos, S.J.M.H. Hulscher</b>	Storm influences on sand wave dynamics: an idealized modelling approach	33 - 37

Authors	Title	Pages
<b>Y. Chen</b> , D.R. Parsons, S.M. Simmons, M.J. Cartigny, J.H. Clarke et al	The influence and interactions of delta slopes and knickpoints on bedforms within submarine channel systems	39 - 44
<b>H. Cheng</b> , L. Teng, W. Chen	Dune dynamics in coarse silt, sand and gravel along the main channel from the estuarine front of the Yangtze River to the Three Gorges Dam.	45 - 50
<b>J. Cisneros</b> , J. Best, T. van Dijk, E. Mosselman	Dune morphology and hysteresis in alluvial channels during long-duration floods revealed using high-temporal resolution MBES bathymetry	51 - 56
<b>A.J. Couldrey</b> , M.A.F. Knaapen, K.V. Marten, R.J.S. Whitehouse	Barchan vs Monopile: what happens when a barchan dune finds an obstacle in its path?	57 - 62
<b>J.H. Damveld</b> , P.C. Roos, B.W. Borsje, S.J.M.H. Hulscher	Phase-related patterns of tidal sand waves and benthic organisms: field observations and idealised modelling	63 - 67
<b>N. Debese</b> , J.J. Jacq, K. Degrendele, M. Roche	Osculatory surfaces applied to systematic errors estimation in repeated MBES surveys	69 - 75
<b>G.A. Díaz</b> , K. Schwarzer	Seabed features on Mecklenburg Bight based on Side-Scan Sonar imagery	77 - 82
<b>R. Durán</b> , J. Guillén, M. Ribó, P. Puig, A. Muñoz	Evolution of offshore sand ridges in tideless continental shelves (Western Mediterranean)	83 - 88
<b>B.W. Flemming</b>	Ripples and dunes: do flumes tell the whole story?	89 - 94
<b>T. Garlan</b> , E. Brenon	Biennial Survey method of marine dunes in the French part of the North Sea shipping channel	95 - 100
<b>M.R.A. Gensen</b> , J.J. Warmink, S.J.M.H. Hulscher	River dune based roughness uncertainty for the Dutch Rhine branches	101 - 106
<b>R.R. Gutierrez</b> , A. Lefebvre, F. Núñez-González, H. Avila	Towards open access of bed forms data, standardization of its analysis, and some steps to these ends	107 - 113
<b>G. Herrling</b> , K. Krämer, M. Becker, A. Lefebvre, C. Winter	Parametrization of bedform induced hydraulic flow resistance in coastal-scale numerical models – an evaluation of Van Rijn's empirical bedform roughness predictors	115 - 120

Authors	Title	Pages
<b>S. Homrani</b> , N. Le Dantec, F. Floc'h, M. Franzetti, M. Sedrati, C. Winter, C. Delacourt	Multi time-scale morphological evolution of a shell sand, dune bank in a shallow mesotidal environment.	121 - 126
<b>L. Kint</b> , N. Terseleer, V. Van Lancker	Multi-scale analysis of sandbank features optimising geomorphological mapping of sandy shelf environments: Belgian part of the North Sea	127 - 133
<b>M.G. Kleinhans</b> , H. Douma, E.A. Addink, R. Jentink	Tidal flats, megaripples and marsh: automated recognition on aerial images	135 - 139
<b>J. Krabbendam</b> , A. Nnafie, L. Perk, B. Borsje, H.E. de Swart	Modelling the past evolution of observed tidal sand waves: the role of boundary conditions	141 - 146
<b>K. Krämer</b> , A. Lefebvre, M. Becker, G. Herrling, C. Winter	Long-term dune dynamics in the Lower Weser Estuary	147 - 149
<b>J. Lang</b> , J. Fedele, D. Hoyal	Bedform successions formed by submerged plane-wall jet flows	151 - 156
<b>J. Le Guern</b> , S. Rodrigues, P. Tassi, P. Jugé, T. Handfus, A. Duperray, P. Berault	Influence of migrating bars on dune geometry	157 - 161
<b>A. Lefebvre</b>	Three-dimensional flow above a natural bedform field	163 - 167
<b>E. Miramontes</b> , G. Jouet, A. Cattaneo, E. Thereau, C. Guerin, S.J. Jorry, L. Droz	Upslope migrating sand dunes in the upper slope of the Mozambican margin (SW Indian Ocean)	169 - 172
<b>S. Naqshband</b> , A.J.F. Hoitink	Observations of low-angle dunes under shallow flow	173 - 175
<b>A. Nnafie</b> , N. van Andel, H. de Swart	Modelling the impact of a time-varying wave angle on the nonlinear evolution of sand bars	177 - 182
<b>M.T.C. Pardal</b> , J.V. Guerra, P.C. Roos, S.J.M.H. Hulscher	Occurrence of tidal sand waves in a Brazilian coastal bay: the Sepetiba case	183 - 187
<b>J.Y. Poelman</b> , A.J.F. Hoitink, S. Naqshband	Improved quantification of sediment transport in lowland rivers	189 - 192
<b>G. Porcile</b> , M. Colombini, P. Blondeaux	Supply-Limited fluvial dunes	193 - 196

Authors	Title	Pages
<b>P.C. Roos</b>	On the crest of sandwave modelling. Achievements from the past, directions for the future	197 - 201
<b>T.V. de Ruijscher, S. Naqshband, A.J.F. Hoitink</b>	Spatial lag effects for dunes migrating over forced bars	203 - 206
<b>L. Scheiber, O. Lojek, J. Visscher, G. Melling</b>	Potential drivers for primary dune growth in the Outer Jade	207 - 211
<b>A. Slootman, M.J.B. Cartigny, A.J. Vellinga</b>	Build-up-and-fill structure: The depositional signature of strongly aggradational chute-and-pool bedforms	213 - 218
<b>N. Terseleer, K. Degrendele, L. Kint, M. Roche, D. Van den Eynde, V.R.M. Van Lancker</b>	Automated estimation of seabed morphodynamic parameters	219 - 224
<b>C.A. Unsworth, D.R. Parsons, C. Hackney, J. Best, S.E. Darby, J. Leyland, A.P. Nicholas, R. Aalto</b>	Testing the state of bedform equilibrium using MBES data from the Mekong River, Cambodia	225 - 230
<b>W.M. van der Sande, P.C. Roos, S.J.M.H. Hulscher</b>	Investigating idealized modelling of estuarine sand waves	231 - 234
<b>T.A.G.P. van Dijk, J. Damen, S.J.M.H. Hulscher, T. Raaijmakers, T. Roetert, J.J. Schouten</b>	Environmental controls on the spatial variation in sand wave morphology and dynamics on the Netherlands Continental Shelf	235 - 238
<b>T. van Veelen, P.C. Roos, S.J.M.H. Hulscher</b>	On shapes and breaks: modelling the transient evolution of tidal sandbanks	239 - 242
<b>L. Wang, Q. Yu, S. Gao</b>	A combined method of 2-D submarine superposed dune morphological parameters calculation	243 - 248
<b>W. de Wouter, F.J. Hernandez-Molina, F.J. Sierro Sánchez, D. Chiarella</b>	Ancient deep-water sand dunes – case study from upper Miocene outcrops in the southern Riffian Corridor, Morocco.	249 - 253
<b>X. Wu, D.R. Parsons, J.H. Baas, D. Mouazé, S. McLlland, L. Amoudry, J. Eggenhuisen, M. Cartigny, G. Ruessink</b>	Near-bed turbulence dynamics and suspended sediment transport over mixed sand-clay substrates	255 - 260
<b>D.R. Parsons</b>	Enigmatic Bedforms in the Deep Sea	261 - 267

# Flow over dunes and its influence on fluid mud entrainment: A concept of the dune-mud transition in tide-controlled, coastal plain estuaries

Marius Becker *Institute of Geosciences, CAU, Kiel, Germany* – [marius.becker@ifg.uni-kiel.de](mailto:marius.becker@ifg.uni-kiel.de)

**ABSTRACT:** In tide-controlled estuaries, slack water settling leads to near-bed stratification and to the formation of ephemeral fluid mud layers. These layers exhibit low consolidation rates and are subject to entrainment by the tidal flow. Due to the tidal excursion and the associated displacement of the turbidity zone, fluid mud is also deposited in troughs of large dunes, upstream and downstream of the center of the turbidity zone. Previously, in-situ observations in the Weser estuary showed that fluid mud entrainment is strongly influenced by local morphology. Here, these results are discussed in view of long-term changes of estuarine conditions, and with respect to the formation of a distinct dune-mud transition in coastal plain estuaries.

## 1 INTRODUCTION

The geodiversity in tide-controlled estuaries is high, partly caused by changes in hydrodynamic conditions from the upper channel to the outer estuary. While tidal channels are naturally often covered by sand, estuarine processes cause accumulation of fine sediments in the turbidity zone (Dalrymple and Choi 2007).

The location of the turbidity zone is linked to the occurrence of fluid mud, frequently observed in tide-controlled estuaries. In addition, deposits of erosion-resistant mud of higher density are found close to the tidally averaged center of the turbidity zone. Further upstream and downstream, fields of large dunes coexist to these mud deposits, in estuarine channels with sandy bed sediments.

Research during the past years emphasized the role of sediment-induced stratification in estuarine mud formation. Settling during slack water leads to near-bed stratification, which effectively dampens turbulence and limits entrainment after slack water (e.g. Winterwerp 2006).

During the cycle of settling and entrainment, the turbidity zone is advected by tidal currents. Ephemeral fluid mud deposits may consequently form (also) in troughs of

large dunes, as observed in the Weser estuary (North Sea, Germany). In this case, the local distribution and intensity of turbulence in dune fields affects the entrainment of fluid mud, which occurs at some point in time after slack water (Becker et al. 2013).

These observations raised the question, if and how the impact of large dunes on fluid mud entrainment influences the along-channel distribution of sedimentary features, as different as dune fields and mud deposits, along an estuarine channel.

A brief summary of previous findings is given in the next chapter. Subsequently, the formation of estuarine mud is revisited, followed by ideas regarding the development of an along-channel transition between dunes and mud. This is discussed with respect to changes of estuaries on longer time scales.

## 2 FLUID MUD IN DUNE TROUGHS

Dynamics of near-bed stratification were analysed in the Weser, Southern North Sea, Germany, based on ADCP and sediment echo sounder data (Becker et al. 2013). Sediment cores were collected during slack water.

Near-bed sediment concentrations were between 25 g/l and 70 g/l, which is close to the gelling concentration of the suspension

of mud flocs. The spatial distribution of these fluid mud layers coincided with the location of the estuarine turbidity zone.

Two types of fluid mud deposits were found. In the center of the tidally averaged location of the turbidity zone, fluid mud was deposited in form of contiguous layers on a predominantly flat river bed of fine grained bed sediments. Due to the tidal excursion, fluid mud formed also further upstream and downstream in troughs of large dunes. There, dune height ( $> 2$  m) exceeded fluid mud layer thickness.

In dune troughs, the average residence time between formation and entrainment of fluid mud was 3.2 h. Entrainment occurred as velocities exceeded 0.45 m/s, measured 1 m above the fluid mud surface (Fig. 1). While these fluid mud deposits were entirely resuspended, less entrainment was observed over flat bed, where near-bed stratification persisted until the following slack water.

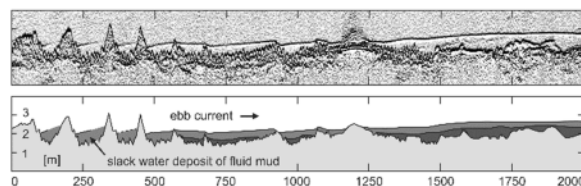


Figure 1. Sediment echo sounder profile of fluid mud during accelerating currents after flood slack water. Note the difference in stratification between dune troughs and the flat bed. In absence of dune crests, the interface between fluid mud and the upper layer appears undisturbed.

According to the local gradient Richardson number, based on mean shear, stratification in dune troughs was stable with respect to shear instabilities during entrainment. After slack water, entrainment is therefore considered to be induced by the development of dune specific turbulence, downstream of the dune crest. Such additional turbulent stress is absent in regions without large dunes, explaining the persistence of contiguous fluid mud layers over a flat river bed.

After fluid mud entrainment, a thin layer of higher concentrated mud was found to remain, adding to the heterogeneity of sediments in due troughs. These heterogeneous

trough deposits are buried by sand during the following period of dune migration. They are seen in sediment echo sounder profiles as a reflector indicating the dune migration base.

### 3 FORMATION OF ESTUARINE MUD

In the subsequent description, the influence of several processes, relevant to fine sediment transport, are taken into account, e.g. flocculation, hindered settling, and entrainment (Winterwerp 2002). On longer time scales, the influence of these processes on the along-channel distribution of sediments depends on subtle balances, between specific processes.

#### 3.1 Entrainment and turbulence damping

The formation of estuarine mud strongly depends on the balance of turbulence damping and entrainment. This is due to the specific vertical density distribution, which results from the settling behaviour of flocculated fine sediments.

Fine sediments reach the bed in form of large mud flocs. Their settling velocity determines the mass settling flux in estuaries (Manning and Dyer 2007, Soulsby et al. 2013). Unlike sand grains, mud flocs are not immediately part of the bed surface once they reach the bed. If the settling flux is high, e.g. at the location of the turbidity zone during slack water, hindered settling causes a reduction of settling velocities near the river bed. A concentrated near-bed suspension is formed, which acts as a buffer layer for fine sediments (Uncles et al. 2006). At its surface, hindered settling leads to a distinct vertical density gradient, the lutocline (e.g. Wolanski et al. 1989).

As concentrations increase near the bed, flocs form a dense network, usually called fluid mud (Winterwerp 2002). Consolidation rates of fluid mud are small, preventing the formation of an erosion-resistant layer of significant thickness and density, at least during slack water.

Due to damping of turbulence at the lutocline, fluid mud may be dynamically decoupled from the turbulent flow in the upper part of the water column (Becker et al.

2018). This decoupling must be effective for a sufficient time during the tidal cycle, to facilitate consolidation despite high current velocities. In most engineering models, this scenario is not explicitly modelled but parameterized by critical shear stresses for deposition and erosion of the respective grain size classes.

### 3.2 Influence of tidal excursion

The region of fluid mud deposition is linked to the location of the turbidity zone during slack water. In case that fluid mud deposition occurs at the end of the flood phase, settling during the following ebb slack water would occur further downstream, due to the tidal excursion and the associated displacement of the turbidity zone.

If the along-channel extent of the turbidity zone exceeds the tidal excursion, two settling periods occur at the tidally averaged location of the turbidity zone (Fig. 2). Note that in this simplified scenario, intratidal variations in the vertical velocity profile, in shear dispersion, and therefore in suspended sediment transport, are neglected.

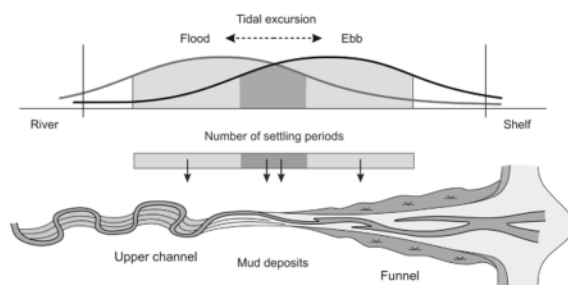


Figure 2. Number of settling periods in relation to tidal excursion and the extent of the turbidity zone.

As already mentioned, freshly deposited fluid mud was observed to persist entrainment during one tidal phase, if fluid mud is deposited over a flat river bed. Taking into account this persistence of fluid mud, slack water settling potentially leads to an increase of sediment concentration in the (remaining) fluid mud layer. Higher concentrations then induce higher stratification, and increase the effect of turbulence damping at the luto-cline.

This quasi-continuous supply of sediments by slack water settling is considered to introduce a positive feedback regarding the persistence of fluid mud to entrainment. As a result, the probability of the formation of erosion-resistant estuarine mud is increased in the tidally averaged location of the turbidity zone.

## 4 DUNE-MUD TRANSITION

Both cohesive and non-cohesive transport processes are relevant to the overall distribution and development of estuarine sedimentary features. In case of fluid mud in dune troughs, cohesive (fluid mud deposition) and non-cohesive (dune migration) transport processes are distinctly separated in time, due to the change of current velocities during the tidal cycle.

One aspect of this interaction of processes is their influence on the shape of the transition between a dune field and adjacent deposits of estuarine mud. The transition is expected to be located close to the tidally averaged location of the turbidity zone.

A scenario is considered, in which estuarine mud is already deposited somewhere in the fluvial-marine transition zone, and in which fields of large dunes coexist up and downstream of the mud deposits.

It is assumed that fine sediments settle in form of large mud flocs, such that deposition of mud occurs only according to the mechanism outlined in the previous chapter. Changes in hydrodynamic conditions and sediment supply on time scales longer than a tidal cycle are neglected. Dune height is assumed to exceed the thickness of fluid mud layers, which results from slack water settling. Dunes are considered to be oriented in direction of the tidal current after slack water.

For this situation it is hypothesized that the observed differences in fluid mud entrainment lead to a sharp transition of dunes and mud. For the Weser estuary, this transition is shown in Fig. 1, upstream of the center of the turbidity zone. The transition is sketched in Fig. 3. It is further suggested that the dune-mud transition is relatively

resistant to changes in environmental conditions.

Any sediment-induced near-bed stratification, formed during slack water, is rapidly destroyed by turbulence in fields of large dunes (Fig. 3 b), at some point in time during the following tidal phase. In other words, dune specific turbulence prevents mud deposition.

By contrast, the same stratification can function as a buffer layer for fine sediments over a flat, muddy river bed, promoting consolidation and mud deposition (Fig. 3 c, d).

Obviously, both bed configurations are associated with mechanisms, which act to sustain the respective state of the river bed. The flat bed in presence of mud supports the persistence of near-bed stratification during the tidal cycle. Dune crests, acting as roughness elements, prevent or at least reduce deposition of mud in dune fields.

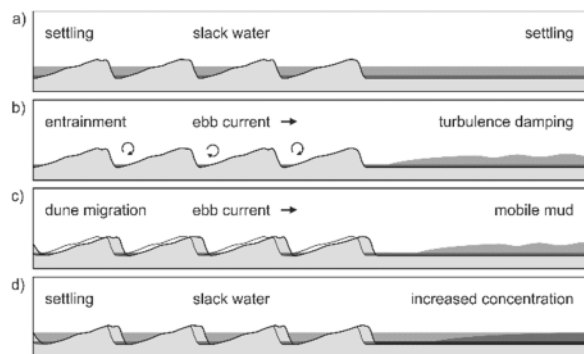


Figure 3. Settling and entrainment of fluid mud upstream and downstream of the dune-mud transition, sketched for the situation upstream of the center of the turbidity zone. Fluid mud is entrained in dune troughs (b). Relatively persistent stratification over the flat bed leads to an increase of near-bed concentration (d).

The dune-mud transition is therefore considered to resist certain changes in environmental conditions, e.g. in the supply of suspended sediments, or in the tidal current regime, which may be caused by variations in river discharge.

## 5 DISCUSSION

The aim to document this concept on the dune-mud transition is to draw attention to

the interaction of cohesive and non-cohesive transport processes, in view of recent changes in estuaries.

In response to channel deepening and extended maintenance work, the transport regime in many estuarine systems changed towards flood-dominant conditions (Burchard et al. 2017, Winterwerp and Wang 2013). The trapping efficiency and suspended sediment concentrations increased, promoting the deposition of estuarine mud. In addition, the turbidity zone is shifted further upstream.

Studies demonstrate that the varying content of mud and the associated cohesive properties of bed sediments change size and dynamics of smaller bedforms, e.g. current ripples (Malarkey et al. 2015). By contrast, almost no information exists on the fate of dune fields for the specific case considered in this study. Recent progress in physical modeling of tide-controlled estuaries shows the effect of mud on large scale morphological features (Leuven et al. 2018). Still, the small scale interaction of dunes and mud is hardly implemented in a physical model, and, at this stage, also not in common numerical models. The response of a field of large dunes to an “invasion” by mud is essentially unknown.

In general, the response of the river bed to a local change in the transport regime depends on the time scale. Neglecting anthropogenic effects, e.g. dredging activities, and assuming a continuous upstream migration of the turbidity zone, the (spatial) transition between dunes and mud may be governed by the processes described in the previous chapters. Accordingly, an abrupt transition is expected between the mud deposit and the dune field, where mud deposition is prevented by dune specific turbulence.

During the upstream shift of the turbidity zone, the locally increased supply of cohesive sediments presumably leads to pronounced stratification in dune fields. To deposit erosion-resistant estuarine mud, this stratification must persist dune related turbulence, in case that the dune height exceeds the thickness of the fluid mud layer. If instead fluid mud thickness exceeds dune height, dunes are decoupled from the flow in the upper layer and cannot act as roughness

elements, potentially leading to a faster infill of dune troughs with fine sediments.

## 6 OUTLOOK

Ideas presented in this contribution are rather speculative. In view of the complexity of the subject, the concept described here is only a starting point, in order to define a model set-up for an appropriate analysis.

The concept of the dune-mud transition stresses the aspect of self-organization, neglecting large-scale boundary conditions. One goal of the analysis would therefore be to show the effectiveness of internal processes, such as the influence of dunes on fluid mud entrainment, in contrast to external processes, e.g. the overall sediment supply.

Sediment supply to the near-bed region depends on the settling flux during slack water. In the turbidity zone, the settling flux probably varies in along-channel direction, with the maximum settling flux expected to occur in the center of the turbidity zone, which is neglected in the conceptual model.

Also neglected is the possibility that dunes are oriented not as assumed but, e.g. in ebb direction downstream of the turbidity zone. This is the case in the Weser estuary. The flood current is directed against these dunes. The structure of turbulence is different (Lefebvre et al. 2016), compared to the situation upstream of the turbidity zone. Fluid mud entrainment might occur later, increasing the time for consolidation around ebb slack water. This may have an impact on the dune-mud transition downstream of the turbidity zone.

However, these aspects can only be investigated with an appropriate model setup. This should be the next step, in view of this and similar questions regarding the interaction of near-bed transport processes in estuaries.

## 7 REFERENCES

Becker, M., Schrottke, K., Bartholomä, A., Ernstsen, V., Winter, C., Hebbeln, D., 2013. Formation and entrainment of fluid mud layers in troughs of subtidal dunes in an estuarine turbidity zone, *Journal*

- of Geophysical Research: Oceans, 118(4), 2175-2187. doi:10.1002/jgrc.20153
- Becker, M., Maushake, C., Winter, C., 2018. Observations of Mud-Induced Periodic Stratification in a Hyperturbid Estuary, *Geophysical Research Letters*, 45. doi: 10.1029/2018GL077966
- Burchard, H., Schuttelaars, H.M., Ralston, D.K., 2017. Sediment Trapping in Estuaries. *Annual Review of Marine Science*. doi: 10.1146/annurev-marine-010816-060535
- Dalrymple, R.W., Choi, K., 2007. Morphologic and facies trends through the fluvial-marine transition in tide-dominated depositional systems: A schematic framework for environmental and sequence-stratigraphic interpretation, *Earth-Science Reviews*, 81(3-4), 135-174. doi:10.1016/j.earscirev.2006.10. 002
- Jay, D.A., Talke, S.A., Hudson, A., Twardowski, M., 2015. Estuarine turbidity maxima revisited: Instrumental approaches, remote sensing, modeling studies, and new directions, in *Developments in Sedimentology*, edited by Philip, J.L.B., Ashworth, J., Daniel R.P., pp. 49-109, Elsevier. doi: 10.1016/B978-0-444-63529-7.00004-3
- Lefebvre, A., Paarlberg, A.J., Ernstsen, V.B., Winter, C., 2014. Flow separation and roughness lengths over large bedforms in a tidal environment: A numerical investigation. *Cont. Shelf Res.* 91, 57-69. doi:10.1016/j.csr.2014.09.001
- Leuven, J.R.F.W., Braat, L., van Dijk, W.M., de Haas, T., van Onselen, E.P., Ruessink, B.G., Kleinhans, M.G. (2018) Growing Forced Bars Determine Nonideal Estuary Planform. *Journal of Geophysical Research: Earth Surface* 123:2971-2992. doi:10.1029/2018JF004718
- Manning, A.J., Dyer K.R., 2007. Mass settling flux of fine sediments in Northern European estuaries: Measurements and predictions, *Marine Geology*, 245(1-4), 107-122. doi: 10.1016/j.margeo.2007.07 005
- Malarkey, J., Baas, J.H., Hope, J.A., Aspden, R.J., Parsons, D.R., Peakall, J., Paterson, D.M., Schindler, R.J., Ye, L., Lichtman, I.D., Bass, S.J., Davies, A.G., Manning, A.J., Thorne, P.D., 2015. The pervasive role of biological cohesion in bedform development. *Nature Communications* 6: 6257. doi: 10.1038/ncomms7257
- Soulsby, R.L., Manning A.J., Spearman J., Whitehouse R.J.S., 2013. Settling velocity and mass settling flux of flocculated estuarine sediments, *Marine Geology*, 339, 1-12. doi: 10.1016/j.margeo.2013.04.006
- Uncles, R.J., Stephens J.A., Law D.J., 2006. Turbidity maximum in the macrotidal, highly turbid Humber Estuary, UK: Flocs, fluid mud, stationary suspensions and tidal bores, *Estuarine, Coastal and Shelf Science*, 67(1-2), 30-52. doi: doi:10.1016/j.ecss. 2005.10.013
- Winterwerp, J.C., 2002. On the flocculation and settling velocity of estuarine mud, *Continental Shelf Research*, 22(9), 1339-1360. doi: 10.1016/S0278-4343(02)00010-9

- Winterwerp, J.C., 2006. Stratification effects by fine suspended sediment at low, medium, and very high concentrations, *Journal of Geophysical Research*, 111(C5), C05012. doi:10.1029/2005JC003019
- Winterwerp, J.C., Wang Z.B., 2013. Man-induced regime shifts in small estuaries - I: theory, *Ocean Dynamics*, 63(11-12), 1279-1292. doi: 10.1007/s10236-013-0662-9
- Wolanski, E., Asaeda T., Imberger J., 1989. Mixing across a lutocline, *Limnology and Oceanography*, 34(5), 931–938. doi: 10.4319/lo.1989.34.5.0931

# Sandwaves and megaripples on Spitsbergenbanken, Barents Sea

Valérie K. Bellec *Geological Survey of Norway (NGU), Trondheim, Norway – valerie.bellec@ngu.no*

Reidulv Bøe *Geological Survey of Norway (NGU), Trondheim, Norway – reidulv.boe@ngu.no*

Lilja R. Bjarnadóttir *Geological Survey of Norway (NGU), Trondheim, Norway – lilja.bjarnadottir@ngu.no*

**ABSTRACT:** Multibeam echosounder data acquired from the shallowest part of Spitsbergenbanken, Barents Sea, reveal a large variety of bedforms indicating sediment erosion and transport. Bedforms with wavelength of a few metres and a few centimetres to a few decimetres height are interpreted as megaripples. These are formed by waves, bottom currents or a combination of the two and occur across most of the study area. Small, medium and large sandwaves occur mainly in the southwestern part of the study area. Different kinds of megaripples are observed on and around the sandwaves, indicating transport processes of different origins.

## 1 INTRODUCTION

The Norwegian seabed mapping programme MAREANO ([www.mareano.no](http://www.mareano.no)) was launched in 2005 to improve the knowledge of the Norwegian seafloor. The programme performs detailed mapping of bathymetry and topography, seabed sediments, contaminants, biodiversity and biotopes. The knowledge gained from MAREANO provides input to ecosystem-based management, organised through integrated management plans covering the Norwegian offshore areas. In the framework of this program, multibeam echosounder data were collected from the shallowest part of the Spitsbergen Bank, which is a large bank area in the Barents Sea, between the Bear Island and Svalbard. A large variety of bedforms was identified, varying from sand ripples to megaripples and sandwaves to sandbanks.

If sandwaves have been described on some places of the Norwegian continental shelf (Bøe et al., 2009, 2015; King et al., 2014), so far sandwaves and megaripples have not been described on the shallow banks in the Norwegian Barents Sea. In general, very little information is found on ripples and megaripples on the open sea, and their connection with sandwaves.

This study focuses on the megaripples and the large sandwaves and presents preliminary interpretation of their connection.

## 2 STUDY AREA AND METHODS

### 2.1 Study area

The study area is situated in the shallowest part of Spitsbergen Bank, close to the center of a clockwise current gyre formed by the cold Polar Water (Loeng, 1989; Slagstad and McClamans, 2005) (figure 1). Tidal currents are particularly strong over the shallow bank, with maximum speeds of up to 1 m/s, amplitude of 20-40 cm and a phase angle of about 330° on the top of the bank (Gjevik et al., 1994; Gjevik, 2008).

### 2.2 Methods

The study area was mapped in 2016 using Kongsberg EM2040 Dual Head multibeam echosounder (200-400 kHz). Both multibeam bathymetry and backscatter data were recorded. The bathymetry data were processed by the Norwegian Hydrographic Service with CARIS, and the backscatter data were processed internally with QPS FMGT software. The high data density allowed gridding at 20 cm.

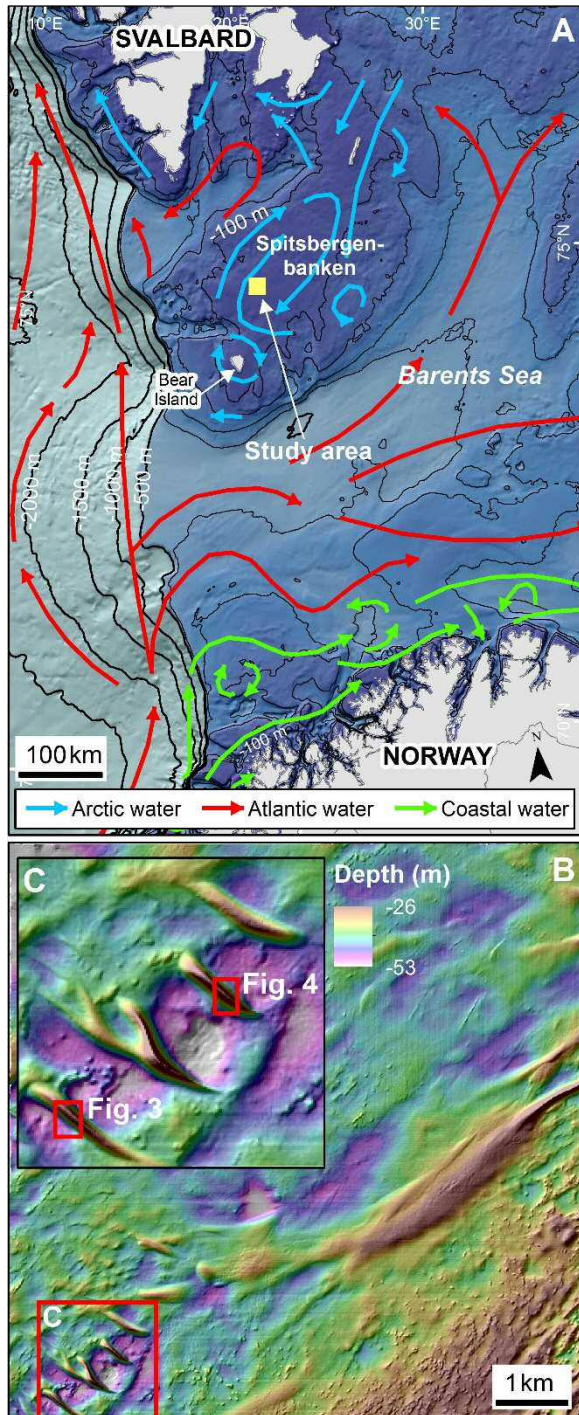


Figure 1. A) Location of the study area (yellow box) and main oceanographic currents (from Loeng, 1989). Background bathymetry: IBCAO (Jakobsson et al., 2012), B) Study area (bathymetry: MAREANO / Kartverket), C) Detail of the sandwave area.

### 3 RESULTS

#### 3.1 Megaripples

Five main types of megaripples occur in our study area (figure 2): elongated megaripples (formed by either wave or bottom

currents), interference megaripples and lingoid/lunate megaripples. The elongated megaripples show various orientations and morphologies. Wave megaripples, with N-S crest orientation, mostly occur on low lying areas, while bottom current megaripples occur on high and low areas. Two main crest orientations are observed: NW-SE (the most common) and NE-SW. The lunate/lingoid megaripples, with generally a NW-SE crest orientation, mostly occur around large sandwaves.

#### 3.2 Sandwaves

Four large sandwaves with NW-SE crest orientation occur in the southwestern part of the study area. The three southernmost sandwaves are the highest and display sharp crests whereas the northernmost sandwave only displays a sharp crest along 250 m. Smaller sandwaves occur around and north of the large sandwaves. Their crests are often smooth and they have generally a NW-SE crest orientation and shows a NE migration.

#### 3.3 Megaripples around sandwaves

Sandwaves have different types of megaripples covering their flanks (figures 3 and 4), but also at their feet. In the example of figures 3 and 4, wave megaripples occur on both sides of the sandwaves. On the west side, they are bordered by lunate/lingoid megaripples, while on the east side, they occur close to interference megaripples and/or lunate/lingoid megaripples. The flanks of the sandwave are mostly covered by current megaripples.

### 4 DISCUSSION

The large sandwaves have sharp crest, indicating that they are active. They show a northward migration which is in accordance with tidal current directions (Gjevik et al., 1994) indicating they are likely of tidal origin. The different types of megaripples around sandwaves indicate different types of transport processes, and that they can evolve quickly from one type to another.

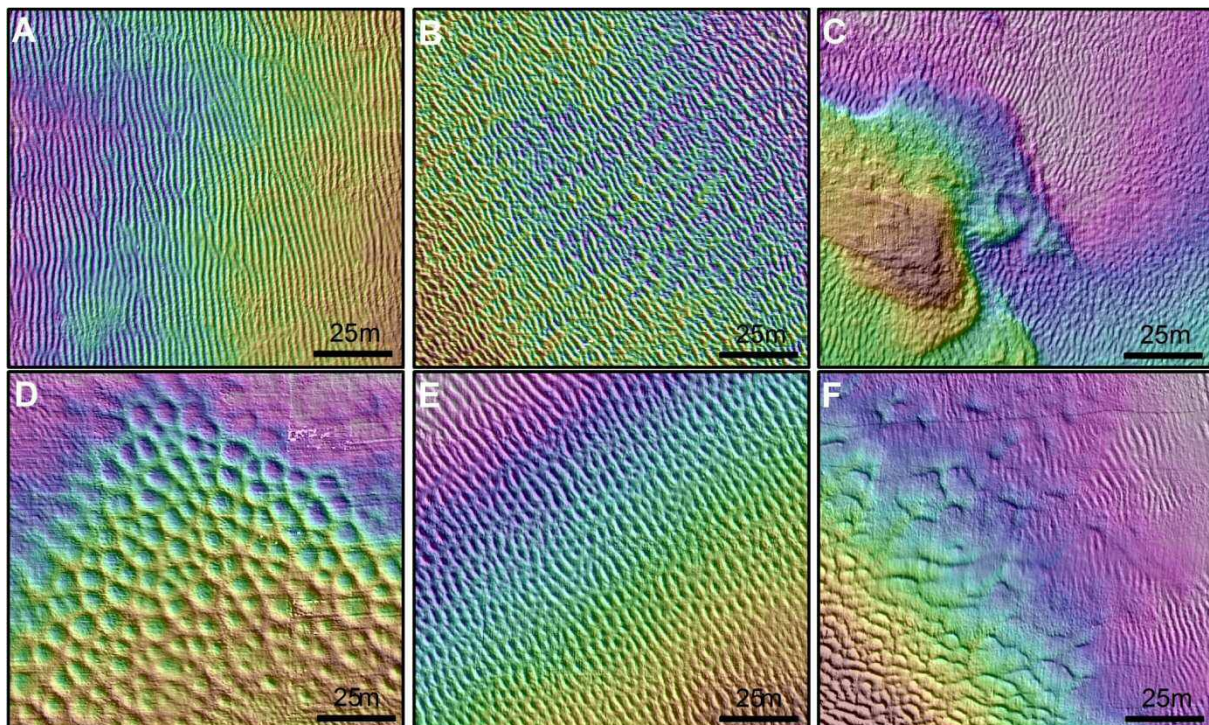


Figure 2. The different types of megaripples observed in the study area. 20 cm bathymetry grids. A) N-S wave megaripples, B) NW-SE current megaripples, C) NE-SW current megaripples, D) Interference megaripples, E) Interference megaripples, F) Lunate/lingoid megaripples. Bathymetry: MAREANO / Kartverket.

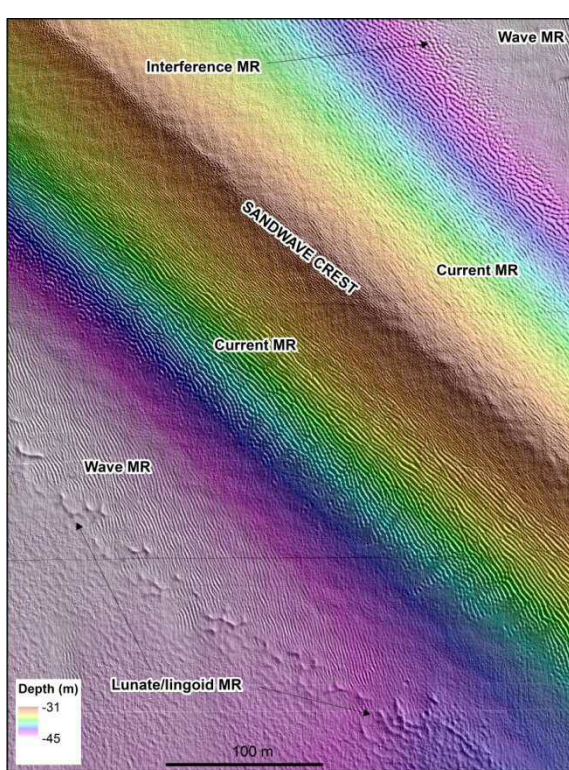


Figure 3. Different types of megaripples occur around and on the flanks of the sandwaves. MR: Megaripples. Bathymetry: MAREANO / Kartverket.

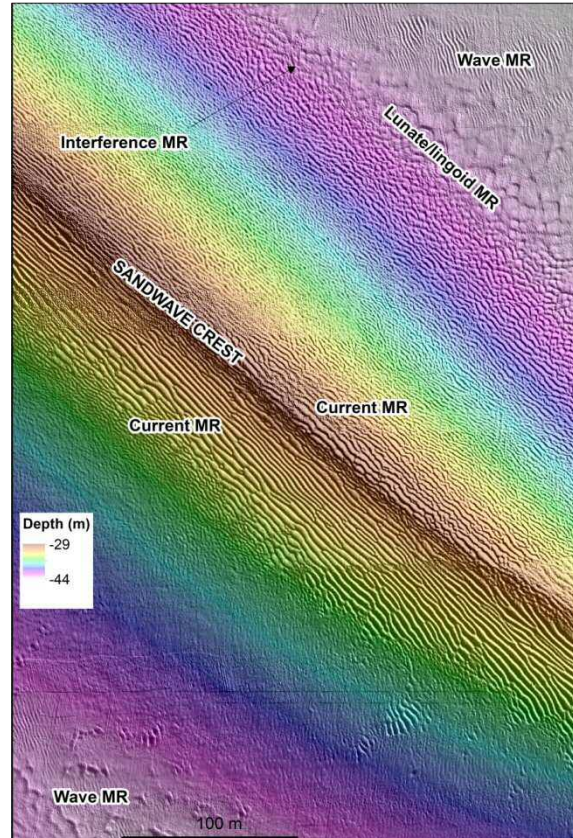


Figure 4. A sandwave showing megaripple pattern similar to the one in figure 4. MR: Megaripples. Bathymetry: MAREANO / Kartverket.

Bottom currents seem to dominate the sandwaves, while wave energy may create megaripples at the feet or between the sandwaves. Interferences megaripples, located at their feet mostly on the east flanks, indicate influence of both processes. Lunate/lingoid megaripples, which normally occur under stronger current than elongated megaripples, only occur between the sandwaves.

## 5 CONCLUSIONS

6 Megaripples are clearly observed on the 20 cm bathymetry grid. Five main types occur in the study area. Wave megaripples indicate a N-S wave energy, while current megaripples are more complex and show two main crest orientations: NW-SE and NE-SW. Wave energy and bottom current together can create interference ripples. Around sandwaves, lunate/lingoid megaripples occur, indicating a stronger current there.

The megaripples pattern is complex around the sandwaves, and four different types of megaripples occur at close range, indicating interactions of different current/wave processes around the sandwaves.

Future research could include more current studies and their influence on the formation of the megaripples and the migration of the sandwaves.

## 7 ACKNOWLEDGEMENT

We acknowledge all participants of the MAREANO programme ([www.mareano.no](http://www.mareano.no)) for their input to this paper. The multibeam data were acquired and supplied by NHS. The data is released under a Creative Commons Attribution 4.0 International (CC BY

4.0): <https://creativecommons.org/licenses/by/4.0/>

## 8 REFERENCES

- Bøe, R., Bellec, V. K., Dolan, M. F. J., Buhl-Mortensen, P., Buhl-Mortensen, L., Slagstad, D., Rise, L., 2009. Giant Sandwaves in the Hola glacial trough off Vesterålen, North Norway). Marine Geology 267, 36-54.
- Bøe, R., Skarðhamar, J., Rise, L., Dolan, M. F. J., Bellec, V. K., Winsborrw, M., Skagseth, Ø., Knies, J., King, E. L., Walderhaug, O., Chand S., Buenz, S., Mienert, J., 2015. Sandwaves and sand transport on the Barents Sea continental slope offshore northern Norway. Marine and Petroleum Geology 60, 34-53.
- Gjevik, B., E. Nøst and T. Straume, 1994. Model simulations of the tides in the Barents Sea. J. Geophysical Research 99, No C2, 3337–3350.
- Gjevik, B., 2008. Tides and topographic waves in the vicinity of the Svalbard islands in the Barents Sea. DNVA-RSE Norway-Scotland Internal Waves Symposium, Oslo 14-15 October 2008, extended abstract.
- Jakobsson, M., L. A. Mayer, B. Coakley, J. A. Dowdeswell, S. Forbes, B. Fridman, H. Hodnesdal, R. Noormets, R. Pedersen, M. Rebesco, H.-W. Schenke, Y. Zarayskaya A, D. Accettella, A. Armstrong, R. M. Anderson, P. Bienhoff, A. Camerlenghi, I. Church, M. Edwards, J. V. Gardner, J. K. Hall, B. Hell, O. B. Hestvik, Y. Kristoffersen, C. Marcussen, R. Mohammad, D. Mosher, S. V. Nghiem, M. T. Pedrosa, P. G. Travaglini, and P. Weatherall, 2012. The International Bathymetric Chart of the Arctic Ocean (IBCAO) Version 3.0, Geophysical Research Letters 39.
- King, E. L., Bøe, R., Bellec, V. K., Rise, L., Skarðhamar, J., Ferré, B., Dolan, M. F. J., 2014. Contour current driven continental slope-situated sandwaves with effects from secondary current processes on the Barents Sea margin offshore Norway. Marine Geology 353, 108-127.
- Loeng, H. 1989. Ecological features of the Barents Sea, in Proc. 6th Conf. Comité Arct. Internat., 13-15 May 1985. E. J. Brill. Leiden, 327-365.
- Slagstad, D. and McClamans, T.A., 2005. Modelling the ecosystem dynamics of the Barents sea including the marginal ice zone: I. Physical and chemical oceanography. Journal of Marine Systems 58, 1-18.

# Experimental study of ripple dimensions under steady current

Ellynn Bouvet<sup>a</sup> *University of Le Havre Normandy, France – ellynn.bouvet@doct.univ-lehavre.fr*

Armelle Jarno<sup>a</sup> *University of Le Havre Normandy, France – jarnoa@univ-lehavre.fr*

Olivier Blanpain *SHOM, Brest, France – olivier.blanpain@shom.fr*

Thierry Garlan *SHOM, Brest, France – Thierry.garlan@shom.fr*

François Marin<sup>a</sup> *University of Le Havre Normandy, France – francois.marin@univ-lehavre.fr*

<sup>a</sup>*Laboratoire Ondes et Milieux Complexes, UMR 6294 CNRS*

**ABSTRACT:** Sand ripples have been the subject of many studies. Numerous empirical formulas exist to describe their dimensions. In this paper, ripple height and length are studied at equilibrium state in a current flume. The impact of the grain size and grain shape are analysed. This work is the first stage to estimate ripple characteristics induced by a current, under simple configurations.

## 1. INTRODUCTION

Ripples are often formed when the shear stress generated by the hydrodynamics is high enough for sediments to be set in motion. They are ubiquitous in coastal seas and river, their dimensions have been widely studied in the past years: e.g. Baas (1994), Baas (2009) and Zhang (2009) studied the morphology of ripples in a laboratory flume. Boguchwal & Southard (1989) and Doucette (2002) studied ripples in their natural environment. The complexity of the subject makes it the subject of many recent studies. Numerous parameters are involved and have an impact on the motion of grains which can depends on the medium grain diameter or grain shape.

Natural environments are extremely complex and ripples are generally formed by a wide range of grain size or an unstable current. Over the years, dimensions of current induced ripples have been widely studied (e.g. Yalin 1977, Flemming 2000, Zhang et al. 2009, Soulsby 2012, Perillo 2014). They suggest that the medium grain size  $D_{50}$  has a key role on the ripple morphology and propose an empirical model to

estimate ripple height and length. The most common formula used is (Yalin 1964):

$$\lambda = 1000 D_{50} \quad (1)$$

$$\eta = 0.08 \lambda^{0.95} \quad (2)$$

Based on Baas (1994) expressions, Soulsby (2012) proposed a revisited empirical model that fits better with his data set:

For  $1.2 < D_* < 16$

$$\eta = D_{50} 202 D_*^{-0.554} \quad (3)$$

$$\lambda = D_{50} (500 + 1881 D_*^{-1.5}) \quad (4)$$

Where  $D_* = D_{50} \left[ \frac{g(s-1)}{\nu^2} \right]^{1/3}$ ,  $g$  is the gravitational acceleration ( $m.s^{-2}$ ),  $s$  is specific density of sand and  $\nu$  the kinematic viscosity ( $m^2.s^{-1}$ ). Zhang (2009) carried out an experimental study with natural sands and suggests that the characteristic height and length depends on the grain size Reynolds number ( $Re_* = \frac{u_* D_{50}}{\nu}$ ):

$$\frac{\lambda}{D_{50}} = 191.76 Re_*^{0.3} \quad (5)$$

$$\frac{\eta}{D_{50}} = 1.97 Re_*^{1.3} \quad (6)$$

The objective of this study is to describe the dimensions of bedforms generated by a unidirectional flow in a laboratory flume. The use of a flume allows the control of a few parameters: the medium grain size, the current speed and a constant depth. Ripple dimensions are measured once the equilibrium time is reached. In the present article, the aim is to quantify the impact of grain size on ripples and therefore, two sands are tested: a very fine sand and a medium sand. Furthermore, the impact of the grain shape is studied as well with the use of a third sand composed of shells debris. The impact of current speed on bedforms morphology is also tested on each sand.

## 2. EXPERIMENTAL SETUP

### 2.1 The flume

Experiments are conducted in the current flume of the University of Le Havre Normandy. It is 10 m long, 0.49 m wide and 0.49 m deep with glass walls (Figure 1). The current is generated with the help of a pump that recirculates the water in a closed circuit. A honeycomb is fixed at the entrance of the channel to break up large-scale turbulent structures in the flow.

Sediments are introduced into the flume and lay above an artificial bottom. A particular attention is paid on the flatness of the initial

sediment bed. Transported particles fall into sediment traps located at the end of the flume, allowing the measurement of bedload transport. A smooth slope is imposed right after the honeycomb so that sediments are not eroded early on and jeopardise the measurements.

### 1. 2.2 Tests conditions

In order to point out the influence of the particle size and shape on bedforms, three natural sands are tested. One is a very fine sand with a  $D_{50}$  of 119  $\mu\text{m}$  and two others have similar sized: one has a  $D_{50}$  of 356  $\mu\text{m}$  and is fully constituted of silica grains while the other has a  $D_{50}$  of 381  $\mu\text{m}$  and contains 39% of carbonate debris. Tests were performed with acid etching to quantify the percentage of carbonate debris. These debris are marine shattered shell and have a flatten shape which distinguish them from silica particles that have a shape more rounded. The three sands are considered well sorted (in accordance with the standard deviation of Soulsby (2012),  $\sigma_g = \sqrt{D_{84}/D_{16}}$ ). Their characteristics are summarized in Table 1.

Tests were realized with three currents speed: 0.33, 0.40 and 0.47  $\text{m s}^{-1}$ . The water depth was set to 25 cm and the thickness of the bed to 7 cm so that all the experiments are performed with an infinite sediment supply. In accordance with Boguchwal & Southard (1989), all the test conditions are made so that the type of bedforms generated in the flume are ripples (Figure 2).

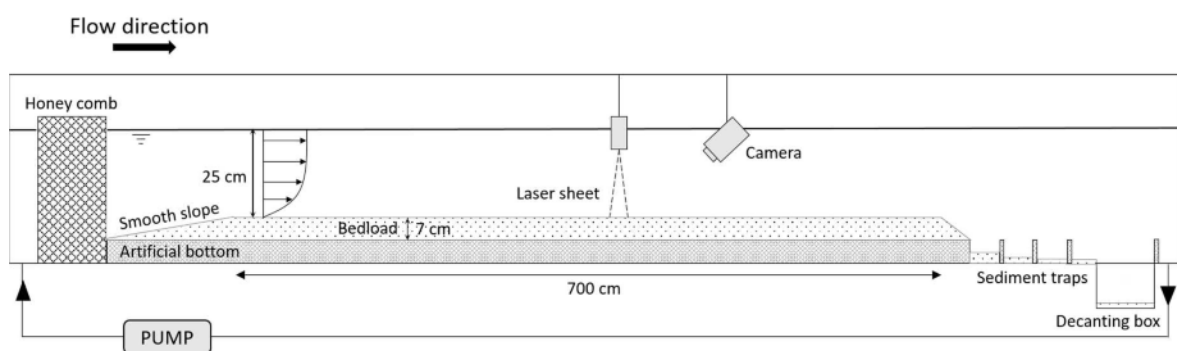


Figure 1. The current flume of the University of Le Havre Normandy

Table 1. Characterization of sands

	Fine	Medium Sand	Medium shell sand
$D_{50}$ ( $\mu\text{m}$ )	119	356	381
$\sigma_g^2$	1.29	2.04	2.98
Shell debris (%)	<1%	<1%	39%

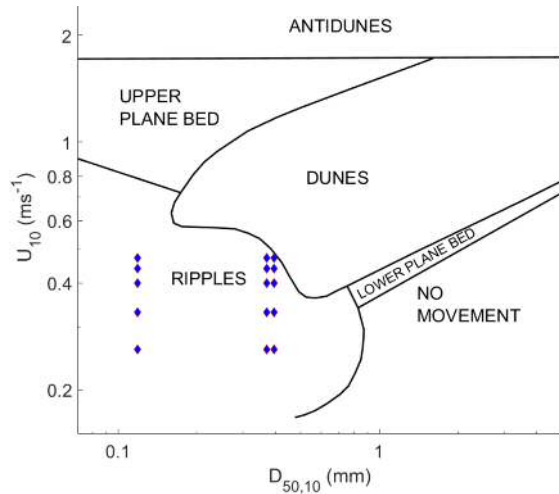


Figure 2. Plot of mean flow velocity against sediment size showing stability fields of bed phases (Modified from Boguchwal & Southward 1989).

### 2.3 Methods

A special care was paid to the experimental protocol (especially with the initial flat bed). The current is slowly increased to avoid an early erosion of the bottom. It takes 300 seconds for the current to reach its full speed. The test lasts until the ripples field is well established (the wavelength and ripple height are frequently monitored until they reach a statistically constant state). Afterwards, the current is stopped. The bathymetry is then acquired using a camera settled on a moving rail above the flume (Fig. 1). The camera records the deformation of a laser sheet projected on the bottom and they both move along the flume and covers about 3 meters of bathymetry. Finally, the full bathymetry is rebuilt in 3D with post-processing methods using MATLAB Software. Ripple heights are measured from one trough to the next crest. The wavelength considered is the total distance between two troughs (Zhang 2009).

## 3. RESULTS

Ripples fields equilibrium state is reached 9 to 17 hours after the beginning of the test depending on the sand: the fine sand reaches the equilibrium conditions more quickly than the two medium-sized sands.

Table 2 summarizes the results of the tests: the three current speeds are named V1, V2, V3 which corresponds respectively to the speeds  $0.33, 0.4$  and  $0.47 \text{ m.s}^{-1}$ . A double value indicates the first and the second mode of the distribution. Height and wavelength are given in centimeters.

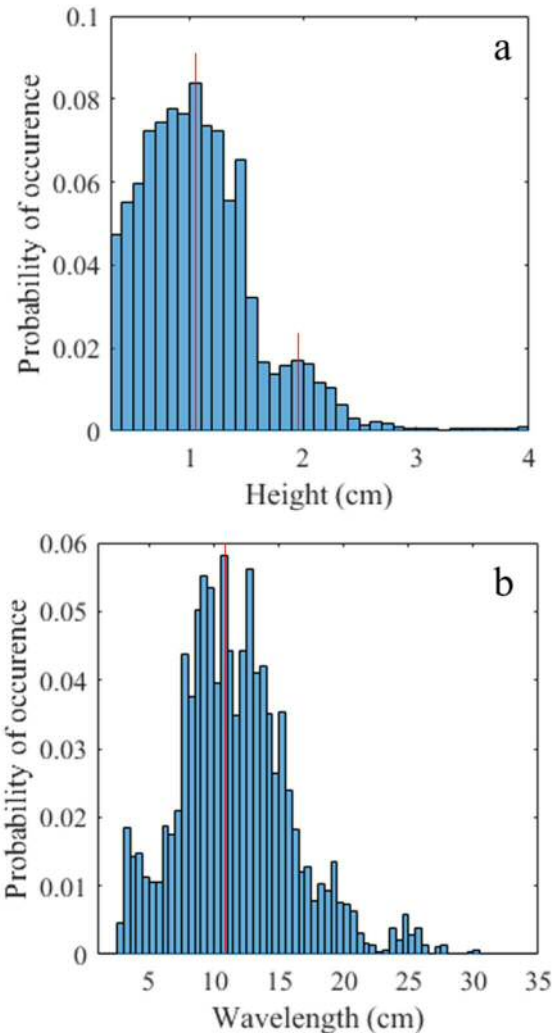


Figure 3. Height (a) and wavelength (b) distribution of the fine sand under low current speed ( $0.33 \text{ m.s}^{-1}$ ). The red lines indicate the most probable values.

Table 2. Bedform dimensions (cm)

	V1	V2	V3
Fine sand			
$H_{mean}$	0.96 / 2.16	0.8 / 2.04	0.99 / 2.13
$H_{mode}$	1.0 / 1.9	0.5 / 1.7	1.1 / 2
$H_{max}$	2.8	3.3	2.7
$L_{mean}$	11.7	13.4	14.1
$L_{mode}$	10.5	12.8	12
$L_{max}$	25.5	26	27
Medium sand			
$H_{mean}$	0.47 / 1.43	0.84 / 2.08	1.11 / 2.84
$H_{mode}$	0.4 / 1.4	0.4 / 2	0.4 / 2.75
$H_{max}$	3.2	2.9	3.7
$L_{mean}$	16	19.8	23.2
$L_{mode}$	12.5	18.5	24
$L_{max}$	31.5	37.5	44
Shell sand			
$H_{mean}$	1.18 / 2.46	1.48 / 3.2	1.27 / 2.94
$H_{mode}$	0.7 / 2.25	0.35 / 3.15	0.5 / 3.15
$H_{max}$	2.9	3.5	3.3
$L_{mean}$	17.7	23.6	25
$L_{mode}$	17	25.5	22
$L_{max}$	35	45	43

Results show that the height distribution for the three sands are multimodal. This means that ripple height can be regrouped and associated with several probable values. Figure 3 is an example of a height distribution that has two distinct modes and a wavelengths distribution that has one mode. Similar results were observed by Baas (1999). The probability of occurrence for a small ripple is higher than for a large one. It is illustrated in Figure 4: there is only a few numbers of large ripples and a majority of small ripples. The results analysis showed that the more the current speed increases the more the height distribution spreads:

Table 3. Height and wavelength theoretical values

Height (cm)	Fine sand	Medium sand	Shell sand
Yalin (1964)	1.1	3.0	3.2
Soulsby (2002)	13.	2.1	2.2
Zhang (2009) V1	1.4	2.3	2.8
Zhang (2009) V2	2.4	3.8	4.6
Zhang (2009) V3	3.5	5.9	7.1
Wavelength (cm)	Fine sand	Medium sand	Shell sand
Yalin (1964)	11.9	35.6	38.1
Soulsby (2002)	10.2	20	21.4
Zhang (2009) V1	6	26	28.6
Zhang (2009) V2	6.6	29	32
Zhang (2009) V3	7.3	32.3	36

heights tend to shift towards medium heights. For each test distribution, the mean and the maximum values are calculated: the maximum is determined by averaging the upper 10% values. Maximum heights are constant.

The same analysis is performed on wavelength: mean wavelength slightly increases with the current and distributions have one distinct probable value. At equilibrium time, the dimensions of a ripple continue to be influenced by the current: vortices set the sediments in motion and erode large ripples. Their height and wavelength are lightly decreased. Eroded sediments create a new ripple with very small height and wavelength which will slowly grow into a large ripple. Figure 5a demonstrates a cross-section of a standard large ripple that developed during the test with the shell sand at a medium speed: it has a wavelength of 23 cm and is 2.6 cm high. An hour later (Figure 5b), its height decreased to 1.8 cm and the lee has changed: a

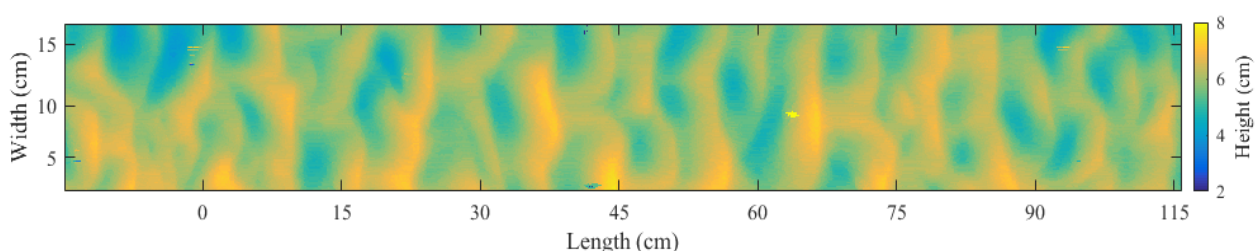


Figure 4. Bathymetry with the fine sand under low current speed ( $0.33 \text{ m.s}^{-1}$ ).

deposition of sediment occurred. On Figure 5c a new ripple is created due to the sediment deposition. It is 0.4 cm high and 5.1 cm long and match with the first height mode of the test.

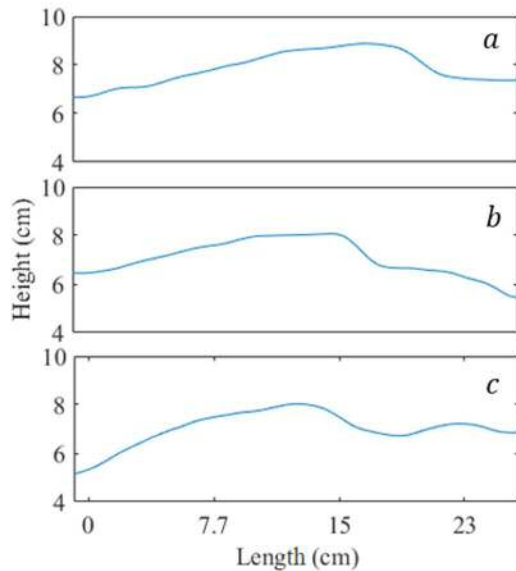


Figure 5. An example of a ripple development with the shell sand with a  $0.4 \text{ m.s}^{-1}$  flow. a: At equilibrium state  $t = 0$ , b: crest has been eroded  $t = +1\text{h}$ , c: a new ripple was created  $t = +2\text{h}$ .

Table 3 summarizes theoretical values of height and wavelength from Yalin (1964), Soulsby (2002) and Zhang (2009) models.

Because of the distribution spreading, a correlation between height of this study and theoretical heights in literature is complex. However, Zhang (2009) found that the grain size Reynolds number can be taken into account to characterize the height and length of ripples. Wavelengths estimated from Equation 5 have same trends as these study wavelengths.

In the early stage of this study, no noticeable difference was observed between medium silica sand and shell sand.

### 3. CONCLUSION AND DISCUSSION

Results show that height and wavelength distributions are complex because of the wide range of bedforms dimensions. A ripple is continuously altered by the current thus vortices can relocate sediments downstream and create a new small ripple. Bedforms dimensions found in this study are nevertheless consistent with

previous studies. Height and wavelength differences between medium silica sand and shell sand are not apparent. To take the analysis one step further, a statistical review will be performed. For instance, the use of the Principal Component Analysis (PCA) might bring new correlations to light.

Further studies will be carried out to investigate the impact of the sand heterogeneity on the bedforms: the very fine sand will be mixed with the medium sands (silica sand and carbonates debris).

In addition, the impact of bedforms on transport (both bedload and suspension) will be studied, each sand individually as well as the mixed sands.

Finally, results will be compared to simulations from a numerical model develop by the SHOM: HYCOM SEDIM.

### 4. ACKNOWLEDGEMENT

This research is part of a Ph. D. project. The authors would like to thanks Région Normandie and the DGA for founding this research project.

### 5. REFERENCES

- Baas, J. A., 1999. An empirical model for the development and equilibrium morphology current ripples in fine sand. *Sedimentology* 46, 123-138.
- Baas, J. H., 1994. A flume study on the development and equilibrium morphology of current ripples in very fine sand. *Sedimentology* 41, 185-209.
- Boguchwal L. A., Southard. J., 1989. Bed configurations in steady unidirectional water flows. Part I. Scale model study using fine sands.
- Doucette, J., 2002. Geometry and grain-size sorting of ripples on low-energy sandy beaches: field observations and model predictions. *Sedimentology* 49, 483-503.

Flemming, B. W., 2000. Marine sandwave dynamics. University of Lille, France: ISBN 2-11-088263-8.

Perillo M.M., Best. J., 2014. A unified model for bedform development and equilibrium under unidirectional, oscillatory and combined-flows. *Sedimentology* 61, 2063-2085.

Soulsby R. L., Whitehouse R. J., 2012. Prediction of time-evolving sand ripples in shelf seas. *Continental Shelf Research* 38, 47-62.

Soulsby, R. L., 1997. Dynamics of marine sands. Springfield: Thomas Telford.

Yalin, M. S., 1964. Geometrical properties of sand waves. *Journal of Hydraulics Div v90*, 105-119.

# Local spatio-temporal bedform patterns on an ebb-tidal delta

Laura Brakenhoff *Utrecht University, Utrecht, The Netherlands* – *l.b.brakenhoff@uu.nl*

Maarten van der Vegt *Utrecht University, Utrecht, The Netherlands* – *m.vandervegt@uu.nl*

Gerben Ruessink *Utrecht University, Utrecht, The Netherlands* – *b.g.ruessink@uu.nl*

**ABSTRACT:** Ebb-tidal deltas are highly complex areas, influenced by both waves and currents. The complex hydrodynamic situation creates an equally complex set of bedforms, varying in both space and time. The present study explores the presence and characteristics of bedforms on the Ameland ebb-tidal delta, which is located along the north coast of the Netherlands. Spatially extensive patterns were determined with a multibeam echosounder, whereas the development of bedforms through time in a limited spatial area was measured with a 3D profiling Sonar. It was found that the area seaward of the shoal consisted of a megaripple field, which disappeared after a storm. Within this area, 3D small-scale wave-current ripples were also found, which recovered within a few days after the storm.

## 1 INTRODUCTION

Ebb-tidal deltas are sand bodies located seaward of tidal inlets, and are therefore affected by both waves and currents, the latter comprising cross- and longshore tidal and wind-driven currents. The combined action of waves and currents creates a wide range of bedforms.

The largest bedforms on ebb-tidal deltas are sandy shoals, which have been studied thoroughly by, for example, FitzGerald (1982) and Ridderinkhof et al. (2016). In the Wadden Sea region, saw-tooth bars are often present on the downdrift side of ebb-tidal deltas, with heights up to 2 m and wavelengths (i.e. spacings) of about 700 m (Brakenhoff et al., 2018). Smaller bedforms like ripples and sand waves are also found on ebb-tidal deltas, but previous studies have only focused on these bedforms in channels and tidal inlets (e.g. Buijsman and Ridderinkhof, 2008). A more general overview of the presence and dynamics of these smaller scale bedforms is still lacking. Nevertheless, these bedforms affect bed roughness and therefore also flow and sediment transport. Thus, an accurate prediction of

bedform characteristics is vital to improve the quality of sediment transport predictions, for example those of models such as Delft3D.

Ebb-tidal deltas are complex environments in both a hydrodynamic and a morphodynamic sense. Forcing conditions vary between wave- and current domination, and waves and currents can interact at different angles. Thus, traditional bedform predictors for wave-only or current-only conditions (e.g. Allen, 1968; Dingler and Inman, 1976) cannot be used. Recently, formulas were developed that incorporate both waves and currents for prediction of bedforms in mixed hydrodynamic environments (e.g. Kleinhans, 2012; Soulsby et al., 2012). However, these predictions have so far not been tested under the complex field conditions of an ebb-tidal delta.

The present study aims to analyse the spatio-temporal behaviour of small-scale bedforms on an ebb-tidal delta and relate these to the hydrodynamic forcing. The research questions are:

1. Which small-scale bedforms are present on the ebb-tidal delta?
2. How do the bedforms change through time?

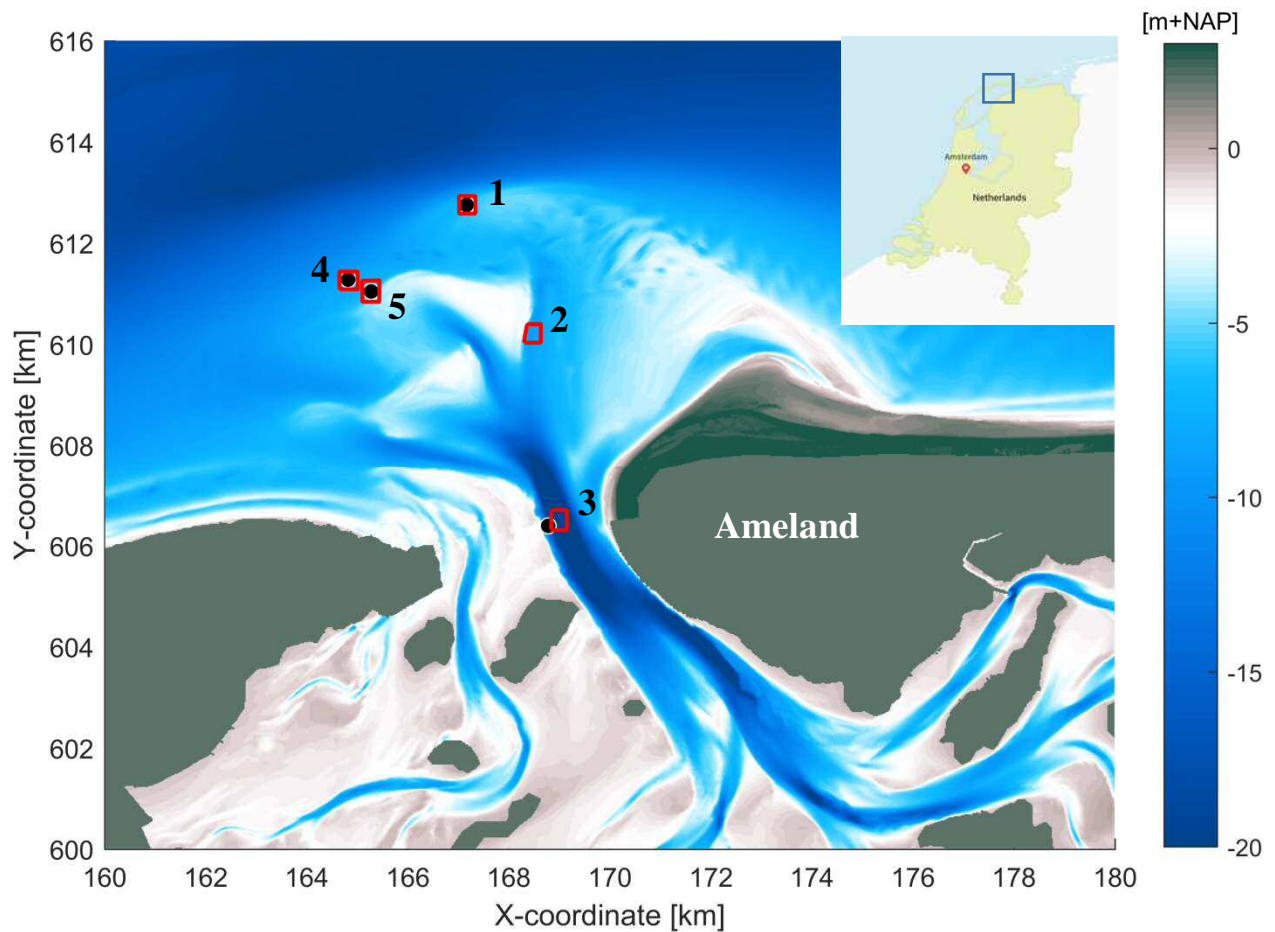


Figure 1. Bathymetry of the Ameland ebb-tidal delta of 2017 (measured by Rijkswaterstaat), including the location of multibeam measurements (red square). The measurement frames are indicated with black dots.

3. What is the relation between bedform characteristics and local hydrodynamics?

## 2 METHODS

The ebb-tidal delta of the Ameland Inlet, which is located in the Dutch part of the Wadden Sea, was studied in two ways. On August 29 and October 24, 2017, several parts of the ebb-tidal delta were mapped with a multibeam echo-sounder, giving an overview of bedform presence in a spatially extensive area, but at only two moments in time (Figure 1). In addition, four frames were installed in or near four of the multibeam survey areas from August 29 to September 27, 2017 (Figure 1). The frames were each equipped with a pressure transducer, three Acoustic Doppler Velocity me-

ters (ADVs) and a Marine Electronics type 2001 3D profiling SONAR. The Sonar was mounted at 1.9 m above the bed, and set to scan the bed once per hour for approximately 15 minutes. This shows bedforms on a small spatial scale of 2x2 m, but with a high resolution in time. The measurement frequency of the pressure transducer was 4 Hz, and wave heights were calculated using the spectral moment per 30 min. Current speeds derived from the ADVs were averaged over 30 minute intervals. Grain size near frame 5 was 185.8  $\mu\text{m}$ , which was determined by a box core sample.

### 2.1 Data analysis

The multibeam point clouds were interpolated onto a grid with 0.5x0.5 m cell size, thus eliminating small-scale ripples but still conserving the megaripples. The images

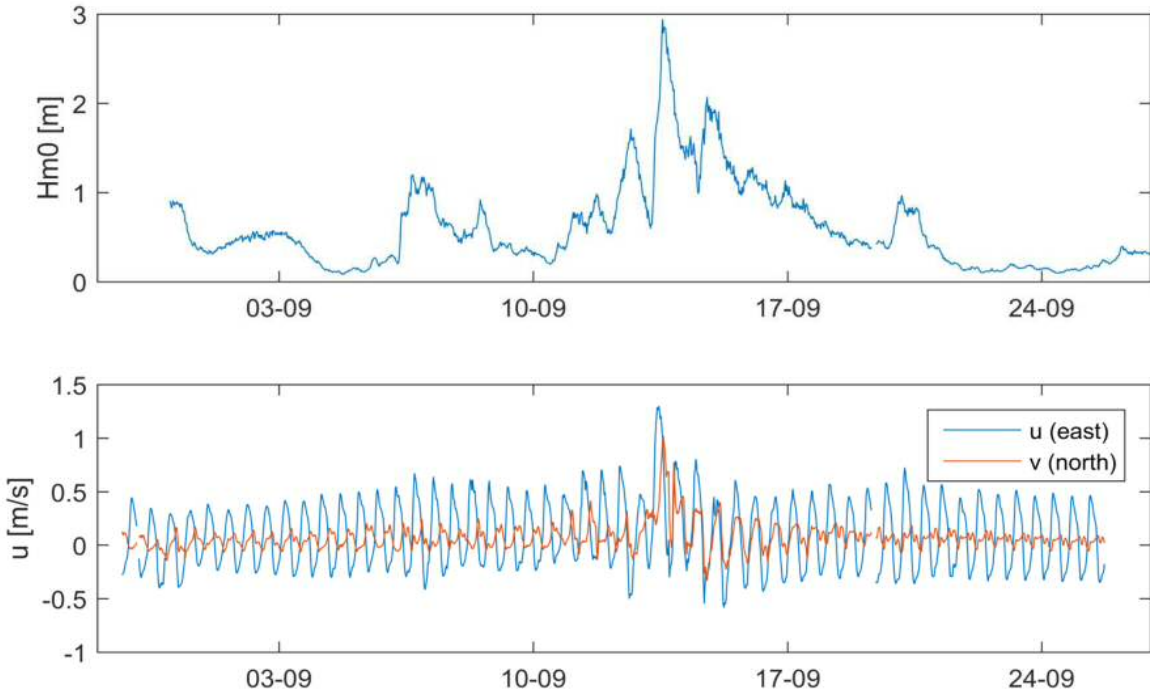


Figure 2. Wave heights and current speeds as measured at frame 5.

were processed in two ways. First, each image was divided into profiles along the x-direction, which were detrended by a second order fit. The bedform wave length  $L$  was determined by a wavelet analysis of the multibeam profiles using the method of Grindsted et al. (2004), which was based on Torrence and Compo (1998). This gives wavelengths along the profile. Combining all profiles results in a 2D image of wavelengths.

Also, the images were divided into moving windows of  $25 \times 25$  m, after which the bed level in each window was detrended. Bedform heights were given by:

$$H = 2\sqrt{2}\sigma \quad (1)$$

with  $\sigma$  being the standard deviation of a window (Smith, 1997).

Following the bed detection procedure described in Ruessink et al. (2015), the SONAR point clouds were processed to a grid with  $0.01 \times 0.01$  m cell size. Smoothing was performed with a loess filter to reveal the ripples. After a first visual inspection revealed that the ripples had length scales between 0.10 and 0.25 m, all bedforms with length scales larger than 0.42 m or smaller

than 0.07 m were removed. After this, the image was detrended by subtracting a second order surface fit.

Bedform steepness was calculated as:

$$s = H/L \quad (2)$$

where  $H$  = bedform height and  $L$  = bedform wave length.

To determine bed shear stresses, wave and current related Shields parameters were calculated following Kleinhans and Grasmeijer (2006).

### 3 PRELIMINARY RESULTS

#### 3.1 Hydrodynamic conditions

The wave height and current speed through time at frame 5 can be found in Figure 2. The average water depth at this frame was 6.5 m. Fair-weather conditions included wave heights between 0 and 1 m, and maximum current speeds of approximately 0.5 m/s. A storm occurred around September 13 (the maximum wave height was reached on September 13 at 13:30 hours), with wave heights up to 3 m and current speeds of

more than 1 m/s in both the u and v direction. Waves during the peak of the storm presumably broke at the frame location.

Figure 3 shows the bed shear stresses related to waves and currents, illustrating that during most of the campaign, the conditions were dominated by both waves and currents ('mixed').

### 3.2 Multibeam

Figure 4 shows the depth as measured by the multibeam on August 29 and October 24, together with the associated wave lengths. On August 29, bedforms with north-south oriented crests were present. These bedforms had wavelengths of 15-25 m and heights of 0.05-0.4 m, resulting in steepness values of 0.01-0.02. These megaripples (classification according to Ashley, 1990) were asymmetric, with the steeper slope pointing to the east. In contrast, no bedforms

were found on October 24.

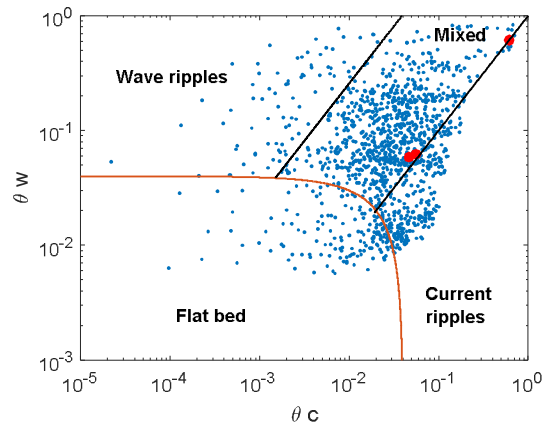


Figure 3. Nondimensional wave- ( $\theta_w$ ) and current- ( $\theta_c$ ) related Shields parameters throughout the measurement period. Red dots indicate the moments visualized in Figure 5. Black lines indicate transition between wave-, wave-current, and current-dominated ripples. Red line indicates threshold for ripples vs flat bed. (Lines reproduced after Amos et al., 1988.)

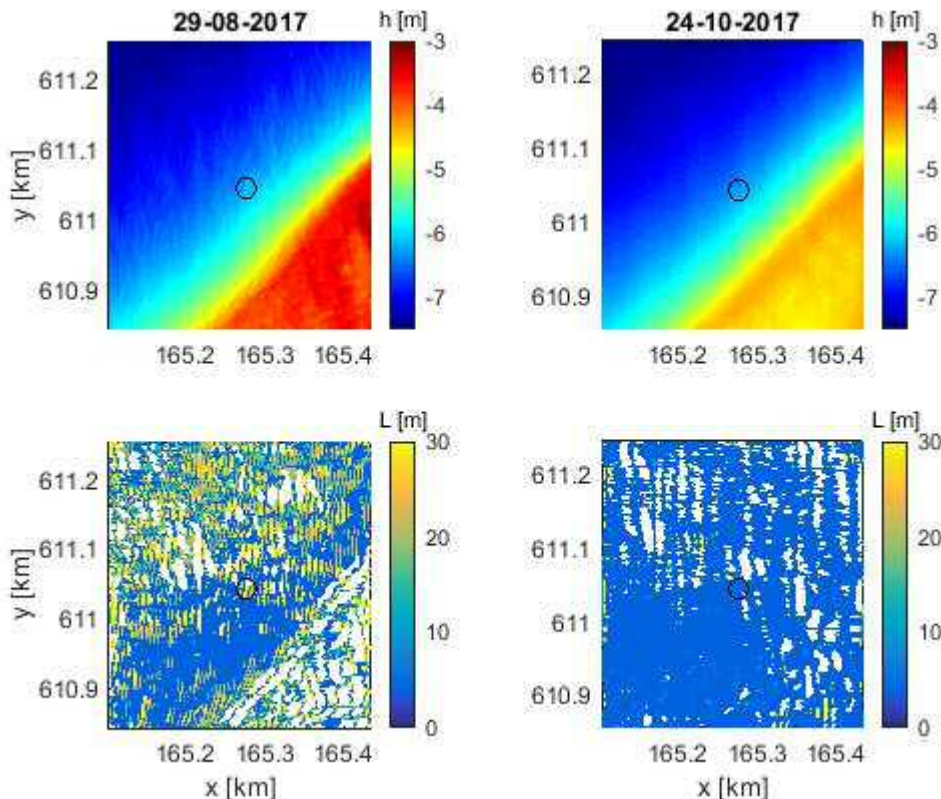


Figure 4. Depths as measured by the multibeam at August 29 (upper left) and October 24 (upper right), and the bedform wave lengths determined with wavelet analysis (bottom). Blank areas indicate that the significance was below the 95% confidence level. Circle shows the location of the frame.

It is highly likely that the storm of September 13 washed out the megaripples and also removed sand from the shoal (note the larger water depths on October 24 compared to August 29 in the lower right corner). While the storm lasted for only a few days, the megaripples were still absent six weeks later.

### 3.3 3D Profiling Sonar

Some typical examples of the 3D Profiling Sonar are given in Figure 5. Before and after the storm, ripples were clearly present, but no ripple crests could be defined as the images consist of disconnected three-dimensional ripples (Figure 5A and C). Ripple heights were approximately 0.05 m, and length scales were in the order of 0.1 m. In both cases, the bed state was dominated by both waves and currents, but tending towards current-dominance ( $\theta_w \approx \theta_c \approx 0.05-0.06$ ). Ripples were active, i.e. their shape and position changed with time.

During the storm, the distinct ripples disappeared, but the bed never flattened out entirely (Figure 5B). The ripple marks decreased in height to less than 0.01 m. The values for the wave- and current-related Shields parameters were both 0.62, indicating that both waves and currents were highly influential (Figure 3).

Finally, it is noteworthy that the image in Figure 5C was measured just a few days after the storm and, contrary to the megaripples, clear small-scale ripples were already present again.

## 4 DISCUSSION

The difference between the presence of ripples and megaripples in space and time emphasizes the need of time-dependent bedform predictors for megaripples. The study area is highly dynamic and dominated by both waves and currents, which will be the basis of further research. First, ripple wave lengths and heights will be calculated, which will then be related to the wave- and current

related bed shear stresses. A similar analysis will be conducted with the orientation and migration direction of all bedforms.

Future work will focus on comparing the results that were shown above to the data of the other measurement locations in Figure 1. In addition, the prediction of ripples and megaripples in both space and time will be studied.

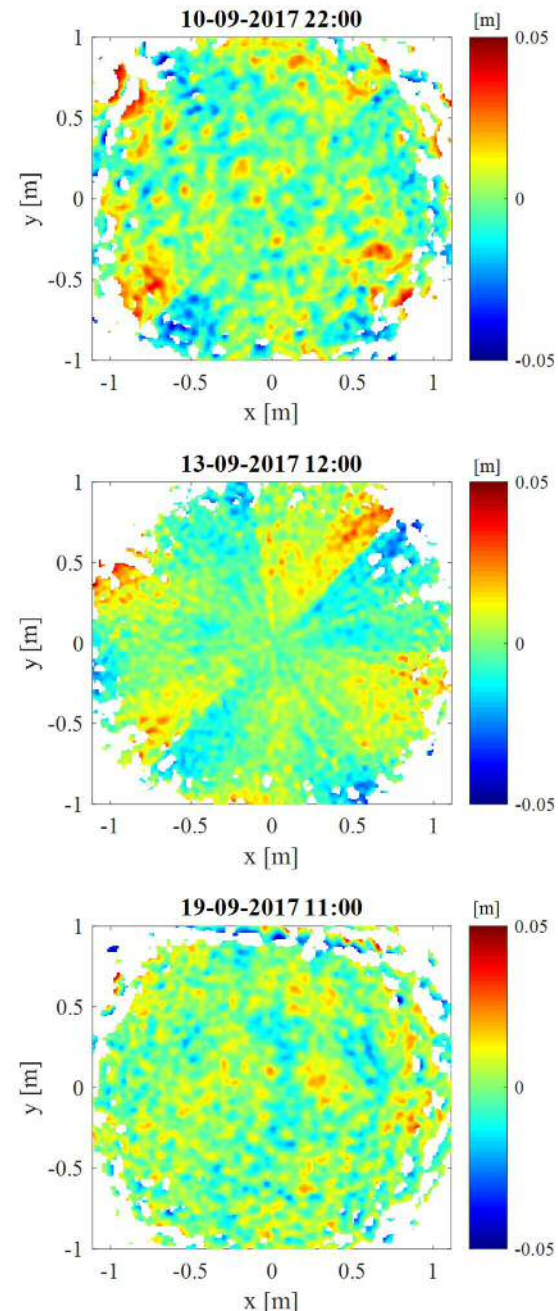


Figure 5. Bed levels as measured by the Sonar on September 10 (upper plot), 13 (middle plot) and 19 (lower plot).

## 5 CONCLUSIONS

At the Ameland ebb-tidal delta, small-scale 3D ripples are present most of the time, which respond quickly to changes in hydrodynamic conditions. Megaripples are not always found, suggesting that they are not only influenced by wave height and current speed, but also by the time that has passed since a storm event has taken place. Further analysis on this topic will provide more insight into the relation between hydrodynamic forcing and bedform presence and dynamics.

## 6 ACKNOWLEDGEMENTS

This project is part of the program SEA-WAD: “SEdiment supply At the Wadden Sea ebb-tidal Delta. From system knowledge to mega-nourishments”. This research is supported by the Dutch Technology Foundation STW, which is part of the Netherlands Organisation for Scientific Research (NWO), and which is partly funded by the Ministry of Economic Affairs. The authors would like to thank Rijkswaterstaat for their support during the field campaign.

## 7 REFERENCES

- Allen, J.R.L., 1968. Current Ripples. New York Elsevier
- Amos, C.L., Bowen, A.J., Huntley, D.A., Lewis, C.F.M., 1988. Ripple generation under the combined influences of waves and currents on the Canadian continental shelf. *Continental Shelf Research* 8(10): 1129-1153.
- Ashley, G.M., 1990. Classification of large-scale subaqueous bedforms: a new look at an old problem. *Journal of sedimentary petrology* 60(1): 160-172.
- Brakenhoff, L.B., Van der Vegt, M., Ruessink, B.G., 2017. Saw-tooth bar dynamics on the Ameland ebb-tidal delta. *Proceedings Coastal Dynamics* 2017: 292-299.
- Buijsman, M.C., Ridderinkhof, H., 2008. Long-term evolution of sand waves in the Marsdiep inlet. I: High-resolution observations. *Continental Shelf Research* 28: 1190-1201.
- Dingler, J.R., Inman, D.L., 1976. Wave-formed ripples in nearshore sands. *Coastal Engineering Proceedings* 15: 2109-2126.
- FitzGerald, D.M., 1982. Sediment bypassing at mixed energy tidal inlets. *Coastal Engineering*, 1094-1118.
- Grinsted, A., Moore, J.C., Jevrejeva S., 2004. Application of the cross wavelet transform and wavelet coherence to geophysical time series. *Nonlinear Processes in Geophysics* 11: 561–566.
- Hine, A., 1975. Bedform distribution and migration patterns on tidal deltas in the Chatham Harbor Estuary, Cape Cod, Massachusetts. *Geology and Engineering*: 235-252.
- Kleinhans, M.G., 2005. Phase diagrams of bed states in steady, unsteady, oscillatory and mixed flows. *EU-Sandpit end-book*, Ed. Leo van Rijn, Aqua Publications, The Netherlands, paper Q
- Kleinhans, M.G., Grasmeijer, B.T., 2006. Bed load transport on the shoreface by currents and waves. *Coastal Engineering* 53(12): 983-996. doi: 10.1016/j.coastaleng.2006.06.009
- Soulsby, R.L., Whitehouse, R.J.S., Marten, K.V., 2012. Prediction of time-evolving sand ripples in shelf seas. *Continental Shelf Research* 38: 47-62. doi:10.1016/j.csr.2012.02.016
- Ridderinkhof, W., Hoekstra, P., Van der Vegt, M., De Swart, H.E., 2016. Cyclic behaviour of sandy shoals on the ebb-tidal deltas of the Wadden Sea. *Continental Shelf Research* 115: 14-26.
- Ruessink, B.G., Brinkkemper, J.A., Kleinhans, M.G. 2015. Geometry of wave-formed orbital ripples in coarse sand. *Journal of Marine Science and Engineering* 3: 1568-1594. doi: 10.3390/jmse3041568
- Smith, S.W., 1997. The Scientist and Engineer's Guide to Digital Signal Processing. California Technical Publishing San Diego, CA, USA, ISBN: 0-9660176-3-3
- Torrence, C., Compo, G.P., 1998. A practical guide to wavelet analysis. *Bulletin of the American Meteorological Society* 79: 61–78.

# Estimation of bedload by tracking supply-limited bedforms

Till Branß, *Leichtweiß-Institut für Wasserbau, Technische Universität Braunschweig, Braunschweig, Germany* – [t.branss@tu-braunschweig.de](mailto:t.branss@tu-braunschweig.de)

Francisco Núñez-González, *Leichtweiß-Institut für Wasserbau, Technische Universität Braunschweig, Braunschweig, Germany* – [f.nunez-gonzalez@tu-braunschweig.de](mailto:f.nunez-gonzalez@tu-braunschweig.de)

Jochen Aberle, *Leichtweiß-Institut für Wasserbau, Technische Universität Braunschweig, Braunschweig, Germany* – [jochen.aberle@tu-braunschweig.de](mailto:jochen.aberle@tu-braunschweig.de)

Dune tracking has been often used for the estimation of bedload sediment transport rates as an alternative for computations with empirical formulas or direct measurements using bedload samplers. With the assumption of a triangular dune shape, the most general form of the tracking method requires the bedform height and migration velocity, as well as the sediment porosity as input parameters. However, the method assumes a tight succession of bedforms, which is not fulfilled under sediment supply-limited conditions. This paper presents results from a study in which the bedform tracking method was applied to supply-limited dunes observed in laboratory experiments. It is shown the gaps between bedforms play a crucial role for the accurate determination of bedload

## 1 INTRODUCTION

Reliable estimates of bedload sediment transport rates are required for the anticipation of the morphological evolution of a stream, as well as for assessing the impact of perturbations on riverbed stability and sedimentation. A large variety of empirical formulas can be found in literature for bedload sediment transport computations; nevertheless, applying these different formulas can result in estimates of the transport rates which can differ in more than one order of magnitude for identical boundary conditions. To overcome this problem, direct field measurements can be used to determine the sediment transport rate of a specific stream section; however, field campaigns are costly and time-consuming, while a large number of samples is required for an accurate characterization of bedload variability and its dependence on flow stage.

An alternative method for the determination of bedload transport rates is the bedform tracking technique. The approach has been successfully applied in laboratory and field conditions by different authors in the last decades (e.g. Simons et al., 1965; Dietrich & Smith, 1984; Gabel, 1993; Blom et

al., 2003; Nittrouer et al., 2008; Aberle et al., 2012). However, no previous experiences or guidelines can be found for applying the method to bedforms under supply-limited conditions.

Supply-limited bedforms occur when the transport capacity of the flow is higher than the amount of available sediment which can be transported. They develop over an immobile bed, as for instance, over armour layers in gravel bed rivers, where they may occur through a gravel-sand transition with supply of suspended sand to the bed, or when there is a persistent sand supply from the floodplain and hillslopes (Venditti et al., 2017). Archetypal supply-limited bedforms include sand-ribbons, barchans, and dunes (Kleinhanß et al., 2002). Their existence depends on sand supply and transport conditions. The tracking technique cannot be applied to sand-ribbons, since these bedforms are oriented parallel to the flow and do not show a traceable regular structure.

In this work we apply the bedform tracking technique to supply-limited dunes. We show that the most commonly used equation to compute the bedload transport rate by tracking bedforms, which is a function of the bedform migration rate, bedform height,

sediment porosity and a shape factor, must be corrected when being applied to supply-limited conditions. In this case, an additional coefficient must be considered which depends on the bedform length and separation distance between the bedforms. We also show that, if high resolution bed scanning data are available, bedload can be computed by integrating the volume fraction of sediment solids from the elevation model and considering the bulk bedform migration celerity, irrespective of the sediment-supply conditions.

## 2 BEDFORM TRACKING METHOD

### 2.1 General equation

Given a train of regular bedforms migrating downstream without changing shape and with a constant celerity  $c_b$ , the volumetric bedload transport rate  $q_b$  per unit width and time, can be computed by

$$q_b = c_b \frac{V \cdot (1-\phi)}{L_b} \quad (1)$$

where  $V$  is the bulk volume of sediment in each bedform,  $\phi$  is the sediment porosity, and  $L_b$  is the bedform length (see Fig. 1a). Equation (1) is valid if there is no sediment movement at the base elevation of the bedforms.

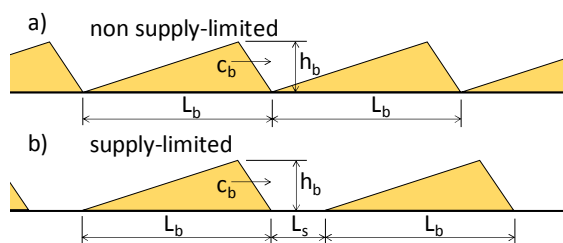


Figure 1. Geometrical variables to calculate the bedload transport rate by bedform tracking in non-supply-limited (a), and in supply-limited bedforms (b).

The volume in each bedform can be expressed as  $V = CL_b h_b$ , where  $h_b$  is the bedform height, and  $C$  is a coefficient dependent on the bedform shape.  $C = 0.5$  for a triangular dune shape which is within the

range of values reported in the literature for both open channel and intertidal dunes (0.3 to 0.8; e.g. van den Berg, 1987; Wilbers, 2004; Knaapen, et al., 2005; Abraham, et al., 2011). Introducing the above definition of  $V$  in Eq. (1) yields:

$$q_b = C c_b h_b \cdot (1-\phi) \quad (2)$$

This is the most general equation that has been used to estimate sediment transport rates by tracking bedforms. It can readily be shown that integration of the Exner equation for sediment continuity leads to the same result. The equation can be applied when the average bedform celerity and height may be accurately determined and when the bedforms cover the entire width of the channel (Simons et al., 1965). Note that this equation does not consider the portion of bedload occurring outside of the bedform migration, as for instance saltating bed material particles.

Cross-correlation techniques have been used by many authors (e.g. Nikora et al., 1997; Henning, et al., 2010) for determining  $c_b$ , while methods like the h-level crossing analysis have been used in defining the average height of the bedforms (e.g. Shen and Cheong, 1977; van der Mark et al., 2008).

### 2.2 Methods for high-resolution bed-surface measurements

A limitation of Eq. (2) is that the results may be biased by the choice of the shape factor and by the method used to determine the bedform height  $h_b$ . To circumvent the latter problem, some authors have used the standard deviation  $\sigma$  of bed elevations as a surrogate measure for  $h_b$  (e.g. Willis & Kennedy, 1977; Coleman et al., 2011); nevertheless, representative values of  $\sigma$  can only be obtained if the bed elevation data have a sufficient spatial and temporal resolution.

Aberle et al. (2012) presented two methods to determine bedload transport from high-resolution measurements of bed surface elevations. The advantage of these methods is that the knowledge of  $h_b$ , which can be

difficult to obtain in 3D-dune fields, is not required and that no assumptions regarding the shape of the bedforms must be made. The first method, requiring information on the distribution of sediment volume concentration, considers the bed layer velocity variation with depth, which is computed by cross-correlation analysis of elevation slices (see also Henning, 2013). The second method is a simplified bulk-surface approach based on the first method. Within this approach, it is assumed that the bed-layer velocity is constant with depth. Testing the two methods with artificially created data and data from laboratory experiments, Aberle et al. (2012) found comparable results. Therefore, only the simplified bulk-surface approach will be considered in the following. Hence, the bedload transport rate can be computed from the integration of the bed elevation model as

$$q_b = c_b \int_{\eta_1}^{\eta_2} \phi_s dz \quad (3)$$

where  $\phi_s$  is the volume fraction of sediment solids in the analysed domain,  $z$  is the vertical coordinate, and  $\eta$  is the bed surface elevation with subscript 1 defining the base of zero transport and 2 the maximum recorded bed-surface elevation.

### 2.3 Application to supply-limited bedforms

Bedforms under supply limited conditions are characterized by gaps between subsequent bedforms, which shrink as the supply increases. These gaps must be considered in the estimation of average bedload transport rates over an entire dune field. Using Eq. (1), this can be done by normalizing the migrating sediment volume with the sum of the bedform length ( $L_b$ ) and the separation distance between two subsequent bedforms ( $L_s$ ) instead of using only  $L_b$  (see Fig. 1b), i.e. for supply-limited conditions one obtains:

$$q_{bSL} = c_b \frac{V \cdot (1-\phi)}{L_b + L_s} \quad (4)$$

Introducing the volume of a bedform into this equation results in:

$$q_{bSL} = C c_b h_b \frac{L_b \cdot (1-\phi)}{L_b + L_s} \quad (5)$$

Note that Eq. (2) is a particular form of the more general Eq. (5) when  $L_s = 0$ . It can be shown that, for the application of Eq. (5) to a surface area or a time domain, the ratio  $L_b/(L_b+L_s)$  must be replaced by  $f_b/(f_b+f_s)$ , where  $f_b$  ( $f_s$ ) is the fraction of surface or time with the bed (not) covered by bedforms. Similarly, referring to the distribution of volume fraction of sediment solids used in Eq. (3), the following equation can be derived:

$$\frac{L_b \cdot (1-\phi)}{L_b + L_s} = \phi_s(\eta_1) \quad (6)$$

The simplified bulk-surface approach described by Eq. (3) does not require any further adjustments to be applied to supply-limited bedforms. The method requires the definition of the vertical extent of the bed that is active in sediment transport; this may not be straightforward when non-supply limited bedforms are highly irregular, but might not pose any complication when supply-limited bedforms are analysed, as in this case the base level of zero transport  $\eta_1$  is the same level as the base of the bedforms.

Equations (2), (3) and (5) are applied and compared below, using laboratory experimental data with supply-limited dunes. The experimental setup and measurements are described first, and later on the results are presented, and compared.

## 3 EXPERIMENTAL DATA

In order to evaluate the performance of the different variants of the bedform tracking method, results of three experimental runs from Branß et al. (2018), in which supply-limited bedforms developed along the main channel of a half trapezoidal compound-section channel, are used. The experiments were performed in a 2 m wide and 30 m long sediment recirculating flume, at the

hydraulics laboratory of the Leichtweiß-Institut für Wasserbau of the Technische Universität Braunschweig, Germany. The main channel of the compound cross-section was 60 cm wide and 10 cm high and was bounded to the left by the flume glass walls and to the right by a 1:1 slope bank covered with 3 cm high flexible artificial grass. The bed of the main channel was constructed from film faced plywood plates which were coated by a single layer of the same granulate material which was used as bedload material. This material consisted of polystyrene grains of cylindrical shape, with a diameter of 2.06 mm, a solid density of 1058 kg/m<sup>3</sup>, and a bulk porosity of 0.38.

The three experimental runs were performed under quasi uniform flow conditions, with a constant discharge of 22 l/s, and a constant bed slope of 0.0005. The duration of each experiment was 19.5 h. Sediment transport rates were continuously monitored within the return pipe of the sediment recirculating system, using a negele four-beam turbidity meter. Bed levels in the main channel were recorded continuously using 16 ultrasonic sensors (SeaTek 5 MHz Ultrasonic Ranging System), in two cross-sections located 17 m and 17.81 m downstream from the flume inlet. In each cross section, 8 sensors were mounted with a spacing of 8 cm. Each recorded value consisted of an average of 10 readings to minimize distortions by suspended sediment. The corresponding recording interval was 0.35 s (2.9 Hz). Further post processing of the signals included smoothing by a moving average over 50 measuring points to reduce noise introduced by particles in suspension.

An important boundary condition was the total amount of polystyrene material in the main channel during each run. Differences in the amount led to different sediment transport rates and bedform characteristics. More details on the experimental setup and measurements can be found in Branß et al. (2018).

## 4 RESULTS

Measured average sediment transport rates and characteristics of the bedforms obtained from the ultrasonic sensors are shown in Table 1. Supply-limited conditions were observed in all three runs. Although particles transported in suspension were observed in all three runs, most of the transport occurred as bedload within the migrating dunes.

Table 1: Experimental results

Run	$q_b$ [g/s·m]	$h_b$ [cm]	$c_b$ [mm/s]	$\phi_s(\eta_1)$ [-]	$\int \phi_s dz$ [cm]
1	24.5	3.6	3.7	0.40	0.8
2	40.4	5.0	4.2	0.45	1.3
3	57.2	5.5	4.6	0.53	1.8

The analysis of the time series of bed elevations showed that bedforms grew in height during the first hour, and that their average dimensions remained stable afterwards. The analysis below refers to the stable period.

Individual bedforms were identified from the time series data. Peak elevations higher than 1 cm above the fixed bed level were interpreted as dune crest level and in order to be validated as bedform, the temporal lag between two peaks had to be larger than 30 s. The median of the cumulative distribution of peak elevations (see Fig. 3 in Branß et al., 2018) from all sensors in the upstream cross-section, was considered as a representative bedform height for each run (see Table 1). The average bedform migration velocities, shown in Table 1, were obtained with a 2D cross correlation analysis between the two cross-sections. As shown in Table 1, bedform celerity and height increased with sediment transport rate.

For each run, the vertical distribution of the volume fraction of sediment solids  $\phi_s(z)$  was obtained from the time-series of bed elevations, following the method described

in Aberle et al. (2012). The obtained distributions, combining the signals of the sensors in the upstream cross-section, are shown in Fig. 2.

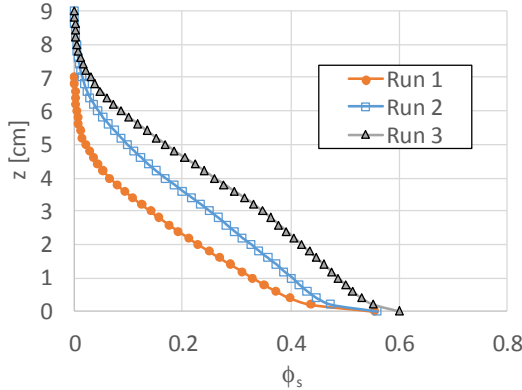


Figure 2. Distribution of the volume fraction of sediment solids with height, for the three experimental runs.

To be able to apply Eq. (3), the bed surface elevation  $\eta_1$ , defining the base of zero transport, must be identified. The unambiguous identification of the level of zero movement is difficult due to the spatial heterogeneity of natural bedforms (e.g., Aberle et al., 2012). Using the lowest measured elevation is not necessarily accurate, since this value depends on both the random nature of the irregular bed and also on bed elevation measurement errors. For supply-limited bedforms migrating over an immobile surface, identification of the zero level is on the other hand straightforward, nevertheless, measurement errors may bias the  $\phi_s$  distribution close to the bed. In the measurements here, particles traveling outside of a bedform in the vicinity of the bed or in suspension, may be picked up by the sensor as a high bed elevation, and thus bias the identification of regions where no bedforms were present. To counteract this effect, the base of zero transport was considered at a bed level of two times the particle diameter, i.e.  $\eta_1 = 4$  mm. This criterion was used for obtaining the values shown in Table 1 from the integral in Eq. (3) and for the volume fraction of sediment solids  $\phi_s(\eta_1)$  to be used in Eq. (6).

Sediment transport rates computed by Eq. (2), Eq. (3), and by the corrected equation for supply-limited conditions Eq. (5), are compared with the measured values in Fig. 3. For both Eq. (2) and (5)  $C = 0.5$  was used. All three equations overpredict the sediment transport rates, which may be related with overestimations on the bed level when the sensors detect particles in suspension. Eq. (5), with an error of circa 20%, performs best, and Eq. (2) shows errors larger than 50%. The error using Eq. (3) increases with the transport rate, performing similarly to Eq. (5) for low  $q_b$  values, and similarly to Eq. (2) for the highest  $q_b$ .

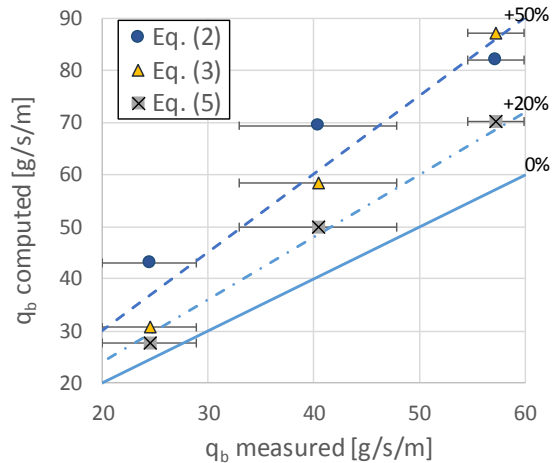


Figure 3. Comparison between sediment transport rates measured and computed with the bedform tracking method. Error bars indicate the maximum and minimum measured transport rates.

## 5 CONCLUSIONS

The results of this paper show that the application of the bedform tracking method under supply-limited conditions to compute bed load transport rates requires the consideration of the gaps between the individual bed forms. A corrected equation to consider this feature was presented (Eq. 5) and applied to experimental data. The corrected equation overestimated the measured transport rates by ca. 20%, but performed much better than the original equation, which overpredicted measured values by circa 50%. Differences between the results

with the new equation and measured values might be associated with the shape factor, determination of bedform height, and measurement errors, especially those on the bed elevation resulting from suspended particles detected by the ultrasonic sensors.

A recently suggested approach for the determination of bedload rates from high resolution bed-surface data was also tested. This approach can be applied either to supply or non-supply limited bedforms. The equation performed well for low transport rates, but largely overestimated high transport rates. The reason for this performance might be the irregularity of the experimental bedforms, the strong dependence of the equation on the distribution of bed elevations, the rather coarse resolution of the measurements (8 points per cross-section), and measurement errors related to particles in suspension (especially in the lee-side of dunes).

## 6 ACKNOWLEDGEMENT

The experimental data were obtained in the framework of the research project "In\_StröHmunG", founded by the German ministry of Education and Research (BMBF). It was part of the support measure "ReWaM", as well as the funding priority "NaWaM".

## 7 REFERENCES

- Aberle, J., Coleman, S., Nikora, V. 2012. Bed load transport by bed form migration. *Acta Geophysica*, 60(6), 1720-1743.
- Abraham, D., Kuhnle, R.A., Odgaard, A.J. 2011. Validation of bed-load transport measurements with time-sequenced bathymetric data. *Journal of Hydraulic Engineering*, 137(7), 723-728.
- Blom, A., Ribberink, J.S., de Vriend, H.J. 2003. Vertical sorting in bed forms: Flume experiments with a natural and a trimodal sediment mixture. *Water Resources Research*, 39(2).
- Branß, T., Núñez-González, F., Dittrich, A., Aberle, J. 2018. A flume study to investigate the contribution of main-channel bedforms on levee formation. In *River Flow 2018*, E3S Web of Conferences (Vol. 40).
- Coleman, S.E., Nikora, V.I., Aberle, J. 2011. Interpretation of alluvial beds through bed-elevation distribution moments. *Water Resour. Res.* 47, W11505, DOI: 10.1029/2011WR010672.
- Dietrich, W.E., Smith, J.D. 1984. Bedload transport in a river meander. *Wat. Resour. Res.*, 20, 1355-1380.
- Gabel, S. 1993. Geometry and kinematics of dunes during steady and unsteady flows in the Calamus River, Nebraska, USA. *Sedimentology* 40, 237-269
- Kleinmans, M.G., Wilbers, A.W.E., De Swaff, A., Van Den Berg, J.H. 2002. Sediment supply limited bedforms in sand-gravel bed rivers. *Journal of Sedimentary Research* 72(5), 629-640.
- Knaapen, M.A.F., van Bergen, H.C.N. 2005. Quantifying bedform migration using multi-beam sonar, *Geo-Marine Lett.* 25, 5, 306-314, DOI: 10.1007/s00367-005-0005-z.
- Henning, M. (2013). Mehrdimensionale statistische Analyse räumlich und zeitlich hoch aufgelöster Oberflächen von Dünenfeldern. Dissertation, TU Braunschweig, Braunschweig, Germany
- Henning, M., Aberle, J., Coleman S. 2010. Analysis of 3D-bed form migration rates. In: A. Dittrich, Ka. Koll, J. Aberle, and P. Geisenhainer, Proc. Int. Conf. on Fluvial Hydraulics River Flow 2010, Braunschweig, Germany, BAW, 879-885.
- Nikora, V.I., Sukhodolov, A., Rowinski, P.M. 1997. Statistical sand wave dynamics in one-directional water flows, *J. Fluid Mech.* 351, 17-39, DOI:10.1017/S0022112097006708.
- Nittrouer, J.A., Mead A.A., Richard C. 2008. Bedform transport rates for the lowermost Mississippi River. *Journal of Geophysical Research: Earth Surface* 113.F3.
- Shen, H.W., Cheong, H.F. 1977. Statistical properties of sediment bed profiles. *Journal of the Hydraulics Division*, 103(ASCE 13348 Proceeding).
- Simons, D.B., Richardson, E.V., Nordin, C.F. 1965. Bedload equation for ripples and dunes. *Prof. Pap. US geol. Surv.*, 462-H, 9 pp.
- van den Berg, J.H. 1987. Bedform migration and bedload transport in some rivers and tidal environments. *Sedimentology*, 34(4), 681-698.
- van der Mark, C.F. Blom, A., Hulscher, S.J. 2008. Quantification of variability in bedform geometry. *J. Geophys. Res.* 113, F03020, DOI: 10.1029/2007JF000940.
- Venditti, J.G., Nelson, P.A., Bradley, R.W., Haught, D., Gitto, A.B. 2017. Bedforms, structures, patches, and sediment supply in gravel-bed rivers. *Gravel-Bed Rivers: Process and Disasters*, Edited by Daizo Tsutsumi and Jonathan B. Laronne. John Wiley & Sons Ltd.
- Wilbers, A. 2004. The development and hydraulic roughness of subaqueous dunes. *Netherlands Geographical Studies* 323, The Royal Dutch Geographical Society, Utrecht, Netherlands, 227.
- Willis, J.C., Kennedy, J.F. 1977. Sediment discharge of alluvial streams calculated from bed form statistics. *IIHR Report No. 202*, Iowa Institute of Hydraulic Research, Iowa City.

# PIV measurements of flow around interacting barchan dunes in a refractive index matched flume

Nathaniel R. Bristow *University of Notre Dame, Notre Dame, IN, USA – nbris@nd.edu*

Gianluca Blois *University of Notre Dame, Notre Dame, IN, USA – gblois@nd.edu*

James Best *University of Illinois at Urbana-Champaign, Champaign, IL, USA – jimb@illinois.edu*

Kenneth T. Christensen *University of Notre Dame, Notre Dame, IN, USA – kchrist7@nd.edu*

...

**ABSTRACT:** Barchan dunes are three-dimensional, crescent shaped bedforms found in both Aeolian and subaqueous environments, including deserts, river beds, continental shelves, and even the craters of Mars. The evolution of and dynamics associated with these mobile bedforms involve a strong degree of coupling between sediment transport, morphological change, and flow, the last of which represents the weakest link in our current understanding of barchan morphodynamics. Their three-dimensional geometry presents experimental challenges for measuring the full flow field, particularly around the horns and in the leeside of the dunes. In this study we present measurements of the turbulent flow surrounding fixed barchan dune models in various configurations using particle image velocimetry in a refractive index matching flume environment. The refractive index matching approach enables near-surface measurements, as well as access to the whole flow field by rendering the solid models invisible. While experiments using solid models are unable to directly measure sediment transport, they allow us to focus solely on the flow physics and full resolution of the turbulent flow field in ways that are otherwise not possible in mobile bed experiments. The results presented here include a statistical analysis, focusing on the spatial structure of coherent motions in the flow through the use of two-point correlations, as well as an analysis of 3D vortical structures in the flow captured using time-resolved cross-plane measurements.

## 1 INTRODUCTION

Barchan dunes typically occur in fields with significant heterogeneity in dune size and migration rate (Lancaster, 2009). In this situation, the interaction between barchans of different sizes produces complex processes such as collisions, amalgamation and breeding. While the morphology of barchan dunes has been widely studied, the interaction between turbulent flows and barchans is limited to a few recent studies (e.g. Palmer et al., 2012; Bristow et al., 2018). “Minimal” models without an adequate simulation of the wake flow structure induced by dunes (Parteli et al., 2014) struggle to accurately predict the morphodynamics of barchans when they come in close proximity, including dune-dune collisions. This model deficiency is readily observed in the Figure 1 which

compares the model results (a-e) (Parteli et al., 2014) of a smaller barchan approaching a larger one (barchan migration rate is inversely proportional to size) with a similar scenario observed in laboratory experiments (f-j) (Hersen and Douady, 2005). Figure 1 highlights the contrasting dynamics, with erosion of the downstream dune occurring prior to contact, indicating that key flow physics associated with such interactions is being missed by these models, and thus further experimental work is needed to elucidate the role of unsteady turbulence in barchan morphodynamics.

In the present work, we study the flow field both in the wake of an isolated barchan and in the interdune space of interacting barchans using a combination of low and high frame-rate measurements with both two-component planar PIV and three-component stereo-PIV. The low frame-rate

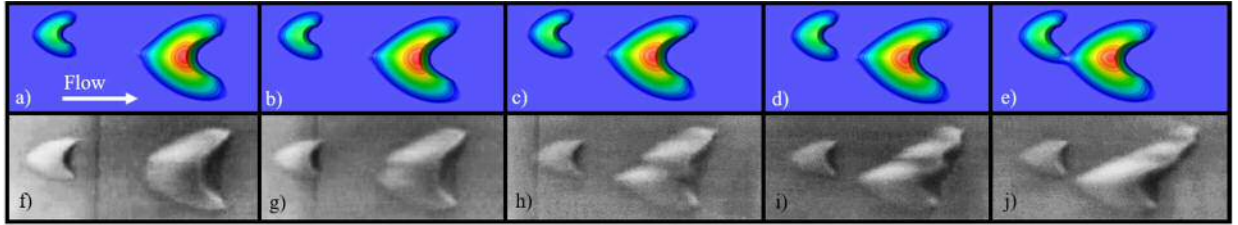


Figure 1. Comparison of (a-e) morphodynamic model and (f-j) mobile-bed flume experiments (Hersen and Douady, 2005), highlighting model deficiencies for a barchan collision. Code courtesy Dr. H. Herrmann (Parteli et al., 2014) (modified by us for this scenario).

measurements are made in all three planes independently ( $x-y$ ,  $x-z$ ,  $y-z$ ), while high frame-rate measurements were limited to the cross-plane ( $y-z$ ), allowing us to reconstruct the 3D flow field using Taylor's hypothesis. Several different configurations of models are investigated, including a baseline isolated case and a series of dune–dune collision configurations where the upstream and downstream barchans are laterally offset from each other.

Access to the flow field around these geometrically complex dunes is achieved using a refractive index matching (RIM) approach. Transparent models of barchan dunes, whose shape was based upon previous work (Palmer et al., 2012), were fabricated by 3D printing positive models, which were used to create negative silicone molds, which in turn were used to cast transparent acrylic models. The models were fixed in a RIM flow tunnel that employs an aqueous solution of sodium iodide (~63% by weight) as the working fluid, and rendered invisible, thus facilitating unimpeded data collection around the entire bedform configuration. The RIM approach also minimizes reflections of the laser sheet off the model and floor surfaces, allowing for higher accuracy measurements in these critical regions.

## 2 RESULTS

Low frame-rate measurements from all three planes ( $x-y$ ,  $x-z$ ,  $y-z$ ) provide an understanding of the mean flow topology (not shown here). For an isolated barchan, flow separates over the crest, forming a

recirculation region in the leeside between the horns, and shear layer which emanates downstream. As flow reattaches in the wake, a vortex structure similar to a horseshoe vortex system develops downstream of the horns, where two counter-rotating streamwise oriented regions of strong swirling strength dominate the flow particularly near the bed. When a smaller barchan is placed upstream, at a lateral offset, a flow that is similar to that in the wake of the isolated barchan is produced as the new inlet condition for the downstream barchan, with its wake veering around the downstream barchan's horn.

In Figure 2 we show an example of calculations of length scales in the flow for the  $y/H = 0.25$  plane, from all four barchan configurations. These calculations are made by computing the spatially inhomogeneous two-point correlation function  $\rho_{uu}$  at each grid point. The contour line of  $\rho_{uu} = 0.5$  is fitted to an ellipse, of which the lengths of the long and short axes, as well as the orientation relative to the  $x$ -axis, can be calculated. The length of the long axis of the ellipse is thus a proxy for the integral length scale in the flow at that grid point. Calculations made at each grid point allow for contour maps of length scales (as well as aspect ratios and orientation angles, not shown here) to be analysed for the entire field of view, in each measurement plane.

Several key features are made evident through these correlation length scale calculations. The wake of the isolated barchan has a very complex structure, with a streak of short length scales aligned with the centerline, and longer length scales

prevailing downstream of each horn. In the wake of the upstream barchan, starting with the first collision stage, the length scales are significantly reducing in the interdune region due to the imposition of the shear layer from flow separation over the upstream barchan. This structure prevails far downstream, with a short length scale “streak” continuing downstream of the downstream barchan’s elongated horn. While this brief abstract is unable to fully explore the results from this statistical analysis of the scales in the flow, these calculations provide a wealth of information about the structure of large scale coherent motions in the flow.

Application of Taylor's frozen field hypothesis to high frame-rate measurements allows for 3D reconstruction of the flow field. In Figure 3 we show an example of this from the wake of the isolated barchan, where isosurfaces of swirling strength,  $\lambda_{ci} \approx 0.2 \lambda_{ci,max}$  are shown and the structures are colored by distance from the wall,  $y/H$ . While rapid dissipation of turbulence in the wake requires careful treatment of this application of Taylor's hypothesis, such reconstructions are at least valid within an integral length scale, which from the previous results is shown to be on the order of several barchan heights. Within this single flow reconstruction we can observe periodically shed structures, as well as elongated vortices near the bed and larger spanwise oriented arches near the crest height.

### 3. CONCLUSIONS

These results demonstrate the utility of the refractive index matching approach for the measurement of flow around complex geometries such as the barchan dune. The ability to capture the entire flow field, particularly close to the model surfaces, such as in the allows analysis of first order flow

features, such as the veering of the wake of the upstream barchan, as well as higher order turbulent statistics of dominant length scales in the flow. The application of high frame-rate cross-plane stereo-PIV enables the fully 3D flow field to be revealed and analysis of the instantaneous structures shed from the shear layer of the barchan dune. Together, such results shed light on the fundamental flow structures associated with the complex morphology of a barchan which are likely to be responsible for determining the erosion of downstream bedforms in close proximity.

### 4. ACKNOWLEDGEMENTS

This work was supported by the National Science Foundation through collaborative grants CBET-1603211 (Notre Dame) and CBET-1604155 (Illinois).

### 5. REFERENCES

- Bristow, N. R., Blois, G., Best, J. L., Christensen, K. T., 2018. Turbulent flow structure associated with collision between laterally offset, fixed-bed barchan dunes. *Journal of Geophysical Research: Earth Surface*, 123, 2157–2188, doi.org/10.1029/2017JF004553
- Hersen, P., Douady, S., 2005. Collision of barchan dunes as a mechanism of size regulation. *Geophysical Research Letters*, 32, L21403, doi: 10.1029/2005GL024179.
- Lancaster, N., 2009. *Dune Morphology and Dynamics*, in *Geomorphology of Desert Environments*. Dordrecht, Springer Netherlands, 557–595.
- Palmer, J. A., Mejia-Alvarez, R., Best, J. L., Christensen, K. T., 2012. Particle-image velocimetry measurements of flow over interacting barchan dunes. *Experiments in Fluids*, 52, 809–829, doi.org/10.1007/s00348-011-1104-4
- Parteli, E. J. R., Kroy, K., Tsoar, H., Andrade, J. S., Pöschel, T., 2014. Morphodynamic modeling of aeolian dunes: Review and future plans. *The European Physical Journal Special Topics*, 223, 2269–2283. doi.org/10.1140/epjst/e2014-02263-2

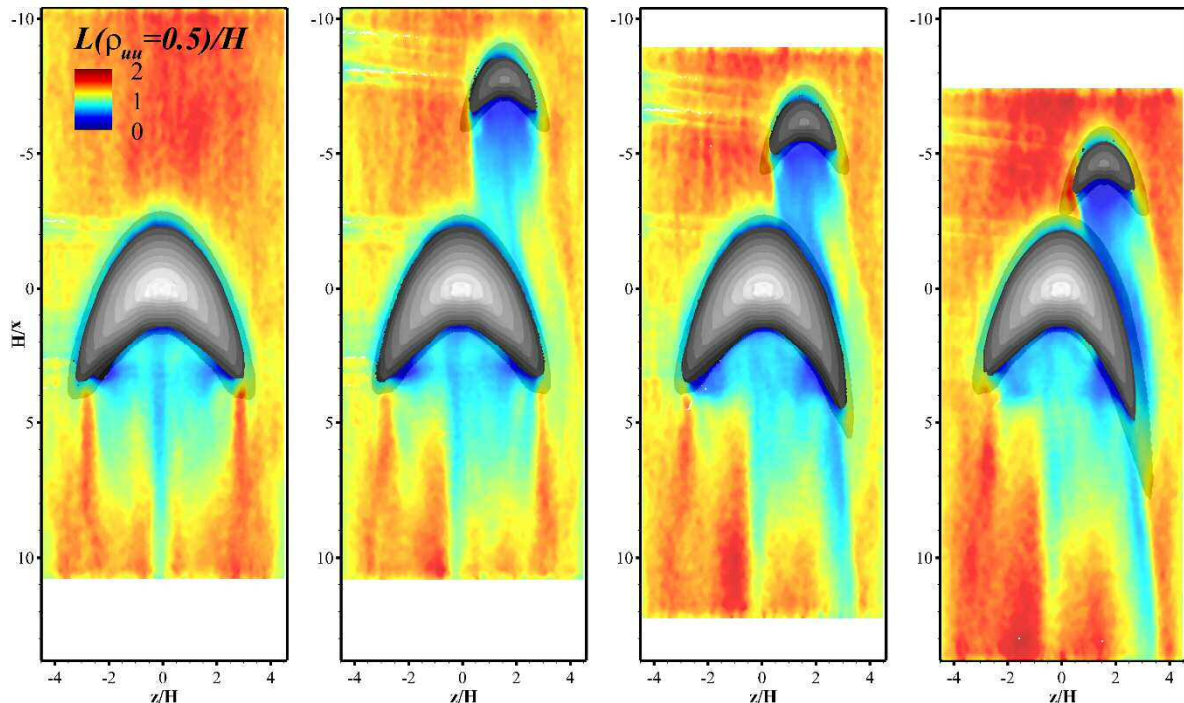


Figure 2. Spatial distribution of length scales,  $L$ , in (a) the isolated case, and (b-d) the collision cases, calculated in the wall-parallel plane  $y/H = 0.25$ .

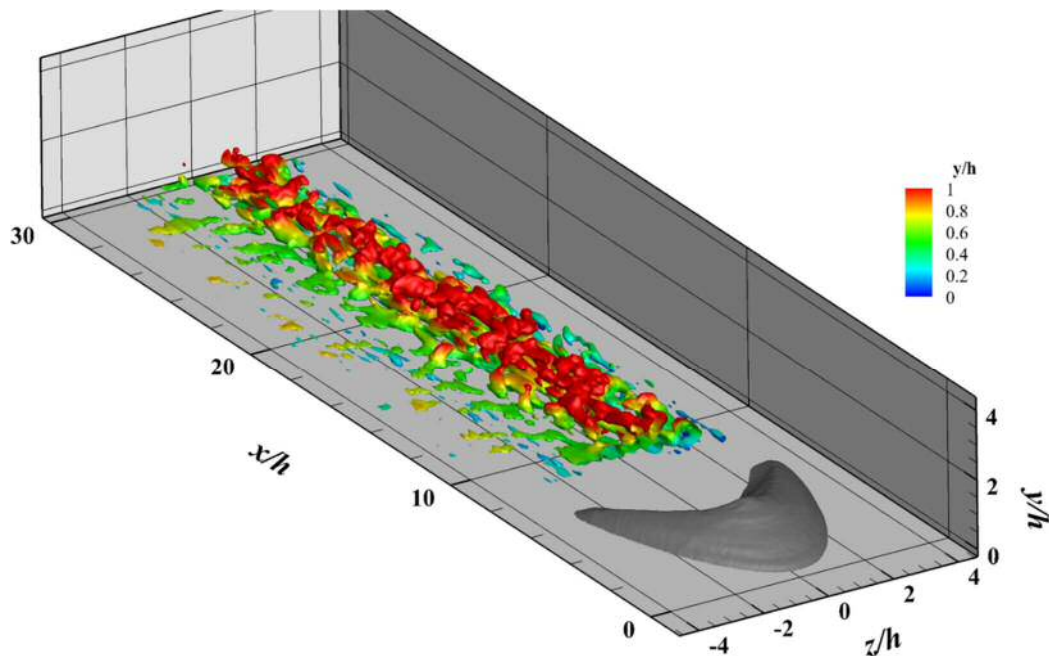


Figure 3. Isocontours of 3D swirling strength,  $\lambda_{ci} \approx 0.2 \lambda_{ci,\max}$ , colored by distance from the wall, in the wake of an isolated barchan, reconstructed using Taylor's hypothesis.

# Storm influences on sand wave dynamics: an idealized modelling approach

Geert Campmans *University of Twente, Enschede, The Netherlands* – [g.h.p.campmans@utwente.nl](mailto:g.h.p.campmans@utwente.nl)

Pieter Roos *University of Twente, Enschede, The Netherlands* – [p.c.roos@utwente.nl](mailto:p.c.roos@utwente.nl)

Suzanne Hulscher *University of Twente, Enschede, The Netherlands* – [s.j.m.h.hulscher@utwente.nl](mailto:s.j.m.h.hulscher@utwente.nl)

**ABSTRACT:** We investigate the influence of wind waves and wind-driven flow on sand wave dynamics using a two-model approach. Using a linear stability analysis, we find that waves decrease sand wave growth and wind causes sand wave migration. Combining linear stability analysis with a typical North Sea wave and wind climate explains variability in sand wave migration rates. Using a nonlinear sand wave model we show that waves reduce sand wave height and wind causes sand wave asymmetry as well as migration.

## 1 INTRODUCTION

Sand waves are dynamic bed forms of hundreds of meters wavelength and several meters in height. They are observed in many tidally dominated seas with sandy beds, such as the North Sea. Offshore activities require a detailed knowledge of sand wave dynamics. Various observational studies suggest that storms affect sand wave height and migration rate (Terwindt, 1971; Fenster et al., 1990).

Our aim is to understand how storms influence sand wave dynamics. We do so by applying an idealized modelling approach that is able to isolate two storm effects: wind waves and wind-driven flow effects. The sand waves that we investigate are generated by a symmetrical tidal current.

To investigate the effects of wind waves and wind-driven flow on sand wave dynamics we applied a two-step approach, in which we systematically analyse storm effects on small-amplitude sand wave dynamics using a linear stability analysis (Campmans et al., 2017), followed by an idealized nonlinear sand wave model to analyse storm effects on

finite amplitude sand wave dynamics (Campmans et al., 2018b).

The linear stability model allows for a large number of model runs due to its semi-analytical solution method. This enabled us to investigate wind wave and wind-driven current scenarios to investigate a real North Sea wave and wind climate (Campmans et al., 2018a).

## 2 MODEL FORMULATION

### 2.1 Tides, wind and waves

The tidal currents in our model are described by shallow-water equations. Hydrostatic pressure balance is assumed in the vertical. Turbulent mixing is modelled by a constant vertical eddy viscosity with a partial slip boundary condition. A uniform pressure gradient is incorporated to force a tidal current. The model domain is spatially periodic in the horizontal.

Wind effects are modelled by a constant uniform shear stress applied at the water surface, causing a wind-driven flow.

Wind waves are modelled using linear wave theory. Near-bed orbital velocities result in an increase in bed-shear stress, but

do not affect the tidally or wind-driven currents.

## 2.2 Sediment transport

Sediment transport is modelled by a bed load transport formula, given by

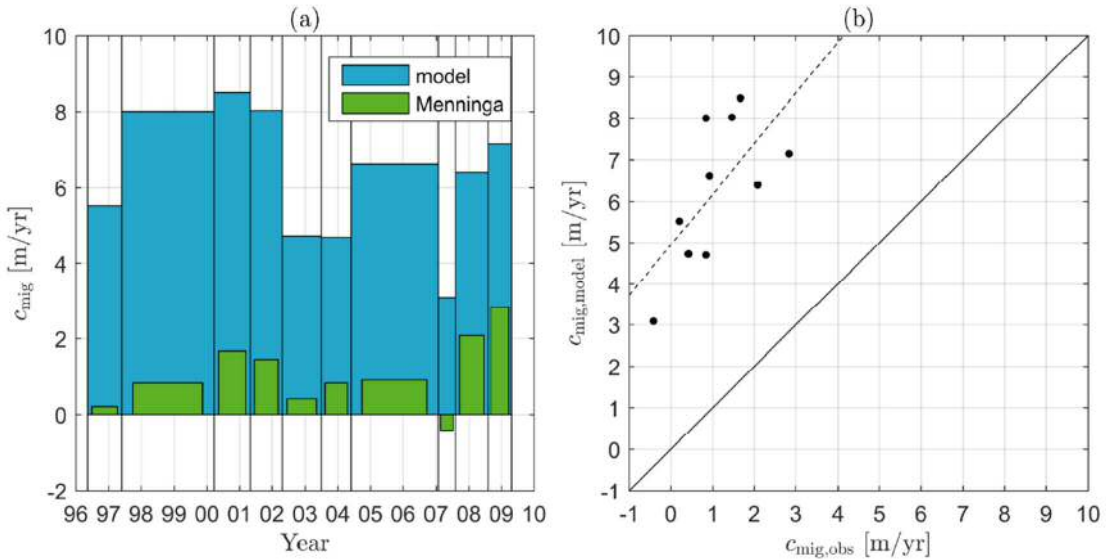


Figure 1. Observed (Menninga, 2012) and modelled sand wave migration  $c_{mig}$  in the North Sea, between 1996 and 2010. Figure after Campmans et al. (2018a)

$$q_b = \alpha |\tau|^\beta \left( \frac{\tau}{|\tau|} - \lambda \nabla h \right), \quad (1)$$

in which  $\alpha$  is a bed load coefficient,  $\tau$  the bed shear stress,  $\beta$  the exponent expressing the nonlinearity of sediment transport,  $\lambda$  the slope correction factor and  $h$  the seabed topography. Here, sediment is transported nonlinearly in the direction of the shear stress, corrected for gradients in the bed slope. Sediment transport is computed on an intra-wave time scale, where the tidal current is assumed constant, and is then averaged over a wave period. Similarly, on the intra-tidal time scale sediment transport is averaged.

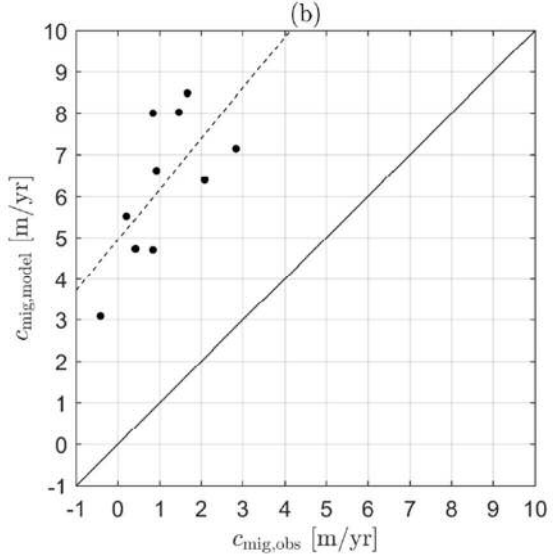
## 2.3 Bed evolution

The seabed evolution is determined by sediment conservation using the wave and tidally averaged sediment transport.

## 3 SOLUTION METHODS

### 3.1 Linear stability analysis

The first method to gain insight into the solution of small-amplitude sand wave dynamics is linear stability analysis. The out-



put for the linear stability analysis is a growth rate and migration rate for a sinusoidal bed perturbation of a chosen wavelength. The growth rate and migration rate describe the small-amplitude behaviour until finite-amplitude effects become important.

### 3.2 Nonlinear solution method

To analyze the finite amplitude dynamics of sand waves, a nonlinear solution method is required. In this solution method the shallow-water equations are transformed to a rectangular computational domain, where the finite-difference method is used to solve the hydrodynamics. In the nonlinear model the bed evolution is numerically integrated to investigate the morphodynamic evolution of finite-amplitude sand waves.

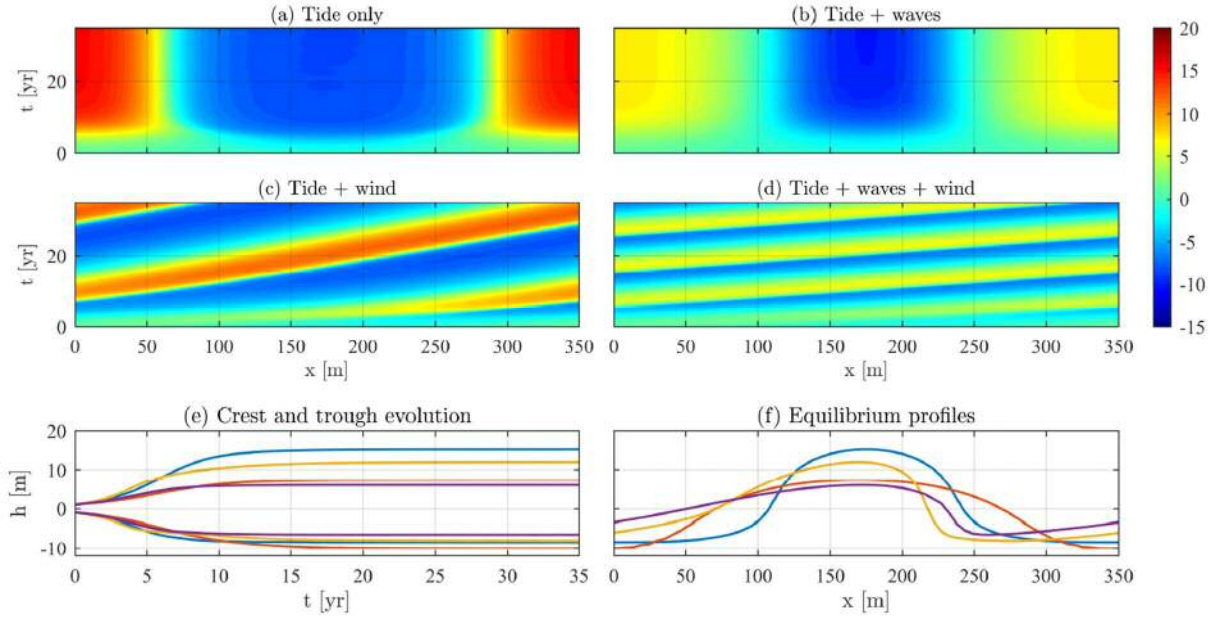


Figure 2. Sand wave evolution  $h(x,t)$  for four forcing conditions: (a) Tide only, (b) Tide + waves, (c) Tide + wind and (d) Tide + waves + wind. The colorbar indicates the seabed topography in meters. The bottom panels show (e) the crest and trough evolution in time and (f) the equilibrium profiles. Where in (e) and (f) the line colors correspond to the colored text in this caption. *Figure after Campmans et al. (2018b)*

## 4 RESULTS

### 4.1 Linear stability analysis

Using the linear stability model the influence of wind waves and wind-driven flow on the growth- and migration-rate was systematically investigated. Both wind and, in particular, waves decrease the growth rate of sand waves. Wind-driven flow generates a residual current that causes sand wave migration. Although waves do not cause sand wave migration, they do enhance migration caused by other mechanisms such as wind-driven flow.

Combining the linear stability sand wave model with 20 years of wave and wind data the influence of a typical North Sea storm climate has been investigated. Using this approach a hindcast of variable sand wave migration, observed by Menninga (2012), showed a qualitative agreement, see Figure 1.

### 4.2 Nonlinear sand wave model

The developed nonlinear sand wave model was used to investigate the effects of storms on the finite amplitude dynamics of sand waves. The evolution of small amplitude bed perturbations towards fully grown sand waves has been investigated for four forcing conditions in Figure 2. It is found that sand wave height is mainly reduced by waves, but also by wind. Wind generates a residual flow component that causes sand waves to migrate and results in a horizontally asymmetric sand wave shape.

In the results above, the sand wave wavelength is restricted by the model domain length of 350 m. This allowed to systematically investigate storm effects. However, to allow sand waves to freely adapt their wavelength similar model simulations were carried out on a longer model domain (4 km), shown in Figure 3.

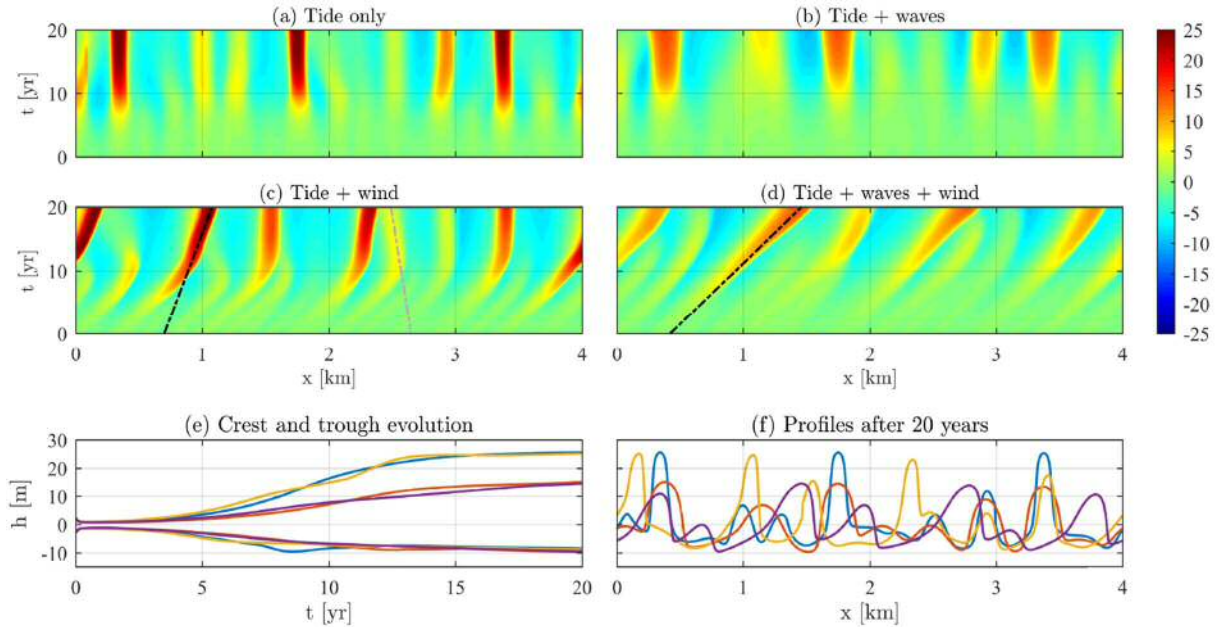


Figure 3. Sand wave evolution  $h(x,t)$  for four forcing conditions: (a) Tide only, (b) Tide + waves, (c) Tide + wind and (d) Tide + waves + wind. The colorbar indicates the seabed topography in meters. The bottom panels show (e) the crest and trough evolution in time and (f) the equilibrium profiles. Where in (e) and (f) the line colors correspond to the colored text in this caption. *Figure after Campmans et al. (2018b)*

Finally we investigated the effect of storm duration. In results thus far, modelled wave and wind conditions are constant in time, whereas in reality storms often occur for a short duration, followed by a period of relatively calm weather. To simulate such storm intermittent behaviour, a storm (*tide + wave + wind*) condition is alternated by a fair-weather (*tide only*) condition for various storm durations. In Figure 4, the crest and trough evolution is shown for six different storm durations: constant fair-weather, 1 week storm, 1 month, 2 months, half a year, and constant storm conditions. For each of the scenarios a single storm is modelled with the remaining part of the year being fair-weather. The model results show that for intermittent storm conditions the sand wave crest and trough height oscillates between the equilibrium crest and trough heights of sand waves in constant fair-weather and constant storm conditions. We interpret this as a storm-dependent *dynamic equilibrium*. Even storms of relatively short

duration already have a significant effect on the sand wave height.

## 5 CONCLUSIONS

By applying the two-model approach in

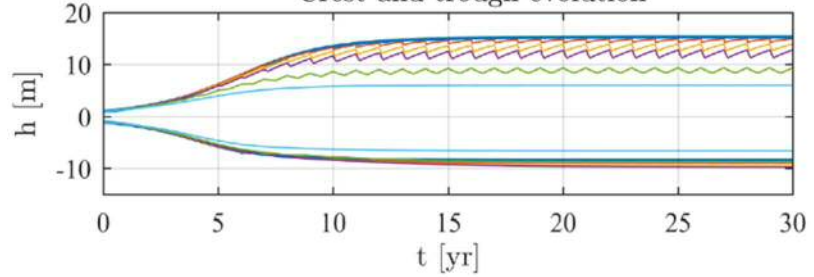


Figure 4. Crest and trough evolution for alternating storm and fair weather conditions. The storm duration for each line is: constant fair-weather, 1 week, 1 month, 2 months, half a year, constant storm. *Figure after Campmans et al. (2018b)*

our research we were able to systematically analyse the wave and wind effects on initial sand wave formation as well as for specific wave and wind conditions on finite amplitude sand wave dynamics. We have shown that particularly wind waves reduce the growth rate and the sand wave height in equilibrium conditions. Wind-induced flow causes sand wave migration, which can be

enhanced by waves. North Sea wave and wind data combined with the linear stability model shows promising results in being able to hindcast sand wave migration. Finally, we show that storms reduce sand wave height, even when they occur for short periods of time.

## 6 ACKNOWLEDGEMENT

This work is part of the research programme SMARTSEA with project number 13275, which is (partly) financed by the Netherlands Organisation for Scientific Research (NWO).

## 7 REFERENCES

- Campmans, G.H.P., Roos, P.C., De Vriend, H.J., Hulscher, S.J.M.H., 2017. Modeling the influence of storms on sand wave formation: A linear stability approach. *Continental Shelf Research* 137, 103-116. DOI: 10.1016/j.csr.2017.02.002
- Campmans, G.H.P., Roos, P.C., Schrijen, E.P.W.J., Hulscher, S.J.M.H. (2018a). Modeling wave and wind climate effects on tidal sand wave dynamics: A North Sea case study. *Estuarine, Coastal and Shelf Science* 213, 137-147. DOI:10.1016/j.ecss.2018.08.015
- Campmans, G. H. P., Roos, P. C., de Vriend, H. J., & Hulscher, S. J. M. H. (2018b). The influence of storms on sand wave evolution: A nonlinear idealized modeling approach. *Journal of Geophysical Research: Earth Surface*, 123, 2070-2086. DOI:10.1029/2018JF004616
- Fenster, M.S., Fitzgerald, D.M., Bohlen, W.F., Lewis, R.S., Baldwin, C.T., 1990. Stability of giant sand waves in eastern Long Island Sound, USA. *Marine Geology* 91, 207-225.
- Menninga, P.J., 2012. Analysis of variations in characteristics of sand waves observed in the Dutch coastal zone: a field and model study. (Master Thesis), Utrecht University (NL) .
- Terwindt, J.H.J., 1971. Sand waves in the Southern Bight of the North Sea. *Marine Geology* 10, 51-67.



# The influence and interactions of delta slopes and knickpoints on bedforms within submarine channel systems

Ye Chen *University of Hull, Hull, UK* – *ye.chen@2016.hull.ac.uk*

Daniel R. Parsons *University of Hull, Hull, UK* – *d.parsons@hull.ac.uk*

Stephen M. Simmons *University of Hull, Hull, UK* – *s.simmons@hull.ac.uk*

Matthieu J. Cartigny *University of Durham, Durham, UK* – *matthieu.j.cartigny@durham.ac.uk*

John Hughes Clarke E. *University of New Hampshire, NH, USA* – *john.hughesclarke@unh.edu*

Cooper Stacey *Institute of Ocean Science, BC, Canada* – *Cooper.Stacey@canada.ca*

Sophie Hage *University of Southampton, Southampton, UK* – *sophie.hage@soton.ac.uk*

Peter J. Talling *University of Durham, Durham, UK* – *peter.j.talling@durham.ac.uk*

Maria Azpiroz-Zabala *University of Southampton, Southampton, UK* – *m.azpiroz@soton.ac.uk*

Mike A. Clare *National Oceanography Centre, Southampton, UK* – *Michael.clare@noc.ac.uk*

Jamie L. Hizzett *National Oceanography Centre, Southampton, UK* – *j.l.hizzett@soton.ac.uk*

James Hunt *National Oceanography Centre, Southampton, UK* – *james.hunt@noc.ac.uk*

Gwyn Lintern *Institute of Ocean Science, BC, Canada* – *gwyn.lintern@canada.ca*

Esther Summer *University of Southampton, Southampton, UK* – *e.j.sumner@soton.ac.uk*

Age J. Vellinga *University of Southampton, Southampton, UK* – *a.j.vellinga@soton.ac.uk*

Daniela Vendettioli *University of Southampton, Southampton, UK* – *d.vendettioli@soton.ac.uk*

Rebecca Williams *University of Hull, Hull, UK* – *rebecca.williams@hull.ac.uk*

**ABSTRACT:** Submarine channels play a vital role in delivering vast quantities of sediment to the deep sea, forming some of the largest sediment deposits on Earth. Knickpoints have been identified as an important morphological feature of many submarine channel systems. Knickpoint features have superimposed crescentic bedforms, which are formed by the action of supercritical turbidity currents. The interactions between bedform dynamics, supercritical flows, and channel morphology remain poorly understood on these environments, and a better understanding of the dynamics would enable improved linkages to be made between the morphological evolution of submarine channels and the deposits they generate. Here we present a suite of wavelet analyses of repeat bathymetric survey data from Bute inlet, British Columbia, Canada, take over a 10 year period, from 2008 to 2018. The results show how dominant crescentic-shaped bedform wavelengths are affected by spatial and temporal changes in delta slope and how knickpoint migration generate down-channel bedforms.

## 1 INTRODUCTION

Submarine channels act as conduits for turbidity currents, which have been identified to be the most volumetrically important processes for the delivery of sediment and organic carbon to the deep sea (Bouma 2000; Peakall et al., 2007; Paull et al., 2010; Hage et al., 2018). Turbidity currents are of great importance not only to our general understanding of global

sediment transport processes, but also because of the environmental hazards they pose to subsea infrastructure such as communication cables or pipelines (Piper et al., 1999, Carter et al., 2014) and tsunamis related to submarine slope failures (Prior et al., 1982). Bathymetric mapping has revealed that proximal sections of submarine channels can be dominated by upslope migrating crescentic bedforms (Symons et al., 2016; Hage, et al., 2018). Another morphological feature of the channels are

knickpoints, which are described as an abrupt change in river gradient (Whipple and Tucker, 1999). Knickpoints are known to play a major role in governing channel adjustment in response to either regional or local perturbations (Gilbert, 1896; Holland, 1974; Hayakawa and Matsukura, 2003; Baynes, 2018). Recent system-scale wide process studies in submarine systems have demonstrated links between seafloor morphology, upward migration of crescentic bedforms, sediment distribution, flow and the depositional record (Hughes Clarke, 2016; Hage et al., 2018).

Here we describe new perspectives on bedform development in submarine channels gained by studying a sequence of bathymetric data acquired over a 10 year period in Bute inlet, British Columbia, Canada. Our study explores the relationships between delta slope, channel knickpoint dynamics and the response of crescentic bedforms in terms of their heights, wavelengths and migration. The results have implications for our understanding of bedforms in these channel systems and furthering our understanding of their development, sediment dispersal and deposition and thus longer-term submarine channel evolution.

## 2 STUDY SITE

Bute inlet, British Columbia, is located on the western coastline of Canada. The fjord has a length of over 40 km and represents a modern example of a submarine channel developing under the modification of turbidity currents (Prior & Bornhold, 1988; Conway, 2012) (Fig. 1). The channel extends to a depth below the water surface of 700 m at the distal part of the fjord, where it terminates in a lobe feature. The two main rivers, the Homathko and Southgate, discharge into Bute Inlet at the head of the fjord. Trites (1995) estimated the total mean annual freshwater flow into the fjord to be approximately  $410 \text{ m}^3 \text{ s}^{-1}$  of which  $280 \text{ m}^3 \text{ s}^{-1}$  is from the Homathko River. Discharge to Bute Inlet is highly seasonal, peaking in July

because of snow and ice melt from the interior watershed. The lowest input occurs in the winter months as the precipitation is stored as snow in the higher elevation of the watershed. The mean annual discharge can also vary year to year (Fig. 2).

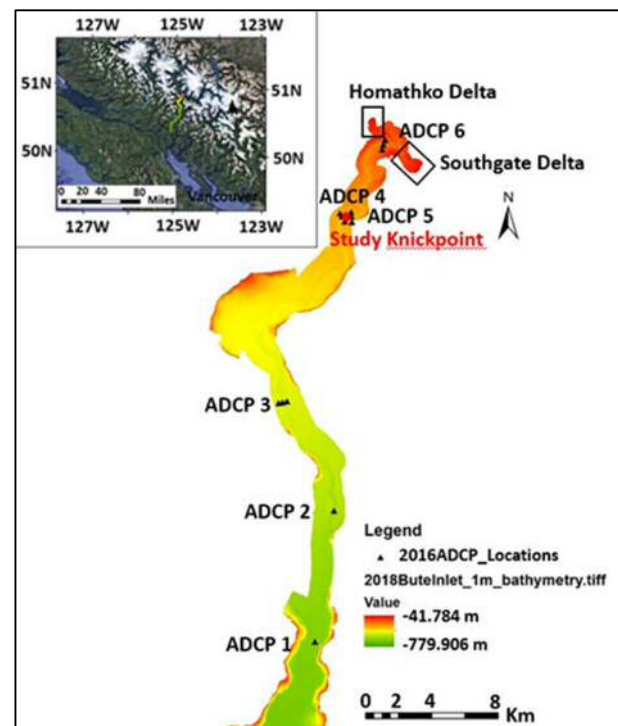


Figure 1. Bute Inlet location in British Columbia

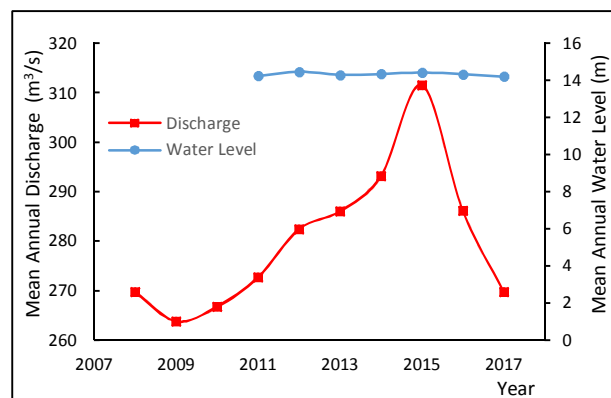


Figure 2. Mean annual discharge and water level of the Homathko River

## 3 METHODOLOGY AND MATERIAL

### 3.1 Bathymetry measurement

Modern bathymetric mapping and sampling techniques are increasingly being applied to submarine channel studies (Sumner et al., 2013; Xu et al., 2014; Dorrell et al., 2016; Clare et al., 2016; Hughes Clarke, 2016;

Azpiroz-Zabala et al., 2017; Paull, 2018; Hage et al., 2018). Here we analyse repeat multibeam bathymetry data from Bute Inlet acquired over a 10 year period from 2008 to 2018. We additionally analyse high resolution multibeam echo-sounder bathymetry data from Homathko and Southgate deltas taken in 2016 and 2018, to compare bedform wavelength evolution with slope patterns formed by supercritical flows and flows with characteristic differences between 2016 and 2018 (Fig. 3.2).

### 3.2 Turbidity currents

Six Acoustic Doppler Current Profilers (ADCP) were deployed on six moorings within the submarine channel axis positioned from the proximal delta to the distal lobe of the system (Fig. 1). Flow at one mooring and acoustic backscatter data were recorded for five months beginning in June 2016. These captured the passage and evolution of episodic supercritical turbidity currents as they progressed through the channel system (Fig. 1). More than 20 turbidity currents were observed during this 5 month period. Most of the flows dissipated in the proximal part of the channel system with 11 events observed at the study knickpoint, 10 km downstream from the proximal delta. The supercritical turbidity currents drive an observed upstream migration of the knickpoint during each event. Thus, this comprehensive system-scale data set enables us to explore the relationship between turbidity current frequency, flow duration, flow velocity and long-term changes in delta morphology and knickpoint retreat.

### 3.3 Wavelet analysis

The wavelet analysis was conducted using the Bedforms-ATM (Bedforms analysis toolkit for multiscale modelling) software (Gutierrez et al., 2018). By adapting the one dimensional continuous wavelet analysis package developed by Torrence et al (1998), the software performs wavelet analysis of along-channel transects containing multiple bedforms. The resulting wavelet spectrum demonstrates information about the dominant constituent wavelengths along the

channel as a function of distance along the channel. Values are screened out that fall outside a cone of influence that discriminates reliable power spectrum results from spurious measurements (Gutierrez et al., 2018).

## 4 RESULTS

### 4.1 Bedform scales in the Homathko and Southgate deltas

The Homathko River contributes around 80% of the discharge that flows into Bute Inlet. Digital elevation model analysis reveals that the delta has experienced periods of both degradation and aggradation during the range of hydrological conditions during the study period. The subaqueous channel geomorphology is shown in Fig. 3a. Dozens of small flow pathways can be observed at the delta lip until the water depth reaches  $\sim 75$  m. The small flow pathways then merge into three main channels in the mid-section, and then into a single channel at the distal end of the delta slope at  $\sim 115$  m depth. Trains of crescentic bedforms occupy the delta slope area and periodically migrate upslope.

Wavelet analysis allows an unravelling of the complex relationship between bedforms of different scales and the underlying channel morphology. Fig. 3b shows the delta slope decreasing from around  $7^\circ$  at the delta lip to  $4^\circ$  at the distal end. Small scale crescentic bedform wavelengths are formed both in the delta lip and close to the distal end of the slope. In the mid-section of the delta slope, the wavelet power spectrum shows dominant bedform wavelength of around 32 m to 50 m. The wavelength increases as the delta slope becomes lower. However, small scale wavelengths and larger wavelengths are both present at the distal part of the delta, which indicates perhaps enhanced variability in the turbidity currents, which flow through this zone.

The wavelet power spectrum of the bedform profiles along the central channel at Southgate (Fig. 4b) shows a greater variation in wavelength from one end of the section to the other, corresponding to a larger decrease in channel gradient, from  $9^\circ$

to  $3.5^\circ$ . The Southgate delta morphology has a deeper delta lip and a flatter delta distal zone compared with the Homathko delta. A main channel with large-scale crescentic bedforms is located at the north side of the delta and few smaller channels exist in the central section. In the south section of the delta a narrower shallow channel exists. All channels merge into one wider conduit at a depth of  $\sim 130$  m. The delta slope declines from around  $9^\circ$  to  $3.5^\circ$  from proximal to distal. As shown in the wavelet analysis results, crescentic bedform wavelengths gradually become longer as the water depth increases and delta slope declines.

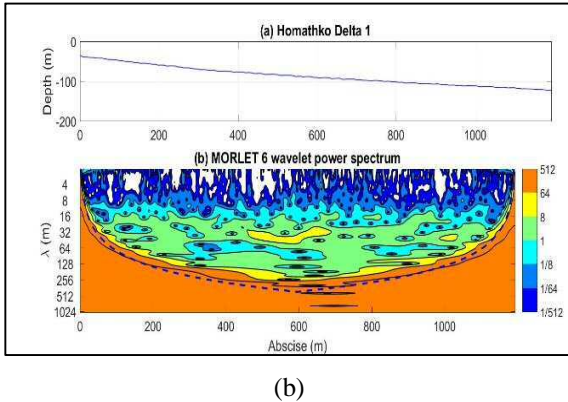
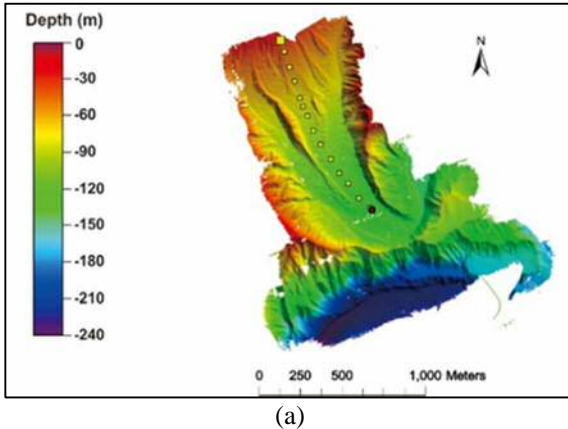
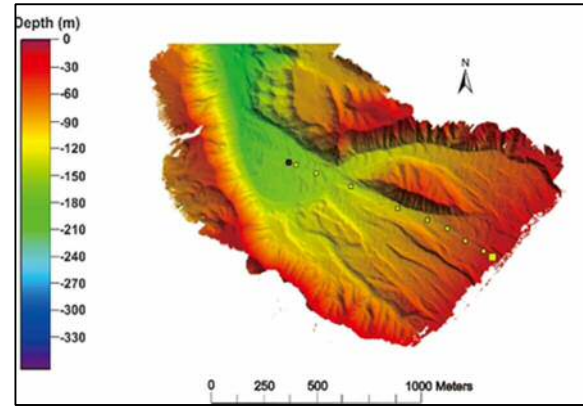
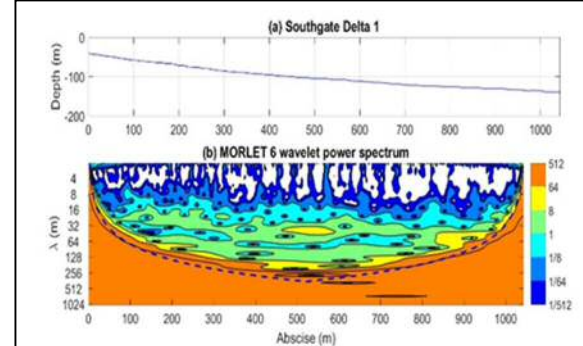


Figure 3: (a) Geomorphology of Homathko delta shown by bathymetry data; (b) Wavelet power spectrum of one profile along the central channel in the delta



(a)

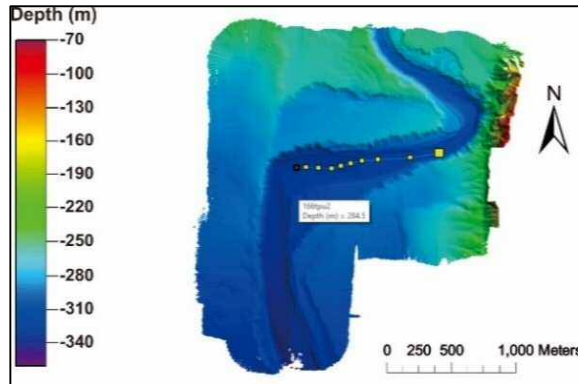


(b)

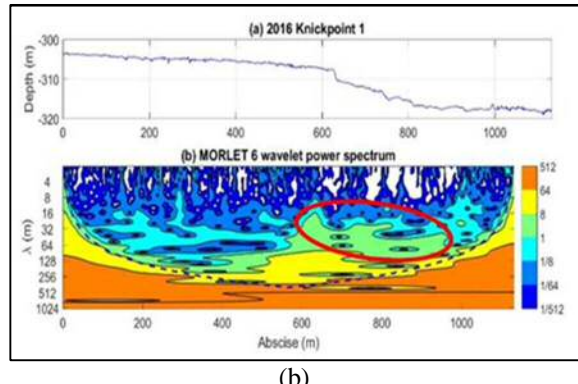
Figure 4: (a) Geomorphology of Southgate delta shown by bathymetry data; (b) Wavelet power spectrum analysis of one profile along the central channel in the delta

#### 4.2 The impact of knickpoint retreat on submarine channel bedforms

The repeat seafloor mapping reveals significantly different knickpoint geometries on June 2016 (Fig. 5a&b) and May 2018 (Fig. 6a&b). Superimposed bedforms patterns of different scales are in evidence before and after knickpoint migration within the wavelet analysis results (Fig. 5). Bedform wavelength in June 2016 increased alongside upstream knickpoint migration. Extended bedforms occurred within a region of  $\sim 380$  m downstream of the knickpoint. Further downstream the bedforms return to a lower wavelength that are similar to the bedforms upstream of the knickpoint. The bedform scale change indicates the influence of the knickpoint morphology on bedform dynamics due to the influence of the knickpoint on passing turbidity currents.



(a)

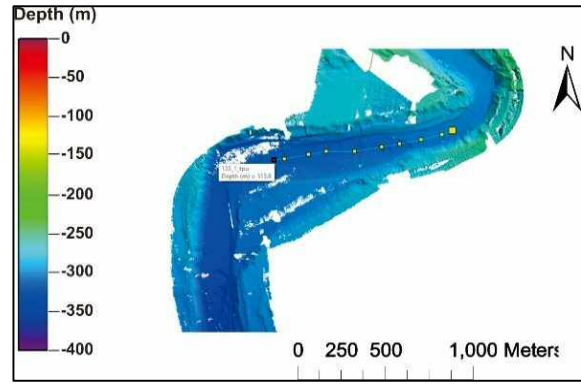


(b)

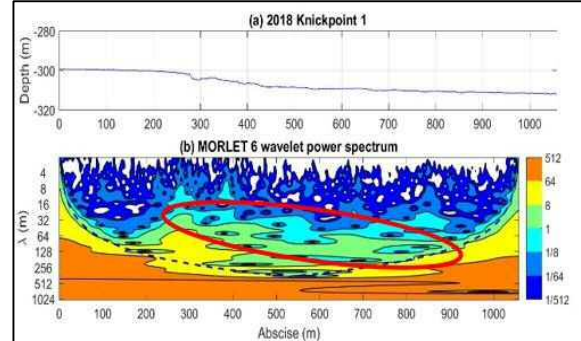
Figure. 5 (a) Geomorphology of the study knickpoint in June 2016; and (b) the wavelet power spectrum of an along-channel transect across the knickpoint from 2016

The wavelet power spectrum from the May 2018 survey (Fig. 6a and b) shows similar bedform scale patterns to June 2016. However, a few extremely long-wavelength bedforms, varying from  $\sim 64$  to  $\sim 150$  m, are present downstream of the knickpoint, perhaps suggesting that the recent set of currents have significantly different hydrological conditions compared to those in 2016.

According to hydrological monitoring data acquired in the Homathko River (Environment Canada), the discharge to the delta was lower 2017 than 2016 (Fig. 2). Therefore the hydraulic parameters of turbidity currents could be different between the two years, which may be a factor in the generation of the longer wavelength bedforms in 2017. However, more work is needed to relate bedform dimensions to the formative currents.



(a)



(b)

Figure. 6 (a) Geomorphology of a study knickpoint in May 2018; (b) the wavelet power spectrum of an along-channel transect across the knickpoint from 2018

## 5 CONCLUSIONS

The results of a wavelet power spectrum analysis demonstrate how delta slope and knickpoint morphologies can influence the scales and geometries of channel bedforms. Upstream knickpoint migration redistributes sediments and the pattern of bedform wavelengths in the channel. Long-wavelength bedforms occurred downstream of the knickpoint following a lower input discharge entering the delta system in 2017, possibly resulting in changes to the turbidity current characteristics and dynamics and subsequent changes in bedform morphology. This study is enabling us to explore the role of delta slope on controlling the size and shape of crescentic bedform geometries and also allows us to explore how knickpoint migration sculpts and influences overall bedform distributions and the links to longer-term submarine channel dynamics.

## 6 ACKNOWLEDGEMENTS

This project is funded by University of Hull and China Scholarship Council. We thank for all the crew members of CCGS Vector and RV John Strickland.

## 7 REFERENCES

- Azpiroz-Zabala, M., et al., 2017. Newly recognized turbidity currents structure can explain prolonged flushing of submarine canyons. *Science Advances* 3(10), e1700200
- Baynes, E.R.C., et al., 2018. River self-organisation inhibits discharge control on waterfall migration. *Scientific Report* 2444
- Bouma, A.H., 2000. Coarse-grained and ® ne-grained turbidite systems as end member models : applicability and dangers. 17, 137–143
- Cartigny, M.J.B. et al., 2014. Morphodynamics and sedimentary structures of bedforms under super-critical-flow conditions: New insights from flume experiments. *Sedimentology* 61(3), 712–748
- Clare, M.A., et al., 2016. Preconditioning and triggering of offshore slope failures and turbidity currents revealed by most detailed monitoring yet at a fjord-head delta. *Earth and Planetary Science Letters* 450, 208–220
- Conway, K.W., et al., 2012. Submarine channel evolution: Active channels in fjords, British Columbia, Canada. *Geo-Marine Letters* 32(4), 301–312
- Carter L., Gavey R., Talling P., Liu J., 2014. Insights into submarine geohazards from breaks in subsea telecommunication cables. *Oceanography* 27, 58–67
- Dorrell, R.M., et al., 2016. Flow dynamics and mixing processes in hydraulic jump arrays: Implications for channel-lobe transition zones. *Marine Geology* 381, 181–193
- Environment Canada (<https://wateroffice.ec.gc.ca>)
- Gilbert, G.K., 1896. Niagara Falls and their history. National Geographic Society. The Physiography of the United States. The American Book Co., New York 203–236
- Gutierrez, R.R., et al., 2018. Bedforms-ATM, an open source software to analyse the scale-based hierarchies and dimensionality of natural bedforms. *SftwareX* 7, 184-189
- Hage, S., et al., 2018. How to recognize crescentic bedforms formed by supercritical turbidity currents in the geological records: Insight from active submarine channels. *Geology* 46(6), 563–566
- Hayakawa, Y., Matsukura, Y., 2003. Recession rates of waterfalls in Boso Peninsula, Japan, and a predictive equation. *Earth Surface Processes and Landforms* 28 (6), 675–684
- Holland, W.N., 1974. Origin and development of hanging valleys in the Blue Mountains, New South Wales. Ph.D. Thesis, Sydney University, Sydney, Australia, 416
- Hughes Clarke, J.E., 2016. First wide-angle view of channelized turbidity currents links migrating cyclic steps to flow characteristics. *Nature Communications* 7, 11896
- Middleton, G.V., 1993. Sediment deposition from turbidity currents. *Annual review of earth and planetary sciences* 21, 80-114
- Peakall, J. et al., 2007. Flow processes and sedimentation in submarine channel bends. *Marine and Petroleum Geology* 24(6–9), 470–486
- Paull, C.K., et al., 2010. Origins of large crescent-shaped bedforms within the axial channel of Monterey Canyon, offshore California. *Geosphere* 6(6), 755–774
- Paull, C.K., et al., 2018. Powerful turbidity currents driven by dense basal layers. *Nature Communication* 4114
- Piper, D.J.W., Cochonat, P., and Morrison, M.L., 1999. The sequence of events around the epicentre of the 1929 Grand Banks earthquake: initiation of debris flows and turbidity currents inferred from sidescan sonar. *Sedimentology* 46, 79–97
- Postma, G. & Cartigny, M.J.B., 2014a. Supercritical and subcritical turbidity currents and their deposits - A synthesis. *Geology* 42(11), 987–990
- Prior D.B., Coleman J.M., Bornhold B.D., 1982. Results of a known seafloor instability event. *Geo-Marine Letters* 2(3-4), 117-122
- Sumner, E.J. et al., 2013. First direct measurements of hydraulic jumps in an active submarine density current. *Geophysical Research Letters* 40(22), 5904–5908
- Symons, W.O., et al., 2016. Large-scale sediment waves and scours on the modern seafloor and their implications for the prevalence of supercritical flow. *Marine Geology* 371, 130-148
- Torrence, C. & Compo, G.P., 1998. A practical guide to wavelet analysis. *Bull Am Meteorol Soc* 79, 61–78
- Trites, A. 1995. The US repeat and VFR – visiting friends and relatives – visitor to Canada: come again, eh! *Journal of Tourism Studies* 6(1), 27-37
- Whipple K.X. & Tucker G.E., 1999. Dynamics of the stream-power river incision model: implications for height limits of mountain ranges, landscape response timescales, and research needs. *Journal of Geophysical Research, Solid Earth* 104 (B8), 17,661-17,674
- Xu, J.P., Sequeiros, O.E. & Noble, M.A., 2014. Sediment concentrations, flow conditions, and downstream evolution of two turbidity currents, Monterey Canyon, USA. *Deep-Sea Research Part I: Oceanographic Research Papers* 89, 11–34

# Dune dynamics in coarse silt, sand and gravel along the main channel from the estuarine front of the Yangtze River to the Three Gorges Dam.

Heqin Cheng *State Key Laboratory of Estuarine and Coastal Research, East China Normal University –*  
*hqch@sklec.ecnu.edu.cn*

Lizhi Teng *State Key Laboratory of Estuarine and Coastal Research, East China Normal University*

Wei Chen *Helmholtz-Zentrum Geesthacht, Max-Planck-Straße 1, 21502 Geesthacht, Germany,*  
*[wei.chen@hzg.de](mailto:wei.chen@hzg.de)*

**ABSTRACT:** Most past studies of dune dynamics have concentrated on dunes in a spatially-homogeneous natural environment. This environmental simplification imposed inherent limitations on understanding of dune form, flow and sediment dynamics in channels affected by human interventions. This paper details a field study of a swath of dunes in a set of particle sizes as coarse silt, sand and gravel in the main channel from the downstream of Three Gorges Dam (TGD) to the estuarine front of Yangtze River (YR), China for recent 22 years. Results show four new types of dune changing in spatial and temporal distribution. They reveal a complicated pattern of dune morphology and associated flow structure mainly attributed to the dam and channel changes by land reclamation. Froude number was applied into the bedform pattern recognition in the low flow velocity regime along the lower reach of the YR and higher accuracy of recognition was achieved.

## 1 INTRODUCTION

Dunes are ubiquitous bedforms in marine and riverine environments and occur in a wide range of bed sediment particle sizes. Numerous studies in natural environments in unidirectional flow (river) and reversing flow (estuaries and other tidal environments) and in controlled settings (flumes) have demonstrated that bedform size is generally related to sediment size: larger dunes form in coarser sediment (Ashley, 1990; Van den Berg and Van Gelder, 1993; Baas, 1994; Best, 2005; Parsons et al., 2005; Malarkey et al., 2015; Hu et al., 2018).

However, most of these dune dynamics studies have concentrated on dunes in a spatially-homogenous natural environment and in the flume (McLean et al., 1994; Kostaschuk and Best, 2005; Lefebvre et al.,

2013). This environmental simplification imposed inherent limitations on the interpretation and understanding of dune form, flow and sediment dynamics in channels affected or controlled by strong human interventions. Examples of anthropologically-modified environments include the main channel downstream of the Three Gorges Dam, Yangtze River (YR) where a strong erosion takes place (Zheng et al., 2018) combined with climate change and sea level rise (Cheng et al., 2018; Shi et al., 2018).

This paper details a field study of dune morphology in a set of particle sizes ranging from coarse silt to sand and gravel in the main channel from downstream of the Three Gorges Dam to the estuarine front of the YR, China. The aim of this work was to characterise flow pattern and bed morphology over a wide range of sedimentological and hydrological conditions.

## 2 STUDY AREA AND METHODS

The Yangtze River (Figure 1) is the longest river in China. It has been strongly affected by anthropogenic works such as the Three Gorges Dam and land reclamation along the main channels for more than 20 years (Zheng et al., 2018; Cheng et al., 2018). Nine survey cruises during May 2014 and September 2017 were conducted with a total length of survey of over 5000 km along the channel from downstream of the Three Gorges Dam to the estuarine front of the YR using a SeaBat 7125 multi-beam echo sounder (MBES). Simultaneously to the MBES survey, flow information was measured using an Acoustic Doppler Current Profiler (ADCP).

Field studies were carried out in order to further improve our understanding of the fundamental sedimentation and morphodynamic processes acting on subaqueous bedforms during the 1997, 1999, 2000, 2002, 2014, 2015 dry season and the 1998, 2013, 2014, 2015, 2016, 2017 flood season in the uppermost estuarine turbidity maxima. Water depth and near surface tidal current speed/direction were measured at 3-minute intervals for 14 hours in 1997 and 26 hours in all other surveyed duration, while near-bottom tidal current speed and direction were measured at 30-minute intervals for 10 hours in 1997 and for 1 minutes in all other surveyed duration. A total of 1648 water samples were collected at 0.6Z, 0.8Z, and 1.0Z (Z being the total water depth), from which the suspended sediment concentration was analysed. Vertical profiles of the suspended sediment concentration were also measured by using an Acoustic Suspended Sediment Monitor. The transverse profiles over the low angle subaqueous bedforms were recorded in the along channel direction. A total of 16 bed sediment samples

were grabbed and analysed for their particle size.

## 3 RESULTS

The surveys revealed a complicated pattern of dune morphology and associated flow structure. Four new types of erosive subaqueous dune are discovered and new transition function of bedform for the recognition.

### (1) Low angle dunes in coarse silt and very fine sand in the estuarine front of the YR and their seaward migration

Analysis results show a tidal asymmetry, i.e., longer period and stronger current speed in ebb than in flood, resulting in a higher suspended sediment concentration during the ebb due to the tidal resuspension of the bed sediment, thus causes a transport of the suspended sediment seaward in the estuarine turbidity maxima (Cheng et al., 2000). It is suggested that resuspension might be a dominant sediment process on the subaqueous bedforms in coarse silt and very fine sand. Ripples and dunes result from the strong resuspension of bed sediments composed of a wide range distribution of particle sizes. Ripples and small scale dunes might be formed in response to long-period resuspension events instead of short-period, burst-like boils over dune crests. Medium scale dunes occurred in a 2-4 minute period of the enhanced bottom sediment suspension. A new conceptual model is proposed for the sediment and morphodynamic processes on the subaqueous bedforms in coarse silt and very fine sand in a semi-diurnal tidal estuary (Cheng et al., 2000).

Moreover, the sets of field-measured records in the main channels of upper estuarine turbidity maxima show that the distributed front of dune in fine sediment migrated seaward for the past 20 years (Li et al., 2008).

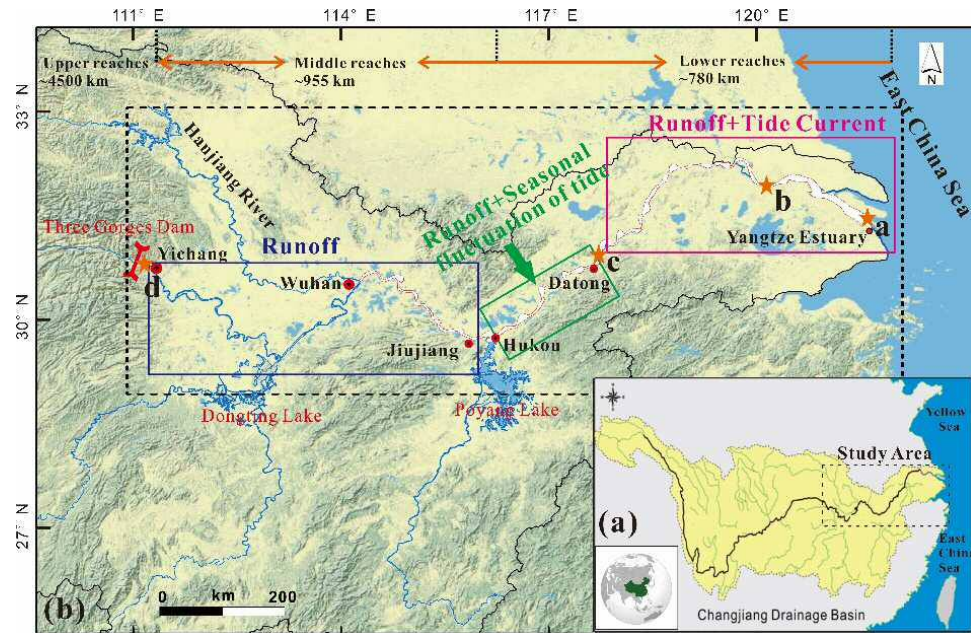


Figure 1 Study area of the dune dynamics along the Yangtze River from the downstream of the Three Gorge Dam to the estuarine front of the Yangtze River. In plot (b), a, b, c, d are the survey locations of subaqueous dune.

## (2) Erosive dunes in very fine sand on the eroded riverbed of channel in lower Yangtze estuary

A new type of dune was defined as a catenary-bead dune, which consists of a catenary dune and its associated elliptical pit (Zheng et al., 2016a). It has a mean height and wavelength of 1.29 m and 31.89 m, respectively; wavelength/height ratio (L/H) of 14 to 56; and elliptical pits of mean and maximum depth 0.98 m and 1.98 m, respectively (Figure 2a). Mean flood and ebb velocities over the dunes are 0.27 and 0.78  $m s^{-1}$ , respectively, with shorter duration of flood tide. The silt, very fine sand, and fine sand fractions were within the ranges 21.6–23.4%, 28.2–32.2%, and 39.7–41.6%, respectively, revealing complex bed material composition. Water depth varies from 13 to 17 m.

## (3) Very large dunes (VLDs) in fine and medium sand in the upper Yangtze estuary and VLDs accompanied by sec-

## ondary dunes in the middle reach of the YR

In the upper estuary and middle reach of the YR, two types of very large dunes were detected in unidirectional flow according to their morphological characteristics (Zheng et al., 2016b). The mean grain size of the riverbed surface sediments is between 0.137 mm and 0.262 mm, named as fine and medium sand.

The first type is the VLDs with a smooth surface and cross-section on the silted riverbed of channel in the upper estuary (Figures 1 and 2b). The average dune spacing is 122.8 m and their mean height is 3.9 m with a mean L/H of 35.4. Water depth ranged from 13.4 m to 17.6 m and simultaneous vertical average flow velocity changed from 0.78 to 0.99  $m s^{-1}$ .

The second type is the VLDs accompanied by secondary dunes and numerous elliptical pits on the eroded riverbed of channel in the upper estuary (Figures 1 and 2c).

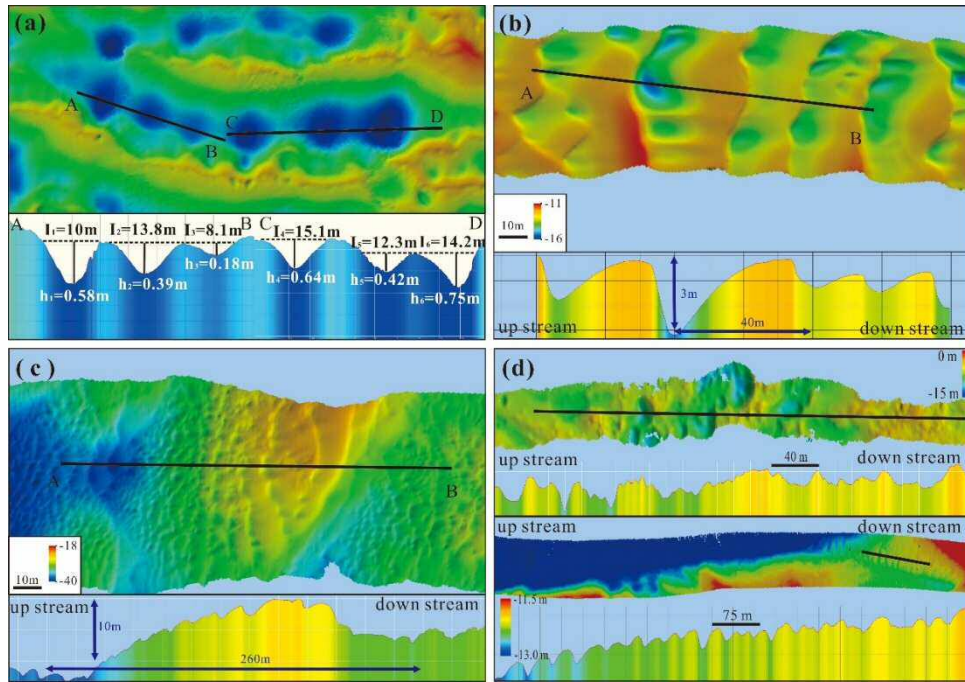


Figure 2. The multi-beam mapping for characteristics of subaqueous dunes along the main channel in the middle and lower reaches of the Yangtze River. (a) Maps of typical characteristics of catenary-bead dunes in very fine sand showing inlaid elliptical pits; (b) Maps of morphology of a very large dune in fine sand with a smooth surface in the silted channel; (c) Maps of morphology of a very large dune in fine sand with a smooth surface imposed on the catenary-bead dunes in the eroded channel; (d) Maps of very large dune in gravel along the channel from downstream the Three Gorge Dam to Yichang.

The mean spacing of dunes changed from 184.5 m to 204.3 m and mean height varied from 4.1 m to 4.3 m with a mean H/L of 55.1 to 56.3. The water depth varied from 17.6 m to 29.9 m and simultaneous vertical average flow velocity ranged from 0.96 to 1.22  $\text{m s}^{-1}$

#### (4) Very large dunes (VLDs) in sandy gravel with strong unidirectional flow along strong eroded channel downstream the Three Gorge Dam (TGD) to Yichang

An area covered with dunes was surveyed downstream of the Three Gorge Dam. The dunes showed a mean spacing of 89 m ranging from 40 m to 267 m and a mean height of 5 m ranging from 5 m to 13 m. Secondary erosive catenary-bead dunes were also imposed on the lee and stoss slope of dunes in gravel (Figure 2d). The mean particle size is 7.90 mm and medium particle

size is 10.52 mm. The sorting coefficient is 12.52. Their scales are larger than most of dunes in gravel studied for the bed load estimation and criteria of flow in the flume experiments and few subaqueous dunes in gravel detected in, e.g., the Severn Estuary (Carling et al., 2006) and the continental shelves in Italy (Iacono and Guillén, 2008).

#### (5) Application of Froude number in the pattern recognition of bedform in low flow velocity regime along the lower reach of the YR

Specific concern is given to the effects of Froude number on the pattern recognition of bedform in low velocity regime. A three-dimensional (3D) phase diagram of dune stability for the recognition is proposed, in Froude number ( $\text{Fr}$ ), Reynolds number ( $\text{Re}_*$ ) and Shields number ( $\Theta$ ) of sediment grains (Figure 3). These parameters are calculated

from flow velocity obtained with ADCP, morphological parameters of bedforms detected by MBES, sediment and particle size, simultaneous real-time water level in typical channels in tidal reach of the YR. The results show an increasing accuracy of bedform pattern recognition with three parameters of Froude number, Reynolds number and Shields number by 35% than two parameters Reynolds number and Shields number. This 3D diagram can also increase the recognition accuracy of bedform by 30% than those with two parameters of dimensionless Shields number and Reynolds number  $Re^*$ . The deviation of dune recognition without Fr ranged from 40% to 80%.

#### 4 CONCLUSIONS

Changes in morphology, flow and sediment dynamics over a main channel ca. 1600 km were examined from the estuarine front of the YR to downstream of TGD, China. The dunes composed of coarse silt, very fine sand, fine sand, medium sand and sandy gravel displayed a complicated pattern of dune morphology and associated flow structure. Four new types of dunes with spatial and temporal changes were discovered with emphasis on the findings of erosive dunes which imply strong effects of the Three Gorges Dam and changes in channel morphology by land reclamation and sand mining, dredging. Application of Froude number into the bedform pattern recognition in the low flow velocity regime can increase the accuracy of bedform recognition. These findings enrich the description and understanding of dune dynamics and provide important data for geomorphological research.

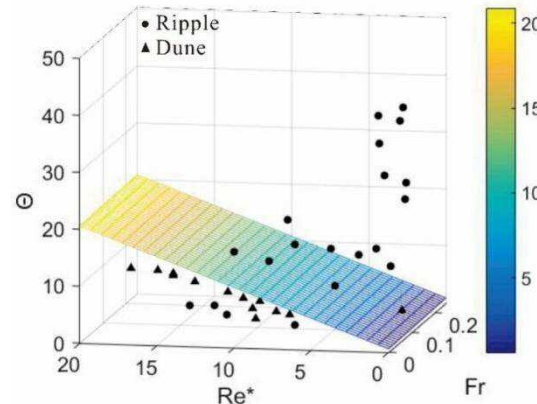


Figure 3. Map showing the stability diagram of dunes with Froude number (Fr), Reynolds number ( $Re^*$ ) and Shields number ( $\Theta$ ).

#### 5 ACKNOWLEDGEMENT

This research was supported by joint research projects NSFC-NOW-EPSRC: Sustainable Deltas (51761135023), China Geological Survey (12120115043101), NSFC (Grant Nos. 41476075, 41340044, 40776056, 40576048), and the 111 Project (B08022). We thank Mr. Y. Z. Xue, B. Song, W. X. Zhang, and H. Y. Xu, J. Zhan who helped in the field data collection. Late Prof. J. Y. Chen is thanked for his encouragement. Prof. H. E. de Swart at Utrecht University, The Netherlands, and Dong Ping at Liverpool University are thanked for their remarks on the helps on this manuscript.

#### 6 REFERENCES

- Ashley, G.M., 1990. Classification of large-scale subaqueous bedforms: A new look at an old problem. *Journal of Sedimentary Research* 60, 160-172.  
doi:10.2110/JSR.60.160
- Baas, J.H., 1994. A flume study on the development and equilibrium morphology of current ripples in very fine sand. *Sedimentology* 41:185-209.
- Best, J., 2005. The fluid dynamics of river dunes: A review and some future research directions. *Journal of Geophysical Research Earth Surface*, 2005, 110(F44S02):  
doi:10.1029/2004JF000218.
- Carling, P.A., Radecki-Pawlak, A., Williams, J.J., Rumble, B., Meshkova, L., Bell, P., Breakspear, R., 2006. The morphodynamics and internal structure of intertidal fine-gravel dunes: Hills Flats, Severn Estuary, UK. *Sedimentary Geology*, 183 (3-4), 159-179

- Cheng, H.Q., Chen, J.Y., Chen, Z.J., Ruan, R.L., Xu, G.Q., Zeng, G., Zhu, J.R., Dai, Z.J., Chen, X.Y., Gu, S.H., Zhang, X.L., Wang, H.M., 2018. Mapping Sea Level Rise Behavior in an Estuarine Delta System: A Case Study along the Shanghai Coast. *Engineering*, 4, 156-163,
- Cheng H.Q., Kostaschuk R., and Shi Z. 2004. Tidal currents, bed sediments, and bedforms at the South Branch and the South Channel of the Changjiang (Yangtze) Estuary, China: implications for the ripple-dune transition. *Estuaries*, 2004, 27(5): 861-866.
- Cheng H.Q., Song B., Xue Y.Z., Mao X.H., 2000. Mechanics on transport of coarser silt and very fine sand in the Changjiang Estuary - Episodic re-suspension and large-scale bedform movement. *Journal of Sediment Research*, 2(1):20-27 (in Chinese with an English abstract)
- Hu H., Wei T.Y., Yang Z.Y., Hackney C.R., Parsons D.R., 2018. Low-angle dunes in the Changjiang (Yangtze) Estuary: Flow and sediment dynamics under tidal influence. *Estuarine, Coastal and Shelf Sciences*, 205: 110-122.
- Iacono C.L., Guillén J., 2008. Environmental conditions for gravelly and pebbly dunes and sorted bedforms on a moderate-energy inner shelf (Marettimo Island, Italy, western Mediterranean). *Continental Shelf Research*, 2008, 28(2):245-256.
- Kostaschuk, R.A., Best, J., 2005. Response of sand dunes to variations in tidal flow: Fraser Estuary, Canada. *Journal of Geophysical. Research: Earth Surface* (2003e2012) 110 (F4).
- Lefebvre A., Ernstsen V.B., Winter C., 2013. Estimation of roughness lengths and flow separation over compound bedforms in a natural-tidal inlet. *Continental Shelf Research*, 61-62: 98-111, doi.10.1016/j.csr.2013.04.030.
- Li W., Cheng H.Q., Li J, Ping, D., 2008. Temporal and spatial changes of dunes in the Changjiang (Yangtze) estuary, China. *Estuarine Coastal and Shelf Science*, 77(1):169-174.
- Malarkey, J., Baas, J.H., Hope, J.A., Aspden, R.J., Parsons, D.R., Peakall, J., Paterson, D.M., Schindler, R.J., Ye, L., Lichtman, I.D., Bass, S.J., Davies, A.G., Manning, A.J. and Thorne, P.D., 2015. The pervasive role of biological cohesion in bedform development. *Nature Communications* 6, 6257. doi:10.1038/ncomms7257
- McLean, S., Nelson, J., Wolfe, S., 1994. Turbulence structure over two-dimensional bed forms: implications for sediment transport. *Journal of Geophysical Research: Oceans* (1978-2012) 99 (C6), 12729-12747.
- Shi, S., Cheng, H., Xuan, X., Hu, F., Yuan, X., Jiang, Y. and Zhou, Q., 2018. Fluctuations in the tidal limit of the Yangtze River estuary in the last decade. *Science China Earth Sciences* 61, 1136-1147. doi:10.1007/s11430-017-9200-4
- Van den Berg, J.H. and Van Gelder, A., 1993. A new bed-form stability diagram, with emphasis on the transition of ripples to plane bed in flows over fine sand and silt. In: M. Marzo and C. Pudefábreas (Eds.), *Alluvial Sedimentation*. Special Publication of the International Association of Sedimentologists 17:11-21.
- Zheng, S., Cheng, HQ., Shi, S., Xu, W., Zhou, Q., Jiang, Y., Zhou, F. and Cao, M., 2018. Impact of anthropogenic drivers on subaqueous topographical change in the Datong to Xulijiang reach of the Yangtze River. *Science China Earth Sciences* 61, 940-950. doi.10.1007/s11430-017-9169-4
- Zheng, S., Cheng, HQ., Wu, S., Liu, G., Lu, X. and Xu, W., 2016a. Discovery and implications of catenary-bead subaqueous dunes. *Science China Earth Sciences* 59, 495-502. doi.10.1007/s11430-015-5194-3
- Zheng, S., Cheng, H.Q., Wu, S., Shi, S., Xu, W., Zhou, Q. and Jiang, Y., 2016b. Morphology and mechanism of the very large dunes in the tidal reach of the Yangtze River, China. *Continental Shelf Research* 139, 54-61. Doi.10.1016/j.csr.2016.10.006

# Dune morphology and hysteresis in alluvial channels during long-duration floods revealed using high-temporal resolution MBES bathymetry

Julia Cisneros *University of Illinois Urbana-Champaign, Champaign, IL – [jcisnrs2@illinois.edu](mailto:jcisnrs2@illinois.edu)*

Jim Best *University of Illinois Urbana-Champaign, Champaign, IL – [jimbest@illinois.edu](mailto:jimbest@illinois.edu)*

Thaiënne van Dijk *Deltares, Utrecht, Netherlands – [Thaienne.vanDijk@deltas.nl](mailto:Thaienne.vanDijk@deltas.nl); University of Illinois Urbana-Champaign, Champaign, IL – [vandijk@illinois.edu](mailto:vandijk@illinois.edu)*

Erik Mosselman *Deltares, Delft, Netherlands; Delft University of Technology, Delft, Netherlands – [Erik.Mosselman@deltas.nl](mailto:Erik.Mosselman@deltas.nl)*

**ABSTRACT:** This paper quantifies how dune morphology changes through flood hydrographs by using high spatial- and temporal-resolution bathymetric data and robust computational analysis methods to produce probability density functions of dune morphology. This quantification aims to provide a better understanding of dune hysteresis by examining river bathymetry from a 16 km reach of the River Waal, Netherlands, in a 6-month time series of bi-weekly multibeam echo sounder surveys. Parameterization includes dune height, wavelength, leeside angle and leeside shape, to assess dune kinematics and hysteresis during different flood hydrographs.

## 1 INTRODUCTION

In rivers and man-made channels, flow discharge may fluctuate across a range of time scales – from diurnal to seasonal – but is often most pronounced in hydrographs that encompass long-duration floods (weeks to months). Under these varying flows, bedforms can be created and modified by the flow without achieving an ‘equilibrium’ state (Ten Brinke et al., 1999). A lag between changes in flow and the morphological response of the bedforms, termed bedform hysteresis, is commonly present. Importantly for channel management and navigation, critical water depths may be reached for inland shipping since dunes may grow larger during floods, but often experience a lagged decay in size during lowering water levels (Ten Brinke et al., 1999; Wilbers & Ten Brinke, 2003). There is also a growing consensus that dunes possess a more flattened shape, and lower leeside angle, than previously assumed in large rivers and that such dunes do not exhibit a region of permanent flow separation downstream of the dune (Roden, 1998; Kostaschuk, 2000; Best & Kostaschuk, 2002; Motamedi et al., 2012,

2014; Lefebvre & Winter, 2016; Lefebvre et al., 2016; Kwoll et al., 2016). This different leeside shape thus questions traditional ideas of flow interactions with dunes, where flow separation in the steep dune leeside leads to energy loss (form drag) that increases flow resistance and energy expenditure within the flow.

The shape of dunes also has the potential to change through the adaptation of dune morphology to the flow, as well as the interaction between neighbouring dunes (Reesink et al., 2018). In variable flow conditions, smaller superimposed dunes can also exist with large dunes (Allen & Collinson, 1974; Allen, 1978; Reesink et al., 2018). As these smaller, superimposed dunes migrate and climb up the stoss side of larger host dunes, they can modify the shape of the larger dunes by eroding the crest and eventually descending down the leeside of host dunes, thus lowering the leeside angle (Allen, 1978; Amsler & Schreider, 1999). In the process of small dune migration up the stoss side of the larger dune, the small dunes can also intermittently increase the leeside angle of the host dune when their leeside is aligned with the crest of the larger dune. This intermittent increase in leeside angle has been

observed from ripple - dune interactions in laboratory experiments and might be reflected in other observations as ‘superelevation’ of the crest, which occurs at time scales of 5 - 15 min (Reesink & Bridge 2007; Reesink et al., 2018; Baar & Cisneros, *in review*). Smaller dunes may also run into, and amalgamate with, larger dunes, leading to large morphological change and complexity for those larger dunes (Allen & Collinson, 1974; Allen, 1978). Thus, whilst previous work has shown that variable flow conditions may cause dunes to increase and decrease in size, the response of dune shape, and specifically leeside angle, to variable flow conditions has not yet been quantified, despite the fact that the leeside has been shown to be of major importance to the flow field over alluvial dunes (Kostaschuk, 2000; Best & Kostaschuk, 2002; Motamedi et al., 2012, 2014; Lefebvre & Winter, 2016; Lefebvre et al., 2016; Kwoll et al., 2016). Understanding such bedform response may also offer important information in teasing out the possible processes of dune formation and dune-dune interactions. This paper aims to investigate dune morphological response to natural variations in flow during a flood in a major navigation channel.

## 2 MBES DATA

Until recently, temporally abundant river bathymetric data were not available, but with the need for accurate riverbed topogra-

phy to assess dredging locations for safer navigation, the River Waal has been surveyed once every two weeks since 2005. These data, along with hydrographs measured at stations along the river, are now available through the Dutch Ministry of Infrastructure and the Environment, Rijkswaterstaat, and Deltares, which offers a unique opportunity to investigate dune morphodynamics under variable flows over long periods of time (weeks to months) (Fig.1). These bathymetric data were obtained using a multibeam echo sounder (MBES) over a period ranging from 1 to several days per survey. Time series MBES data in 2010-2011 were analyzed (Fig. 1), yielding 12 bathymetric maps that reveal the morphologic response in the Waal River at two weekly time steps through a compound, long-duration flood, lasting ~6 months and reaching peak flow of *c.* 6,000  $\text{m}^3\text{s}^{-1}$  (3x the average flow discharge) (Fig.1).

## 3 METHODS

A bedform analysis (Cisneros et al., *in prep.*; Baar & Cisneros, *in review*) was implemented on all 12 river bathymetric surveys of the River Waal. This method measures dune morphology by running automated profile line measurements spaced at the resolution of the bathymetric grid (0.5 m grid cells) across the width of the surveyed area and interrogates the value of each data point along each dune profile (Cisneros et al., *in prep.*). Thus, dune height, wavelength, leeside angle, and leeside shape (location of

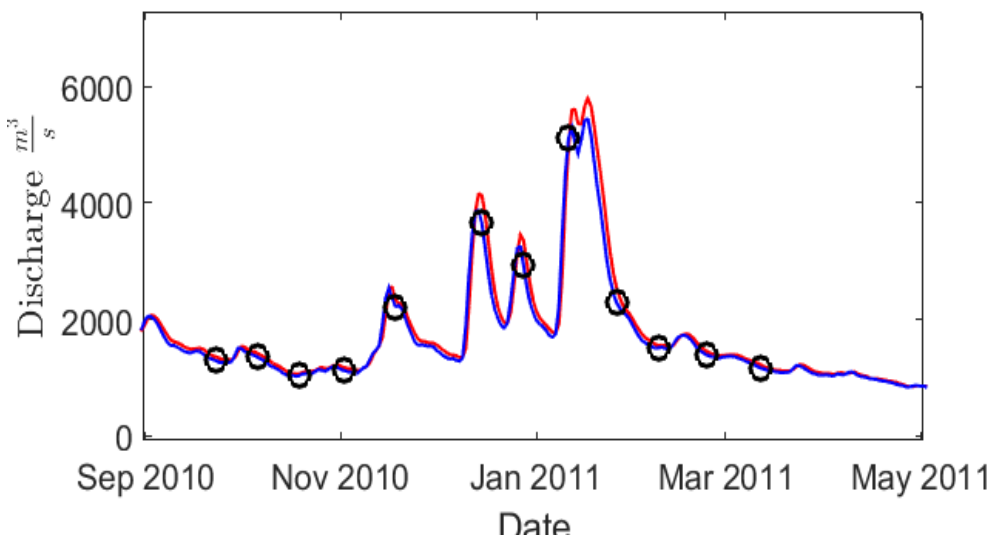


Figure 1. Discharge hydrograph of the River Waal at stations upstream (Pannerdense Kop) and downstream (Tiel) of the survey area, with the survey dates throughout the flood denoted by black circles.

possible brink points or changes in slope), as well as the flow depth for each dune, are measured along its width, thereby quantifying the morphology of the dunes and indicators of dune shape complexity in the streamwise and spanwise directions.

#### 4 RESULTS AND DISCUSSION

From the bedform analysis method, ~100,000 measurements of dune morphology were made for each survey date through the flood. Distributions of the mean and maximum leeside angle (Figure 2) represent all measured values of the average slope of the leeside (mean) and the singular, maximum slope on the leeside (maximum) of each dune. In this plot, the shapes of the distributions appear similar and the peaks of the distributions fall in the same ranges. A normal probability density function was also fitted to each of the distributions. These data (Table 1) show that the shape of the distributions changes through the flood. Notably, at the peak of the flood, on January 11, 2011, the shape parameters of the distribution indicate that the mean and maximum distributions are shifted to higher values ( $\mu$  is  $13.48^\circ$  &  $19.26^\circ$ , for mean and maximum angle, respectively). After the peak of the flood, on January 26<sup>th</sup>, 2011, a long tail on the high end of the distribution of maximum leeside angles is present and demonstrates that more dunes with higher angle leesides exist at this time, even though the majority of leeside angles are lower (mean value of  $16.65^\circ$ ).

In addition, dune height, wavelength, and aspect ratio (height/wavelength) were quantified through time (Figure 3). A sharp distinction between dunes was observed between the northern and southern parts of the river, with large dunes in the north and small dunes in the south. Thus, analysis of the data was split between the dunes occupying the north and south of the channel, using a channel centreline for differentiation. This north-south division has been previously

noted by Wilbers & Ten Brinke (2003), irrespective of any natural bends in the channel. The northern and southern dunes react differently to the changes in flow (Figure 3). Initially, the dunes on both sides of the channel grow in height with increasing discharge, but during the falling stage of the flood (after January 11, 2011), the northern dunes decay in size at a much slower rate than the southern dunes. Thus the heights of the northern dunes are lagged behind changes in river flow during the falling stage, with dunes being higher during the falling stage than the rising stage. In terms of dune wavelength, the northern and southern dunes also possess different responses through the flood. The northern dunes are shorter in wavelength during the rising stage and longer during the falling stage, whereas the southern dunes show the opposite behaviour.

Table 1. The shape factors ( $\mu$  = mean &  $\sigma$  = sigma) of the probability density function normal fit to the mean and maximum angle distributions for each survey.

Date	Mean ( $\mu$ )	Mean ( $\sigma$ )	Max ( $\mu$ )	Max ( $\sigma$ )
Sept. 23, 2010	10.79	4.20	14.92	5.59
Oct. 6, 2010	10.93	4.64	14.95	5.70
Oct. 19, 2010	10.79	4.02	14.56	5.09
Nov. 2, 2010	10.87	4.13	14.62	5.01
Nov. 18, 2010	11.73	4.50	16.43	5.41
Dec. 15, 2010	13.39	4.55	19.19	5.28
Dec. 26, 2010	12.80	4.44	18.22	5.28
Jan. 11, 2011	13.48	4.03	19.26	4.65
Jan. 26, 2011	11.70	4.63	16.65	6.16
Feb. 8, 2011	10.34	4.18	14.01	5.49
Feb. 23, 2011	10.53	4.00	14.14	4.99
Mar. 12, 2011	10.66	3.77	14.22	4.63

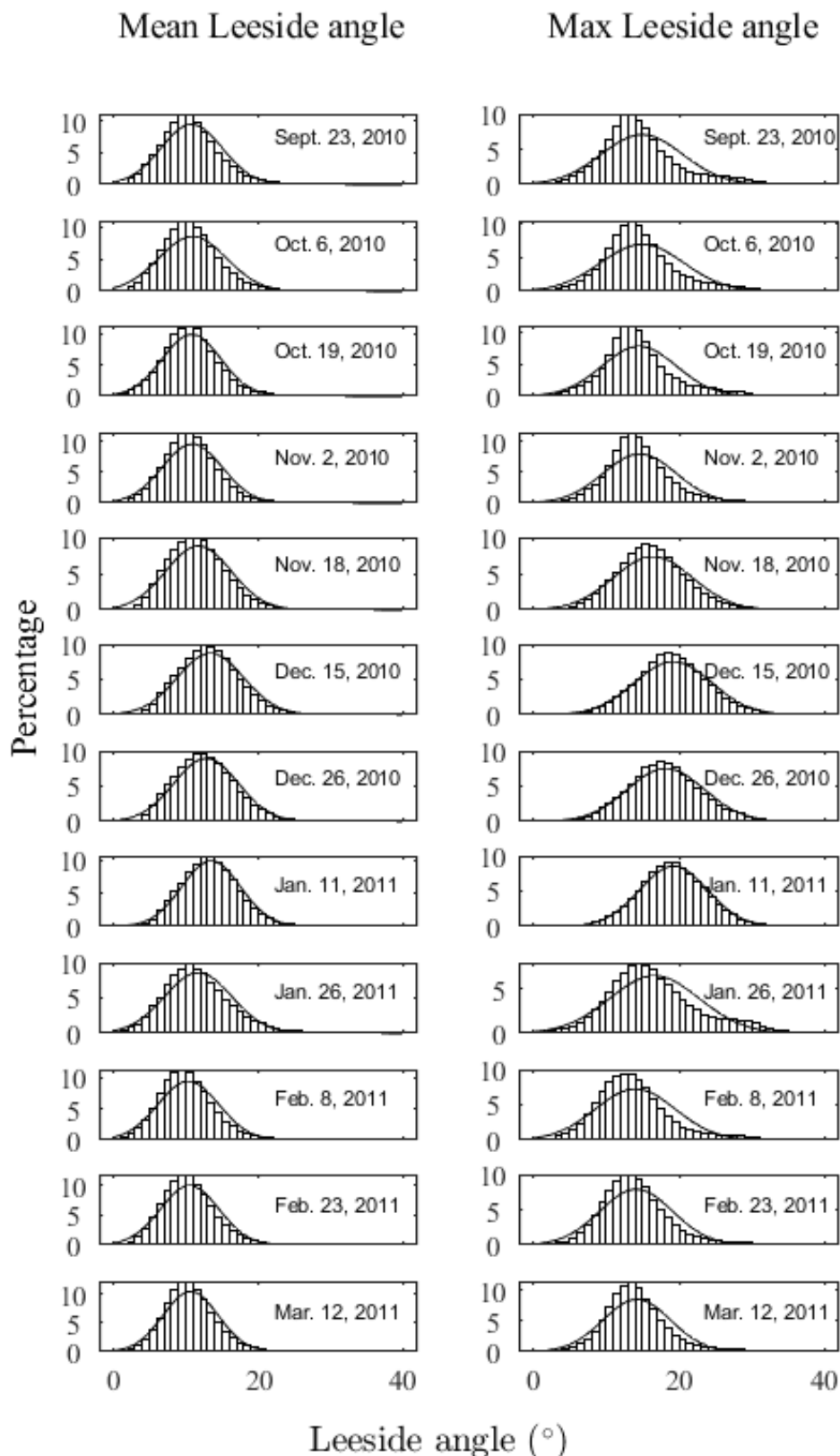


Figure 2. The distributions of mean and maximum leeside angle representing all dunes measured across the river width for each survey date. Note each distribution represents ~100,000 data points. Black lines are normal pdf's fitted to each distribution.

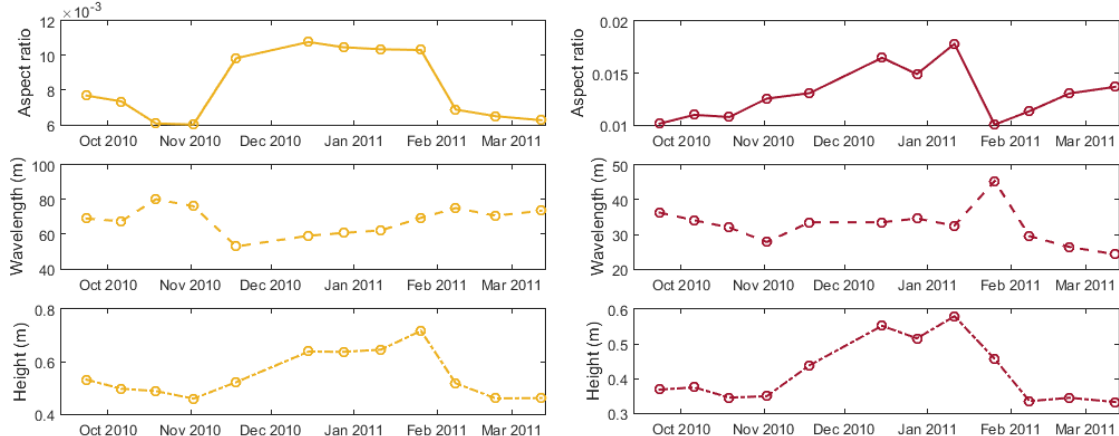


Figure 3. Dune population characteristic values (mean values) of aspect ratio, wavelength, and height determined for each survey through the flood for northern (yellow) and southern (red) dunes.

The northern dunes range in their mean wavelength by 30 meters through the flood, with the southern dunes range being 20 meters, but the change between successive surveys is only a few meters, i.e. the rate of change is relatively mild (Figure 3). One exception occurs in the southern dunes immediately after the peak of the flood, on January 26<sup>th</sup> 2011, when the wavelength increased from ~30 meters to the maximum wavelength during this time, ~50 meters, and then decreased just as abruptly by the following survey date. This time represents a period of large change in the morphology of the southern dunes – the dunes almost double in wavelength and then decrease in wavelength by a factor of 2. In addition to dune height and wavelength, their aspect ratio is also plotted in Figure 3 and shows how the height and wavelength change together through the flood. Overall, the aspect ratio thus increases and decreases through the rising and falling stage, but the aspect ratio notably remains constant in the northern dunes during the peaks of the flood, which corresponds to discharges greater than  $2,000 \text{ m}^3 \text{s}^{-1}$  (Figures 1 and 3).

## 5 CONCLUSIONS

Dune morphology was measured in the River Waal over a 16 km reach using MBES bathymetric data taken every 2 weeks through a long-duration (6-month long)

flood. During this flood, three major morphological features are apparent:

1. Dune leeside angles are largest during the peak of the flood. Such an increase in leeside angle during the flood peak suggests more significant contributions to flow resistance by dunes, and changing leeside angle should be considered in future flow models.

2. Dunes grow and decay in size in the northern half of the channel, whereas in the southern half dunes show little to no hysteresis in dune height and wavelength. Previously, the hydrodynamic effects of laden ships travelling eastbound (on the south side of the river) and unladen ships travelling westbound (on the north side) have been proposed to explain such a distinction in dune scale. This hypothesis is now under investigation by comparing this bathymetry against ship tracks with information on ship loading.

3. Large morphological change occurs immediately after the peak of the flood in the southern dunes, where wavelength firstly increases and then decreases by a factor of two. This may indicate possible amalgamation and splitting processes are occurring at this time for the southern dunes.

These preliminary findings demonstrate how the distributions of the dune dimensions and population characteristic values can be used to make morphologic and process-based interpretations of dune response during a

long-duration flood, which may not be apparent by an analysis of solely mean values. It is clear that the former approach is required to more fully quantify dune-flow hysteresis, and its effects, over the temporal scale of a flood wave.

## 6 ACKNOWLEDGEMENTS

This work is part of the Ph.D. research of JC. JC is supported by National Science Foundation Graduate Research Fellowship (NSF GRF). This material is based upon work supported by the National Science Foundation Graduate Research Fellowship under Grant No. DGE – 1746047, and supported by the Department of Geology, Illinois, and the Jack and Richard Threet chair in Sedimentary Geology to JB. This work was also supported by the Graduate Research Opportunities Worldwide collaborative grant scheme awarded to JC through the NSF, Netherlands Organization for Scientific Research (NWO), Delft University of Technology, and Deltares.

## 7 REFERENCES

- Allen, J., 1978. Polymodal dune assemblages: An interpretation in terms of dune creation– destruction in periodic flows. *Sedimentary Geology*, 20, 17–28
- Allen, J., Collinson, J., 1974. The superimposition and classification of dunes formed by unidirectional aqueous flows. *Sedimentary Geology*, 12 (3), 169–178
- Amsler, M., Schreider, M., 1999. Dune height prediction at floods in the Parana' River, Argentina. *River sedimentation: Theory and applications*, 615–620
- Baar, A., Cisneros, J., In Review. Influence of grain size-dependent bedform morphology on flow and downslope sediment transport in river bends. *Journal of Geophysical Research*
- Best, J., Kostaschuk, R., 2002. An experimental study of turbulent flow over a low-angle dune. *Journal of Geophysical Research: Oceans*, 107 (C9)
- Cisneros, J., et al., In prep. The shape of dunes in the World's big rivers.
- Kostaschuk, R., 2000. A field study of turbulence and sediment dynamics over subaqueous dunes with flow separation. *Sedimentology*, 47(3), 519–531.
- Kwoll, E., Venditti, J., Bradley, R., Winter, C., 2016. Flow structure and resistance over sub-aqueous high-and low-angle dunes. *Journal of Geophysical Research: Earth Surface*, 121(3), 545–564
- Lefebvre, A., Winter, C., 2016. Predicting bed form roughness: The influence of lee side angle. *Geo-Marine Letters*, 36(2), 121–133
- Lefebvre, A., Paarlberg, A. J., Winter, C., 2016. Characterising natural bedform morphology and its influence on flow. *Geo-Marine Letters*, 36 (5), 379–393
- Motamed, A., Afzalimehr, H., Gallichand, J., Abadi, E. F. N., 2012. Lee angle effects in near bed turbulence: An experimental study on low and sharp angle dunes. *International Journal of Hydraulic Engineering*, 1(6), 68–74
- Motamed, A., Afzalimehr, H., Zenz, G., Galoie, M., 2014. Rans simulations of flow over dunes with low lee and sharp lee angles. in *Advances in Hydroinformatics*, Springer, 525–533
- Reesink, A. J. H., Bridge, J. S., 2007. Influence of superimposed bedforms and flow unsteadiness on formation of cross strata in dunes and unit bars. *Sedimentary Geology*, 202(1-2), 281–296.
- Reesink, A., Parsons, D., Ashworth, P., Best, J., Hardy, R., Murphy, B., McLelland, S., Unsworth, C., 2018. The adaptation of dunes to changes in river flow. *Earth-Science Reviews*, 185, 1065–1087
- Roden, J. E., 1998. The sedimentology and dynamics of mega-dunes, Jamuna River, Bangladesh. Ph.D., University of Leeds
- Ten Brinke, W., Wilbers, A., Wesseling, C., 1999. *Dune growth, decay and migration rates during a large-magnitude flood at a sand and mixed sand-gravel bed in the Dutch Rhine River System. Fluvial Sedimentology VI*, 15–32
- Wilbers, A., Ten Brinke, W., 2003. The response of subaqueous dunes to floods in sand and gravel bed reaches of the Dutch Rhine. *Sedimentology*, 50(6),

# Barchan vs Monopile: what happens when a barchan dune finds an obstacle in its path?

Amelia J. Couldrey *HR Wallingford, Oxfordshire, UK* – *A.Couldrey@hrwallingford.com*

Michiel A. F. Knaapen *HR Wallingford, Oxfordshire, UK* – *M.Knaapen@hrwallingford.com*

Kerry V. Marten *HR Wallingford, Oxfordshire, UK* – *K.Marten@hrwallingford.com*

Richard J. S. Whitehouse *HR Wallingford, Oxfordshire, UK* – *R.Whitehouse@hrwallingford.com*

**ABSTRACT:** The impact of barchan dunes colliding with one another has been well observed, understood and modelled. But what happens when there is an immobile obstacle, an Offshore Wind Farm (OWF) monopile foundation, in one's path? At the case study OWF a monopile was installed ~45 m downstream of the slip-face of an approaching barchan dune. Six bathymetric surveys, over a 20 year period, are analysed capturing the impact of the monopile on the dune's evolution. The dune migrated relatively consistently, at a rate of 20 to 25 m/year. The re-appearance of the jack-up rig spudcan footprints in the wake of the barchan indicates that the dune does not exchange material with the seafloor and that the sedimentary composition of the two must be distinct.

## 1 INTRODUCTION

Barchan dunes have been studied in subaerial settings, both terrestrial e.g. deserts (Hugenholtz & Barchyn, 2012) and extra-terrestrial e.g. on the surface of Mars (Parteli et al. 2014); as well as in subaqueous settings (Berné et al. 1989, Ma et al. 2014). The advent of repeat satellite observations has made documenting the behaviour of subaerial dune migration less challenging in comparison with their subaqueous counterparts, which have attracted fewer studies due to the limited number of repeat observations in the marine environment.

The crescent-shaped barchan dunes form when the current (or wind) cannot set in motion all sedimentary particles or when there is a sand deficit. They can be formed under a unidirectional current or a bi-directional current where there is a strong asymmetry. In Figure 1 the terminology used to describe the dune morphology is defined. Material is transported from the toe of the dune up the stoss slope, where it is then deposited on the slip face, the result of which is a net migration towards the direction that the horns point. Barchan dunes in marine environments can have annual

migration rates of upwards of 70 m/year (Berné et al. 1989). Commonly barchan dunes are described by their horn-to-horn distance (width) and horn-to-toe distance (length).

Typically dunes are found in large groups, known as fields. Within a field barchans vary in both size and mobility, with small dunes migrating at faster rates. As a result, smaller dunes frequently catch-up to larger dunes resulting in collisions. Rather than combining into a singular larger dune, a smaller dune ejects from the larger dune. If a barchan dune gains material from the surrounds it can eventually become destabilised. Once sufficiently large a dune may 'calve' a smaller barchan dune from their downstream side (Worman et al. 2013).

Whilst the collision of one barchan with another is well documented and understood the impact of a barchan colliding with a physical obstacle has not yet been documented in scientific literature. However, the interaction between non-barchan bedforms, e.g. linear sandwaves, with objects, e.g. a cylinder, has been studied numerically (Margalit, 2017). In Margalit's model it is observed that the presence of a monopile mostly affects sandwave migration on the lee-side of the monopile by limiting the migration speed and blocking the sediment transport. In the same

model sand is observed to build up on the upstream side of the monopile.

The main aim of this study is to analyse the morphological evolution of a barchan dune as it passes an obstacle (in this case a monopile). The secondary aim is to assess the impact of the dune on the scour pit at the base of the monopile of interest for the management of wind farm assets.

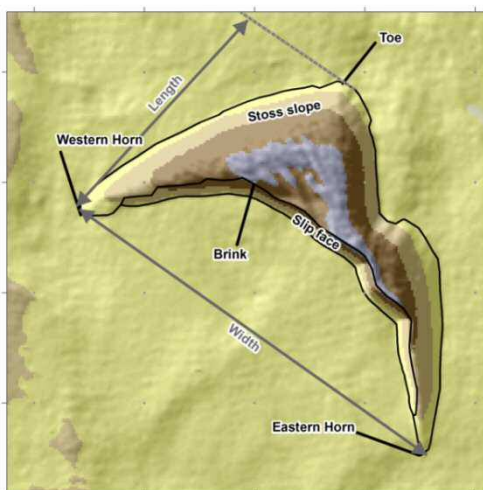


Figure 1. Nomenclature used to describe barchan dune.

## 2 BACKGROUND

### Infrastructure

The study area is in a windfarm development off the east coast of the UK. In this paper a singular monopile foundation will be considered, this foundation was installed in 2010 (ahead of the passage of a barchan dune). The pile has an outer diameter of 5.8 m and was installed using a jack-up rig, leaving spudcan depressions to the northeast of the pile (Fig. 2f).

### Site conditions

The seabed level at the case study monopile foundation is on average -25 m relative to the Lowest Astronomical Tide (LAT). Locally spring tidal ranges are typically around 3.4 m.

The site is tidally dominant with a tidal flow towards the northeast during the ebb phase and to the southwest during the flood phase. Tidal

velocities are flood dominated, with average bed current speeds approximately 0.4 m/s, whilst peak current speeds are approximately 1 m/s.

The wave distribution is bimodal and is proximally aligned with the tidal flow, with waves approaching both from the north-northeast and south-southwest. The largest waves approach the site from the north-northeast, with a 1 in 10 year significant wave height of 4.0 m.

One kilometre to the northwest of the study barchan is a northeast-southwest aligned linear sandbank with a height of 18 m. This sandbank is still active and sediment mobility calculations confirm that locally sediments are mobile for approximately 80% of the time.

The seabed around the sandbank comprises largely sand and gravelly sand, which makes up a veneer generally not exceeding 1 m thickness. Beneath this is a layer of London Clay.

### Data

Six surveys are available for analysis (Table 1, Fig. 2). Five of these (2004, 2009, 2013, 2014 and 2014) were collected using commercial operations related to the wind farm development, these have a vertical uncertainty of  $\pm 0.3$  m or less. Whilst the 1995 data have been sourced from the UKHO INSPIRE portal and likely have a much larger vertical and horizontal uncertainty.

Table 1: Details of surveys

Survey	Grid resolution (m)
(a) 1995	25
(b) July 2004	20
(c) March to May 2009	2
(d) May 2013	1
(e) July to August 2014	0.5
(f) August to September 2015	0.5

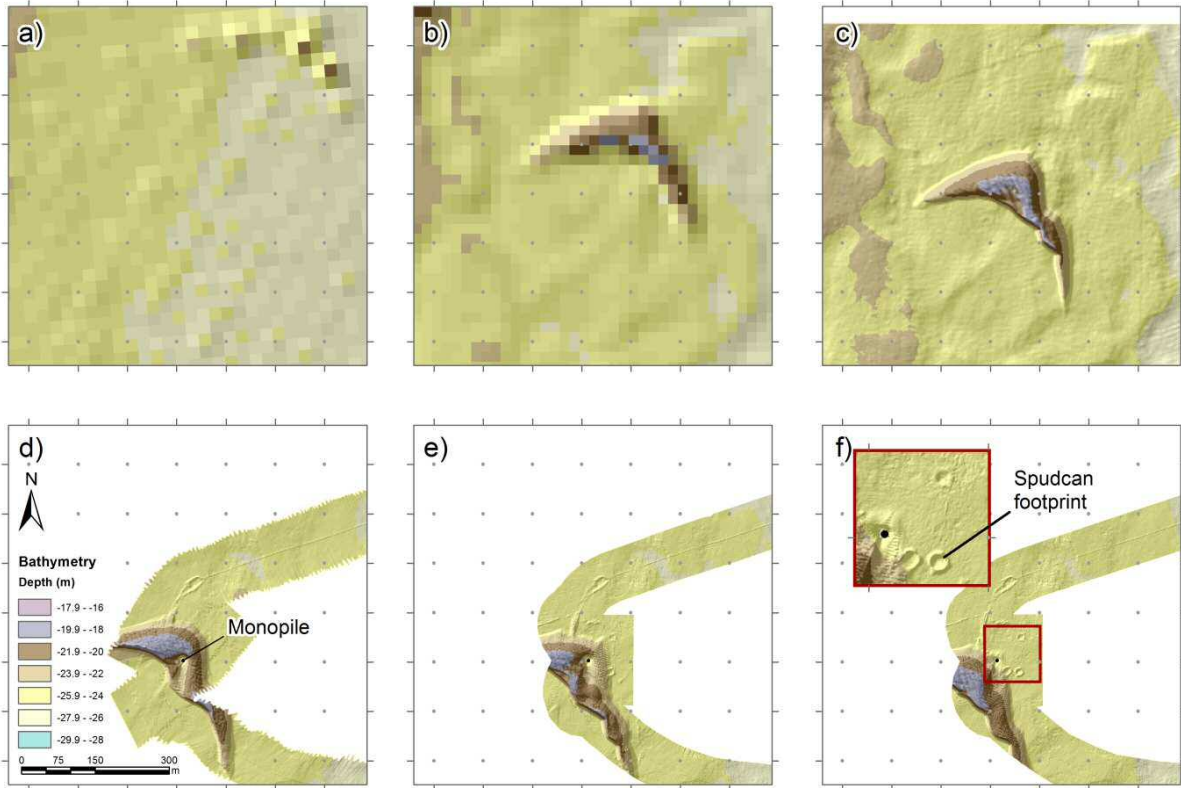


Figure 2. Panels showing the bathymetry for a) 1995, b) 2004, c) 2009, d) 2013, e) 2014 and f) 2015

### 3 RESULTS AND DISCUSSION

#### Dune morphology

Whilst barchan dunes are often found grouped with numerous other dunes (fields) the dune studied here had only two neighbouring dunes, one 1.8 km and another 3.2 km to the north-northeast.

The case study dune was moderately asymmetrical with the eastern horn being 1.4 times the width of the western horn in 2009. The dune had a width of approximately 370 m and a length of approximately 190 m. A peak in dune height, 6.9 m, was observed in 2013 when the crest dune was aligned with the monopile.

Superimposed atop the stoss slope of the dune were megaripples with a height of 0.1 – 0.3 m and a wavelength of 5 – 7 m. These were visible in the latest three surveys, though are likely still present in the earlier years and are

not visible due to lower resolutions of the surveys.

The slip face of the dune had an average slope of 30°, near the angle of repose (~32°), and hence consistent with an actively migrating bedform. In the 2015 data a 5 m long step can be seen in the slip face (Fig. 3), which similarly to the top of the dune, had bedforms superimposed.

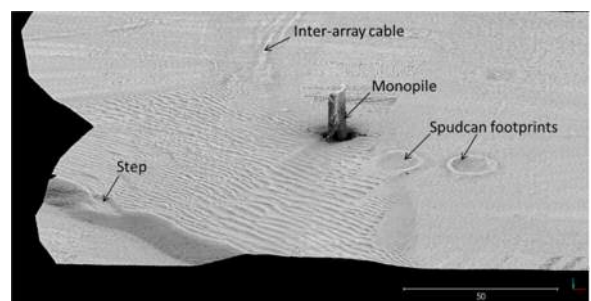


Figure 3. 2015 bathymetry with PCV hillshade. Horizontal scale is in metres.

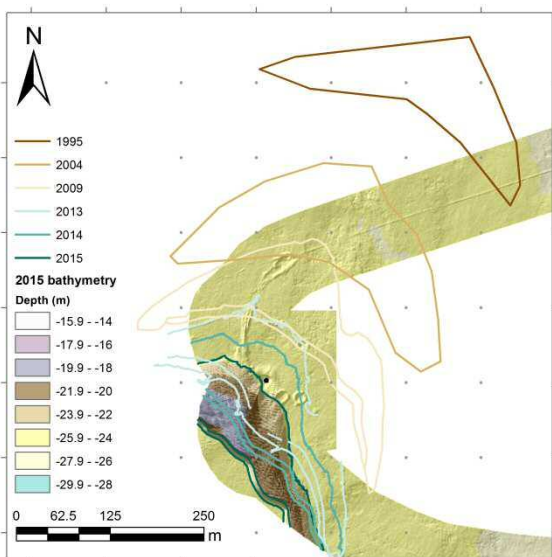


Figure 4. Outline of barchan footprint for each survey overlaid on the 2015 bathymetry.

### Dune evolution

Figure 4 shows the outline of the footprint of the dune identified from each repeat bathymetry survey overlaid on the latest, 2015, bathymetry. The dune displayed a fairly constant rate of migration towards the southwest, ranging between 20 and 25 m/yr, with the exception of 2014 to 2015 period where the toe migrated by 42 m/yr. During this period the dune migrated more towards the west-southwest.

For the 2013/2014 period considerably large waves with significant wave heights greater than 5 m approached from the south-southwest. Potentially these waves may have prevented the horns from keeping up with the rest of the dune body, causing the dune to flatten out.

From 2009 onwards the barchan dune presented a sinusoidal face, similar to that of a transverse bedform. Since this pattern is observed in 2009 it cannot be as a response to the installation of the monopile. Equally, at this point in time the eastern horn was elongated relative to the western and there was a second, smaller eastern toe. From 2009 to 2013 the eastern horn continued to break away from the main dune. This event appeared to mimic the stages leading up to a ‘calving’ event as described by Ma et al. (2014).

However, by 2014 the main western dune had caught up to re-join the eastern horn. A smaller dune will calve off a large dune’s horn

when the host barchan cannot supply enough sand. It is unknown as to why in this case the calving event did not go through to completion. This could be related to the disturbance in the flow field due to the monopile.

### Scour at the base of monopile

Scour is the process by which flow past an obstacle (in this case the monopile) is altered initiating flow acceleration and an increase in turbulent intensity, which in turn leads to the suspension and removal of sediment.

A relatively symmetrical circular scour pit had formed at the base of the pile by 2013 (three years after the installation of the monopile), although it likely formed almost immediately after the pile was installed but this time-step is missing. Whilst the local scour was relatively symmetrical, with an average extent of 6 m, the scour pit had formed a downstream wake through the barchan dune which extended to a distance of 70 m from the pile (see Fig. 2d). We note that the direction of the scour wake is to the south, oblique to the southwest-erly migration direction of the dune reflecting the direction of the residual transport as well. This shows that scour wakes around hard objects in bedform fields do not necessarily make an accurate indication for the residual transport direction. The dominant flow to the southwest interacts with the dune form, leading to flow divergence downstream of the brink of the dune (Allen, 1968) which controls the southerly scour wake direction.

Commonly the level at the base of a scour pit is compared with the ambient seabed level to give a scour depth. However, at the study location the bed level locally will have changed as the dune passed the pile. Therefore, care must be taken when choosing the level with which the base of the scour pit is compared with. If the scour level compared with the bed level at the edge of the scour pit (which aligned with the crest position in 2013) then we see much larger scour depth, reaching a maximum of 6.8 m in 2013 (Table 2). This is comparable with empirical observations which suggest a scour depth on the order of 1.3 times the pile diameter in sand (Sumer et al. 1992). This suggests that scouring through the barchan dune is similar to scouring in a flat bed of sandy sediments.

Table 2: Scour development

Year	Maximum scour pit level (mLAT)	Ambient sea-bed level (mLAT)	Bed level at edge of scour pit (mLAT)	Maximum scour depth compared with ambient level (m)	Maximum scour depth compared with edge of scour pit (m)
2013	-26.3	-24.7	-19.5	1.6	6.8
2014	-26.5	-24.7	-21.7	1.8	4.8
2015	-27.0	-24.7	-24.4	2.3	2.6

Relative to the ambient seabed the scour depth progressed at a rate comparable to neighbouring monopiles, giving a maximum scour depth of 2.3 m in 2015 (Table 2). Even from the first time-step after the installation of the monopile (2013) the level at the base of the scour pit was deeper than the ambient bed level, i.e. it had scoured the full depth of the barchan dune and then maintained scour into the underlying seabed.

On average for the four nearest monopile foundations the maximum local scour depth was 1.5 m in 2013, 1.7 m in 2014 and 2.1 m in 2015. The scour depths observed at the study site are all within 0.2 m of the average observed scour depths. This suggests that potentially the presence of the barchan dune has had a limited impact on the progress of the scour into the underlying seafloor and that the maximum scour depth is limited by the rate at which the scouring can occur, which is limited by the presence of London Clays found at a depth of 0.5 to 1 m.

#### Spudcan depressions

The monopile was installed using a jack-up rig, with four feet (spudcans), positioned to the east of the monopile location. At the time of installation of the monopile the northern most two legs of the jack-up rig would have penetrated into the dune, whilst the southern two were to the south of the dune.

Remarkably the southern two and the north-eastern spudcan depressions were still visible even after the dune had passed over them. The spudcan footprint consists of a 0.2 m deep circular depression with a 0.8 m high ring formed from the displaced material. Locally at foundations which have not been disturbed by bed-forms the depth of the spudcan footprints range between 0.5 and 1.7 m. Therefore, it is likely that the depressions at the study site have filled in by 0.3 to 1.5 m.

In 2013 the western-most spud-can depression would have had over 4 m of sand atop it. The re-appearance of a spudcan footprint in the wake of the barchan indicates that the dune does not exchange material with the seafloor and that the composition of the two sediments must be distinct. In the next section the potential source of material for the dune is explored to test this hypothesis.

#### Formation and degradation of dunes

Whilst the dune studied here is not part of a field of dunes there are two other dunes in the vicinity of the barchan: one 1.8 km to the north-northeast (partially attached to the sandbank) and another 3.2 km to the north-northeast. The dune still partially attached to the sandbank may give a clue as to the origins of the dunes. It seems plausible that dunes might calve off this bank to form solitary barchan dunes.

Geophysical surveys of the wind farm site indicate that the central sandbank is made up of a much higher proportion of sands than the material that makes up the seafloor at the study foundation. This would explain why only the barchan dune is mobile and not the veneer of more gravelly sand at the site.

Barchans are observed to lose sediment from their horns over time (Tsoar, 2001). In most cases this material is replaced by sediment lost from the horns of other upstream barchan dunes. However, it is questioned whether or not the two dunes more than 1 km away will be supplying sediment to our barchan dune. As a result it is likely that the dune will lose material with time and will ultimately degrade or rejoin the bank.

## 4 CONCLUSIONS

In this paper six repeat bathymetric surveys have been used to track and describe a singular barchan dune as it passes a wind farm monopile foundation. The impact on both the barchan dune itself and the scour at the base of the monopile have been documented.

Even before the installation of the monopile the barchan displayed signs that it was about to undergo a calving event; the eastern horn elongated and a second toe developed. However, in subsequent time-steps the barchan dune gradually reformed into a singular feature. After the slip face of the dune had passed the pile the dune face became flatter, with the western horn lagging behind the central body. The monopile appeared to have a fairly limited impact on the evolution of the dune. Instead it is theorised that the modifications of the dune's morphology result from variations in the prevailing wave regime.

Scouring at the base of the monopile progressed unhindered through the full depth of the barchan dune and into the underlying seafloor. The scour depth relative to the ambient bed level was comparable with that observed around neighbouring monopile foundations. This indicates that the presence of the barchan had a limited impact on the scouring into the seabed.

The depressions made by the jack-up rig spudcan footprints survived the passage of the barchan dune. This implies that utilising the presence of spudcan footprints to infer a benign seafloor environment through site investigations (Harris & Whitehouse, 2015), is incorrect, as here the footprints survive intact even after buried by 4 m sand.

The lack of exchange of material between the spudcan footprints and the barchan dune it is hypothesised that the barchan comprises a higher proportion of sand than the underlying seafloor. This supports the reasoning that the barchan dune has shed from the central sandbank in the wind farm site. This has implications for the longevity of both the sandbank and the barchan dune.

## 5 ACKNOWLEDGMENTS

We are grateful to the Client who provided permission to present their data and HR Wallingford for research funding.

Contains public sector information, licensed under the Open Government Licence v3.0, from the Maritime and Coastguard Agency.

## 6 REFERENCES

- Allen, J.R.L., 1968. Current Ripples. North-Holland Publishing Company.
- Berné, S., Allen, G., Auffert, J.-P., Chamley, H., Durand, J., Weber, O., 1989. Essai de synthèse sur les dunes hydrauliques géantes tidales actuelles. Bulletin de La Société Géologique de France 6, 1145–1160.
- Harris, J.M., Whitehouse, R.J.S., 2015. Marine scour : Lessons from Nature's laboratory. 201(2014), 19–31.
- Hugenholtz, C. H., Barchyn, T. E., 2012. Real barchan dune collisions and ejections. Geophysical Research Letters 39(2), 1–6. doi: 10.1029/2011GL050299.
- Ma, X., Yan, J., Fan, F., 2014. Morphology of submarine barchans and sediment transport in barchans fields off the Dongfang coast in Beibu Gulf. Geomorphology. Elsevier B.V. 213, 213–224. doi: 10.1016/j.geomorph.2014.01.010.
- Margalit, J., 2017. Development of natural seabed forms and their interaction with off shore wind farms. Technical University of Denmark.
- Parteli, E. J. R., Durán, O., Bourke, M. C., Tsoar, H., Pöschel, T., Herrmann, H., 2014.. Origins of barchan dune asymmetry: Insights from numerical simulations. Aeolian Research 12, 121–133. <https://doi.org/10.1016/j.aeolia.2013.12.002>
- Sumer, B. M., Fredsøe, J., Christiansen, N., 1992. Scour Around Vertical Pile in Waves. Journal of Waterway, Port, Coastal, and Ocean Engineering 118(1), 15–31. doi: 10.1061/(ASCE)0733-950X(1992)118:1(15).
- Tsoar, H., 2001. Types of Aeolian Sand Dunes, Geomorphological Fluid Mechanics. 403–429. doi: 10.1007/3-540-45670-8\_17.
- Worman, S. L., Murray, A. B., Littlewood, R., Andreotti, B., Claudin, P., 2013. Modeling emergent large-scale structures of barchan dune fields. Geology 41(10), 1059–1062. <https://doi.org/10.1130/G34482.1>

# Phase-related patterns of tidal sand waves and benthic organisms: field observations and idealised modelling

Johan H. Damveld *University of Twente, Enschede, NL – j.h.damveld@utwente.nl*

Pieter C. Roos *University of Twente, Enschede, NL – p.c.roos@utwente.nl*

Bas W. Borsje *University of Twente, Enschede, NL – b.w.borsje@utwente.nl*

Suzanne J. M. H. Hulscher *University of Twente, Enschede, NL – s.j.m.h.hulscher@utwente.nl*

**ABSTRACT:** Observations from the field show that the spatial distribution of benthic organisms is strongly correlated to the morphological structure of tidal sand waves. In particular the troughs of sand waves are typified by a large benthic community, in contrast to the crest. In this paper, we present an idealised process-based model to study these patterns of biota and sand waves. Our model results agree with the observations that these phase-related patterns can arise on the seabed. Moreover, we show that local topography disturbances may lead to spatial patterns of both sand waves and biomass.

## 1. INTRODUCTION

Tidal sand waves are common features which occur on the bottom of sandy coastal shelf seas, such as the North Sea. They can grow up to 25% of the local water depth, and migrate at a speed of several meters per year (van Dijk & Kleinhans, 2005). Due to these dynamic properties, they endanger offshore engineering structures, shipping lines and cables.

Moreover, coastal areas are covered by large communities of benthic organisms, living on top and within the seabed (Rabaut et al., 2007). Field observations often show a strong temporal and spatial relationship between marine bed patterns and these organisms (Baptist et al., 2006), while on the other hand, benthic organisms are able to influence hydro- and sediment dynamics. In addition, a wide range of activities in coastal seas (e.g., the ones mentioned above) put an increasing pressure on the long-term stability of the marine ecosystem.

For the planning and execution of offshore engineering projects, knowledge of the distribution of these organisms over sand waves is of great importance. Predictions about the spatial

response of benthic habitats to interventions can have considerable consequences regarding the time needed to process new licences for these offshore projects.

The combination of morphodynamic modelling and field surveys can increase our understanding of the governing processes responsible for the spatiotemporal patterns of benthos over sand waves. In this paper we first present an overview of field studies which analysed spatial patterns of biotic as well as abiotic parameters in the marine environment. Second, we use an idealised two-way coupled biogeomorphological model to study the observed phase-related patterns by means of a linear stability analysis.

## 2. FIELD OBSERVATIONS

The seabed of coastal areas harbours a rich ecosystem, and the benthic organisms living here show a great variety in both space and time (Widdows & Binsley, 2002). These patterns are usually related to the presence of marine bed forms of various dimensions.

For large-scale tidal ridges, van Dijk et al. (2012) reported that the benthic community structure in the troughs was much richer and much denser than on the crests. Small-scale

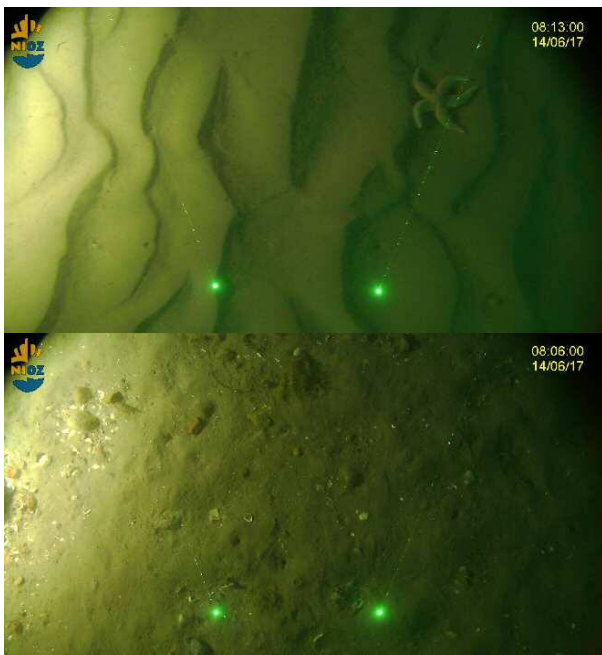


Figure 1. Typical seabed structure within a sand wave area, displaying the crest (top) and trough (bottom). The green dots represent a horizontal distance of 30 cm. Pictures from Damveld et al. (2018b)

bedforms, such as megaripples, are shown to drive the distribution of benthos as well (van der Wal et al., 2017).

Also for sand waves (meso-scale bedforms) a clear relation has been established between the occurrence of benthic organisms and the morphological structure of the bedforms. Baptist et al. (2006) looked into seasonal spatial variations and found evidence that endobenthic organisms occur in higher densities in sand wave troughs. Moreover, using a video system, Damveld et al. (2018a) found that the number of both epi- and endobenthic organisms are significantly higher in sand wave troughs, compared to the crests (see Figure 1).

Apart from directly monitoring the distribution of benthic organisms, it is also possible to look into other parameters. It is widely known that various abiotic parameters (e.g. sediment type and size, silt content and permeability) are strongly related to the habitat structure of benthos (Reis et al., 2010). Several studies analysed the distribution of grain sizes over sand waves and both a coarsening and a fining of the crests were reported (van Oyen et al., 2013, and references therein). In addition to these abiotic variations in crest/trough, also abiotic patterns

have been found on a smaller spatial scale. Cheng et al. (2018) reported that silt content is higher in both the troughs and on the lee side slope of (strongly asymmetrical) sand waves, compared to the crests and stoss slope. Due to the expected spatial correlation between these abiotic variables and the benthos, it follows that benthic habitats are also related to the spatial structure of sand waves.

### 3. METHODOLOGY

#### a. Stability methods

To study the evolution of bed and benthic organisms we follow a linear stability approach, which is often used to study morphodynamic rhythmic patterns (Dodd et al., 2003). This method assesses the response of small-amplitude perturbations to a so-called basic state (i.e. a flat bed in morphodynamics). The typical result is a range of modes which show either exponential growth or decay. The mode with the largest positive growth rate is considered the fastest growing mode. The corresponding wavelength, orientation, migration and growth rate are assumed to be the properties occurring in the field.

Using this method, Hulscher (1996) explained the process leading to the formation of sand waves. The interaction of the oscillatory tidal flow with small disturbances on the seabed gives rise to steady recirculation cells in the water column. The direction of these cells near the bed is directed towards the crests of the perturbations, resulting in a net sediment displacement in the same direction. In contrast, gravity favours a downward sediment transport, such that the balance between these two forces eventually leads to either growth or decay of the perturbation.

Various model studies have extended this approach in order to determine the effect of a wide range of physical processes on the initial formation of sand waves. These processes are, for instance, migration due to tidal asymmetry (Besio et al., 2004), sediment sorting (van Oyen & Blondeaux, 2009) and biological activity (Borsje et al., 2009).

Also the formation of biological spatial patterns can be explained using stability analysis. For a fluvial environment, Bärenbold et al. (2016) showed that the interaction between riverbed vegetation and hydrodynamics leads to the emergence of riverine bar patterns.

## b. The biogeomorphological model

Building upon the methodology described above, we present an idealised, process-based model, in which hydro- and sediment dynamics are described by the 2DV Navier-Stokes equations, flow and sediment continuity equations and are supplemented with appropriate boundary conditions. The evolution of the bed  $h$  is governed by the Exner equation, which reads

$$\frac{\partial h}{\partial t} = -\frac{1}{(1-p)} \frac{\partial q(\phi)}{\partial x}. \quad (1)$$

Here,  $p$  is the bed porosity and  $q$  is the sediment transport rate.

Next, the evolution of benthic organisms (represented by the biomass  $\phi$ ) is described by logistic growth, according to

$$\frac{\partial \phi}{\partial t} = \alpha_g \phi (\phi_{eq}(\tau) - \phi), \quad (2)$$

with  $\alpha_g$  as the logistic growth rate and  $\phi_{eq}$  as the biological carrying capacity (equilibrium biomass) which depends on the local shear stress  $\tau$ .

Moreover, the sediment transport depends, amongst other parameters, on the biomass ( $q(\phi)$ , see eq. 1). It turns out that both evolutionary equations are two-way coupled. As a consequence, the problem can be written as the following linear eigenvalue problem

$$\frac{\partial}{\partial t} \begin{bmatrix} \tilde{h} \\ \tilde{\phi} \end{bmatrix} = \Gamma(t) \begin{bmatrix} \tilde{h} \\ \tilde{\phi} \end{bmatrix}, \quad (3)$$

where the breve  $\tilde{\cdot}$  denotes the perturbation amplitude. The complex growth rate of the perturbations  $\Gamma(t) = \Gamma_r(t) + i\Gamma_i(t)$  is a function of flow, sediment and biological parameters. The real part  $\Gamma_r$  describes the exponential growth of the perturbations, whereas the imaginary part  $\Gamma_i$  is related to the migration.

An important property of this methodology is that this problem leads to two distinct eigenvalues ( $\Gamma_1$  &  $\Gamma_2$ ). The actual perturbation amplitudes are thus a superposition of two

eigenmodes, each displaying its own growth and migration. For further details, we refer the reader to Damveld et al. (submitted).

In next section, we study the evolution of bed and biomass by imposing random perturbations to the flat bed, while keeping the biomass spatially uniform. Furthermore, the system is asymmetrically forced by a combination of the M2 tide and an M0 residual current (0.05 m / s).

## 4. RESULTS

We present our results in Figure 2, where each panel describes the temporal evolution of the topography and biomass profile. In (a) we define the initial state, where the bed profile displays a random pattern. The biomass has a spatially uniform value of  $\phi = 0.1$  kg / m. Other than the basic bed, the basic biomass evolves autonomously due to logistic growth. This is best visible in (a, b and c), where  $\phi$  uniformly increases over time, independent of the perturbations.

When looking at the bed development, it can be seen that, initially, the perturbations with shorter wavelengths decay. After this, the modes that display growth evolve into a bed pattern with wavelengths in the range of hundreds of meters, corresponding to sand wave wavelengths in the field.

It stands out that, independent of the autonomous benthic growth, spatial patterns for the biomass develop as well. Moreover, the phase of these patterns is the opposite of that of the bed. More specific, the biomass crests are concentrated on the lee side slope of the sand wave troughs. Other results, which are not shown here, show that the residual current strength is responsible for this phase shift. In case of a symmetrical tidal forcing, the phase difference is exactly 180°, whereas for an increasing residual current strength, this phase difference decreases towards 90°. However, as residual currents in the field are often on the order of the presented values here, it is to be expected that the phase differences are somewhere in between.

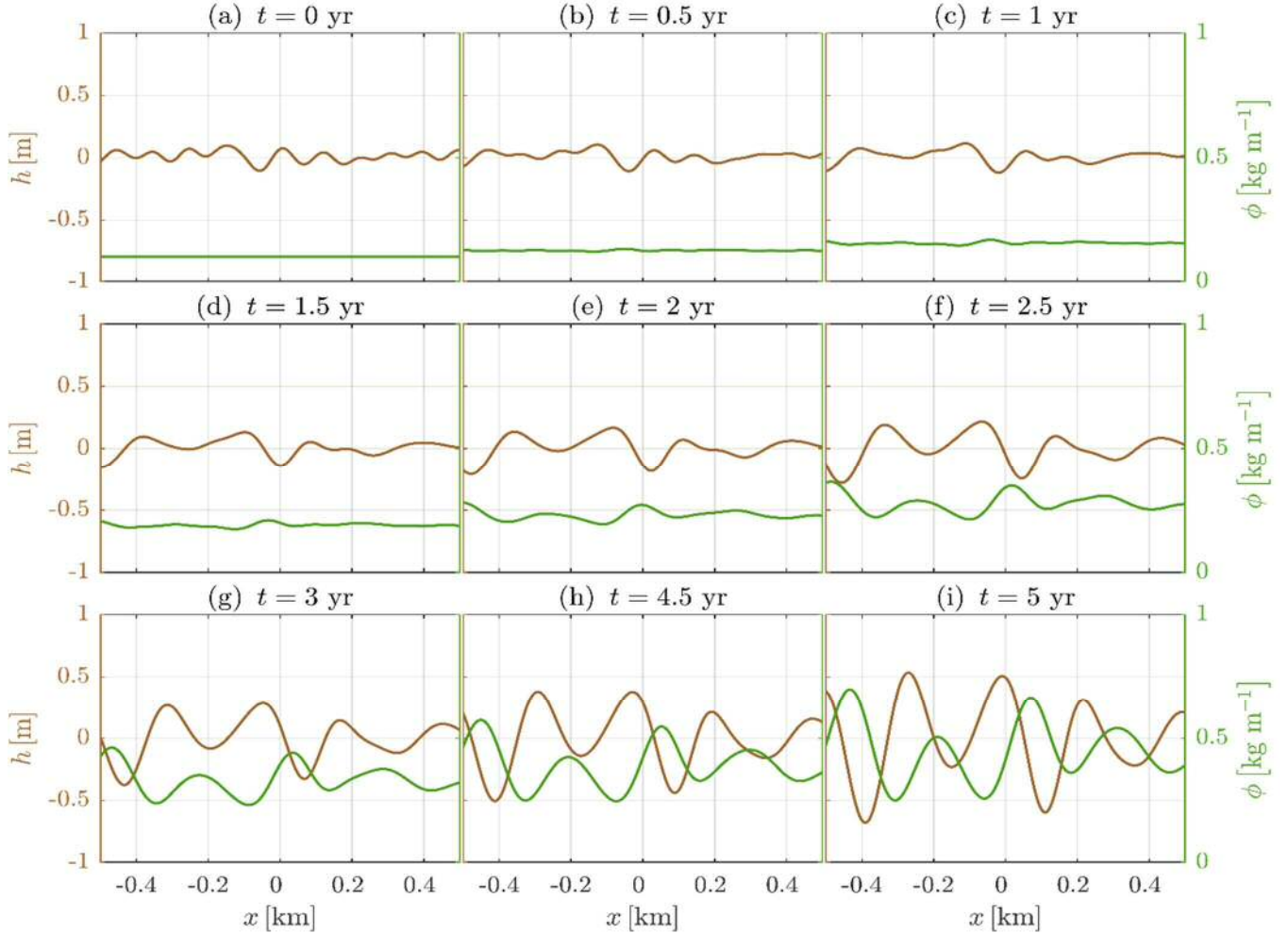


Figure 2. Topography (brown line) and biomass (green line) evolution, where each panel indicates a time step of 0.5 yr. The initial bed (a) is perturbed with a random signal, whereas the initial biomass has a spatially uniform value of  $\phi = 0.1 \text{ kg} / \text{m}^2$ .

## 5. CONCLUSIONS

In this paper we summarise observed spatial patterns of both benthic organisms and other abiotic parameters over marine bed forms, in particular over sand waves. These field surveys show a clear distinction in habitat characteristics between troughs and crests of sandwaves, while even variations on an even smaller spatial scale (slopes) have been observed.

With the biogeomorphological model presented here we are able to simulate these observed patterns. Based on the results from the model we expect overall higher biomass in the troughs of the sand waves. In addition, the lee side of the sand waves is likely to harbour a higher biomass compared to the stoss side.

Although we can successfully model the two-way interactions between sand waves and

benthic organisms, more detailed information is needed on the exact species distribution over sand waves. Current knowledge is still scarce, and mainly focusses on top/trough differences. Moreover, the implemented biological parameterisations are still strongly idealised. Nevertheless, this methodology allows us to predict the spatial distribution of benthic organisms over sand waves, valuable information from both an engineering and ecological perspective.

## 6. ACKNOWLEDGEMENTS

The authors greatly acknowledge the financial support of this research from NWO, Royal Boskalis Westminster N.V. and NIOZ.

## 7. REFERENCES

- Baptist, M.J., van Dalsen, J., Weber, A., Passchier, S., van Heteren, S. (2006). The distribution of macrozoobenthos in the southern North Sea in relation to meso-scale bedforms. *Estuarine Coastal and Shelf Science*, 68(3-4), 538-546. doi:10.1016/j.ecss.2006.02.023
- Bärenbold, F., Crouzy, B., Perona, P. (2016). Stability analysis of ecomorphodynamic equations. *Water Resources Research*, 52(2), 1070-1088. doi:10.1002/2015wr017492
- Besio, G., Blondeaux, P., Brocchini, M., Vittori, G. (2004). On the modeling of sand wave migration. *Journal of Geophysical Research*, 109(C4). doi:10.1029/2002jc001622
- Borsje, B.W., de Vries, M.B., Bouma, T.J., Besio, G., Hulscher, S.J.M.H., Herman, P.M.J. (2009). Modeling bio-geomorphological influences for offshore sandwaves. *Continental Shelf Research*, 29(9), 1289-1301. doi:10.1016/j.csr.2009.02.008
- Cheng, C.H., Soetaert, K., & Borsje, B.W. (2018). Small-scale variations in sediment characteristics over the different morphological units of tidal sand waves offshore of Texel. Paper presented at the NCK Days 2018, Haarlem.
- Damveld, J.H., van der Reijden, K.J., Cheng, C., Koop, L., Haaksma, L.R., Walsh, C.A.J., Soetaert, K., Borsje, B.W., Govers, L.L., Roos, P.C., Olff, H., Hulscher, S.J.M.H. (2018a). Video Transects Reveal That Tidal Sand Waves Affect the Spatial Distribution of Benthic Organisms and Sand Ripples. *Geophysical Res. Letters*. doi:10.1029/2018gl079858
- Damveld, J.H., van der Reijden, K.J., Cheng, C., Koop, L., Haaksma, L.R., Walsh, C.A.J., Soetaert, K., Borsje, B.W., Govers, L.L., Roos, P.C., Olff, H., Hulscher, S.J.M.H. (2018b), "Replication Data for: Video transects reveal that tidal sand waves affect the spatial distribution of benthic organisms and sand ripples", hdl:10411/4OARYB, DataverseNL, V1
- Damveld, J. H., Roos, P. C., Borsje, B. W., Hulscher, S. J. M. H. (submitted). Modelling the two-way coupling of tidal sand waves and benthic organisms A linear stability approach.
- Dodd, N., Blondeaux, P., Calvete, D., De Swart, H.E., Falques, A., Hulscher, S.J.M.H., Rozynski, G., Vittori, G. (2003). Understanding coastal morphodynamics using stability methods. *Journal of coastal research*, 19(4), 849-866.
- Hulscher, S.J.M.H. (1996). Tidal-induced large-scale regular bed form patterns in a three-dimensional shallow water model. *Journal of Geophysical Research: Oceans*, 101(C9), 20727-20744. doi:10.1029/96jc01662
- Rabaut, M., Guilini, K., Van Hoey, G., Vincx, M., Degraer, S. (2007). A bio-engineered soft-bottom environment: The impact of Lanice conchilega on the benthic species-specific densities and community structure. *Estuarine, Coastal and Shelf Science*, 75(4), 525-536. doi:10.1016/j.ecss.2007.05.041
- Reiss, H., Degraer, S., Duineveld, G.C.A., Kröncke, I., Aldridge, J., Craeymeersch, J., Eggleton, J.D., Hillewaert, H., Lavaleye, M.S.S., Moll, A., Pohlmann, T., Rachor, E., Robertson, M., vanden Berghe, E., van Hoey, G., and Rees, H.L. (2010). Spatial patterns of infauna, epifauna, and demersal fish communities in the North Sea. *ICES Journal of Marine Science*, 67(2), 278-293. doi:10.1093/icesjms/fsp253
- van Dijk, T.A.G.P., Kleinhans, M.G. (2005). Processes controlling the dynamics of compound sand waves in the North Sea, Netherlands. *Journal of Geophysical Research: Earth Surface*, 110(F4). doi:10.1029/2004JF000173
- van der Wal, D., Ysebaert, T., Herman, P.M.J. (2017). Response of intertidal benthic macrofauna to migrating megaripples and hydrodynamics. *Marine Ecology Progress Series*, 585, 17-30. doi:10.3354/meps12374
- van Oyen, T., Blondeaux, P. (2009). Tidal sand wave formation: Influence of graded suspended sediment transport. *Journal of Geophysical Research: Oceans*, 114(C7). doi:10.1029/2008JC005136
- van Oyen, T., Blondeaux, P., van den Eynde, D. (2013). Sediment sorting along tidal sand waves: A comparison between field observations and theoretical predictions. *Continental Shelf Research*, 63, 23-33. doi:10.1016/j.csr.2013.04.005
- Widdows, J., Brinsley, M. (2002). Impact of biotic and abiotic processes on sediment dynamics and the consequences to the structure and functioning of the intertidal zone. *Journal of Sea Research*, 48(2), 143-156. doi:10.1016/S1385-1101(02)00148-X



# Osculatory surfaces applied to systematic errors estimation in repeated MBES surveys

N. Debese *ENSTA Bretagne, Brest, France* – *nathalie.debese@ensta-bretagne.fr*

J. J. Jacq *Mines-Telecom Institute / IMT-Atlantique, Brest, France* – *jj.jacq@imt-atlantique.fr*

K. Degrendele *Federal Public Service Economy, SMEs, Self-employed and Energy – Continental Shelf Service, Brussel, Belgium* – *koen.degrendele@economie.fgov.be*

M. Roche *Federal Public Service Economy, SMEs, Self-employed and Energy – Continental Shelf Service, Brussel, Belgium* – *marc.roche@economie.fgov.be*

**ABSTRACT:** In the Belgium part of the North Sea, regular multibeam echosounder (MBES) surveys are carried out on reference areas to control the environmental impact of the sand extraction. The volume of sand extracted can be estimated from Electronic Monitoring System (EMS) installed aboard the dredging vessels. The correction of potential systematic errors affecting the MBES bathymetric measurements is a prerequisite for precisely analyzing the correlation between EMS and MBES volume. This paper presents a new approach, based on osculatory surfaces, to estimate and correct the bathymetric data from these potential biases. Osculatory surfaces are smooth virtual surfaces giving access to the envelop surface of the sandbank. Systematic errors are estimated by taken into account the morphological impact of the suction hopper dredgers and assuming a bathy-morphology stability of the sandbank on a decadal scale. Once applied to MBES bathymetric data, the volumes of sand extracted estimated from EMS data are in very high accordance with those deduced from MBES survey.

## 1. INTRODUCTION

The Continental Shelf Service of the FPS Economy, SMEs, self-employed and Energy (Belgium) is in charge of the management and control of the sand extraction within the Belgian part of the North Sea. To this end, monitoring areas defined where the extraction is concentrated are regularly surveyed with a multibeam echosounder (MBES - RV *Belgica* EM3002D 300kHz) to evaluate the impact of dredging on the seabed bathymetry, morphology and habitat on a local scale. In each monitoring area, variations in sediment volumes as a function of time are derived from the bathymetric time series composed of the Digital Bathymetric Models (DBM) derived from MBES surveys.

The dredging activity itself is controlled by an Electronic Monitoring System (EMS - informally called “black-boxes”) installed aboard each dredging vessel. The EMS records both the vessel position and pump activity at a frequency rate of one record per 30s, allowing an estimation of the extracted volume over any monitoring area for any

time interval assuming that dredging vessels are always using their maximum capacity (Roche et al., 2017 and Van den Branden et al., 2017).

The correlation between MBES and EMS data has been analyzed with different approaches and at different spatial resolution (Roche et al., 2011 and 2017 and Terseleer et al., 2016). At the local spatial scale of the monitoring areas the volume variation measured by MBES is strongly correlated with the volume variation estimated from the EMS data, implying that most of the bathymetric variation is explained by the extraction itself. With respect to this high average correlation, the residuals are of the same decimetric order of magnitude as the uncertainty associated with the RV *Belgica* EM3002D bathymetric measurements which meet IHO S44 Special Order (IHO, 2008). On the other side, the strong concordance between the volumes derived from the EMS data and the volumes officially declared by the dredging companies suggest, on a first approach, that a negligible bias can be considered for the volume estimation derived from the EMS data.

To clarify the respective importance of the extraction and the sediment-dune dynamics in the overall volume variation estimated from the bathymetric time-series, it is necessary to correct as much as possible the systematic errors affecting the MBES bathymetric measurements. Through a case study, this contribution proposes an original approach to correct these systematic errors which are independent from one survey to another.

Section 2 describes the dataset used. Section 3 presents a number of preliminary considerations. Section 4 gives an operational description of osculatory surfaces applied to systematic errors estimation.

## 2. DATASET DESCRIPTION

The Oosthinder bank is localized in the north of the Belgian part of the North Sea and is part of a group of elongated parallel sandbanks known as the Hinderbanken. Our study area, the monitoring area HBMC is located on the Oosthinder bank, within the extraction area 4c from which is extracted each spring since 2012, a large volume of sand for the beach maintenance.

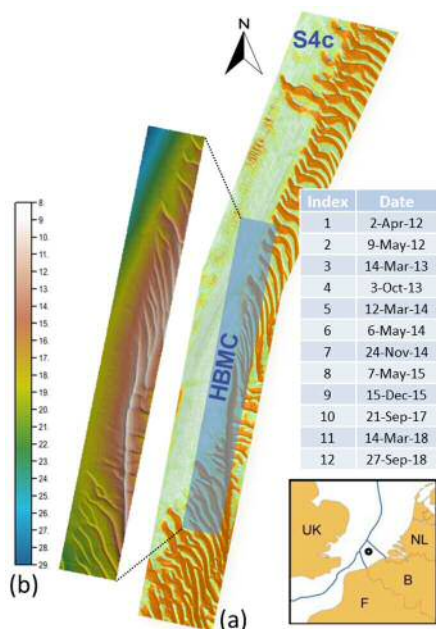


Figure 1. (a) Location of HBMC monitoring area and RV *Belgica* EM3002D MBES survey dates; (b) DBM#1

The evolution of the bathymetry based on the MBES survey data, is due to: (1) short periods of intense extraction, visible by large trailing suction hopper dredgers marks along and across the sandbank; (2) natural sediment transport processes, resulting in changes in shape and migration of very large dunes (*sensu* Ashley 1990) superimposed on the bank.

## 3. PRELIMINARY CONSIDERATIONS

A complex mechanism of maintenance of the tidal sandbanks related to the hydrodynamic and sediment transport regimes is mentioned by many authors (De Moor, 1984, Berné et al., 1998, Dyer & Huntley, 1999). The displacement of linear offshore banks is extremely variable from one bank group to another (see Kenyon and Cooper, 2005) and some tidal banks show stability phases alternating with dynamic phases (Van Cauwenberghe, 1971). The bathymetric profiles along perpendicular lines (old “DECCA” lines) to the Oosthinder using the available surveys from 2004 to 2014 allow an estimation of the overall sandbank variation in vertical and horizontal direction on a decadal scale. The bathymetric profiles are displayed in Figure 2. Locally, the profiles on the north and south flanks of the sandbank in areas without large dune pattern and where extraction is negligible show variations of about ten meters in the horizontal direction. In the vertical plan, fluctuations of about twenty centimeters are observed, the latter being in the order of magnitude of the uncertainty associated with the MBES bathymetric measurements. But no significant trend is present: these variations, both in the vertical plane and in the horizontal plane, do not follow any drift as a function of time. From 2004 to 2014, in the investigated area, the Oosthinder bank is stable: oscillating randomly around a mean position.

The volume changes induced by natural net influx will then be considered as being negligible compared to those induced by anthropogenic activities. In this context,

estimating the volume variation on HBMC only requires the change in overall mean depth of the area, or equivalently, the thickness variation computed over the HBMC area.

In HBMC monitoring area, EMS data show that the volume of sand extracted between two successive MBES surveys brought to the surface of the area can amount to 20 cm. Accordingly, MBES soundings depth uncertainty should be at least one order of magnitude less to achieve the initial objective. Hence a technique to eliminate the systematic errors that contribute to this uncertainty is required. To obtain this, robust techniques are proposed to adjust the global depths of the DBM, using the first survey as a reference. In this manner, at the spatial scale of the HBMC area, systematic errors affecting MBES data will be a posteriori compensated.

The dune migration and the sand extraction greatly complicate the registration of DBM's since they reduce the redundant information between DBM's. The technique we propose aims to restore the missing information by using an intermediate surface, referred as bottom-osculatory surface. Such a surface allows to virtually remove the dunes superimposed on the sandbank.

The osculatory surface that surrounds the sandbank tangentially at the base – toe of the dunes represents a hypothetic boundary between a dynamic upper part shaped by the mobile dunes and a stable internal part. Given the stability of the Oosthinder Bank in the HBMC area, this concept of an osculatory surface separating vertically the bank in a dynamic part, where the sand is mobile, of a stable part takes here all its meaning.

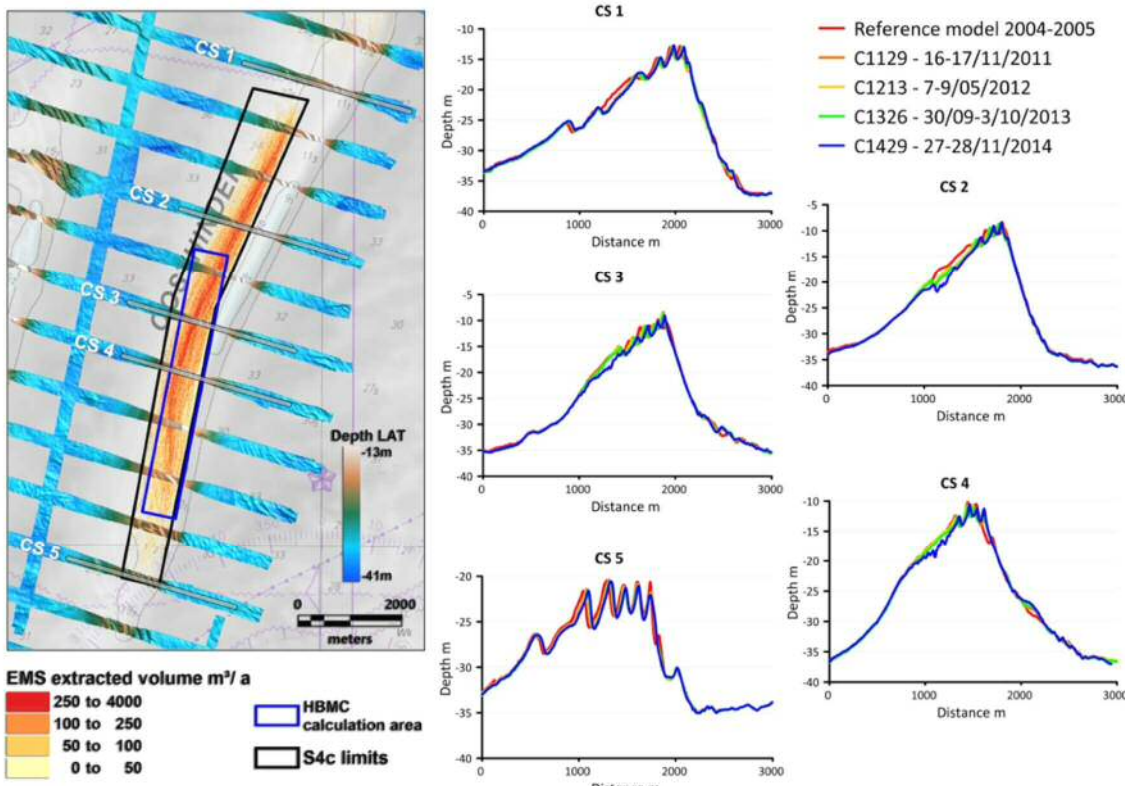


Figure 2. Bathymetric profiles on S4c Extraction Sector across the Oosthinder bank (crossection: average value calculated on a corridor of 25 m on both sides of the central position of the profile).

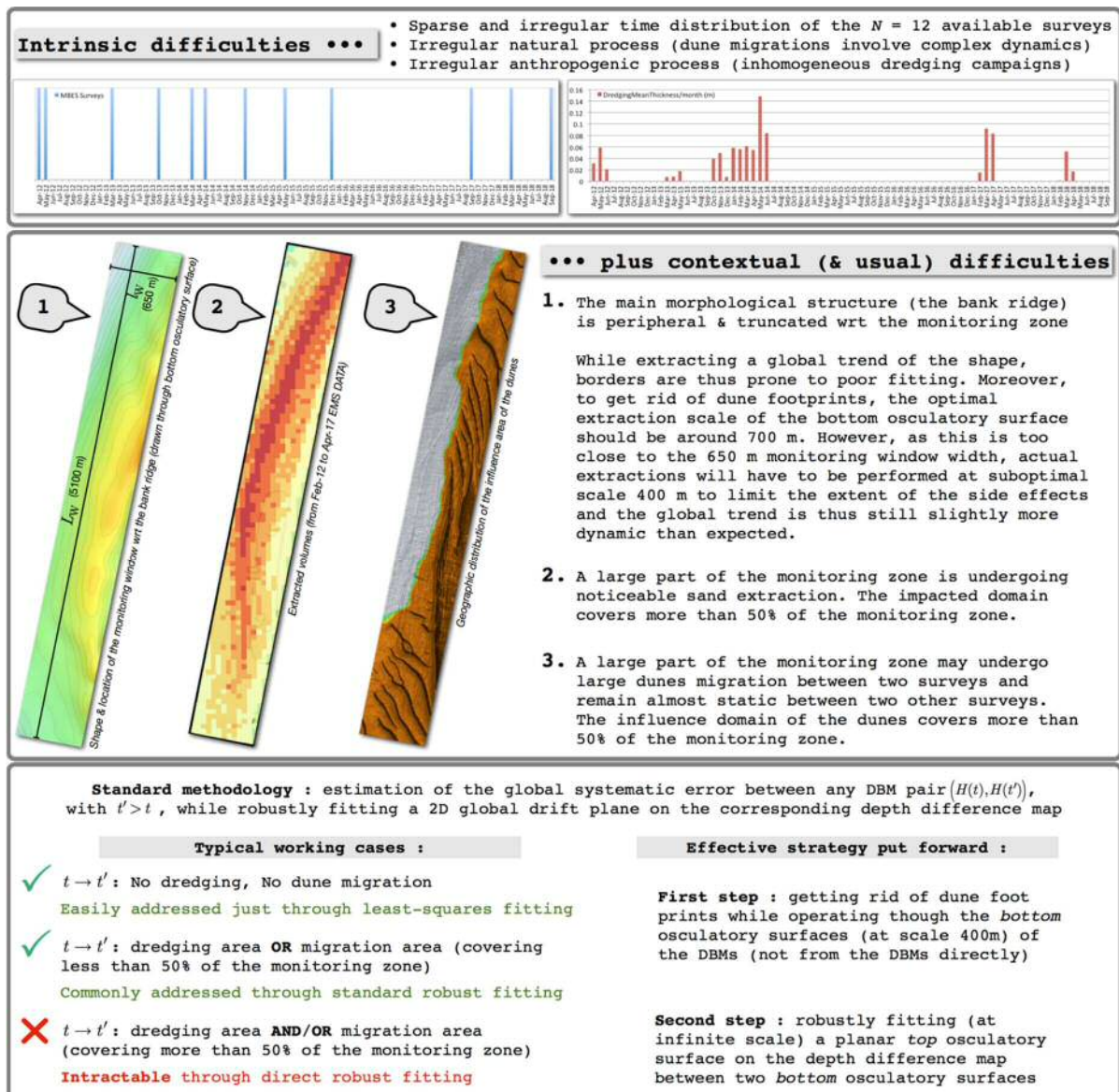


Figure 3. Actual challenges w.r.t. robust estimation of MBES systematic errors and corresponding strategy

#### 4. OSCULATORY SURFACES

Osculatory surfaces are robust trend surfaces derived from DBM. The methodology aiming at deriving osculatory surfaces from DBM is fully described in Debese et al. (2018b). This shape transform operates through only two non-optional parameters: its scale length  $\lambda$  and the corresponding degree of the local representations.

Extracting HBMC osculatory surface is a challenging task. As displayed in Figure 1, HBMC area is a narrow strip of seabed, which only partially covers the sandbank.

This makes it difficult to define the entire shape of the bank and avoid edge effects. Very large dunes located in HBMC area are highly dynamic. The volume of sand involved in the dynamics is estimated to 1.8 million of meter cube. The very large dunes migrate at a speed of 30 m per year in the South west of more than 1 m locally from April 2012 to September 2018.

Besides the better understanding of sand bedform dynamics this technique provides, the osculatory surfaces are useful for the detection and quantification of systematic errors in bathymetric time series.

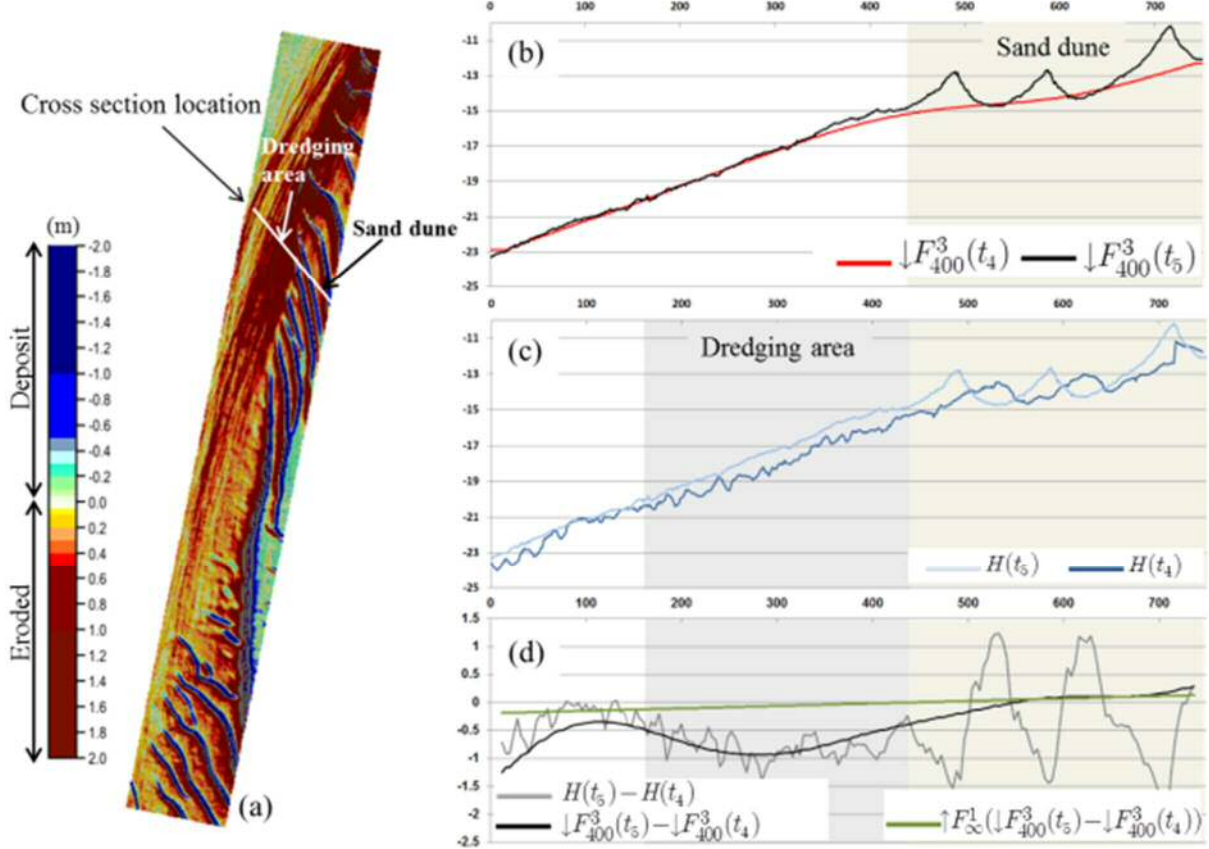


Figure 4. (a) DTM of differences (DoD) between DBM#5 and DBM#4 and location of the cross section; (b) Bathymetric and osculatory resulting profiles for the survey#4; (c) DBM#4 and DBM#5 cross sections; (d) Cross sections in DoD between DBM#5 and DBM#4 and in DoD between their corresponding osculatory surfaces.

Figure 3 attempts to intuitively highlight both the actual data limitations and the methodological choices made to work around them while aiming at robustly tracking the volume variation of the remaining sand resource over time. The corresponding key operational step addresses the extraction of the set of bottom osculatory surfaces built from the DBMs ( $4 \times 4$  m) issued from the 12 MBES surveys  $H(t_1), \dots, H(t_N)$  currently available. As they get rid of the dune structures, the former are expected to deliver a reasonably stable shape with respect to the non-anthropogenic processes insofar as their common extraction scale is carefully chosen (Debese et al., 2018b). This study makes use of the bottom osculatory model  $\downarrow F_{400}^3(H(t))$  – that is, operating through an extraction scale set to 400 m and with local 2D models of degree 3 (Figure 4b). The key hypothesis made in this work expects that the distribution of the remaining differences between a pair of bottom osculatory surfaces

$(\downarrow F_{400}^3(t), \downarrow F_{400}^3(t'))$ , should then mostly result from potential systematic errors and/or possible dredging campaigns. The global systematic error component is extracted through a top osculatory planar global model  $\uparrow F_\infty^1(\downarrow F_{400}^3(t') - \downarrow F_{400}^3(t))$  fitted on the bottom osculatory difference map (Figure 4d). This robust trend extractor is expected to be immune against outliers patches resulting from dredging erosion since these patches are always concavities within the difference map. A scalar indicator  $\delta(t, t')$  of the apparent volume change from  $t$  to  $t'$  (or its equivalent thickness upon divided by the area of the monitoring zone) due to systematic errors is then just built as the mean value of the map  $\uparrow F_\infty^1(\downarrow F_{400}^3(t') - \downarrow F_{400}^3(t))$ .

Using this generic approach, preliminary results were already published in (Debese et al., 2018a). However, since the volume corrections were computed from the  $N-1$  first-order indicators  $\delta(t, t+1)$  only, these results were still prone to large estimation drifts

along time. Indeed, although the bias operator  $\delta(t, t')$  is expected to be robust w.r.t. the comparison of two successive surveys, its linear concatenation  $\Delta(t_1, t_N) = \sum_{i=1}^{N-1} \delta(t_i, t_{i+1})$  over the time sequence does not provide the global robustness required to address the whole sequence of surveys, as displayed in Figure 5a by the dotted curve.

To this end, this paper proposes to explicitly pre-compute the whole set of indicators  $\delta(t, t')$ , with  $t' > t$ , i.e., getting  $N(N-1)/2$  independent estimations. An estimation  $\Delta(t_1, t_N)$  is then got as the weighted average of its  $2^{N-2}$  possible cumulative evaluations, each summation result depending on the directed graph path (without loops) currently chosen between  $t_1$  and  $t_N$  – the shortest and longest corresponding graph lengths between  $t_1$  and  $t_N$  being 1 and  $N-1$ , respectively. The weight of an estimation is taken as the inverse of its corresponding graph path length.

HBMC osculatory surfaces were extracted using a polynomial degree of three by setting to 400 m. As displayed in Figure 4a, this pair of parameters fully assimilates the ridge of the bank.

The temporal evolution of the volume changes estimated from MBES and EMS data are displayed on Figure 5. The black curve represents the volume changes estimated from EMS data while the red one represents the volume changes deduced from the bathymetric models issued from MBES surveys. The green curve represents the volume changes deduced from MBES bathymetric data after removal of the residual bias estimated through this global approach.

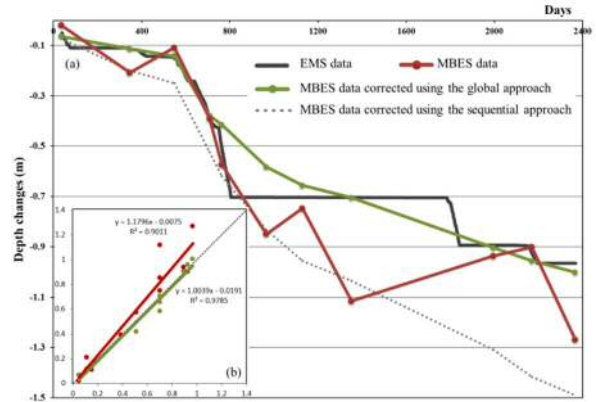


Figure 5. (a) The temporal evolution of the MBES-based volume changes measurements w.r.t. their predictions issued from the EMS system database – the time origin is the date of the first survey; (b) Linear regression applied to the differences of the depth changes between EMS and each of the MBES datasets (raw and corrected).

## 5. CONCLUSIONS

A method is proposed to correct residual bias associated with bathymetric models derived from MBES data. The correction process makes use of a top osculatory planar model fitted on a bottom osculatory difference map. A robust estimation of these biases is achieved through a global approach.

This method applied to the HBMC monitoring area located on the Oosthinder bank where sand is extracted since 2012, significantly improves the estimation of the volume variation w.r.t. time.

The correlation between the volumes measured by MBES and corrected with the volumes estimated from EMS data is very significant (Pearson's  $r^2 = 0.99$ ). In the HBMC zone, sand extraction explains 99% of the variation of bathymetry during the period considered.

This contribution, which is rather hydrographic in nature, uses advanced morphometric techniques to correct the intrinsic errors associated with MBES bathymetric data. It is a first step in a long-term project whose ultimate objective is to accurately and reliably quantify in routine the sand volumes involved in the sandbanks dynamics and to make a link between the sand volume in-

volved in the dune dynamics and the hydrodynamic regime. This method will be applied soon to all MBES data acquired as part of the monitoring of sand extraction in the Belgian part of the North Sea.

## 7 REFERENCES

- Ashley, G.M. 1990. Classification of large-scale subaqueous bedforms: a new look at an old problem. *Journal of Sedimentary Petrology*, 60, 1: 160-172.
- Berné, S., Lericolais, G., Marsset, T., Bourillet, J.-F. and De Batist, M., 1998. Erosional offshore sand ridges and lowstand shorefaces: Examples from tide- and wave-dominated environments of France. *Journal of Sedimentary Research*, 68(4): 540-555.
- Debese, N., Jacq, J.J., Degrendele, K., Roche, M., 2018a. "Toward Reliable Volumetric Monitoring of Sandbanks", In *Proc. of the 5th International Conference of the Int. Society for Geomorphometry*, Aug. 13-17, 2018, Boulder, USA.
- Debese, N., Jacq, J.J., Degrendele, K., Roche, M., Garlan, T., 2018b. "Osculatory Surfaces Extraction applied to Monitoring of Submarine Sand Materials", *Marine Geodesy*, doi:10.1080/01490419.2018.1509161.
- De Moor, G., 1984. Morfodynamiek en sedimentodynamiek rond de Kwintebank. Brussel, Ministerie Economische Zaken, Vol. I, II, III, IV, V ; 219, 71, 65, 39, 36 p.
- International Hydrographic Organization, 2008. Special Publication No. S-44, "IHO Standards for Hydrographic Surveys", 5th Ed., Monaco.
- Kenyon, N.H. and Cooper, B., 2005. Sand banks, sand transport and offshore wind farms. Technical Report. ABP Marine Environmental Research Ltd (ABPmer). pp 106.
- Roche, M., Degrendele, K., De Mol, L., Schotte, P., Vandenreyken, H., Van Den Branden, R. and De Schepper, G., 2011. Synthesis of the monitoring of the impact from the aggregate extraction on the Belgian Continental Shelf. Brussels: Marine aggregate extraction: needs, guidelines and future prospects. Belgian FPS Economy – Study day 5 October 2017 : 5-37
- Roche M., Degrendele K., Vandenreyken H., Schotte, P., 2017. Multi time and space scale monitoring of the sand extraction and its impact on the seabed by coupling EMS data and MBES measurements. Belgian marine sand: a scarce resource? Belgian FPS Economy – Study day 7 June 2017: 5-37 [http://economie.fgov.be/fr/binaries/Articles-study-day-2017\\_tcm326-283850.pdf](http://economie.fgov.be/fr/binaries/Articles-study-day-2017_tcm326-283850.pdf)
- Terseleer, N., Roche, M., Degrendele, K., Van den Eynde, D., Van Lancker, V.R.M., 2016. ICES Annual Science Conference, Theme session K: Make marine sediment extraction sustainable by mitigation of related processes, CM 2016/K:617.
- Van Cauwenbergh, C., 1971. Hydrografische analyse van de Vlaamse banken langs de Belgisch-Franse kust. *Ingenieurstijdingen*, 4, 141-149.
- Van den Branden, R., G. DeSchepper, and L. Naudts (this volume). The Electronic Monitoring System (EMS) as a minimum requirement for monitoring the extraction of an increasingly scarce raw material. Belgian marine sand: a scarce resource? Belgian FPS Economy – Study day 9 June 2017 : 39-45 [http://economie.fgov.be/fr/binaries/Articles-study-day-2017\\_tcm326-283850.pdf](http://economie.fgov.be/fr/binaries/Articles-study-day-2017_tcm326-283850.pdf)



# Seabed features in Mecklenburg Bight based on Side-Scan Sonar Imagery

Giuliana A. Díaz Mendoza *Christian-Albrechts-Universität zu Kiel, Institute of Geosciences, Coastal Geology and Sedimentology, Kiel, Germany* - [stu205563@mail.uni-kiel.de](mailto:stu205563@mail.uni-kiel.de).

Klaus Schwarzer *Christian-Albrechts-Universität zu Kiel, Institute of Geosciences, Coastal Geology and Sedimentology, Kiel, Germany* - [klaus.schwarzer@ifg.uni-kiel.de](mailto:klaus.schwarzer@ifg.uni-kiel.de).

**ABSTRACT:** Mecklenburg Bight (Baltic Sea) has various natural, geomorphological and sedimentological features reflecting hydrodynamic processes, sediment dynamics, biological activities and coastal development. This area is also strongly influenced by human activities like military exercises, professional fishing, dumping of dredged material and touristic activities. Bedforms such as small subaqueous dunes and sediment transport patterns, as well as features resulting from anthropogenic disturbances of the seafloor have been identified using hydroacoustic mapping techniques. A catalogue was prepared, showing different disturbances of natural seafloor conditions due to anthropogenic pressure. The sustainability of these features will be discussed.

## 1 INTRODUCTION

Nowadays, coastal areas are used in many different ways. They can be under natural protection, allowing no anthropogenic activity, or they can be heavily used by different type of industries. This use often has an impact on seafloor conditions. The inner Mecklenburg Bight (SW Baltic Sea, Germany, Fig. 1) is a confined area, where all these different activities are archived in the seafloor conditions. Here, anthropogenic activities such as trawling, anchoring due to military and touristic activities, dumping of dredged material and others activities can be observed in the seabed environment.

Side-scan Sonars (SSS) are hydroacoustic devices which are suitable tools for mapping sea bottom properties. They emit and collect high-frequency acoustic pulses which are scattered back from the seafloor. The intensity of sound scattered from obstacles on the seafloor, from the sediment due to its properties, from benthic organisms or other features gives a picture of the characteristics of the seafloor. The backscatter is affected by the local geometry of ensonification, the

physical seabed characteristics and the intrinsic properties of the seafloor (Blondel, 2009). Therefore, the compilation of numerous backscatter measurements results in an image of backscatter intensities, providing information of the substrate characteristics. Furthermore, the characterisation of SSS imagery may be used to identify dynamical processes controlling seabed morphology by observing bedforms and surface sediment distribution patterns.

This work aims to provide a catalogue of SSS images of the seafloor in the area of inner Mecklenburg Bight and to identify distinctive features in a shallow water environment under the influence of human activities.

## 2 STUDY AREA

The hydroacoustic surveys are distributed in an area of approximately 1.260 km<sup>2</sup> in the Mecklenburg Bight (Fig. 1), located in the south-western Baltic Sea with a maximum depth of -28 m NHN. Lübeck Bight and Neustadt Bight are part of Mecklenburg Bight and the present morphology is the

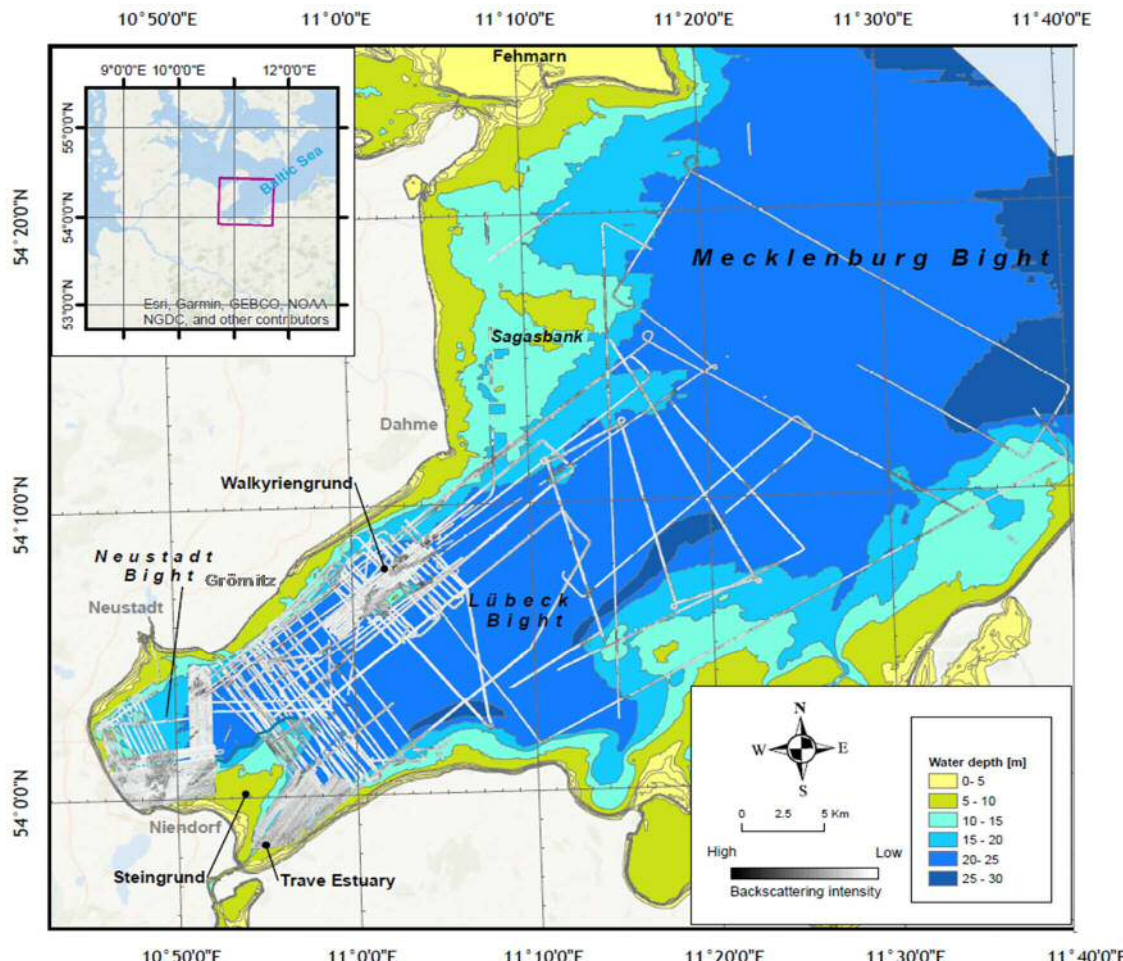


Figure 1 Location of the study area and side-scan sonar survey lines. Bathymetry source: BSH ([www.geoseaportal.de](http://www.geoseaportal.de)).

result of various depositional processes occurring since the late Pleistocene deglaciation (Schwarzer et al., 2003). Wide areas of the seafloor are built up of Pleistocene deposits, mainly glacial till (Niedermeyer et al., 2011). Common features in the area are active cliffs alternating with lowlands which are fronted by nearshore bars. Additional morphological features include abrasion platforms in front of cliffs, submarine channels, detached abrasion platforms and the Trave River which empties into Lübeck Bight.

All abrasion platforms are predominantly composed of soft boulder clay of Pleistocene origin, sometimes with intermediary melt

water deposits (Schrottke et al., 2006). On these platforms stones are occurring. Active cliffs and abrasion platforms are supporting the nearshore environment with sediment.

The surface sediment distribution in Mecklenburg Bight is a function of geological prerequisites, water depth, energy input due to waves and resulting currents. Significant wave height can reach 3.12 m in between a 10 years return period (Fröhle, 2000) or a maximum height of 5.5 m during storms from NE (Dette & Stephan, 1979). In deeper areas, muddy material predominates while the shallower areas on detached shoals and along the coast are dominated by coarse sediment including boulders. Also, lag deposits cover large areas of the seafloor especially in areas close to the coast and down to water depths of about -20 m NHN like NE of Sagasbank or NW of Steingrund

(Fig. 1). They are the result of the abrasion of the underlying till and mainly consist of gravel, stones and boulders, often surrounded by well-sorted fine to medium sand (Zeiler et al., 2008).

Walkyriengrund is a protected natural marine structure with typical communities of reefs and sandbanks (according to FFH regulations) located in central Lübeck Bight. It is a shoal rising up to about -5 m NHN water depth. This shoal is densely covered by boulders, benthic macrophytes such as *Laminaria saccharina* and the seagrass *Zostera marina*, as well as mussel beds of *Mytilus edulis*, which provide a marine invertebrate habitat and substrate (Christiansen & Körner, 2013).

In addition, Lübeck Bight is a busy area due to harbours and marinas, a shipyard, the mouth of the Trave River and the multiple activities developed in the regions which include dredging, anchoring, dumping of material, fishing and testing military devices.

## 2 METHODS

Mosaic generation is based on SSS raw data obtained from different cruises carried out during student exercises since 2001 (for database see Fig. 1). The acoustic devices employed are the Teledyne Benthos Dual Frequency 1624 (100 and 400 kHz), the Side-Scan Sonar Benthos C3D (200 kHz) and the Klein 595 Dual Frequency (100 kHz and 500 kHz). All systems were towed behind the ship with a vessel speed of 4-5 knots and with altitudes which equals 10 % of the range which was applied. However, in shallow areas, the altitude sometimes was only 3 m above the seafloor. The SSS towfish was fixed underneath a larger buoyancy to maintain the system in a stable position, minimising the effect of ship motion (Schwarzer et al., 1996). In general, the survey profiles were recorded with a range between 50 and 100 m to each side.

Data was recorded in digital form employing the software package ISIS (Triton Erics Int.). This allowed to construct georeferenced mosaics of the investigated seafloor. Corrections due to the distance of the fish to the seabed (the slant range) and layback/offset were settled according to survey characteristics. The raw data in extended Triton Format (.xtf) was processed in Sonar Wiz 7.0.

Due to the complexity in the compilation of data with different frequencies and gain settings obtained from different devices, individual files for every cruise were exported as GeoTIFF files with 0.25 m resolution and consequently assembled and characterised in ArcGIS 10.1.

## 3 RESULTS

The seabed features observed in the SSS images in Mecklenburg Bight include bedforms and human-induced seabed structures which are generated on a variety of seafloor types ranging from mud to boulders fields.

Bedforms such as small subaqueous dunes according to Ashley (1990) were found at the end of the abrasion platform, offshore of the Trave river mouth. They are found in depth of about -20 m NHN and they have sinuous to tongue-shaped crestlines (linguoid) with variable wavelengths from 1 m and 3.5 m. In sandy areas offshore Dahme (Fig. 2a) between -15 m and -20 m NHN small subaqueous dunes are asymmetrical and present straight crests partly showing bifurcation with wavelengths up to 1.5 m. Also, on the Walkyriengrund, a ripple field showed small subaqueous dunes straight to sinuous-crested with wavelengths between 0.5 to 1.1 m.

Other features recognised in the SSS images in Lübeck Bight consist of high-backscattering elongated, sinuous- structures composed of coarse material (Fig. 2b). Probably, these structures are related to bends of mussel beds of *Mytilus edulis* observed in video profiles.

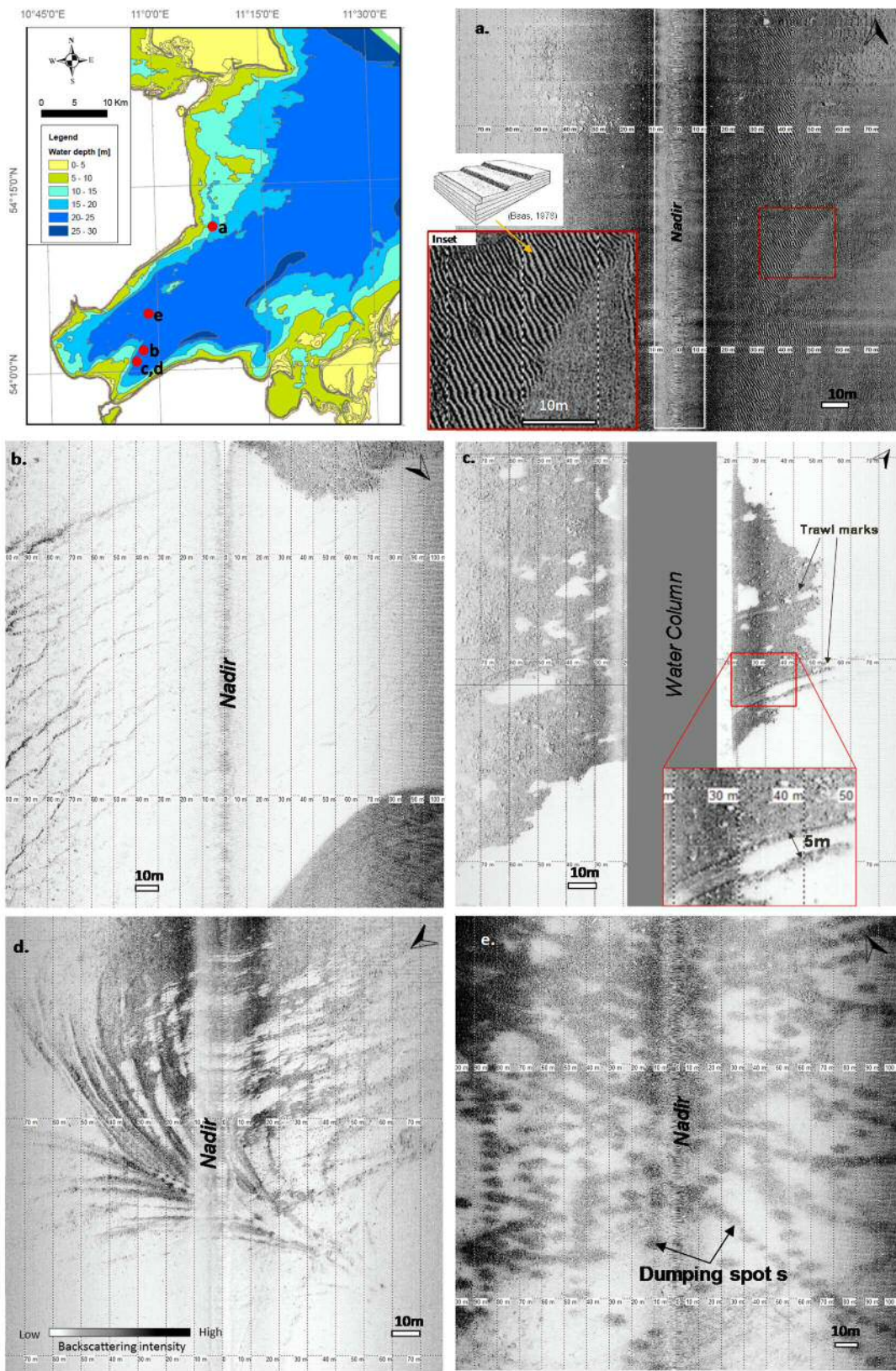


Figure 2 High resolution acoustic images showing a) bedforms, frequency: 400 kHz b) elongated bends of coarse material, c) trawl marks, d) anchor scars and e ) dumping spots.

The source of the coarser material forming the elongated bends might be associated with the higher backscattering area of the

nearby region (see Fig. 2b). Thus, probably the elongated bends are the result of deposition of shells and shell fragments transported

from elevated areas during storm conditions. They are building a settlement of new and active communities on the surficial sediment layer and provide a new hardground for other species.

On the other hand, anthropogenic activities such as trawling or anchoring also influence the interaction between water flow and seabed surface by sediment reworking and redistribution, furrow formation and sometimes scouring affecting the seafloor severely. Particularly in Lübeck Bight, sonographs demonstrate strong seabed sediment disturbance (Figs 2c-e). Fishing activities using bottom contact gears such as otter trawlers, demersal seiners, beam trawlers, and dredgers have a significant impact on the seafloor. During the trawling operation, a trawl is towed behind the ship over long distances. It is weighed down on the seafloor by heavy steel doors, and the resulting erosion creates linear parallel features or furrows (Fig. 2c). The seafloor vulnerability to the trawling impact depends on sedimentological conditions and consolidation, geomorphological gradient, benthic fauna, sedimentation rates and the degree of reworking of sediments. Consequently, seabed disturbance includes scouring, furrow formation, creating roughness, increase in surface relief, flattening of ripples, sediment mobilisation, seabed smoothing, boulder displacement, and sediment penetration (Eigaard et al., 2016).

Similarly, anchoring creates furrows, reworks and redistributes strongly the sediment (Fig. 2d). The purpose of anchoring is to attach a ship to the seabed at a specific location, avoiding vessel drifting due to wind, waves or currents, which happens quite often in the military exercise area. The operation consists in dropping the anchor attached by the anchor chain. When the anchor hits the bottom, it is embedded into the seabed. As the ship is moving due to currents, the anchor also moves, dragging all sediment around it. Thus, anchoring affects the seabed morphology, creating depressions and redistributing sediment.

Additionally, the SSS images show distinctive conical and elliptical geometries

which have been related to dumping sites in Lübeck Bight, east of Neustadt and Grömitz and south of Walkyriengrund in water depths of about -22 m NHN (Fig. 2e). These features are the result of dumping, and their morphology depends on multiple factors such as: the ship velocity, currents, the type of material, and water depths. Dumping areas can include dredged or excavated soil from sea or land, mainly from the dredging of harbours or harbour entrances. Old dumping sites might contain weapons, munitions and warfare agents. Today, dumped munitions and warfare agents are in different stages of decomposition which is a risk for the marine ecosystem due to corrosion (Brenner et al., 2017).

#### 4 CONCLUSIONS

SSS technique has a high potential to identify natural and anthropogenic features on the seabed. The SSS constitutes a useful tool to image the seafloor letting us recognise the spatial distribution and character of different sediment types, bedforms and objects. Small subaqueous dunes were found in depths between - 10 to -25 m NHN with variable wavelengths and with straight to tongue-shaped crestlines. Furthermore, the acoustic imagery showed traces of intense human activity in the study area. Trawling marks, anchor scars and distinct conical to elliptical features were recognised in the acoustic images suggesting that anthropogenic activities strongly modify the seabed. As trawling marks cross fine-grained cohesive material and coarse-grained sediment, it can be easily observed that the disturbance last for a much longer time in the muddy deposits. With the growing demand of maritime traffic, touristic use and economic development these disturbances might increase.

#### 5 ACKNOWLEDGEMENT

We thank master and crew of RV AL-KOR and FK LITTORINA for excellent support during all cruises. Thanks as well to the group of Coastal Geology and Sedimentology and especially to Daniel Unverricht

for the support during the realisation of this project.

## 6 REFERENCES

- Ashley, G.M., 1990. Classification of large-scale subaqueous bedforms; a new look at an old problem. *J. Sediment. Res.* 60, 160–172. <https://doi.org/10.2110/jsr.60.160>
- Baas, J.H., 1978. Ripple, ripple mark, ripple structure, in: *Sedimentology*. Springer Berlin Heidelberg, pp. 921–925. [https://doi.org/10.1007/3-540-31079-7\\_172](https://doi.org/10.1007/3-540-31079-7_172)
- Blondel, P., 2009. *The Handbook of Sidescan Sonar*. Springer Berlin Heidelberg, Berlin, Heidelberg. <https://doi.org/10.1007/978-3-540-49886-5>
- Brenner M., Bostelmann A. & Klöpper S. 2017. Military activities. In: Wadden Sea Quality Status Report 2017. Eds.: Kloepper S. et al., Common Wadden Sea Secretariat, Wilhelmshaven, Germany. Last updated 21.12.2017. Downloaded 08.08.2018. [qsr.waddensea-worldheritage.org/reports/military-activities](http://qsr.waddensea-worldheritage.org/reports/military-activities)
- Bundesamts für Seeschifffahrt und Hydrographie (BSH), Baltic Sea Bathymetry. Downloaded from [www.geoseaportal.de](http://www.geoseaportal.de) (accessed 05.27.18).
- Christiansen, S. & Körner, E. 2013. Steckbrief Natura 2000 Gebiete Ostsee, Walkyriengrund. Available in: World Wide Fund For Nature (WWF). [http://www.wwf.de/fileadmin/fmw/wfw/Publikationen-PDF/6-Steckbrief\\_FFH\\_Walkyriengrund.pdf](http://www.wwf.de/fileadmin/fmw/wfw/Publikationen-PDF/6-Steckbrief_FFH_Walkyriengrund.pdf).
- Dette, H.-H., Stephan, H.-J. 1979. About waves and wave-induced effects in the nearshore zone of the Baltic Sea,. - Mitt. Leichtweiss-Inst. d. TU Braunschweig, 65, 89 - 136.
- Eigaard, O.R., Bastardie, F., Breen, M., Dinesen, G.E., Hintzen, N.T., Laffargue, P., Mortensen, L.O., Nielsen, J.R., Nilsson, H.C., O'Neill, F.G., Polet, H., Reid, D.G., Sala, A., Sköld, M., Smith, C., Sørensen, T.K., Tully, O., Zengin, M., Rijnsdorp, A.D., 2016. Estimating seabed pressure from demersal trawls, seines, and dredges based on gear design and dimensions. *ICES J. Mar. Sci. J. Cons.* 73, i27–i43. <https://doi.org/10.1093/icesjms/fsv099>.
- Fröhle, P., 2000. Einfluß von Steiluferabbrüchen an der ostsee auf die Prozessdynamik angrenzender Flachwasserbereiche, Teilprojekt Hydrodynamik. Abschlussbericht, 62 S. (unveröff.).
- Niedermeyer, R.-O., Lampe, R., Janke, W., Schwarzer, K., Duphorn, K., Kliewe, H. and Werner, F., 2011. Die Deutsche Ostseeküste. Sammlung geologischer Führer, 105, 370 p
- Schrottke, K., Schwarzer, K., Fröhle, P., 2006. Mobility and Transport Directions of Residual Sediments on Abrasion Platforms in Front of Active Cliffs (Southwestern Baltic Sea). *J. Coast. Res.* 6.
- Schwarzer, K.; Ricklefs, K., And Schumacher, W. and Atzler, R., 1996. Beobachtungen zur Vorstrand-dynamik und zum Küstenschutz sowie zum Sturmer-eignis vom 3./4.11.1995 von dem Streckelsberg/Use-dom. Meyniana, 48, 49-68.
- Schwarzer, K., Diesing, M., Larson, M., Niedermeyer, R.-O., Furmanczyk, K., 2003. Coastal evolution in different time scales - examples from the Mecklenburg Bight (Baltic Sea). - *Mar. Geol.* 194, 79 - 101.
- Zeiler, M., Schwarzer, K., Bartholomä, A., Ricklefs, K., 2008. Seabed Morphology and Sediment Dynamics 14.

# Evolution of offshore sand ridges in tideless continental shelves (Western Mediterranean)

Ruth Durán *Institut de Ciències del Mar, CSIC, Barcelona, Spain* –rduran@icm.csic.es

Jorge Guillén *Institut de Ciències del Mar, CSIC, Barcelona, Spain* –jorge@icm.csic.es

Marta Ribó *Macquarie University, Sydney, Australia* –marta.ribogene@mq.edu.au

Pere Puig *Institut de Ciències del Mar, CSIC, Barcelona, Spain* –ppuig@icm.csic.es

Araceli Muñoz *Tragsa-SGP, Madrid, Spain* –amur@tragsa.es

**ABSTRACT:** An extensive dataset of vibrocores and high-resolution seismic data were analysed to characterise offshore sand ridges on the Gulf of Valencia and the Murcia continental shelves, in the western Mediterranean Sea, with the aim of improving knowledge about the formation and evolution of these bedforms. Sediment coring revealed a layer of coarse sand and gravel with pebbles corresponding with the basal reflector of the sand ridges and interpreted as the Holocene ravinement surface. The architecture of the sand ridges reveals the presence of small, mound-like features interpreted as coastal deposits that could have served as a precursor for the sand ridges genesis. The different degree of preservation of the precursor within the sand ridges observed in the western Mediterranean reveals a gradation from partially to fully evolved sand ridges with increasing water depth. The offshore sand ridges represent valuable potential sand resources that must be preserved as strategic sand reservoirs.

## 1. INTRODUCTION

Sand ridges are widespread bedforms found on many continental shelves at a wide range of water depths from the nearshore to the shelf edge. Shoreface-connected sand ridges are observed on the shoreface and inner shelf in water depths shallower than 20 m (McBride and Moslow, 1991, Guerrero et al., 2018). Offshore sand ridges, or shoreface-detached ridges, are located on the middle and outer shelf (e.g. Goff et al., 1999; Simarro et al., 2015). They are interpreted as formed in shallow waters and detached from the shoreface during the transgression (McBride and Moslow, 1991).

A depositional model for the evolution of shoreface-connected sand ridges into detached sand ridges was developed by McBride and Moslow (1991) and subsequently expanded by Snedden et al. (1999). The model includes three stages of development, based on the extent to which a ridge retains evidence of its initial irregularity: a) juvenile, where the initial irregularity forms; b) partially evolved, where ridges migrate

enough to erode the precursor; and c) evolved, with limited to no trace of the initial stage of development.

In this work, we present the detailed characterization of offshore sand ridges located on the Gulf of Valencia (GoV) and the Murcia continental shelves in the western Mediterranean Sea based on the analysis of an extensive vibrocore dataset and high resolution seismic data. The aim of this study is to provide additional information about the formation and evolution of these bedforms in tideless continental shelves.

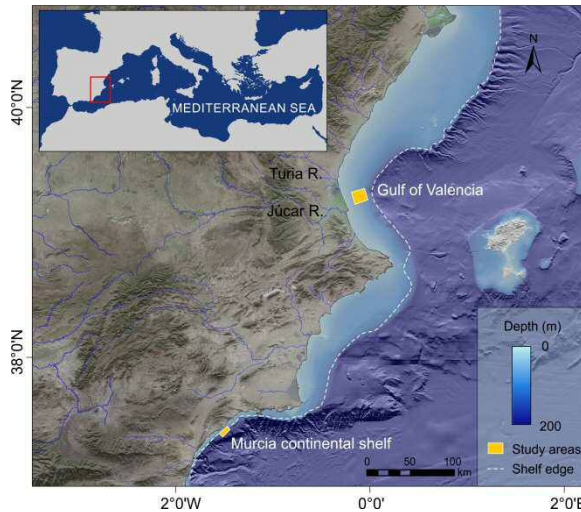
## 2. STUDY AREA

The GoV and Murcia continental shelves are storm-dominated, microtidal (< 0.2 m) environments with a low sediment input by rivers. The main river discharging into the GoV is the Turia River (Fig. 1), with a small mean discharge of 14 m<sup>3</sup>/s. Only small, ephemeral streams flow into the Murcia continental shelf (Fig. 1).

The GoV continental shelf has a variable width up to 30 km, with the shelf edge lo-

cated at ~150 m water depth (Fig. 1). The Murcia continental shelf is narrower; it has an average width of 4 km, locally up to 10 km with the shelf edge located at 80-120 m water depth (Acosta et al., 2013). Surficial sediments in both shelves are characterized by a mud blanket that extends along the middle and outer shelf, with the exception of two isolate areas of sandy sediments, where the sand ridges were observed.

Figure 1. Shaded-relief colour map of the Medi-



tean margin of the Iberian Peninsula showing the location of the study areas. Topographic data provided by the Spanish National Geographic Institute ([www.ign.es](http://www.ign.es)). Bathymetric data downloaded from the EMODnet portal (<http://portal.emodnet-bathymetry.eu/>).

Sand ridges in the GoV continental shelf are located between 55 and 85 m water depth, covering an area of 35 km<sup>2</sup>. The sand ridges show a predominant NE-SW orientation, obliquely to the isobaths (Maldonado et al., 1983) (Fig. 2). The ridge height (H) ranges from 1.5 to 7 m, with a spacing (L) between 600 and 1,100 m (Simarro et al., 2015). The sand ridges are asymmetric with the lee face on the south side of the crest.

Sand ridges in the Murcia continental shelf are observed between 58 and 78 m water depth, covering an area of 13 km<sup>2</sup> (Durán et al., 2018) (Fig. 3). They are 1.5 to 3 m high and show E-W orientation oblique to the shoreline. Smaller-scale subaqueous

dunes (0.3-1.3 m high) appear superimposed on the sand ridges (Fig. 3). The dunes are asymmetric with the lee side facing southwest. The comparison of two bathymetric surveys 10 years apart revealed that the dunes are migrating towards the southwest at very low rates (~3 m yr<sup>-1</sup>).

### 3. DATA AND METHODS

The analysis of the sand ridges is based on the interpretation of very-high resolution seismic reflection data, surficial sediment samples and sediment cores (Figs. 2 and 3).

Seismic data were acquired in 2011 onboard the R/V Vizconde de Eza and in 2013 onboard the R/V Angeles Alvariño in the GoV and Murcia continental shelves, respectively, using a Kongsberg TOPAS PS018 parametric sub-bottom profiler.

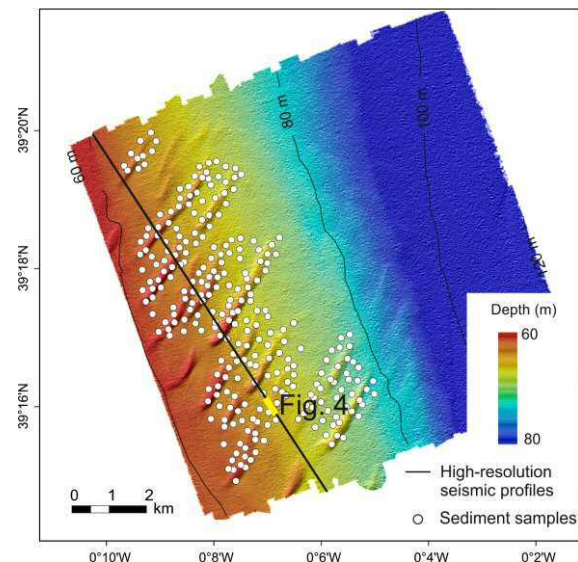


Figure 2. Shaded-relief colour bathymetry of the GoV sand ridges including the location of the high-resolution seismic profile and the sediment cores. Modified from Durán et al., 2015.

A total of 279 vibrocores were retrieved in the GoV continental shelf in 2007 by the Spanish Ministry of Agriculture, Food and Environment (Sub-Directorate General for Coastal Protection) (Fig. 2). Vibrocores, usually 4-5.5 m long, were sub-sampled every 0.5 m. for grain size analysis. In addition, 20 surficial sediment samples were collected on the Murcia continental shelf.

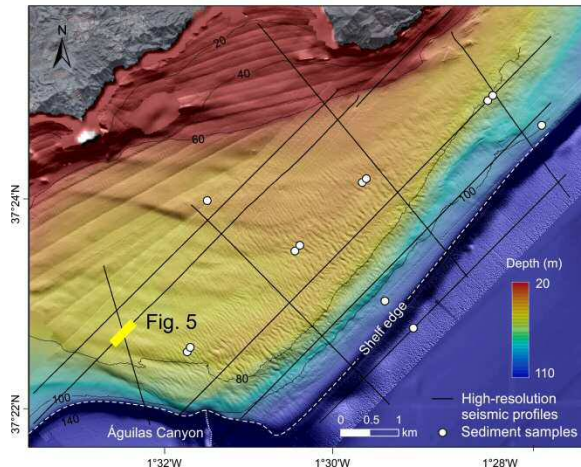


Figure 3. Shaded-relief colour bathymetry of the Murcia continental shelf including the location of the high-resolution seismic profiles and the surficial sediment samples. Modified from Durán et al., 2018.

## 4. RESULTS

### 4.1 Sediment characteristics

The analysis of the sediment cores provides information about the sedimentary structure of the sand ridges. The sand ridges are composed of well-sorted medium and coarse sand (85% on average) with a low content of mud (<20%) and gravel (<10%). A coarse layer composed of coarse sand and gravel (up to 98%) with presence of pebbles and cobbles is observed at the base of the sand ridges (Fig. 4). Locally, the sandy facies display interbedded mud layers at different depths.

In the flank of the sand ridges, the sand layer appears covered by a surficial layer of fine-grained sediments (0.3-1 m thick) composed of sand (33% on average) and mud (69% on average) (Fig. 4). The mud content of this layer increases up to 98% in the troughs between ridges, where it can be up to 3.5 m thick.

In the Murcia continental shelf, surficial sediment samples are mostly composed of medium to coarse sand (33%-60%) with a mud content lower than 40%. Only in some locations, the sediment is composed of coarse sand and gravel (about 64%).

### 4.2 Seismic data

The high-resolution seismic profiles display a strong reflector that truncates the underlying seismic units and locally emerges at the seafloor in the deeper parts of the troughs between ridges (Figs. 4 and 5). It corresponds to a major erosional surface that can be traced along the whole study areas. It shows an irregular topography with local relieves up to 3 ms, or ~2.5 m.

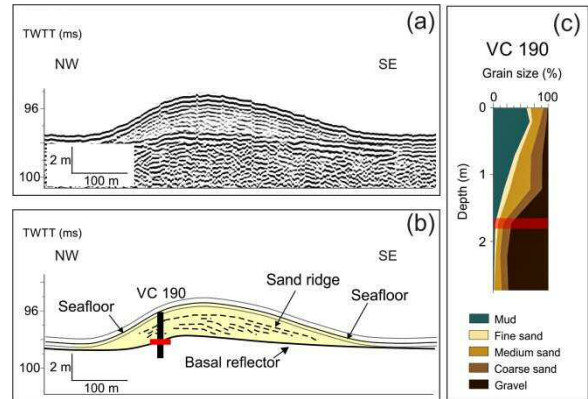


Figure 4. (a) Uninterpreted and (b) interpreted high-resolution seismic profile of a small sand ridge. (c) Sediment corer description. Red line indicates the location of the basal reflector identified in the seismic profile. A sound velocity of 1550 m/s was used. Solid grey lines indicate parallel reflectors mimicking the seafloor surface. See figure 2 for location.

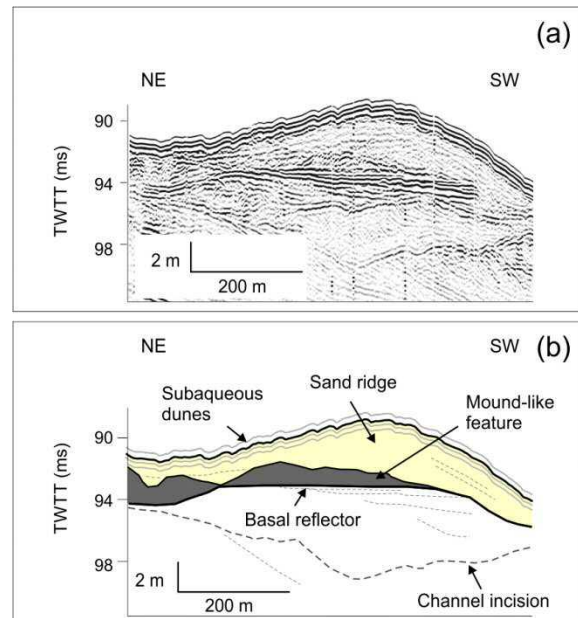


Figure 5. (a) Uninterpreted and (b) interpreted high-resolution seismic profile of sand ridges. Note that the basal reflector locally outcrops at the seafloor. Location is shown in Fig. 3.

In the GoV, this reflector corresponds to the coarse lag identified in the sediment cores at the base of the sand ridges (Fig. 4). In the Murcia continental shelf, the coarse nature of this surface is evidenced by the presence of coarse sand and gravel in the areas where the erosional surface is exposed.

Internally, the sand ridges are characterized by high-amplitude, high-angle internal reflectors dipping towards the south (Figs. 4 and 5). Locally, small mound-like features with low relief (up to 1 m high) are identified at the base of the sand ridges, showing a high degree of acoustic impedance. They are commonly observed in the Murcia sand ridges (Fig. 5) but also in some ridges in the GoV.

## 5. DISCUSSION

### 5.1 Sand ridge formation on tideless continental shelves with limited sediment supply

The sand ridges identified in the GoV and Murcia continental shelves rest on a regionally recognized erosional surface. In the Murcia shelf sector, this surface caps channel fill deposits, suggesting a transition from fluvial to marine conditions. In the GoV, it corresponds to a coarse sand or pebble lag that is overlain by a thick layer of sandy-sediments in the sand ridges and fine-grained sediments in the troughs. This basal surface is interpreted as the ravinement surface associated with the Holocene sea level rise. Accordingly, the sand ridges might have formed during the Younger Dryas at about 10,000 years BP, favoured by the deceleration of sea-level rise.

The architecture of the sand ridges also reveals the presence of small, mound-like features. Based on their acoustic signature, these features are interpreted as coast-associated features such as cemented beach deposits or armoured shallow-water deposits that may act as the nucleus for sand ridge genesis through the interaction between flow and seabed roughness. Their preservation within the sand ridges indicates that these ridges have not migrated enough to erode the precursor.

The formation of sand ridges on the GoV and Murcia continental shelves suggests that despite the low fluvial sedimentary contribution, enough sand was locally available for ridge development, most likely derived from marine reworking of coastal deposits during transgression. However, the limited sediment availability determines the reduced areal extent of the sand ridge fields in comparison with other storm-dominated sand ridges developed in areas with higher sediment availability, such as the Atlantic shelves of North America (Goff et al., 1999; Li and King, 2007), where sand ridges spread over tens of kilometres along the continental shelf.

### 5.2 Sand ridge evolution

Internally, the sand ridges display SE dipping oblique reflectors indicating long-term migration towards the south. These reflections appear associated with mud layers interbedded in sand sediment suggesting episodic ridge migration, with intervals of reactivation after relatively calm periods dominated by mud deposition.

The comparison of the sand ridges observed in the GoL and Murcia continental shelves with those described in the Gulf of Lions (GoL), north of the study areas, reveals some differences in their architecture (Fig. 6). On the Murcia continental shelf, most sand ridges contain evidence of their precursor (Fig. 6b), whereas in the GoV only some ridges display evidence of their initial irregularity (Durán et al., 2015) (Fig. 6c). In fact, where the precursor is preserved, it is smaller than that those observed in the Murcia sand ridges. Sand ridges in the GoL show no traces of the initial stages of development (Bassetti et al., 2006) (Fig. 6d).

Based on the differences in the sand ridge location and the preservation of the precursor, we can establish a gradation from partially evolved sand ridges on the Murcia continental shelf to more evolved ones in the GoV and the fully evolved ones in the GoL. These observations agree with the sand ridge evolution described on the New Jersey continental shelf (McBride and Moslow, 1991;

Snedden et al., 1999), where sand ridges are found today in three stages of development, the deeper sand ridges being older and more evolved than the shallower ones.

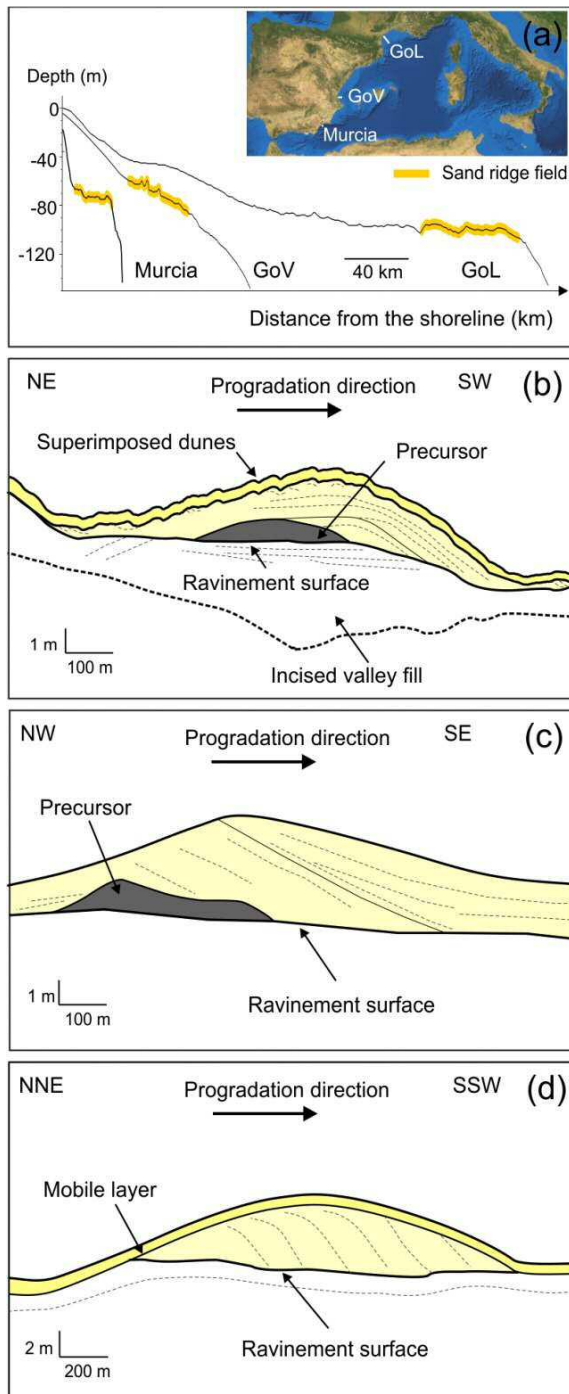


Figure 6. (a) Bathymetric profiles across the Murcia, GoV and GoL continental shelves indicating the location of sand ridges. (b to d) Schematic diagrams illustrating sand ridge architecture observed on the: (b) Murcia, (c) GoV and (d) GoL shelves. Modified from Durán et al., 2018.

### 5.3 Sand ridges as potential borrow areas

Understanding the formation and evolution of these bedforms is of high interest because of their potential as sources of sediment for beach nourishment and coastal restoration. During the last years, the increasing shortage of sand around the world has led the governments to go further out into the sea to obtain new sand supplies. Shoals, sand ridges and other sediment bodies developed on the middle shelf represent valuable strategic sand resources.

In Europe, around 50 million m<sup>3</sup> of sand and gravel are extracted each year from the inner continental shelf (Sutton and Boyd, 2009). Along the Spanish Mediterranean coast, only between 1997 and 2002, a total fill volume of about 110 millions of m<sup>3</sup> were used for coastal protection (Hamm et al., 2002). In the Valencia sand ridge field, it was defined a potential sand borrow area of 22 million m<sup>3</sup> (Durán et al., 2015). It constitutes a valuable potential sand resource because of the high quality of sediment. However given the level of demand of the region, about 3 million m<sup>3</sup>/year since 1950s (Yepes and Medina, 2005), the stored volume of sand only would cover the huge nourishment requirements for recreational purposes for about 7 years.

On that basis, even though offshore sand ridges developed in these continental shelves represent strategic potential sand borrow areas, their use for such an unsustainable goal as artificial beach nourishment is discouraged because of the limited volume of sand.

## 6. CONCLUSIONS

The architecture of the GoV and Murcia sand ridges provides a better understanding of the formation and evolution of sand ridges in tideless environments.

The sand ridges developed over an erosional surface composed of coarse sand with pebbles that is interpreted as the Holocene ravinement surface.

Coast-associated features can act as a precursor of sand ridge genesis. Their preservation within the sand ridges indicates that these ridges have not migrated enough to erode the precursor.

The formation of sand ridges on the GoV and Murcia continental shelf demonstrates that sand ridges can develop on tideless shelves with a reduced sediment supply when local conditions favour the accumulation of sediment.

The sand ridges observed in the western Mediterranean are found in three stages of development from partially evolved to fully evolved sand ridges with increasing water depth.

Despite the offshore sand ridges constitute valuable potential sand borrow areas, it is recommended to preserve them as strategic sand reservoirs.

## 7. ACKNOWLEDGEMENT

This research was supported by the ABIDES (CTM2015-65142-R) project. The authors thank Instituto Español de Oceanografía the Murcia oceanographic cruise and Secretaría General para el Territorio y la Biodiversidad (Ministerio de Agricultura, Alimentación y Medio Ambiente) the sediment cores information.

## 8. REFERENCES

- Acosta, J., Fontán, A., Muñoz, A., Muñoz-Martín, A., Rivera, J., Uchupi, E., 2013. The morpho-tectonic setting of the Southeast margin of Iberia and the adjacent oceanic Algero-Balearic Basin. *Mar. Pet. Geol.* 45, 17–41. doi: 10.1016/j.marpetgeo.2013.04.005
- Bassetti, M. A., Jouet, G., Dufois, F., Berné, S., Rabineau, M., Taviani, M., 2006. Sand bodies at the shelf edge in the Gulf of Lions (Western Mediterranean): Deglacial history and modern processes. *Marine Geology* 234, 93–109. doi: 10.1016/j.margeo.2006.09.010
- Durán, R., Guillén, J., Simarro, G., Ribó, M., Puig, P., Muñoz, A., Palanques, A., 2015. Sand ridges in the mid-outer shelf as potential sand borrows areas (NW Mediterranean). *Proceedings of Coastal Sediments*. doi: 10.1142/9789814689977\_0111
- Durán, R., Guillén, J., Rivera, J., Lobo, F.J. Muñoz, A., Fernández-Salas, L.M., Acosta, J., 2018. Formation, evolution and present-day activity of offshore sand ridges on a narrow, tideless continental shelf with limited sediment supply. *Marine Geology* 397, 93–107. doi: 10.1016/j.margeo.2017.11.001.
- Guerrero, Q., Guillén, J., Durán, R., Urgeles, R., 2018. Contemporary genesis of sand ridges in a tideless erosional shoreface. *Marine Geology* 395, 219–233. doi: 10.1016/j.margeo.2017.10.002
- Goff, J. A., Orange, D.L., Mayer, L. A., Hughes Clarke, J.E., 1999. Detailed investigation of continental shelf morphology using a high-resolution swath sonar survey: the Eel margin, northern California. *Marine Geology* 154, 255–269. doi: 10.1016/S0025-3227(98)00117-0
- Hamm, L., Capobianco, M., Dette, H.H., Lechuga, A., Spanhoff, R., Stive, M.J.F., 2002. A summary of European experience with shore nourishment. *Coastal Engineering* 47, 237–264. doi: 10.1016/S0378-3839(02)00127-8
- Li, M.Z., King, E.L., 2007. Multibeam bathymetric investigations of the morphology of sand ridges and associated bedforms and their relation to storm processes, Sable Island Bank, Scotian Shelf. *Marine Geology* 243, 200–228. doi: 10.1016/j.margeo.2007.05.004
- Maldonado, A., Swift, D.J.P., Young, R.A., Han, G., Nittrouer, C.A., DeMaster, D.J., Rey, J., Palomo, C., Acosta, J., Ballester, A., Castellvi, J., 1983. Sedimentation on the Valencia Continental Shelf: Preliminary results. *Continental Shelf Research* 2, 195–211. Doi: 10.1016/0278-4343(83)90016-X
- McBride, R.A., Moslow, T.F., 1991. Origin, evolution and distribution of shoreface sand ridges, Atlantic inner shelf, U.S.A. *Marine Geology* 97, 57–85. doi: 10.1016/0025-3227(91)90019-Z
- Simarro, G., Guillén, J., Puig, P., Ribó, M., Lo Iacono, C., Palanques, a., Muñoz, a., Durán, R., Acosta, J., 2015. Sediment dynamics over sand ridges on a tideless mid-outer continental shelf. *Marine Geology* 361, 25–40. doi: 10.1016/j.margeo.2014.12.005
- Snedden, J.W., Dalrymple, R.W., 1999. Modern shelf sand ridges: From historical perspective to a unified hydrodynamic and evolutionary model. *SEPM Concepts of Sedimentology and Paleontology*. 6, 13–18. doi: 10.2110/pec.99.64.0013
- Sutton, G. and Boyd, S. (Eds), 2009. Effects of Extraction of Marine Sediments on the Marine Environment 1998 – 2004. ICES Cooperative Research Report No. 297, 180 pp.
- Yepes, V., Medina, J.R., 2005. Land use tourism models in Spanish coastal areas. A case study of the Valencia region. *Journal of Coastal Research* 49, 83–88.

# Ripples and dunes: do flumes tell the whole story?

Burg W. Flemming *Senckenberg, Wilhelmshaven, Germany* – [bflemming@senckenberg.de](mailto:bflemming@senckenberg.de)

**ABSTRACT:** Field observations have revealed the existence of small ripples ( $L=8$  cm) in coarse sand ( $D=0.87$  mm). This contradicts the conventional perception that ripples, defined as  $L < 0.6$  m, do not occur in sediments coarser than about 0.7 mm. As the currently accepted dimensional differentiation between ripples and dunes has essentially been based on flume observations, the contradictory evidence suggests that flumes, i.e. very shallow flows, suppress or inhibit the development of the smallest ripple-sized bedforms across all grain sizes. A plausible explanation for this could be that, in depth-limited flows, the turbulence generated by friction along the bed is confined to the small flow cross-sections and thereby prevents the formation of very small ripples.

## 1 INTRODUCTION

Phase diagrams of flow-transverse bedforms observed in flumes and shallow natural flows commonly distinguish between ripples and dunes (Figure 1). The main morphological criterion for this distinction is that ripples have spacings  $<0.6$  m (Allen, 1984; Sumer and Bakioglu, 1984), whereas dunes have spacings larger than 0.6 m (Costello and Southard, 1981; Allen, 1984; Sumer and Bakioglu, 1984; Ashley, 1990). Earlier, Yalin (1977) had, in addition, defined dunes as bed forms that interacted with the water surface, whereas ripples did not. He did not, however, provide any boundary conditions for which this definition was supposed to be valid. There is now overwhelming evidence that this criterion does not apply in deep flows (e.g. Flemming and Bartholomä, 2012, and citations therein). At the same time, Yalin (1977) suggested that, at initiation, flow-transverse bed forms had spacings of about 1000 grain diameters ( $L_{\min} = 1000D$ ), a concept that fitted the implied dimensional differentiation between ripples and dunes.

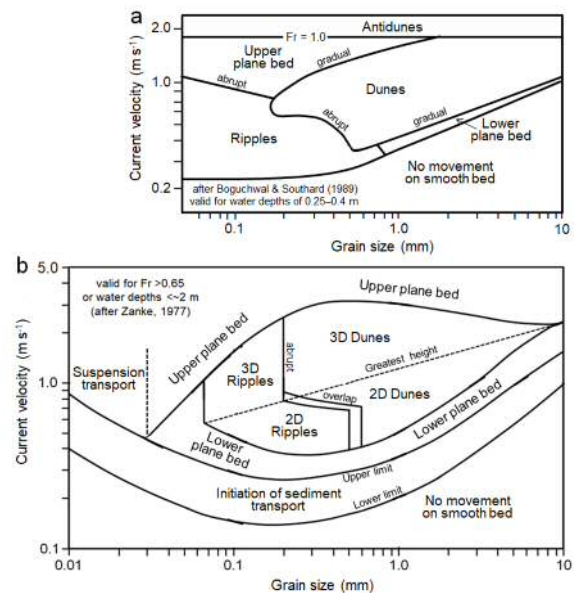


Figure 1. a) Bedform phase diagram of North American researchers (based on Boguchwal and Southard, 1989). b) Bedform phase diagram of German hydraulic engineers (based on Zanke, 1977). Note identical vertical and horizontal scales.

Finally, also on the basis of flume experiments, Simons and Richardson (1966), Costello and Southard (1981), Allen (1984), Sumer and Bakioglu (1984), Chiew (1991), van den Berg and van Gelder (1993) and Kleinhans (2002) concluded that, at grain

sizes larger than about 0.65–0.7 mm, ripples no longer formed and the initial bedforms were dunes ( $L>0.6$  m). Good reviews of these definitions and delimitations can be found in Carling (1999) and Best (2005).

In this context, it is instructive to compare standard bedform phase diagrams constructed by different researchers, here from Boguchwal and Southard (1989), USA, and Zanke (1976), Germany, in each case on the basis of their respective flume data (Figure 1a, b). While the diagrams have much in common, they also show significant deviations from each other, which seem to reflect different perceptions in data interpretation and presentation.

Thus, in diagram a, the initiation of movement is based on Shields (1936), while that in diagram b is based on Hjulström (1935). Furthermore, lower plane bed transport is restricted to grain sizes larger than about 0.7 mm in diagram a, whereas diagram b shows lower plane bed transport at all grain sizes. Furthermore, considering the shallow water, the pinching out of the dune stability field towards larger grain sizes in diagram b is a clearly more realistic representation of the observations than in diagram a, where the stability field to the right remains open-ended. The larger vertical phase scaling of diagram b reflects its validity for water depths up to 2 m, whereas the validity of diagram a is restricted to water depths up to 0.4 m. A particularly interesting aspect of diagram b is the distinction between 2D and 3D forms, the diagonal broken line indicating the maximum bedform height reached by ripples and dunes in those experiments.

In the light of the above, the main purpose of this investigation is to present new observational data that questions the validity of the conventional distinction between ripples and dunes, and to discuss the implications thereof.

## 2 METHODS

In this article the information presented in standard phase diagrams of flow-transverse bedforms observed in flumes and shallow flows is analysed in the light of recently published and new observational data concerning initial bedform spacing as a function of grain size.

## 3 RESULTS

In the course of a field trip to the Valdez Peninsula (Argentina) in 2016, the author spotted ripple formations in evidently coarse sand on a channel bar at low tide (Figure 2). The spacing of the bed forms ranged from 30 cm to a smallest size of 8–9 cm. A subsequent sieve analysis produced a median grain size of  $D_{50} = 0.87$  mm, which would correspond to an approximate minimum spacing ( $L_{\min}$ ) of  $100D$ .



Figure 2. Ripples in coarse sand ( $D_{50} = 0.87$  mm) on a tidal channel bar (southwestern San José Gulf, Valdez Peninsula, Argentina). Note that the smallest examples have spacings of 8–9 cm.

According to the morphological criteria for the distinction between ripples and dunes outlined above, and consistent with the bed phase diagrams of both Boguchwal and Southard (1989) and Zanke (1977), ripples should not occur at all in such coarse sediment, let alone such small ones. As both the flume and the field evidence must be accepted as being true representations of the respective observations, something must be

amiss with the flume data. The only explanation would seem to be that in flumes, and probably also very shallow natural flows in general, the development of initial ripple-size bedforms is, for some reason, suppressed or inhibited. This not only applies to grain sizes larger than 0.7 mm but also to finer sediment, as can be deduced from Figure 3 (cf. data points of Baas, 1994, 1999).

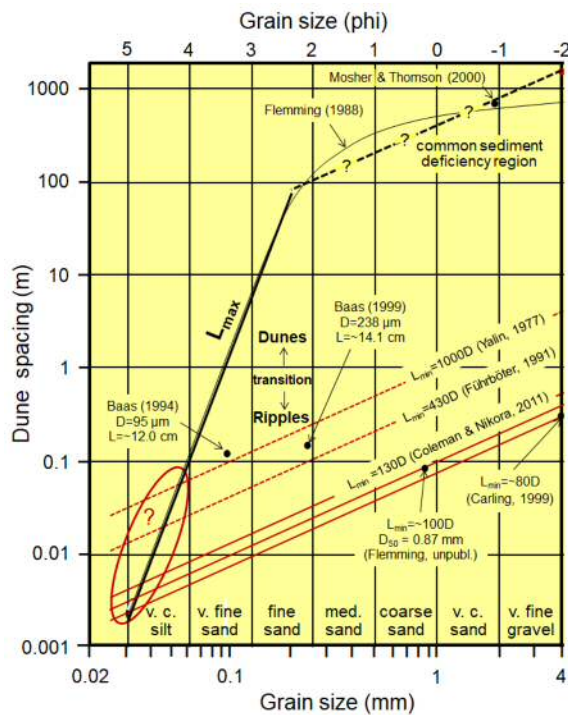


Figure 3. Initial and largest spacings of ripples and dunes as a function of grain size. Initial spacings ( $L_{\min}$ ) as defined by grain diameters (D) after various researchers; largest spacings ( $L_{\max}$ ) as observed in nature (modified after Flemming, 1988).

The above discrepancy has in recent years also been fuelled by the suggestion that minimum spacings of flow-transverse bedforms can be expressed in terms of grain diameters (Figure 3). The  $L_{\min} = 1000D$  relation proposed by Yalin (1977) has already been mentioned. Führbörter (1991) suggested a relation of  $L_{\min} = 450D$ . More recently, Coleman and Nikora (2011) proposed the relation of  $L_{\min} = 130D$ , while  $L_{\min} = 80D$  for a mean grain size of 4 mm can be inferred from data published in Carling (1999). A point of interest here is the progressive reduction in the grain scaling over past decades. The narrow band defined by

the relations of Coleman and Nikora (2011), Carling (1999) and Flemming (this article) can be viewed as the initiation zone within which initial bedforms appear to evolve (Figure 3). It should also be noted that the 1000D and 450D proposals are in conflict with the size of ripples known to occur in very coarse silt. Furthermore, the data compiled in Figure 3 contradict the view that dunes do not scale with grain size (Ashley, 1990), this contention having been exclusively based on observations made in depth-limited flows.

The trend lines tracing the largest bed forms ( $L_{\max}$ ) in Figure 3 are based on multiples of the 100D criterion. If, instead, the 130D or 80D criteria were used, the corresponding  $L_{\max}$  trend lines would lie slightly above or below those trend lines. For comparison, the  $L_{\max}$  trend line of Flemming (1988), which was based on rather scarce observational data, is also shown (thin grey line).

#### 4 DISCUSSION

A first point to be discussed concerns the question as to why very small bedforms apparently do not develop in very shallow flows. A plausible explanation for this could be the interference of turbulence generated by friction at the bed. In shallow or depth-limited flows the vertical expansion of the frictional boundary layer terminates at the water surface. In deep, depth-independent flows, by contrast, the thickness of the boundary layer can be approximated by the relation  $\delta_{bl} = 30U_{mff}$ , where  $\delta_{bl}$  is the thickness of the boundary layer in metres and  $U_{mff}$  is the mean free flow velocity above the boundary layer in m/s (Flemming, unpublished). Thus, already at a critical velocity of 0.25 m/s, the boundary layer would expand to a height of 7.5 m above the bed if given sufficient water depth. In deep flows, the turbulence generated at the bed can thus spread across the entire boundary layer (in the above case across 7.5 m). In depth-limited flows such as flumes (e.g. 0.4

m in the case of Figure 1a), the turbulence is concentrated near the bed, which may result in the suppression or inhibition of the development of very small bedforms.

A second point to discuss is whether the conventional distinction between ripples and dunes can be upheld in the light of the grain scaling concept of initial bedform spacing ( $L_{\min}$ ) outlined above and illustrated in Figure 3. In fact, Figure 3 suggests that ripples (as currently defined) occur in grain sizes up to at least 8 mm, although this does not appear to be reproduced in flume experiments. A consequence of this is that the assumed genetic difference between ripples and dunes turns out to be entirely artificial, being simply due to the incomplete nature of data generated in severely depth-limited flows. An interesting point to be made here is that the small ripples in Figure 2 were preserved at low tide, i.e. in the course of decelerating flow. This may explain the formation and preservation of the smallest forms.

A final point of discussion is the question of how large flow-transverse bedforms can become ( $L_{\max}$ ) under ideal conditions, i.e. where flow velocities and water depths are large enough. The field evidence clearly shows that the growth of ripples and dunes is ultimately limited by grain size. This is illustrated in Figure 3 by plotting  $L_{\max}$  against grain size based on multiples of 100D. The steeper trend line represents grain sizes up to about 0.2 mm and is well constrained by observational data (cf. Flemming and Bartholomä, 2012). For coarser grain sizes the trend line follows a substantially lower gradient, running almost parallel to the  $L_{\min}$  trend lines. Although both trends are to variable extent supported by field data, the data base for the lower-gradient trend line is much poorer because of the increasing sediment deficiency with increasing grain size and dune size. Nevertheless, the single data point from Mosher and Thomson (2000) shows good agreement with this trend.

Flemming (2000a) suggested that dune growth is terminated when the flow velocity above the crest reached the point where part of the bedload began to bypass the crest in suspension. It was assumed that this condition was fulfilled when the settling velocity of the average grain size ( $w_s$ ) was equal to the shear velocity ( $u_*$ ). According to Graf and Acaroglu (1966), approximately 40% of the bed material would be in suspension when this condition is reached. The choice of this criterion by Flemming (2000b) was thought to be justified by the fact that, when two dunes of similar size amalgamate, the geometric relationships dictate that about 40% of the larger dune body is initially missing. However, without sediment bypassing, the missing sediment is gradually regained by lowering of the base level through trough scouring in the course of amalgamation (Flemming, 2000b).

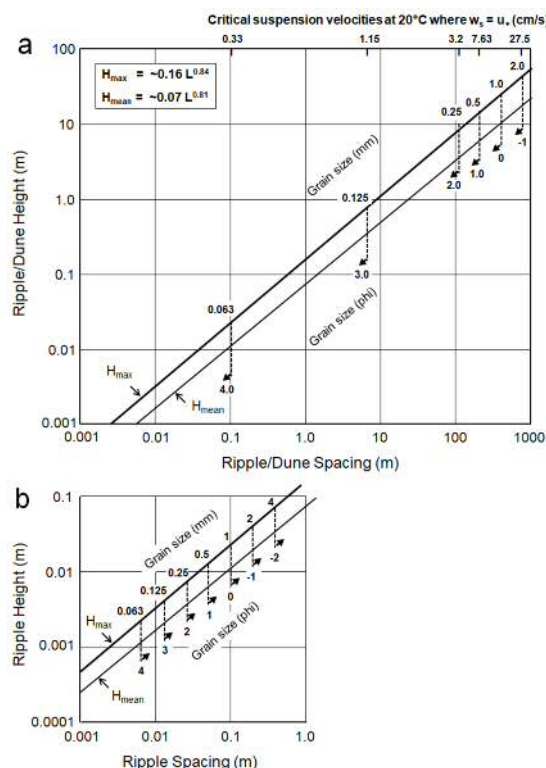


Figure 4. Size ranges (H vs L) of ripples/dunes as a function of selected mean grain sizes; **a** maximum dimensions; **b** initial dimensions. Note that for all grain sizes shown here the initial forms are ripples. Also shown are the corresponding suspension velocities for  $w_s = u_*$  valid at a water temperature of 20°C.

To illustrate the dependence of ripple and dune dimensions on grain size, the  $L_{\max}$  and  $L_{\min}$  values generated by the 100D criterion were plotted into the height versus spacing diagram of Flemming (1988) for grain sizes corresponding to full phi steps (Figure 4). To avoid confusion between the two, the  $L_{\max}$  and  $L_{\min}$  limits were plotted separately in Figure 4a, b, respectively. From the diagrams it can be seen that both the size range and the maximum size of dunes increase with increasing grain size. This is supported by numerous observations in nature.

## 5 CONCLUSIONS

The main conclusions of this investigation are:

- Flumes evidently do not tell the whole story.
- Flumes (and probably shallow flows in general) appear to suppress the initial development of ripple-size bedforms, especially in sediments coarser than about 0.6 mm.
- A possible reason could be the high concentration of turbulence near the bed in shallow flows.
- The initial spacing of flow-transverse bed forms appears to follow the rule of  $L_{\min} = 100\text{--}130D$ , which appears to be valid for all grain sizes.
- Carefully designed studies are required to gain a better understanding and a more definitive explanation of this phenomenon.
- A promising approach could be the investigation of bedform evolution in decelerating flows, i.e. working backwards from higher to lower velocity regimes.

## 6 ACKNOWLEDGEMENTS

The author thanks Senckenberg and, in particular, the Department of Marine Research in Wilhelmshaven, for providing work space and access to their sophisticated analytical instrumentation for grain-size analysis.

## 7 REFERENCES

- Allen, J.R.L., 1984. Sedimentary structures: their character and physical basis. Elsevier, Amsterdam, 539 pp.
- Ashley, G.M., 1990. Classification of large-scale subaqueous bedforms: A new look at an old problem. *Journal of Sedimentary Research* 60, 160–172. doi:10.2110/JSR.60.160
- Baas, J.H., 1994. A flume study on the development and equilibrium morphology of current ripples in very fine sand. *Sedimentology* 41, 185–209.
- Baas, J.H., 1999. An empirical model for the development and equilibrium morphology of current ripples in fine sand. *Sedimentology* 46, 123–138.
- Best, J., 2005. The fluid dynamics of river dunes: a review and some future research directions. *Journal of Geophysical Research* 110, F04S02.
- Boguchwal, L.A., Southard, J.B., 1989. Bed configurations in steady unidirectional water flows. Part 1. Scale model study using fine sands. *Journal of Sedimentary Research* 60, 649–657.
- Carling, P.A., 1999. Subaqueous gravel dunes. *Journal of Sedimentary Research* 69, 534–545.
- Chiew, Y.M., 1991. Bed features in nonuniform sediments. *Journal of Hydraulic Engineering* 117, 116–120.
- Coleman, S.F., Nikora, V.I., 2011. Fluvial dunes: initiation, characterization, flow structure. *Earth Surface Processes and Landforms* 36, 39–57.
- Costello, W.R., Southard, J.B., 1981. Flume experiments on lower-flow-regime bed forms in coarse sand. *Journal of Sedimentary Petrology* 51, 849–846.
- Flemming, B.W., 1988. Zur Klassifikation subaquatischer, strömungstransversaler Transportkörper. *Bochumer geologische und geotechnische Arbeiten* 29: 44–47.
- Flemming, B.W., 2000a. The role of grain size, water depth and flow velocity as scaling factors controlling the size of subaqueous dunes. In: Trentesaux, A., Garlan, T. (eds.), *Marine Sandwave Dynamics*, 23–24 March 2000, University of Lille 1 (France), Proceedings, pp. 55–60.
- Flemming, B.W., 2000b. On the dimensional adjustment of subaqueous dunes in response to changing flow conditions: a conceptual process model. In: Trentesaux, A., Garlan, T. (eds.), *Marine Sandwave Dynamics*, 23–24 March 2000, University of Lille 1 (France), Proceedings, pp. 61–67.
- Flemming, B.W., Bartholomä, A., 2012. Temporal variability, migration rates, and preservation potential of subaqueous dune fields on the southeast African continental shelf. *International Association of Sedimentologists Special Publication* 44: 229–247.
- Führbötter, A., 1991. Theoretischen und experimentelle Untersuchungen zum Entstehungsprozess von Strömungsriffeln. *Leichtweiss-Institut für Wasserbau, Braunschweig, Mitteilungen* 111, 185–268.

- Graf, W.H., Acaroglu, F.R., 1966. Settling velocities of natural grains. International Association d'Science Hydraulique, Bulletin 11, 27–43.
- Hjulström, F., 1935. Studies on the morphological activity of rivers as illustrated by the River Fyris. Geological Institute, University of Uppsala, Bulletin 25, 221–527.
- Kleinmans, M.G., Wilbers, A.W.E., de Swaaf, A., van den Berg, J.H., 2002. Sediment supply-limited bedforms in sand–gravel bed rivers. Journal of Sediment Research 72, 629–640.
- Mosher, D.C., Thomson, R.E., 2000. Massive submarine sand dunes in the eastern Juan de Fuca Strait, British Columbia. In: Trentesaux, A., Garlan, T. (eds.), Marine Sandwave Dynamics, 23–24 March 2000, University of Lille 1 (France), Proceedings, pp. 131–142.
- Shields, A., 1936. Anwendung der Ähnlichkeitsmechanik und der Turbulenzforschung auf die Geschiebebewegung. Preußische Versuchsanstalt für Wasserbau und Schiffbau, Mitteilungen 26, 26 pp.
- Simons, D.B., Richardson, E.V., 1966. Resistance to flow in alluvial channels. US Geological Survey, Washington D.C., Professional Paper 422-J.
- Sumer, B.M., Bakioglu, M., 1984. On the formation of ripples on an erodible bed. Journal of Fluid Mechanics 144, 177–180.
- Van den Berg, J.H., van Gelder, A., 1993. A new bedform stability diagram, with emphasis on the transition of ripples to plane bed in flows over fine sand and silt. IAS Spec. Publ. 17, 11–21.
- Yalin, M.S., 1977. Mechanics of Sediment Transport (2nd Edition). Oxford, Pergamon Press, 295 pp.
- Zanke, U., 1976. Über den Einfluß von Kornmaterial, Strömung und Wasserständen auf die Kenngrößen von Transportkörpern in offenen Gerinnen. Franzius-Institut, Hannover, Mitteilungen 44, 111 pp.

# Biennial survey method of marine dunes in the French part of the North Sea shipping channel

Thierry Garlan *Shom, Brest, France – Thierry.garlan@shom.fr*

Emeric Brenon *Shom, Brest, France – Emeric.Brenon@shom.fr*

**ABSTRACT:** After a period of recurrence of three years for surveying and charting sand dune dynamics of some areas of the French part of the North Sea shipping channel, a decennial survey of the entire channel was realized. The measured movements served to propose a new monitoring approach of the channel based on the Multibeam Echo Sounder biennial survey of a few selected dunes. It was then decided that after a 10-year period, from 2013 to 2023, a decision would be made regarding the method of monitoring of this shipping lane. This paper presents the first results from the study of these 15 dunes surveyed in 2013, 2015 and 2017.

## 1. INTRODUCTION

During the 1980s, in the context of an agreement with the North Sea Hydrographic Commission (NSHC), the French Hydrographic Office conducted surveys of eight areas of the North Sea shipping lane which represents a quarter of all the area. Initially, survey recurrence was of one, three and five years, but as dune movements were of the same order as the location precision of this time, it was rapidly decided to perform these surveys only every three years. After data analysis, it appeared that the boundaries of these areas did not match the most hazardous sectors for shipping; in 1997 we proposed to replace these surveys by a decennial hydrographic survey of the entire shipping channel, in order to produce an extensive overview of the dunes distribution.

The data analysis of these surveys provided knowledge on dunes, for example whether they are isolated or grouped in fields. The measured movement speeds on 113 dunes that had been surveyed several times gave values between 0 and 30 me-

ters/year, with slower movement observed in the dune fields compared to isolated dunes and the highest speeds in the underflow shear areas. Our results, obtained by the classical method of crest location to analyse rhythmic bed patterns, are comparable to those of scientific literature (Knaapen, 2004). This analysis was used to define a number of indicators characterising those dunes which are considered a hazard to shipping. Subsequently, a suggestion was made to monitor channel based on a few selected dunes, instead of the initially considered indefinite repeat of the decennial survey. Based on studies conducted since the 1990s a list of 15 dunes requiring biennial surveys was drawn up. It was then decided that, after a 10-year period (2013 – 2023), a decision would be made regarding the monitoring of this shipping lane. Indeed, as dune movements are slow, we need to wait at least 10 years to be able to draw any conclusion from this new mode of dune monitoring. The purpose of this paper is to present the results from the study of these 15 dunes surveyed in 2013, 2015 and 2017. This new method for the resurveying of sand dunes areas is different from the one used in other Hydrographic Offices of the North Sea (Dorst *et al* 2013). This is not due to the

reduction in bathymetric survey capacity, but to the necessity to deploy the hydrographic survey capacities in other zones of the French continental shelf where the last bathymetric data were acquired before the Second World War.

## 2. DUNES BIENNIAL SURVEYS

The complete survey of the French part of the North Sea shipping channel displayed a number of sediment cells (Figure 1), which can be distinguished by the north-easterly or south-westerly direction of dune movement. In these cells, fifteen dunes were selected as the most representative of these cells and more generally of this part of this channel. Hydrographic surveys of these dunes were done in 2013, 2015 and 2017. We present here these initial data which have been studied to assess the need to adapt the survey procedure.

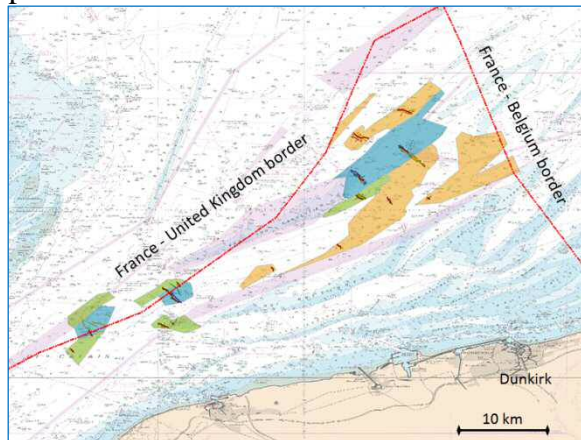


Figure 1. Location of sediment cells according to the direction of dune movement (■: movement towards the south-west; ■: movement towards the north-east; ■: undetermined movement).

### Overview of initial guidelines

Geographical cells have been defined all along the French part of the North Sea shipping channel according to their depth, height and movement speed characteristics. One or two dunes have been selected in each of these cells. For each dune, the hydrographic survey starts with one or two cross profiles that allows marking the position of the crest and its external limits. The survey continues with a series of profiles, longitudinal to the crest, to cover the entire dune. A Digital

Elevation Model (DEM) constructed from the data is intended to allow the calculation of volumes and slope angles required for the study of sediment dynamics and to configure future models.

The dune surveys are conducted:

- always at the same period of the year, in order to ensure similar hydrodynamic conditions and to guarantee similar times between surveys. So the three first surveys were all done in July;
- in a single survey operation (i.e. over a period of one to two weeks), such that all the dunes may have experienced the same tide and storm conditions.

As one of the surveys of Dune 3 is not complete, the three surveys of 2013, 2015 and 2017 were compared for each of the 14 other dunes, between themselves and against previous MBES data (Figure 2).

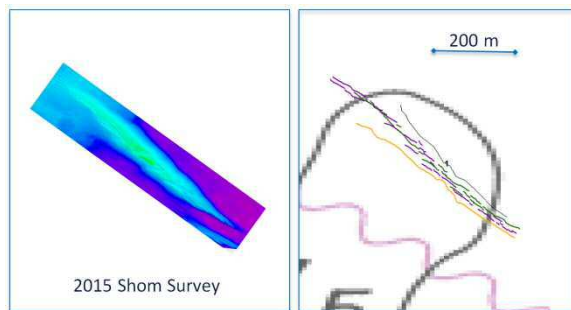


Figure 2. DEM of D1 in 2015 and evolution of the crest of Dune 1 in 2002: —, 2013: —, 2015: —, 2017: —)

### Midway overview of biennial surveys of North Sea dunes

The Shom (French National Hydrographic and Oceanographic Office) is developing a new software to calculate dune parameters (Ogor, 2018), to replace the previous software "DuneS". For this initial study, mean dune travel is calculated from between crest measurements made at 10 points regularly spaced along previously digitised crests. Dunes do not move in a uniform manner and different sections of a dune may move in opposite directions. By convention, northwards movements are considered to be positive, while southwards movements are negative. Dune movement is thus expressed as a mean movement, which is reduced in the presence of such inversions.

### i. Direction of dune movement

The first observation derived from the study of biennial surveys is that the dunes occasionally display inversion in their direction of movement (Figure 2). Table 1 summarizes these observations (Table 1). Grey cells indicate movement to the north-east or north, while the others represent movement to the south-west or south.

Our previous studies established that the movements of dunes 1, 4, 6 and 10 were to the north-east or north, that the dunes 2, 5, 7, 8, 11 and 14 movements were to the south-west or south, that the dunes 9, 12, 13 and 15 were stable.

Table 1: Direction of dune movements for the various time periods: to the north-east or north (N to NE), to the south-west or south (S to SW), and stable dunes (*Stable*).

	X-2013	2013-2015	2015-2017	X to 2017
D1	S to SW	N to NE	S to SW	S to SW
D2	S to SW	N to NE	S to SW	S to SW
D4	N to NE	N to NE	S to SW	S to SW
D5	S to SW	N to NE	N to NE	N to NE
D6	S to SW	N to NE	N to NE	N to NE
D7	S to SW	N to NE	S to SW	S to SW
D8	S to SW	N to NE	S to SW	S to SW
D9	<i>Stable</i>	N to NE	<i>Stable</i>	<i>Stable</i>
D10	N to NE	N to NE	N to NE	N to NE
D11	S to SW	S to SW	S to SW	S to SW
D12	<i>Stable</i>	N to NE	<i>Stable</i>	<i>Stable</i>
D13	<i>Stable</i>	N to NE	<i>Stable</i>	<i>Stable</i>
D14	S to SW	S to SW	S to SW	S to SW
D15	<i>Stable</i>	N to NE	S to SW	S to SW

Upon completion of the analysis of biennial surveys (Table 1), it appears that:

- the 2013-2015 period displayed overall northward movement,
- only dunes 11 and 14 did not move in this northward direction during this period, possibly due to their protection by the *Sandettié* shoal,
- dunes 9, 12 and 13, classified as stable, i.e. displaying speeds of less than or equal to 1 m/year, displayed for the 2013-2015 period a northward movement at speeds of 6 to 8 m.

With the exception of dunes 10, 11 and 14, all of the dunes display back and forth

movements, as had already been observed on several dunes in the south of this zone (Le Bot et al., 2000). As the number of spring tides is of the same order each year, tidal forcing is similar and cannot explain such movement inversions. The observed movements are thus likely to be the result of surge currents caused by storms.

The inversion in the direction of movement observed here shows that the phenomenon is at a regional scale. That or those storm(s) amplified the speed of dunes which has a similar direction of movement to that of the storm (D10), it generated a slower apparent movement for dunes conventionally moving towards the south (D1, 2, 7, 8, 11, 14) and it triggered the movement of normally immobile dunes (Dune 9, 12 and 13). The too large time period between the surveys prevents us from determining whether this northward movement arose from the impact of several storms or from the cumulative impact of a powerful storm during a spring tide. Subsequent surveys, along with the studies that will be conducted on the relation between inversion and climate would enable us to determine the storm conditions that generated this phenomenon. The quarterly surveys scheduled in the context of the DUNES project, submitted to the latest France Energie Marine call for tenders, could supplement the biennial surveys to provide information regarding the short-term effects of storms.

### ii. Speed of dune movement

The mean annual movement for the various periods (Table 2) shows that the storm phenomenon, previously mentioned, causes dune 10, which is the only one to systematically have northward movement, to display during the 2013-2015 period a speed 11 m higher than its usual speed. Over this period, it displayed a movement of 34 m/year. Conversely, the speed of movement of those dunes that usually move southwards dropped during this period, even reversing for dunes with a usually low southward dynamic. Finally, the 3 stable dunes displayed mean northward migration rate of 6 to 8 m/year during this period.

Table 2: Migration rates in meters per year of the 14 dunes included in the biennial surveys

	X - 2013	2013-2015	2015-2017	X-2017
D1	7.1	<b>23.1</b>	2.3	2.5
D2	8.3	11.5	13.8	6.8
D4	4.1	15.5	9.7	4.0
D5	1.5	<b>22.9</b>	9.1	5.8
D6	7.2	<b>22.4</b>	6.7	1.0
D7	5.6	6.2	7.7	2.7
D8	7.5	8.7	4.0	4.6
D9	0.4	7.7	1.0	0.6
D10	<b>24.6</b>	<b>34.4</b>	<b>22.8</b>	26.3
D11	12.3	10.5	9.5	11.8
D12	0.4	8.3	0.0	0.4
D13	0.5	6.1	0.3	0.7
D14	7.8	2.3	6.0	5.8
D15	0.6	5.2	3.3	2.3
<i>Mean</i>	6.3	13.2	6.9	

From this table we can put forward the following hypothesis:

- the storm or storms generated a movement of all dunes of circa 15 m northward.
- stable dunes may in fact move, but the slow southward movements of only a few meters per year caused by the tidal currents would appear to compensate by the inverse currents of storm surges.

To be confirmed, these hypotheses will obviously need to be substantiated by new data and by a study of storm activity.

A previous analysis of MBES surveys conducted by the Shom from 2000 to 2007 allowed the migration rate of 113 dunes to be measured. Those rates, compared to the results of the biennial survey (Table 3), show that movements for the 2013-2015 period are comparable to the means obtained for the 113 dunes of the previous surveys. As the extreme and mean values are comparable, this confirms that the group of 14 dunes is relatively representative of the shipping lane, but we need more recurrences to draw further conclusions.

Table 3: Comparison of mean dune speeds in meters/year from previous surveys with those from the biennial surveys

	Speed of 113 dunes	Speed of the 14 biennial dunes		
		2000-2007	X-2013	2013-2015
min	0.0	0.4	2.3	0.0
mean	10.2	6.3	13.2	6.9
max	32.1	24.6	34.4	22.8

### iii. Dune height variability

During the pre-2011 studies on the few available MBES surveys, it was noted that dune height appeared to vary from one survey to the next. Megaripple dynamics superimposed on dunes and dune deformation during migration may cause longitudinal changes in the high point of the dune along its crest over time. While the crest-line can easily be digitized, calculating dune height is more complicated: the results must be reworked with the dune automatic parameter calculation software not to be attributable to human interpretation. The height of the 14 dunes, defined between the base of the dune and its highest point for the 3 biennial surveys provide new elements regarding dune height. The observed variations are greater than previous data had suggested, so it seems that the risk, from a hydrographic standpoint, seems to be significant (Table 4).

Table 4: Maximum dune height of the dunes in meters

	2013	2015	2017	$\Delta$ max
D1	7.0	7.6	8.7	1.7
D2	6.7	8.5	7.9	1.8
D4	5.1	6.7	7.4	2.3
D5	4.0	6.0	6.4	2.4
D6	5.0	5.9	8.3	3.3
D7	7.3	8.0	8.0	0.7
D8	6.4	8.0	7.2	1.6
D9	5.5	4.9	4.0	1.5
D10	4.0	3.4	4.5	1.1
D11	4.3	6.0	6.4	2.1
D12	2.5	3.4	5.2	2.7
D13	3.0	2.0	2.0	1.0
D14	5.0	7.3	6.7	2.3
D15	5.0	8.2	8.6	3.6
<i>Mean</i>	5.1	6.1	6.5	

As a first approximation, the mean height of the 14 dunes increased progressively between 2013 and 2017; this progression was very clear for dunes 1, 4, 5, 6, 11, 12 and 15. This appears correlated neither to the direction, nor to the speed of movement. With the exception of dune 7, this increase seems major as the height difference for some dunes is greater than 50%. This change in dune height may come from:

- the improvement in MBES accuracy, leading to improved integration of mega-ripples covering the dunes,
- the action of storms, which tend to level the tops of the dunes, and from tidal currents which tend to rebuild them,
- the faster movement of small dunes, which, by combining with the larger dunes, can in theory increase their volume,
- changes in sediment granularity; an increase in grain size leading to an increase in height (Flemming, 2000).

It first appears important to be able to confirm these observations through an automated calculation, which should be more precise thanks, for example, to the integration of the slope effect. This software calculation will serve to consolidate the results, to allow comparison to previous surveys and to supplement this parameter with the study of dune top depth. It will also be necessary to study the behaviour of small dunes located upstream. This already implies that the survey area around each dune must be increased to systematically encompass the entire dune and dune crest located upstream.

#### Addition of 6 new dunes

The north eastern part and the region bordering Belgium were recently surveyed, leading to the definition of 5 new dunes selected for their height and their representativeness. They will be added to upcoming biennial surveys. Moreover, an area close to the Sandettié Sandbank presents barchans which display the highest movement speeds observed in this region (more than 50 m/y).

So, 21 dunes will be studied for the next biennial surveys (Figure 3).

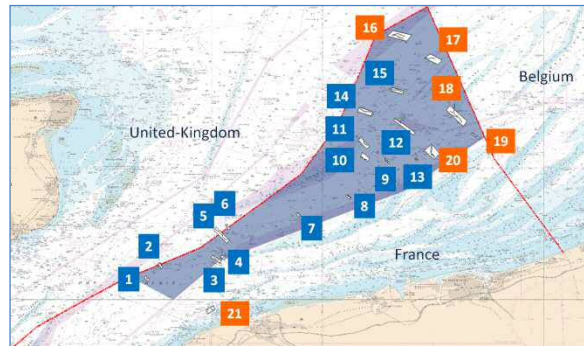


Figure 3: the shipping lane and tracking of dunes to survey during the biennial surveys

### 3. CONCLUSIONS

Dune movements obtained by analysis of the latest surveys are nearly all smaller than those predicted in 2011 based on the analysis of older surveys. This may be ascribed to improved tracking precision and better accuracy of the MBES, allowing the observation of previously difficult to distinguish mega-ripples. The dune crests, which appeared continuous and linear in previous low resolution Multibeam Echo-Sounder survey, are now frequently defined by series of sections separated by several meters. The speed change is, however, also due to an exceptional storm, or to several storms that occurred during the 2013-2015 period. This event leading to a generalized dune migration to the north, whereas the dune movement is usually variable. This phenomenon may be exceptional, but it could also be caused by climate change and the evolution of storm activity.

Of all the fifteen monitored dunes, the one that display the greatest movement is dune 10, which travelled 290 m in 11 years. This represent a difference of 0.4 cm on the local chart at 1/75000 scale. All the other dunes give a difference in positioning on the chart of less than 1.6 mm after a period of 10 years. Those results support shipping safety and confirm that an exhaustive survey of the shipping lane is not at this stage necessary.

Analysis of the 2013, 2015 and 2017 surveys shows that the survey methods need to be refined. It appears necessary, in particular, to specify the areas to be covered rather than defining the survey areas on location. Therefore polygons within which the dunes should be located in the next 6 years have been defined for the future surveys.

As dune height is linked to sediment grain size, it would appear necessary to collect sediment samples from at least 2 or 3 of the dunes most sensitive for this parameter. The aim of future models will mainly be to calculate dune height variability along with the theoretical maximum height. During the upcoming three surveys, sediment samples should be collected from 2 dunes displaying significant heat variations.

From now to 2023, we shall conduct the following studies:

- about temporal variation of dune grain size distribution and height
- on survey procedure according to dangerousness of dunes defined by height, depth and relation between the movement speed to the representation chart scale.

Upon completion of the 10-year biennial survey period, i.e. in 2023, the North Sea hydrographic survey procedure will be redefined. It does not currently appear possible to further reduce the hydrographic surveys. The possibilities considered for the 2023-2033 period are:

- to continue the biennial surveys.
- to adapt these biennial surveys during a further decennial cycle by performing surveys every 2 years for dunes having displayed movements of more than 20 m, and every 4 years for all the 21 dunes.
- to continue the biennial surveys, supplementing them with some surveys of sectors having displayed large changes.
- if the height variability studies confirm the increase observed over the 2013-2017 period, to resume the surface survey of all sectors where the dune tops are, or could

have been, at a depth of less than or equal to 26 meters; international regulations impose that such depths must be guaranteed.

The biennial survey data acquired between 2013 and 2023 will provide a sufficient dataset to enable the sediment dynamics modelling expert to study and validate the modelling of the shipping lane dunes. The aim is to have, by 2025, a model capable of calculating dune movements and height changes in order to predict the date and location of surveys to conduct.

## ACKNOWLEDGEMENT

We would like to thank the Officers and crew of BH2 Lapérouse, Laplace and Borda, and the hydrographers of the Group Hydrographique et Océanographique de l'Atlantique (Shom/GHOA).

## 4. REFERENCES

- Dorst, L., Dehling, T., Howlett, C., 2013. Developments in North Sea wide resurveying and charting of dynamic sand wave areas. Proc. Marine and River Dune Dynamics (MARID IV), Bruges, Belgium, 81-88.
- Flemming, B.W., 2000. The role of grain size, water depth and flow velocity as scaling factors controlling the size of subaqueous dunes. Proc. Marine Sandwave Dynamics, Lille, France, 55-61.
- Knaapen, M.A.F., 2004. Measuring sand wave migration in the field. Comparison of different data sources and an error analysis. Proc. Marine Sandwave and River Dune Dynamics (MARID II), Enschede, the Netherlands, 152-160.
- Le Bot, S., Trentesaux, A., Garlan, T., Berné, S., Chamley, H., 2000. Impact of storms on tidal dune mobility on the Pas-de-Calais strait. Oceanologica Acta, 23/2, 129-141.
- Ogor, J., 2018. Design of algorithms for the automatic characterization of marine dune morphology and dynamics. PhD Thesis, University of Bretagne Occidentale-DGA, 255 pp.

# River dune based roughness uncertainty for the Dutch Rhine branches

Matthijs R.A. Gensen *University of Twente, Enschede, Netherlands – m.r.a.gensen@utwente.nl*

Jord J. Warmink *University of Twente, Enschede, Netherlands – j.j.warmink@utwente.nl*

Suzanne J.M.H. Hulscher *University of Twente, Enschede, Netherlands – s.j.m.h.hulscher@utwente.nl*

**ABSTRACT:** This work aims to establish discharge-dependent main channel roughness scenarios due to dune dynamics for the four largest Dutch river Rhine branches. Roughness predictions were made using three roughness predictors with dune measurements as input. Although a large scatter in the roughness predictions was observed, roughness scenarios were established for all branches. These scenarios indicate a bandwidth of expected roughness values. As expected from literature, increasing main channel roughness is observed with increasing discharge. The large spreading in main channel roughness is expected to significantly affect local water levels in the river system.

## 1. INTRODUCTION

Hydraulic models are widely used to predict water levels in river systems (Warmink et al. 2013). These hydraulic models are an interpretation of the physical river system. Any model representation goes hand in hand with model uncertainties. For river systems the most important sources of uncertainty are the upstream discharge and the main channel roughness (Warmink et al. 2013, Bozzi et al. 2015). Under the new Dutch probabilistic flood risk approach it is required to explicitly account for these uncertainties in the design and assessment of flood protection systems (Ministerie van Infrastructuur & Milieu, 2016).

In hydraulic modelling the main channel roughness is widely used as a calibration parameter, thereby marginalizing the connection with actual physical behaviour of river dunes. However, this connection is required for accurate uncertainty assessment. Physically, it is expected that dunes grow in height for an increasing discharge and slowly decrease in size for the falling stage of a discharge wave (Julien et al. 2002). This general discharge-dependent behaviour is observed in various large

rivers, e.g. the Mississippi river (Julien et al. 1995) and the Upper Rhine (Julien et al. 2002, Warmink et al. 2013). Observations have shown that dunes in some rivers do not show this consistent behaviour, e.g. the river Waal (Frings & Kleinhans, 2008). At the same time a large spread in dune heights for the same hydraulic conditions is often observed. These uncertain dune dynamics strongly affect the predictions of main channel roughness.

This study aims to quantitatively estimate the uncertainty range in main channel roughness due to the presence of river dunes for a range of hydraulic conditions. This uncertainty is expressed in roughness scenarios for various river branches. The purpose of these scenarios is using them in a system analysis of a bifurcating river system. Predictions for hydraulic roughness due to river dunes are carried out for 7 locations in the three branches in the Dutch river Rhine after the river has bifurcated (Fig. 1).

The outline of this paper is as follows. In section 2, the domain is characterized, the available data sources are shown, the roughness predictors are introduced and the method to construct roughness scenarios is described. In section 3 the results are shown

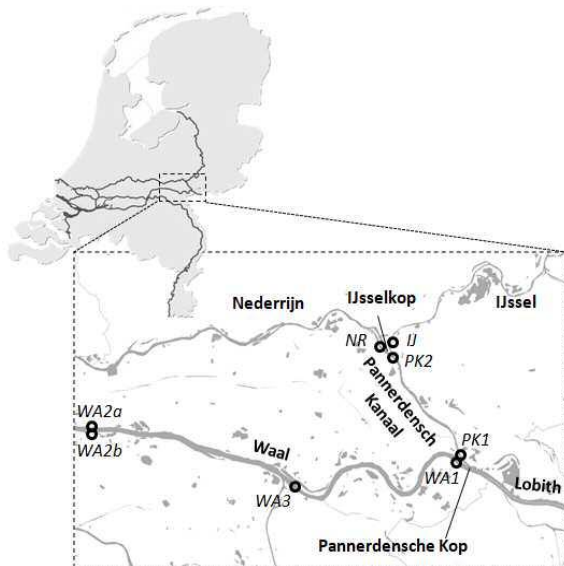


Figure 1. Area of interest. The circles indicate the locations at which dune measurements are available (Table 2). Locations WA2a and WA2b are the northern and southern half of the local main channel.

if the data is implemented in the roughness predictors. From these data points roughness scenarios for every branch are set up. The final two sections are a discussion and a conclusion, respectively.

## 2. METHODOLOGY

### 2.1 Domain description

The domain for this study consists of the four largest Dutch Rhine branches shown in Figure 1. Just after entering the Netherlands at Lobith, the Rhine splits into the Waal and the six kilometer long Pannerdensch Kanaal. Subsequently, the Pannerdensch Kanaal splits into the Nederrijn and IJssel. General characteristics of these Rhine branches are shown in Table 1.

Table 1: General characteristics of the Dutch Rhine branches

Branch	Discharge [m <sup>3</sup> /s]	Water depth [m]	Mean flow velocity [m/s]	D50 [mm]
Waal	500-11000	1.5-17	0.7-2.0	0.5-2.0
Pan.Kan.	50-6000	1.5-17	0.3-1.5	2.0-9.0
IJssel	50-2700	1.5-13	0.5-2.0	1.0-9.0
Ned.Rijn	0-3400	1.5-13	0-1.5	0.5-5.0

Table 2: Available dune measurements of Wilbers & Ten Brinke (2003; WB03), Sieben et al. (2008; SI08) and Frings & Kleinhans (2008; FK08). The locations are shown in Figure 1.

Source	# data points	Location	Period
WB03	38	WA1	1997-1998
WB03	84	WA2a	1989-1998
WB03	49	WA2b	1994-1998
WB03	31	PK1	1997-1998
SI08	94	WA3	2002-2003
FK08	5	PK2	Jan. 2004
FK08	5	IJ	Jan. 2004
FK08	5	NR	Jan. 2004

### 2.2 Available data

In several studies the elevation of the river bed of the Dutch Rhine branches has been measured, from which dune characteristics were deduced (Table 2). Additionally, corresponding data on discharges, water levels, flow velocities in the main channel and grain characteristics are available. The amount of available data differs significantly between the branches. Dunes in the river Waal have been measured multiple times, for different hydraulic conditions and at different locations. However, for the rivers IJssel and Nederrijn dune characteristics are only available for a short period in 2004 during low discharge and at one location per branch.

### 2.3 Roughness predictors

The dune characteristics are translated into main channel roughness values using the formulation of Van Rijn (1993). This method is widely used due to its good match with both flume data as well as data from rivers. To account for uncertainty in the choice of roughness predictor the predictors of Wright & Parker (2004) and Vanoni & Hwang (1967) are added. Along with Van Rijn's predictor these predictors perform well for a section of the Upper Rhine between Lobith and Pannerdensch Kop (Warmink et al. 2013). While the Van Rijn predictor uses only dune characteristics, the Vanoni & Hwang predictor additionally uses water

depths and flow velocities. The Wright & Parker predictor is only based on water level and flow velocity data along with general grain characteristics. For location WA3 only the Van Rijn predictor is applied as water depth and flow velocity data is not available for this location.

The Nikuradse roughness height was selected as roughness parameter, because in a conversion to a different roughness parameter the water depth is required, which cannot be obtained objectively for all hydraulic conditions as it would always require the use of a hydraulic model for extreme conditions.

#### 2.4 Roughness scenarios

For each branch an upper and a lower roughness scenario is defined for the range of discharges (Table 1). The two scenarios per branch present the realistic bandwidth of main channel roughness values. Therefore, they be used as input for hydraulic modelling in which the propagation of uncertainties to water levels can be determined.

The scenarios are defined based on dune theory as well as a visual inspection of the data. Wherever unrealistic roughness values are predicted by a predictor, which is the case for the Wright & Parker predictor, these values are discarded from the analysis. Linear functions of discharge versus roughness height are chosen as a first order estimate of the discharge-dependency. Hysteresis is expected to cause non-linear effects which are not taken into account in this analysis.

As theory predicts increasing dune heights and associated roughness for an increasing discharge the roughness scenarios are defined with a positive slope. The slopes are based on the average trend in the data of the river Waal as for this branch sufficient data is available. For the other branches the slopes of the scenarios are assumed equal to that of the Waal as for these branches insufficient data is available to independently estimate a slope. It is thus assumed that the discharge-dependent behaviour of the dunes is similar.

For the Pannerdensch Kanaal the intercept of the upper scenario is changed to represent the observed roughness values. Subsequently, this upper scenario for the Pannerdensch Kanaal is also used for the IJssel and Nedderrijn as for these branches too little data is available and the characteristics are more similar to that of the Pannerdensch Kanaal than to the Waal (Table 1).

### 3 RESULTS

Figure 2 shows the defined roughness scenarios along with the roughness predictions for the available dune data using the three roughness predictors.

It is observed that the dunes are higher in the Waal river compared to the other branches, which also leads to higher main channel roughness values. This is likely caused by the relatively coarse-grained river beds of the Pannerdensch Kanaal, IJssel and Nedderrijn.

It is also observed that the Wright & Parker formulation predicts significantly different roughness heights compared to the other two predictors. It predicts unrealistically high and unrealistically low roughness values for the fine-grained and coarse-grained branches respectively.

### 4 DISCUSSION

Using the roughness predictors of Van Rijn (1993), Vanoni & Hwang (1967) and Wright & Parker (2004) roughness scenarios were defined using dune and hydraulic data from the Dutch Rhine branches. Even though little data was available for the IJssel and Nedderrijn branches, roughness scenarios for these branches were defined using information from the other branches.

The results indicate a discharge-dependent main channel roughness, which is consistent with literature (Julien et al. 2002, Naqshband et al. 2014). However, this discharge-dependency is not as large as for the upper Rhine (Warmink et al. 2013).

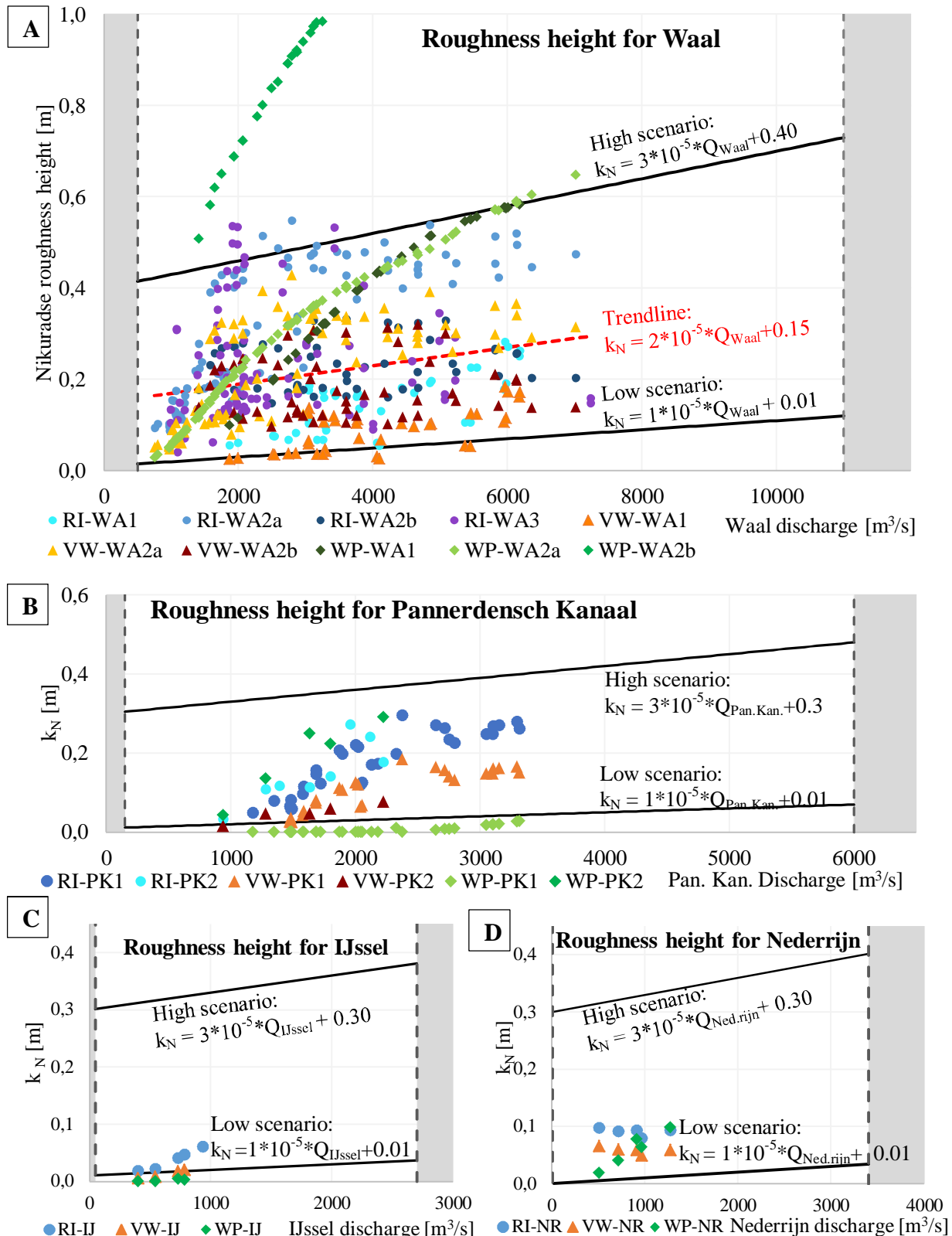


Figure 2: Nikuradse roughness heights calculated with the Van Rijn (RI), Wright & Parker (WP) and Vanoni & Hwang (VW) roughness predictors for the available data in the respective branches: (A) Waal, (B) Pannerdensch Kanaal, (C) IJssel, (D) Nederrijn. The black lines indicate the visually constructed roughness scenarios constructed. For the IJssel and Nederrijn branch the roughness scenarios are similar to those of the Pannerdensch Kanaal. The red dotted line in plot (A) shows the linear trend through the RI and VW data. The Wright & Parker predictor is discarded from the analysis wherever it gives unrealistic roughness values.

This inconsistency was also observed by Frings & Kleinhans (2008). In cases where the flow strength is large enough during very high discharges, upper stage plane bed (USPB) may develop. It is not known whether this will occur in any of the Dutch Rhine branches (Hulscher et al. 2017). If it is able to develop at high discharges, grain roughness may be an indication of the roughness values. With 90<sup>th</sup> percentile grain sizes in the order of 10 mm (Frings & Kleinhans, 2008), the grain roughness is in the order of 0.03 m ( $k_N = 3*D90$ . Van Rijn, 1993). For the smaller IJssel and Nederrijn branches, the lower scenario is in the same order of magnitude and may be an estimate for the roughness under the influence of upper stage plain bed.

Furthermore, a large spreading in dune heights and subsequent roughness predictions is observed. This demonstrates the large uncertainty involved with main channel roughness. Partly this uncertainty is caused by inaccuracies in the methods to deduce dune characteristics from longitudinal river profiles.

In this paper the roughness scenarios have been defined under the assumption of similar dune dynamics on the various branches. The stronger discharge-dependency of main channel roughness for the Pannerdensch Kanaal is an indication that differences between the dune dynamics for the branches exist. Such variations in dune dynamics in the considered branches have also been found by Frings & Kleinhans (2008). It is therefore possible that the assumption of similar dune dynamics in the branches is not fully valid.

The roughness scenarios serve as input for a sensitivity analysis in the bifurcating river system. It is expected that the wide ranges of main channel roughness values expressed in the roughness scenarios cause a large spread in modelled water levels for the analysed river branches.

## 5. CONCLUSIONS

This abstract has presented roughness predictions and extreme scenarios for the Dutch Rhine branches. The results showed that the dune dynamics and its resulting main channel roughness are not significantly discharge-dependent for the analysed branches, with the exception of the Pannerdensch Kanaal. The uncertainty in main channel roughness is large, which is indicated by the large spread in the roughness predictions.

Future work should aim at improving the roughness scenarios by including more dune data, especially for the IJssel and Nederrijn branches. Subsequently, the roughness scenarios can be used to estimate the effect of the main channel roughness on the water levels in the river Rhine system.

## 6. ACKNOWLEDGEMENTS

This work is part of the Perspectief research programme All-Risk with project number P15-21, which is (partly) financed by the Applied and Engineering Sciences domain of The Netherlands Organisation for scientific research (NWO-TTW).

## 7. REFERENCES

- Bozzi, S., Passoni, G., et al., 2015. Roughness and discharge uncertainty in 1D water level calculations. *Environmental Modeling and Assessment* 20, 343-353. doi:10.1007/s10666-014-9430-6
- Frings, R.M., Kleinhans, M.G., 2008. Complex variations in sediment transport at three large river bifurcations during discharge waves in the river Rhine. *Sedimentology* 55, 1145-1171. doi: 10.1111/j.1365-3091.2007.00940.x
- Hulscher, S.J.M.H., Daggenvoorde R.J., Warmink J.J., Vermeer, K., Van Duin, O., 2017. River dune dynamics in regulated rivers. 4th ISSF, Eindhoven.
- Julien, P.Y., Klaassen, G.J., 1995. Sand-dune geometry of large rivers during floods. *Journal of Hydraulic Engineering* 121, 657-663
- Julien, P.Y., Klaassen, G.J., Ten Brinke, W.B.M., Wilbers, A.W.E., 2002. Case study: bed resistance of Rhine river during 1998 flood. *Journal of Hydraulic Engineering* 128, 1042-1050

- Ministerie van Infrastructuur en Milieu, 2016. Achtergronden bij de normering van de primaire waterkeringen in Nederland.
- Naqshband, S., Ribberink, J.S., Hulscher, S.J.M.H., 2014. Using both free surface effect and sediment transport mode parameters in defining the morphology of river dunes and their evolution to upper stage plane beds. *Journal of Hydraulic Engineering* 160. 06014010.
- Sieben, J., 2008. Taal van de rivierbodem. Rijkswaterstaat.
- Van Rijn, L.C., 1993. Principles of sediment transport in rivers, estuaries and coastal areas. Blokzijl, Aqua Publications.
- Vanoni, V.A., Hwang, L.S., 1967. Relation between bedforms and friction in streams. *Journal of the Hydraulics Division* 93, 121-144
- Warmink, J.J., Booij, M.J., Van der Klis, H., Hulscher, S.J.M.H., 2013. Quantification of uncertainty in design water levels due to uncertain bed form roughness in the Dutch river Waal. *Hydrological Processes* 27, 1646-1663. doi:10.1002/hyp.9319
- Wilbers, A.W.E., Ten Brinke, W.B.M., 2003. The response of sub-aqueous dunes to floods in sand and gravel bed reaches of the Dutch Rhine. *Sedimentology* 50, 1013–1034. doi: 10.1046/j.1365-3091.2003.00585.x.
- Wright, S., Parker, G., 2004. Flow resistance and suspended load in sand-bed rivers: simplified stratification model. *Journal of Hydraulic Engineering* 130, 796-805. doi: 10.1061/(ASCE)0733-9429(2004)130:8(796)

# Towards open access of bed forms data, standardization of its analysis, and some steps to these ends

Ronald R. Gutierrez *University of the North, Barranquilla, Colombia* – [rgutierrezll@uninorte.edu.co](mailto:rgutierrezll@uninorte.edu.co)

Alice Lefebvre *MARUM, University of Bremen, Bremen, Germany* – [alefebvre@marum.de](mailto:alefebvre@marum.de)

Francisco Núñez-González, *Leichtweiß-Institut für Wasserbau, University of Braunschweig, Braunschweig, Germany* – [f.nunez-gonzalez@tu-braunschweig.de](mailto:f.nunez-gonzalez@tu-braunschweig.de)

Humberto Avila *IDEHA, University of the North, Barranquilla, Colombia* – [havila@uninorte.edu.co](mailto:havila@uninorte.edu.co)

**ABSTRACT:** This contribution highlights the challenges and opportunities for the community of coastal and fluvial engineers and morphologists to consolidate a paradigm of open and data-intensive scientific culture through for example data sharing, formal recognition of scientists who collect the data, free accessible code, and standardized procedures to collect and analyze data. We stress that the technical challenges can be tackled through the body of knowledge being built on the matter by some institutions such as the Federation of Earth Science Information Partners. We also underline the potential of Bedforms-ATM to standardize some bed forms data analysis techniques and enumerate the applications that could be developed and incorporated into it in the short term.

## 1 INTRODUCTION

Many rivers and coastal areas around the World are facing increasing demands on both land and water resources for human settlement growth, navigability, and energy. Thus, there is a necessity for improving the prediction of flow and sediment transport for a wide range of river sizes and coastal seas. Bed forms are ubiquitous features in shallow and deep-water environments, having a strong influence on flow properties and sediment transport; as such, a better understanding of their dynamics is of relevance for engineers, geomorphologists, and planners (Best, 2005; ASCE, 2002).

Despite the significant improvement on the scientific understanding of bed form dynamics from field, laboratory and numerical investigations performed in the last decades, many aspects remain obscure (Allen, 1983; Best, 2005). The availability of more sophisticated equipment (such as multibeam echo sounder) and data analysis techniques played an important role in this evolution by providing a large amount of detailed measurements which can be analyzed to help improve our knowledge on

the mutual interaction of bed forms and flow. However, these data may not always be freely available and are certainly not all analyzed in a standardized manner.

In recent years, the necessity for the scientific community to move towards a paradigm for open and free sharing of scientific data and software has been underlined (McNutt et al., 2016). Although some disciplines (e.g., astronomy and oceanography) have a long tradition of sharing data, we believe that it is fair to state that it is still a pending challenge for the community of engineers and scientists devoted to the analysis of river and coastal dynamics, as well as the community dealing with bed forms dynamics, which regularly meets at the MARID conference.

The objectives of this contribution are twofold, namely: [1] to discuss on the challenges and opportunities of open and free sharing of bed form data based on similar experiences from other disciplines, and [2] to identify the applications that can be added to Bedforms-ATM that potentially would help improve our understanding of bed form dynamics and/or standardize bed form data analysis.

## 2 CHANGING OUR PARADIGMS

### 2.1 The opportunity

To date, two paradigms are becoming more prevalent in scientific research, namely: openness, and data-intensive scientific approach, which may even turn into a big-data-intensive scientific approach soon. Openness [1] enhances the productivity and efficiency of research by preventing to repeat scientific studies; [2] is essential to the validation of hypothesis, theories, data, and results; and [3] helps to promote trust among scientists by fostering cooperation and collaboration. Openness demands not only allocating information but also allocating the necessary resources to understand, validate, and apply information such as data, results, methods, and tools (Resnik, 2006; McNutt et al., 2016).

Data-intensive scientific approach has called the attention of the scientific community and has become a new opportunity and incentive to knowledge discovery because it expands the correlations among multi-disciplinary data, which subsequently triggers the discovery of new models, new rules, and new knowledge (Hey et al., 2009; Guo et al., 2017). Some researchers (e.g., Peng et al., 2016) even propose that “universities, research institutions, and funding agencies should develop new measures to evaluate a research project’s success not only based on publications and other outcomes it produces but also based on the amount and quality of data it makes available for the wider user community and society.”

As it is the case in many disciplines, we believe that the aforementioned paradigms are not currently fully present in the coastal and river geomorphology community, and thus, it represents a pending challenge.

### 2.2 The challenges

Some cultural, institutional, and technological constraints limit openness in many scientific disciplines and possibly, by

extension, the evolution towards big-data-driven science. Based on the experience of some of the co-authors of this contribution, these limitations are more deeply present in the scientific community from developing countries. Cultural and institutional constraints will possibly be forced to change as many funding agencies and peer-reviewed journals have adopted regulations that require scientists to share data, results, methods, and tools (Resnik, 2006).

Data are often shared within a working group or with close collaborators before being published and declared to be openly available after publication (Buys et al 2015). This step of openly sharing of the data however is rarely completed. For instance, less than 1% of the collected ecological data is accessible after publication (Reichman et al., 2011), even though important discoveries were made by integrating large data sets from many systems, for example in ecology, and the potential benefits of data reuse and open data citation are widely recognized (Hey et al., 2009; Lindenmayer & Likens, 2013, Piwowar & Vision, 2013). Other disciplines, such as genomics, have shared repositories, chiefly due to the homogeneity of their data (Reichman et al., 2011). Past research has underlined the necessity for having access to large amounts of bed form data from well-documented theoretical and experimental case histories, and the need for integrated interdisciplinary studies to fully understand the morphodynamics of bed forms (Allen, 1983; Dalrymple and Rhodes 1995; Best, 2005).

Some researchers (e.g., Kowall et al., 2014; Lefebvre & Winter, 2016; Winter et al., 2016; Gutierrez, 2017) have made bed form data publicly available. For instance, Gutierrez (2017) published synthetic bed form data, which contains ripple, dune, and bar-like features that can be used to assess bed form hierarchization techniques. Likewise, Gutierrez et al. (2018) reported the development of Bedforms-ATM, a free available software for bed forms data analysis, which also provides field bed forms data from the Parana River, Argentina.

We believe that two major technological challenges will arise in the effort to changing our paradigms, namely: [1] dealing with the heterogeneity of bed form data that results from the lack of common experimental practices, field measurement standards, and data analysis (Reichman et al., 2011; Gutierrez et al, 2013); and [2] tracking the provenance of data derived from original data sets, and the scientific outcomes stemming from them through quality control, analysis, and modeling (Reichman et al., 2011).

Despite the potential benefits of having access to massive bed form data collections, we must be aware that it might induce the proliferation of inductive science (i.e., developing research questions after having data), which, although a valid research method, may contradict the current workflow of science. It also opens the door for the existence of scientists who might hardly be motivated to gather data, because it is time and resource consuming, and who might simply take data gathered by others (Lindenmayer & Likens, 2013). This might be prevented nonetheless by following a good practice that those using open-access data sets must work in close collaboration with those who collected these data sets through co-authorship, attribution, or citation (Lindenmayer & Likens, 2013). Overall, it is recognized that data sharing increases citation rate (Piwowar et al., 2007) and we believe that it would advance bed form research in general and profit to all, those who initially collect and analyze the data and those who subsequently reuse them.

### **2.3 Tackling the technological challenges**

Data need to be stewarded throughout the entire data lifecycle, i.e. from data collection, to management of active data sets, to long-term archive. However, most disciplines still lack the technical, institutional, and cultural frameworks to support open data access (Peng et al., 2016).

The Federation of Earth Science Information Partners (ESIP) aims at making earth science data more discoverable, accessible, and usable. In this vein, the ESIP Data Stewardship Committee has provided a set of recommendations, best practices, and guidelines allowing to influence data management carried out by government agencies and other data stewards (Downs et al., 2015). ESIP proposed a provenance and context content standard (PCCS) which lists all content items required to fully represent the provenance and context of the data products resulting from earth science missions, namely: content item name, descriptive definition, rationale (why a given item is needed), criteria (how good the content should be), priority, user community (who would most likely use the item), source, project phase capture, representation (word files, numeric files, etc.), and distribution restrictions (e.g., proprietary concerns). PCCS presented these items in a matrix that is considered a good starting point for developing a standard to offer guidance for data producers, data managers, and others (Ramapriyan et al., 2012). ESIP has stated its openness to apply PCCS standards to other types of data and has encouraged the organizational and individual membership-based participation of earth science data providers (Downs et al., 2015). ESIP has also tested the data stewardship maturity matrix developed by Peng et al. (2015), which can be applied by data centers and other data-holding organizations.

We believe that the MARID conferences could be a unique platform to discuss on the creation, management, distribution, use, and citation of bed form data, which eventually might lead to devising an organization that can work in partnership with, for instance, ESIP. We are aware that for this end, funding, a cooperative attitude from the community of engineers and scientists, and the collaboration with public and private institutions, nongovernmental organizations, among others, will be necessary.

The bed form data set that can be potentially built does not necessarily have to be a single system. Instead, it can be made up of centralized multiple crowdsourced

open-access data entities. Large complex platforms such as the Digital Earth are usually built this way (Guo et al., 2017). It is expected that stewarded bed form data would potentially encompass heterogenous, multi-source, multi-temporal, multi-scale, high dimensional, highly complex, and unstructured geospatial data sets, which are typical characteristics of many geophysical signals datasets (Nativi et al., 2015).

### 3 TOWARDS BED FORM DATA ANALYSIS STANDARDIZATION

With more openly accessible bed form data, scientists will require more complex processing and data analysis tools. In this regard, code used to analyze, and process data will be a fundamental requirement for transparency and reproducibility (McNutt et al., 2016). We believe that the Bedforms-ATM platform by Gutierrez et al. (2018) could potentially be used to build such code.

Bedforms Analysis Toolkit for Multiscale Modeling (Bedforms-ATM) currently comprises the following applications: [1] Bed forms wavelet analysis; [2] Power Hovmöller analysis; [3] Bed forms multiscale discrimination, which discriminates bed form fields into three scale-based hierarchies (e.g., ripples, dunes, bars); and [4] Three-dimensionality analysis, which quantifies the three-dimensionality of bed form fields. Herein we enumerate the applications that can be incorporated into Bedforms-ATM in the short term for the analysis of both marine and fluvial bed forms.

#### 3.1 Atomization of bed form fields

The atomization of bed form fields, i.e. the identification and extraction of single bed form entities from bed form fields, and subsequent quantification of its geometric characteristics (e.g., stoss and lee side slopes, wavelengths, and amplitudes) provides information on the interactions of flow field, and suspended sediment (Best, 2005). Some researchers (e.g., van der Mark, 2008; Gutierrez et al., 2013) have

already presented methodologies to perform the atomization of bed form fields. These methods are easily reproducible or openly available and can therefore be used to standardize the atomization of bed form fields. They could be incorporated into Bedforms-ATM and be expanded to include, for example, a three-dimensional atomization.

#### 3.2 Bed form statistical analysis

Bed forms atomization is also necessary for identifying fully developed bed form fields in experimental environments and quantifying the variability of natural bed forms through statistical analysis (van der Mark, 2008; Gutierrez et al., 2013; Perillo et al., 2014; LeRoy et al., 2016). There is a body of evidences that suggest that large rivers are characterized by bed forms with leeside slope lower than the angle of repose. Thus, Best (2005) stated that the study of low-angle bed forms constitutes one of the main future research topics in the understanding of bed forms dynamics. To this end, sharing data from worldwide large rivers and standardizing bed forms atomization will be needed. A statistical analysis of bed form fields and their characteristics will enable a better characterization of their properties and provide possible explanation of their dynamics.

LeRoy et al. (2016) reported the development of SABAT (Slope-aspect bedform analysis tool), a Matlab tool that does not identify superimposed bed forms but performs a variety of statistical analyses on bed form' wavelengths and amplitudes. However, to the best of our knowledge, SABAT is not publicly available. Van der Mark et al (2008) quantified the variability in bedform geometry from a series of bathymetric measurements in the lab, in a small river (0.25 m water depth) and the Rhine (8 m water depth). Their analysis could be expanded and deepened in a variety of environment, especially in diverse large and small rivers, in order to statistically describe bed form parameters and their variability.

### 3.3 Characterization of experimental bed forms

Dumas et al. (2005) proposed a discrimination scheme for experimental bed forms resulting from oscillatory and combined flows. It is based on a wavelength threshold of 0.5 m for characterizing symmetrical small ripples, asymmetrical small ripples, symmetrical large ripples, and asymmetrical large ripples. This scheme has been successfully used in the past (e.g. Perillo et al., 2014). We believe that after developing a methodology for atomizing bed form fields, the scheme of Dumas et al., (2005) can be used to: [1] perform statistical analysis over single entities of bed forms, and [2], provided that enough information is available, study the time it takes for bed forms to become fully developed, which is of special concern for the understanding of bed forms morphodynamics (Allen, 1983; Best, 2005; Doré et al., 2016).

### 3.4 Characterization of marine bed forms

Bed forms in marine environments have a great variety of dimensions and shapes, for example small-scale ripples, tidal dunes and sand waves. They are found at a wide range of depth, from the intertidal zone to the continental rise and are subjected to diverse hydrodynamic forcings (e.g., regular and storm waves, and tidal, wave-induced or contourite currents). They also form in diverse sedimentary settings such as sand, mixed sediment or sediment starved. Extensive bed form fields are now well-known and the control of their morphology by environmental parameters is better understood (e.g. Damen et al, 2018). However, Garlan et al. (2016) invites for a renewed classification of marine bed forms following the recent improvement of bed form mapping and characterization. This could be done in the framework of a large collaboration bringing marine bed form data together to be analyzed in a standardized and comprehensive way.

## 4 CONCLUSIONS

Scientific openness, and data-intensive science are becoming more important in today's scientific inquiry; however, they are not currently prevalent in the community of fluvial and coastal morphologists and engineers. We believe that these paradigms open a myriad of possibilities to better understand the spatio-temporal mechanisms that govern the dynamics of bed forms, which, at present, remain obscure.

A change towards scientific openness will pose some technical challenges such as handling copious data, which involves transferring, storing, managing, processing, computing, and sharing such data. We believe that MARID represents a unique platform to discuss on the opportunities and challenges related to changing our scientific paradigm.

Bedforms-ATM can potentially be used as a common platform for standardizing bed form data analysis methodologies via the contribution of river and coastal engineers and scientists. In our opinion the following applications could be developed on the Bedforms-ATM platform in the short term: [1] an application to atomize bed form fields (i.e., identifying single bed form entities), [2] an application to perform statistical analysis over single bed form entities, [3] an application to discriminate experimental bed forms based on the Dumas et al. (2005) classification scheme, and [4] an application to classify marine bed forms.

## 5 ACKNOWLEDGEMENT

We acknowledge the Universidad del Norte and the IDEHA research group for funding this contribution. Alice Lefebvre is founded by the German Research Foundation (Deutsche Forschungsgemeinschaft, DFG), project number 345915838.

## 6 REFERENCES

- Allen, J. R. L. (1983). River bedforms: progress and problems. Modern and ancient fluvial systems, 6, 19-33.

- ASCE Task Committee on Flow and Transport over Dunes (2002). Flow and transport over dunes. *Journal of Hydraulic Engineering*, 128(8), 726-728.
- Best, J. (2005). The fluid dynamics of river dunes: A review and some future research directions. *Journal of Geophysical Research: Earth Surface*, 110(F4).
- Buyss, C. M., Shaw, P. L. (2015). Data Management Practices Across an Institution: Survey and Report. *Journal of Librarianship & Scholarly Communication*, 3(2).
- Dalrymple, R. W., & Rhodes, R. N. (1995). Estuarine dunes and bars. In *Developments in sedimentology* (Vol. 53, pp. 359-422). Elsevier.
- Damen, J. M., van Dijk, T. A. G. P., & Hulscher, S. J. M. H. (2018). Spatially varying environmental properties controlling observed sand wave morphology. *Journal of Geophysical Research: Earth Surface*,
- Doré, A., Bonneton, P., Marieu, V., & Garlan, T. (2016). Numerical modeling of subaqueous sand dune morphodynamics. *Journal of Geophysical Research: Earth Surface*, 121(3), 565-587.
- Downs, R. R., Duerr, R., Hills, D. J., & Ramapriyan, H. K. (2015). Data stewardship in the earth sciences. *D-Lib Magazine*, 21(7/8).
- Dumas, S., Arnott, R. W. C., & Southard, J. B. (2005). Experiments on oscillatory-flow and combined-flow bed forms: implications for interpreting parts of the shallow-marine sedimentary record. *Journal of Sedimentary research*, 75(3), 501-513.
- Garlan T., Brenon E., Marchès E., Blanpain O., 2016. From regional variability of the morphology of dunes to a new method of their classification. *Proceedings of Marine and River Dune Dynamics – MARID V – 4 & 5 April 2016 – North Wales, UK*, 4pp
- Guo, H., Liu, Z., Jiang, H., Wang, C., Liu, J., & Liang, D. (2017). Big Earth Data: a new challenge and opportunity for Digital Earth's development. *International Journal of Digital Earth*, 10(1), 1-12.
- Gutierrez, R. R., Abad, J. D., Parsons, D. R., & Best, J. L. (2013). Discrimination of bed form scales using robust spline filters and wavelet transforms: Methods and application to synthetic signals and bed forms of the Río Paraná, Argentina. *Journal of Geophysical Research: Earth Surface*, 118(3), 1400-1418.
- Gutierrez, R. R. (2017): Synthetic data for the Bed-forms Analysis Toolkit for Multiscale Modeling (Bedforms-ATM). PANGAEA, <https://doi.org/10.1594/PANGAEA.873304>.
- Gutierrez, R. R., Mallma, J. A., Núñez-González, F., Link, O., & Abad, J. D. (2018). Bedforms-ATM, an open source software to analyze the scale-based hierarchies and dimensionality of natural bed forms. *SoftwareX*, 7, 184-189.
- Hey, T., Tansley, S., Tolle, K. M. (2009). The fourth paradigm: data-intensive scientific discovery (Vol. 1). Redmond, WA. Microsoft research.
- Huang, N. E., & Wu, Z. (2008). A review on Hilbert Huang transform: Method and its applications to geophysical studies. *Reviews of geophysics*, 46(2).
- Kwoll, E., Becker, M. and Winter, C. (2014). With or against the tide: The influence of bed form asymmetry on the formation of macroturbulence and suspended sediment patterns. *Water Resources Research*, 50(10), pp.7800-7815.
- Lefebvre, A. and Winter, C. (2016). Predicting bed form roughness: the influence of lee side angle. *Geo-Marine Letters*, 36(2), pp.121-133.
- LeRoy, J.Z., Rhoads, B.L., Best, J.L., Cisneros, J. 2016. Bed morphology and sedimentary dynamics at chute cutoffs: A case study of McKey Bend, lower Wabash River, IL-IN. *River Flow 2016: Iowa City, USA*, July 11-14, 2016, 469-481.
- Lindenmayer, D., & Likens, G. E. (2013). Benchmarking open access science against good science. *The Bulletin of the Ecological Society of America*, 94(4), 338-340.
- Masselink, G., et al. (2007). Geometry and dynamics of wave ripples in the nearshore zone of a coarse sandy beach. *Journal of Geophysical Research: Oceans* 112.C10 (2007).
- McNutt, M., Lehnert, K., Hanson, B., Nosek, B., Ellison, A., and King, L. (2016). Liberating field sciences samples and data. *Science*, 351 (6277). Doi: 10.1126/science.aad7048.
- Nativi, S., Mazzetti, P., Santoro, M., Papeschi, F., Craglia, M., & Ochiai, O. (2015). Big data challenges in building the global earth observation system of systems. *Environmental Modelling & Software*, 68, 1-26.
- Peng, C., Song, X., Jiang, H., Zhu, Q., Chen, H., Chen, J. M., ... & Zhou, X. (2016). Towards a paradigm for open and free sharing of scientific data on global change science in China. *Ecosystem Health and Sustainability*, 2(5), e01225.
- Peng, G., Privette, J. L., Kearns, E. J., Ritchey, N. A., & Ansari, S. (2015). A unified framework for measuring stewardship practices applied to digital environmental datasets. *Data Science Journal*, 13, 231-253.
- Perillo, M. M., Best, J. L., Yokokawa, M., Sekiguchi, T., Takagawa, T., & Garcia, M. H. (2014). A unified model for bedform development and equilibrium under unidirectional, oscillatory and combined flows. *Sedimentology*, 61(7), 2063-2085.
- Piwowar, H. A., Day, R. S., & Fridsma, D. B. (2007). Sharing detailed research data is associated with increased citation rate. *PLoS one*, 2(3), e308.
- Piwowar, H. A., & Vision, T. J. (2013). Data reuse and the open data citation advantage. *PeerJ*, 1, e175.
- Ramapriyan, H., Moses, J., & Duerr, R. (2012). Preservation of data for Earth system science—Towards a content standard. In *Geoscience and Remote Sensing Symposium (IGARSS)*, 2012 IEEE International (pp. 5304-5307). IEEE.

- Reichman, O. J., Jones, M. B., Schildhauer, M. P. (2011). Challenges and opportunities of open data in ecology. *Science*, 331(6018), 703-705.
- Resnik, D. B. (2006). Openness versus secrecy in scientific research. *Episteme*, 2(3), 135-147.
- van der Mark, C. F., Blom, A. and Hulscher, J.S. (2008). Quantification of variability in bedform geometry. *J. Geophys. Res.*, 113, doi:10.1029/2007JF000940.
- Winter, Christian; Lefebvre, Alice; Benninghoff, M; Ernstsen, Verner Brandbyge (2016): German Bight bedform reconstructions. PANGAEA, <https://doi.org/10.1594/PANGAEA.858716>



# Parametrization of bedform induced hydraulic flow resistance in coastal-scale numerical models – an evaluation of Van Rijn’s empirical bedform roughness predictors

Gerald Herrling *Inst. of Geosciences, Kiel University, Germany* – [gerald.herrling@ifg.uni-kiel.de](mailto:gerald.herrling@ifg.uni-kiel.de)

Knut Krämer *MARUM, University Bremen, Bremen, Germany* – [kkraemer@marum.de](mailto:kkraemer@marum.de)

Marius Becker *Inst. of Geosciences, Kiel University, Germany* – [marius.becker@ifg.uni-kiel.de](mailto:marius.becker@ifg.uni-kiel.de)

Alice Lefebvre *MARUM, University Bremen, Bremen, Germany* – [alefebvre@marum.de](mailto:alefebvre@marum.de)

Christian Winter *Inst. of Geosciences, Kiel University, Germany* – [christian.winter@ifg.uni-kiel.de](mailto:christian.winter@ifg.uni-kiel.de)

**ABSTRACT:** Bedforms (dunes and ripples) constitute a form roughness, i.e. hydraulic flow resistance, which has a large-scale effect on hydrodynamics and sediment transport of coastal environments. This hydraulic effect of bedforms needs to be parameterized in coastal-scale process-based models, since individual numerical grid cell sizes of typically 20 to 200 meters do not allow a proper discretization of bedform elements. State-of-the-art empirical bedform roughness predictors (Van Rijn 1984, 2007) are tested in numerical model simulations of both a simplified flume experiment and on the estuarine domain scale. A sensitivity analysis shows the performance of the bedform roughness predictors at variable water depths, flow velocities and mean grain-sizes. Predicted dune heights and lengths in a model of the Weser estuary are compared to dune dimensions observed by high-resolution multibeam measurements.

## 1. INTRODUCTION

Bedforms, such as ripples, megaripples or large dunes, cause a local hydraulic flow resistance which has a large-scale effect on hydrodynamics and sediment dynamics of rivers, estuaries and coastal seas. The resistance to the flow induced by bedforms, i.e. hydraulic bedform roughness, is associated with the flow expansion on their lee side resulting in kinetic energy loss, as exemplified for river dunes by Engelund and

Fredsøe (1982). Additional turbulence generated in case of flow separation behind the bedform crest and recirculation on the downstream side greatly enhances this effect (e.g. Vanoni and Hwang, 1967). The expansion loss and the rate of velocity decrease downstream of the bedform crest can be related to the lee slope angle (Best and Kostaschuk, 2002; Motamed et al., 2013; Paarlberg et al., 2007; Lefebvre and Winter, 2016).

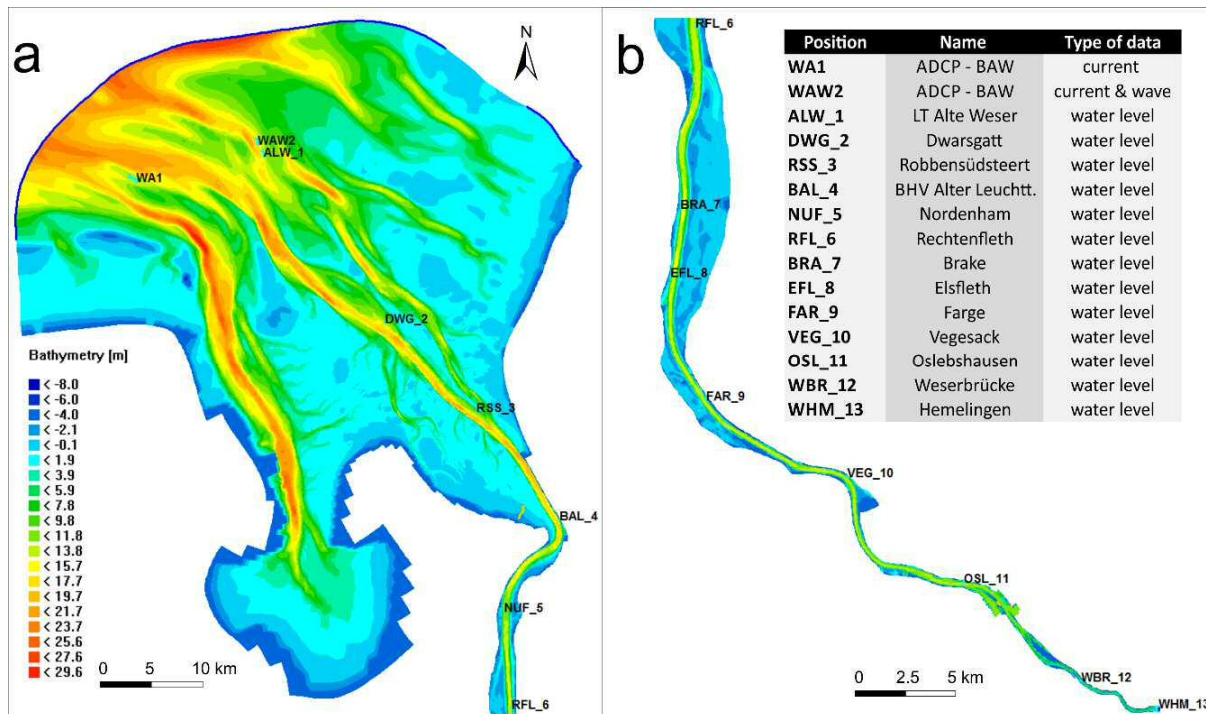


Figure 1. Bathymetry of the model domain and position of measurements (a) from the open sea boundary (blue line) to Rechtenfleth (RFL\_6) and (b) from Rechtenfleth to the tidal barrier at Hemelingen, Bremen (WHM\_13). Note the different spatial scales selected to improve the presentation of the outer and inner part of the estuary.

Energy loss above bedforms must be taken into account in numerical hydro- and morphodynamic model simulations in the form of bed friction coefficients that are associated with grain and form roughness. Particularly the applicability and performance of form roughness predictors has received little attention in large-scale model applications. Although computer power increases gradually, numerical coastal domain models are typically still restricted in horizontal and vertical grid resolutions to properly represent all topographical and morphological features; common grid cell sizes of process-based models are between 20 and 200 meters. This implies the parameterisation of the effect of bedform roughness elements that are of the length of a model grid cell or less. Thus bedforms are usually considered as of ‘sub-grid-scale’ (Sandbach et al., 2012). It should be noted that even at high spatial resolution and adequate 3-dimensional discretization of bedforms, their resistance to the flow may not be taken into account; flow separation and turbulence

generation over bedforms requires simulations with a fully non-hydrostatic model configuration (Lefebvre et al., 2014, 2016).

Although common in fluvial studies, there are very few numerical model studies in coastal settings that apply bedform roughness predictors and deal with the effect of bedform roughness on the hydro- and morpho-dynamics. Van Rijn’s bedform roughness predictor (2007), and particularly the dune roughness predictor, have primarily been developed for riverine conditions. The scheme has already been applied in a few large-scale coastal area models and appears to be robust (Davies and Robins, 2017; Herrling et al., 2017; Villaret et al., 2011; Wang et al., 2016).

Hydraulic bedform roughness predictors commonly are based on the ratio of height and length (i.e. steepness) of a bedform (e.g. Julien and Klaassen, 1995; Karim, 1999; van Rijn, 1984; Yalin, 1964) and thus require field data or a prediction of bedform geometries. Yet the predictor of van Rijn (2007) directly expresses the bedform roughness

height depending on current velocity, surface sediment grain-size and water depth. Thus, in tidal environments, variations of current speed and water depth may result in variations of bedform roughness over a tidal cycle.

This study explores the parameterisation of bedform hydraulic roughness in a simple flume experiment (sensitivity study) and a model of the Weser estuary, Germany, using the Delft3D (Deltares, 2014) modelling system. Well-established bedform roughness predictors of van Rijn (1984, 2007) are evaluated and predicted bedform dimensions are compared to observations from high-resolution multi-beam bathymetry.

overall bedform roughness. The overall bedform roughness predicted by VR07 is known as a combination of the roughness from ripples, megaripples and dunes and may vary spatially in its composition and magnitude. In this study only the bedform roughness of dunes (VR07) is considered and is compared to the dune roughness predicted by VR84. For a detailed description of the formulae used in these predictors and the implementation into the modelling system, it is referred to the original publications (van Rijn 1984, 2007) and the manual of the model system Delft3D (Deltares, 2014).

#### Numerical flume experiment

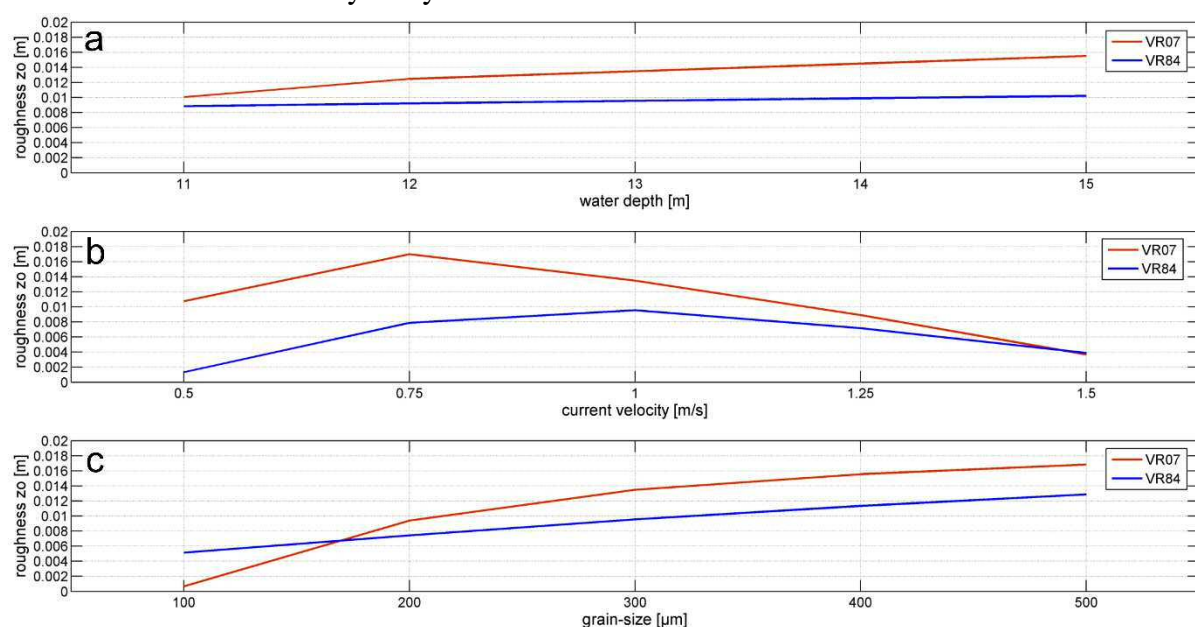


Figure 2. Bedform (dune) roughness height  $z_0$  predicted by VR84 and VR07 for simulations with (a) variable water depths, (b) variable current velocities and (c) variable mean grain-sizes in a numerical flume experiment.

## 2. METHODS

### Bedform roughness prediction

Predictors of bedform dimension (van Rijn, 1984) and bedform roughness (van Rijn 1984, 2007) were tested. While the predictor after van Rijn 2007 (VR07) directly estimates the bedform roughness height  $z_0$ , van Rijn 1984 (VR84) determines bedform dimensions (height and length) in an intermediate step before calculating the

Sensitivity tests were conducted in a simple numerical flume experiment with unidirectional flow to study the predicted bedform roughness (VR84 and VR07) as a response to variable water depths (11 to 15 m), current velocities (0.5 to 1.5 m/s) and mean grain-sizes (100 to 500  $\mu\text{m}$ ). These conditions are within typical ranges of the parameters found in the Lower Weser estuary. For each model run, only one parameter has been altered at a time; the reference condition is a water depth of 13 m, a flow velocity of 1 m/s and mean grain-size of 300

μm. The model domain has a width of 100 m and length of 5000 m, the simulations are performed in depth-averaged (two-dimensional horizontal, 2DH) and three-dimensional (3D) configurations applying velocity forcing at the upstream open boundary and a stationary water level at the downstream boundary. Bedform roughness heights are extracted at 1000 m downstream of the upstream end after a hydrodynamic spin-up of 12 hours.

model of the Weser estuary forced by real-time tidal flow and upstream discharge (Herrling et al., 2017).

Predicted bedform dimensions of VR84 and VR07 were compared to dune observations in the Lower Weser estuary. Predicted dune heights and lengths were determined from VR84. For VR07 a backward calculation based on Van Rijn (1984) determined bedform dimensions.

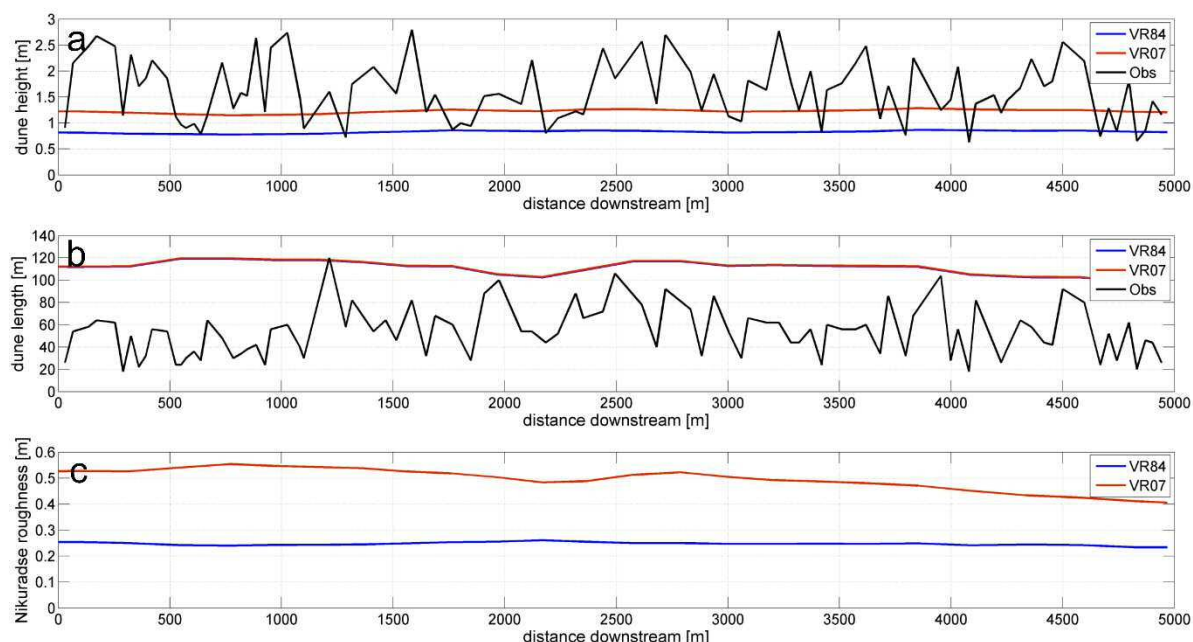


Figure 3. Predicted (at max. ebb flow, VR07, VR84) and observed (a) dune heights and (b) dune lengths along a section of 5 km downstream of Rechtenfleth in the Lower Weser estuary in Sept. 2012; (c) Predicted Nikuradse dune roughness.

As expected both formulae predict larger roughness with increasing water depth and/or grain-size with an order of magnitude range (Fig. 2). The case of variable current magnitudes shows that under Weser estuarine conditions the critical conditions occur, where bedform roughness has a maximum. It is noted that the application of VR07 results in significantly higher dune roughness values compared to VR84.

### Evaluation of bedform roughness prediction in the estuarine domain model

The performance and effect of uncalibrated bedform predictors at estuarine scale is shown with a numerical morphodynamic

High-resolution multi-beam bathymetric data surveyed by local authorities (WSA Bremerhaven) in September 2012 resolve a bedform field at a section of 5 km downstream of Rechtenfleth in the Lower Weser (RFL\_6, Fig. 1). Dune heights and lengths were determined by filtering and zero-upcrossing (Krämer et al., abstract MARID 2019).

## 3. PRELIMINARY RESULTS

Predicted dune height and length from the uncalibrated model simulations are compared to measured bedform dimensions. In September 2012, measured dune heights of

the observed dune field are between 0.6 and 2.8 m with overall mean heights of 1.6 m. Mean dune lengths are 53 m with absolute lengths varying between 18 and 120 m.

Predictions of dune heights are consistent along the section with mean values of 0.83 and 1.23 m for VR84 and VR07, respectively; thus underestimating observations. Predicted dune lengths are very similar for both formulae and vary between 100 and 120 m. These values in turn are at the upper limit of observed values. From a physical understanding, results imply a possible underestimation of bedform roughness, as the underestimated heights and over-estimated lengths would result in lower steepness of the modelled dunes compared to the measured ones.

Nikuradse dune roughness heights are predicted to be significantly larger for VR07 compared to VR84.

Although maximal current magnitudes are simulated to be similar for ebb and flood, dune height and roughness are predicted to be larger during flood than ebb, particularly for VR07 (not shown here). It is noted that upstream discharges about 105 m<sup>3</sup>/s are low in September 2012 in relation to long-time mean discharges of 323 m<sup>3</sup>/s. Maximal ebb currents occur at late ebb when water levels are lower compared to maximal flood currents at late flood.

#### 4. SUMMARY AND OUTLOOK

Dynamic dune roughness prediction has a significant effect on simulated hydrodynamics. In this study two empirical bedform roughness predictors, developed by Van Rijn (1984, 2007), primarily for riverine, unidirectional flow conditions, have been tested and evaluated.

Applied for tidal flow conditions, dune heights predicted by VR07 and VR84 underestimate observed mean dune heights by 23% and 48%, respectively. Predicted mean dune lengths are overestimated by both formulae by approximately 50% with respect to

measurements. A smaller dune steepness is thus predicted compared to observations.

For a section of 5 km in the Lower Weser, predicted dune roughness and dimensions are consistent; however on the entire estuarine scale predictions vary spatially. An upcoming evaluation of predicted dune dimensions in relation to measurements of dune fields along the Outer and Lower Weser estuary will reveal the spatial performance of bedform roughness predictors. Variations of roughness height on annual time scales with seasonal and event-driven discharges will be evaluated against estimations of dune dimensions analysed from monthly bathymetric surveys.

#### 5. ACKNOWLEDGEMENTS

This study was funded by the research projects MorphoWeser and FAUST being financed by the German Federal Waterways Engineering and Research Institute (BAW). We thank the relevant authorities (WSA Bremerhaven) for providing data on Weser bathymetry. AL is funded by the German Research Foundation (Deutsche Forschungsgemeinschaft, DFG), project number 345915838.

#### 6. REFERENCES

- Best, J., Kostaschuk, R.A., 2002. An experimental study of turbulent flow over a low-angle dune. *J. Geophys. Res.* 107, 3135.  
doi:10.1029/2000jc000294
- Davies, A.G., Robins, P.E., 2017. Residual flow, bedforms and sediment transport in a tidal channel modelled with variable bed roughness. *Geomorphology* 295, 855–872.  
doi:10.1016/j.geomorph.2017.08.029
- Deltaires, 2014. Delft3D-FLOW, User Manual, Simulation of multi-dimensional hydrodynamic flows and transport phenomena, including sediments. The Netherlands.
- Engelund, F., Fredsoe, J., 1982. Hydraulic theory of alluvial rivers. *Adv. Hydrosci.* 13, 187–215.  
doi:<http://dx.doi.org/10.1016/B978-0-12-021813-4.50009-3>
- Herring, G., Benninghoff, M., Zorndt, A., Winter, C., 2017. Drivers of channel-shoal morphody-

- namics at the Outer Weser estuary, in: Coastal Dynamics Conference, Helsingør, Denmark. Helsingør, Denmark.
- Julien, P.Y., Klaassen, G.J., 1995. Sand-dune geometry of large rivers during floods. *J. Hydraul. Eng.* doi:10.1061/(ASCE)0733-9429(1995)121:9 (657)
- Karim, F., 1999. Bed-Form Geometry in Sand-Bed Flows. *J. Hydraul. Eng.* 125, 1253–1261. doi:10.1061/(ASCE)0733-9429(1999)125:12 (1253)
- Lefebvre, A., Paarlberg, A.J., Ernstsen, V.B., Winter, C., 2014. Flow separation and roughness lengths over large bedforms in a tidal environment: A numerical investigation. *Cont. Shelf Res.* 91, 57–69. doi:10.1016/j.csr.2014.09.001
- Lefebvre, A., Winter, C., 2016a. Predicting bed form roughness: the influence of lee side angle. *Geo-Marine Letters* 36:121-133. doi:10.1007/s00367-016-0436-8
- Lefebvre, A., Paarlberg, A.J., Winter, C., 2016b. Characterising natural bedform morphology and its influence on flow. *Geo-Marine Lett.* 36, 379–393. doi:10.1007/s00367-016-0455-5
- Motamedi, A., Afzalimehr, H., Gallichand, J., Fazel Najaf Abadi, E., 2013. Lee Angle Effects in Near Bed Turbulence: An Experimental Study on Low and Sharp Angle Dunes. *Int. J. Hydraul. Eng.* 1, 68–74. doi:10.5923/j.ijhe.20120106.02
- Paarlberg, A.J., Dohmen-Janssen, C.M., Hulscher, S.J.M.H., Termes, P., 2007. A parameterization of flow separation over subaqueous dunes. *Water Resour. Res.* 43. doi:10.1029/2006WR005425
- Sandbach, S.D., Lane, S.N., Hardy, R.J., Amsler, M.L., Ashworth, P.J., Best, J.L., Nicholas, A.P., Orfeo, O., Parsons, D.R., Reesink, A.J.H., Szupiany, R.N., 2012. Application of a roughness-length representation to parameterize energy loss in 3-D numerical simulations of large rivers. *Water Resour. Res.* 48. doi:10.1029/2011WR011284
- van Rijn, L.C., 1984. Sediment Transport, Part III: Bed forms and Alluvial Roughness. *J. Hydraul. Eng.* 110, 1733–1754. doi:10.1061/(ASCE)0733-9429(1984)110:12(1733)
- van Rijn, L.C., 2007. Unified view of sediment transport by currents and waves. I: Initiation of motion, bed roughness, and bed-load transport. *J. Hydraul. Eng.* 133, 649–667.
- Vanoni, V.A., Hwang, L.-S., 1967. Bed forms and friction in streams. *J. Hydraul. Div.* Vol 93, 121–144.
- Villaret, C., Huybrechts, N., Davies, A.G., Way, O., 2011. Effect of bed roughness prediction on morphodynamic modelling: Application to the Dee estuary (UK) and to the Gironde estuary (France), in: Proceedings of the 34th World Congress of the International Association for Hydro-Environment Research and Engineering: 33rd Hydrology and Water Resources Symposium and 10th Conference on Hydraulics in Water Engineering. Engineers Australia, p. 1149.
- Wang, Y., Yu, Q., Jiao, J., Tonnon, P.K., Wang, Z.B., Gao, S., 2016. Coupling bedform roughness and sediment grain-size sorting in modelling of tidal inlet incision. *Mar. Geol.* 381, 128–141. doi:10.1016/J.MARGEOL.2016.09.004
- Yalin, M.S., 1964. Geometrical Properties of Sand Wave. *J. Hydraul. Div.* 90, 5105–119.

# Multi time-scale morphological evolution of a shell sand, dune bank in a shallow mesotidal environment.

Sabrina Homrani, Nicolas Le Dantec, France Floc'h, Marcaurelio Franzetti, Christophe Delacourt *Université de Bretagne Occidentale, Plouzané, France*– [sabrina.homrani@univ-brest.fr](mailto:sabrina.homrani@univ-brest.fr)

Mouncef Sedrati *Université de Bretagne Sud, Vannes, France*– [mouncef.sedrati@univ-ubs.fr](mailto:mouncef.sedrati@univ-ubs.fr)

Christian Winter *Christian-Albrechts-Universität, Kiel, Germany*, [christian.winter@ifg.uni-kiel.de](mailto:christian.winter@ifg.uni-kiel.de)

**ABSTRACT:** Dune banks are ubiquitous systems in coastal areas. Understanding their morphodynamics and the associated sediment fluxes is still scientifically challenging. To address these questions, we use a multi time-scale bathymetric dataset of a dune bank located in a very shallow area inside a semi-enclosed bay, where the tidal current is strong and unsteady. The bank is composed of coarse shell sand, has a steady sediment volume, and is not migrating. The bank can be seen as a two-component system, featuring a ridge oriented along the bank, and a series of dunes orthogonal to the ridge. These two types of bedforms exhibit different dynamics. The transverse dunes are migrating toward SW (ebb current orientation) with a mean migration distance on the order of a meter over a month. At multiyear time scale, the orientation of the ridge is stable except for the central area of the bank, where the bedform configuration is quite variable.

## 1. INTRODUCTION

Submarine banks and dunes are ubiquitous sedimentary systems in coastal areas (Ernstsen et al., 2006; Horrillo-Caraballo et al., 2008; Ferret et al., 2010). Understanding their morphodynamics, and the associated sediment fluxes and sediment transport pathways, is crucial for various applications such as the safety of navigation, the exploitation of marine resources, or the conservation of benthic and pelagic species (Trentesaux et al., 1999; Hequette and Aernoult, 2010; Todd et al., 2014). However, due to the lack of monitoring data and the difficulty in measuring or evaluating sediment transport for these systems, dune morphodynamics still poses some scientific challenges. Here, we focus on a very shallow sand bank, consisting of shell sand, and that is only subject to tidal forcing, the wave climate being characterized by very small significant wave heights. The bank is located on a narrow margin between two channels near the inlet of a large, semi-closed gulf. While tidal currents are strong and un-

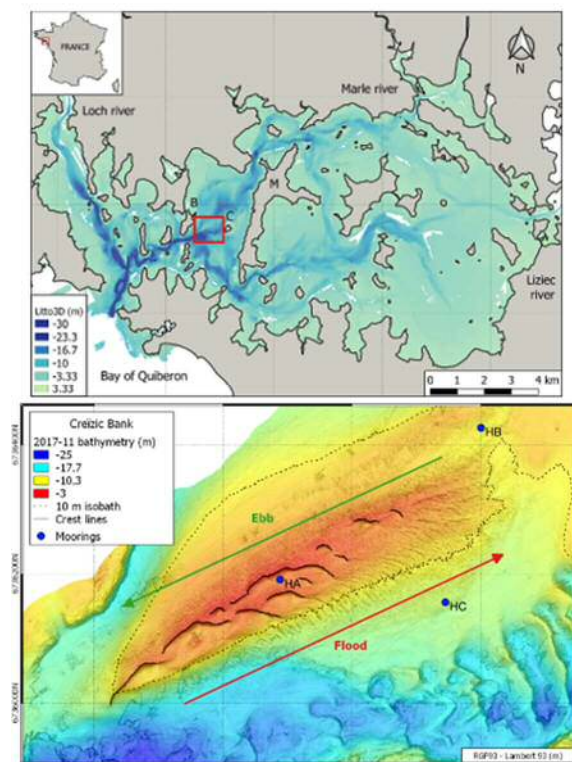
steady in this shallow area, and the dunes located in the central area of the bank are highly dynamic, the bank exhibits a very low migration rate and its sediment volume is conserved. Using bathymetric datasets covering multiple time scales, both multi-annual and over a month, this paper aims to study the morphodynamic behavior and sediment transfer of the bank and dunes.

## 2. STUDY SITE

The study site, the *Creïzic* submarine dune bank (fig. 1), is located in the western part of the Gulf of *Morbihan* (South Brittany, France). This gulf is connected to the Atlantic Ocean by a very narrow inlet. Due to this configuration, the semi-diurnal tide generates a residual current above the seafloor, with the ebb current being predominant in the outer part of the Gulf (Marcos et al., 1996). The Gulf of *Morbihan* is a bedrock-controlled lagoonal basin with low sediment supply, incised by a complex network of tidal channels (Menier et al., 2011). The last marine transgression led to the infilling of the incised palaeo-valleys, with ero-

sion at the entrance of the Gulf and sediment deposition (lithic and biolithic material) inside the Gulf. On the outer part of the Gulf (between its entrance and the island *Île aux Moines*) hydrodynamics conditions were highly energetic, leading to sediment deposits on the margins of the tidal channels only, such as the *Creïzic* bank (Menier et al., 2011).

The *Creïzic* bank is situated in water depths ranging from 3 m to 25 m (fig. 1). It is about 1200 m long, 600 m wide, with a mean sediment thickness over the bed-rock



estimated to 11 m (Perez-Belmonte, 2008).

The volume of the bank is about  $1.7 \times 10^6$

Figure 4. The *Creïzic* bank (Gulf of Morbihan, France) with the main orientation of the tidal current.

$m^3$  and has been quasi steady over the last decade (sediment volume variations inferior to 1 % from 2003 to 2014) (Moal, 2015). The sand bank features large superimposed bedforms, with dune wavelengths up to 116 m and dune heights up to 3.8 m. The bank is mainly composed of shelly, coarse sand comprising both shell fragments and whole shells of the species: *Bittium*, *Littorina*,

*Spisula elliptica* amongst others. The median sediment diameter is 1 mm for the central area of the bank. The *Creïzic* bank used to be exploited as a sand resource for oyster farming in the gulf until 2003.

The main hydrodynamic forcing factor at play on the bank is a strong and unsteady tidal current, typically 50 cm/s and up to 2 m/s, with a tidal range of about 3 m at spring tide. The ebb current is directed toward the SW and the flood current toward the NE. The eastern channel exhibits a classical bidirectional tidal current with a short reversal time; the western channel features a unidirectional, ebb orientated current. On the central area of the bank where active dunes are found, the flood current varies in direction, whereas the current ebb has stable direction and is stronger than the flood in magnitude. Fourteen other sand banks are located in the Gulf, all in the outer part. Hence, sediment exchanges might potentially occur between the *Creïzic* bank and these other sedimentary systems.

### 3. DATASET AND METHOD

The dataset used for this study consists of a series of Digital Elevation Models (DEM) obtained from Multibeam echo sounder bathymetric surveys from 2003, 2010, 2011, 2014, October 2017, and November 2017, with resolution from 1 m for 2003 to 25 cm for the two 2017 DEM, allowing diachronic analyses at different time scales. In addition, instrumented moorings were deployed on the bank during one month in the fall 2017, with the objective of measuring the hydrodynamic forcing. Sediment samples were collected in spring 2015 and June 2017 using an orange peel bucket. The collected samples were rinsed, dried off and sieved.

The picking of dune crest lines was performed manually on a GIS, using slope rasters to help visualize the crests (Franzetti et al., 2013). Using the bathymetry of November 2017, representative profiles drawn perpendicular to the crest lines were extracted for each dune in the central area. The profiles were analysed using Matlab in order to

estimate the morphological parameters of the dunes: height  $H$ , stoss side length  $a$ , lee side length  $b$ , dune length  $a+b$ , stoss side angle  $\alpha$ , lee side angle  $\beta$ , aspect ratio  $H/L$  and asymmetry  $a/b$  (Berné et al., 1989; Le Bot, 2001).

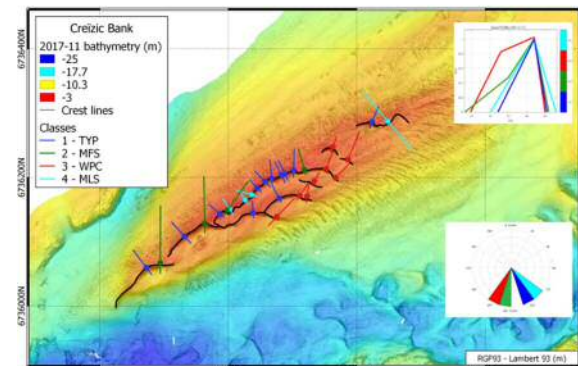
On a monthly time scale the bedform configuration remains relatively unchanged, so that bedforms can be individually identified and tracked between successive DEM. Therefore, two complementary methods were used to compute the distances and rates of bedform migration between the October and November 2017 surveys: 1) the migration distances from crest lines were computed using an algorithm implemented in Python for two consecutive datasets. A raster of Euclidian distances is generated for the crest lines of the first dataset, giving for each pixel of the raster the distance to the crest (within a range and resolution selected by the user). The distance raster of the first dataset is then intersected with the crest lines of the second dataset, directly giving the corresponding migration distances. The sampling step along the crest line is also chosen by the user ; 2) the migration distances and directions were also derived directly from two consecutive DEMs using the image correlation algorithm implemented by Stumpf et al. (2018) with a search radius of 10 m, degrading the DEM resolution to 1 m so that the algorithm could properly match features.

## 4. RESULTS

### 4.1 Morphological parameters

The *Creïzic* Bank comprises three main sectors: a central dune field featuring dunes with heights between 1 m and 3.8 m for wavelengths between 23 m and 116 m, and two dune fields on either side of the bank with dunes of decimetric lengths and metric wavelengths. A field of stable fossil mega ripples is located SE of the bank with a mean height of 5 m and a mean wavelength of 60 m (Moal, 2015).

Particular attention was paid to the central area of the bank where 28 dune profiles (over 8 dunes) were extracted from the November 2017 DEM. These profiles were classified into 4 classes according to their shape (fig. 2): typical submarine dunes with a well-defined avalanche slope (TYP, 12 profiles), dunes with Milder slope at the Foot of Stoss side (MFS, 4 profiles), dunes with Wider Plateau at the Crest (WPC, 8 profiles) and dunes with both Milder slopes on the Stoss and Lee sides (MSL, 4 dunes). The mean morphological parameters of each class of dunes are presented in table 1. Except for the MSL class, all dunes do exhibit maximum lee-side slope angles consistent with avalanche mechanisms. The mean lee-side slope angles are rather small, as was observed dunes of similar shell sand composition in the Banc du Four (Franzetti et al.,



2013). Lee-side angles of MSL dunes are

Figure 5. Bathymetric profiles extracted from the November 2017 DEM, categorized by morphological classes. The dots show the location of the dune profile highest points, chosen manually when analysing the profiles in Matlab. The characteristics of the four classes are sketched in the upper left insert; the mean orientation by class is displayed in the lower left insert.

even lower, which could be due to the tide reversal. There is a relationship between the location of the dunes and their class for some dunes types. The TYP dunes are located on the ridge with crest lines oriented along the bank. The WPC dunes have crest lines orthogonal to the axis of the bank and consequently to the ridge.

A power law relationship between dune height and dune length has been investigated

comparing the best fit for each dune class to the law  $H=0.0677L^{0.8098}$  proposed by Flemming (2000). All classes are consistent with the maximum threshold given by Flemming, except for the WPC class where the morphological measurements were too scattered to determine a satisfying power law, so that no particular trend can be assessed. The TYP class is the closest to the Flemming relationship with an exponent of 0.85 against 0.81. Considering this classification, the central area of the bank can be seen as a two-component system, composed of the ridge on the western part (TYP dunes), oriented toward SE, almost parallel to the direction of the ebb current, and the series of dunes (WPC type) orthogonal to the ridge, with lee sides oriented to the SW.

As the asymmetry of the smaller, active bedforms is expected to adjust to the oscillating tidal currents according to the instantaneous direction of the flow (Winter et al., 2016), several terrain profiles have been examined at different steps of the tide throughout the bank to assess the bedforms' polarity. Bedforms on the eastern side of the bank are mainly symmetrical, or slightly changing their orientation with tidal current direction. Bedforms on the western side of the bank are all ebb oriented; indicating that sediment transport mainly occurs in ebb direction for that area. The smaller bedforms on the central area, located in the troughs of metric-size dunes, are also mainly ebb oriented, which is consistent with the orientation of the dunes that are orthogonal to the axis of the bank. Thus, the polarity of smaller bedforms has the signature of a main sediment transport pathway oriented toward SW, in the ebb current direction. The asymmetry of the ridge, with steeper slopes of the eastern side, is indicative of sediment transport in SE direction. Sediment transport is possibly occurring toward NE on the outer parts of the bank on the eastern side.

#### 4.2 Multiyear evolution

The overall bank is very slowly migrating toward SE, with a migration of 40 m from

Table 1: Mean morphological parameters for dune profiles extracted from the November 2017 bathymetric dataset.

	$\alpha_{mean}$	$\alpha_{max}$	$\beta_{mean}$	$\beta_{max}$	$H/L$	$a/b$
ALL	4.3	11.5	12.6	27.0	0.05	3.1
TYP	5.3	12.9	13.5	27.8	0.07	2.3
MFS	2.8	12.8	14.6	30.0	0.04	5.4
WPC	2.4	9.1	13.1	30.0	0.04	4.0
MSL	4.8	10.9	6.6	15.1	0.04	1.7

2003 to November 2017 for the Southern extremity of the bank.

The configuration of the central area of the bank and the position of the primary dunes have been significantly evolving over the 2003-2017 period. Different dynamics were identified depending on the sectors of the bank. In the southern part of the bank, the orientation of the ridge is slightly changing with time, turning to North from 2003 to 2011 and going back to South thereafter. On the contrary, on the central area of the bank the ridge orientation is significantly changing. On the northern part of the bank, the ridge exhibits a stable orientation over time.

Tracking each dune from a DEM to another is not always feasible when the DEM are more than 1 year apart. When possible, migration distances have been computed using a profile along the main axis of the bank and crossing orthogonally the dunes. Migration distances are of decametric order (max. 54 m between 2011 and 2014). They vary from one dune to another and give different annual migration rates depending on the two DEM used within the series of datasets. For the ridge, the migration is toward SE but slower (max. 24 m between 2003 and 2010).

#### 4.3 Monthly time scale migration

The migration of the crest lines of the central area of the bank between October and November 2017 has been investigated (fig. 3), with a range and resolution set to 10 m and 0.25 m respectively, showing a significant migration at the time scale of a

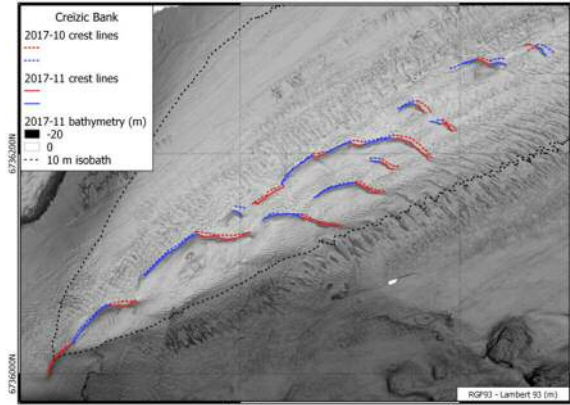


Figure 6. Crest lines of the central area of the Creizic bank used for the computation of migration distances.

month. The dune crest line sections that are orthogonal to the ridge exhibit higher migration distances than the ridge itself, with the maximum migration distance up to 4.5 m and a weighted mean of 2 m for a same standard deviation of 0.5 m (mean value of the std for considered sections, table 2). Few migration distances were negative considering all the sections of orthogonal dunes, confirming that they are migrating toward SE. The dunes constituting the ridge are undergoing a deformation rather than actually migrating, since the weighted mean migration of the ridge line sections is low, close to the crest line picking error, and the percentage of negative values is higher.

Using the image correlation algorithm with the two 2017 DEMs, displacement ranges of several meters have been computed at the bank scale. On the central and northern area, migration distances are the highest, up to 7 m over the small dunes that are not connected to the ridge. On the southern part of the bank, around the extremity of the bank, migration is between 0 and 2 m, mainly oriented toward South. At the Northern extremity of the bank, beyond the 10 m isobath, a counter clock-wise motion is seen, going first to the North, then to the West and finally joining the general motion of the central area toward South-West. Migration distances close to zero on the western part of the bank are possibly an artefact due to the high degree of similarity of the small dunes in this area, which could prevent the algorithm from properly correlating objects. Altogether, a general motion of migration toward SW is observed. This global migration

Table 2: Migration distances of the crest lines. The mean was computed by weighting the migration distance with the ratio of the length of the line section and the length of all the line sections considered.

	Interval [m]	std [m]	% negative	Mean [m]	Total length [m]
All	0 ; 4.5	0.5	6.2	1	608
Ridge	0 ; 3.5	0.5	8.8	0.5	345
Orthogonal	0 ; 4.5	0.5	2.8	2	263

pattern could be seen as a recirculation pathway around the bank, the sediment being redistributed from the South of the bank to the North in a counter clockwise loop crossing the deeper parts of the eastern side of the bank.

## 5. CONCLUSION

This study focuses on the multiyear and monthly time scales, morphological evolution and dynamics of a submarine dune bank located in the Gulf of Morbihan, in a shallow area where the tidal currents are strong and unsteady. The bank exhibits a low migration rate and a steady volume, whereas the superimposed dunes are undergoing deformation and/or migration. The bank can be seen as a two-component system, featuring a ridge oriented along the bank, and a series of dunes that are orthogonal to the ridge. At the multiyear time scale, the orientation of the ridge is quite stable except for the central area of the bank, where it is quite variable, with the junction points between the ridge and the orthogonal dunes also changing rapidly. Migration distances for the orthogonal dunes are up to 54 m in three years, and display mean migrating distances of 2 m in one month, whereas the ridge is rather undergoing a deformation at monthly scale. The orthogonal dunes are migrating to the SW, in the direction of the ebb current which is dominant on the area. This migration direction is confirmed by results of an image correlation algorithm applied between October and November 2017. Furthermore, a recircu-

lation pattern over the bank can be inferred from the migration directions of the smaller bedforms. Sediment could be recirculated from the South point of the bank to its North extremity in a wide counter clock wise loop in the tidal channel east of the bank. This hypothesis could be investigated, as well as the longitudinal orientation of the ridge dunes in the central and southern part of the bank, using a local hydrodynamic model.

## 6. ACKNOWLEDGEMENT

This work was supported by the Labex-MER (ANR-10-LABX-19-01, IUEM, Brest), and by the ANR MESURE project. The authors would like to give a special thanks to the Pôle Image and diving teams of IUEM (Institut Universitaire Européen de la Mer), and to the crew of the Sépiola research vessel (L. Allano).

## 7. REFERENCES

- Berné, S., Allen, G., Auffert, J.-P., Chamley, H., Durand, J., & Weber, O., 1989. Essai de synthèse sur les dunes hydrauliques géantes tidales actuelles. Bulletin de La Société Géologique de France, (6), 1145–1160.
- Ernstsen, V. B., Noormets, R., Winter, C., Hebbeln, D., Bartholomä, A., Flemming, B. W., & Bartholdy, J., 2006. Quantification of dune dynamics during a tidal cycle in an inlet channel of the Danish Wadden Sea. *Geo-Marine Letters*, 26(3), 151–163.
- Ferret, Y., Le Bot, S., Tessier, B., Garlan, T., Lafite, R., 2010. Migration and internal architecture of marine dunes in the eastern English Channel over 14 and 56 year intervals: the influence of tides and decennial storms. *Earth Surface Processes and Landforms* 35, 1480–1493.
- Flemming, B. W., 2000, March. The role of grain size, water depth and flow velocity as scaling factors controlling the size of subaqueous dunes. In *Marine sandwave dynamics, international workshop* (pp. 23-24).
- Franzetti, M., Le Roy, P., Delacourt, C., Garlan, T., Cancouët, R., Sukhovich, A., & Deschamps, A. 2013. Giant dune morphologies and dynamics in a deep continental shelf environment: example of the banc du four (Western Brittany, France). *Marine Geology*, 346, 17-30.
- Hequette, A., Aernoult, D., 2010. The influence of nearshore sand bank dynamics on shoreline evolution in a Macrotidal coastal environment, Calais, France. *Continental Shelf Research*. 1349-1361.
- Horrillo-Caraballo, J. M., & Reeve, D. E., 2008. Morphodynamic behaviour of a nearshore sandbank system: The Great Yarmouth Sandbanks, UK. *Marine Geology*, 254(1-2), 91-106.
- Le Bot, S., 2001. Morphodynamique de dunes sous-marines sous influence des marées et des tempêtes: processus hydro-sédimentaires et enregistrement: exemple du Pas-de-Calais. PhD Thesis, Université Lille 1.
- Letort S., 1999. Extension de la spartine anglaise dans le Golfe du Morbihan : répartition actuelle, tendances d'évolution et impact potentiels. Rapport d'étude. ODEM
- Marcaillou, B., Camus, P., Daniel, F., 1996. Caractéristiques sédimentaires du Golfe du Morbihan : granulométrie, teneur en haut, matière organique et phosphate total. ODEM, IFREMER : 46 pages.
- Marcos F., Janin J.M., Le Saux J.M., 1996. Modélisation hydrodynamique du Golfe du Morbihan. EDF (Laboratoire National Hydraulique), Conseil général du Morbihan : 47 pages.
- Menier, D., Tessier, B., Dubois, A., Goubert, E., & Sedrati, M., 2011. Geomorphological and hydrodynamic forcing of sedimentary bedforms- Example of Gulf of Morbihan (South Brittany, Bay of Biscay). *Journal of Coastal Research*, 1530-1534.
- Moal, F., 2015. Étude hydro-morpho-sédimentaire d'un banc tidal en milieu semi-fermé, cas du banc du Creïzic dans le Golfe du Morbihan. Master Thesis. Université de Bretagne Sud.
- Perez-Belmonte, L., 2008. Caractérisation environnementale, morphosédimentaire et stratigraphique du Golfe du Morbihan pendant l'Holocène terminal: Implications évolutives. PhD Thesis. Université de Bretagne Sud.
- Stumpf, A., Michéa, D., & Malet, J. P., 2018. Improved Co-Registration of Sentinel-2 and Landsat-8 Imagery for Earth Surface Motion Measurements. *Remote Sensing*, 10(2), 160.
- Todd, B. J., Shaw, J., Li, M. Z., Kostylev, V. E., & Wu, Y., 2014. Distribution of subtidal sedimentary bedforms in a macrotidal setting: The Bay of Fundy, Atlantic Canada. *Continental Shelf Research*, 83, 64-85.
- Trentesaux, A., Stolk, A., & Berne, S., 1999. Sedimentology and stratigraphy of a tidal sand bank in the southern North Sea. *Marine Geology*, 159(1-4), 253-272.
- Winter, C., Lefebvre, A., Becker, M., Ferret, Y., Ernstsen, V. B., Bartholdy, J., Kwoll, E., & Flemming, B., 2016. Properties of active tidal bedforms. In *Fifth International Conference on Marine and River Dune Dynamics* (pp. 205-208). Bangor University and SHOM.

# Multi-scale analysis of sandbank features optimising geomorphological mapping of sandy shelf environments: Belgian part of the North Sea

Lars Kint *Royal Belgian Institute of Natural Sciences, Belgium – lkint@naturalsciences.be*

Nathan Terseleer *Royal Belgian Institute of Natural Sciences, Belgium – nterseleerlillo@naturalsciences.be*

Vera Van Lancker *Royal Belgian Institute of Natural Sciences, Belgium – vvanlancker@naturalsciences.be*

**ABSTRACT:** Low- and high-resolution digital bathymetry models are freely available as interoperable gridded data layers and data products. The higher resolution data, together with increasing data analyses tools, give new impetus to a more uniform geomorphological mapping of wider marine areas. To test approaches in sandy shelf areas, a multi-scale analysis is performed on data from the Belgian part of the North Sea using the Bathymetric Position Index (BPI). A comparative study of the calculated surface area and the perimeter (or contour) of sandbank features is illustrated using measures of accuracy, complexity or detailedness.

**Keywords:** Bathymetric Position Index (BPI), marine geomorphology, resolution, sandbank features, scale factor.

## 1. INTRODUCTION

Rapid access to reliable and accurate data is vital in addressing threats to the marine environment (e.g., in relation to policy and legislation-oriented measures, understanding trends and rare events, forecasting future changes). European marine data projects such as Geo-Seas (FP7), EMODnet (DG MARE), SeaDataNet (FP7, Horizon 2020) are influential in standardizing and harmonizing marine datasets allowing subsequent use by scientific institutes, organisations and services, authorities, industry, universities and schools.

An abundance of bathymetric charts has been released in the last decade, comprising single beam and/or multibeam datasets at low to high resolution and combined over several sea basins. This evolution triggers the re-awakening and renewal of geomorphological mapping over wider areas, but also at higher resolution for dedicated applications (e.g., Marine Spatial Planning, Habitat Directive; or supporting industrial design). Still ‘no one size fits all approach’ exists and testing of most suitable parameterization is needed.

Determining geomorphological seabed features from bathymetric datasets is strongly dependent on the resolution and the scale factor of the bathymetry, as well as its data quality. A case study on sandbank features on the Belgian part of the North Sea (BPNS) has been worked out in a GIS environment using the Benthic Terrain Modeler (Lundblad et al., 2006).

A tidal wave of bathymetric data and charts

Under the impetus of Europe’s Integrated Maritime Policy, the European Marine Observation and Data Network (EMODnet) collects fragmented and scattered marine data. Harmonization and standardization allow use of the data by a wider community, creating new opportunities for research and innovation in ‘blue growth’. Data archives are managed by regional and national organisations, whilst the data products, interoperable and quality-controlled, are managed centrally (e.g., [www.emodnet.eu](http://www.emodnet.eu)).

The gateway to bathymetry data is EMODnet Bathymetry (<http://www.emodnet-bathymetry.eu>), bringing together hydrographic surveys and other professionals in bathymetric data collection, processing and management. The main data product, the

Digital Terrain Model (DTM) or Digital Elevation Model (DEM), is based on three types of bathymetric data sources: 1. High-resolution bathymetric data from single and multibeam echo sounding, combined with historic leadline soundings where needed; 2. Gridded bathymetry datasets, provided by Hydrographic Offices producing and maintaining nautical charts following international procedures; 3. GEBCO Digital Bathymetry as the minimum resolution (1/2 arc minutes interval grid), where data gaps still exist.

In October 2016 EMODnet Bathymetry released a major update of the European digital bathymetry model. The grid resolution of the DTM was increased from the 1/4 x 1/4 arc minutes of the February 2015 version to a grid with 1/8 x 1/8 arc minutes ( $\pm 230$  by 230 meters) covering all European seas (e.g., Adriatic Sea, Aegean Sea, Baltic Sea, Barents Sea, Black Sea, Celtic Sea, Ionian Sea, Icelandic Sea, Levantine Sea, Mediterranean Sea, North Sea, Norwegian Sea). A new version is available for download since mid-September 2018, upgrading the grid resolution to 1/16 x 1/16 arc minutes ( $\pm 115$  by 115 meters). Both digital bathymetry models are available via the viewing and downloading service of the EMODnet Bathymetry data portal (<http://portal.emodnet-bathymetry.eu>).

Apart from international initiatives, Hydrographic Services may still release higher resolution data and/or gridded datasets. For the BPNS, a first DTM, at a resolution of 80 m, was produced in 2006 based on data from the Maritime Services and Coast Agency, Flemish Hydrography, completed with data from the Hydrographic Office of the Netherlands and the United Kingdom. This grid was used for the mapping of sandbank features (Verfaillie et al., 2007; Verfaillie, 2008), as well as marine landscapes (Verfaillie et al., 2009). Recently, Flemish Hydrography made available a DTM at a grid resolution of 20 by 20 meters, combining single beam (2004-2010) and more recent multibeam (post 2010) echo sounding data (table 1), a high-resolution patchwork quilt.

Table 1. Resolution of available digital bathymetry models.

Name	Year	Resolution [m]
EMODnet bathymetry	2016	230x230
	2018	115x115
Flemish Hydrography	2006	80x80
	2016	20x20

Sandbank features off the Belgian part of the North Sea

The BPNS, with a coastline of approximate 65 km and an area covering 3454 km<sup>2</sup>, is situated in the southern bight of the North Sea and is geomorphologically characterized by the presence of four sandbank systems, several swales and many sand waves and (mega)ripples formed by the interaction between water movement, i.e. local tidal and wind-driven currents, sediment transport and seabed nature. The overall water depth reaches from 0 to 40 meters LAT (Lowest Astronomical Tide).

A series of NE-SW trending linear sandbanks are developed in the BPNS, commonly asymmetric in cross-section and kinked in their plan view, but rather stable in position (Van Cauwenberghe, 1971). With a height up to 20 meters and display angles of 0 to 20 degrees relative to the main axis (Kenyon et al. 1981), these long ridges of tens of kilometres in length are often overlain by superimposed NW-SE trending sand waves and (mega)ripples with spatially-variable asymmetric patterns. Their height and wavelengths are typically 4 to 8 meters, and 200 meters respectively. Their migration changes over relatively short time intervals (Trentesaux, 1993; Houthuys et al., 1994; Lanckneus et al., 1994; Terseleer et al., this volume), but is typically in the order of 20 meters (Lanckneus et al. 2001).

Four systems with elongated sandbanks are distinguished: the Coastal Banks nearshore, the Flemish Banks located in the southwest, the Zeeland Banks in the north-east and the Hinder Banks offshore (figure 1). The Coastal and Zeeland Banks are quasi parallel to the coastline, while the Flemish

and Hinder Banks have a rather oblique position.

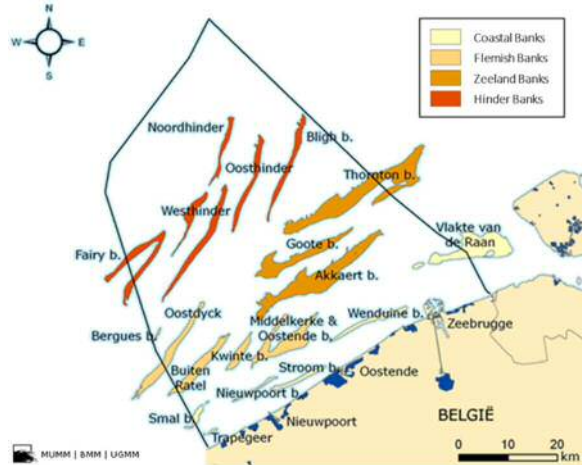


Figure 1. Simplified representation of the sandbanks on the Belgian part of the North Sea, based on the main contour lines. Small-scale sandbanks are missing.

## 2 BENTHIC TERRAIN MODELER

The Bathymetric Position Index (BPI) (Lundblad et al., 2006), part of the Benthic Terrain Modeler (BTM) toolbox in ArcGIS, is a marine modification of the Topographic Position Index (TPI) algorithm developed by Weiss (2001), and was initially used to classify the terrain on land. It allows metric calculations where a georeferenced location with a defined elevation is relative to the overall surrounding landscape, the second order derivative of the surface from an input single or multibeam bathymetric dataset. The algorithm compares each cell's elevation to the mean elevation of the surrounding cells within a user defined inner and outer radius of a rectangle, annulus (donut shape) or circle. Using negative bathymetry data, a cell lower than its neighbouring cells gets a negative BPI (valleys), a cell higher than its neighbouring cells a positive BPI (ridges). This results in a map with geomorphological features like crests (+BPI), depressions (-BPI), constant slopes and flat areas (zero BPI). Distinction between flats and slopes, the first order derivatives, is based on a user-defined threshold. For the BPNS this is 0.65 degrees, a value equal to the mean slope value of the slope map multiplied by 0.6 standard deviation (Burrough & McDonnell, 1998; slope classification

from Burrough & McDonnell, 1999). A broad-scale BPI (B-BPI) is used to determine the large geomorphology structures, a fine-scale BPI (F-BPI) for the smaller features (figure 2). For the standardization of the raw BPI, both B-BPI and F-BPI are needed. The bathymetric data tend to be spatially autocorrelated (i.e. locations that are closer together are more related than locations that are farther apart), allowing classifications against a defined dictionary of fine- and broad-scale BPI values, slopes and depths on almost any scale (Weiss, 2001).

Verfaillie et al. (2007) applied the BPI on datasets of the Belgian and Netherlands part of the North Sea (NPNS). A scale factor of  $\pm 1600$ , an outer radius of 20 meters multiplied by the grid resolution of 80 meters, for the B-BPI and a scale factor of  $\pm 240$  for the F-BPI, outer radius of 3 meters, was found most appropriate for the sandbank features on the BPNS and NPNS (Verfaillie et al., 2007). Comparative scale factors are now used for the EMODnet bathymetry datasets with a resolution of 230 by 230 meters and 115 by 115 meters, as well as for the Flemish Hydrography data grid with a resolution 20 by 20 meters. Also, other scale factors (table 2) were tested for the latter high-resolution bathymetry. Results were filtered with a minimum surface of 1 km<sup>2</sup> (1 000 000 m<sup>2</sup>) to distinguish the sandbank crests from

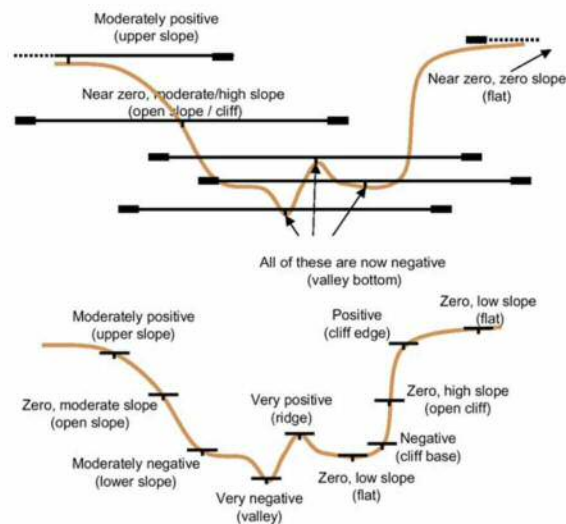


Figure 2. Top: a broad-scale BPI (B-BPI) is used to determine the large-scale geomorphological structures. Bottom: a fine-scale BPI (F-BPI) represents the smaller features.

the smaller remaining features (e.g., sand waves and other small crests). Depressions, slopes and flats have not yet been charged. On the 80 by 80 meters resolution map of Verfaillie et al. (2007), based on only single beam echo sounding data, a threshold of 300 000 m<sup>2</sup> was used.

### 3 RESULTS

Analysis of the 230 by 230 meters resolution dataset of the BCS, resulted in extra ridges in front of the Bergues Bank, Fairy Bank, Leopold Bank, Smal Bank, the northernmost bank and the bank north of the Fairy Bank, creating an extension of the sandbanks. The surface area in km<sup>2</sup> and perimeter (contour) in km, without those low-resolution additions, are listed in table 3. Even though the resolution gets a dozen times better in the 20 by 20 meters resolution, several sandbanks remain having a constant surface area (+/- 15 %). This is the case for the Bergues Bank, Bligh Bank, Buiten Ratel, Fairy Bank, Hinder Banks (Noord-, Oost- and Westhinder) and Oostdyck. A 15 to 60 % increase of the perimeter was instead calculated. For all other sandbanks, the surface area decreased drastically with better resolution. High contours are representative in the highest resolution for the Broers Bank (+98.4 %), Kwinte Bank (+65.2 %), Leopold Bank (+89.6 %), Middlekerke Bank (+36.9 %), Smal Bank (+69.6 %) Stroom Bank (+10.4 %), Thornton Bank (+135.8 %), the intermediate bank between the Buiten Ratel and Oostdyck (+34.2 %), the northernmost bank (+136.0 %) and the bank north of the Fairy Bank (+262.9 %), while lower contours are consistent for the nearshore banks, Nieuwpoort Bank (-9.8 %) and the intermediate sandbank between the Nieuwpoort and Wenduine Bank (-28.8 %). The coastal banks, Oostende Bank and Wenduine Bank, only occur from the analysis on the lowest resolution (230 by 230 meters), similar to the appearance of the extensional ridges as described above. The Akkert Bank and Goote Bank are topographically expressed as sandbanks. However, they disappear or shred in two or three with higher resolutions (115 by 115 meters and 20 by 20 meters).

Table 2. Broad- and fine-scale BPI applied to the digital bathymetry models.

	Inner [m]	Outer [m]	Resolution [m]	Scale factor
<b>B-BPI</b>				
20x20	1	80	20	1600
20x20	1	60	20	1200
20x20	1	40	20	800
20x20	1	20	20	400
80x80	1	20	80	1600
115x115	1	14	115	1610
115x115	1	7	115	805
230x230	1	7	230	1610
<b>F-BPI</b>				
20x20	1	12	20	240
20x20	1	9	20	180
20x20	1	6	20	120
20x20	1	3	20	60
80x80	1	3	80	240
115x115	1	2	115	230
115x115	1	1	115	115
230x230	1	1	230	230

### 7. 4 DISCUSSION

A fitted scale factor of 1600 for the B-BPI and 240 for the F-BPI, as proposed by Verfaillie et al. (2007) for the BPNS, was adopted. With decreasing scale factors on the same resolution of 20 by 20 meters (B-BPI: 1600-1200-800-120; F-BPI: 240-180-120-60), the surface area and perimeter of the sandbank features minimized, until some of them disappeared by the BPI algorithm. Sandbanks were thinning out, fell apart in multiple parts and faded or disappeared when using lower scale factors.

The sandbank features created by Verfaillie et al. (2007), based only on single beam bathymetry data at the time, proved to be not usable for comparing the surface area and perimeter in the multi-scale analysis. Although, the 80 meters resolution is much higher than the 230 by 230 meters or 115 by 115 meters bathymetry available via EMODnet, the fact that the latter also comprises multibeam overrules the importance of the resolution.

The sandbank extensions of Bergues Bank, Fairy Bank, Leopold Bank, Smal

Bank, the northernmost bank and the bank north of the Fairy Bank created in the lowest resolution analysis (230 by 230 meters), needed to be removed to make a correct comparison with the sandbanks at other resolutions (115 by 115 and 20 by 20 meters).

The results confirm that the surface area of the sandbank crests decrease with higher resolutions (or lower scale factors). The complexity or detailedness is reflected in the contours. With constant surface area, the higher the perimeter, the more complex the sandbank will be delineated. As such sandbank protrusion (large sand waves and small crests) will become more visible, being indicative for the varying tide-topography interaction (e.g., Bligh Bank, Buiten Ratel, Hinder Banks (Noord-, Oost- and Westhinder) and Oostdyck). And vice versa, the lower the perimeter, the less detailed and complex the sandbank will appear. (e.g., Nieuwpoort Bank and the intermediate sandbank between the Nieuwpoort and Wenduine Bank).

Some other coastal sandbanks, the Oostende Bank and Wenduine Bank, degraded with higher resolution from sandbanks to smaller and scattered sand crests, resulting in their disappearance on the 115 by 115 meters and 20 by 20 meters resolution map. The same applies for the reduction of the Akkaert Bank and Goote Bank, and the additional ridges of some sandbanks. This highlights the importance of resolving sandbanks on low-resolution datasets (e.g., 230 by 230 meters), and combine the results with a higher resolution analysis of small sand crests (e.g., 20 by 20 meters).

## 5 CONCLUSION

- Sandbank features off the BPNS are delineated with a fitted scale factor of 1600 B-BPI and 240 F-BPI.
- Multi-scale analyses are still needed, since the resolution will determine how a sandbank is delineated: continuous or as a grouping of multiple consecutive smaller crests.
- The perimeter (contour) can be a measure of accuracy, complexity or

detailedness giving insight into varying tide-topography interactions.

- Since the delineations are dependent on the resolution and data quality up-front (e.g., single beam, multi-beam), BPI outcomes may become obsolete with future improvements of available datasets.
- The revisited BPI analysis assists in the creation of a new geomorphological map for the southern bight of the North Sea. It is envisioned to further incorporate the two-part classification system for seabed geomorphology of Dove et al. (2016).
- For the BPNS, smaller-scale bedforms and their dimensions will be included as well. Other topographical highs or lows will be incorporated, together with their origin, where possible.

## 6 ACKNOWLEDGEMENT

The research is in view of the EMODnet Geology project (EASME/EMFF/2016/1.3.1.2 - Lot 1/SI2.750862). Data bathymetry is used from the Flemish Hydrography and EMODnet Bathymetry data portals.

## 9. 7 REFERENCES

- Burrough, P.A., McDonnell, R.A., 1998. Principles of Geographical Information Systems. Oxford University Press. New York. 190-193.
- Dove, D., Bradwell, T., Carter, G., Cotterill, C., Gafeira, J., Green, S., Krabbendam, M., Mellet, C., Stevenson, A., Stewart, H., Westhead, K., Scott, G., Guinan, J., Judge, M., Monteys, X., Elvenes, S., Baeten, N., Dolan, M., Thorsnes, T., Bjarnadóttir, L., Ottesen, D., 2016. Seabed Geomorphology: a two-part classification system. Marine Geoscience Programme. Open Report OR/16/001. British Geological Survey, Edinburgh, UK.
- Houthuys, R., Trentesaux, A., de Wolf, P., 1994. Storm influences on a tidal sandbank's surface (Middelkerke Bank, southern North Sea). Marine Geology 123, 23-41.
- Kenyon, N.H., Belderson, R.H., Stride, A.H., Johnson, M.A., 1981. Offshore tidal sand banks as indicators of net transport and as potential deposits. In: S.-D. Nio R.T.E. Schüttenhelm and T.C.E. van

- Weering (Editors), Holocene Marine Sedimentation in the North Sea Basin, 257-268.
- Lanckneus, J., De Moor, G., Stolk, A., 1994. Environmental setting, morphology and volumetric evolution of the Middelkerke Bank (southern North Sea). *Marine Geology* 121, 1-21.
- Lanckneus, J., Van Lancker, V., Moerkerke, G., Van den Eynde, D., Fettweis, M., De Batist, M., Jacobs, P., 2001. Investigation of the natural sand transport on the Belgian Continental Shelf (BUDGET). Final report. Federal Office for Scientific, Technical and Cultural Affairs (OSTC).
- Lundblad, E., Wright, D.J., Miller, J., Larkin, E.M., Rinehart, R., Anderson, S.M., Battista, T., Naar, D. F., Donahue, B.T., 2006. A Benthic Terrain Classification Scheme for American Samoa. *Marine Geodesy*, 29 (2), 89-111.
- Trentesaux, A., 1993. Structure et dynamique sédimentaire du Middelkerke Bank, Mer du Nord méridionale. Unpublished PhD Thesis. Université des Sciences et Technologies de Lille, France, 229pp.
- Van Cauwenberghe, C., 1971. Hydrographische analyse van de vlaamse Banken langs de Belgische-Franse kust. *Ingenieurstijdingen Blatt* 20, 141-149.
- Verfaillie, E., Degraer, S., Schelfaut, K., Willems, W., Van Lancker, V., 2009. A protocol for classifying ecologically relevant marine zones, a statistical approach. *Estuarine, Coastal and Shelf Science* 83 (2), 175-185. doi:10.1016/j.ecss.2009.03.003.
- Verfaillie, E., Doornenbal, P., Mitchell, A.J., White, J., Van Lancker, V., 2007. The bathymetric position index (BPI) as a support tool for habitat mapping. Worked example for the MESH Final Guidance, 14pp.
- Verfaillie, E., 2008. Development and validation of spatial distribution models of marine habitats, in support of the ecological valuation of the seabed. PhD Thesis. Ghent University, Belgium, 207 pp.
- Weiss, A. D. 2001. Topographic Positions and Landforms Analysis (Conference Poster). ESRI International User Conference. San Diego, CA, July 9-13.

Table 3. Surface area and perimeter (contour) of BPNS sand banks (crest only) delineated on the basis of datasets with a resolution of 230 meters, 115 meters, 20 meters and B-BPI = ± 1600, F-BPI = ± 240.

Name	230x230		115x115		20x20	
	Area [km <sup>2</sup> ]	Contour [km]	Area [km <sup>2</sup> ]	Contour [km]	Area [km <sup>2</sup> ]	Contour [km]
<b>COASTAL BANKS</b>						
Broers Bank	7.98	17.09	2.25 -71.8%	13.32 -22.1%	2.87 -64.1%	33.90 98.4%
Nieuwpoort Bank	9.12	29.28	5.47 -40.0%	23.22 -20.7%	5.66 -38.0%	26.41 -9.8%
Nieuwpoort-Wenduine Bank	4.20	17.59	1.37 -67.3%	10.14 -42.3%	1.78 -57.6%	12.52 -28.8%
Smal Bank	9.71	24.92	5.09 -47.6%	21.62 -13.2%	6.48 -33.3%	42.26 69.6%
Stroom Bank	8.13	27.88	4.17 -48.7%	26.07 -6.5%	4.16 -48.8%	30.78 10.4%
Wenduine Bank	2.85	16.80	Na Na	Na Na	Na Na	Na Na
<b>FLEMISH BANKS</b>						
Bergues Bank	5.25	14.81	3.82 -27.4%	12.97 -12.4%	4.59 -12.7%	17.15 15.8%
Buiten Ratel	26.84	42.75	22.37 -16.7%	50.64 18.5%	25.27 -5.9%	58.92 37.8%
Kwinte Bank	23.99	73.00	14.46 -39.7%	56.65 -22.4%	19.79 -17.5%	120.60 65.2%
Middelkerke Bank	10.87	29.96	6.47 -40.5%	26.55 -11.4%	8.20 -24.6%	41.02 36.9%
Oostdyck	31.02	65.57	24.19 -22.0%	71.03 8.3%	27.72 -10.6%	93.35 42.4%
Oostdyck-Buiten Ratel	6.64	18.37	4.18 -37.0%	14.59 -20.5%	5.21 -21.6%	24.65 34.2%
Oostende Bank	8.79	41.33	Na Na	Na Na	Na Na	Na Na
Smal-Kwinte-Middelkerke Bank	3.74	12.94	2.35 -37.2%	10.24 -20.8%	2.56 -31.6%	12.90 -0.2%
<b>HINDER BANKS</b>						
Bligh Bank	18.80	59.09	12.64 -32.8%	60.33 2.1%	21.25 13.0%	93.43 58.1%
Fairy Bank	20.05	51.06	16.20 -19.2%	54.29 6.3%	17.88 -10.8%	62.15 21.7%
Noordhinder	32.35	94.81	22.78 -29.6%	94.24 -0.6%	31.67 -2.1%	125.85 32.7%
Oosthinder	31.18	89.96	21.31 -31.7%	102.86 14.3%	32.35 3.7%	125.74 39.8%
Westhinder	27.64	62.05	23.66 -14.4%	70.08 12.9%	28.67 3.7%	79.54 28.2%
bank north of the Fairy Bank	7.88	19.23	5.79 -26.5%	26.40 37.3%	6.07 -22.9%	69.79 262.9%
northernmost bank	11.79	31.50	6.87 -41.7%	38.22 21.3%	6.26 -46.9%	74.33 136.0%
<b>ZEELAND BANKS</b>						
Akkaert Bank	19.91	69.37	7.06 -64.6%	51.38 -25.9%	9.47 -52.4%	80.28 15.7%
Goote Bank	10.91	39.31	Na Na	Na Na	2.18 -80.0%	24.88 -36.7%
Leopold Bank	10.29	31.75	5.78 -43.8%	30.04 -5.4%	7.92 -23.1%	60.20 89.6%
Thornton Bank	25.13	55.96	17.44 -30.6%	62.40 11.5%	20.25 -19.4%	131.94 135.8%



# Tidal flats, megaripples and marsh: automated recognition on aerial images

Maarten G. Kleinhans *Utrecht University, Utrecht, the Netherlands* – *m.g.kleinhans@uu.nl*

Harke Douma *Utrecht University, Utrecht, the Netherlands* – *h.douma@uu.nl*

Elisabeth A. Addink *Utrecht University, Utrecht, the Netherlands* – *e.a.addink@uu.nl*

Robert Jentink *Rijkswaterstaat CIV, Middelburg, the Netherlands* – *robert.jentink@rws.nl*

**ABSTRACT:** Intertidal areas in estuaries are highly dynamic and ecologically important. Here we present a novel method for automated recognition of saltmarsh, pioneer vegetation, megaripples and plane bed from aerial photographs and bathymetry. Results are compared with manual classification. The two methods agree for about 73% of the whole area, and 95% for (partly) vegetated areas. The distinction between the bare bar surface classes is more difficult and often vague due to the existence of gradients and temporal transitions. The distinction between (nearly) plane sand bed and megaripples does not improve much with the use of slope and slope variation calculated from bathymetry, but further improvements may be possible with data derived from stereo photography. Nevertheless, the high degree of agreement shows that the automated method is highly promising for application to large systems such as the Wadden Sea.

## 1 INTRODUCTION

Intertidal areas in estuaries are ecologically valuable, but their dynamics are poorly understood because they are determined by complex interactions between:

- shallow flow over tidal bars with large bedforms,
- sand-mud sedimentation with macrobenthic bioturbation effects,
- disposed sediment advection following fairway maintenance, and
- saltmarsh.

The most striking characteristic is the spatiotemporal variation in surface properties in close proximity. While saltmarsh has been studied extensively, understanding of the tidal flats is limited because these large areas are difficult to access for fieldwork and difficult to model numerically because of the shallow flows and continuous drying and wetting.

The intertidal surface area in the Western Scheldt is protected by law (e.g. Natura

2000), but it is under threat of reduction. Since large-scale fairway dredging has been conducted, the channels deepened and the bars accreted, so that bar margins steepened and the intertidal area has reduced, which is mitigated by shoal margin disposal strategies. To gain system behaviour understanding and monitor these important areas, Rijkswaterstaat developed a manual methodology of biogeomorphology with protocols for mapping from aerial photography and fieldwork for the entire system (Bouma et al. 2005). An automated method would be beneficial for efficient and objective application to other tidal systems, including the much larger Wadden Sea.

Our objectives are 1) to explore whether a semi-automated classification using Object-Based Image Analysis (OBIA, Addink et al. 2012) and a ruleset produces similar maps as the manual classification, and 2) to study spatial extent and temporal change of megaripples and flats.

## 2 METHOD AND RESULTS

After extensive testing the following novel method was developed (Douma et al. 2018). Tiles of merged false-colour aerial photographs were segmented to yield a few tens of thousands of objects with a minimum degree of spectral heterogeneity. We developed a ruleset in eCognition to classify the objects into seven classes (Figure 1). Main steps are illustrated in Figure 2. Vegetated surfaces were recognised through a ratio between near-infrared and red reflection: the Normalised Difference Vegetation Index. The bare surface was further classified on the basis of brightness, object shape and context (neighbouring objects). For present conditions and the entire system the total computation time is 24 hours.

The automated classification based on the ruleset produces a similar map as the visual method. The total surface areas of the classes are fairly similar (Figures 3,4,5). For saltmarsh areas including partially covered areas the agreement is about 95%, where differences arise due to objectified thresholds for partial cover and the detail in the boundaries in the automated method. However, the total area of perfect agreement between the manual and automatically produced maps is about 73%.

Most of the disagreement between the maps occurs in the bare surface classes that were difficult to distinguish. We tested whether the use of bed slope and variation thereof calculated from bathymetry improved the classification of the bare surfaces (Figure 6). However, this added megaripple area corresponding on both maps, but also added low-energy and high-energy plane shoal areas to the megaripple class in disagreement with the manually drawn map. Visual inspection shows that the boundaries between sand flat and megaripples are sometimes poorly recognised in the automated method.

Map inspection and field site visits show that all three possible transitions between megaripples, high-energy plane bed and low-energy plane bed occur. The nature of the transitions varies. In some cases there

appear to be relic megaripple fields, sometimes covered by mud (consisting of clay and silt). Another frequently occurring transition occurs due to the migration of a sand body, covered in megaripples, onto a low-energy tidal flat. Clearly, further study of spatiotemporal transitions on intertidal flats are needed.

## 3 CONCLUSIONS

Object-Based Image Analysis of aerial photographs of intertidal areas allows fast automated mapping of biogeomorphology that corresponds well with visual interpretations for about three quarters of the surface.

While two-dimensional bedforms are fairly well detectable by automated methods on bathymetries, the recognition of three-dimensional megaripple fields in complex intertidal areas remains challenging.

Spatial and temporal transitions have various causes and natures that need to be unravelled, and that are reflected by differences between visual and automated mapping.

## 4 ACKNOWLEDGEMENTS

HD did most of the analyses and was funded by RWS-CIV. MGK was funded by NWO-TTW (grant Vici 016.140.316/13710 to MGK).

## 5 REFERENCES

- Addink, E.A., Van Coillie, F.M.B., and De Jong, S.M., 2012. Introduction to the GEOBIA 2010 special issue: From pixels to geographic objects in remote sensing image analysis. International Journal of Applied Earth Observation and Geoinformation 15, 1-6.
- Bouma, H., de Jong, D.J., Twisk, F. and Wolfstein, K., 2005. Zoute wateren EcotoenStelsel (ZES.1) voor het in kaart brengen van het potentiële voorkomen van levensgemeenschappen in zoute en brakke rijkswateren. Report of Rijkswaterstaat RIJKZ/2005.024.
- Douma, H., Addink, E.A. and Kleinhans, M.G., 2018. Verkenning productie Geomorfologische Kaart met behulp van Object Based Image Analysis. Universiteit Utrecht, Departement Fysische Geografie, report for Rijkswaterstaat CIV.



Figure 1. Biogeomorphology classes with map legend.

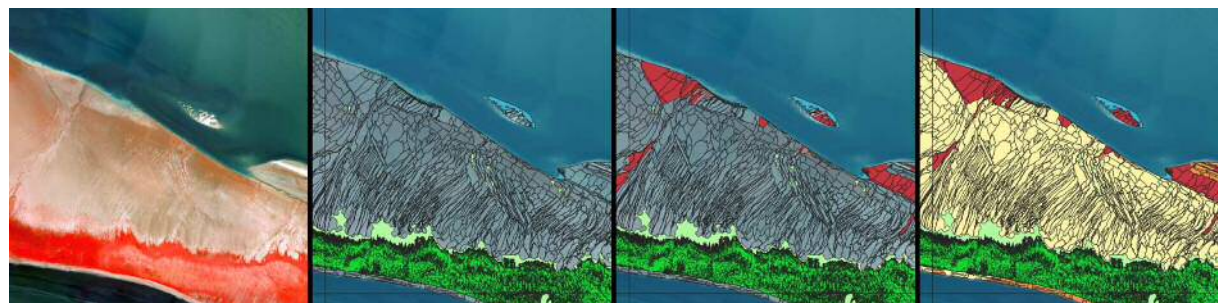


Figure 2. Main steps in the classification: (stretched) aerial photograph; vegetation, megaripples (includes height information), bare surface classes.

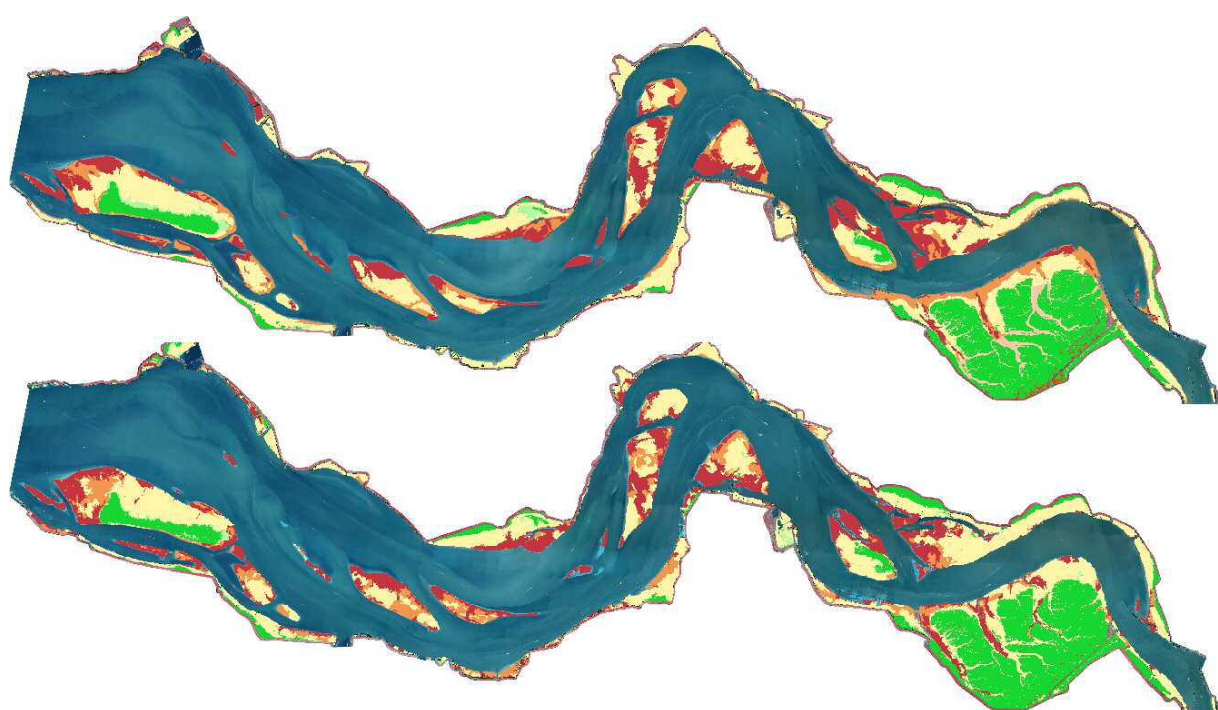


Figure 3. Maps of the Western Scheldt (Netherlands) classified automatically (top) and manually (bottom).

\*

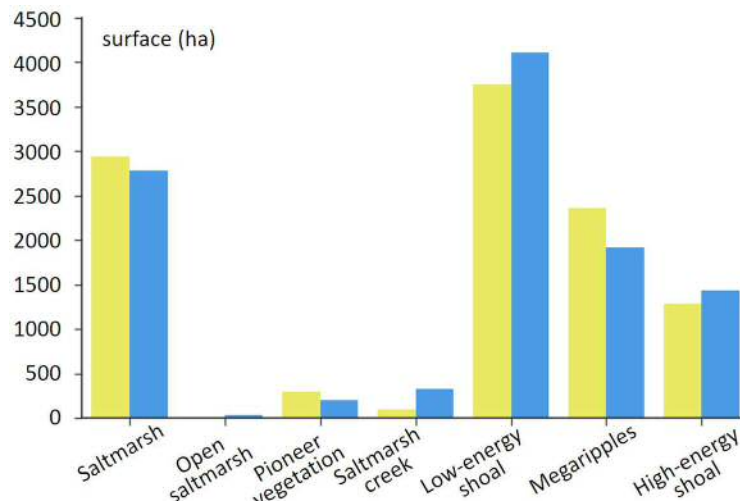


Figure 4. Total area per class in 2016 for the manual (yellow) and automatic (blue) classification including elevation data.

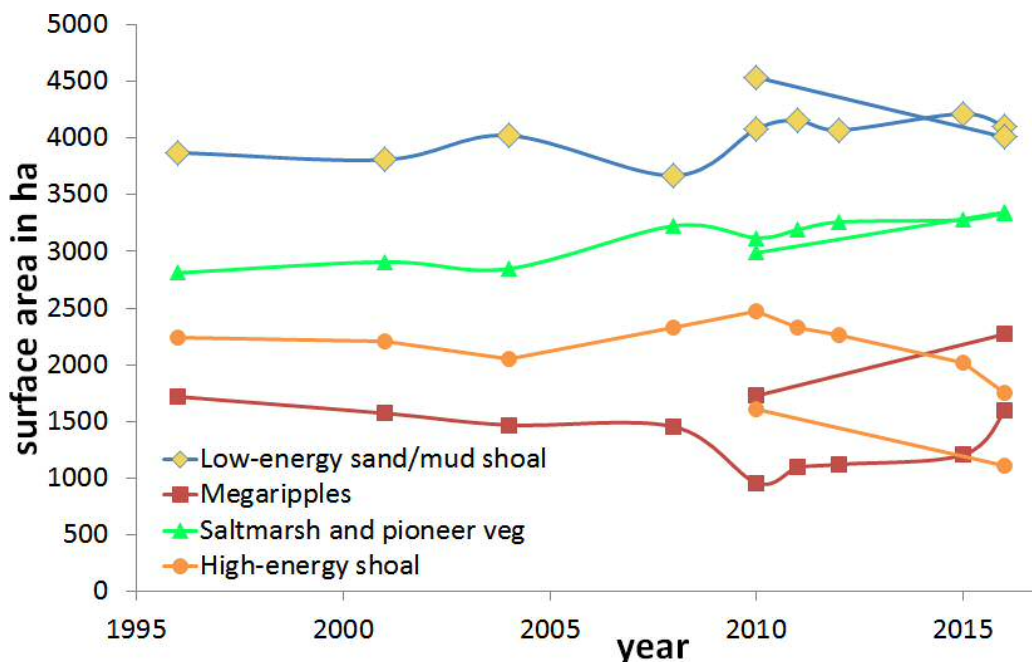


Figure 5. Development of surface area. Straight lines with points at 2010 and 2016 are from the automatic classifications presented here.

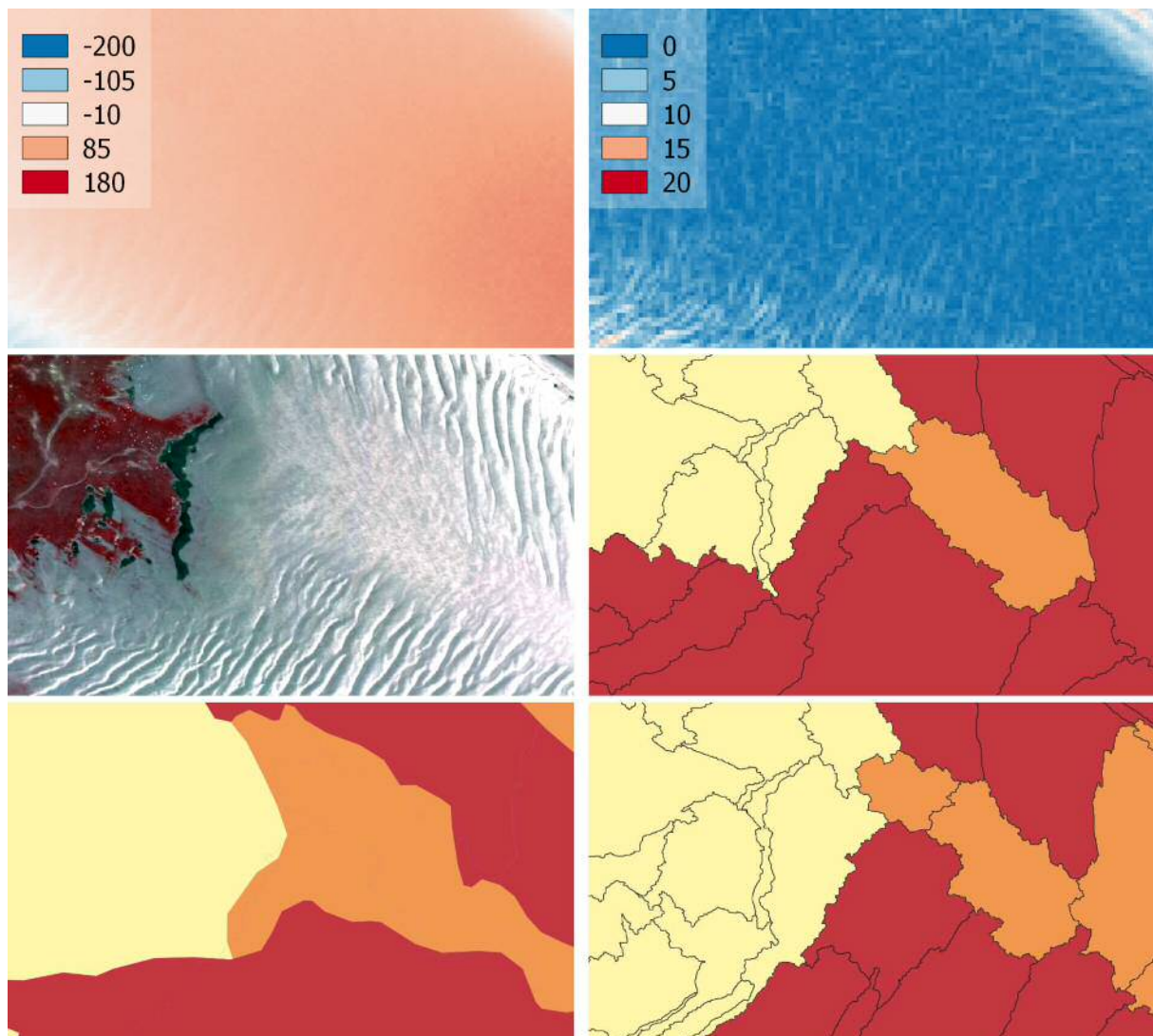


Figure 6. Classification of bare surface on the basis of bed elevation data (top left, in cm+NAP, 2 m horizontal resolution), bed slope (top right, in degrees), and aerial photograph (stretched image middle left). Width of the image is about 300 m. Classification by visual interpretation (bottom left), automated image segmentation alone (middle right) and by inclusion of bed slope and bed slope variation in the automated method (bottom right).



# Modelling the past evolution of observed tidal sand waves: the role of boundary conditions

Janneke M. Krabbendam *Utrecht University, Utrecht and WaterProof B.V., Lelystad, the Netherlands* – *j.m.krabbendam@uu.nl*

Abdel Nnafie *Utrecht University, Utrecht, the Netherlands* – *A.Nnafie@uu.nl*

Luitze M. Perk *WaterProof B.V., Lelystad, the Netherlands* – *luitze.perk@waterproofbv.nl*

Bas W. Borsje *University of Twente, Enschede, the Netherlands* – *b.w.borsje@utwente.nl*

Huib E. de Swart *Utrecht University, Utrecht, the Netherlands* – *H.E.deSwart@uu.nl*

**ABSTRACT:** Tidal sand waves are rhythmic bed forms located in many coastal seas. These bed forms have heights up to ten meters and migration rates of several meters per year. Due to their dynamic nature, sand waves can uncover buried cables and pipelines, thereby making them subject to risk of damage. This study aims at developing a new numerical 2DV model (Delft3D) to simulate the past evolution of tidal sand waves on a decadal timescale (hindcast study). In particular, the effect of imposing different types of boundary conditions (time series of currents, water levels and Riemann invariants) on sand wave evolution is investigated. Simulations are conducted for a period of ten years, whereby an observed sand wave field is used as an initial bathymetry. Model results show that imposing time series of Riemann invariants at one boundary and of water level at the other yields the best agreement with bed level observations.

## 1 INTRODUCTION

Coastal seas are often characterized by the presence of a large variety of rhythmic bed forms with different spatial and temporal scales (Van Dijk et al., 2008). One type of these bed forms are tidal sand waves, which have wavelengths of 100-1000 m, heights of 1-10 m and migration speeds of up to 10 m/year (McCave, 1971).

Because of their dynamic behaviour, variations in the characteristics of sand waves (e.g. crest height, trough depth, migration rate) pose a hazard to offshore activities, for example by uncovering originally buried cables and pipelines, by changing the depth of navigation channels and scouring offshore platforms (Németh et al., 2003). Therefore, increasing knowledge of the dynamics of sand waves could lower costs related to these offshore activities, e.g. by optimizing burial depths of cables and pipelines.

Currently, when planning the burial of cables and pipelines, predictions of sea bed evolution are used that result from extrapolation of historical trends. As this method has large uncertainties, alternative predictions are needed. Process-based models are suitable tools for such a purpose, as they contain the physical processes driving tidal sand wave evolution.

Various modelling studies have been conducted over the past and these can be divided into linear and non-linear models. The first models used linear stability analysis to study the initial formation of tidal sand waves (see Besio et al. 2008 for an overview). In these studies it was shown that the interaction of the oscillating tidal flow with a small amplitude wavy bottom results in residual circulation cells in the vertical plane. Because of the higher instantaneous velocity up the crest and the non-linear relation between sand transport and velocity, the sand transport is always higher up the crest than down. This results in a net convergence

of sand at the crest when averaged over a tidal cycle. This growth process is counteracted by the divergence of slope-induced transport. Borsje et al. (2013) used a complex numerical model (Delft3D) to investigate the initial formation. However, linear stability analysis is only valid for sand waves with small amplitudes.

Non-linear effects cause the growth rate to slow down and need to be included in order to study long-term evolution of tidal sand waves. Idealized non-linear models, such as the one presented by Campmans et al. (2018 and references therein), showed promising results, but sand wave amplitudes tended to grow larger than observed. Van Gerwen et al. (2018) analysed the model of Borsje et al. (2013) for longer timescales and sand waves were able to grow from an initial perturbation to an equilibrium height. However, the only initial states considered in these studies were sinusoidal sand waves with small amplitudes. In order to simulate the evolution of observed sand waves, sand waves with a finite height should be used as initial state.

The aim of this study is to develop a new numerical model based on the modelling system Delft3D that is able to simulate the past evolution of observed tidal sand waves, i.e. a hindcast study. In particular, the effect of imposing different types of boundary conditions on sand wave evolution is investigated. To this end, simulations are conducted for a period of ten years, whereby an observed sand wave field is used as an initial bathymetry. The simulated bed level after ten years is compared with observations. Comparison between model results and observations includes sand wave height, wavelength, shape and migration rate.

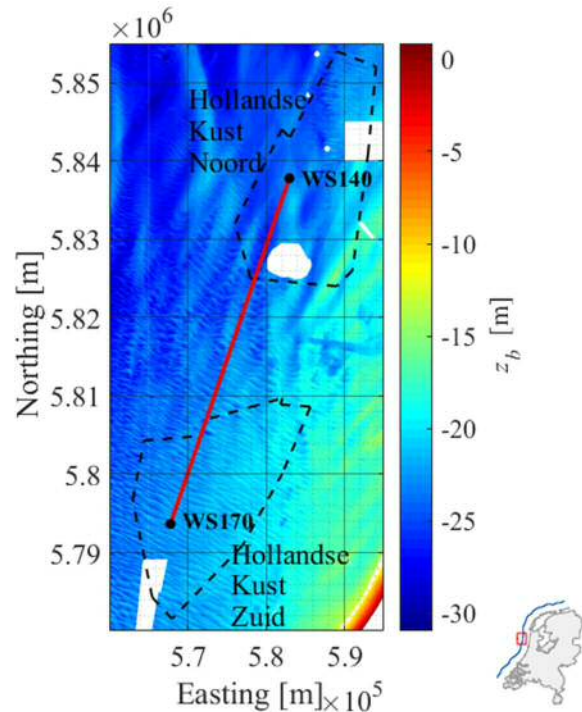


Figure 1. Bed level  $z_b$  of 2010 (Netherlands Hydrographic Office, 2017) and location of future wind farms Hollandse Kust Zuid and Noord. The red line corresponds to the transect under investigation.

## 2 MATERIAL AND METHODS

### Study area

The study area consists of a 45.5 km transect located between two measuring buoys (WS170 and WS140) in the North Sea (Fugro, 2018a and b). The first buoy is located in the area of the future wind park Hollandse Kust Zuid (HKZ) and the second in Hollandse Kust Noord (HKN), as shown in Figure 1. In this area, bathymetrical surveys were performed by the Netherlands Hydrographic Office of the Royal Netherlands Navy (2017).

### Model description

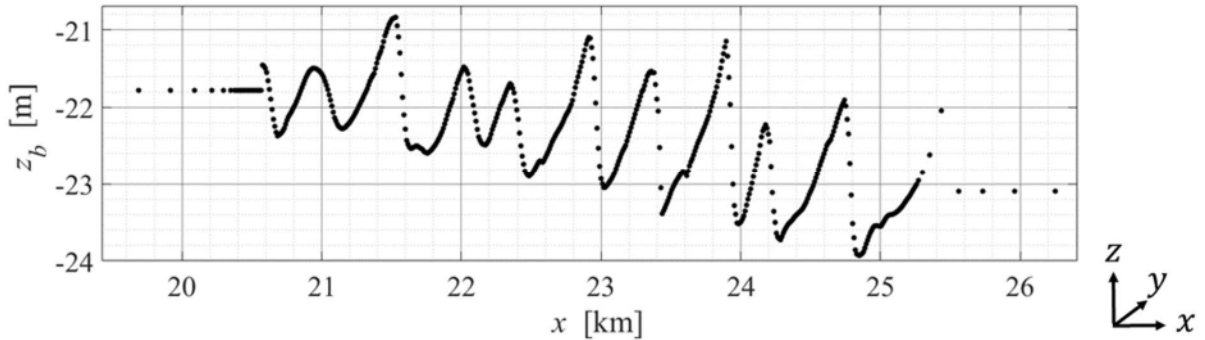


Figure 2. The initial bed level  $z_b$  ( $t=0$ ) (Netherlands Hydrographic Office, 2017) over  $x$ , which is the distance from boundary point WS170 in the HKZ area. Figure is a close-up of the middle of the domain where the sand waves under investigation are located.

The formation of sand waves is modelled using the numerical shallow water model Delft3D-FLOW (Lesser et al., 2004). It consists of a horizontal momentum equation, a continuity equation, a bed load and suspended load transport equation and a sediment continuity equation. The model equations are solved by applying sigma layering in the vertical direction. In this study, the model is run in the 2DV mode, i.e. considering flow and variation in the  $x$ - and  $z$ -direction only, while assuming zero flow and uniformity in the  $y$ -direction. This is valid as the crests and the migration are oriented perpendicular to the direction of the principal tidal current. The  $x$ -coordinate is defined as distance from boundary point WS170 in the HKZ area. For turbulence closure the  $k - \varepsilon$  model is chosen.

In order to study the evolution of observed sand waves, bathymetric data as measured in 2000 (Netherlands Hydrographic Office, 2017) along the transect in Figure 1 were used as initial bed level. To minimize boundary effects, only the sand waves in the middle 5 km of the domain were retained (Fig. 2).

The tidal flow was forced with a three-month time series of water level and depth-averaged velocity measured by the two buoys (Fugro, 2018a and b). A snapshot of this data as measured in HKZ (WS170) is shown in Figure 3, with depth-averaged velocity  $U$  in blue and the water level  $\zeta$  in red.

These time series were imposed in four different ways: (1)  $U(t)$  and  $\zeta(t)$  combined into two Riemann invariants  $R(t)$  at both boundaries; (2)  $U(t)$  at the Southern boundary ( $x = 0$ ) and  $\zeta(t)$  at the Northern boundary ( $x = L_x$ ); (3) a water level time series  $\zeta(t)$  at both boundaries and (4) a Riemann invariant  $R(t)$  at  $x = 0$  (S) and  $\zeta(t)$  at  $x = L_x$  (N). The Riemann invariants, which are constant along the characteristic curves of the system of equations, are implemented by combining water level and velocity timeseries as follows (Deltaires, 2013):

$$R(t) = U(t) + \zeta(t) \sqrt{\frac{g}{d(t)}}. \quad (1)$$

The median sand grain size  $d_{50}$  was set to 0.25 mm (Fugro, 2016). The bed slope factor  $\alpha_{bs}$  is a correction parameter and is included to account for the fact that sand is transported more easily downhill than uphill. The value of  $\alpha_{bs}$  was set to 3, which corresponds to an angle of repose of sand of  $19^\circ$ . The Chézy roughness  $C$  was set to  $75 \text{ m}^{1/2} \text{ s}^{-1}$  after Van Gerwen et al. (2018).

The horizontal grid spacing varies from  $\Delta x = 1500 \text{ m}$  at the boundaries to  $\Delta x = 10 \text{ m}$  in the area of the sand waves (Fig. 2). In the vertical direction, the domain is divided into 50  $\sigma$ -layers in such a way that the vertical resolution is highest near the bed and decreases towards the surface. To speed up the computation time, a morphological acceleration factor (MF) of 100 was intro-

Table 1: Model parameters

Parameter	Symbol	Value
Horizontal domain length	$L_x$	45.5 km
Chézy roughness	$C$	$75 \text{ m}^{1/2} \text{ s}^{-1}$
Median sand grain size	$d_{50}$	0.25 mm
Bed slope parameter	$\alpha_{bs}$	3
Hydrodynamic time step	$\Delta t$	6 s
Horizontal grid spacing	$\Delta x$	10-1500 m
No of sigma layers	-	50
Morphological acceleration factor	MF	100

duced. The hydrodynamic time step was set to  $\Delta t = 6$  s. The hydrodynamic runtime was 10 years in order to compare the output with

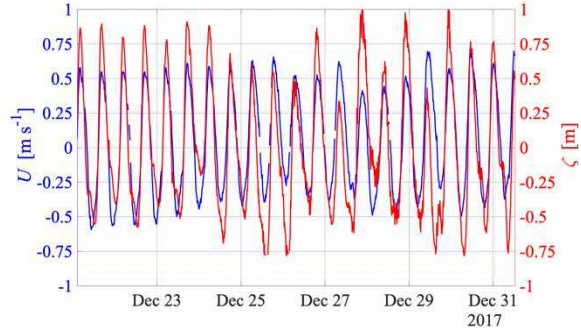


Figure 3. Snapshot of time series of depth-averaged velocity  $U$  (blue) and water level  $\zeta$  (red) over time (Fugro, 2018a), measured at HKZ (WS170).

the bathymetry data of 2010. An overview of the main model parameters and their values is provided in Table 1.

### 3 RESULTS AND DISCUSSION

From Figure 4, which shows the ob-

served bed levels in 2000 and 2010 (black and blue

lines, respectively), it appears that sand waves migrate in the positive  $x$ -direction, at rates ranging between 0.5 m/year and 2 m/year. Two sand waves have not migrated in this period (indicated by black arrows in Figure 3), but they underwent changes in their shape. Most of the sand waves retained their trough depth over the period 2000-2010, but their crest height decreased in some locations and increased in others.

Figure 5 shows the simulated bed levels  $z_b$  for different cases of boundary conditions (a), as well as bed level differences  $\Delta z_b$  with respect to observations of the bed level in 2010 (b). From this figure, it turns out that simulated bed levels are rather sensitive to the type of boundary conditions imposed. Best agreement between model results and observations is obtained in the case of using a time series of Riemann invariants  $R(t)$  at both boundaries (Case 1 in Table 2) and in case of using  $R(t)$  at the Southern boundary and  $\zeta(t)$  at the Northern boundary (Case 4). In these cases, the simulated sand crest heights and trough depths agree well with observations, although the model over (under)-predicts crest height at some locations. The simulated sand wave field migrates in the same directions as the observed field. In the other cases (Cases 2 and 3), the simulated sand wave field migrates in the opposite direction compared to observations, and its shape is considerably different from the one observed, particularly in Case 3. The achievement of best model performance in Cases 1 and 4 is also

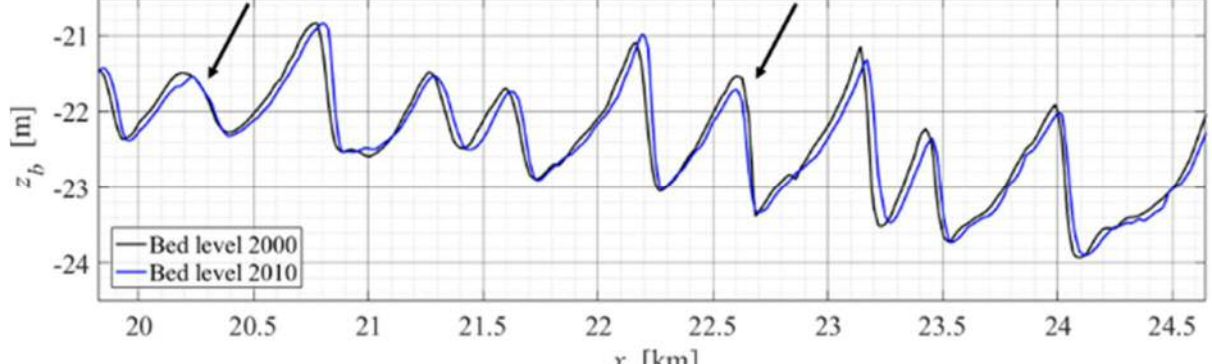


Figure 4. Observed bed level of 2000 and the observed bed level of 2010. Figure is a zoom-in of the transect.

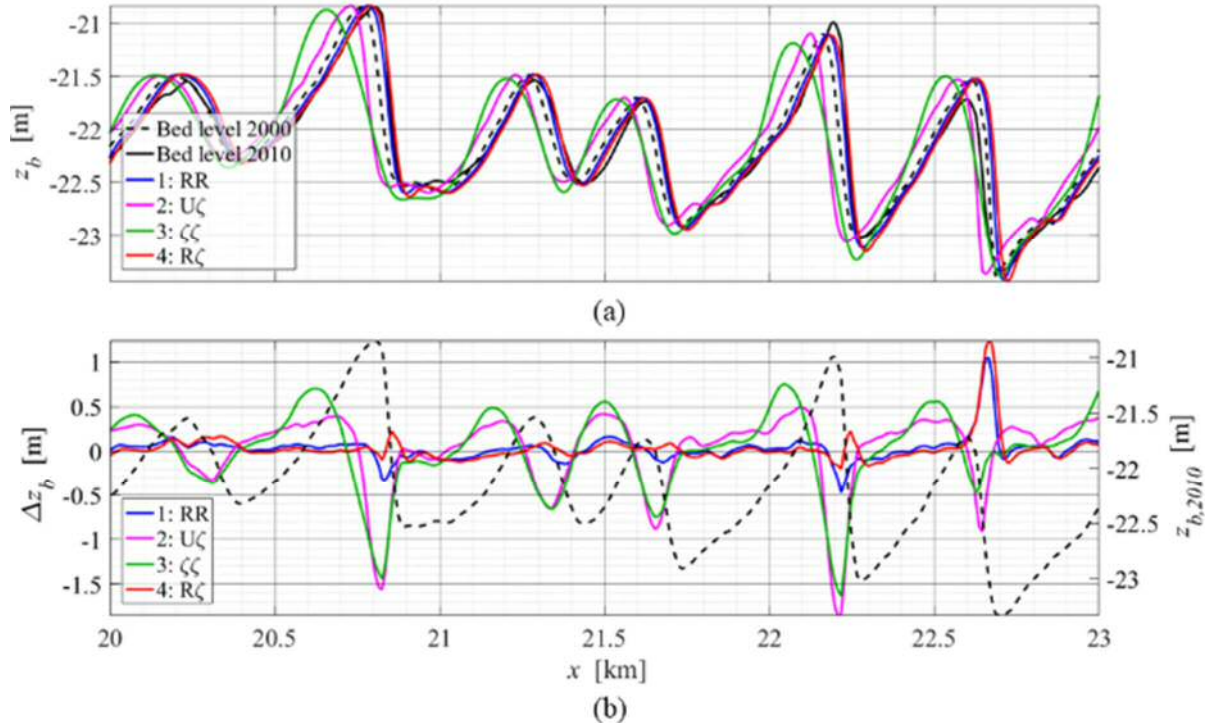


Figure 5. (a) Bed level  $z_b$  measured in 2000 and 2010 (dashed and solid black lines, respectively) over  $x$ , and simulated  $z_b$  for the different types of boundary conditions: 1. two Riemann invariants  $R(t)$  (blue); 2. depth-averaged velocity  $U(t)$  and water level  $\zeta(t)$  (magenta); 3. two water level time series  $\zeta(t)$  (green); 4. Riemann invariants  $R(t)$  and water level  $\zeta(t)$  (red). (b) Difference between modelled and measured bed level  $\Delta z_b$  for different sets of boundary conditions. The right y-axis corresponds to bed level as measured in 2010 ( $z_{b,2010}$ ) (black dotted line).

confirmed by the smallest root-mean-square-error (RMSE), compared with other cases (Table 2).

Sand wave migration is caused by differences in ebb- and flood velocity and/or duration (Besio et al. 2008). These differences can arise from the presence of a residual current ( $M_0$ ) or the phase difference between the principal tidal component  $M_2$  and its first overtide  $M_4$ . The results in Figure 5 demonstrate that the type of boundary conditions imposed significantly affects the migration rate. This is surprising, as these boundary conditions are based on the same time series, meaning that residual currents and the phase difference between  $M_2$  and  $M_4$  should be the same. Apparently, different types of boundary conditions translate into different residual velocity fields and can therefore result in opposing migration directions.

Table 2 Root mean square error

Boundary conditions	RMSE (m)
1 S: $R(t)$ and N: $R(t)$	0.15
2 S: $U(t)$ and N: $\zeta(t)$	0.48
3 S: $\zeta(t)$ and N: $\zeta(t)$	0.46
4 S: $R(t)$ and N: $\zeta(t)$	0.14

There are several model limitations. Firstly, one horizontal dimension is neglected, while sand waves are in fact a 3D phenomenon (see for example Figure 1). Also, a morphological acceleration factor is introduced, which is convenient for the computation time, but can cause errors. Thirdly, the effects of wind driven currents and waves are neglected (Campmans et al. 2018). Furthermore, the median grain size is assumed to be constant throughout the whole domain, while measurements by Fugro (2016) and surveys elsewhere in the North Sea (see e.g. Van Oyen and Blondeaux (2009) and references therein) indicate that sorting patterns

occur along sand waves. Including these sorting patterns might affect the magnitude and direction of sand transport. Finally, this model was only tested for one location and it is a topic of future research to apply it to other places in the North Sea.

#### 4 CONCLUSIONS

The model results are rather sensitive to the type of boundary conditions imposed; especially the migration rate is affected by changing the boundary conditions. The best agreement between the observed and simulated bathymetry results from a combination of a time series of Riemann invariants and of water levels. Using the latter, the model is able to mimic the evolution of mature sand waves in the HKZ-HKN area in the North Sea and can therefore provide a valuable tool in the planning of cable burial depths provided that velocity and/or water level measurements are available.

#### 5 ACKNOWLEDGEMENT

This research is part of NWO project NWA.ID.17.038 of the Netherlands Organisation of Scientific Research.

#### 6 REFERENCES

- Besio, G., Blondeaux, P., Brocchini, M., Hulscher, S. J. M. H., Idier, D., Knaapen, M. A., Németh., A. A., Roos, P. C., Vittori, G. 2008. The morphodynamics of tidal sand waves: A model overview. *Coastal Engineering*, 55(7-8), 657–670.
- Blondeaux, P., Vittori, G. 2016. A model to predict the migration of sand waves in shallow tidal seas. *Continental Shelf Research*, 112, 31-45.
- Borsje, B. W., Roos, P. C., Kranenburg, W. M., Hulscher, S. J. M. H. (2014). Modeling tidal sand wave formation in a numerical shallow water model: The role of turbulence formulation. *Continental Shelf Research*, 60, 17–27.
- Campmans, G., Roos, P. C., de Vriend, H. J., Hulscher, S. M. J. H. , 2018. The influence of storms on sand wave evolution: a nonlinear idealized modelling approach. *Journal of Geophysical Research: Earth Surface*. doi: 10.1029/2018jf004616.
- Deltares, 2013. User manual Delft-3D FLOW. Technical report. Deltares, Delft.
- Fugro, 2016. Geophysical Site Investigation Survey, Wind Farm Site I. Technical Report. Fugro, Leidschendam.
- Fugro., 2018a. HKN Metocean Campaign Data & Reports. Retrieved from <https://offshorewind.rvo.nl/windwaternh>
- Fugro., 2018b. HKZ Metocean Campaign Data & Reports. Retrieved from <https://offshorewind.rvo.nl/windwaterzh>
- Lesser, G., Roelvink, J. v., Van Kester, J., Stelling, G., 2004. Development and validation of a three-dimensional morphological model. *Coastal Engineering*, 51(8-9), 883–915.
- McCave, I. N., 1971. Sand waves in the North Sea off the coast of Holland. *Marine Geology*, 10(3), 199–225.
- Németh, A. A., Hulscher, S. J. M. H., De Vriend, H. J., 2003. Offshore sand wave dynamics, engineering problems and future solutions. *Pipeline and Gas Journal*, 230(4), 67–69.
- Netherlands Hydrographic Office., 2017. Hydrographic surveys. Retrieved from [http://opendap.deltares.nl/thredds/catalog/opendap\\_hydrografie/surveys/catalog.html](http://opendap.deltares.nl/thredds/catalog/opendap_hydrografie/surveys/catalog.html)
- Van Dijk, T. A. G. P., Lindenbergh, R. C., Egberts, P. J. P., 2008. Separating bathymetric data representing multiscale rhythmic bed forms: A geostatistical and spectral method compared. *J. of Geophys. Res.: Earth Surface*, 113(4), 1– 16.
- Van Gerwen, W., Borsje, B. W., Damveld, J. H., Hulscher, S. J. M. H., 2018. Modelling the effect of suspended load transport and tidal asymmetry on the equilibrium tidal sand wave height. *Coastal Engineering*, 136, 56–64.
- Van Oyen, T., Blondeaux, P., 2009. Grain sorting effects on the formation of tidal sand waves. *Journal of Fluid Mechanics*, 629, 311–342.

# Long-term dune dynamics in the Lower Weser Estuary

Knut Krämer *MARUM, University of Bremen, Bremen, Germany* – kkraemer@uni-bremen.de

Alice Lefebvre *MARUM, University of Bremen, Bremen, Germany* – alefebvre@marum.de

Marius Becker *Institute of Geosciences, CAU, Kiel, Germany* – marius.becker@ifg.uni-kiel.de

Gerald Herrling *Institute of Geosciences, CAU, Kiel, Germany* – gerald.herrling@ifg.uni-kiel.de

Christian Winter *Institute of Geosciences, CAU, Kiel, Germany* – christian.winter@ifg.uni-kiel.de

**ABSTRACT:** The dynamics of primary dunes in the Lower Weser Estuary have been studied for over 40 years due to their importance for sediment transport and the safety of navigation. In this work, a dataset of monthly bathymetric surveys over a period of 10 years is analyzed to investigate the relations between hydrological parameters and corresponding dune morphodynamics. Dune heights show a negative correlation with freshwater discharge whereas dune lengths exhibit a positive correlation. The tidal range inversely correlates to dune height and length. The dune migration celerity increases with increasing discharge and is independent of tidal range across temporal scales from individual discharge events to decadal trends.

## 1 INTRODUCTION

The Weser is a 452 km long river which flows in northwestern Germany and discharges into the German Bight, southern North Sea (Fig. 1). The lower reach of the river is tidally-influenced over 130 km from the river mouth until the tidal weir in Bremen. The fresh water discharge at gauge station Intschede ranges from 120 to 1,200 m<sup>3</sup>/s with an annual average of 320 m<sup>3</sup>/s. The mean tidal range of 3.76 m in Bremerhaven classifies the Weser Estuary as mesotidal. The riverbed is mainly covered by medium to coarse sand with an exception of a muddy stretch between river kilometers 50 and 65. The morphology of the sandy reaches is dominated by dunes with lengths of up to 100 m and heights of around 2 m.

The estuary is an important waterway connecting the ports of Bremen and Bremerhaven to the North Sea. To guarantee access for the large number of ships sailing through the Weser Estuary, the navigational channel has been repeatedly shifted and deepened over the last 100 years (Garrelts et al., 1973). Its depth is periodically monitored by the responsible authorities and maintained by dredging when required. A large part of the annual dredging costs is

expended for removing individual dune crests by water-injection dredging.

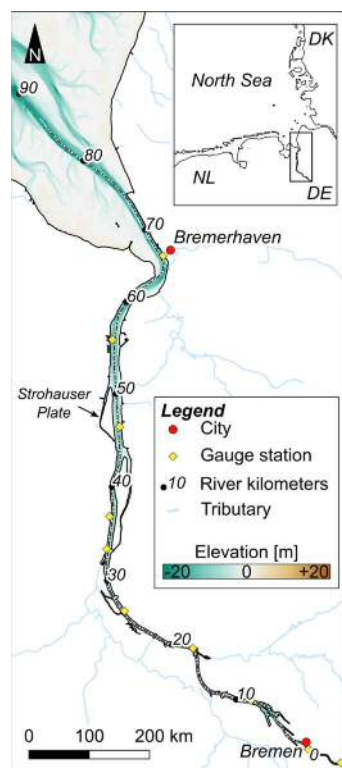


Figure 1. The Lower Weser Estuary

The tidal bedforms which cover most of the Weser Estuary are not only important for the navigational hazard they cause. They are also the main transport agent of bed material

and are the main constituents of hydraulic roughness. Therefore, they are of high importance for the understanding and modeling of estuarine hydrodynamics, transport and morphological evolution.

Bedforms in estuaries are influenced by fresh water discharge as well as tidal forcing. Nasner (1974) and Allen (1976) investigated relations and time-lags between discharge and dune geometry and migration in the Lower Weser, but the contribution of tidal flow has received little attention.

This study analyzes the state and variability of bedform parameters based on monthly measurements of high-resolution bathymetry, upstream freshwater discharge, and tidal characteristics to improve the understanding of bedform related roughness and the performance of hydro-numerical models of estuarine scale.

## 2 DATA AND METHODS

### 2.1 Bathymetry data

Bathymetric surveys in the Lower Weser are carried out by the waterway and shipping administration (WSV) on a monthly basis to guarantee safe navigation. Bathymetry data from multibeam echosounder surveys with RTK-DGPS positioning were made available by Waterways and Shipping Agency (WSA) Bremerhaven, for the reach between river kilometer 40 and 120, for the period between January 2008 and December 2017. The preprocessed data was provided as xyz ASCII. The overall reach was divided into twenty sections of 2.4–4.6 km length. Surveys were repeated for individual sections. The ASCII data were gridded to obtain digital elevation models (DEMs) with a resolution of 2x2 m in GMT (Generic Mapping Tools) compatible NetCDF format.

### 2.2 Extraction of transects

The federal waterway (Bundeswasserstraße) in the Lower Weser marks the cen-

terline of the navigational channel. For a 2D analysis of dune geometries, three profiles were extracted from the DEMs: One following the centerline and two at a lateral distance of  $\pm 50$  m from the centerline.

### 2.3 Dune dimensions and celerity

To separate different bedform regimes (small dunes, large dunes and bars), the extracted transects were bandpass filtered with a passband of 250 to 10 m. Dune dimensions were then extracted from the individual transects by picking local crests and troughs as peaks with a minimum along-profile distance of 10 m and a minimum prominence of 10% of the overall profile elevation range. Mean and standard deviation for dune height and length were calculated (Fig. 2a,b,d,e).

The average migration celerity was determined for the entire section by cross-correlation of successive profiles (Fig. 2c,f).

### 2.4 Hydrological data

Time series of freshwater discharge were obtained from gauge station Intschede, 31 km upstream of the tidal weir. Time series of the tidal range were obtained from gauge stations along the estuary (Fig. 1).

## 3 PRELIMINARY RESULTS

A 10 km long test section in the area Strohauser Plate (Fig. 1) was evaluated over a period of 3 years. Dune heights, lengths and migration rates were compared to the hydrological parameters freshwater discharge and tidal range. Dune heights show a negative correlation with freshwater discharge (Fig. 2a) whereas dune lengths exhibit a positive correlation (Fig. 2b). The tidal range measured at a gauge station in the middle of the transect exhibits a negative effect on both dune height and length (Fig. 2d,e). The dune migration celerity increases with increasing discharge (Fig. 2c) and is independent of tidal range (Fig. 2f).

## 4 CONCLUSIONS AND OUTLOOK

Dimensions and migration celerities of large bedforms in the Lower Weser Estuary have been shown to depend on river discharge and tidal range. While a general correlation can be shown, the short-term effect of individual discharge events, in combination with the concurrent tidal forcing and wind setup, remains to be investigated.

## 5 ACKNOWLEDGEMENTS

Bathymetry data has been kindly provided by WSA (Waterways and Shipping Agency) Bremerhaven.

## 6 REFERENCES

- Allen, J.R.L., 1976. Time-lag of dunes in unsteady flows: an analysis of Nasner's data from the R. Weser, Germany. *Sedimentary Geology*, 15(4), 309–321. doi: 10.1016/0037-0738(76)90037-3
- Garrelts, E., Harten, H., Hovers, G., Lucht, F., Oebius, H., Ohlmeyer, F., Rohde, H., Sindern, J., Vollmers, H.-J., Wigand, V., 1973. Die Ausbauteile der Mündungsstrecken der deutschen Tideströme und deren Einfluss auf die Sandbewegung, in Deutsche Beiträge 23. Internationaler Schifffahrtskongress, Ottawa, Kanada, Juli 1973. Bonn, PIANC Deutschland, 197–228. doi: 20.500.11970/104781
- Nasner, H., 1975 Prediction of the height of tidal dunes in estuaries. *Coastal Engineering* 1974, 1036–1050. doi: 10.1061/9780872621138.063

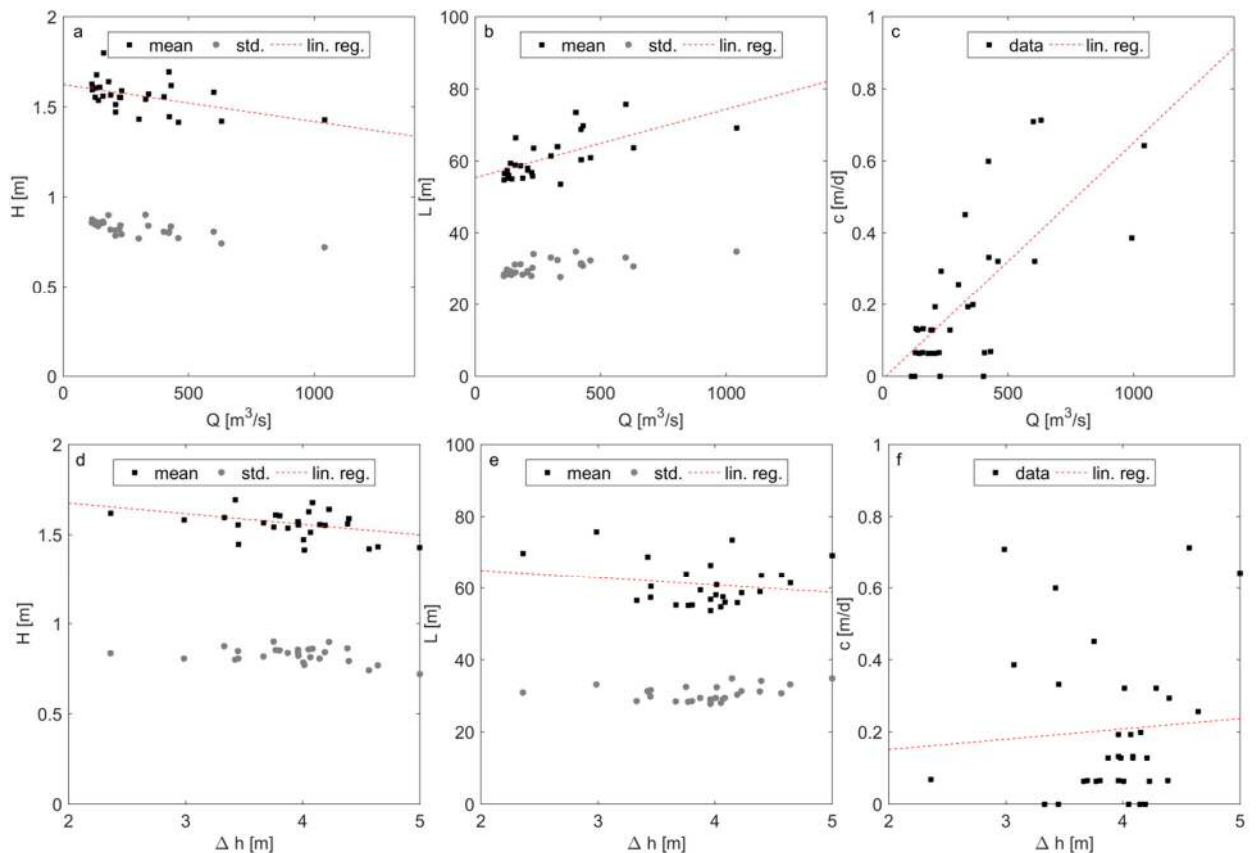


*Figure 2. Correlations of dune dimensions (height  $H$  and length  $L$ ) and celerity  $c$  with hydrological parameters discharge  $Q$  and tidal range  $\Delta h$ .*



# Bedform successions formed by submerged plane-wall jet flows

Jörg Lang *Leibniz Universität Hannover, Institut für Geologie, Hannover, Germany – lang@geowi.uni-hannover.de*

Juan Fedele *ExxonMobil Upstream Research Company, Spring, Texas, USA  
juan.j.fedele@exxonmobil.com*

David Hoyal *ExxonMobil Upstream Research Company, Spring, Texas, USA  
david.c.hoyal@exxonmobil.com*

**ABSTRACT:** Jet flows, expanding from an orifice into a standing water body, are considered as scale-independent model for clastic depositional processes. We conducted 3D experiments with Froude supercritical jet flows, systematically varying several of the controlling parameters such as bed slope, grain size, and flow variables that define the initial densimetric Froude number. The initial inertia-driven jets evolved into gravity-driven flows by rapid expansion and deceleration, thereby forming scours, mouth bars and trains of bedforms. Hydraulic jumps were absent in the flow transition. The geometries of the mouth bar and bedforms were primarily controlled by the initial densimetric Froude number. Further control was exerted by the bed slope, sediment supply and grain sizes. Gravity-controlled processes rapidly take-over the control on the morphodynamic evolution of the flow and are responsible for deposition on the lee side of the mouth bar and beyond.

## 1. INTRODUCTION

Jet flows are flows that emerge from an orifice into a standing water body and decelerate and expand due to the entrainment of ambient water. They can be considered as a basic model for clastic depositional processes independent of scale and environment, for example deltas (Bates, 1953), submarine fans (Beaubouef et al., 2003; Hoyal et al., 2003; Terlaky et al., 2016) and subaqueous ice-contact fans (Powell, 1990; Russell & Arnott, 2003; Winsemann et al., 2009). The evolution from inertia-driven jet flows into gravity-driven density flows is primarily controlled by the initial momentum and the density difference between the flow and the ambient water (Powell, 1990; Hoyal et al., 2003). The rates of jet flow deceleration and expansion and the expansion angle are primarily controlled by the orifice densimetric Froude number ( $Fr'$ ). Secondary controlling factors for jet flows and their deposits include discharge, sediment concentration and grain size (Bates, 1953; Powell, 1990; Hoyal

et al., 2003). Jet flows and their deposits display a distinct proximal to distal zonation. Jet-flow deposits are generally characterized by a mouth bar that develops downflow of a scour. The downflow facies tracts reflect the deceleration of the flow and pass from a region of by-pass and erosion via a region of bedform formation into a region of suspension settling (Powell, 1990; Hoyal et al., 2003; Russell & Arnott, 2003; Winsemann et al., 2009). After the transition from an inertia-driven jet flow into a gravity-driven density flow, the density flow may either evolve into an underflow or rise as a buoyant plume, depending on the density difference to the ambient water (Powell, 1990).

## 2 METHODS

We conducted 3D tank experiments with submerged plane-wall jet flows in an experimental domain, which comprised an 8 m long and 5 m wide plate placed in a 10 m long, 7 m wide and 2 m deep glass-walled tank (Fig. 1A). The evolving flows and de-

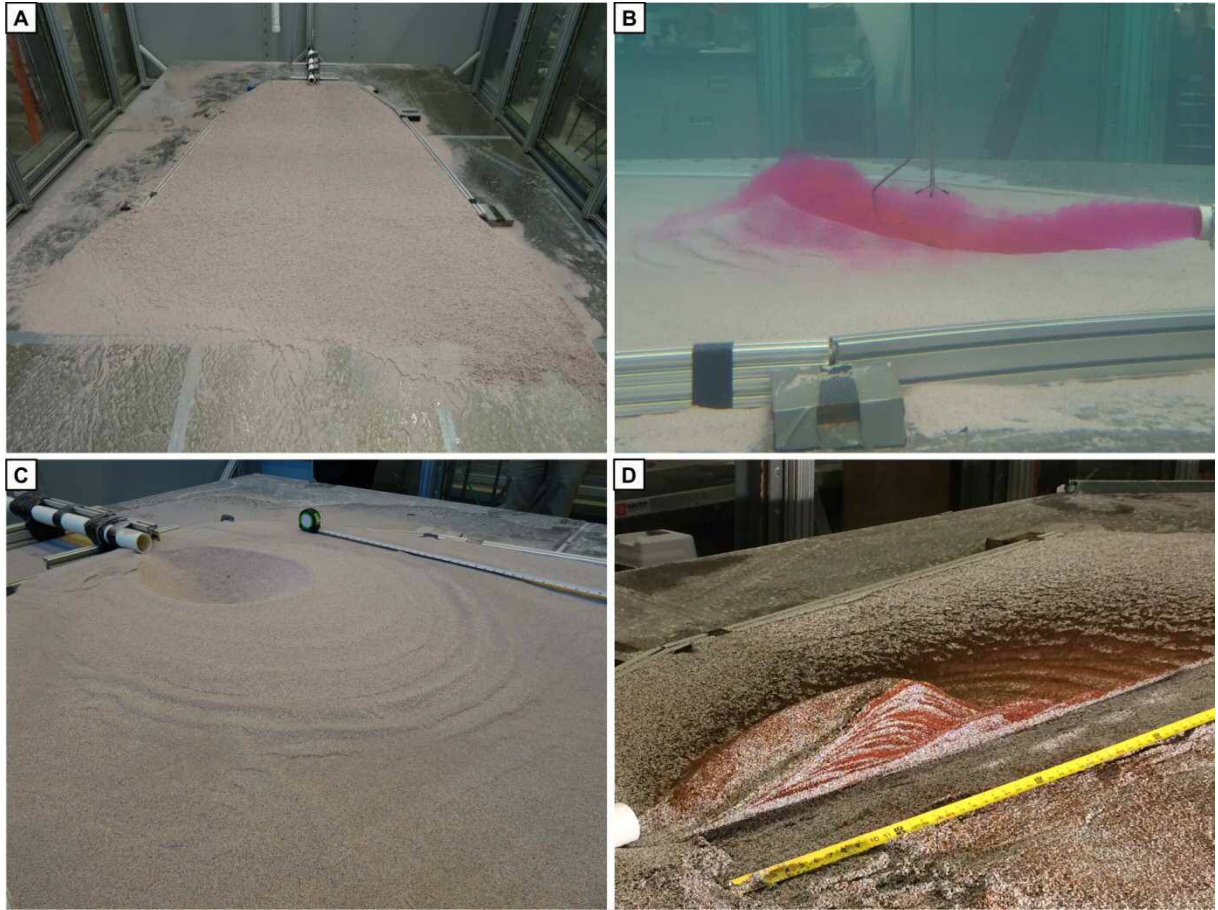


Figure 1. Experimental jet flows and their deposits. **A)** Experimental set-up for jet flows. A leveled sediment bed is prepared on the plate. Flows are released from the inlet pipe. **B)** The expanding jet flow forms a scour and a mouth bar (densimetric Froude number  $Fr' = 4$ ). Flows passing over the mouth bar have already evolved into gravity-controlled density flows. **C)** Scour and mouth bar of a experimental jet flow ( $Fr' = 2$ ). **D)** Cross-section of a jet-flow deposit ( $Fr' = 4$ ).

Posits were documented by photographs through the tank walls. Velocity (point ADV and profiler) and density (conductivity) probes enabled the collection of flow data during the experiments. After the experiments the tank was drained and the external and internal geometry of the deposits was measured.

The controlling parameters were systematically varied to test their impact on the flow dynamics and the resulting deposits. These controlling parameters include bed slope, sediment-grain size and the flow variables (discharge, density difference and pipe diameter) that define the initial densimetric Froude number. The tested experimental conditions were classified as follows: (i) non-aggrading jet flows on non-erodible beds, (ii) non-aggrading jet flows on erodi-

ble beds, and (iii) aggrading jet flows on erodible beds.

### 3 RESULTS

The initial inertia-driven jet flows evolved into gravity-driven density flows by rapid flow expansion and deceleration (Fig. 1B). The turbulent jet flows rapidly expanded from the orifice by the entrainment of ambient water into large turbulent eddies that develop at the flow interface. Hydraulic jumps were never observed in the expanding Froude supercritical jet flow or at the transition into a density flow. The transition from jet to density flow was observed to occur at a short distance from the orifice, typically at the crest of the evolving mouth bar.

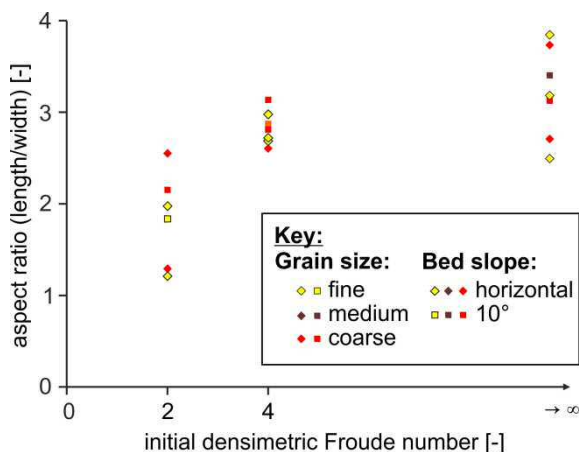


Figure 2. Aspect ratio (length/width) of the mouth-bar crest plotted against the initial densimetric Froude number.

The decelerated density flow was pushed away by the jet flow, promoting the formation of an underflow (Fig. 1B). Underflows were observed to flow all the way to the distal margins of the plate. In experiments with low-density jet flows, a rise of a buoyant plume was observed. However, rising plumes were also observed to develop from high-density jet flow.

Successions formed by the experimental flows comprised early-stage bedforms, scours and mouth bars and bedforms deposited by the distal density flow (Figs. 1C). Concentric early-stage bedforms commonly preceded the formation of the scour and mouth bar. The formation of these bedforms was very rapid and occurred within few minutes after the start of the flow or sediment feed, respectively. The geometry of the bedforms was primarily controlled by the densimetric Froude number. The aspect ratio (length vs. width) of the bedforms crests increased with increasing densimetric Froude number, displaying a logarithmic-style trend (Fig. 2). During the experiments the early stage bedforms showed an interaction with the flow thickness, indicating that they represent small-scale dunes (Fedele et al., 2017).

The formation of scours and mouth bars was observed in all experiments with erodible beds, regardless if sediment was fed into the jet or not. The geometry and dimensions of the scour and mouth bar were controlled

by the initial densimetric Froude number, the sediment-grain size and the sediment supply. The aspect ratio (length vs. width) was controlled by the densimetric Froude number and increased with higher Froude numbers (Fig. 2). The depth of the scour increased with decreasing densimetric Froude number and more gravitationally-dominated flows. The mouth-bar height increased with increasing scour depth and was therefore also controlled by the densimetric Froude number. Experiments with aggrading jet flows led to the vertical and lateral growth of the mouth bar and an infilling of the scour (Fig. 1D). The dimensions and steepness of the mouth bar and bedforms were further related to the sediment-grain size with coarser grain sizes causing the formation of higher and steeper bars and bedforms. Internally, mouth bars were characterized by prograding foreset-like geometries (Fig. 1D).

Very low-relief rounded bedforms were observed to form on the distal slope of the mouth bar, where the flow had transitioned to a fully gravity-dominated density flow. The rounded bedforms on the mouth-bar front appeared to be in-phase with the density flow. On horizontal plates the mouth-bar deposits passed distally into the early-stage bedforms. The movement and growth of these bedforms was very slow and they were starved of sediment, receiving only a small fraction of sediment that bypassed the mouth bar. At high sediment supply the mouth bar prograded over the early-stage bedforms.

In experiments on inclined plates density flows were observed to flow all the way to the distal margins of the plate and led to the formation of small scours and bedforms between the base of the mouth bar and the distal margin of the plate, which were aligned along preferential flow pathways.

Bedform trains downflow of the mouth bar were prominent in runs with fine-grained sediment and low sediment supply, where mouth-bar aggradation was low. The proximal bedforms were symmetrical, while the distal bedform were asymmetrical with steeper lee sides. In plan-view the bedforms displayed straight crests. Superimposed onto

these bedform trains smaller-scale asymmetrical bedforms occurred. Observations during the runs showed an in-phase relation between the bedform trains and the upper interface of the density flow, indicating that they represented antidunes (Fedele et al., 2017).

Bedform fields laterally adjacent to the mouth bar were prominent when coarse-grained sediment was supplied at high rates, leading to high mouth-bar aggradation and flow splitting around the mouth bar. The bedform trains comprised scours separated by low symmetrical bedforms, which were laterally followed by asymmetrical bedforms. An in-phase relation with the upper flow interface indicates that these bedforms represent antidunes (Fedele et al., 2017).

#### 4 IMPLICATIONS FOR FIELD STUDIES

Glacigenic jet flows triggered by the release of meltwater at the grounding line of a glacier can be considered as an ideal field example of plane-wall jet flows. Subaqueous ice-contact fan successions related to glacigenic jet flows are commonly characterized by deposits of aggrading supercritical flows (e.g., Russell & Arnott, 2003; Winsemann et al., 2009; Lang & Winsemann, 2013; Lang et al., 2017b). Depositional processes in glacigenic jet-flow settings have been deduced from outcrop-based studies. The proximal to distal zonation of glacigenic jet flows is reflected in the zonation of the sedimentary facies. Many sedimentary facies in subaqueous ice-contact fan successions indicate supercritical flows, hydraulic jumps and highly aggradational conditions. The most proximal fan zone is dominated by erosion and bypass of sediment. In the proximal fan, coarse-grained (gravel-rich) deposits display crude stratification and cross-stratification and are interpreted as pointing to the rapid infilling of scours. Winsemann et al. (2009) reconstructed large-scale (several km long, 10's of meters deep) scours beneath the proximal parts of a Pleistocene glacilacustrine ice-contact fan, closely resembling the scours formed by the experimental jet flows. Distally, the deposits become more sand-

rich and bedform successions are indicative of rapidly waning flows, including deposits of hydraulic jumps, antidunes and humpback dunes (Powell, 1990; Russell & Arnott, 2003; Winsemann et al., 2009; Lang & Winsemann, 2013; Lang et al., 2017b). Farther downflow, deposits indicate waning flow and deposition by migrating dunes, (climbing) ripples and suspension fall-out (Powell, 1990; Russell & Arnott, 2003; Winsemann et al., 2009). However, in field-based studies it may be ambiguous if deposits are derived from the glacigenic jet flow or the associated density flow (Lang et al., 2017b).

Gravity-driven density flows, which switch from confined to unconfined settings, may also be modeled as submerged plane-wall jets. Field examples of such expanding density flows occur across several orders of magnitude, including submarine fans, lobes and crevasse splays, where flows expand from the mouths of canyons, distributary channels and crevasse channels, respectively (Beaubouef et al., 2003; Hoyal et al., 2003; Terlaky et al., 2016). In these settings, density flows are prone to become supercritical and the resulting deposits are strongly affected by the flow morphodynamics. Erosion and deposition in the zone of flow expansion are commonly associated with the occurrence of bedforms indicating supercritical flow conditions (Postma et al., 2014, 2015; Hamilton et al., 2015, 2017; Lang et al., 2017a). The deposition of mouth bars in front of channels is strongly controlled by the densimetric Froude number within the channel (Hamilton et al., 2015, 2017).

#### 4. 5 CONCLUSIONS

Our experiments show the rapid evolution from inertia-driven jet flows to gravity-driven density flows by flow expansion and deceleration. The results show that gravity-controlled processes rapidly take-over the control on the morphodynamic evolution of the flow and are responsible for deposition on the lee side of the mouth bar and beyond. The experiments indicate that hydraulic jumps are absent.

The experimental jet-flow deposits comprise early-stage bedforms, scours and mouth bars. Flows with higher incoming densimetric Froude numbers produced scours with larger aspect ratios (length vs. width). Conversely, the scours were deeper for lower incoming densimetric Froude numbers. Scours formed by the entrainment of sediment by turbulent eddies. The entrained sediment was typically flushed out of the scour to build a mouth bar around the scour margin. The aspect ratio and the depth of scours provide indicators for the flow conditions at the orifice. The dimensions and steepness of the mouth bar and bedforms were controlled by the sediment-grain size, with coarser grain sizes causing the formation of higher and steeper bars and bedforms. Bedforms developed beyond the mouth-bar crest were related to the density flow. Their formation was controlled by the bed slope, sediment-grain size and sediment supply.

## 6 ACKNOWLEDGEMENTS

This study was funded by Leibniz Universität Hannover (“Wege in die Forschung” program; Grant II-05-2014-05) and the German Research Foundation (DFG; Grant LA 4422/1-1). ExxonMobil Upstream Research Company is thanked for providing access to the experimental facility. J. Winsemann is thanked for discussion.

## 7 REFERENCES

- Bates, C.C., 1953. Rational theory of delta formation. AAPG Bulletin 37, 2119-2162.
- Beaubouef, R.T., Van Wagoner, J.C., Adair, N.L., 2003. Ultra-high resolution 3-D characterization of deep-water deposits - II: Insights into the evolution of a submarine fan and comparisons with river deltas. Search and Discovery Article #40085.
- Fedele J.J., Hoyal, D.C., Barnaal, Z., Tulenko J., Awalt, S., 2017. Bedforms created by gravity flows, in SEPM Special Publication 106, 95-121.
- Hamilton, P.B., Strom, K.B., Hoyal, D.C., 2015. Hydraulic and sediment transport properties of autogenic avulsion cycles on submarine fans with supercritical distributaries. Journal of Geophysical Research: Earth Surface 120, 1369-1389. doi:10.1002/2014JF003414
- Hamilton, P., Gaillot, G., Strom, K., Hoyal, D., 2017. Linking hydraulic properties in submarine distributary channels to depositional lobe geometry. Journal of Sedimentary Research 87, 935-950. doi:10.2110/jsr.2017.53
- Hoyal, D.C., Van Wagoner, J.C., Adair, N.L., Defenbaugh, M., Li, D., Sun, T., Huh, C., Giffin, D.E., 2003. Sedimentation from jets: a depositional model for clastic deposits of all scales and environments. Search and Discovery Article #40082
- Lang, J., Winsemann, J., 2013. Lateral and vertical facies relationships of bedforms deposited by aggrading supercritical flows: from cyclic steps to humpback dunes. Sedimentary Geology 296, 36-54. doi:10.1016/j.sedgeo.2013.08.005
- Lang, J., Brandes, C., Winsemann, J., 2017a. Erosion and deposition by supercritical density flows during channel avulsion and backfilling: Field examples from coarse-grained deepwater channel-levée complexes (Sandino Forearc Basin, southern Central America). Sedimentary Geology 349, 79-102. doi: 10.1016/j.sedgeo.2017.01.002
- Lang, J., Sievers, J., Loewer, M., Igel, J., Winsemann, J., 2017b: 3D architecture of cyclic-step and antidune deposits in subaqueous fan and delta settings: Integrating outcrop and ground-penetrating radar data. Sedimentary Geology 362, 83-100. doi: 10.1016/j.sedgeo.2017.10.011
- Postma, G., Kleverlaan, K., Cartigny, M.J.B., 2014. Recognition of cyclic steps in sandy and gravelly turbidite sequences, and consequences for the Bouma facies model. Sedimentology 61, 2268-2290.
- Postma, G., Hoyal, D.C., Abreu, V., Cartigny, M.J.B., Demko, T., Fedele, J.J., Kleverlaan, K., Pederson, K.H., 2015. Morphodynamics of supercritical turbidity currents in the channel-lobe transition zone, in Submarine Mass Movements and their Consequences. Springer, 469-478.
- Powell, R.D., 1990. Glacimarine processes at grounding-line fans and their growth to ice-contact deltas, in Glacimarine Environments: Processes and Sediments. Geological Society of London, Special Publication 53, 53-73.
- Russell, H.A.J., Arnott, R.W.C., 2003. Hydraulic jump and hyperconcentrated-flow deposits of a glaciogenic subaqueous fan: Oak Ridges Moraine, Southern Ontario, Canada. Journal of Sedimentary Research 73, 887-905. doi:10.1306/041103730887
- Terlaky, V., Rocheleau, J., Arnott, R.W.C., 2016. Stratigraphic organization of stratal elements in an ancient deep-marine basin-floor succession, Neoproterozoic Windermere Supergroup, British Columbia, Canada. Sedimentology 63, 136-175. doi:10.1111/sed.12222
- Winsemann, J., Hornung, J.J., Meinsen, J., Asprion, U., Polom, U., Brandes, C., Bußmann, M., We-

ber, C., 2009. Anatomy of a subaqueous ice-contact fan and delta complex, Middle Pleistocene, NW Germany. *Sedimentology* 56, 1041-1076. doi:10.1111/j.1365-3091.2008.01018

# Influence of migrating bars on dune geometry

Jules. Le Guern *UMR CNRS CITERES, University of Tours, Tours, France* – *leguern@univ-tours.fr*

Stéphane Rodrigues *UMR CNRS CITERES & Polytechnic School of Engineering Polytech Tours, University of Tours, Tours, France* – *srodrigues@univ-tours.fr*

Pablo Tassi *EDF R&D – National Laboratory for Hydraulics and Environment (LNHE) & Saint-Venant Laboratory for Hydraulics, Chatou, France* – *pablo.tassi@edf.fr*

Philippe Jugé *CETU Elmis ingénierie, University of Tours, Tours, France* – *juge@univ-tours.fr*

Timothée Handfus *CITERES, University of Tours, Tours, France* – *Handfus@univ-tours.fr*

Antoine Duperray *CETU Elmis ingénierie, University of Tours, Tours, France* – *duperray@univ-tours.fr*

Patrick Berrault *CETU Elmis ingénierie, University of Tours, Tours, France* – *berrault@univ-tours.fr*

**ABSTRACT:** Authors investigate the effect of migrating bars on dune geometry in a sandy gravel bed river (Loire River, France). Bathymetric survey were carried out in order to determine dune geometry. Preliminary results show that superimposed dunes geometry is not only governed by water depth. Bars could provide enough sediment to the development of dunes on their stoss sides despite decreasing water depth.

## 1 INTRODUCTION

Bedforms are commonly superimposed in river channels (Figure 5). Many authors have described this phenomenon in both, field and flume studies (McCabe & Jones 1977, Carling et al. 2000, Parson et al. 2005, Villard & Church 2005, Fernandez et al. 2006, Rodrigues et al. 2015, Wintenberger et al. 2015). However, there is a gap in the understanding of interactions between two scales of superimposed bedforms, specifically between bars (macroforms sensu Jackson 1975) and dunes (mesoforms sensu Jackson 1975).

Bars induce spatial forcing of flow depth, velocity and direction (Claude et al. 2014) that impact superimposed dunes geometry, celerity and sediment transport. Bars also influence sediment supply locally by defining the thickness of the active layer (Carling et al. 2000, Kleinhans et al. 2002, Tuijnder



Figure 5. Bar front and superimposed dunes in the Loire River (near Saint-Mathurin-sur-Loire-, Source: J. Le Guern).

et al. 2009). Dunes located on bars influence time and spatial variation of flow resistance (roughness) and sediment supply that feedback on migration rates of the bars. One point specifically needs attention: how bar and dune configuration influence sediment transport and how they interact? This paper, is focused on the first type of interactions mentioned above.

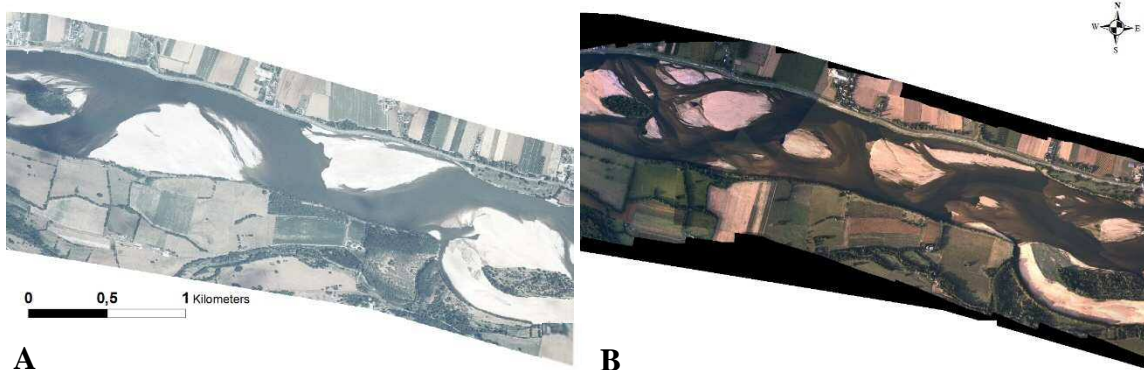


Figure 6. Aerial photographs of the study reach. A. July 2002  $Q=200 \text{ m}^3.\text{s}^{-1}$ , alternate bars ( $m=1$ ). B. September 2017  $Q=160 \text{ m}^3.\text{s}^{-1}$ , multiple bars ( $1.5 < m < 2.5$ ).

## 2 STUDY SITE

The study site is located near Saint-Mathurin-sur-Loire, in the downstream part of the Loire River (France), about 150 km upstream of the estuary. The study reach is 2.5 km long and nearly straight with a bed slope of  $0.0002 \text{ m m}^{-1}$ . The aspect ratio  $\beta$ , which is the width to depth ratio of the channel, ranges between 120 and 750 and decreases with discharge. This large variation of the aspect ratio with hydrological conditions lead to a reach with different bar modes: multiple bars (Figure 2, study site in 2017) with one to two bars per cross section; and alternate bars (Figure 2, study site 2002) with one bar per cross section (respectively  $m=1.5$  to 2.5 and  $m=1$ , Crosato & Mosselman 2009). From a theoretical point of view, alternate bars cannot occur for such high  $\beta$  ratio values. When the bar mode of the reach is greater than one, it is difficult to determine bar wavelength but height is about 1.5 m. When bars are alternate, the wavelength is about 1.3 km.

Superimposed dunes are about 4 m long and 0.2 m height. They migrate with a mean celerity of 30 meter per day during flood events. The bed is composed of sands and gravels with a mean diameter of 0.8 mm.

## 3 METHODS

To assess the effect of bars on dunes, 12 single-beam bathymetric surveys were car-

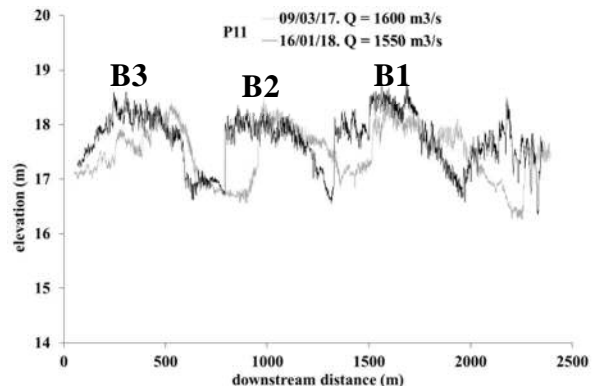


Figure 3. Examples of BEP surveyed in March 2017 and January 2018. Note the presence of dunes on bars stoss side and migration of bars.

ried out along the reach for different discharge conditions (Figure 4). Geometry of dunes have been extracted from three longitudinal bed elevation profiles (BEP, see Figures 3 and 4) with the Matlab code Bedform Tracking Tools (van der Mark et al. 2008).

The geometry of each dune, determined by the program with a zero crossing method, was extracted from the stoss side of each bar present on the site. Stoss side of bars were intentionally delimited using the lowest water level surveyed to exclude the lower parts of the channel that are subject to transverse sediment reworking at low flows.

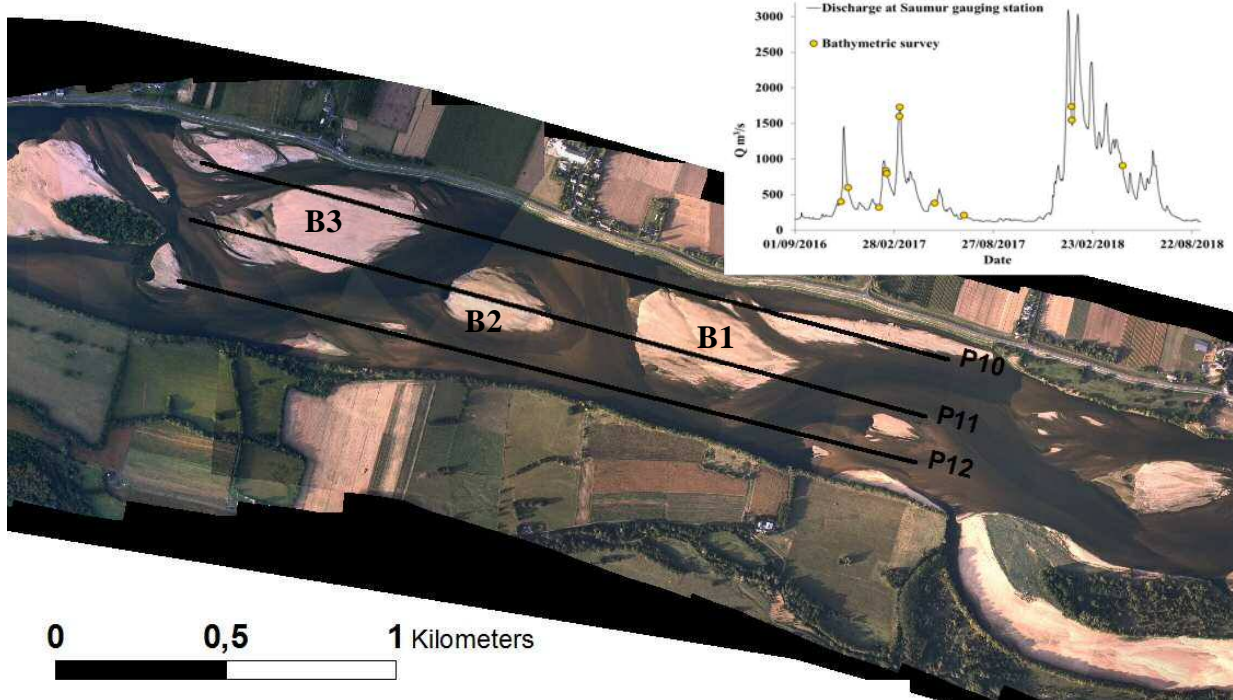


Figure 4. Study reach and profiles followed along the reach during bathymetric surveys and discharge of the Loire at Saumur gauging station (located about 30 km upstream, mean discharge =  $680 \text{ m}^3 \cdot \text{s}^{-1}$ ) with bathymetric surveys.

#### 4 RESULTS

During low flows, when present on stoss sides of bars, dunes are small (about 1.4 m long and 0.04 m height). During flood events, the height of dunes is about 0.2 m and the wavelength is about 4.4 m. Mean parameters on each bar stoss side show that dune height and length increase with the water depth (Figure 5). Mean water depth

gradually decrease from banks to the center of the channel. Consequently, height of dunes follows the same evolution even if bedforms appears to be more asymmetric where mean depth is higher (left bank). These observations are in line with predictive models of dune height based on water depth (e.g. Yalin 1964) even if those models overestimate the height of dunes (Figure 5).

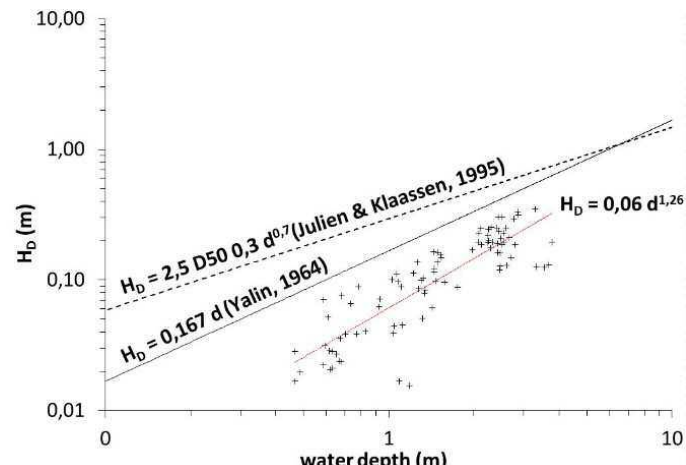


Figure 5. Relationship between mean flow depth and mean dune height for each bar. Comparison models by Yalin (1964) and Julien & Klaassen (1995).

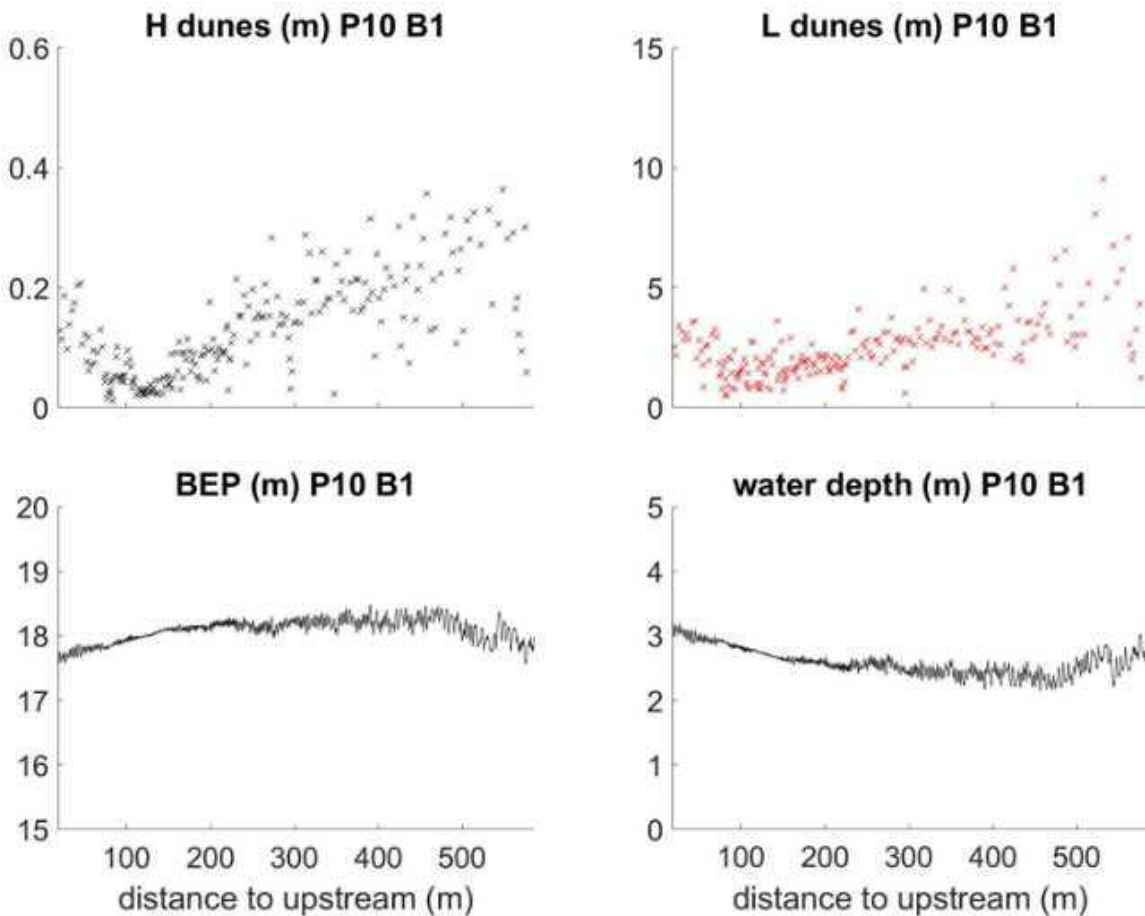


Figure 6. Evolution of dunes geometry along the stoss side of bar B1 on profile P10 (see figure 4) during the survey of 10/03/2017 (discharge at Saumur was  $1740 \text{ m}^3 \cdot \text{s}^{-1}$ ).

By a closer look, we consider one survey during a flood event (Figure 4, 10/03/2017). During this survey, bar in the upstream part of P10 (B1) denote that sediment availability could control dune geometry because dunes height and wavelength increase when the water depth decrease (towards the crest of the bar, see Figure 6). These observations show that the increase of dune height is not necessarily linked to water depth and suggest that other parameters are involved. For instance, dune height can also be a function of sediment supply and availability (Tuijnder et al. 2009, Claude et al. 2014). The availability of sediment depends on the presence of bars that provide a sedimentary stock/active layer that allow the formation of larger dunes near the bar crest although water depth is shallower. The position of bars between them can also affect the development of dunes on bar located downstream by

decreasing sediment supply or hydraulic constraints: lee side effect (Reesink et al. 2014). Upstream of B1, bars could affect hydraulic constraints and limit dune development immediately downstream.

## 5 CONCLUSION

Preliminary results of this study show different behavior of dunes geometry according to their location on the stoss side of bars. It is suggested that water depth is not always the governing parameter of superimposed dune height. It could be interesting to investigate effect on steepness, in order to better understand the impact of bar on dunes geometry. Moreover, we have to investigate evolution of dunes geometry for different flood stage (Reesink et al. 2018) and take into account history of floods on bars and superimposed dunes.

## 6 ACKNOWLEDGEMENT

This work is part of the RTEMUS I & II research programs co-funded by the Agence de l'Eau Loire-Bretagne (*convention n°150569501*) and European Union (FEDER *convention n° 2016-110475*). This work is part of the PhD thesis of the first author.

## 7 REFERENCES

- Carling, P.A., Götz, E., Orr, H.G., Radecki\_Pawlik, A., 2000. The morphodynamics of fluvial sand dunes in the River Rhine, near Mainz, Germany. I. Sedimentology and morphology. *Sedimentology* 47, 227-252.
- Claude, N., Rodrigues, S., Bustillo, V., Bréhéret, J.-G., Tassi, P., Jugé, P., 2014. Interactions between flow structure and morphodynamic of bars in a channel expansion/contraction, Loire River, France, *Water Resour. Res.*, 50, doi: 10.1002/2013WR015182.
- Crosato, A., Mosselman, E., 2009. Simple physics-based predictor for the number of river bars and the transition between meandering and braiding, *Water Resour. Res.*, 45, W03424, doi: 10.1029/2008WR007242.
- Fernandez, R., Best, J., Lopez, F., 2006. Mean flow, turbulence structure, and bed form superimposition across the ripple-dune transition, *Water Resour. Res.*, 42, W05406, doi: 10.1029/2005WR004330.
- Jackson, R.G.II, 1975. Hierarchical attributes and a unifying model of bed forms composed of cohesionless material and produced by shearing flow. *Geological Society of America Bulletin*, v. 86, p. 1523-1533.
- Julien, P.Y., Klaassen, G.J., 1995. Sand-Dune geometry of large rivers during floods. *Journal of Hydraulic Engineering*, Vol. 121, Issue 9, doi:10.1061/(ASCE)0733-9429(1995)121:9(657).
- Kleinhans, M.G., Wilbers, A.W.E., De Swaaf, A., van den Berg, J.H., 2002. Sediment supply-limited bedforms in sand-gravel bed rivers. *Journal of Sedimentary Research*, Vol. 72, 5, 629-640.
- McCabe, P.J., Jones C.M., 1977. Formation of reactivation surfaces within superimposed deltas and bedforms. *Journal of sedimentary petrology*, Vol. 47, No. 2, 707-715.
- Parsons, D.R., Best, J.L., Orfeo, O., Hardy, R.J., Kostaschuk, R., Lane S.N., 2005, Morphology and flow fields of three-dimensional dunes, Rio Parana', Argentina: Results from simultaneous multibeam echo sounding and acoustic Doppler current profiling, *J. Geophys. Res.*, 110, F04S03, doi: 10.1029/2004JF000231.
- Reesink, A.J., Parsons, D.R., and Thomas, R.E., 2014. Sediment transport and bedform development in the lee of bars: Evidence from fixed- and partially-fixed bed experiments. Presented at: River Flow 2014, International Conference on River Hydraulics, 3-5 September 2014 Lausanne, Switzerland.
- Reesink, A.J.H., Parson, D.R., Ashworth, P.J., Best, J.L., Hardy, R.J., Murphy, B.J., McLelland, S.J., Unsworth, C., 2018. The adaptation of dunes to changes in river flow. *Earth Science Reviews*, Vol. 185, 1065-1087, doi: 10.1016/j.earscirev.2018.09.002.
- Rodrigues, R., Mosselman, E., Claude, N., Wintenberger, C.L., Jugé, P., 2015. Alternate bars in a sandy gravel bed river: generation, migration and interactions with superimposed dunes. *Earth Surf. Process. Landforms* 40, 610–628, doi: 10.1002/esp.3657.
- Tuijnder, A.P., Ribberink, J.S., Hulscher, S.J.M.H., 2009. An experimental study into the geometry of supply-limited dunes. *Sedimentology*, 56, 1713-1727, doi: 10.1111/j.1365-3091.2009.01054.x.
- van der Mark, C.F., Blom, A., Hulscher, S.J.M.H., 2008. Quantification of variability in bedform geometry. *J. Geophys. Res.*, 113, F03020, doi: 10.1029/2007JF000940.
- Villard, P.V., Church, M., 2005. Bar and dune development during a freshet: Fraser River estuary, British Columbia, Canada. *Sedimentology*, 52, 737-756, doi: 10.1111/j.1365-3091.2005.00721.x.
- Wintenberger, C.L., Rodrigues, S., Claude, N., Jugé, P., Bréhéret, J.-G., Villar, M., 2015. Dynamics of nonmigrating mid-channel bar and superimposed dunes in a sandy-gravelly river (Loire River, France). *Geomorphology*, 248, 185-204, doi: 10.1016/j.geomorph.2015.07.032.
- Yalin, S.M., 1964. Geometrical properties of sand wave. *Proc. Am. Soc. Civil Eng.*, 90, 105-119.



# Three-dimensional flow above a natural bedform field

Alice Lefebvre *MARUM, University of Bremen, Bremen, Germany* – alefebvre@marum.de

**ABSTRACT:** Large bedforms in rivers and coastal seas usually develop as extensive fields of three-dimensional (3D) dunes. The mutual interaction of flow and 3D bedforms has until now been studied mainly above idealised bedforms. The present work examines 3D flow over a natural bedform field from the Rio Paraná (Argentina) using the Delft3D modelling system. The presence and position of flow reversal and turbulent wake are found to be related to the presence and properties of the slip face (portion of the lee side having a slope  $> 15^\circ$ ) and not to that of the crest or the bedform height, as is usually assumed. Therefore, in order to correctly describe and model the effect of bedforms on flow, detailed bedform morphology, including slip face presence and 3D properties, needs to be calculated.

## 1 INTRODUCTION

Traditionally, the effect that bedforms have on flow has been investigated in laboratory flumes over two-dimensional (2D) bedforms having an angle-of-repose ( $30^\circ$ ) lee side and a relatively simple shape (e.g. Lefebvre et al., 2014b, Lefebvre and Winter, 2016, Maddux et al., 2003, Omidyeganeh and Piomelli, 2013, Venditti, 2007). Over such bedforms, the flow field shows different regions (Best, 2005); (1) a flow separation zone over the bedform lee side in which flow reversal is observed; (2) a shear layer and turbulent wake region, originating at the crest, extending, and expanding downstream; (3) an internal boundary layer that grows from the reattachment point beneath the wake toward the crest; and (4) an outer, overlying region. The flow separation zone and associated turbulence production in the wake are largely responsible for the so-called form roughness, which constitutes an important part of the shear stress in environments where bedforms are present and thus a major factor in the calculation and prediction of hydrodynamics and sediment transport.

It is now recognised that many large rivers are characterised by low-angle bedforms with lee side slopes lower than the angle of repose (Best, 2005). Over such bedforms flow no permanent flow separation is observed; no distinct wake is found, only a region of slightly elevated turbulence (Lefebvre et al., 2016). The threshold between low and high-angle bedforms is usually given to be between  $10$  and  $20^\circ$  (Lefebvre and Winter, 2016). Natural bedforms also have a complex shape, frequently showing a lee side made up of a gentle upper lee side, or crestral platform, and a steeper slip face (Lefebvre et al., 2016).

Bedforms in rivers and in coastal tidal environments often develop into large fields. These fields are inherently three-dimensional (3D), with only special conditions leading to two-dimensional bedform fields (Rubin, 2012).

Bedform three-dimensionality has been recognised by the early work of Allen (1968); since then, only some aspects of three-dimensionality, mainly the influence of crest line sinuosity and height variations,

have been systematically studied however only over regular geometric pattern and at laboratory scale (Maddux et al., 2003, Omidyeganeh and Piomelli, 2013, Venditti, 2007) with the notable exception of the field study of Parsons et al. (2005). These studies allowed to characterise some aspects of flow over regular 3D bedforms (Maddux et al., 2003, Omidyeganeh and Piomelli, 2013, Venditti, 2007). Over profiles having the little height variations, or over nodes, streamwise flow is accelerated, crosswise flow develops, and a strong downward directed flow induces a vertical suppression of turbulence with a reduced flow separation zone and a suppressed wake. Over profiles with strong height variations, or over a lobe, crosswise flow is limited and vertical flow is positive; flow separation and wake are strong and diffused upward. Although variations of flow patterns are seen depending on bedforms three-dimensionality in the field, they are more difficult to precisely interpret due to instrument limitations (Parsons et al., 2005).

The present work aims at investigating the details of 3D flow over a natural bedform field using numerical modelling.

## 2 NUMERICAL MODEL

### 2.1 Modelling system

Delft3D is a process-based open-source integrated modelling system developed to simulate flow and transport in river, estuarine and coastal areas (Deltares, 2014). In the Delft3D-FLOW module the 3D non-linear shallow water equations derived from the three-dimensional Navier-Stokes equations for incompressible free surface flow are solved. The non-hydrostatic Delft3D modelling system has already been successfully used in 2DV to simulate horizontal and vertical velocities, turbulent kinetic energy

(TKE) and water levels above fixed bedforms (Lefebvre et al., 2014a, Lefebvre et al., 2014b, Lefebvre et al., 2016, Lefebvre and Winter, 2016).

The model is now set up to simulate three-dimensional flows over bedform fields by extending the model domain into the cross-stream direction. All simulations are performed on a 3D Cartesian model grid discretising a fixed bed, i.e. no sediment transport is modelled. The model has been calibrated against laboratory measurements of flow above idealised 3D bedforms from Maddux et al. (2003).

### 2.2 Model set up

The model is used to simulate flow over a natural bedform field collected in the Rio Paraná, Argentina by Parsons et al. (2005). The investigated river bed is covered with large dunes (1.2 to 2.5 m high and 45 to 85 m long) as well as smaller bedforms mainly situated on the stoss side of the large dunes. The chosen domain excludes local morphological features and is detrended to exclude any large scale slope. Two open boundaries are set, one entrance and one exit, and two closed boundaries, to make the domain model resemble, to some extent, a field-scale flume.

The chosen domain size is 675 m long and 200 m wide, with a grid cell of 0.5 m. Forty non-equidistant vertical layers are set, having a size of 0.15 m from the lowest point of the bed to 0.5 m above the highest crest, before slowly increasing to 0.45 m at the water surface. The entrance boundary is set with velocities of  $1 \text{ m s}^{-1}$  to resemble flow conditions during data collection, which supposedly created and maintained the measured bedforms.

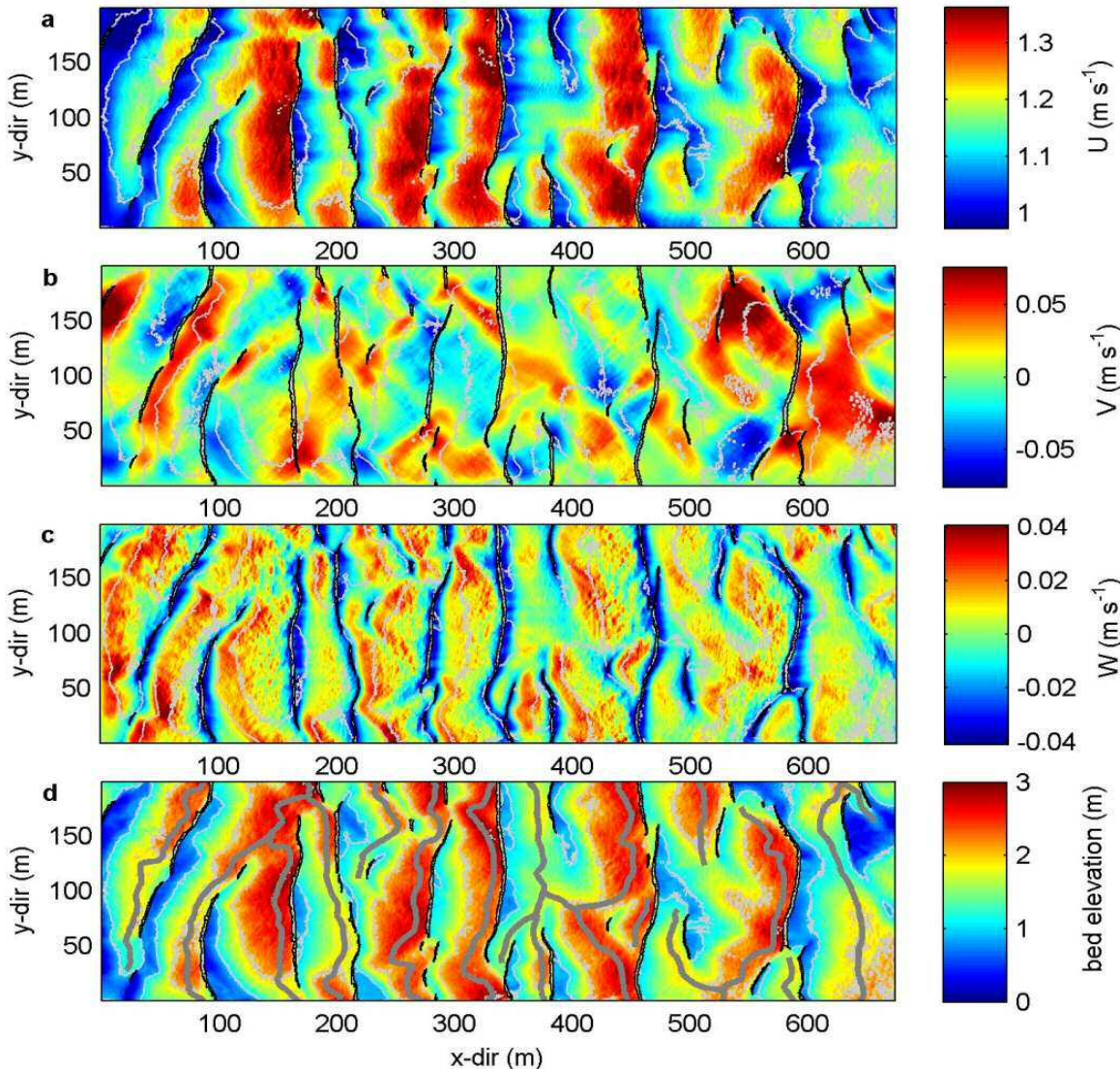


Figure 1. Depth-averaged stream wise velocity  $U$  (a), crosswise velocity  $V$  (b) and vertical velocity  $W$  (c) over the model domain (d); in all figures, the black lines show the position of the slip faces and the thin grey lines highlights the bed elevation contours; in Figure d, the thick grey lines show the crest line positions; flow is from left to right

### 3 RESULTS

The depth-averaged stream wise velocity (Figure 1a) shows the expected patterns of flow acceleration over the stoss side and flow deceleration over the lee side; more precisely, fast flow before the slip face and slow flow over the slip face. The topographic forcing of the flow is seen as a strong crosswise velocity observed in the regions where the slip faces are curved (Figure 1b).

The depth-averaged vertical velocity (Figure 1c) follows the expected patterns above bed-forms, with upward velocity above the stoss sides and downward above the lee sides, with the strongest downward velocity being found over the slip faces.

In order to better assess the mutual influence of bed morphology and flow properties, the positions of the flow separation zones and turbulent wakes are calculated. The flow separation zones are defined as

portions of the flow where negative stream wise velocity are found. The height of the flow separation zone is calculated for each point where a negative velocity is found as the height where the upstream directed flow is compensated by the downstream directed flow. Along each transect, the length of the flow separation zone,  $L_{FSZ}$ , is calculated as the horizontal distance between the first and the last negative point between each crest and trough. The wake is detected as positions where TKE is higher than the TKE 98th percentile. Along each transect and between each successive crest, the length of the wake is calculated as the horizontal distance between the beginning of the slip face and the maximum extent of the wake.

Figure 2a shows the position of the detected flow separation zones and wakes in relation the bedform crestlines and slip faces. Flow separation zones and turbulent wakes are found behind slip faces and are absent above bedforms with a gentle lee side. The length of the flow separation zone

is only poorly related to the bedform height but it is strongly related to the height of the slip face ( $H_{sp}$ )  $L_{FSZ} = 4.99 H_{sp}$  ( $R^2 = 0.74$ , Figure 2b).

Although a flow separation zone is found behind most slip faces, 18% of the slip faces are not followed by flow reversal. These are mainly slip faces with a strong angle compared the flow (i.e. not transverse to the flow), or relatively gentle and small slip faces. The presence of a flow separation zone is therefore predicted to happen behind slip faces with an absolute direction less than  $25^\circ$ , a height greater than 0.3 m and maximum angle steeper than  $18^\circ$ .

The length of the wake shows a weak relation to bedform height but a strong relation the slip face height  $L_w = 13.3 H_{sp}$  ( $R^2 = 0.68$ , Figure 2c). Similarly to the flow separation zone, the wake is more likely to appear behind high and steep slip faces than behind gentle and low ones.

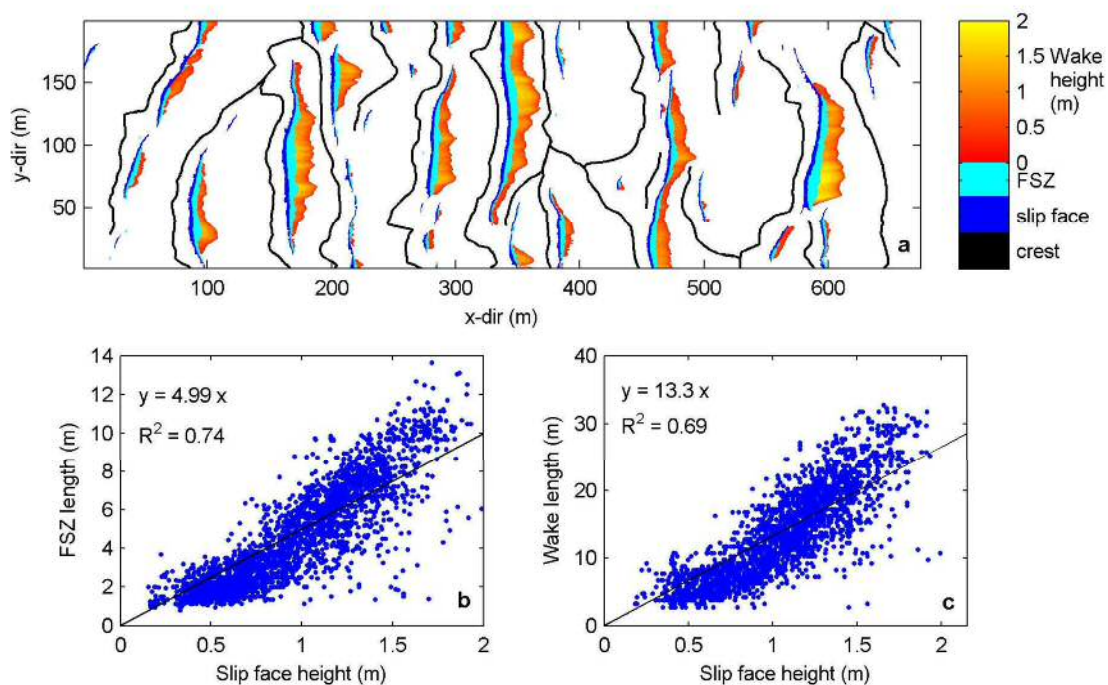


Figure 2. (a) position the crest lines, slip faces and flow separation zone (FSZ) and height of the wake (vertical distance between the lowest and highest point of the wake) across the model domain, flow is from left to right; (b) flow separation zone length as a function of slip face height and (c) wake length as a function of slip face height.

However, the direction of the slip face compared to the flow does not seem to have a strong effect on the presence of a turbulent wake. A wake is therefore predicted to form behind slip faces with a height greater than 0.6 m and maximum angle steeper than 20°.

#### 4 CONCLUSIONS

A three-dimensional numerical model was used over a bedform field from the Rio Paraná to bring insights in the relation between complex 3D bed morphology and flow properties. The main conclusions of this work are:

- The presence and size of the flow separation zone and turbulent wake depends on the presence and properties of the slip face (lee side angles >15°) and not on those of the crest.

- A flow separation zone forms preferably over steep and high slip faces with a direction transverse to the flow; the flow separation length can be estimated as being 5 times the height of the slip face.

- A wake develops over steep and high slip faces, with only little influence of the slip face direction. The length of the wake is around 13 times the slip face height.

A detailed description of the bedform morphology including the presence and properties of the slip face is therefore necessary to correctly represent the complex interaction of flow and bedform.

#### 5 ACKNOWLEDGEMENT

This study was funded by the German Research Foundation (Deutsche Forschungsgemeinschaft, DFG), project number 345915838. The author is grateful to Tim Maddux and Dan Parsons for sharing their data, and Christian Winter for constructive feedback.

#### 6 REFERENCES

Allen, J.R.L. 1968. Current Ripples. New York, NY.

- Best, J., 2005. The fluid dynamics of river dunes: A review and some future research directions. *Journal of Geophysical Research* 110, 21. doi:10.1029/2004JF000218
- Deltires. 2014. User Manual Delft3D-FLOW. Delft, The Netherlands.
- Lefebvre, A., Paarlberg, A.J., Ernstsen, V.B. and Winter, C., 2014a. Flow separation and roughness lengths over large bedforms in a tidal environment: a numerical investigation. *Continental Shelf Research* 91, 57-69. doi:10.1016/j.csr.2014.09.001
- Lefebvre, A., Paarlberg, A.J. and Winter, C., 2014b. Flow separation and shear stress over angle of repose bedforms: a numerical investigation. *Water Resources Research* 50, 986-1005. doi:10.1002/2013WR014587
- Lefebvre, A., Paarlberg, A.J. and Winter, C., 2016. Characterising natural bedform morphology and its influence on flow. *Geo-Marine Letters* 36, 379–393. doi:10.1007/s00367-016-0455-5
- Lefebvre, A. and Winter, C., 2016. Predicting bed form roughness: the influence of lee side angle. *Geo-Marine Letters* 36, 121-133. doi:10.1007/s00367-016-0436-8
- Maddux, T.B., Nelson, J.M. and McLean, S.R., 2003. Turbulent flow over three-dimensional dunes: 1. Free surface and flow response. *Journal of Geophysical Research: Earth Surface* 108, doi:10.1029/2003JF000017
- Omidyeganeh, M. and Piomelli, U., 2013. Large-eddy simulation of three-dimensional dunes in a steady, unidirectional flow. Part 1. Turbulence statistics. *Journal of Fluid Mechanics* 721, doi:10.1017/jfm.2013.36
- Parsons, D.R., Best, J.L., Orfeo, O., Hardy, R.J., Kostaschuk, R. and Lane, S.N., 2005. Morphology and flow fields of three-dimensional dunes, Rio Paraná, Argentina: results from simultaneous multibeam echo sounding and acoustic Doppler current profiling. *Journal of Geophysical Research* 110, F04S03. doi:doi:10.1029/2004JF000231
- Rubin, D.M., 2012. A unifying model for planform straightness of ripples and dunes in air and water. *Earth-Science Reviews* 113, 176-185. doi:10.1016/j.earscirev.2012.03.010
- Venditti, J.G., 2007. Turbulent flow and drag over fixed two- and three-dimensional dunes. *Journal of Geophysical Research* 112, F04008. doi:10.1029/2006JF000650



# Upslope migrating sand dunes in the upper slope of the Mozambican margin (SW Indian Ocean)

E. Miramontes *UMR6538, CNRS-UBO, IUEM, Laboratoire Géosciences Océan, Plouzané, France*  
*elda.miramontesgarcia@univ-brest.fr*

G. Jouet *IFREMER, Géosciences Marines, Plouzané, France – gwenael.jouet@ifremer.fr*

A. Cattaneo *IFREMER, Géosciences Marines, Plouzané, France – antonio.cattaneo@ifremer.fr*

E. Thereau *IFREMER, Géosciences Marines, Plouzané, France – estelle.thereau@ifremer.fr*

C. Guerin *IFREMER, Géosciences Marines, Plouzané, France – charline.guerin@ifremer.fr*

S.J. Jorry *IFREMER, Géosciences Marines, Plouzané, France – stephan.jorry@ifremer.fr*

L. Droz *UMR6538, CNRS-UBO, IUEM, Laboratoire Géosciences Océan, Plouzané, France – laurence.droz@univ-brest.fr*

**ABSTRACT:** The upper slopes of continental margins are very energetic areas where nepheloid layers are often observed. Multibeam bathymetry, sub-bottom profiler and multi-channel high-resolution seismic reflection data acquired during the PAMELA-MOZ04 survey in the Mozambique Channel revealed the presence of sand dunes on the upper slope at 120-250 m water depth. The dunes migrate upslope and their crests are oblique to the contours. They are medium to large dunes, with wavelengths between 20 and 150 m and heights between 0.15 and 1.50 m, and their size decreases upslope. Seismic reflection data of the water column show internal solitary waves travelling offshore in the depth range of the dune field. The formation of the dune field could be related to the interaction of the barotropic tide with the upper slope that results in the generation of internal tides.

## 1 INTRODUCTION

Sediment transfer from land to ocean basins is strongly controlled by sea-level fluctuations, especially in areas with extended continental shelves such as the Mozambican margin. During sea-level lowstands, the Zambezi river, one of the longest and largest river systems of eastern Africa (Fekete et al., 1999), supplied high amounts of fine-grained sediment to the continental slope (Schulz et al., 2011). However, at present, during the sea-level highstand, the sediment is redistributed by currents, and winnowed sand is accumulated along the upper slope (Schulz et al., 2011). Currents in the Mozambique Channel (SW Indian Ocean; Fig. 1) are very complex and intense. They comprise a southward-bound, western boundary current that forms sand dunes at the Mozambican outer continental shelf (Flemming & Kudrass, 2018), and large ( $\geq 300$  km diameter), southward migrating, anticyclonic eddies affecting the entire water column (Halo et al., 2014).

The presence of nepheloid layers on continental slopes has often been related to the elevated bottom shear stresses generated by internal tides (Cacchione & Drake, 1986; Puig et al., 2004). We propose that, in addition to geostrophic currents, internal tides can also affect the sedimentation of continental slopes.

## 2 MATERIALS AND METHODS

The multibeam bathymetry and the related backscatter used for this study were acquired with a Kongsberg EM710 system in 2015 during the PAMELA-MOZ04 survey (Jouet and Deville, 2015). The horizontal resolution of the bathymetry is 3 m, and 5 m for the backscatter. The seismic data used in this study were acquired during the same survey with a sub-bottom profiler (1800-5300 Hz) and with a 72-channels high-resolution mini GI system (50-250 Hz), which also imaged the water column.

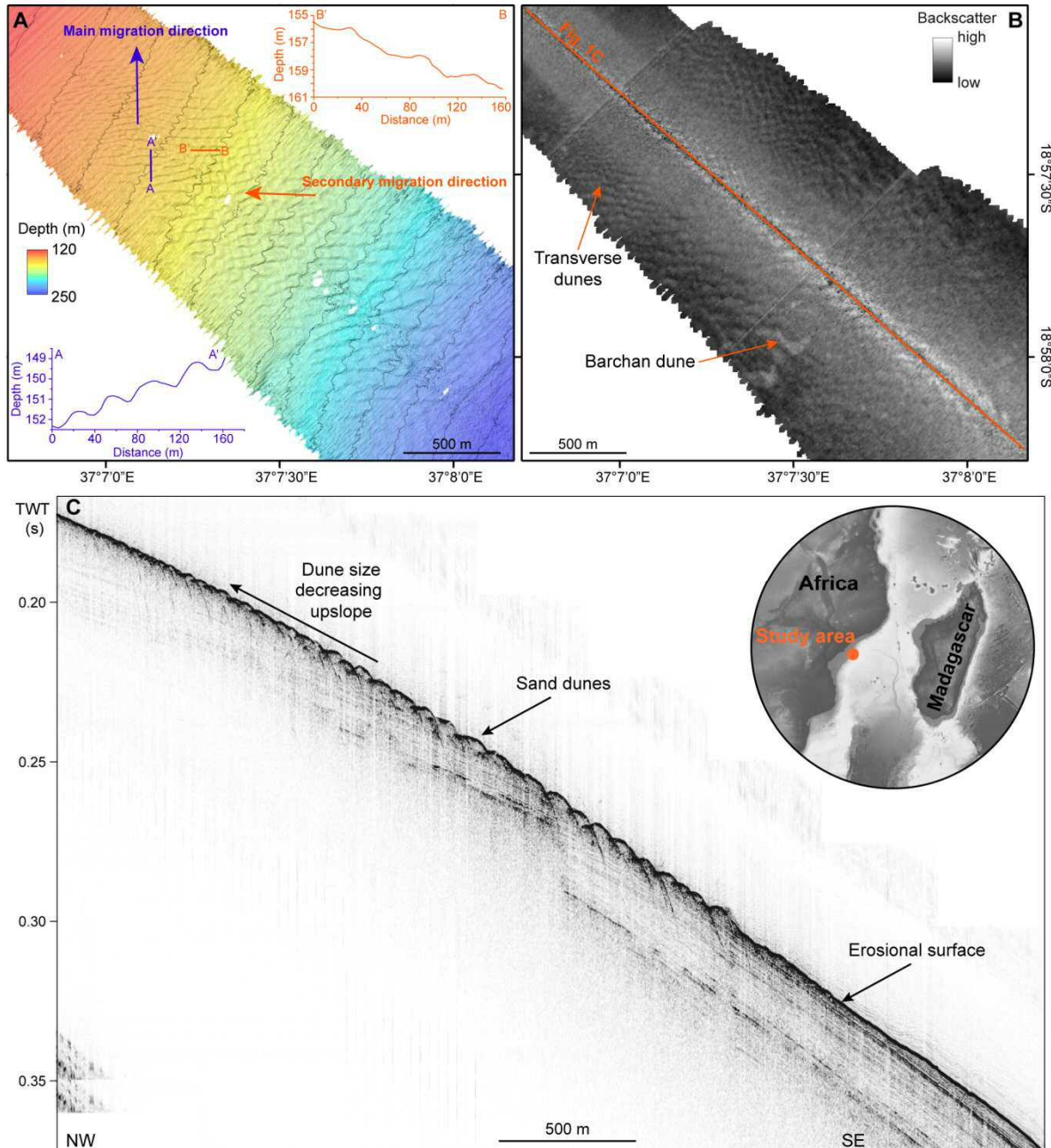


Figure 1. (A) Multibeam bathymetry and topographic profiles of the dune field. Depth contours are shown every 10 m; (B) Backscatter of the dune field; (C) Sub-bottom profiler image MOZ04-SDS-0102a showing an erosional surface in the deep part of the dune field and an upslope decrease in dune size.

### 3 RESULTS

A sand dune field was observed on the upper slope of the Mozambican margin (western Mozambique Channel) at water depths ranging between 120 and 250 m (Fig. 1A). The dunes are medium to large dunes, with wavelengths between 20 and 150 m and heights between 0.15 and 1.50 m. The dune crests are mainly oriented E-W (oblique to the contours), although some of

them show a N-S orientation (Fig. 1A). Both orientations are superimposed, but the E-W orientation is dominant (Fig. 1A). The dune field is composed mainly of transverse dunes and only two barchan dunes were observed in the SW part of the dune field (Fig. 1B). The dunes migrate upslope, and their size decreases upslope (Figs. 1A, C). The deepest limit of the dune field is characterised by an erosional surface, indicating the presence of more energetic conditions in

this area. The progressive change from erosion to large dunes and finally to medium dunes, suggests an upslope decrease of energy.

A multi-channel high-resolution seismic reflection profile acquired in the study area shows that the dune field is located above a plastered drift, which has a convex morphology (Fig. 2). The lower part of the plastered drift is characterised by low amplitude continuous reflections. In contrast, the area of the dune field (above the plastered drift) is characterised by high amplitude discontinuous and chaotic reflections (Fig. 2). These differences suggest a change in sedimentary facies, the upper part of the plastered drift being probably composed of coarser sediment.

The upper Mozambican slope has been previously identified as a hot spot for the generation of internal tides and internal waves (Da Silva et al., 2009). A seismic image of the water column confirms the presence of Internal Solitary Waves (ISW) at the water depth of the dune field (Fig. 2). Their amplitude is bigger offshore, indicating that they were moving toward the ocean (eastwards) (Fig. 2). The interaction of the barotropic tide with the continental slope may result in the generation of internal tides, that can radiate horizontally in the form of ISW (as observed in Figure 2) or as rays into the stratified water column (Da Silva et al., 2009). Internal tides generate turbulence near the seafloor and currents flowing across the slope (Gayen & Sarkar 2010), that may be strong enough to erode the seafloor and generate upslope migrating sand dunes.

#### 4 CONCLUSIONS

4.1 A dune field composed of medium to large sand dunes was identified in the upper continental slope of the Mozambican margin at 120-250 m water depth. The dune migrate upslope and their size also decreases upslope. High-resolution seismic reflection data showed the presence of internal solitary waves at the depth of the dune field. The formation of the observed dune field may be related to the currents near the seafloor cre-

ated by the generation of internal tides on the slope.

#### 5 ACKNOWLEDGEMENT

We thank the Captain and the crew of the PAMELA-MOZ04 survey onboard the R/V Pourquoi pas?. The oceanographic survey PAMELA-MOZ04 and Elda Miramontes' Post-Doctoral fellowship were co-funded by TOTAL and IFREMER as part of the PAMELA (Passive Margin Exploration Laboratories) scientific project. The PAMELA project is a scientific project led by Ifremer and TOTAL in collaboration with Université de Bretagne Occidentale, Université Rennes 1, Université Pierre and Marie Curie, CNRS and IFPEN.

#### 6 REFERENCES

- Cacchione, D.A., Drake, D.E., 1986. Nepheloid layers and internal waves over continental shelves and slopes. *Geo-Marine Letters* 6(3), 147-152.
- Da Silva, J.C.B., New, A.L., Magalhaes, J.M., 2009. Internal solitary waves in the Mozambique Channel: Observations and interpretation. *Journal of Geophysical Research: Oceans* 114(C5).
- Fekete, B.M., Vörösmarty, C.J., Grabs, W., 1999. Global composite runoff fields based on observed river discharge and simulated water balances. *WMO-Global Runoff Data Centre Report*, 22, Koblenz, Germany.
- Flemming, B.W., Kudrass, H., 2018. Large dunes on the outer shelf off the Zambezi Delta, Mozambique: evidence for the existence of a Mozambique Current. *Geo-Marine Letters* 38, 95–105.
- Gayen, B., Sarkar, S., 2010. Turbulence during the generation of internal tide on a critical slope. *Physical review letters* 104(21), 218502.
- Halo, I., Backeberg, B., Penven, P., Ansorge, I., Reason, C., Ullgren, J.E., 2014. Eddy properties in the Mozambique Channel: A comparison between observations and two numerical ocean circulation models. *Deep Sea Research Part II: Topical Studies in Oceanography* 100, 38–53.
- Jouet, G., Deville, E., 2015. PAMELA-MOZ04 cruise, RV Pourquoi pas?, <http://dx.doi.org/10.17600/15000700>.
- Puig, P., Palanques, A., Guillén, J., El Khatab, M., 2004. Role of internal waves in the generation of nepheloid layers on the northwestern Alboran slope: implications for continental margin shaping. *Journal of Geophysical Research: Oceans* 109(C9). doi: 10.1029/2004JC002394
- Schulz, H., Lückge, A., Emeis, K. C., Mackensen, A., 2011. Variability of Holocene to Late Pleistocene Zambezi riverine sedimentation at the upper

continental slope off Mozambique, 15–21° S.  
Marine Geology 286(1-4), 21-34.

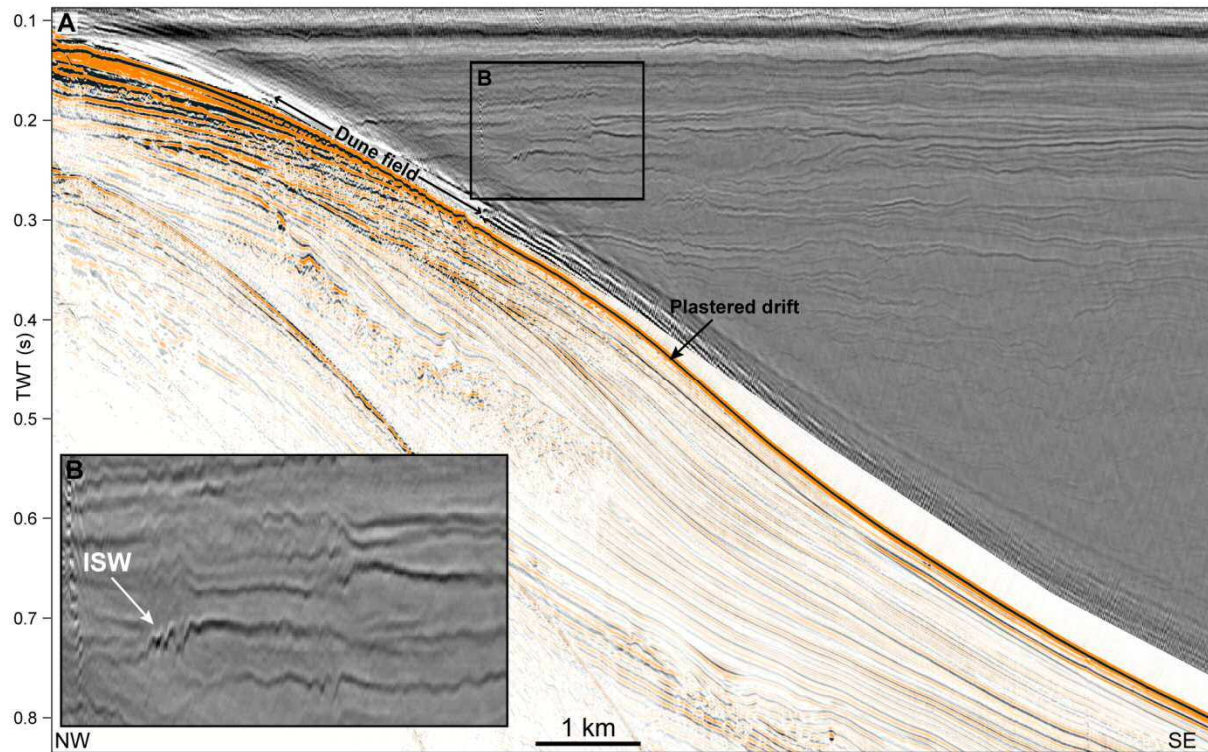


Figure 2. Multi-channel high-resolution mini GI gun seismic reflection profile MOZ04-HR-102 showing the dune field at the upper part of a plastered drift and Internal Solitary Waves (ISW) moving offshore at the water depth of the dune field.

# Observations of low-angle dunes under shallow flow

Suleyman Naqshband *Wageningen University, Wageningen, Netherlands – suleyman.naqshband@wur.nl*

A.J.F. (Ton) Hoitink *Wageningen University, Wageningen, Netherlands – ton.hoitink@wur.nl*

**ABSTRACT:** Dunes commonly dominate the bed of sandy rivers and they are of central importance in predicting flow resistance and water levels. In the present study, we show that by using light-weight polystyrene particles as substrate in a laboratory setting, promising morphodynamic similarity is obtained between dunes in shallow flow (flume) and deep flow (field) conditions. In particular, results from our flume experiments show that dune lee-side angles, which are crucial in turbulence production and energy dissipation, better approximate dune lee-side angles observed in natural channels.

## 1 INTRODUCTION

River bedforms arise from the interaction between flow and the underlying sandy river bed. Dunes are the most common bedforms observed in rivers. Due to their large dimensions relative to flow depth and the formation of turbulent flow separation zones, dunes are the main source of flow roughness and they are the essential ingredient for accurate predictions of water levels during floods (Warmink, 2014). Particularly under increasing river discharges, dunes grow rapidly and reach heights up to several meters, resulting in a significant rise of water levels and, consequently, increase flood risk.

Dunes are traditionally studied in sand-bedded flumes, in which Froude numbers are relatively high due to limited flow depths (e.g. Venditti et al., 2016; Naqshband et al., 2017). Dunes under these conditions are asymmetric and possess lee-side angels at the angle of repose of sand ( $\sim 30^\circ$ ). Consequently, most of our understanding of dune morphodynamics, kinematics, flow resistance, and sediment transport originates from shallow flows with high Froude numbers. However, field studies over the past decades have illustrated that dunes in natural

rivers are predominantly symmetric with much lower lee-side angles ( $\sim 10^\circ$ ) and more complex lee-side morphology (Hendershot et al., 2016). These low-angle dunes (LADs) are associated with intermittent flow separation zones, whereas laboratory generated, high-angle dunes (HADs) show a permanent zone of flow separation (Kwoll et al., 2016). Such difference in dune morphology and lee-side flow separation zone has major implications for flow resistance and water levels.

Using light-weight polystyrene particles as a substrate, in this study, we were able to generate low-angle dunes under shallow laboratory flow conditions. By limiting the Froude number, low-angle dune morphodynamics were studied for a wide range of flow and sediment conditions.

## 2 METHODS

Experiments were conducted in the Kraijenhoff van de Leur laboratory for Water and Sediment dynamics of Wageningen University & Research. A tilting flume of 14.4 m long and 1.20 m wide was used. At the downstream end of the flume, a sediment trap is connected to a sediment recirculation

pump. At the upstream point where the sediment-rich water re-enters the flume, a diffuser is placed to distribute the inflow over the full width of the flume. Furthermore, turbulence is suppressed by a laminator located at the upstream end of the flume.

A 15 cm thick layer of light-weight polystyrene particles was installed at the flume bed with a  $D_{50}$  of 2.1 mm and a  $D_{90}$  of 2.9 mm, and a specific gravity of 1.1. A filter was installed at the end of the flume to prevent loss of polystyrene particles over the flume edge and to make sure that all particles were fully recirculated. Flow conditions were chosen such to represent the natural variability of observed suspension numbers and Froude numbers in large rivers ( $u_*/w_s$  range of 0.50 to 3.2, Fr number up to 0.15).

Flow discharge was measured continuously with an electromagnetic flow meter. Flow depths along the entire flume were measured using stilling wells. Water levels in the stilling wells were continuously recorded using magnetostrictive linear position sensors. Bed morphology was measured during certain phases of the experiment, being the initial dry-bed condition, the initial submerged condition and after reaching dynamic dune equilibrium. A line laser scanner mounted on a semi-automatic carriage was used for this purpose (for details see de Ruijsscher et al., 2018). The entire flume bed was scanned with a streamwise resolution of 2 mm and a crosswise resolution of 3 mm, in four parallel partly-overlapping swipes, within a period of 2 minutes. Three transects, evenly distributed from the centre of the flume towards both side walls, were selected to monitor dune morphology (height and length statistics, together with lee-side angles) using bedform tracking tool developed by van der Mark et al., 2008. Average and standard deviations of dune height and length were determined over the effective measurement section of the flume.

### 3 RESULTS AND DISCUSSION

Flume experiments with light-weight polystyrene particles show that dune lee-side angles considerably vary across the width of

a dune, and also between successive dunes downstream as recently observed in world's large rivers, including the Amazon, Mississippi, Parana, Mekong, Columbia and Jamuna rivers. Furthermore, for a wide range of flow and sediment conditions, dune lee-side angles are predominantly lower than the 30° angle of repose found under traditional flume experiments with sand.

In addition to the promising dune dynamic similarity observed between shallow flow and deep flow, using light-weight particles further result in a more realistic dune height evolution towards upper stage plane bed. By compiling and analysing a large data set, Naqshband et al., 2014 showed that dune heights under shallow laboratory flow conditions (high Froude number) decay and dunes reach upper stage plane bed at much lower suspension numbers compared to dunes under deep flow in natural channels (low Froude number). For the investigated range of suspension numbers, average dune heights closely follow dune height evolution as observed in the field. Figure 1 further illustrates a sequence of dune development over time, for the effective measurement section of the flume, corresponding to a suspension number of approximately 2.5.

### 4 CONCLUSIONS

In the present study, we showed that by using light-weight polystyrene particles as substrate in a laboratory setting, promising morphodynamic similarity is obtained between dunes in shallow flow (flume) and deep flow (field) conditions. In particular, for a wide range of flow conditions, lee-side angles obtained in the present flume investigations better approximate dune lee-side angles observed in natural channels. Furthermore, dune height evolution towards upper stage plane bed observed in the present experimental study, closely follows dune height evolution as observed in world's large rivers.

## 5 ACKNOWLEDGEMENT

Partial funding for this research was provided by the Department of Environmental Sciences at Wageningen University, and the Dutch Ministry of Infrastructure and Environment (Rijkswaterstaat, Fund 5160957319).

## 6 REFERENCES

- Hendershot, M.L., Venditti, J.G., Bradley, R.W., Kostaschuk, R.A., Church, M., and Allison, M.A., 2016. Response of low angle dunes to variable flow. *Sedimentology* 63, 743–760.
- Van der Mark, C. F., Blom, A., & Hulscher, S. J. M. H., 2008. Quantification of variability in bedform geometry. *Journal of Geophysical Research* 113, F03020.
- Naqshband, S., Ribberink, J. S., Hurther, D., and Hulscher, S. J. M. H., 2014. Bed load and suspended load contributions to migrating sand dunes in equilibrium. *Journal of Geophysical Research* 119, 1043–1063.
- Naqshband, S., Hoitink, A.J.F., McElroy, B., Hurther, D., and Hulscher, S. J. M. H., 2017. A Sharp View on River Dune Transition to Upper Stage Plane Bed. *Geophysical Research Letters* 44, 437–444.
- Kwoll, E., Venditti, J.G., Bradley, R.W., and Winter, C., 2016. Flow structure and resistance over subaqueous high- and low-angle dunes. *Journal of Geophysical Research: Earth Surface* 121, 545–564.
- de Ruijsscher, T.V., Hoitink, A. J. F., Dinnissen, S., Vermeulen, B. and Hazenberg, P. Application of a Line Laser Scanner for Bed Form Tracking in a Laboratory Flume. *Water Resources Research* 54, 2078–2094.
- Venditti, J. G., Lin, C.-Y. M., and Kazemi, M., 2016. Variability in bedform morphology and kinematics with transport stage. *Sedimentology* 63, 1017–1040.
- Warmink, J.J., 2014. Dune dynamics and roughness under gradually varying flood waves, comparing flume and field observations. *Advances in Geoscience* 39, 115–121.

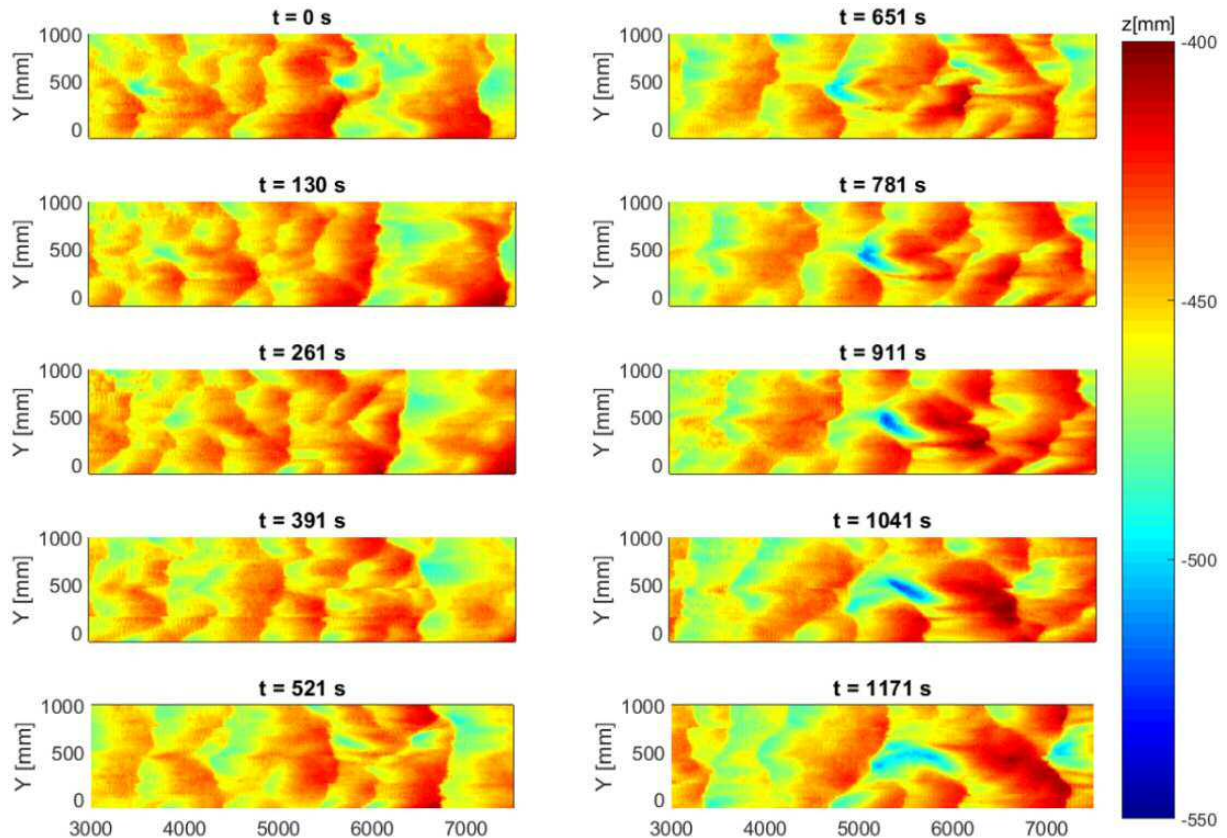


Figure 1. Sequence of dune development over time for the suspended load dominant experimental condition ( $u_*/w_s = 2.5$ ). X is the streamwise direction, Y is the cross-stream direction, and z is the vertical distance with respect to the mean bed elevation.



# Modelling the impact of a time-varying wave angle on the nonlinear evolution of sand bars

Abdel Nnafie *IMAU, Utrecht University, Netherlands – a.nnafie@uu.nl*

Niek van Andel *IMAU, Utrecht University, Netherlands – j.p.c.vanandel@students.uu.nl*

Huib de Swart *IMAU, Utrecht University, Netherlands – H.E.deSwart@uu.nl*

**ABSTRACT:** Sandy beaches are often characterized by the presence of sand bars, whose characteristics (growth, migration, etc.) strongly depend on the wave conditions (wave height, angle of wave incidence, etc.). This study addresses the impact of a periodically time-varying wave angle of incidence with different time-means on the long-term evolution (order days to months) of sand bars. Model results show that heights of sand bars that form in the case of a time-varying angle around a zero-mean are on average larger than those in the cases of time-varying angles around an oblique mean, particularly for large variations in the angle of wave incidence.

## 1 INTRODUCTION

The surf zone of many sandy uninterrupted beaches often features the presence of several sand bars that are aligned perpendicularly or obliquely to the coast (Fig. 1). These bars display a rhythmic pattern along the shore, with alongshore spacings (distance between successive bar crests) in the order of tens to hundreds of meters. Their migration rates, which depend on the strength of the alongshore current, might reach tens of meters per day along the shore, and their lifetimes range between days to months (e.g., Wright & Short 1985). The presence of sand bars has a direct impact on the shoreline by, among other things, creating areas of erosion and deposition (Komar, 1998). Therefore, increasing our knowledge of the dynamics of these bedforms is important to enhance our insight into coastal processes and, thereby, our capacity to accurately simulate the evolution of coastal systems.

Fair weather conditions favour the growth of sand bars, of which the characteristics (e.g. growth and migration rates) strongly depend on the wave conditions (e.g., Wright & Short, 1985). During severe

storms, or during moderate-energy waves with highly oblique wave angle of incidence (with respect to the shore-normal), the bars are wiped away or they are reshaped into linear features without longshore variability (Lippman & Holman 1990, Van Enckevort et al., 2004; Price & Ruessink, 2011).

Various models have been developed to study the initial formation and long-term evolution of sand bars (see review by Ribas et al., 2015). These models simulate waves, currents, sand transport and bed evolution in the surf zone, with incoming waves being the main driver. In most of these studies, wave conditions (wave height, angle of wave incidence, etc.) have been assumed to be time-invariant (constant in time), whereas in reality, these conditions change continuously with time. Exceptions are the studies by Smit et al. (2005) and Castelle & Ruessink (2011), which addressed the impact of time-varying wave conditions on the dynamics of sand bars. The latter study (Castelle & Ruessink, 2011, hereafter referred to as CR2011) presents a systematic analysis of the impact of a time-varying wave forcing on the evolution of finite-amplitude sand bars. It was demonstrated that especially periodic variations in the wave angle of incidence were crucial in the development of

bars in terms of their finite amplitude behaviour, migration and their alongshore spacing. A drawback in the study by CR2011 was that the angle of wave incidence was limited to variations around a zero mean (normal incidence). Obviously, in real physical situations, the mean angle is not necessarily 0 degrees. In fact, the nonlinear modelling study by Garnier et al. (2008) demonstrated that beyond a critical wave angle of incidence ( $\theta = 7^{\circ}$ ), sand bars do not grow, revealing the importance of this angle for sand bar dynamics.

This study will build on the work of CR2011, with the main extension that also oblique mean angles of wave incidence are considered. Specifically, the following question is addressed: What is the impact of a periodically time-varying wave angle of incidence with a non-zero mean on the growth of sand bars? To this end, simulations will be performed with an available numerical model (morfo55), developed by Caballeria et al. (2002) and Garnier et al. (2006), who simulated the evolution of finite-amplitude sand bars in the nearshore zone in the case of time-invariant wave forcing. Morfo55 uses depth-averaged shallow water equations, including sediment transport and bed updating. Moreover, it includes fully detailed wave-topography feedbacks, wave shoaling and refraction, wave breaking and wave radiation stresses. Further details are given in Garnier et al. (2006). This model will be extended such that it includes a time-varying wave angle of incidence.

Section 2 describes the methodology applied in this study, followed by a presentation and discussion of model results (section 3). In Section 4, the conclusions are given.

## 2 METHODOLOGY

Following Garnier et al. (2006), the study area is schematized as a rectangular domain with dimensions  $L_x \times L_y (= 250 \text{ m} \times 2000 \text{ m})$ , which is bounded by a straight coast at  $x = 0$  (Fig. 2). Periodic boundary conditions are applied at the lateral boundaries ( $y = 0$  and  $y = L_y$ ) for each variable in the model

(e.g. water level, velocity, bed level, etc), as well as for their  $y$ -derivative (e.g.,  $z_b(x, 0, t) = (x, L_y, t)$  and  $\partial z_b / \partial y(x, 0, t) = \partial z_b / \partial y(x, L_y, t)$ ). At the shore boundary ( $x = 0$ ), a vanishing cross-shore flow is assumed. At the offshore boundary ( $x = L_x$ ), a constant significant wave height ( $H_{\text{rms}}$ ), wave period ( $T_p$ ) and a time-varying angle of wave incidence  $\theta$  are imposed. The latter varies with time according to:

$$\theta(t) = \theta_0 + \hat{\theta} \sin(2\pi/Tt) \quad (1)$$

with  $\theta_0$  the time-mean angle,  $\hat{\theta}$  is the amplitude of the variation in the angle and  $T$  is the period of this variation. Different values for the mean angle  $\theta_0$ , amplitude  $\hat{\theta}$  and period  $T$  are considered, in the ranges  $0 \leq \theta_0 \leq 4^{\circ}$ ,  $0 < \hat{\theta} \leq 8^{\circ}$  and  $7 < T \leq 224$  days. For the sake of comparison, additional simulations are conducted without time variation in  $\theta$ , i.e.,  $\theta = \theta_0$ .

Non-cohesive sediment is assumed with a single size  $d_{50} = 250 \mu\text{m}$ . The equations are solved on a computational grid with spacing  $\Delta x \times \Delta y = 10 \text{ m} \times 5 \text{ m}$ . The hydrodynamic time step  $\Delta t = 0.05 \text{ s}$ , while the morphodynamic time step is increased by a morphological amplification factor (Moac) of 90. Test simulations with lower Moacs do not yield different results.

Model simulations start from the Yu & Slinn (2003) single barred beach bottom profile with superimposed random bottom perturbations  $h$  (with amplitude 2 cm). This profile, which is uniform in the longshore direction ( $y$ ), is given by the following equation:

$$z_b^0(x) = -a_0 - a_1 \left( 1 - \frac{\beta_2}{\beta_1} \right) \tanh \left( \frac{\beta_1 x}{a_1} \right) - \beta_2 x + a_2 \exp \left[ -5 \left( \frac{(x - x_c)}{x_c} \right)^2 \right], \quad (2)$$

with  $x_c$  the bar location ( $= 80 \text{ m}$ ),  $a_2$  is the bar amplitude ( $= 1.5 \text{ m}$ ),  $a_0$  is the water depth at the coast ( $= 0.25 \text{ m}$ ). Other coefficients are

$a_1 = 2.97 \text{ m}$ ,  $\beta_1 = 0.075$  and  $\beta_2 = 0.064$ .

The simulation time is approximately 300 days. An overview of the important model parameters is presented in Table 1. Further details are given in Garnier et al. (2006).

Finally, analysis of model results focuses on growth of sand bars, which is expressed by their root-mean-square height as follows:

$$|h| = \left[ \frac{1}{L_x L_y} \iint h^2 dx dy \right]^{1/2}. \quad (3)$$

### 3 RESULTS AND DISCUSSION

Figure 3 shows the root-mean-square height  $|h|$  of the sand bars versus time in the cases of imposing a time-varying angle of wave incidence  $\theta$  with different periods  $T$  and different time-mean angles  $\theta_0$  (panels a-b). Amplitude of the variation in the angle  $\hat{\theta} = 2^\circ$ . After a period of about 20 days of a rapid bar growth, saturation of this growth appears in the subsequent period. Note the oscillating behaviour in the height of the bars, reflecting the time variation in the angle of wave incidence  $\theta$ . This figure reveals that in the case of a time-varying angle around a zero-mean ( $\theta_0 = 0$ ), the saturation height of the bars is on average larger than that in the case of a constant  $\theta$  (see also Fig. 3c, black line), particularly for small periods  $T$ . In contrast, in the cases of  $\theta_0 = 2^\circ$  and  $\theta_0 = 4^\circ$  (panels b and c), the saturation height of the bars is generally smaller than their corresponding heights in case of constant angles  $\theta$ . Figure 3b further shows that in the case of a time-varying angle  $\theta$  with an oblique mean angle, bar growth is weaker compared with that of the case with constant  $\theta$ , particularly for large periods  $T$ . This difference in bar growth does not occur in the case of variations around a zero mean (Fig. 3a).

Regarding the impact of using different amplitudes  $\hat{\theta}$  of angle variation, model results (Fig. 4) demonstrate that with respect

to the case of a constant angle  $\theta$ , the saturation height of sand bars of the cases with oblique mean angles becomes smaller with increasing amplitude  $\hat{\theta}$ . The larger this mean angle, the stronger is the decrease in height (panels b, c). In contrast, the height of the bar of the case with zero-mean angle initially becomes larger with increasing variation  $\hat{\theta}$ , after which it decreases for large variations  $\hat{\theta}$ .

These outcomes contradict the results obtained by CR2011, who found that saturation height of sand bars of the case of a time-varying angle of wave incidence  $\theta$  (with zero-mean) is always smaller than that in the case of constant  $\theta$ . Their model results show that the larger the amplitude of angle variation  $\hat{\theta}$ , the smaller the saturation height. This contrast between the outcomes of the present study and those of the study by CR2011 might be due to differences that exist between model configurations of two studies. These differences are mainly that 1) the initial bathymetry used in morfo55 is deeper than that in CR2011; 2) morfo55 uses a rigid coastline, while CR2011 uses a dynamic coastline (changes in time); 3) morfo55 applies the sediment transport formulation of Soulsby (1997), while CR2011 uses the formulation of Bailard (1981); and finally 4) the wave model implemented in morfo55 is based on linear wave theory (narrow spectrum with one frequency and one direction), while CR2011 uses the spectral wave SWAN, which accounts for a broad spectrum with multiple frequencies and directions. Which differences are causing the contradiction between outcomes from the present study and those of CR2011 remain to be quantified, and are subject of further research.

### 4 CONCLUSIONS

1. To conclude, the saturation height of sand bars of the case of a time-varying angle around a zero-mean is on average larger than that in the case of a constant  $\theta$ . In contrast, the saturation height of bars of the cas-

es of time-varying angles around an oblique time-mean are generally smaller than their corresponding heights in the case of a constant angle, particularly for large variations in the angle of wave incidence.

Table 1: Overview model parameters

Parameter	Value
Domain dimensions $L_x \times L_y$	250 m × 2000 m
Significant wave height $H_{\text{rms}}$	1 m
Wave period $T_p$	6 s
Sediment size $d_{50}$	250 µm
Grid spacing $\Delta x \times \Delta y$	10 m × 5 m
Time step $\Delta t$	0.05 s
Amplification factor Moac	90

## 5 REFERENCES

- Bailard, J., 1981. An energetics total load sediment transport model for a plane sloping beach, *Journal of Geophysical Research*, 86, 10,93810,954.
- Caballeria, M., G. Coco, A. Falqués, and D. A. Huntley, 2002. Self-organization mechanisms for the formation of nearshore crescentic and transverse sand bars, *Journal of Fluid Mechanics*, 465, 379–410.
- Castelle, B. and B.G. Ruessink, 2011. Modeling formation and subsequent nonlinear evolution of rip channels: Time-varying versus time-invariant wave forcing. *J. Geophys. Res.* 116F04008, doi:10.1029/2011JF001997.
- Garnier, R., D. Calvete, A. Falqués, and M. Caballeria, 2006. Generation and nonlinear evolution of shore-oblique/transverse sand bars, *J. Fluid Mech.*, 567, 327–360.
- Komar, P. D., 1998. *Beach Processes and Sedimentation*, 2nd ed., Prentice Hall, Englewood Cliffs, N. J.
- Lippman, T.C. and R.A. Holman, 1990. The spatial and temporal variability of sandbar morphology. *J. Geophys. Res.* 95C7, 11575–11590.
- Price, T. D., and B. G. Ruessink, 2011. State dynamics of a double sandbar system, *Cont. Shelf Res.*, 31, 659–674.
- Ribas, F. A. Falqués, H.E. de Swart, N. Dodd, R. Garnier and D. Calvete, 2015. Understanding coastal morphodynamic patterns from depth-averaged sediment concentration. *Rev. Geophys.* 53, doi: 10.1002/2014RG000457.
- Smit, M. W. J., A. J. H. M. Reniers, and M. J. F. Stive, 2005. Nearshore bar response to time-varying conditions, paper presented at Coastal Dynamics '05, Am. Soc. of Civ. Eng., New York
- Soulsby, R. L., 1997. *Dynamics of Marine Sands*, Thomas Telford, London.
- Van Enckevort, I. M. J., B. G. Ruessink, G. Coco, K. Susuki, I. L. Turner, N. G. Plant, and R. A. Holman, 2004. Observations of nearshore crescentic sandbars, *J. Geophys. Res.*, 109, C06028, doi:10.1029/2003JC002214.
- Wright, L. D., and A.D. Short, M., 1984 Morphodynamic variability of surf zones and beaches: A synthesis. *M. ar. Geol.*, 56, 93-118.
- Yu, J., Slinn, D.N., 2003. Effects of wave-current interaction on rip currents. *J. Geophys. Res.* 108 (C3), 3088. doi:10.1029/2001JC001105.



Figure 1. Transverse sand bars at Horn Island, Mississippi, USA. (Source: <http://www.coastalwiki.org>).

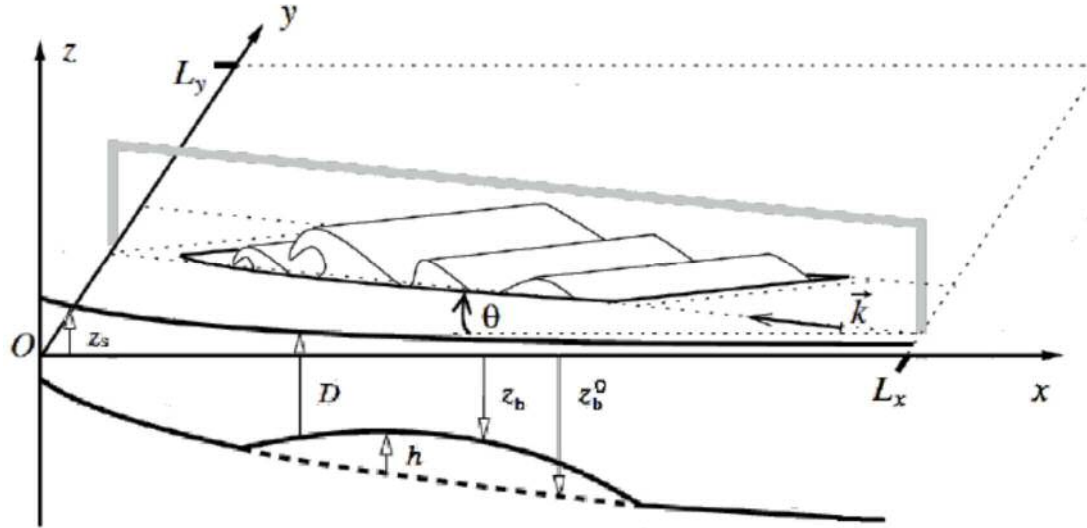


Figure 2. Schematic view of the study area, which is represented as a rectangular domain with dimensions  $L_x \times L_y$ . The coordinate system, with origin  $O$ , is defined such that  $x$  indicates a cross-shore,  $y$  an alongshore, and  $z$  a vertical position. Depth  $D$  is the difference between sea level  $z_s$  and bed level  $z_b$ . Furthermore, bottom perturbation  $h$  defined with respect to initial bed level  $z_b^0$ , i.e.,  $h = z_b - z_b^0$ . Waves propagate in the direction of wave vector  $\vec{k}$ , with an angle  $\theta$  with respect to  $x$ -axis. Figure modified after Garnier et al. (2006).

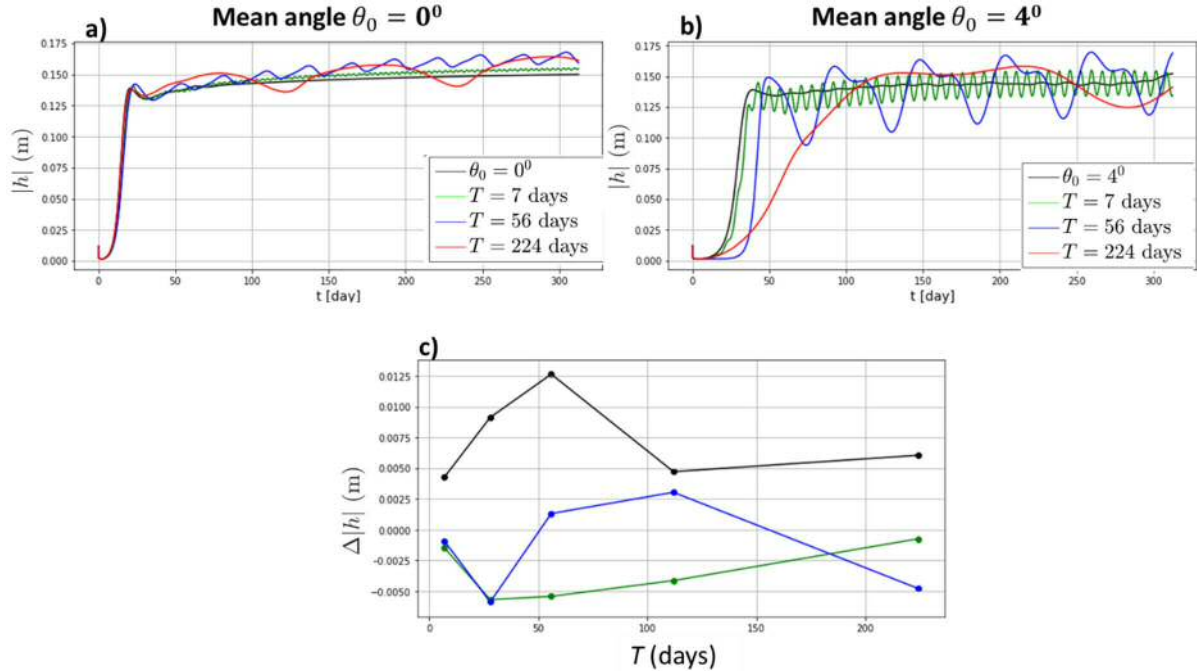


Figure 3. a) Root-mean-square height of the sand bars  $|h|$  versus time in the case of a time-varying angle of wave incidence  $\theta$  with zero-mean ( $\theta_0 = 0^\circ$ ), and which varies with different periods  $T$ . Amplitude of the variation in the angle  $\hat{\theta} = 2^\circ$ . The case of a time-invariant angle  $\theta$  is also shown (black line). b) As in a), but in the case of a time-varying angle  $\theta$  with a mean  $\theta_0 = 4^\circ$ . e) Difference between finite heights  $|h|$  of the sand bars of cases with and without a time varying angle  $\theta$  for different mean angles ( $\theta_0 = 0^\circ$ , black;  $\theta_0 = 2^\circ$ , green;  $\theta_0 = 4^\circ$ , blue)

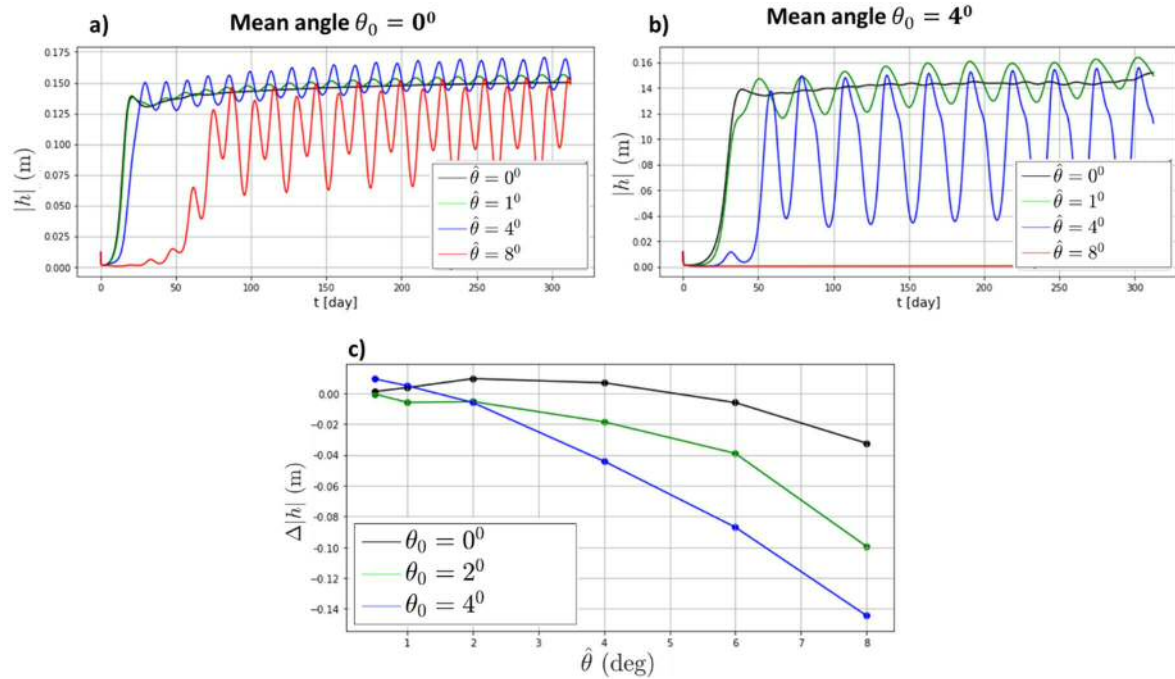


Figure 4. As in Figure 3, but for different amplitudes of angle variation  $\hat{\theta}$ .

# Occurrence of tidal sand waves in a Brazilian coastal bay: the Sepetiba case

Mariana T.C. Pardal *Universidade do Estado do Rio de Janeiro, Rio de Janeiro, Brasil* – [maripardal@gmail.com](mailto:maripardal@gmail.com)

Josefa V. Guerra *Universidade do Estado do Rio de Janeiro, Rio de Janeiro, Brasil* – [josie.guerra@gmail.com](mailto:josie.guerra@gmail.com)

Pieter C. Roos *University of Twente, Enschede, The Netherlands* – [p.c.roos@utwente.nl](mailto:p.c.roos@utwente.nl)

Suzanne J.M.H. Hulscher *University of Twente, Enschede, The Netherlands* – [s.j.m.h.hulscher@utwente.nl](mailto:s.j.m.h.hulscher@utwente.nl)

**ABSTRACT:** Sepetiba Bay is one of the most important bays in southeastern Brazil mainly because of several economic activities such as fishing, tourism, and the presence of important ports. The occurrence of sand waves in Sepetiba Bay was studied using two multibeam bathymetric datasets obtained during surveys carried out between November and December 2011, and in December 2012. The sand wave field was divided into seven areas and 104 individual sand waves were identified with heights varying between 0.1 and 5.7 m and wavelengths ranging from 9 to 228 m. Coarse sands occur in the crests whereas medium to fine sands are found in the troughs. Near-bed current velocities measured at the northern limit of the sand wave field reached 1.02 m/s during spring tides, and exhibit flood dominance. In this work were used a linear process-based sand wave model to improve the understanding about their occurrence and the relation with environmental

## 1 INTRODUCTION

Bedforms are common features in the bottoms of shallow seas where tidal currents are present and sands are available. Here we focus on features known as subaqueous dunes or tidal sand waves (Terwindt, 1971).

The presence of bedforms in Sepetiba Bay was first mentioned by Belo (2002) and later studied by Oliveira (2013). Belo (2002) described small bedforms in the entrance of the bay (height ranging from less than 0.2 until 0.55 m and wavelength between 8.6 and 60 m).

Oliveira (2013) was the first to conduct an observational study focused on the subaqueous dunes from Sepetiba Bay. The author identified 62 subaqueous dunes distributed close to Sepetiba's bay main navigational channel with heights varying between 0.2 and 4.6 m and wavelengths ranging from 18 to 164 m. In his study, Oliveira (2013) could not determine if the bedforms are still fully active or not.

The available bathymetric data show a great diversity in sand wave morphology occurring in a small area ( $\approx 34 \text{ km}^2$ ). Therefore, the main goal of this study is to understand how this morphological variability is related to the modern environmental characteristics and which conditions favour the formation and development of such bedforms. Here, we first present the study area (§2), followed by data and methods (§3), some first observational and modelling results (§4), as well as a discussion and conclusions (§5).

## 2 STUDY AREA

### a. 2.1 General Description

Sepetiba bay is located in the southern part of Rio de Janeiro State between the coordinates  $043^{\circ}30'W/44^{\circ}10'W$  and  $22^{\circ}50'S/23^{\circ}05'S$ . It has an ellipsoidal shape being 40 km long and 16 km wide (Villena et al., 2012) (Fig. 1). depths are mostly less than 10 m except in the main channel area (water depth greater than 25 m maintained by dredging).

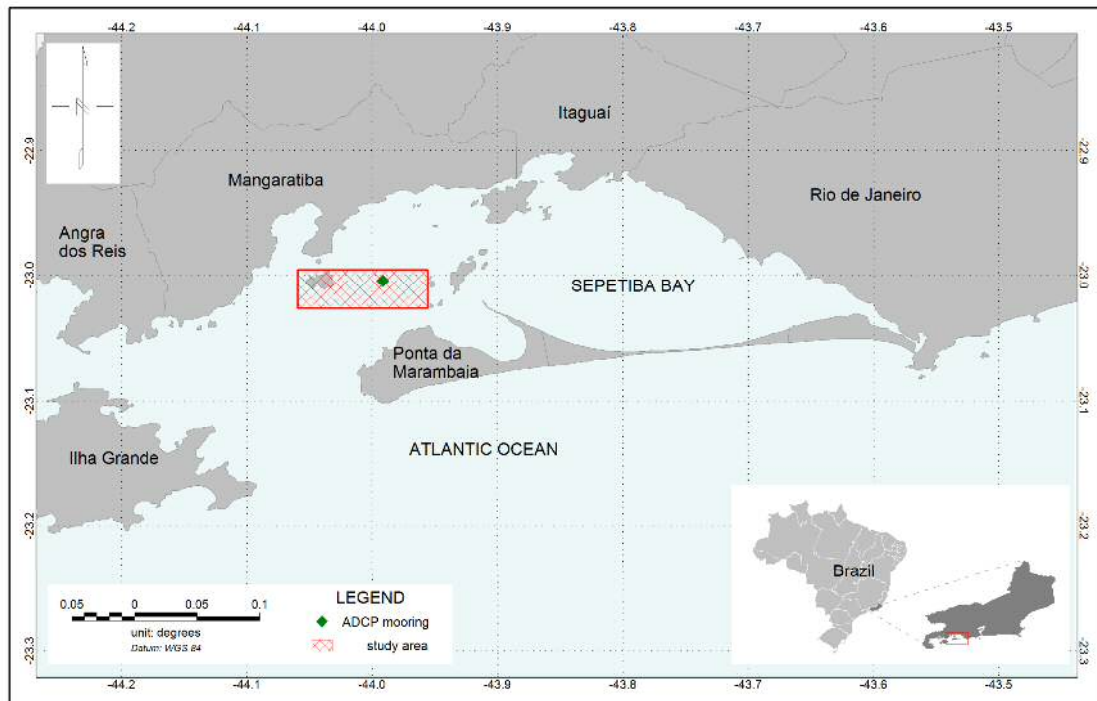


Figure 1: Sepetiba bay location, study area, and ADCP mooring position.

Its origin is associated to structural events occurred during the Cenozoic (Zalán & Oliveira, 2005), whereas its geologic evolution and present morphology are related to sea level oscillations during the Quaternary (Villena et al, 2012).

According to Signorini (1980), the circulation mechanism follows the partially-mixed estuarine system with components of gravitational, residual and tidal circulations.

In Sepetiba Bay, there is a lag between the tide wave in its entrance and its head, generating both sea level elevation gradients and strong tidal currents (Fragoso, 1999). Winds acting on the continental shelf can have an important role in this area affecting the currents in the interior of the bay (Fragoso, 1999). Vertical profiles of the currents were documented at the northern limit of the study area and revealed that floods are up to 2 hours shorter than ebbs and are associated with the strongest flows (Fonseca, 2013).

The bay is covered by sediments ranging from clay to sands, which have multiple

sources such as (i) past and modern rivers flowing into the bay, (ii) the nearby shelf, and (iii) coastal erosion. Sands are more abundant between Ilha Grande and Ponta da Marambaia, being a mixture of modern and relict deposits (Fig. 2).

The study area is approximately 34 km<sup>2</sup> (red rectangle in Fig. 1); it is limited eastward by Jaguanum island, southward by Ponta da Marambaia and north/westward by Guaíba island, encompassing sectors of the main navigation channel.

### 3 DATA AND METHODS

#### a. 3.1 Available data

In this study, the data acquired during three multibeam bathymetric surveys (Fig. 3) and five Teledyne-RDI 600 kHz ADCP moorings was used. The first two multibeam surveys were carried out in December 2010 and November 2011 by the Brazilian Navy. The data was acquired with a Kongsberg EM 3000 multibeam echosounder. The third survey was carried out in December 2012 by Microars, working for the mining company Vale, using an R2Sonic 2024 multibeam echosounder.

The horizontal resolutions in these datasets are different: the first one has a 0.3 m resolution for both horizontal directions (X and Y) while the second one has a 1.44 m resolution in the same directions.

The ADCP dataset corresponds to five moorings deployed intermittently between December 2010 and September 2012 for 3- to 4-month long periods in the main navigation channel (Fig. 1).

### 3.2 Bathymetric data analysis

For this work, all the bathymetric datasets are provided in XYZ format. The analysis of these data was carried out using Geosoft Oasis montaj 8.5.5.

Firstly, the data was gridded using the minimum curvature method respecting the X-Y spacing of each dataset resulting in a surface model. The study area was divided into seven areas with distinct properties in terms of dune occurrence and dune morphology.

For each area, one or more transects were extracted obtaining a total of 12 transects (white traces in Fig.3). The dunes in each transect were identified by visual inspection revealing the characteristics of each subaqueous dune (height H, wavelengths L) and calculated the parameters H/L, L/H (ripple index) and the asymmetry (Knappen, 2005).

Both characteristics and parameters were plotted in scatterplot graphs to correlate each pair of data using Golden Software Grapher 12.

### 3.5 Current data

The ADCP mooring was deployed with transducers on an upward-looking configuration, positioned 0.64 above the seafloor.

The water column was sampled with 0.5 m bin sizes and four-minute sampling rate. The blank distance corresponds to 0.88 m, then measurements were taken between 2.26 m above the bottom and 3 m below the surface.

### b. 3.4 Sand wave modelling

The modeling used in this work is the process-based morphodynamic model developed by Campmans et al. (2017) which uses linear stability analyses to explain sand wave formation considering environmental parameters such as currents and waves.

The modelling process can be briefly described in five steps: (1) model formulation, including all necessary hydrodynamic and sediment parameters to describe the problem; (2) basic state, which consists of a flat bed without sediment movement and no spatial variation; (3) perturbation of the basic state expressed as a superposition of modes with a sinusoidal structure; (4) calculation of the linear response to this perturbation leading to growth and migration rates of these modes and (5) interpretation of the model results. In particular, the so-called *fastest growing mode* provides insight in the preferred sand wave characteristics.

## 4. 4 RESULTS

From the bathymetric data 104 subaqueous dunes were identified with heights varying between 0.1 and 5.7 m and wavelengths ranging from 9 to 233 m. The crests of the subaqueous dunes are located in an average depth of 17.2 m.

Sand wave morphology is not spatially uniform: different shapes are observed. Small bedforms superimposed to the sand waves are present in some areas. The crests are oriented in different directions.

The sand waves occur in depths ranging from 4 to 31 metres. Furthermore, the available sedimentary record show that sand waves are formed by very fine to coarse sands. Finally, the current data and sand wave modelling are work in progress and no results are currently available.

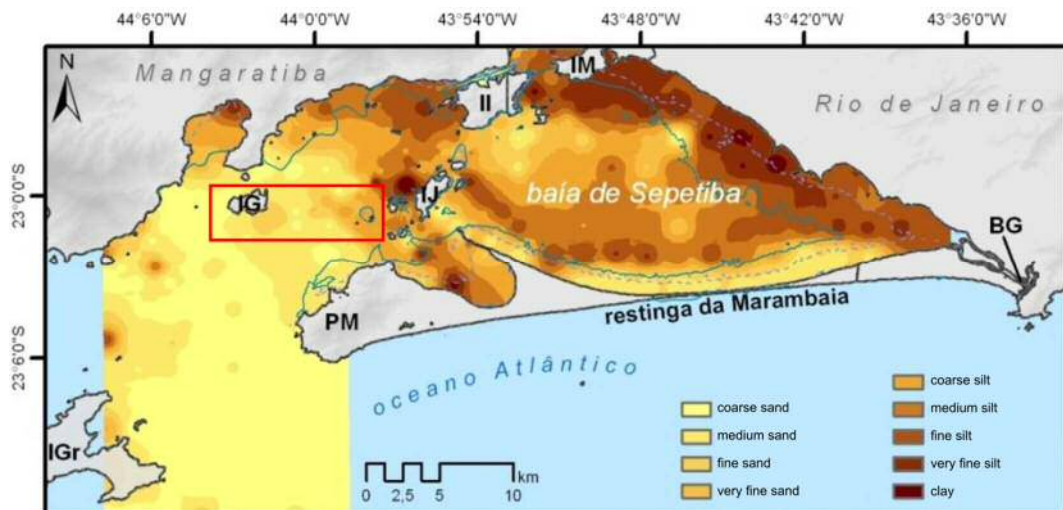


Figure 2: Sediment distribution in Sepetiba bay and study area (red rectangle) (modified from Carvalho, 2014)

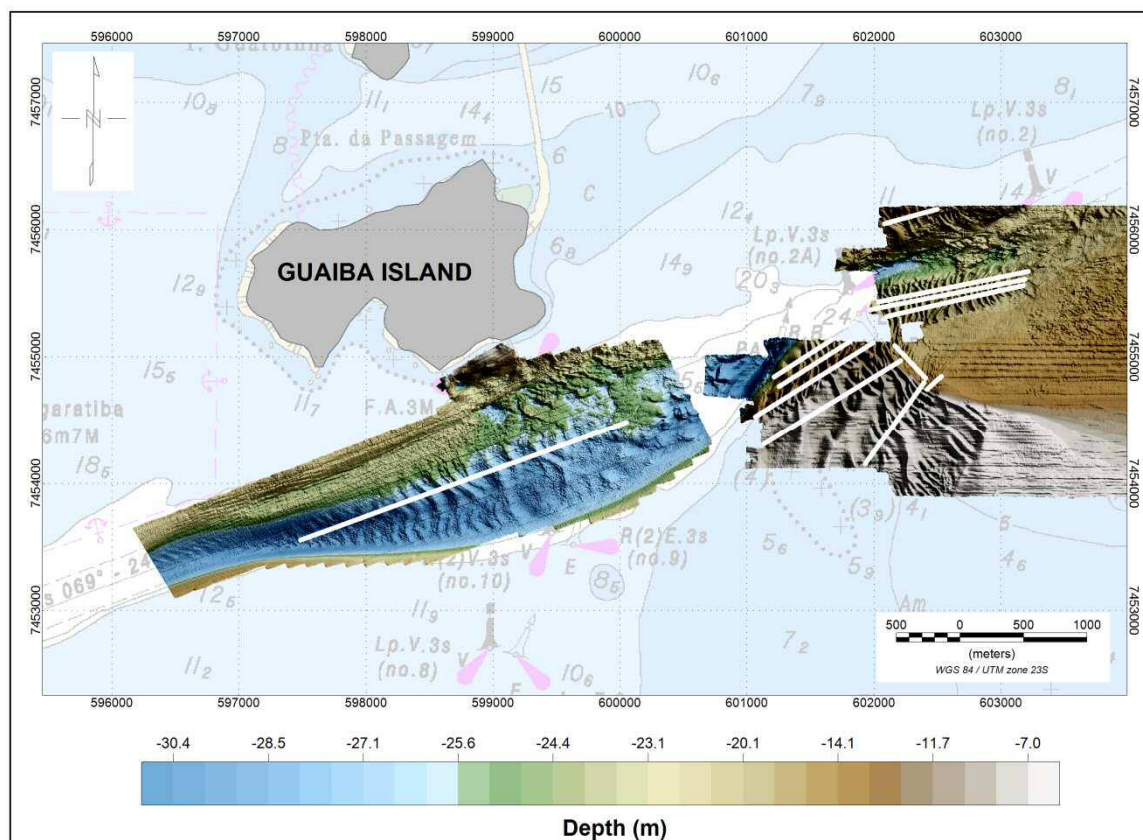


Figure 3: Available bathymetric data superimposed on the nautical chart and transects position (white traces). Southward from Guaiba island: VALE data; eastward: Brazilian Navy data.

## 5 DISCUSSION AND CONCLUSIONS

The sand waves are present in a small area of the bay (but it is not possible to say if it is restricted to this area) with a strong morphological variation, e.g. with bedforms disappearing abruptly in the east sector.

According to previous studies (see Fig. 2), in this sector the sediments become finer and the navigation channel narrower (Fig. 3).

The greatest sand wave heights occur in the areas with an average depth of 8 metres (Fig. 3) while the longest wavelengths occur in the deepest areas.

The crest orientation and shape variability suggest a complex hydrodynamic scenario acting in the study area. The current data and the modelling results will help to better describe and understand the processes associated with the sand wave presence in this area.

## 6 ACKNOWLEDGMENT

This study was financed in part by the Coordenação de Aperfeiçoamento de Pessoal de Nível Superior – Brasil (CAPES) – Finance Code 001.

This work is part of the research programme SMARTSEA with project number 13275, which is (partly) financed by the Netherlands Organisation for Scientific Research (NWO).

## 7 REFERENCES

- Belo, W.C. (2002). O fundo marinho da Baía da Ilha Grande, RJ: evidências da ação das correntes e de ondas no canal central com base em formas de fundo observadas em registros de sonar (100kHz). Revista Brasileira de Geofísica, 20 (1), pp.18-30. In Portuguese.
- Carvalho, B.C. (2014). Aplicação de múltiplas ferramentas no estudo do transporte de sedimentos na margem interna da restinga da Marambaia (baía de Sepetiba, RJ). Universidade do Estado do Rio de Janeiro. Faculdade de Oceanografia, Dissertação de Mestrado. 137p. In Portuguese.
- Campmans, G.H.P.; Roos, P.C.; Vriend, H.J. de, Hulscher, S.J.M.H. (2017), Modeling the influence of storms on sand wave formation: a linear

stability approach. *Continental Shelf Research* 137:103-116.

Fragoso, M.R. (1999). Estudo numérico da circulação marinha da região das baías de Sepetiba e Ilha Grande (RJ). Universidade de São Paulo, Instituto Oceanográfico, Dissertação de Mestrado. 115p.

Fonseca, S.A.R. (2013). Circulação e fluxo de material particulado em suspensão no principal canal de acesso à baía de Sepetiba. Dissertação de Mestrado (Oceanografia), UERJ. 78p. In Portuguese.

Knaapen, M. A. F. (2005). Sandwave migration predictor based on shape information. *Journal of Geophysical Research*, 110, F04S11. <https://doi.org/10.1029/2004JF000195>

Oliveira, R.F. (2013), Caracterização de dunas subaquosas no canal de navegação da baía de Sepetiba (RJ). Dissertação de Mestrado (Geologia e Geofísica Marinha), UFF. 110p.

Signorini, S.R.(1980). A study of circulation in Bay of Ilha Grande and Bay of Sepetiba. Bolm. Instituto Oceanográfico, São Paulo, 29 (1), pp.41-55.

Terwindt, J.H.J., 1971. Sand waves in Southern Bight of the North Sea. *Mar.Geol.* 10, 51-67.

Villena, H.H., Pereira, S.D., Chaves, H.A.F., Dias, M.S., Guerra, J.V. (2012). Indícios da variação do nível do mar na Baía de Sepetiba In: Rodrigues, M.A.C., Pereira, S.D., Santos, S.B. (Eds.), Baía de Sepetiba Estado da Arte, Corbá Editora, Rio de Janeiro, 264p. In Portuguese.

Zalán, P.V., Oliveira, J.A.B. (2005). Origem e evolução estrutural do Sistema de Riftes Cenozoicos do Sudeste do Brasil. Boletim de Geociências – Petrobrás 13(2):269-300. In Portuguese.

# Improved quantification of sediment transport in lowland rivers

Judith Y. Poelman *Wageningen University, Wageningen, The Netherlands* – [judith.poelman@wur.nl](mailto:judith.poelman@wur.nl)

A. J. F. (Ton) Hoitink *Wageningen University, Wageningen, The Netherlands* – [ton.hoitink@wur.nl](mailto:ton.hoitink@wur.nl)

Suleyman Naqshband *Wageningen University, Wageningen, The Netherlands* –

[suleyman.naqshband@wur.nl](mailto:suleyman.naqshband@wur.nl)

**ABSTRACT:** Quantifying sediment transport is essential for understanding large-scale morphological developments as well as for the calibration of numerical models and long-term river management. A research proposal is developed that aims to improve the quantification of sediment transport in lowland rivers by improving acoustical measurement methods and by investigating the relation between bedforms, both geometry and superimposed bedforms, and total sediment transport.

## 1 INTRODUCTION

The management of river sediments is of vital importance for many reasons: flood protection, navigation, infrastructure and ecology. This results in a need for research on river morphodynamics, sediment transport processes and fluxes and the use of numerical tools for prediction of morphological development of the river. Currently, river managers face the oncoming challenge of sea-level rise and climate change, which will have large, but uncharacterized, effects on lowland rivers. Recently, a Dutch national research program *Rivers2Morrow* has been initiated, which focusses on the long-term development of the Dutch delta.

To enable river management and long-term numerical prediction, continuous observations of suspended sediment load and bed load transport are essential, enabling the explanation of observed morphological trends and the calculation of multiyear budgets. However, available observations are often scarce. This holds for many delta's worldwide, including the Dutch delta (Becker, 2015). The reason for this is that measuring is usually time- and labour intensive. It is difficult to get precise and accurate measurements, for instance because sediment fluxes are highly variable in time and space and because instruments are intrusive or are based on optical or acoustical measurements that not only depend on

sediment concentration, but are influenced by other variables, hindering the interpretation of such measurements (Guerrero et al., 2016; Hoitink and Hoekstra, 2004; Thorne and Hurther, 2014).

To complement observations, sediment fluxes can be estimated through sediment transport equations (*e.g.* Van Rijn, 1993; Meyer-Peter and Müller, 1948; Engelund and Hansen, 1967), whether or not implemented in numerical morphological models. However, transport equations are to a large extent based on flume data and tested for a limited range of parameters. Furthermore, dune geometry to determine bedform roughness is estimated and their form is simplified (Bradley and Venditti, 2017). Superimposed secondary bedforms are not taken into account. The added complexity in real rivers systems can limit the applicability of sediment transport modelling.

In fine-grained estuaries, well-accepted transport equations can lead to an underestimation of transport by an order of magnitude, as recently shown for the Yellow River (Ma et al. 2017). Ma et al. (2017) attributed this underestimation to a relation between bedforms and sediment transport efficiency. Schindler et al. (2015) have shown that a small fraction of cohesive sediment can have a dramatic effect on bed form dimensions, decreasing height and steepness. This is crucial in numerical modelling of sediment transport, as dune

dimensions have a large effect on flow and sediment fluxes.

A recent study on the sediment budget of the Rhine-Meuse estuary further illustrated that current availability of sediment transport observations and numerical modelling tools is insufficient to get accurate information on sediment fluxes (Becker, 2015). This emphasizes the need for reliable transport modelling and continuous measurements to calibrate and validate morphological models.

## 2 RESEARCH AIM

This project aims to improve the quantification of sediment transport in lowland rivers, with a focus on acoustical measuring methods, bedforms and sediment dynamics in the Rhine-Meuse estuary and with that, the applicability of sediment transport equations and sediment rating curves throughout the river system.

First, the improvement of acoustical measuring methods includes the inversion of ADCP (Acoustic Doppler Current Profiling) backscatter to suspended sediment concentration with multimodal sediment distribution, measuring bedload transport with the bottom track feature of an ADCP and measuring bedload with MBES (multibeam echosounder).

Secondly, the improvement of estimating sediment flux using transport equations is focused on the relation between bedform geometry and transport efficiency in the lower delta, as well as the relation between superposed secondary bedforms and flow, dune migration and sediment transport.

Third, combining improved methodology to infer sediment transport from acoustical measurements and increased understanding of transport dynamics in the lower delta, total sediment discharge estimations are gathered from available data.

## 3 WORK PLAN

### 3.1 Suspended sediment concentration (SSC) from ADCP backscatter.

Due to the large spatial and temporal variation of suspended sediment, sampling is usually not sufficient to estimate the total suspended sediment discharge through a channel. As an alternative, suspended sediment can be estimated by inversion of ADCP backscatter intensity. However, the acoustic signal is largely dependent on the particle size distribution. For a measuring frequency of 1.2MHz, common for moving-boat deployment, finer sediment fractions mainly contribute to attenuation of the signal, where coarser fractions form the largest contribution to scattering. We aim to improve the estimation of suspended sediment concentration by quantifying the attenuation by fine sediment, through employing a tilted sensor. The following two questions were defined:

*How can inversion of backscatter to SSC be improved using a tilted transducer?*

*How can ADCP be used to estimate SSC in areas with a multimodal sediment distribution?*

A dataset will be analysed that is gathered through a 13-hour survey at a junction in the Rhine-Meuse estuary (the Netherlands) and data from a measurement campaign in the Ems-Dollard estuary. Reference sediment concentration and particle size distribution are determined from water samples.

### 3.2 Laboratory experiments

A series of laboratory experiments aims at answering two questions:

*How do ripples contribute to dune migration and sediment transport?*

*How can ADCP-BT be used to measure bedload transport and with what accuracy?*

A first objective of the laboratory study is to elucidate the role of superimposed ripples to dune migration and sediment transport.

The common assumption when estimated bed load transport through dune tracking is that superimposed ripples dissipate at the lee side of dunes and thus contribute to dune migration. The experiments offer the opportunity to investigate how ripples contribute to sediment transport, especially in the case of low-angle dunes.

Secondly, we aim to improve the method of estimating bedload transport using the bottom track feature of an ADCP, building on previous work that included both field and laboratory experiments (Gaeuman and Jacobson, 2006; Rennie and Millar, 2004).

Experiments will be conducted at the Kraijenhoff van de Leur laboratory (Wageningen University) and we plan to include measurements with multiple ADCPs and an AVCP (Acoustic Concentration and Velocity Profiler), which enables very precise measurements of sediment fluxes and flow velocity (Hurther et al., 2011).

### 3.3 Field campaign: MBES and ADCP

A second method to estimate bedload transport based on acoustics is dune tracking using multibeam echo sounding. Here we aim to include the movement of superimposed bedforms.

A recently obtained dataset includes simultaneous MBES and ADCP measurements over five neighbouring transects in the River Waal. Based on this data we aim to answer two questions:

*Can continuous MBES be used to measure bedload transport over a transect (both ripples and dunes)?*

*What is the relation between cross-varying flow, bedform dimensions and transport?*

### 3.4 Bedforms and sediment transport equations

To determine what the relation between bedforms and sediment transport is, and with that, the applicability of transport equations, we aim to answer the following question:

*What is the relation between bed form geometry and transport efficiency in the Dutch delta and how does this affect the accuracy of transport equations?*

A first approach to answer this question is to analyse available bed elevation data, which is measured with MBES, two-weekly, in a major part of the Dutch river system. This analysis focuses on bedform geometry through the delta, from up- to downstream. Secondly, the presence and dimensions of superimposed secondary bedforms are determined.

Based on this analysis, field campaigns will be designed at two contrasting locations in the Dutch Rhine-Meuse delta. Those field campaigns will also be used to test developed acoustical methods.

## 4 CONCLUDING REMARKS

By answering the defined research questions, we aim to improve transport measurements through acoustics, already used for regular discharge and bathymetry measurements. Secondly, through investigating the relation between bedforms—dune geometry and superimposed secondary bedforms—and sediment transport, numerical modelling will be improved.

## 5 REFERENCES

- Becker, A. (2015) Sediment in (be)weging. deel 2 (periode 2000-2012). Deltares report 1208925-000  
Engelund, F., & Hansen, E. (1967). A monograph on sediment transport in alluvial streams. Technical University of Denmark Østervoldsgade 10, Copenhagen K.  
Gaeuman, D., & Jacobson, R. B. (2006). Acoustic bed velocity and bed load dynamics in a large sand bed river. *Journal of Geophysical Research: Earth Surface*, 111(F2).  
Hurther, D., Thorne, P.D., Bricault, M., Lemmin, U., Barnaud, J. (2011). A multi-frequency Acoustic Concentration and Velocity Profiler (AVCP) for boundary layer measurements of fine-scale flow and sediment transport processes. *Coastal Engineering* 58, 594-605. doi:10.1016/j.coastaleng.2011.01.006  
Latosinski, F. G., Szupiany, R. N., Guerrero, M., Amsler, M. L., & Vionnet, C. (2017). The ADCP's

- bottom track capability for bedload prediction: Evidence on method reliability from sandy river applications. *Flow Measurement and Instrumentation*, 54, 124-135.
- Ma, H., Nittrouer, J.A., Naito, K., Fu, X., Zhang, Y., Moodie, A.J., Wang, Y., Wu, B., Parker, G. (2017). The exceptional sediment load of fine-grained dispersal systems: Example of the Yellow River, China. *Science Advances* 3(5). doi: 10.1126/sciadv.1603114
- Meyer-Peter, E., & Müller, R. (1948). Formulas for bed-load transport. In IAHSR 2nd meeting, Stockholm, appendix 2. IAHR.
- Rennie, C. D., & Millar, R. G. (2004). Measurement of the spatial distribution of fluvial bedload transport velocity in both sand and gravel. *Earth Surface Processes and Landforms: The Journal of the British Geomorphological Research Group*, 29(10), 1173-1193.
- Schindler, R. J., Parsons, D. R., Ye, L., Hope, J. A., Baas, J. H., Peakall, J., ... & Paterson, D. M. (2015). Sticky stuff: Redefining bedform prediction in modern and ancient environments. *Geology*, 43(5), 399-402. doi: 10.1130/G36262.1
- Van Rijn, L. C. (1993). Principles of sediment transport in rivers, estuaries and coastal seas (Vol. 1006). Amsterdam: Aqua publications.

# Supply-Limited Fluvial Dunes

Gaetano Porcile, *University of Genoa, Genoa, Italy* – *gaetano.porcile@edu.unige.it*

Marco Colombini, *University of Genoa, Genoa, Italy* – *col@dicca.unige.it*

Paolo Blondeaux, *University of Genoa, Genoa, Italy* – *blx@dicca.unige.it*

**ABSTRACT:** Among the parameters affecting the morphology of fluvial dunes is the volume of mobile sediment. Fluvial dunes have an important practical relevance since they give a substantial contribution to flow resistance by inducing a hydraulic roughness which depends on their shape and dimensions. Although supply-limited dunes present similarities with typical fluvial dunes, the scaling of their wavelength and their three-dimensional evolution differs from that of alluvial dunes observed where the volume of mobile sediment is not limited. The present investigation is intended to be a contribution to the theory of sand dune stability which comprises the effect of supply limitation on the formation of fluvial dunes.

## 1 INTRODUCTION

The motion of natural fluids interacts with the erodible surface of the Earth by sediment transport. When the bottom shear stress exceeds its threshold value for sediment entrainment, sediment particles begin to move. In response to this movement, sedimentary patterns might appear. Among the various morphological patterns, the present study focus on transverse fluvial dunes, the crests of which are usually perpendicular with the main direction of the river stream. Formation and migration of fluvial dunes are very important because they give a substantial contribution to flow resistance, they affect the sediment transport and they have significant interactions with human activities. Fluvial dunes are a primary source of roughness and therefore a major factor in determining river stages. Moreover, their practical interest arises also in connection with fluvial structures the safety of which could be endangered by their dynamics. The appearance of sand dunes and their characteristics have been dealt with in great details by various researchers over the years. Investigations on the morphology and dynamics of fluvial dunes include both

theoretical and physical modelling. The knowledge of dune dynamics is in constant progress thanks to the development of new techniques for laboratory and field observations and the improvement of its theoretical modelling. Field surveys clearly show that these patterns are repetitive both in time and space, so that typical wavelengths, amplitudes and migration speeds can be assigned to them. Although no theoretical models have yet been able to reproduce all the characteristics of sand dunes correctly, idealised models exist which are capable of predicting their spacing. By describing their appearance as a free instability of cohesion-less river beds forced by steady currents, these models, based on a linear stability analysis, predict dune wavelengths in fair agreement with both laboratory and field observations. One of the main limitation of stability-based models is the assumption of full mobility conditions, i.e. unlimited sediment supply. Under supply-limited conditions, i.e., limited sediment supply, they are not valid. How fluvial dunes react to a limitation in the sediment supply is the main research question this study tries to address. The investigation described below consists of a first part in which a physical modelling of the formation of fluvial

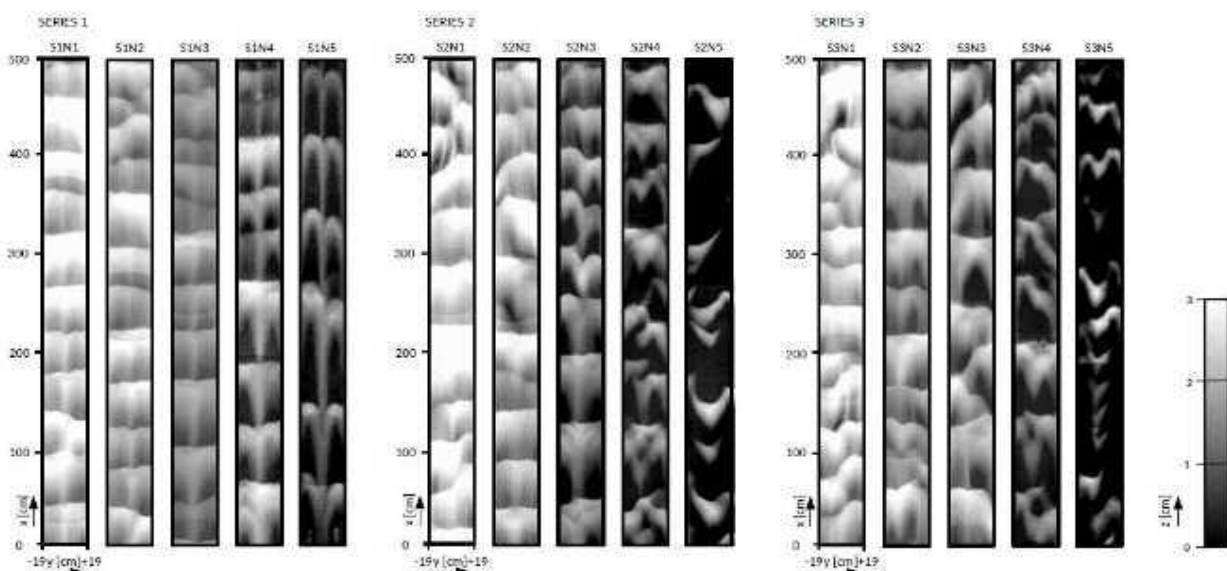
dunes is presented. Then in a second part a numerical modelling is described that is intended to be a contribution to the theory of sand dune stability which accounts for sediment supply limitation.

## 2 PHYSICAL MODELLING

In many fluvial environments supply-limited sediment transport is common. When a sediment mixture is subject to a discharge wave or a period of low flow, the bed-level undergoes a transient degradation until it is fully armoured leading to the natural formation of a motionless substratum over which sandy patterns grow and migrate. In sand-gravel mixtures, such transport conditions are common and supply limited dunes have been observed both by field surveys (Carling et al., 2000) and by flume experiments (Tuijnder et al., 2009). While the field surveys by Carling et al. (2000) seem to indicate that a decrease in the sediment availability causes an increase in dune length as well as in the irregularity of their morphology, the experimental data by Tuijnder et al. (2009) show an opposite trend.

In order to provide data on a topic in which measurements are limited and to use this data to shed light on the apparent contradiction found in the literature, a set of laboratory experiments are presented which investigate the

relation between dune morphology and sediment availability. An open-channel free-surface flow forcing an erodible hydraulically rough sandy bottom is described for a flow regime in which a continuous intermittent sediment transport occurs. The experiment is conducted in a slope varying laboratory flume. The entire flume is mounted on a beam, the slope of which can be easily adjusted. Cohesion-less sand is used as artificial roughness. At the beginning of each experiment the same sediment is uniformly spread on the flume bottom to generate an initial layer of sediment with a constant thickness. Three series of experiments are realised by fixing hydrodynamic and morphodynamic parameters and in particular the duration of the experiments but varying the thickness of the initial layer of mobile sediment and therefore the sediment supply. Each run is stopped after half an hour from the beginning of the experiment allowing sand dunes to develop over the entire length of the channel. Their geometry varied significantly depending on the initial volume of mobile sediment. In the first experiment of each series, the volume of mobile sediment is enough to allow the formation of sand dunes under alluvial conditions. Progressively decreasing the initial sand layer thickness, the formation of supply-



elevation is shown in shades of grey, lighter colours corresponding to higher values. Rigid bottom level is black. Flow is from bottom to top.

limited dunes is observed. The physical modelling of the formation of supply-limited dunes indicates that the presence of a motionless substratum strongly affects the morphology of the dunes, the average wavelength of which increases with a decreasing sediment supply.

### 3 NUMERICAL MODELLING

The linear stability analysis by Colombini (2004) has been extended to take into account the effect of supply limitation on the formation of fluvial dunes. A steady turbulent free-surface water flow through a wide straight channel is studied in two-dimensional Cartesian coordinate system with the horizontal axis along the channel axis and the vertical axis over the depth pointing upwards with the origin at the bottom. The presence of two-dimensional dunes with crests orthogonal to the direction of the flow is considered. Assuming that the dune amplitude is much smaller than the local water depth, the flow field can be evaluated by means of a perturbation approach. Such assumption seems reasonable since supply limitation should keep bottom forms low. Regarding the bottom geometry as periodic, the sandy bed can be expressed as superposition of different spatial components, the number of which should be large enough to describe the discontinuity of the supply limited bottom profile. Analogously to the above described physical modelling, the dune profile is thought to be the result of the instability of a thin layer of sand of given thickness which at first is homogeneously lying on a motionless substratum. The hydrodynamic problem can be split into the evaluation of a basic flow field, which describes the steady flow over a flat bottom, and a set of linearly independent differential problems, which describe the perturbation of the flow field owing to the presence of sand dunes. Since fluvial streams are characterized by high values of the Reynolds number, the determination of the flow field requires the introduction of a turbulence model. The two-dimensional Reynolds-Averaged-Navier-Stokes equations are numerically integrated to evaluate the basic flow field, under the shallow water approximation, and the perturbed flow field, which is solved fully two-dimensional. At the free surface, the dynamic

boundary condition forces the vanishing of the shear stresses and the kinematic boundary condition is considered as well. Close to the bottom, the velocity vanishes at a distance from the seabed related to the bed roughness. The hydrodynamic problem is closed by introducing a self-similar solution for the kinematic eddy viscosity, and, finally, Reynolds stresses are quantified by the Boussinesq relationship. Directly from the knowledge of the perturbed flow field, information on the net sediment transport can be obtained by the evaluation of the bed shear stress and relative Shields parameter introducing sediment transport predictor formulae. Suspended sediment transport is neglected at this first stage of the modelling. Only bed-load sediment transport is considered, including a correction in the threshold value for sediment motion, in order to account for the role of gravity, which opposes uphill motion and favour downhill motion. The Shields stress is evaluated at the interface between the flowing fluid and the very thin saltation layer, where grains are involved in transport processes. The sediment discharge is computed by the classical Mayer-Peter & Müller formula. The time-development of the sandy bottom can be estimated introducing the sediment continuity equation (Exner equation), which is the heart of the morphodynamic model. Linearising all the morphodynamic formulae and coupling them with the linear hydrodynamics previously described, it is possible to perform a linear stability analysis. Such a linear stability analysis entails few main steps. Small amplitude bottom perturbations and related sediment transport rates are expressed as exponential functions in time and space and investigated one separately from the other. Directly from the linearised sediment continuity equation a dispersion relationship is deduced. The morphodynamic time dependent amplitude of the bottom perturbation turns out to be exponential, and, in turn, its complex argument is able to describe the growth (decay) of the amplitude, with its imaginary part, and the migration of the crest, with its real part. Finally, assuming the most unstable mode to prevail on the other, the main features of the sand dune which is more likely to occur can be predicted depending on the values of the flow and sediment parameters.

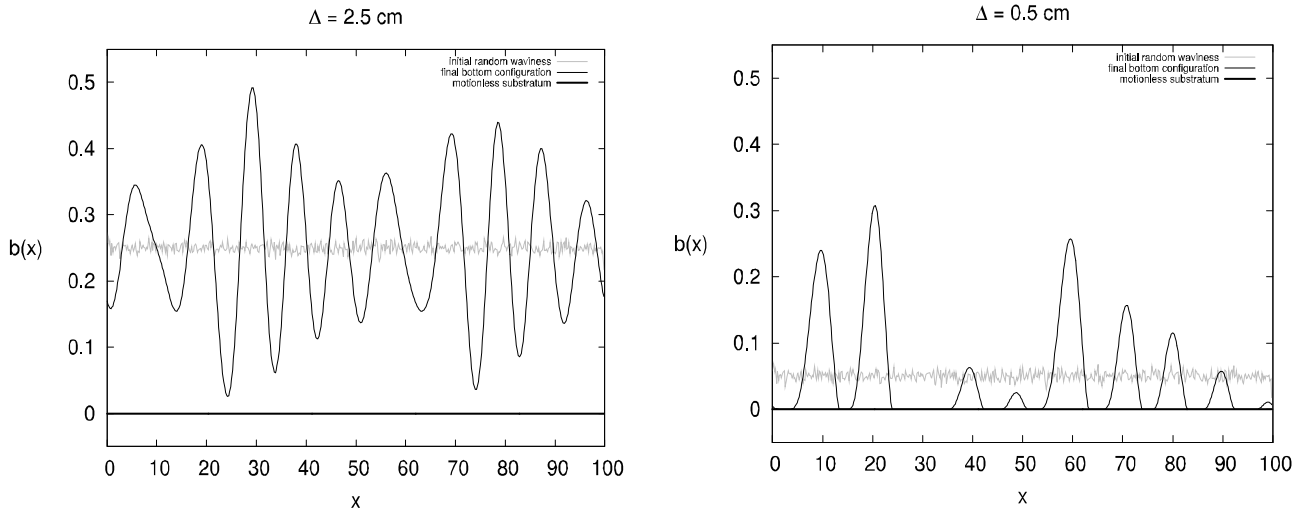


*Illustration 2: Time development of an initial random bottom waviness for a conductance coefficient  $C = 15$ , a Froude number  $F_r = 0.5$  and an angle of repose of the sand  $\Psi = 50^\circ$ . The bottom profile is plotted in the horizontal direction at the beginning (grey lines) and at the end of each numerical simulation (black thin lines). The motionless substratum is represented by the thick black lines.*

The numerical approach described by Blondeaux et al. (2016) is adopted to take into account the effect of supply limitation on the sediment transport. When local entrainment of sediment is prevented by the presence of a motionless substratum, and, therefore, the amount of sediment in motion is smaller than the local transport capacity, the sediment flux is evaluated by numerical means. Where locally no sand is available, the sediment transport depends on the bed shear stress and its spatial derivative. If the shear decreases in the direction of the main flow, the sediment transport rate is provided by the sediment transport predictor formulas and some deposition occurs accordingly with the sediment continuity equation. Conversely, if the shear stress increases in the flow direction, the sediment transport rate cannot increase because locally no further sediment is available, and, therefore, its local value should be equal to the upstream value.

Numerical simulations of the bottom time-development starting from an initial random small-amplitude perturbation are presented. The length of the computational domain, the initial thickness of the sand layer and the simulation time-window are free parameters. The bottom time-development is computed for a simulation time-window of the same order of the duration of the laboratory experiments.

Flow and sediment parameters has been chosen so that they fall in the range of values typical of the above described flume experiments. The main outcome of the model is the lengthening of the supply-limited dunes owing to the decrease of the volume of mobile sediment. This finding is qualitatively and quantitatively in fair agreement with the experimental measurements.

#### 4 REFERENCES

- Blondeaux, P., Vittori, G. and Mazzuoli, M. (2016) Pattern formation in a thin layer of sediment. *Marine Geology*, Vol. 376, 39-50.
- Carling, P. A., Williams, J. J., Golz, E. and Kelsey, A. D. (2000). The morphodynamics of fluvial sand dunes in the River Rhine, near Mainz Germany. Hydrodynamics and sediment transport. *Sedimentology*, Vol. 47, 253-278.
- Colombini, M. (2004) Revisiting the linear theory of sand dune formation. *J. Fluid Mech.*, Vol. 502, 1-16.
- Tuijnder, A. P., Ribberink, J. S. and Hulscher, S.J.M.H. (2009). An experimental study into the geometry of supply-limited dunes. *Sedimentology*, Vol. 56, 1713-1727.

# On the crest of sandwave modelling. Achievements from the past, directions for the future

Pieter C. Roos *University of Twente, Enschede, The Netherlands – p.c.roos@utwente.nl*

**ABSTRACT:** Tidal sandwaves form a prominent bed pattern in shallow sandy shelf seas. Here the class of idealised process-based models, aimed at obtaining generic insight in sandwave dynamics, is reviewed. Since many model studies focus on the instability underlying sandwave formation, first an outline of linear stability analysis is given. Then, an overview of model results is presented, highlighting two ongoing research projects (SMARTSEA and SANDBOX) and followed by suggestions for future research.

## 1 INTRODUCTION

Tidal sandwaves are large-scale bed features observed in many shallow shelf seas, such as the North Sea (Fig. 1) and many other locations. Examples include Messina Strait in the Mediterranean, San Francisco Bay, Bahía Blanca Estuary in Argentina, Sepetiba Bay in Brazil, the Yellow Sea, Taiwan Strait and Bisanseto Sea in Asia, and Bass Strait near Australia. Sandwaves occur in more or less regular patterns, with wavelengths of 100-1000 m, heights of several metres, and migration rates up to ten metres

per year (Terwindt, 1971). They are commonly found to co-exist with other bed forms, both larger (tidal sandbanks) and smaller (megaripples).

Due to their combination of location, dimensions and dynamics, tidal sandwaves may interfere with offshore activities and structures, such as navigation, pipelines and (cabling for) wind farms. The sustainable design and maintenance of these activities and structures requires insight in sandwave dynamics. For example, efficient dredging strategies in nautical channels should be based on knowledge of sandwave migration

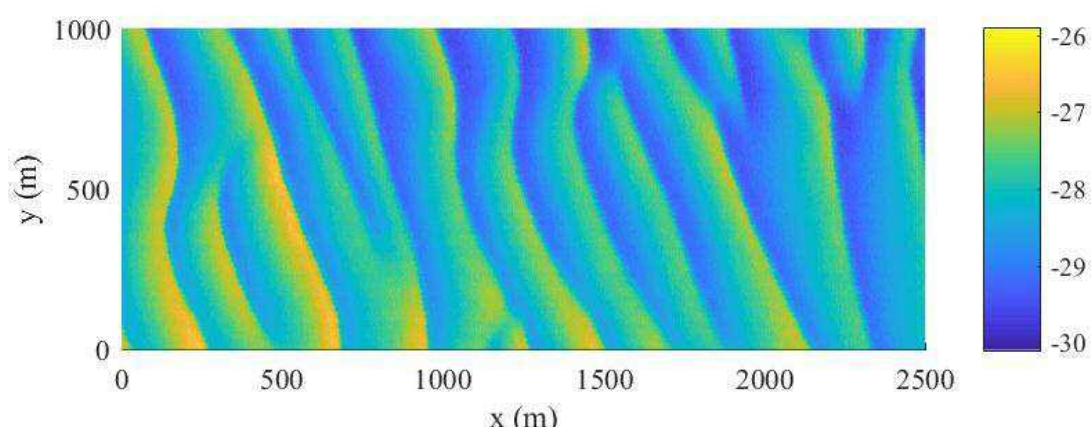


Figure 1. Example of a sandwave field from the Netherlands Continental Shelf (North Sea), showing crests in yellow, troughs in blue and depth below MSL (bathymetric data from Rijkswaterstaat, The Netherlands).

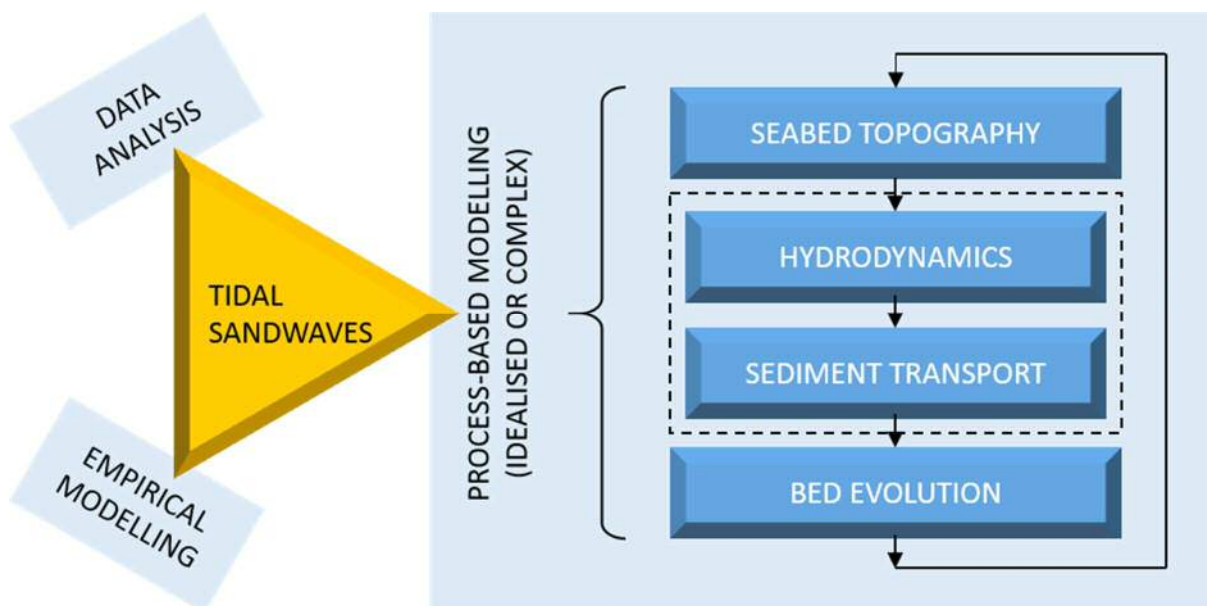


Figure 2. Overview of research approaches in the study of tidal sandwaves, distinguishing data analysis, process-based modelling and empirical modelling (left). Topic of this key note is *process-based modelling*, which – either idealised or complex – follows the classical morphodynamic loop (right).

and regeneration processes. The growing awareness of interaction with benthic activity, and the nature value associated with it, adds to the complexity of sandwave-related problems (Borsje et al., 2009).

Research methods to study tidal sandwave dynamics include (i) analysis of measured data, (ii) process-based modelling and (iii) empirical modelling (Fig. 2). Ideally, they are applied in a strongly integrated way: correlations revealed by data analysis form the inspiration for process-based model studies, which – in turn – are validated against observations. Alternatively, analysis of observations and these model results may give rise to simplified empirical models that can be used in practise. Also, it should be noted that process-based models usually contain various empirical elements such as the parameterisations of bottom friction, turbulence closure and sediment transport. Despite these apparent links, it is meaningful to zoom in on one of the research approaches: here the class of *process-based models*.

Building on the so-called morphodynamic loop (Fig. 2), process-based sandwave models rely on partial differential equations expressing the governing laws of wa-

ter/sediment motion, supplemented with appropriate boundary conditions. As noted above, this may include empirical laws. Within the class of process-based modelling, one typically distinguishes two types (e.g., Murray, 2003): (i) *idealised* or exploratory models, (ii) *complex* simulation models.

Herein, idealised models are essentially aimed at gaining generic insight in a specific physical mechanism. They involve strong schematisations of physical processes and geometry, aimed at enabling efficient solution techniques (e.g., analytical in the horizontal direction), which in turn enables extensive sensitivity analyses. The vast majority of sandwave model studies belongs to this class and is based on stability methods. Alternatively, complex simulation models are generally aimed at solving site-specific engineering problems, with detailed geometries and using state-of-the-art process formulations. Although useful, the above classification is also blurred by idealised model development becoming more and more complex, and complex simulation models also being applied in highly idealised settings.

This keynote contains an outline of linear stability analysis (§2), an overview of sand-

wave modelling results (§3), and suggestions for future research (§4).

## 2 LINEAR STABILITY ANALYSIS

Sandwave formation can be explained as an inherent instability of a sandy seabed subject to tidal motion (3D model study by Hulscher, 1996). The method to investigate this is known as *linear stability analysis* (e.g., Dodd et al., 2003), which can be summarised in five steps:

1. Model formulation, describing the time evolution  $\partial\phi/\partial t$  of the system's state  $\phi$ , which is a vector quantity containing all flow, sediment and topography variables. Herein, scaling arguments may motivate the use of certain approximations such as ‘rigid lid’, spatially uniform forcing, and the quasi-stationary approach separating the time scales of hydrodynamics and bed evolution.
2. Identification of a so-called *basic state*  $\phi_0$ , describing the tide-driven water and sediment motion over a horizontally flat bed in an offshore environment far away from coastal boundaries. This flat seabed remains flat as the divergence of sediment transport vanishes.
3. Perturbation of the basic state:

$$\phi = \phi_0 + \epsilon\phi_1, \quad (1)$$

with *perturbed state*  $\phi_1$  and expansion parameter  $\epsilon$ , assumed small. Higher order terms in  $\epsilon$  are neglected.

4. Solution of the (linear) *eigenvalue problem* posed by the morphodynamic evolution of  $\phi_1$ . Eigensolutions turn out to be sinusoidal in space, characterised by topographic wave numbers  $k_x$  and  $k_y$ . In time, they display exponential growth or decay as well as migration at a constant rate. The growth and migration rates of these ‘modes’ depend on the topographic wave numbers and model parameters.
5. Interpretation of the growth rates. If modes with positive growth rates exist, the basic state is *unstable*. The ‘fastest

growing mode’, i.e. the one with the largest growth rate, is likely to emerge from a flat bed. Alternatively, if all modes have negative growth rates, the basic state is *stable*.

The spatiotemporal structure of the eigenfunctions provides insight in the initial tendencies and in the underlying physical mechanisms. For example, tide-averaged flow patterns show vertical circulation cells with near-bed flow directed from trough to crest. Importantly, the validity of linear analysis is restricted to small amplitude dynamics. The properties of the fastest growing mode have been successfully compared with observations from, e.g., the North Sea.

## 3 ACHIEVEMENTS IN PAST AND PRESENT

The linear stability model by Hulscher (1996) has been extended in many respects: solution method, hydrodynamics (symmetric vs asymmetric forcing, turbulence model, wind waves), sediment transport (bed load vs suspended load, grain size sorting), influence of benthic activity. Also, the results from a linear analysis have been applied to describe the evolution of a sandpit. Finally, they have inspired finite amplitude studies of tidal sandwaves involving nonlinear dynamics. For an overview of related studies before 2008, see the review paper by Besio et al. (2008). Among the more recent studies, I mention the systematic comparison of linear model results with sandwave data (Van Santen et al., 2011), the inclusion of a non-erodible rock layer underneath the mobile sediment (Porcile et al., 2017), and the recent complex simulation study using Delft3D (Van Gerwen et al., 2018).

Here I further highlight two research projects: SMARTSEA and SANDBOX (§5). The former develops knowledge of seabed dynamics in support of safe navigation, the latter investigates seabed dynamics in relation to offshore dredging operations. Both projects combine process-based modelling

and measurements, and involve a variety of users from practise.

In the process-based modelling part of the SMARTSEA-project, the influence of storm processes on sandwave dynamics has been studied. Observations have shown that sandwave height decreases and their migration rate increases during periods of stormy weather compared to calm conditions. In the linear regime, wind waves are found to decrease growth rates and enhance migration, whereas wind-driven currents particularly affect sandwave migration (Campmans et al., 2017). Forcing this linear model with typical wave and wind conditions from the North Sea, using a statistical weighting averaging method shows that storms mainly affect sandwave migration (Campmans et al., 2018a). In the nonlinear regime, wind waves tend to reduce the equilibrium height. Furthermore, simulations with an intermittent occurrence of storms and fair-weather conditions display a dynamic equilibrium, in which sandwaves intermittently grow/decay toward (but have insufficient time to reach) the equilibrium states corresponding to fair-weather and stormy conditions, respectively (Campmans et al., 2018b). Two other sub-projects in SMARTSEA deal with data analysis of sandwave characteristics on the Netherlands Continental Shelf in relation to dredging operations (Damen et al., 2018) and the translation of seabed dynamics into a risk chart (Toodesh & Verhagen, 2018).

In the process-based modelling part of the SANDBOX-project, the linear stability analysis was extended by incorporating two-way interaction between benthos and sandwave topography: flow intensity affects benthic activity, whereas benthic biomass affects bottom roughness and thus the flow. In addition to the hydro- and morphodynamic time scales, this involves a new time scale of biological evolution. It was shown that a benthic perturbation only (i.e., without any topographic perturbation) or a topographic perturbation only (i.e., without any benthic perturbation) may both trigger the joint growth of topographic and benthic patterns (Damveld et al., submitted). Related to this,

video analysis has revealed spatial variations of benthos over sandwave profiles (Damveld et al., 2018).

#### 4 DIRECTIONS FOR THE FUTURE

Among a variety of possible suggestions for future research on sandwave modelling, I propose the following topics.

Firstly, the two-way coupling between co-existing sandbanks and sandwaves deserves further study. On the one hand, sandbanks determine the ‘background’ conditions (flow and sediment characteristics, water depth, Van Veen et al., 2018) in which sandwaves develop. On the other hand, migrating sandwaves constitute part of the sediment circulation over sandbanks. The autonomous dynamics of this coupled system is of interest, and so is its relation to interventions such as sand extraction (e.g., for the Belgian Continental Shelf).

Secondly, a not yet understood technical aspect deals with linear and nonlinear model behaviour on large model domains, e.g., the system’s tendency to gradually develop high bed forms with a wavelength equal to the domain size. This is sometimes termed the ‘ $k = 0$ -problem’, referring to the related fact that positive growth rates occur for topographic wave numbers close to zero. It should be noted that on these length scales some of the model assumptions are no longer valid, such as the spatial uniformity of the tidal wave that forces the system.

Thirdly, the immense complexity and computational effort has so far prevented long-term and large-scale studies of nonlinear dynamics of sandwave fields, i.e. with spatial variations in two horizontal directions. This is partly due to the need to resolve the vertical flow structure in sufficient detail. To overcome this limitation, one may seek adequate parameterizations of certain aspects of sandwave dynamics. In turn, this may lead to a new type of ‘hybrid’ process-based/empirical model of tidal sandwave dynamics that can also be applied to engineering applications.

Fourthly, the topic of estuarine sand waves deserves to be explored from a process-based perspective, to unravel the complexities associated with forcing (flow with strong tidal and residual components) and sediment dynamics (mixtures of sand and mud).

Finally, turning back to the three research approaches and specifically to the two process-based model types introduced in §1, it remains a challenge to integrate the idealised and complex simulation models in relation to the increasing amount of data available from the field.

## 5 ACKNOWLEDGEMENTS

This work is part of the research programme SMARTSEA with project number 13275, which is (partly) financed by the Netherlands Organisation for Scientific Research (NWO). It further fits in the SANDBOX research programme, funded by NOW, Royal Boskalis Westminster NV and Royal Netherlands Institute for Sea Research (NIOZ).

In the framework of these projects (see §3), I am grateful to Geert Campmans, Johan Damveld, John Damen, Suzanne Hulscher and Bas Borsje (University of Twente), Thaiënne van Dijk (Deltares) as well as Reenu Toodesh, Ramon Hanssen and Sandra Verhagen (Delft University of Technology).

## 6 REFERENCES

- Besio, G., P. Blondeaux, M. Brocchini, S.J.M.H. Hulscher, D. Idier, M.A.F. Knaapen, A.A. Németh, P.C. Roos & G. Vittori (2008). The morpho-dynamics of tidal sand waves: A model overview, *Coast. Eng.* **55** (7-8), 657–670.
- Borsje, B.W., M.B. de Vries, T.J. Bouma, G. Besio, G., S.J.M.H. Hulscher & P.M.J. Herman (2009). Modelling bio-geomorphological influences for offshore sand waves. *Cont. Shelf Res.* **29** (9), 1289–1301.
- Campmans, G.H.P., P.C. Roos, H.J. de Vriend & S.J.M.H. Hulscher (2017). Modeling the influence of storms on sand wave formation: A linear stability approach, *Cont. Shelf Res.* **137**, 103–116.
- Campmans, G.H.P., P.C. Roos, E.P.W.J. Schrijen & S.J.M.H. Hulscher (2018a). Modelling wave and wind climate effects on tidal sand wave dynamics: a North Sea case study, *Est. Coast. Shelf Sci.* **213**, 137–147.
- Campmans, G.H.P., P.C. Roos, H.J. de Vriend & S.J.M.H. Hulscher (2018b). The influence of storms on sand wave evolution: a nonlinear idealized modeling approach, *J. Geophys. Res.* **123** (9), 2070–2086.
- Damen, J. M., T. A. G. P. van Dijk & S.J.M.H. Hulscher (2018). Spatially varying environmental properties controlling observed sand wave morphology, *J. Geophys. Res.* **123**, 262–280.
- Damveld, J.H., K.J. van der Reijden, C. Cheng, L. Koop, L.R. Haaksma, C.A.J. Walsh, K. Soetaert, B.W. Borsje, L.L. Govers, P.C. Roos, H. Olff, S.J.M.H. Hulscher (2018). Video transects reveal that tidal sand waves affect the spatial distribution of benthic organisms and sand ripples, *Geophys. Res. Lett.* **45**.
- Damveld, J. H., P.C. Roos, B.W. Borsje & S.J.M.H. Hulscher. Modelling the two-way coupling of tidal sand waves and benthic organisms. A linear stability approach, *submitted*.
- Dodd, N., P. Blondeaux, D. Calvete, H.E. de Swart, A. Falquès, S.J.M.H. Hulscher, G. Rozynski & G. Vittori (2003). Understanding coastal morphodynamics using stability methods. *J. Coast. Res.* **19** (4), 849–866.
- Hulscher, S.J.M.H. (1996). Tidal-induced large-scale regular bed form patterns in a three-dimensional shallow water model. *J. Geophys. Res.* **101** (C9), 20727–20744.
- Murray, A.B. (2003). Contrasting the goals, strategies, and predictions associated with simplified numerical models and detailed simulations, in Prediction in Geomorphology, edited by R.M. Iverson and P.R. Wilcock, pp. 151–165, Vol. 135 of Geophysical Monograph, AGU, Washington, D.C.
- Porcile, G., P. Blondeaux & G. Vittori (2017). On the formation of periodic sandy mounds, *Cont. Shelf Res.* **145**, 68–79.
- Terwindt, J.H.J. (1971). Sand waves in the Southern Bight of the North Sea. *Mar. Geol.* **10**, 51–67.
- Toodesh, R. & A.A. Verhagen (2018). Adaptive, variable resolution grids for bathymetric applications using a quadtree approach, *J. Appl. Geodesy* **12**(4), 311–322.
- Van Gerwen, W., B.W. Borsje, J.H. Damveld & S.J.M.H. Hulscher (2018). Modelling the effect of suspended load transport and tidal asymmetry on the equilibrium tidal sand wave height. *Coast. Eng.* **136**, 56–64.
- Van Santen, R.B., H.E. de Swart & T.A.G.P. van Dijk (2011). Sensitivity of tidal sand wavelength to environmental parameters: A combined data analysis and modelling approach, *Cont. Shelf Res.* **31** (9), 966–978.
- Van Veen, T.J., P.C. Roos & S.J.M.H. Hulscher (2018). Process-based modelling of bank-breaking mechanisms of tidal sandbanks, *Cont. Shelf Res.* **167**, 139–152.



# Spatial lag effects for dunes migrating over forced bars

Timo V. de Ruijsscher *Wageningen University, Wageningen, Netherlands* – *timo.deruijsscher@wur.nl*

Suleyman Naqshband *Wageningen University, Wageningen, Netherlands* –

*suleyman.naqshband@wur.nl*

A.J.F. (Ton) Hoitink *Wageningen University, Wageningen, Netherlands* – *ton.hoitink@wur.nl*

**ABSTRACT:** A fortnightly morphological dataset was used to analyse the relation between dune characteristics and forced bars in the river bend. Using a cross-correlation technique, it is shown that for a slight negative lag, dune height is negatively correlated with the bed level of the bar profile. This indicates that dunes reach their minimum height just downstream of a bar top, when migrating over a forced bar.

## 1 INTRODUCTION

In fluvial morphodynamics, bed forms have been a popular research topic for years. However, there appears to be a clear separation between studies dealing with bed forms on different spatial scales, being focussed on in different communities. The dune community focusses on e.g. the relation between dune dimensions and flow characteristics (Shields, 1936) three-dimensionality of dunes (Venditti et al., 2005) and the transition to upper stage plane bed (Naqshband et al., 2016). On the other side of the spectrum, the bar community focusses on e.g. the (slower) evolution of alternate bars (Lanzoni, 2000), the regime change from meandering to braiding (Crosato and Mosselman, 2009) and the relation between bars and sediment supply (Nelson et al., 2015).

Interestingly, both communities operate largely independently, filtering out bed forms of other spatial scales as a first step. In the dune community, the study of superimposed bed forms (dunes and ripples) is a topic of interest (Best, 2005), yet the interac-

tion with larger scale features is relatively unexplored. Dunes and alternate bars often coexist and will therefore most probably have an influence on each other's evolution. In the present study, the authors aim to quantify the effect of bars on both dune height and dune length using an extensive dataset of multi-beam echo-sounding measurements on a large domain both in space and in time.

## 2 METHODS

### Data and measurement location

For the present study, an extensive bed level dataset from the Waal River is used. The Waal River is the main Rhine branch in the Netherlands. This dataset consists of fortnightly multi-beam echo-sounding (MBES) measurements of the fairway of the Waal River, covering a width of 170 m. A total length of 80 km is available, over a period from March 2011 onwards. The data is gridded on a 1 m x 1 m grid, with at least 95% of the cells containing ten or more data points.

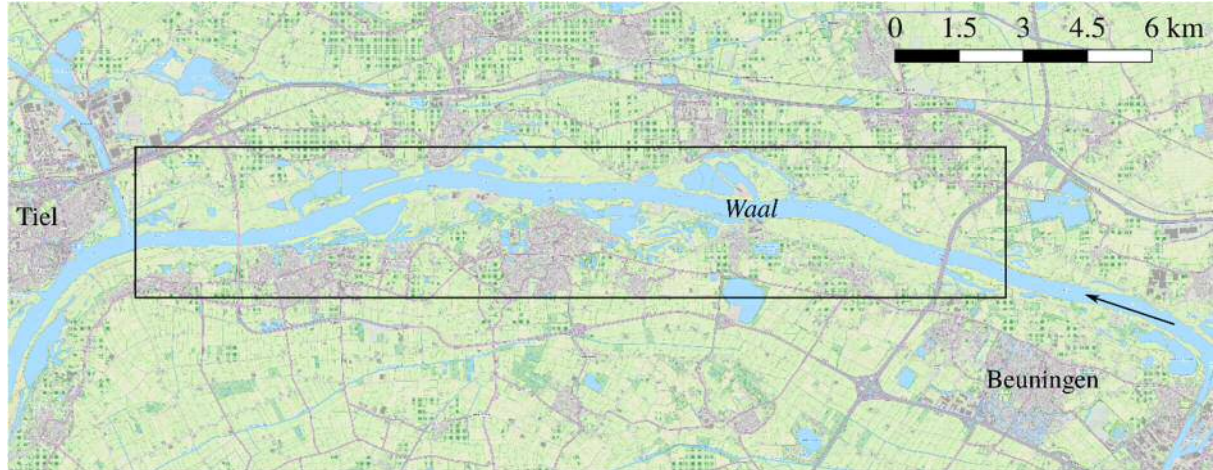


Figure 1. The part of the Waal River under study, with the arrow indicating the flow direction.

Only part of the total river length is taken into account, to make sure that factors like for instance changes in grain size distribution along the river and varying bar wavelengths do not have a large influence on the quality of the results. Moreover, for the time being only the first year of the dataset has been studied. The region of the river under study is shown in Figure 1.

#### Data analysis

##### Bed form characteristics

For the present study, we determined dune characteristics by using the bed form tracking tool by Van der Mark & Blom (2007). After detrending the bed level profile, using a moving average filter, this tool detects individual bed forms by means of a zero-crossing method. For each dune, both height and length are determined.

##### Cross-correlation

To determine whether bars influence dune characteristics, we performed a cross-correlation analysis between dune height and the bar profile. The latter is determined as the bed level profile after removal of the dune signal. For each of the profiles, a confidence bound (at the 0.05 level) was determined. Moreover, the  $p$ -value was determined using Student's  $t$ -distribution. The same procedure was followed for dune length.

### 3 RESULTS

Figures 2 and 3 show the distribution of dune height and length in the region and period under study. Median values are a dune height of 0.94 m and a dune length of 76.8 m.

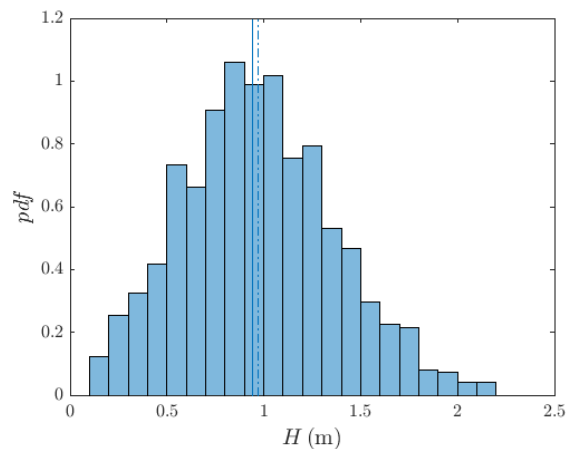


Figure 2. Probability density function of the dune height in the region under study, where values outside a band of 5 standard deviations are omitted. The solid and dash-dotted lines represent median and mean values, respectively.

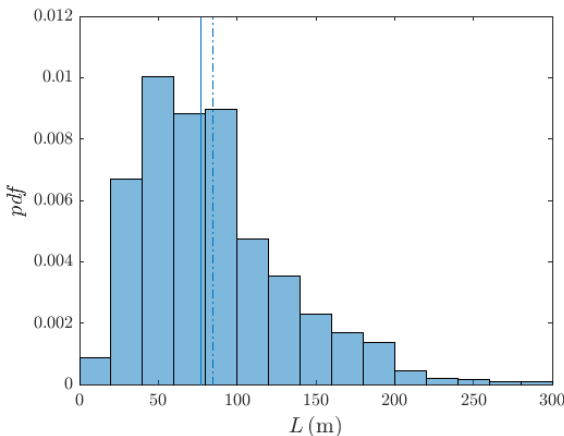


Figure 3. Probability density function of the dune length in the region under study, where values outside a band of 5 standard deviations are omitted. The solid and dash-dotted lines represent median and mean values, respectively.

The cross-correlation between the dune height and the bar profile has a negative peak for a slightly negative lag (Figure 4).

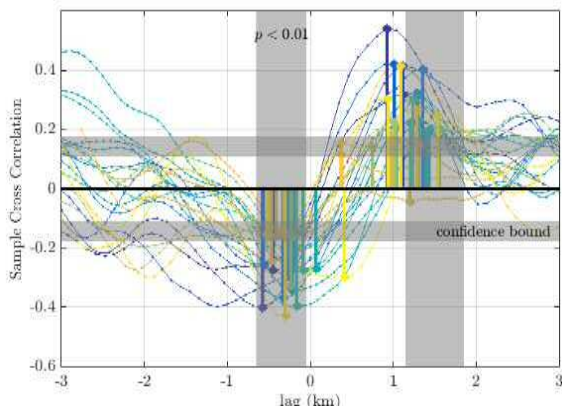


Figure 4. Cross-correlation of dune height and bar profile for one year of biweekly data 41 m right of the river axis. Values of the cross-correlation exceeding the confidence bound and within regions of  $p < 0.01$  are considered significant.

This is the case for all biweekly bed profiles under consideration. Most of the peaks of the individual profiles are above the confidence bound and fall within the band of  $p < 0.01$ , indicating that the result is significant. A negative cross-correlation at a lag less than 1 km indicates that dune height is lowest just downstream of the bar top.

For the dune length, the same analysis is carried out, although no clear relationship with the bar profile is found.

## 4 DISCUSSION

Although only one year of data is taken into account, containing one discharge peak, a relation between the dune height and the bar profile is found. The negative correlation with slightly negative lag suggests that dunes have a decreased height just downstream of the bar top. Physically, this can be explained by a reduced water depth on the bar top, reducing the dune height as dune height generally scales with water depth (Allen, 1968; Yalin, 1992). The spatial lag might be a result of the adaptation time of the dunes needed to adjust to the changing hydraulic conditions while migrating over the bar.

The fact that no clear correlation is found between dune length and the bar profile, might be due to the skewed distribution (Figure 3). For both dune height and length, an investigation with the lag expressed in units of bar length might also reduce the noise in the results. This might also allow for taking into account a larger stretch of the river, where forced bars range in wavelength from 4 km to 10 km.

## 5 CONCLUSIONS

From a cross-correlation of dune height and bar profile, it follows that dune height reaches its minimum value just downstream of the bar top. For dune length, no clear relationship is found, which deserves attention in future analysis.

## 6 ACKNOWLEDGEMENT

This research is part of the research programme RiverCare, supported by the Dutch Technology Foundation STW, which is part of the Netherlands Organization for Scientific Research (NWO), and which is partly funded by the ministry of Economic Affairs under grant number P12-14 (Perspective Programme). We thank Rijkswaterstaat for making available the morphological dataset of the Waal River and the Python script for

converting the data to profiles parallel to the river axis.

## 7 REFERENCES

- Allen, J.R.L., 1968. Current Ripples. New York, Elsevier
- Best, J., 2005. The fluid dynamics of river dunes: A review and some future research directions. *Journal of Geophysical Research* 110, F04S02
- Crosato, A., Mosselman, E., 2009. Simple physics-based predictor for the number of river bars and the transition between meandering and braiding. *Water Resources Research* 45(3), W03424
- Lanzoni, S., 2000. Experimental on bar formation in a straight flume. 1. Uniform sediment. *Water Resources Research* 36, 3337–3349
- Naqshband, S., van Duin, O., Ribberink, J., Hulscher, S., 2016. Modeling river dune development and dune transition to upper stage plane bed. *Earth Surface Processes and Landforms* 41, 323–335
- Nelson, P. A., Brew, A. K., Morgan, J. A., 2015. Morphodynamic response of a variable-width channel to changes in sediment supply. *Water Resources Research* 51, 5717–5734
- Shields, A., 1936. Anwendung der Ähnlichkeitsmechanik und der Turbulenzforschung auf die Geschiebebewegung. Preussische Versuchsanstalt für Wasserbau und Schiffbau 26, 1–26.
- Van der Mark, C.F., Blom, A., 2007. A new and widely applicable tool for determining the geometric properties of bedforms. *Civil Eng. & Man. Res. Reports* 2007R-003/WEM-002; No. 1568-4652. Enschede: Water Engineering & Management (WEM)
- Venditti, J. G., Church, M., Bennett, S. J., 2005. On the transition between 2D and 3D dunes. *Sedimentology* 52, 1343–1359
- Yalin, M.S., 1992. River Mechanics. Oxford, Pergamon Press

# Potential drivers for primary dune growth in the Outer Jade

Leon Scheiber *Ludwig-Franzius-Institute, Hannover, Germany* – *scheiberleon@gmail.com*

Oliver Lojek *Ludwig-Franzius-Institute, Hannover, Germany* – *lojek@lufi.uni-hannover.de*

Jan Visscher *Ludwig-Franzius-Institute, Hannover, Germany* – *visscher@lufi.uni-hannover.de*

Gregor Melling *Federal Waterways Engineering and Research Institute, Hamburg, Germany* – *gregor.melling@baw.de*

**ABSTRACT:** This study examines 47 navigational safety surveys of the Outer Jade. The bathymetric data is utilized for an analysis of local bedforms and a volume balancing study. The obtained cumulative volume differences from consecutive surveys are used to test for correlations with metocean influences and documented maintenance activities. For the relationship between bathymetric changes and maintenance works a statistically significant connection is found indicating a recirculation of dredge spoil as suggested in previous studies. However, additional research has to be undertaken, especially in terms of a coupled numerical simulation, to facilitate a verification of the described hypothesis.

## 1 INTRODUCTION

The Jade Bight is a tidal bay cutting deep into the marshland of northern Germany with no notable freshwater discharge and a tidal range of up to 3.69 m in Wilhelmshaven. Stretches of the Jade navigational channel, specifically along fairway kilometers (fkm) 14.8 - 23.6 and fkm 28.7 - 41.6, are characterized by compound subaqueous dunes. The aforementioned bedforms are of particular interest to the Federal Waterways and Shipping Administration (WSV), as dune crests tend to reduce the navigational depth of the fairway and thereby impede safe navigation towards the transhipment complex of Wilhelmshaven (Götschenberg & Kahlfeld 2008). The navigational depth along the Outer and Inner Jade is maintained at - 18.5 m below chart datum (CD). Dunes with crest heights reaching - 17.6 mCD jeopardize maritime traffic and are dredged by the local Waterways and Shipping Office (WSA). To enhance the understanding of the underlying morphodynamic processes, areas of increased morphological activity have been successfully identified by Kubicki &

Bartholomä (2011). In 2017, subsequent investigations revealed the existence of a dune field of some 20 km<sup>2</sup> in the Outer Jade comprising a remarkable zone of dune convergence that indicated a potential recirculation of dredging spoils dumped nearby (Kubicki et al. 2017). Numerical simulations conducted by the Federal Waterways Engineering and Research Institute (BAW) further substantiated the hypothesis of a recirculation relating to hydrodynamics and transport capacities (Melling & Kösters 2017). Based on regular navigational safety surveys, the present study tests the hypothesis of a dune convergence zone by means of an analysis of bedform asymmetries and migration directions. Moreover, potential causes for the formation and growth of the respective bedforms are investigated. To this end, all echo-sounding data, sampled within the area of interest between 2012 and 2016, is analyzed and tested for correlations between the observed morphological changes on the one hand and metocean and/or operational factors on the other.

## 2 METHODS

### 2.1 Study area

The focus area of the present study is delineated by the intersection of all analyzed echo-sounding surveys and the domain specified by the previous investigations of Kubicki et al. (2017). It is situated in the Outer Jade fairway between the islands of Oldeoog/ Minsener Oog in the west and the lighthouse of Mellumplate in the east.

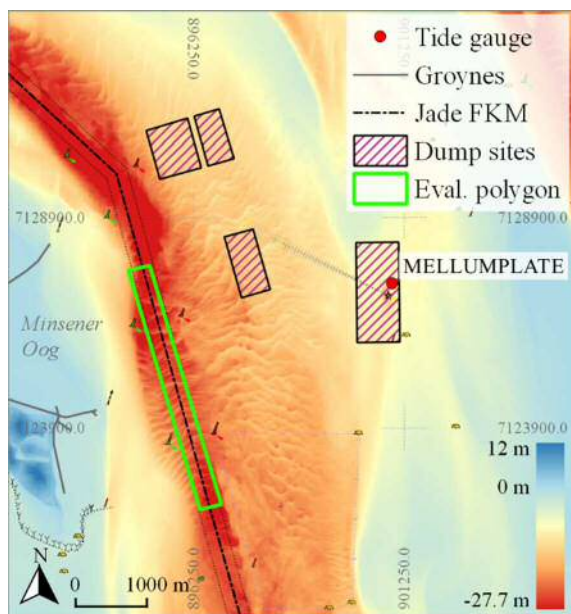


Figure 1. Location of the study area in the Jade navigational channel between the islands of Oldeoog/ Minsener Oog in the west and the lighthouse of Mellumplate in the east.

As depicted in Figure 1 the intersection polygon stretches roughly from fkm 29 to 32.5 of the Jade navigational channel and has a width of about 300 m. To allow for the analysis of longitudinal geodetic profiles, an intersection line is defined along the central axis of the fairway.

### 2.2 Data sources

At regular intervals of about one month, the Jade fairway bathymetry is monitored by the responsible German authority, namely the WSA Wilhelmshaven (Götschenberg & Kahlfeld 2008). For this purpose, the whole navigational channel is surveyed in distinct sections using a ship-mounted *Atlas Fansweep 20-200* multibeam echosounder

(Kubicki et al. 2017). For the present study, 47 echo-sounding datasets, composed of gridded coordinate-elevation pairs at a horizontal resolution of 2 x 2 m, were provided by the WSA. This data is utilized to investigate the temporal morphodynamic evolution of primary dunes forming along the bottom of the fairway.

For subsequent examinations of potential correlations, comprehensive information on the conducted maintenance works, i.e. dredging and dumping activities in the vicinity of the study area, was available from the federal maintenance monitoring database *MoNa*. The unfortunate fact, that maintenance volumes moved by private companies were not quantified, is addressed by estimating these values to be of similar magnitude as the overall mean volume.

Furthermore, metocean data was collected from various adjacent measuring stations. In detail, information on current velocities and directions was obtained from an official monitoring station located at fkm 21. Wind and wave conditions are constantly measured by the National Meteorological Service of Germany (DWD) at the lighthouse of Alte Weser and can be downloaded from a public database. Finally, tidal water level data is readily available from the measuring station at Mellumplate (fkm 31.1) about 3 km east of the study area.

### 2.3 Data processing

In the course of this study, various bathymetric analyses of the survey domain are conducted. In a first step, geodetic profiles along the intersection line are assessed, identifying distinct bedforms according to an automated approach presented by Zorndt et al. (2011). After detecting dune crests and troughs on the basis of local extrema, the bedform dimensions, specifically the heights and lengths of large to very large dunes as defined by Ashley (1990), are computed. Asymmetries, as a proxy for migration directions, are calculated from the relative upstream dune side lengths (cf. Zorndt et al. 2011) and migration rates are derived from the horizontal displacement of dune crests between the individual echo-soundings.

Thereafter, the morphological changes between consecutive echo-soundings are computed by means of a volume balancing study and the temporal course of observed volume differences inside the survey domain is used as one variable of the correlation analysis. In detail, the bathymetric changes are examined for linear and cross correlations with the cumulative maintenance volume and with data on the local metocean conditions, respectively.

### 3 RESULTS

#### 3.1 Bedform characteristics

The examination of monthly geodetic profiles shows an average number of 83 primary dunes along the 3.5 km fairway axis adding up to a total of 3885 analyzed bedforms for the four-year period between 2012 and 2016. The corresponding dune dimensions vary between 0.8 m and 7.6 m of height, and between 17.7 m and 336.7 m of length, respectively. Figure 2 illustrates the relative frequency of observed dune dimensions and reveals an average dune height of 2.5 m and an average dune length of 67.0 m inside the study area. As previously suggested by van der Mark et al. (2008), the distribution of dune dimensions can be adequately described by a Weibull function.

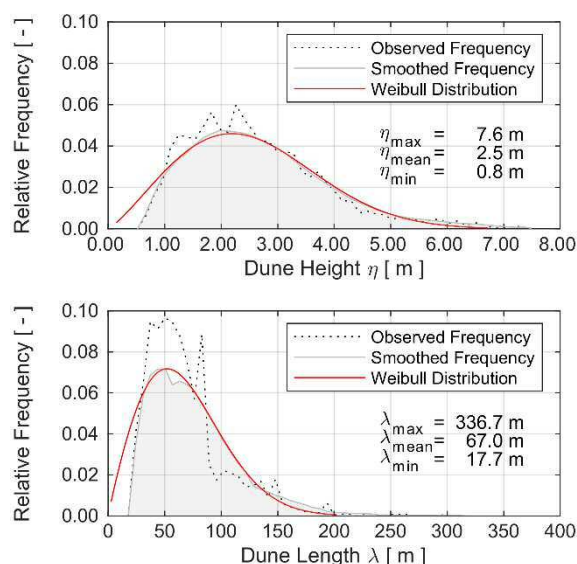


Figure 2. Observed and smoothed frequency of prevailing dune dimensions inside the fairway segment and the corresponding Weibull distribution.

Investigations of the spatial distribution of bedform characteristics, in particular of dune asymmetries and migration rates, indicate a distinct segmentation of the analyzed domain. Whereas primary dunes in the southern half of the survey area (fkm 29.0 - 30.7) mainly show northward directed migration at an average rate of  $u_{\text{mig}} = 8.7$  cm/d and a mean asymmetry of  $A = 0.576$ , dunes between fkm 31.1 and 32.5 are characterized by southward migration ( $u_{\text{mig}} = -9.1$  cm/d) and a mean asymmetry of  $A = 0.408$ . The average migration rate and asymmetry of the fairway segment between fkm 30.7 and 31.1 are of a minor order of magnitude ( $u_{\text{mig}} = -0.1$  cm/d,  $A = 0.498$ ) and, thus, support the hypothesis of a dune convergence zone in this area.

#### 3.2 Bathymetric changes

In a second step, the morphological changes between consecutive echo-sounding surveys are analyzed by assessing the gridded elevation data of the defined fairway segment cell-by-cell and comparing the respective sediment volumes. This volume balancing study results in a list of consecutive volume differences documenting both erosive periods with sediment losses, such as 53,400 m<sup>3</sup> in September 2013, and intervals of intense sediment deposition of up to 107,600 m<sup>3</sup> in March 2015. However, in general the morphological situation of the study site can be characterized as depositional with an overall sediment accretion of 883,700 m<sup>3</sup> implying a reduction of the average depth by  $\Delta h = 0.84$  m within 47 months.

#### 3.3 Investigation of causes

The temporal course of sediment volume changes is used, subsequently, to check for potential correlations with the corresponding metocean data, i.e. prevailing wind, wave and current conditions. In this context, the coefficient of determination  $R^2$  varies between 0.00 and 0.33 for the available parameters (see Table 1) and, hence, no significant correlation is evident, neither linear nor phase-shifted.

Table 1. Achieved coefficients of determination  $R^2$ 

	2012	2013	2014	2015
Max. wind speed [m/s]	0.05	0.03	n.a.	n.a.
Max. wave height [cm]	0.00	0.00	n.a.	n.a.
Max. ebb current [m/s]	0.09	0.03	n.a.	n.a.
Max. flood current [m/s]	0.06	0.33	n.a.	n.a.
Maintenance volume [ $\text{m}^3$ ]	0.09	0.76	0.67	0.62

Concerning a relationship between the observed bathymetric changes in the fairway segment and the documented maintenance activities, no evidence for a distinct phase-shifted dependency could be obtained from the cross-correlation analysis. However, investigations regarding a linear correlation indicate a significant similarity between cumulated mean elevation changes and maintenance volumes; the corresponding coefficient of determination reaches a value of  $R^2 = 0.96$  for the complete analyzed period (see Figure 3).

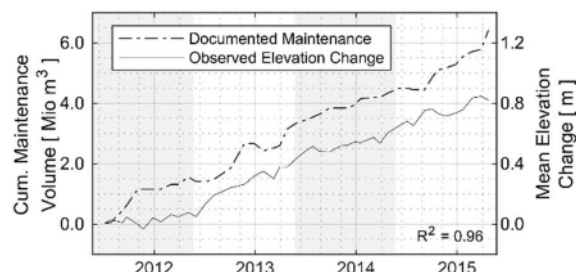


Figure 3. Temporal course of the cumulated maintenance volume and the cumulated mean elevation change inside the fairway segment, respectively; the coefficient of determination reaches  $R^2 = 0.96$  for the period between 2012 and 2016.

#### 4 DISCUSSION

After comparing the computed dune characteristics with historical data on bedform dimension ratios (Flemming 1988), the present results are considered plausible. Moreover, the observed dune dimensions meet the codomain of the bedforms reported by Kubicki et al. (2017) fairly well, likewise implying that the automated approach applied in this study renders feasible.

With respect to metocean causes for the evolution of primary dunes, no correlation could be established from the available point measurements. However, it is obvious that extreme events, such as storm surges, have an impact on the hydrodynamic processes in the Outer Jade and, thus, on the transport regime inside the survey domain as well. Preliminary results on the temporal variation of dune migration rates indicate that the horizontal movement of large bedforms may be influenced by the storm season. Further investigations will clarify, whether metocean factors may also influence the net sediment transport in this area, e.g. in combination with longshore transport.

With regard to the positive correlation between cumulated maintenance volumes and morphological changes, the present results suggest a causal connection, namely the hypothesized recirculation of dredge spoil from the dump sites close to the fairway segment. However, the purely mathematical correlation between the two time-series is not tantamount to a causal nexus. And although previous numerical model simulations indicate a zone of recirculation relating to hydrodynamics and transport capacities (Melling & Kösters 2017), the behavior of the dumped sediment volumes should be further investigated by simulations respecting the specific dynamics of dredge dispersion at the adjacent spoil grounds. As prior studies concluded before (e.g. Kubicki et al. 2017), a high-resolution model coupling hydrodynamic and sediment transport processes seems essential for the understanding of the fate of dumped sediments. Nevertheless, if the recirculation hypothesis holds, significant changes have to be applied regarding the official sediment management strategy and especially concerning the location of spoil grounds.

#### 5 CONCLUSIONS

Within the scope of this study echosounding datasets of 47 consecutive navigational safety surveys in the Outer Jade are examined. The obtained bathymetric information is utilized for an analysis of local

bedforms and a volume balancing study. The temporal variation of sediment volume differences from consecutive bathymetric surveys inside a predefined fairway segment is used to test for potential correlations with the corresponding metocean time-series and with documented maintenance activities, respectively. In this context, significant correlations are observed for the linear relationship between bathymetric changes and reported maintenance works, yielding a high coefficient of determination of  $R^2 = 0.96$ . This finding indicates a recirculation of dredge spoil dumped in the vicinity of the navigational channel as previously suggested by other authors. However, further research has to be undertaken on this topic, especially in terms of numerical simulations, to facilitate a verification of the described hypothesis.

## 6 ACKNOWLEDGEMENT

The described investigations were undertaken in the course of a Master's Thesis at the Gottfried Wilhelm Leibniz University. The joint project was supervised by associates of the Ludwig-Franzius-Institute in Hannover and the Federal Waterways Engineering and Research Institute of Germany, Hamburg. Therefore, sincere thanks are given to these competent supporters of the present paper. Moreover, special thanks go to the experts of the Waterways and Shipping Office of Wilhelmshaven who generously shared their "digital treasure", i.e. navigational safety surveys and MoNa reports, with us.

## 7 REFERENCES

- Ashley, G.M. (1990): Classification of large-scale subaqueous bedforms; A new look at an old problem. In: *Journal of Sedimentary Research* 60 (1), S. 160–172. doi:10.2110/JSR.60.160
- Flemming, B.W. (1988): Zur Klassifikation subaquatischer, strömungstransversaler Transportkörper. In: *Bochumer geologische und geotechnische Arbeiten* 29 (93-97).
- Götschenberg, A.; Kahlfeld, A. (2008): The Jade. In: *Die Küste*, 74 ICCE (74), S. 263–274.
- Kubicki, A.; Bartholomä, A. (2011): Sediment dynamics in the Jade tidal channel prior to port construction, southeastern North Sea. In: *Journal of Coastal Research* SI 64, S. 771–775. ISSN 0749-0208
- Kubicki, A.; Kösters, F.; Bartholomä, A. (2017): Dune convergence/divergence controlled by residual current vortices in the Jade tidal channel, south-eastern North Sea. In: *Geo-Marine Letters* 37 (1), S. 47–58. doi:10.1007/s00367-016-0470-6
- Melling, G.; Kösters, F. (2017): Voruntersuchungen zum Sedimentmanagement in der Jade. Internal Report. Federal Waterways Engineering and Research Institute (BAW), Germany.
- Van der Mark, C.F.; Blom, A.; Hulscher, S.J.M.H. (2008): Quantification of variability in bedform geometry. In: *Journal of Geophysical Research (Earth Surface)* 113. doi: 10.1029/2007JF000940
- Zorndt, A. C.; Wurpts, A.; Schlurmann, T. (2011): The influence of hydrodynamic boundary conditions on characteristics, migration, and associated sand transport of sand dunes in a tidal environment. In: *Ocean Dynamics* 61 (10), S. 1629–1644. doi:10.1007/s10236-011-0452-1



# Build-up-and-fill structure: The depositional signature of strongly aggradational chute-and-pool bedforms

Arnoud Slootman *College of Petroleum Engineering & Geosciences, King Fahd University of Petroleum and Minerals, Dhahran, Saudi Arabia – arnoudslootman@gmail.com*

Matthieu J.B. Cartigny *Department of Geography, Durham University, Durham, United Kingdom – matthieu.j.cartigny@durham.ac.uk*

Age J. Vellinga *National Oceanography Centre, University of Southampton Waterfront Campus, Southampton, United Kingdom – age.vellinga@gmail.com*

**ABSTRACT:** Chute-and-pools are unstable, hybrid bedforms of the upper flow-regime, populating the stability field in between two stable end-members (antidunes and cyclic steps). Chute-and-pools are manifested by supercritical flow (chute) down the lee side and subcritical flow (pool) on the stoss side, linked through a hydraulic jump in the trough. The associated sedimentary structures reported here were generated at the toe-of-slope of a Pleistocene carbonate platform dominated by resedimentation of skeletal sand and gravel by supercritical density underflows. It is shown that wave-breaking on growing antidunes occurred without destruction of the antidune like commonly observed for antidunes in subaerial flows. This led to the formation of chute-and-pools that were not preceded by intense upstream scouring, interpreted to be the result of high bed aggradation rates. The term *aggradational chute-and-pool* is proposed for these bedforms, associated with *build-up-and-fill structures* consisting of interstratified convex-upward (in-phase wave regime) and concave-upward (hydraulic jump regime) lenses.

## 1 INTRODUCTION

The upper flow-regime spans between two stable bedform end-members: short-wavelength antidunes and long-wavelength cyclic steps (wavelength measured relative to flow thickness) (Spinewine et al. 2009; Kostic et al. 2010; Yokokawa et al. 2016). Antidunes form under in-phase (standing) waves, whereas cyclic steps are marked by the permanent presence of hydraulic jumps in the troughs between successive steps (Taki and Parker 2005; Fildani et al. 2006; Cartigny et al. 2011).

A continuum of hybrid bedforms exists between the two end-members of the upper flow-regime (Yokokawa et al. 2011; Cartigny et al. 2014). Such hybrid bedforms develop in trains of antidunes affected by the occasional breaking of in-phase waves. In the unstable antidune regime, the surges that follow wave breaking perish rapidly. In contrast, surges in the chute-and-pool regime evolve into transient hydraulic jumps (Alexander et al. 2001; Cartigny et al. 2014).

The flow pattern in chute-and-pools mimics the flow between two successive crests in a series of cyclic steps, characterised by a Froude-supercritical chute down the lee side and a pool filled with Froude-subcritical flow on the stoss side (Simons et al. 1965; Hand 1974; Taki and Parker 2005). The transition from the supercritical to the subcritical regime is situated in the upstream region of the pool and is embodied by the hydraulic jump. In contrast to cyclic steps, the pool of chute-and-pools is progressively filled and the hydraulic jump is eventually flushed downstream.

Chute-and-pool bedforms are often associated with the formation of scour-and-fill structures (Hand 1974; Alexander et al. 2001; Lang and Winsemann 2013; Cartigny et al. 2014). On the basis of outcrops situated along the toe-of-slope off a carbonate platform covered with skeletal debris, this paper advocates that chute-and-pools generate *build-up-and-fill structures* under high aggradation rates.

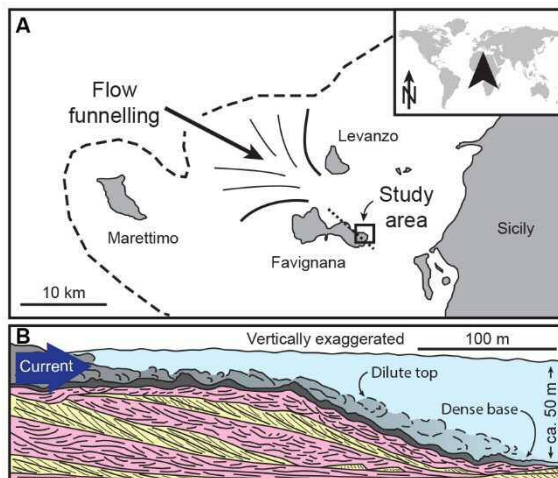


Figure 1. (A) The studied outcrops are located in the Egadi Archipelago in the Central Mediterranean Sea offshore western Sicily. Eastward flows were funnelled over a cool-water carbonate platform between the palaeo-islands Favignana and Levanzo during the Lower Pleistocene. Dashed line shows present-day 200 metres isobath. Stippled line indicates location of the cross-section. (B) Off-platform transport of skeletal debris was bimodal, hence progradation of the platform slope generated a repeated alternation of two types of clinoform units: (1) Numerous low-energy events formed up-to-10-m-thick stacks of subaqueous dune deposits (shown in yellow). (2) Single high-energy events produced Froude-supercritical density flows that deposited up-to-6-m-thick beds composed of sedimentary structures formed by upper flow-regime bedforms (shown in pink). The *build-up-and-fill structures* in these beds are the topic of the present study.

## 2 STUDY AREA

The studied sedimentary structures are located in the Lower Pleistocene calcirudites and calcarenites of Favignana Island; the largest island of the Aegadian Archipelago offshore western Sicily in the Central Mediterranean (Fig. 1). Continuous sea cliffs show that these heterozoan remains (*sensu* James 1997) adopt a large-scale clinoform architecture consisting of southeastward prograding units up to 50 m high, 500 m long, several m thick and dipping 5-20 degrees (Fig. 1).

The series of clinoform units is marked by a bimodal facies stacking pattern consisting of an alternation of bioturbated subaqueous dune deposits and thick supercritical density flow beds, which occur in approximately equal proportions (Slootman et al. 2016). Flow funnelling between the palaeo-

islands during high-energy events (e.g. tsunamis) is suggested to have swept the platform and to lie at the origin of the large-scale sediment density flows (Slootman et al. in review).

Palaeoflow direction of the supercritical density flows is inferred from the orientation of the base and top of the beds, and compares well with the southeastward migration direction of subaqueous dunes, which is more straightforward to interpret.

## 3 BEDFORM RECONSTRUCTION

Line drawing of the internal stratification of density flow beds enabled the geometrical analysis at lamina-level, which forms the basis for the reconstruction of the timewise evolution of bed topography and the development of bedforms. This revealed the concept of the composite erosion surface and the alternation of convex-up and concave-up stratified lenses forming the main architectural elements of density flow beds. Two beds in two different exposures are presented.

### 3.1 Bed C27 in Balena outcrop

#### 3.1.1 Observations

*Convex and concave lenses.* Bed C27 (ca. 2 m thick) is underlain and overlain by fossil subaqueous dunes. A downstream-dipping erosion surface dissects the section into two parts (Fig. 2). Different stratification patterns define the main architectural elements of density flow beds: convex-up-stratified lenses and concave-up-stratified lenses (sub-units 1-3 in Fig. 2).

*Composite erosion surface and nature of stratification.* The convex-up backset-beds of subunit 1 are slightly concave-up at their upstream termination, where laminae erode the underlying fossil subaqueous dune and truncate the laminae of subunit 3. Most laminae of subunits 1 and 2 also truncate the underlying lamina at its upstream end, generating a composite erosion surface (Fig. 2). The nature of the stratification varies. In subunit 3, laminae are relatively thin and well pronounced. On the downstream side of

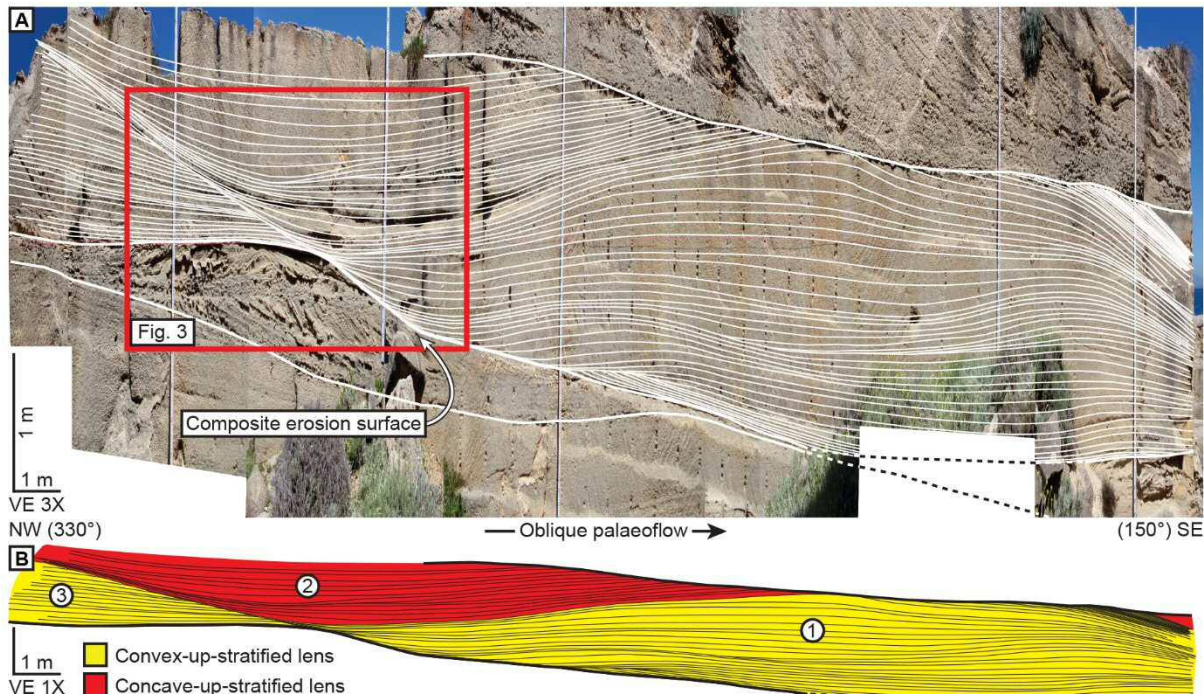


Figure 2. (A) Balena outcrop. Width of view is 24 m. Internal stratification of density flow bed C27 and bed boundaries are shown. Note the composite erosion surface at the upstream termination of strata. Three times vertically exaggerated. (B) Main architectural elements of bed C27. Subunits indicated by encircled numbers.

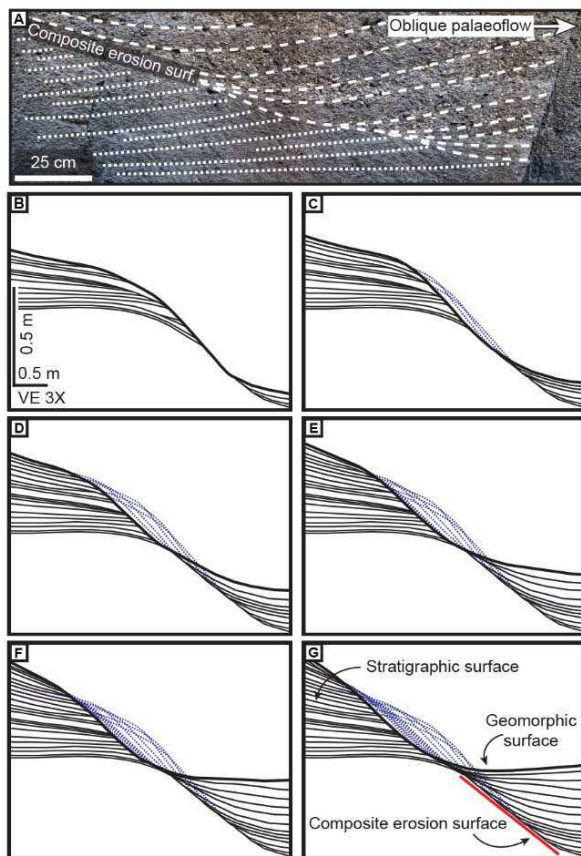


Figure 3. (A) Composite erosion surface juxtaposing

the composite erosion surface, strata are calcirudites (left) with biogenic conglomerates (right). (B) Timewise reconstruction of bed-flow interfaces (geomorphic surfaces) in red box in Fig. 2.

invariably marked by an erosional lower boundary that commonly becomes less sharp toward the crest of the step, accompanied with a decrease in grainsize and an increase in sorting.

### 3.1.2 Interpretation

*Strata correlation.* A method useful for the correlation of strata is the ‘barcode principle’, which is based on the assumption that laminae have certain characteristics, such as relative thickness, grainsize distribution and sharpness of boundaries that can be used as a tracer along exposures. A high-frequency pulsation intrinsic to the flow led to a cyclic alternation of (in most cases) erosion and deposition related to the formation of individual laminae. A temporal variation in the intensity of such fluctuations and herewith the rate of deposition created a bar-code-like pattern in the deposit, occurring on both sides of (composite) erosion surfaces or

even in different outcrops, albeit with a slightly different character depending on the local conditions of deposition.

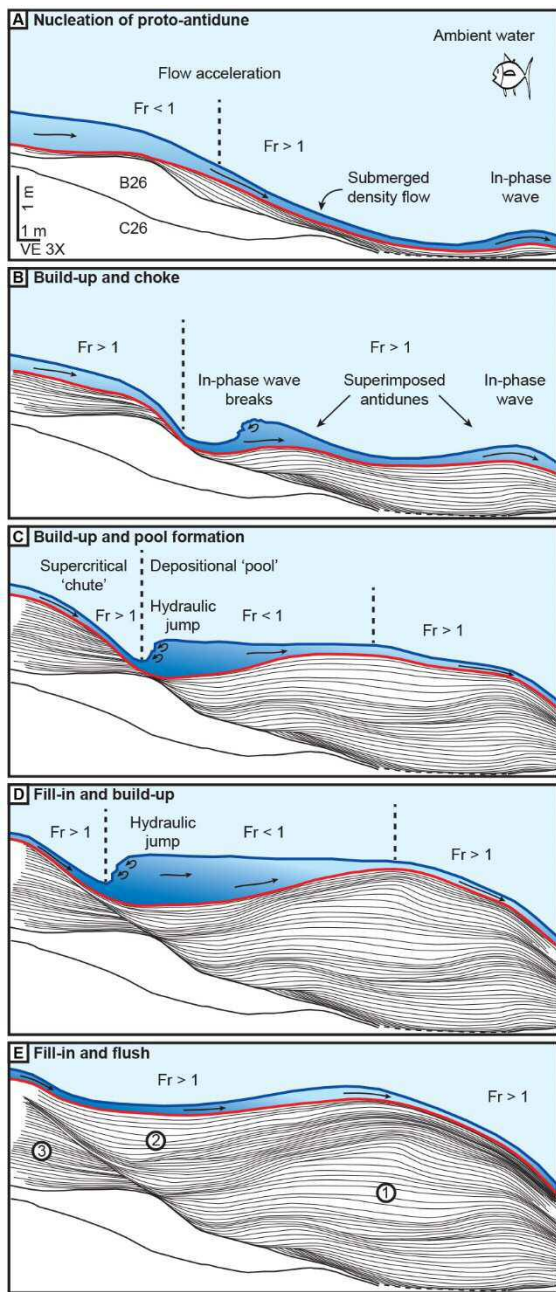


Figure 4. Morphodynamic reconstruction of the Balena outcrop and the evolution of the build-up-and-fill structure. See text for explanation.

The missing part of laminae comprised within the erosion surface can be inferred from the non-eroded portion.

**Geomorphic surfaces.** This introduces the concept of geomorphic surfaces (Sylvester et al. 2011), representing time lines of the bed-flow interface (Fig. 3). Geomorphic

surfaces are key to the reconstruction of the morphodynamic evolution of bedforms. It is proposed that the foreset-beds of subunit 3 were continuous into the backset-beds of subunits 1 and 2 such that a convex-up step connected both sides. The concave-up portion that linked the upstream slope with the downstream step was thus the trough of a bedform, which migrated upward by deposition on the stoss-side and upstream by erosion of the lee side. This style of deposition is characteristic of a hydraulic jump on an aggrading mobile substrate (e.g. Alexander et al. 2001; Duller et al. 2008; Cartigny et al. 2014; Dietrich et al. 2016). Hydraulic-jump-related deposition was preceded by the build-up of the step and succeeded by the infill of the trough, altogether generating the build-up-and-fill structure.

**Bedform evolution.** The evolution of the build-up-and-fill structure is reconstructed by the stepwise stacking of laminae, reconstructed using the bar-code principle. The bed went through the following five phases (Fig. 4): (a) Nucleation: establishment of an asymmetrical proto-antidune under an in-phase wave. (b) Build-up and choke: the antidune developed into a long-wavelength step superimposed by two short-wavelength antidunes. As the short-wavelength antidune at the upstream side built-up, the overriding flow thickened because supercritical flows tend to amplify the topography of the bed. Such thickening co-occurred with flow deceleration, until the densimetric Froude number fell below unity. The transition from supercritical to subcritical flow at the crest of the antidune, involved the breaking of the in-phase wave and the formation of a hydraulic jump (flow-choking, e.g. Fedele et al. 2017). Retention of water in the hydraulic jump reduced the discharge over the second superimposed antidune, which led to the build-up and subsequent breaking of the overriding in-phase wave. (c) Build-up and pool formation: the two antidunes progressively merged into a single, large step governed by asymmetrical deposition over its entire length that resulted in its vertical growth. The trough between the 'chute' and

the crest of the step developed into a ‘pool’ by the accumulation of water, herewith enhancing the intensity of the hydraulic jump. The configuration now established is referred to as a chute-and-pool. Deposition from the hydraulic jump induced the upward migration of the trough, whereas erosion by the chute forced the trough to migrate upstream. This continued the creation of the downstream-dipping composite erosion surface, the formation of which already started in the antidune configuration. (d) Fill-in and build-up: the trough filled with sediment as a result of deposition rate in the trough outpacing that on the crest. Erosion no longer governed the chute, which had become depositional, herewith overstepping the composite erosion surface. (e) Fill-in and flush: the depth of the trough abated and the trough eventually disappeared. Deceleration of the chute no longer caused the transition to subcritical flow and the hydraulic jump was flushed downstream, re-establishing supercritical flow conditions throughout.

### 3.2 Bed C28 in Pappagallo outcrop

#### 3.2.1 Observations

Bed C28 reaches over 7 m and is underlain by two fossil subaqueous dunes in the Pappagallo outcrop. Reconstruction using the barcode-principle reveals the continuity of some laminae over the entire ca. 60 m length of the outcrop, enabling the reconstruction of a few key geomorphic surfaces thus representing time lines (encircled numbers in Fig. 5). Laminae with an upward-decreasing concavity overlie the upstream subaqueous dune. This concave-up lens evolves upward into a near-horizontal bed (1) and then into a convex-up shape (2), which grades downstream into another concave fill (top of which is 3). The thickness of lenses may be strongly reduced in upstream direction from a few metres down to a few tens of cm or less. The marked timelines illustrate that the ‘build-up’ and ‘fill-in’

phases alternate in a timewise sense. The build-up phase commonly initiates from a semi-horizontal surface (e.g. 1,3). The succeeding fill-in phase (partly) restores the near-horizontal bed (e.g. 3,5).

#### 3.2.2 Interpretation

The stacked build-up-and-fill structures composing bed C28 in the Pappagallo outcrop reflect a periodicity in bedform behaviour: build-up and fill-in phases alternate in both horizontal and vertical direction (Fig. 5). The 3 m elevation drop over the lee side of the underlying fossil subaqueous dune at the upstream side (0) dictates that the first phase in this exposure is a fill-in phase. The composite erosion surface at the upstream limit of the concave lens suggests that a hydraulic jump was involved in its formation. A convex lens that formed during the subsequent build-up phase overlies the horizontal top of the concave lens (1). This pattern continues in horizontal and vertical direction, illustrating the periodic alternation of build-up and fill-in phases.

## 8 DISCUSSION AND CONCLUSIONS

There is a fundamental difference between antidunes and cyclic steps (Fildani et al., 2006; Spinewine et al., 2009; Kostic, 2010; Cartigny et al. 2014; Yokokawa et al. 2016). Antidunes are short-wavelength bedforms that develop under trains of in-phase surface waves. Cyclic steps are long-wavelength bedforms associated with series of steps marked by supercritical flow down the lee side and subcritical flow on the stoss side, separated by hydraulic jumps in the intervening troughs (e.g. Cartigny et al., 2011).

Hybrid bedforms that have more in common with cyclic steps than with antidunes are predominately characterised by hydraulic jumps and less so by in-phase waves.

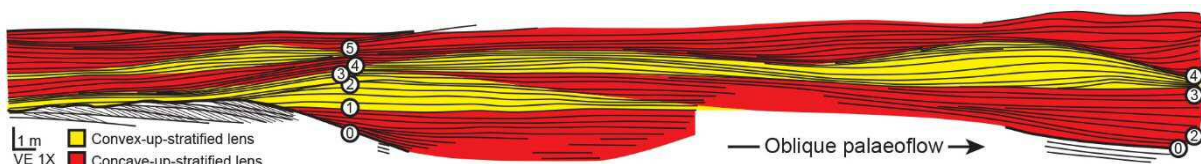


Figure 5. Main architectural elements bed C28 in the Pappagallo outcrop (58 m wide). See text for explanation.

This morphology is referred to as chute-and-pool (Simons et al., 1965) and is commonly associated with the formation of scour-and-fill structures.

The density flow beds of the Lower Pleistocene carbonate slope of Favignana Island are composed of *build-up-and-fill structures*, defined by interstratified convex and concave lenses as main architectural elements. On the basis of detailed morphodynamic reconstructions, it is suggested that convex lenses represent deposition under in-phase waves in the antidune-regime, and that concave lenses were formed by deposition from hydraulic jumps situated in the trough between bedforms. Such hydraulic jumps formed by the breaking of the in-phase antidune wave. Unlike wave-breaking in subaerial flows, wave-breaking was not accompanied with antidune destruction due to high rates of bed aggradation. Hence, the term *aggradational chute-and-pools* is proposed for these bedforms.

## 9 REFERENCES

- Alexander, J., Bridge, J.S., Cheel, R.J. and Leclair, S.F. (2001) Bedforms and associated sedimentary structures formed under supercritical water flows over aggrading sand beds. *Sedimentology*, 48, 133-152.
- Cartigny, M.J.B., Postma, G., Van den Berg, J.H. and Mastbergen, D.R. (2011) A comparative study of sediment waves and cyclic steps based on geometries, internal structures and numerical modeling. *Mar. Geol.*, 280, 40-56.
- Cartigny, M.J.B., Ventra, D., Postma, G. and Den Berg, J.H. (2014) Morphodynamics and sedimentary structures of bedforms under supercritical flow conditions: New insights from flume experiments. *Sedimentology*, 61, 712-748.
- Dietrich, P., Ghienne, J.F., Normandeau, A. and Lajeunesse, P. (2016) Upslope-Migrating Bedforms In A Proglacial Sandur Delta: Cyclic Steps From River-Derived Underflows? *J. Sediment. Res.*, 86, 113-123.
- Duller, R.A., Mountney, N.P., Russell, A.J. and Cassidy, N.C. (2008) Architectural analysis of a volcanoclastic jökulhlaup deposit, southern Iceland: sedimentary evidence for supercritical flow. *Sedimentology*, 55, 939-964.
- Fedele, J.J., Hoyal, D.C., Barnaal, Z., Tulenko, J., Awalt, S. (2017) Bedforms created by gravity flows. In: Budd, D., Hajek, E., Purkis, S. (Eds.), *Autogenic Dynamics and Self-Organization in Sedimentary Systems*. SEPM Spec. Pub., 106, 95-121.
- Fildani, A., Normark, W.R., Kostic, S. and Parker, G. (2006) Channel formation by flow stripping: large-scale scour features along the Monterey East Channel and their relation to sediment waves. *Sedimentology*, 53, 1265-1287.
- Hand, B.M. (1974) Supercritical flow in density currents. *J. Sed. Petrol.*, 44, 637-648.
- James, N.P. (1997) The cool-water carbonate depositional realm. In: *Cool-water carbonates* (Eds. N.P. James and J. Clarke), SEPM Spec. Pub, 56, 1-20.
- Kostic, S., Sequeiros, O., Spinewine, B. and Parker, G. (2010) Cyclic steps: A phenomenon of supercritical shallow flow from the high mountains to the bottom of the ocean. *J. Hydr-Environ. Res.*, 3, 167-172.
- Lang, J. and Winsemann, J. (2013) Lateral and vertical facies relationships of bedforms deposited by aggrading supercritical flows: from cyclic steps to humpback dunes. *Sediment. Geol.*, 296, 36-54.
- Simons, D.B., Richardson, E.V. and Nordin, C.F. (1965) Sedimentary structures generated by flow in alluvial channels. In: Primary sedimentary structures and their hydrodynamic interpretation (Ed. G.V. Middleton), SEPM Sp. Pub., 12, 34-52.
- Slootman, A., Cartigny, M.J.B., Moscariello, A., Chiaradia, M. and De Boer, P.L. (2016) Quantification of tsunami-induced flows on a Mediterranean carbonate ramp reveals catastrophic evolution. *Earth Planet. Sc. Lett.*, 444, 192-204.
- Slootman, A., De Boer, P.L., Cartigny, M.J.B., Samankassou, E. and Moscariello, A. (in review) Evolution of a carbonate delta generated by gateway-funnelling of episodic currents. *Sedimentology*.
- Spinewine, B., Sequeiros, O.E., Garcia, M.H., Beaujouef, R.T., Sun, T. and Savoye, B. (2009) Experiments on wedge-shaped deep sea sedimentary deposits in minibasins and/or on channel levees emplaced by turbidity currents. Part II. Morphodynamic evolution of the wedge and of the associated bedforms. *J. Sediment. Res.*, 79, 608.
- Sylvester, Z., Pirmez, C. and Cantelli, A. (2011) A model of submarine channel-levee evolution based on channel trajectories: Implications for stratigraphic architecture. *Mar. Petrol. Geol.*, 28, 716-727.
- Taki, K. and Parker, G. (2005) Transportational cyclic steps created by flow over an erodible bed. Part 1. Experiments. *J. Hydraul. Res.*, 43, 488-501.
- Yokokawa, M., Y. Takahashi, H. Yamamura, Y. Kishima, G. Parker and N. Izumi. (2011) Phase diagram for antidunes and cyclic steps based on suspension index, non-dimensional Chezy resistance coefficient and Froude number. In: Int. Assoc. Hydro-Envir. Engin. and Res., 7th RCEM Symposium, Beijing, China (2011), Proceedings, 1789-1794.
- Yokokawa, M., Izumi, N., Naito, K., Parker, G., Yamada, T. and Greve, R. (2016) Cyclic steps on ice. *J. Geophys. Res.-Earth*, 121, 1023-1048.

# Automated estimation of seabed morphodynamic parameters

Nathan Terseleer *Royal Belgian Institute of Natural Sciences (Operational Directorate Natural Environment), Brussels, Belgium – nterseleer@naturalsciences.be*

Koen Degrendele *Continental Shelf Service, Federal Public Service Economy, S.M.E.s, Self-Employed and Energy, Brussels, Belgium – koen.degrendele@economie.fgov.be*

Lars Kint *Royal Belgian Institute of Natural Sciences (Operational Directorate Natural Environment), Brussels, Belgium – lkint@naturalsciences.be*

Marc Roche *Continental Shelf Service, Federal Public Service Economy, S.M.E.s, Self-Employed and Energy, Brussels, Belgium – marc.roche@economie.fgov.be*

Dries Van den Eynde *Royal Belgian Institute of Natural Sciences (Operational Directorate Natural Environment), Brussels, Belgium – dries.vandeneynde@naturalsciences.be*

Vera R. M. Van Lancker *Royal Belgian Institute of Natural Sciences (Operational Directorate Natural Environment), Brussels, Belgium – vera.vanlancker@naturalsciences.be*

**ABSTRACT:** An automatic procedure is described to estimate seabed morphodynamic parameters (main bedform wavelength, height, migration direction and magnitude) from repeated multibeam echosounder (MBES) bathymetric data. The method explores successive bathymetric profiles to assess seabed morphodynamics based on wavelet analysis and cross-correlation. It is applied on 143 successive MBES surveys from a monitoring program in 10 areas of marine aggregate extraction in the Belgian part of the North Sea, resulting in 355 observations of morphodynamic parameters. These can be used to explore specific patterns such as the decrease in dune height in areas experiencing more extraction. Altogether, this method appears efficient to quickly and automatically map seabed bedforms, investigate their temporal dynamics, and points towards interesting features for further analysis.

## 1 INTRODUCTION

Repeated MBES measurements over time allow the investigation of seabed morphodynamics at possibly high spatial and temporal resolutions. In the Belgian part of the North Sea, the monitoring program accompanying the aggregate extraction activity (Roche et al., 2017) provides such data. When investigating the evolution of the seabed over time in the monitored areas, two main sources of bathymetric variation are observed: the human extraction and the migration of very large dunes. In order to assess the remaining variability of the seabed and the possible depletion or repletion dynamics, a method was previously developed to extract the effect of dune migration (Terseleer et al., 2016): morphodynamics were considered as homogeneous over the

investigated areas, and an overall dune migration (magnitude and direction) was derived from an optimization procedure. Yet, variations in seabed morphodynamics within the investigated areas (a few square km) called for a more local approach.

In this contribution, an automated approach is presented to estimate morphodynamics parameters such as dune migration and magnitude as well as wavelengths and heights. This allows mapping bedforms as well as assessing the prospective evolution over time of such parameters. The method is applied on a MBES dataset from the monitoring program of marine aggregate extraction in Belgium, and thereafter exploited to investigate the seabed behaviour over time (and more specifically the evolution of dune heights) in extracted areas.

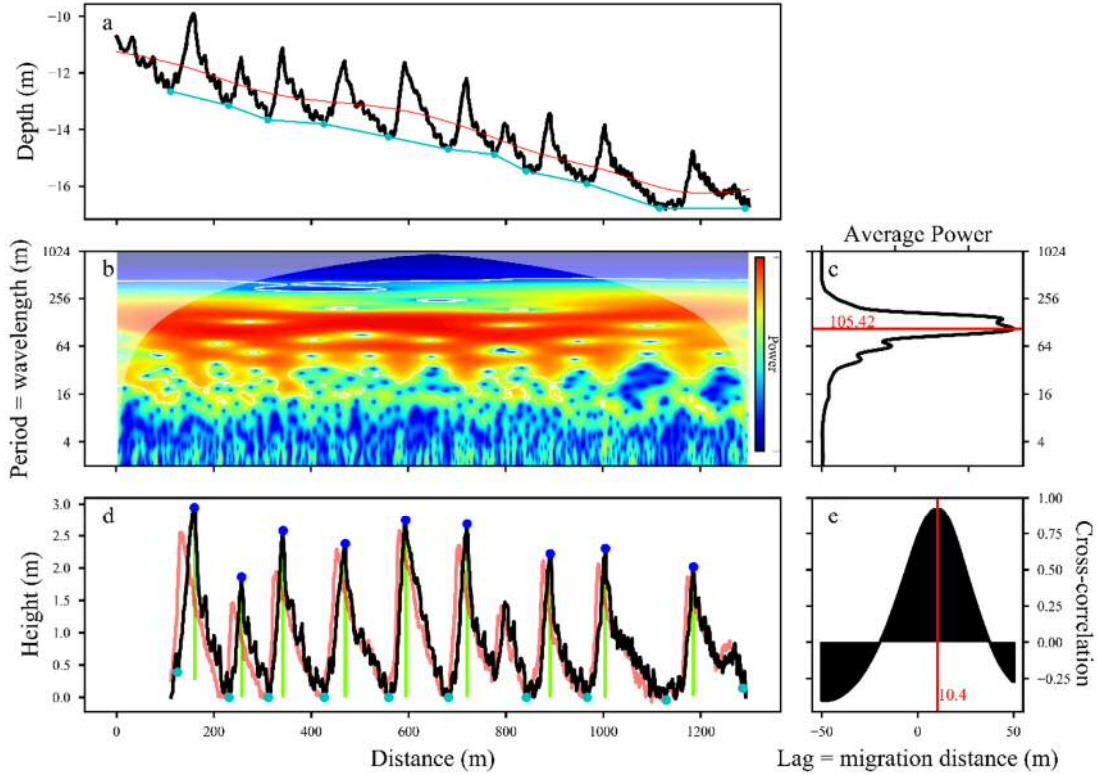


Figure 1. Automatic treatment of a bathymetric profile. (a) The original bathymetric profile (black line) is considered to be composed of one stable part corresponding to the sandbank (under the cyan line) and one mobile part on top of it (between the cyan and black lines) which is used for later analysis. The red line is a cubic regression spline used to detrend the bathymetric profile for the wavelet analysis. (b) Wavelet analysis of the detrended bathymetric profile: at each location on the profile (x axis), it indicates the preponderance (power, colour scale) of each wavelength (y axis) in the bathymetric profile. (c) Average power (x axis) of each wavelength (y axis) over the bathymetric profile. The maximum (red line) identifies the dominant wavelength (here, ~105 m). (d) Profile of the upper, mobile part of the seabed (black) with automatic detection of crests (blue) and trough (cyan) points, allowing the estimation of dune heights (vertical green lines). The bathymetric profile of the next survey is shown in red. (e) Cross-correlation between the red (old) and black (recent) profiles of (d). The maximum correlation (red line) identifies the spatial gap (i.e., migration distance) between the two profiles (here, ~10 m).

## 2 METHODS

Two sources of data can be used to investigate the seabed behaviour in marine aggregate extraction areas of the Belgian part of the North Sea. First, MBES surveys are regularly conducted over monitoring areas, providing a time series of bathymetric data (1 m horizontal resolution and 1 to 4 surveys per year; see Roche et al., 2017). Second, an electronic monitoring system (Van den Branden et al., 2017) is placed onboard of extraction vessels and records their activity and position, providing a spatio-temporal dataset of extraction in the areas.

In Terseleer et al. (2016), the dune migration was estimated based on an optimization

process comparing pairs of successive bathymetric surfaces, with the older one being horizontally shifted to find the best match with the most recent one. Consequently, a unique migration pattern (magnitude and direction) was estimated for the whole area. Here, a similar principle is applied but more locally: in order to allow deriving different migration patterns (in magnitude and direction) within a single area, the comparison is done between successive bathymetric profiles taken in all directions around different centroids within the areas. Thus, contrary to other approaches where the migration is measured in the direction perpendicular to the bedforms crests, the direction here freely emerges from the automatic procedure. Successive profiles are compared on the basis of

their cross-correlation, as if two time series were compared (similarly to McElroy & Mohrig, 2009): the best match corresponds to the highest correlation (i.e., the profiles are the most alike), while the migration distance is estimated from the spatial gap between them (similarly to the temporal lag separating two time series).

The procedure is fully automatic. It can be summarized into four steps which are detailed hereafter and illustrated in Figure 1.

## 2.1 Definition of the centroids and profiles

The centroids are the centres of the bathymetric profiles (which are distributed in all directions). They are regularly positioned over the main axis of the rectangular monitored areas. To allow the detection of bedforms with typical wavelengths up to ~300 m (very large dunes), the profiles are between 800 and 1300 m long (depending on the actual extent of the areas). Depending on the size of the monitored areas, between 1 and 6 centroids are used. For each centroid, profiles explore the bathymetry over the full 0-360° directions with intervals of 5°.

## 2.2 Distinction between the mobile seabed and the stable sandbank underneath

Two components are separated in a bathymetric profile: the sandbank body, which is assumed to be stable over time, and the overlaying seabed, composed of different bedforms and considered to be the mobile part of the seabed. Only the latter is thus conserved for further analysis. The approach is similar to Debese et al. (2018), who introduced the geomorphometric concept of osculatory surface matching the sandbank tangentially to the dune feet and representing a boundary between a dynamic upper part shaped by the mobile dunes and a stable internal part. Here, the sandbank body is obtained by joining all the troughs (i.e., the deepest points) between the largest successive bedforms (typically, very large dunes with wavelengths ~150-300 m; cyan line in Fig. 1a). To automatically identify the troughs and to distinguish them from other

local bathymetric minima (corresponding to neighbouring seabed features or measurement noise), a wavelet analysis (Fig. 1b) is conducted on the detrended bathymetric profile. A moving window is then used over the profile to assess the corresponding dominant periodicity (i.e., wavelength of the largest bedforms) inside which the deepest minimum is selected as the trough of the bedform (Fig. 1a, cyan). This step is important to avoid the problematic influence of the sandbank signal (with a very long wavelength) on the cross-correlation analysis of the next step. The use of wavelet analysis allows the adaptive identification of the troughs of bedforms with different properties.

## 2.3 Cross-correlation and estimation of the migration amplitude and direction

Once the dynamic upper part of the oldest and most recent profiles is obtained (Fig. 1d, red and black lines), a cross-correlation analysis is carried out (as if they were considered as two univariate time series; Fig. 1e). Between the different investigated pairs of profiles, the one with the highest correlation is selected, assuming that migration occurs in the direction maintaining the highest degree of similarity between successive profiles. The migration distance is then provided by the spatial lag between the two profiles obtained from the cross-correlation (as would be the case for the time lag between two time series).

## 2.4 Bedform wavelength and height

A wavelet analysis is carried on the selected profile from step 2.3. Similarly to step 2.2, the wavelet analysis is used to scan the bathymetric profile with a moving window and select only one minimum (trough) and maximum (crest) corresponding to the dominant wavelength at each segment of the profile. Once troughs and crests are identified, the bedform height (green vertical lines in Fig. 1c) is then computed as the vertical height between the crest point (blue points) and its base joining the two neighbouring

trough points (cyan points). The dominant wavelength over the bathymetric profile correspond to the period averaging the highest power of the wavelet analysis over the full profile (Fig. 1c; similar approach to e.g. Gutierrez et al., 2013).

### 3 RESULTS

The four-step procedure described above allows to automatically estimate morphodynamic parameters (bedform height, wavelength, migration rate and direction) upon availability of successive MBES datasets. This study incorporates 143 campaigns, distributed over 10 different areas over a monitoring period of 16 years, leading to 355 observations. The obtained lag correlations range from 0.80 to 0.99 (median = 0.96), indicating an appropriate match between successive profiles.

#### 3.1 Dune migration rate and direction

Figure 2 shows the resulting dune migration rate (y axis) as a function of its direction (x axis). The largest migration rates are essentially directed towards the NNE-NE or the SSW-SW, corresponding to the main axis of the tidal ellipse in the area.

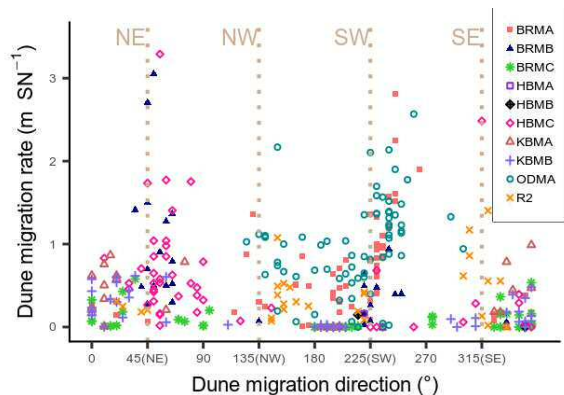


Figure 2. Results from the automatic procedure: dune migration rate (in m per spring-neap cycle, SN) vs the dune migration direction ( $0^\circ$  being the East). Legend: names of the monitored areas (see Roche et al., 2019).

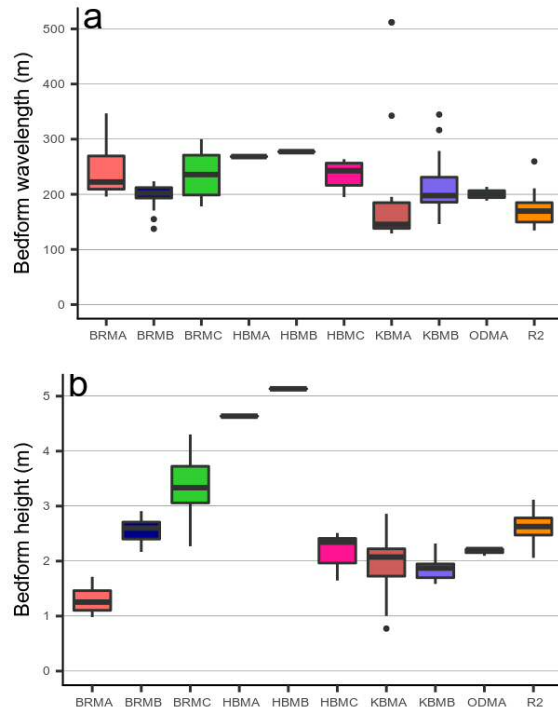
These dominant migration directions were identified previously and related to currents, meaning that dune migration essentially

occurs as a function of the relative morphological position of the area on the sandbanks, leading to an ebb- or flood-dominated tidal regime (Terseleer et al., 2016). Some areas seem to experience a unidirectional migration (e.g., HBMC towards the NE) while others experience multidirectional migration (e.g., BRMC).

Within a same area, while the preferred dune migration direction is preserved over the area, a gradient in its magnitude can be observed, typically with higher migration rates on top of the shallower central part of the sandbank and lower ones in deeper parts (e.g., BRMA and ODMA; not shown).

#### 3.2 Morphological parameters

Obtained bedform wavelengths and heights are shown in Figure 3. Most wavelengths range from 150 to 300 m, and observed maximum height over each profile range from 1 to 5 m. No relationship was observed between wavelength and dune heights in this dataset of limited bedforms



(mostly very large dunes; not shown).

Figure 3. Morphological parameters: boxplots of (a) the dune wavelengths and (b) the dune maximum height observed over each profile.

The estimation of dune heights is affected by two main sources of uncertainty. First, the automatic procedure itself (more specifically Section 2.4 above) can be a source of uncertainty. Visual inspection of the intermediate results revealed that, while the largest bedforms are usually well depicted by the procedure, mistakes may sometimes appear: more specifically, depending on the migration distance between two successive profiles, different bedforms may occasionally be selected, leading to a spurious comparison. The procedure is under further development to improve this behaviour. Second, an uncertainty of about 20 to 30 cm may be associated to the MBES data acquired with a Kongsberg EM1002 and EM3002d, which are compliant respectively with IHO S44 order 1 and special order (IHO, 2008). The difference between two successive bathymetric models can thus be up to 60 cm wrong in the worst case. Successive profiles may for example show a different smoothing degree and measurement noises, which affect estimated bedforms characteristics. Nevertheless, investigation of intermediate results suggests that the obtained parameters are realistic. These can help describing general morphological characteristics of the areas (Fig. 3), and are now used to investigate some dynamics occurring over time.

### 3.3 Seabed dynamics

As an illustration of the possible use of the parameters provided by the automatic procedure presented here, Figure 4 shows the difference in maximum dune heights between successive profiles. When this difference is negative, it suggests (beyond the error margin mentioned above) a decrease in bedform heights between two successive campaigns.

Among all areas, most values are centred around zero, suggesting relatively stable bedforms (Fig. 4a). Yet, some areas appear to present more negatively distributed values, mostly BRMC (and, to some extent, HBMC and ODMA). Figure 4b shows the difference in dune heights between suc-

sive campaigns as a function of the aggregate extraction occurring in the area during this period. A loess smoothing is applied (in grey) to illustrate a prospective trend: bedform heights seem to decrease with increasing extraction values. Logically, the trend is mostly influenced by the areas experiencing larger extraction intensities (BRMC and HBMC), which tend to present a more important decrease in bedform height between surveys experiencing more extraction (Fig. 4b). For BRMC, the height decrease (beyond the depth difference due to extraction only) of the very large dunes located in the neighbourhood of an extraction spot which, on the contrary, exhibited sediment accretion, was indeed reported before (Terseleer et al., 2016). This suggests that the present automatic approach is suitable to detect such overall morphodynamic behaviours.

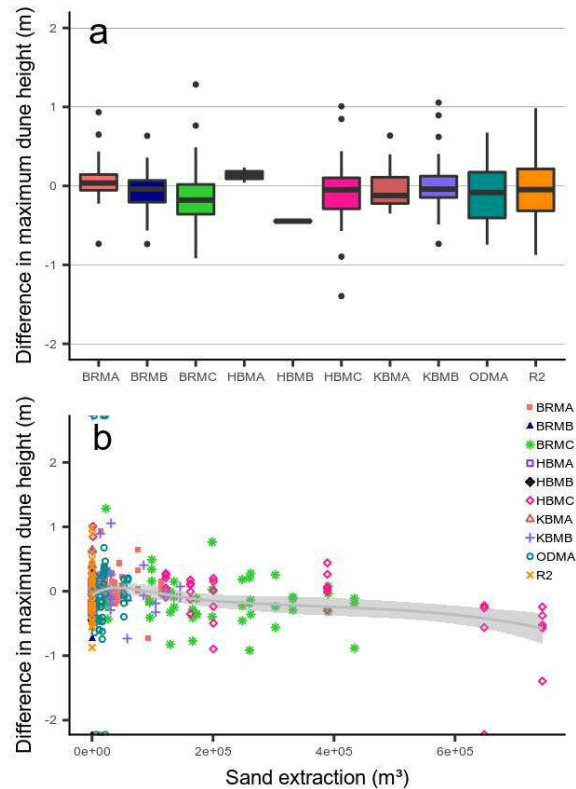


Figure 4. Seabed behaviour in areas of marine aggregate extraction: (a) boxplots of the difference in maximum dune height between successive surveys; (b) difference in maximum dune height between successive surveys *vs* aggregate extraction intensity.

### 3.4 Advantages and limitations of the approach

The use of the wavelet analysis, allowing bedforms of different characteristics to be identified over the bathymetric profile, has proved to be efficient. It allows the procedure to autonomously adapt to bathymetric profiles with different characteristics. Although it would theoretically be possible to use this approach to also map smaller bedforms (bedforms with wavelength between ~15 and 60 m were often detected as secondary signal), their temporal evolution would be more difficult to assess. Indeed, the cross-correlation step, which provides the estimate of the migrated distance between two surveys, relies on the agreement between successive profiles. Preliminary tests on separated profiles for larger (wavelength > 150 m) and smaller (wavelength ~15-60 m) bedforms showed that the procedure was not able to properly discriminate smaller bedforms and to estimate their spatial lag between successive profiles. At this scale, the procedure would require more frequent surveys to be able to identify smaller bathymetric patterns over time. The temporal resolution of the MBES data (and, to some extent, the vertical resolution) therefore limits the type of bedforms that can be studied with such an approach.

## 4 CONCLUSIONS

The procedure described in this contribution allows to efficiently and quickly process the vast amount of data being made available by repetitive MBES surveys such as those provided by the monitoring program of the marine aggregate extraction in the Belgian part of the North Sea. Effort was concentrated on the automated and adaptive nature of the process, which can treat data with different morphometric characteristics. Yet, it remains dependent on the intrinsic quality of the MBES data, more specifically the temporal and vertical resolutions. The procedure can be used to quickly map and classify bathymetric data, and to assess sea-

bed dynamics. Future analyses will investigate differences in dynamics between impacted and non-impacted areas, and will account also for the morphological position of an area upon a sandbank.

## 1. 5 ACKNOWLEDGEMENT

This is a contribution to the Brain-be project TILES (Transnational and Integrated Long-term marine Exploitation Strategies), funded by Belgian Science Policy (Belspo) under contract BR/121/A2/TILES. The research is fully supported by the ZAGRI project, a federal Belgian program for continuous monitoring of sand and gravel extraction, paid from private revenues.

## 2. 6 REFERENCES

- Debese, N., Jacq, J.J., Degrendele, K., Roche, M., Garlan, T., 2018b. Osculatory Surfaces Extraction applied to Monitoring of Submarine Sand Materials. *Marine Geodesy*, 41:6, 605-631.
- Gutierrez, R. R., Abad, J. D., Parsons, D. R., Best, J. L., 2013. Discrimination of bed form scales using robust spline filters and wavelet transforms: Methods and application to synthetic signals and bed forms of the Río Paraná, Argentina. *Journal of Geophysical Research: Earth Surface*, 118(3).
- International Hydrographic Organization, 2008. Special Publication No. S-44, “IHO Standards for Hydrographic Surveys”, 5th Ed., Monaco.
- McElroy, B., Mohrig, D., 2009. Nature of deformation of sandy bed forms. *Journal of Geophysical Research: Earth Surface*, 114(F3).
- Roche, M., Degrendele, K., Vandenreyken, H., Schotte, P., 2017. Multi time and space scale monitoring of the sand extraction and its impact on the seabed by coupling EMS data and MBES measurements, in Degrendele, Vandenreyken, Belgian marine sand: a scarce resource, Brussels, 5-37.
- Terseleer, N., Degrendele, K., Roche, M., Van den Eynde, D., Van Lancker, V., 2016. Dynamics of very-large dunes in sandbank areas subjected to marine aggregate extraction, Belgian continental shelf, in Van Landeghem, K.J.J., Garlan T., Baas, J.H., 2016. MARID 2016, Caernarfon, UK, 4–6 April 2016. Bangor University and SHOM. 216 pp. ISBN 978-2-11-128417-3.
- Van den Branden, R., De Schepper, G., Naudts, L., 2017. The Electronic Monitoring System (EMS) as a minimum requirement for monitoring the extraction of an increasingly scarce raw material, in Degrendele, Vandenreyken, Belgian marine sand: a scarce resource?, Brussels, 39-45.

# Testing the state of bedform equilibrium using MBES data from the Mekong River, Cambodia

Christopher A. Unsworth *University of Hull, Hull, UK – christopher.unsworth@hull.ac.uk*

Daniel R. Parsons *University of Hull, Hull, UK – d.parsons@hull.ac.uk*

Christopher Hackney *University of Hull, Hull, UK – c.hackney@hull.ac.uk*

James Best: *Departments of Geography and Geographic Information Science, Mechanical Science and Engineering and Ven Te Chow Hydrosystems Laboratory, University of Illinois, 1301 W. Green St., Urbana, IL 61801, USA - jimbest@illinois.edu*

Stephen E. Darby *Geography and Environment, University of Southampton, Southampton SO17 1BJ, UK - S.E.Darby@soton.ac.uk*

Julian Leyland *Geography and Environment, University of Southampton, Southampton SO17 1BJ, UK - J.Leyland@soton.ac.uk*

Andrew P. Nicholas *Department of Geography, University of Exeter, Exeter EX4 4RJ, UK - A.P.Nicholas@exeter.ac.uk*

Rolf Aalto *Department of Geography, University of Exeter, Exeter EX4 4RJ, UK- Rolf.Aalto@exeter.ac.uk*

**ABSTRACT:** In this short paper, we demonstrate a new method of deciphering the state of non-equilibrium bedforms using Semi-Variograms. Semi-variograms allow us to take a measure of uniformity in repeating features; therefore, the technique implicitly assumes that equilibrium is defined by uniformity. Comparison of the semi variogram produced from 5 selected profiles of dunes at different states of equilibrium and boundary conditions from the Mekong River (Cambodia) is compared against the semi variogram produced from an idealised and identical train of bedforms. We find that the empirical semi-variogram of a bedform profile is more than adequate at estimate the mean length of the bedforms, can decipher the dominant scales of bedforms. Moreover, this technique opens up the possibility of quantifying the degree of dis-equilibrium in the bed state that departs from basic geometric measurement of height, length and aspect ratio, and also does not require a series of repeated measurements: which is uncommon in large MBES surveys.

## 1 INTRODUCTION

Equilibrium in bedform state is described as a series of repeating bed features with consistent height, length and shape in time and space, and whilst many definitions attempt to describe predict the geometric size of the bedform in relation to grain size, flow depth or bed shear stress (Baas, 1994, 1999; Bartholdy et al., 2002; Dreano et al., 2010; Flemming, 2000; Martin & Jerolmack, 2013; Myrow et al., 2018; Perillo et al., 2014; Reesink et al., 2018), here we are only investigating the consistency in bedform shape in space. Such a definition of equilibrium requires a geometric uniformity perhaps unlikely with some definitions of equilibrium and three-dimensional bedforms

(Myrow et al., 2018; Reesink et al., 2018) but no less can define the end member to the

broad spectrum of bedform disequilibrium. A fundamental property of uniquely repeating shapes is that they are “self-similar” at their own spatial and temporal scales, implying a measure of equilibrium (or disequilibrium) is plausible from their correlation. For features which display spatial linkages, the semi-variogram is preferred over auto-correlation due to the semi-variograms’ inherent spatial-dependency (Clifford et al., 1992; Matheron, 1965; Oliver & Webster, 1986; Qin et al., 2015). A train of dunes, for instance, displays a range of spatial linkages:

1) alteration of the downstream pressure gradient and the production and dissipation rates of turbulence over bedforms (Engel,

1981; Kadota & Nezu, 1999; Unsworth et al., 2018).

2) changing the rate of sediment supply though altering the ratio of suspended to bedload fraction (Naqshband et al., 2014; Reesink et al., 2018; Schindler & Robert, 2005; Wren et al., 2007), largely a response to bedform interactions in or out of equilibrium (Blois et al., 2012; Ewing & Kocurek, 2010; Reesink et al., 2018).

The semi-variance  $\gamma(h)$  of a random function ( $G(X)$ ) is described by half the variance of the increment:

$$2\gamma(h) = \text{Var}[G(x + h) - G(x)] \quad (1)$$

Where  $G$  is the random variable of interest,  $h$  is the lag or distance with respect to  $x$ . The empirical semi variance is estimated by:

$$2\gamma(h) = \left[ \frac{1}{N-h} \right] \sum_{i=1}^{N-h} [(x_i + h) - G(x_i)]^2 \quad (2)$$

Where  $N$  is the number of observations.

The semi-variogram of three types of dune shapes is described in Figure 1. In this figure the maximum lag distance  $h_{max}$  has been set to the same length scale as the length of the bedform profiles so any variation in the shape of the dunes would be picked up.

The shape of the variogram appears to not correspond to the shape or asymmetry of the bedform – it is always a sine wave when given identical repeating bedform. This is a useful feature as we wish to test this method of quantifying equilibrium on a range of bedform shapes.

To provide a range of realistic bed states to test these ideas on, Multibeam echosounder (MBES) bathymetry from the Mekong River in Cambodia is used as it provides a range of flow discharges, bedform states and is large enough that superimposed bedforms are well resolved in the bathymetry.

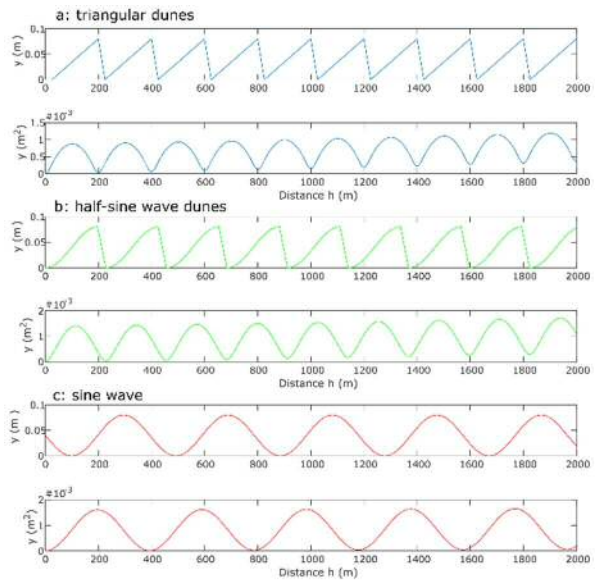


Figure 1. Three sets of idealised repeating dune shapes and their semi-variogram. The triangular dunes in a) are those form (Unsworth et al., 2018); b) half-sine wave shape is from (Nelson et al., 1993). The repeating dune shapes produce a sine-wave in the semi-variogram that is correlated to the dune troughs – where the profiles begin. The location of each trough in the semi-variograms directly corresponds to the wavelength of the bedform. The sine wave bedforms in c) provide a symmetrical bedform profile, the semi-variogram of which produces a sine wave 45 degrees out of phase.

## 1 2 METHODS

### 2.1 Study Area

The Mekong is one of the world's largest rivers, with a mean annual discharge of 457 km<sup>3</sup> draining an area of 795,000 km<sup>2</sup> and a mean annual sediment load of 1.68 t (MRC 2010; Gupta & Liew 2007; Milliman & Meade 1983). Annual rainfall is high over the northern and eastern basin (2000–4000+ mm yr<sup>-1</sup>), decreasing over the lowland areas, (~1000mm a year) (Gupta & Liew, 2007). However this rainfall is highly seasonal with 85-90% falling between June and October in the South-western monsoon season. This produces large flood events on the order of 30,000 to 60,000 m<sup>3</sup>s<sup>-1</sup> that provide 80% of the mean annual discharge for the river (MRC 2005). The Mekong River basin north of the town of Kratie, Cambodia, is largely bedrock controlled. The Mekong travels 4000km from its source (out of a total length of 4880km) before reaching the Cambodian

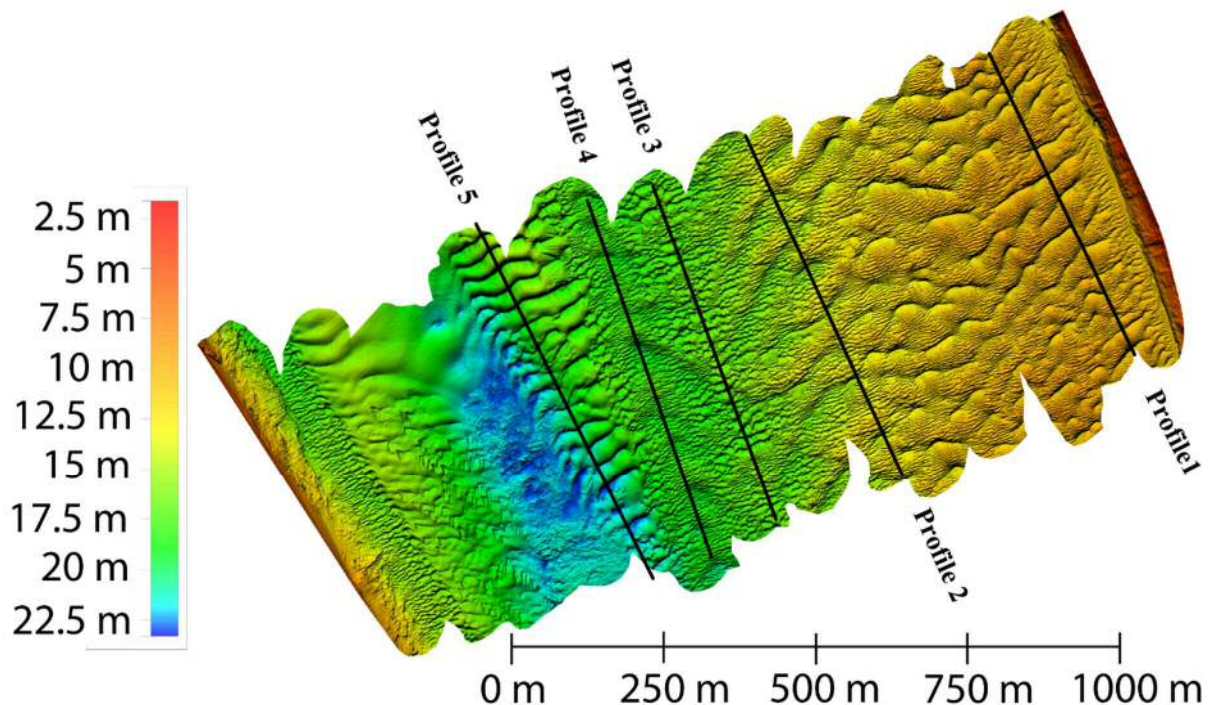


Figure 2 MBES bathymetry of the Mekong River, near Kratie 24/09/2013 at a flood peak discharge of  $\sim 60,000 \text{ m}^3 \text{s}^{-1}$ . Gridded resolution is 0.5 m.

alluvial plain near Kratie (Gupta & Liew 2007). By this point, 95% of the total Mekong flow has entered the river (MRC 2005) and the mostly bedrock nature of the upper reaches means the Mekong at Kratie receives the peak flood flows with little upstream attenuation. The inter-annual river discharge changes dramatically between monsoon and dry seasons, with changes in stage of 20-30m being common and corresponding discharge changes from  $<5,000 \text{ m}^3 \text{s}^{-1}$  in the dry season to an average of  $35,000 \text{ m}^3 \text{s}^{-1}$  in the wet which peaks at  $\sim 60,000 \text{ m}^3 \text{s}^{-1}$ .

## 2.2 Data Collection Instruments, accuracy and correction.

An MBES field survey was undertaken on the Mekong river, Cambodia  $\sim 12\text{km}$  south of the transition from bedrock channel to gravel and sand. The complex river bed bathymetry was measured with a Reson<sup>©</sup> SeaBat<sup>©</sup> SV2 7125 Multibeam (MBES) at a gridded horizontal resolution of 0.5m on 24/09/2013. The MBES positioning was measured using a real-time kinematic GPS accurate to 0.02

m horizontally and 0.03 m vertically. The manufacturer reported that depth resolution of the MBES is 1.25 cm [Reson Inc., 2009]. The head generates 512 equidistant beams and measures relative water depths over a  $150^\circ$  wide swath perpendicular to the vessel track. Navigation, orientation, and attitude data (heave, pitch, and roll) were recorded using an Applanix POS MV V3 gyroscope inertial guidance system mounted inside the vessel. The MBES data was measured and corrected concurrently using this dGPS and gyroscope setup, with additional acoustic correction using a RESON SVP sound velocity profiler.

## 3 RESULTS:

Figure 3 displays the bed profile and empirical semi-variogram of bed Profile 1 (see Figure 1 for location). In this section of the DEM, group average dune height = 0.84 m; Length = 38 m; Stoss slope =  $3.2^\circ$ ; Lee slope =  $19^\circ$ ) with mildly sinuous crest lines. This section of the river is often exposed or  $<1\text{m}$  deep in the dry season. At the time of measurement, flow stage was at its 3rd high-

est on record and all the river bed was fully submerged. This section of dunes has superimposed bedforms with group average dimensions of ~0.17 m height, 5.17 m length, stoss side angle of 7° and lee side angle of 14°. The empirical semi-variogram in Figure 3F displays zero nugget, a gaussian curve with a range of 37m– very closely matching the hand measured mean wavelength. At longer lag distances than the range, a distorted sine wave is produced, indicating divergence from ideal equilibrium.

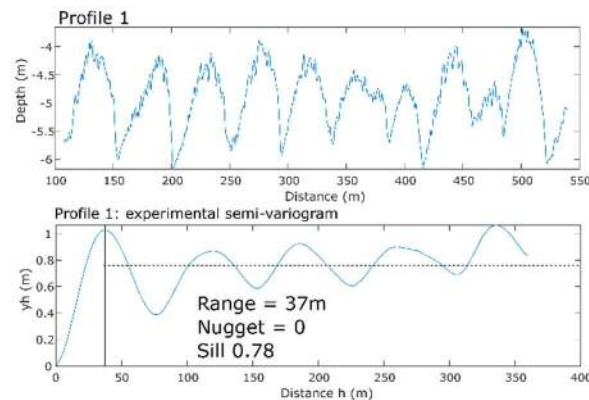


Figure 3. Displays the de-trended bed profile 1 (top) and its empirical semi-variogram (bottom).

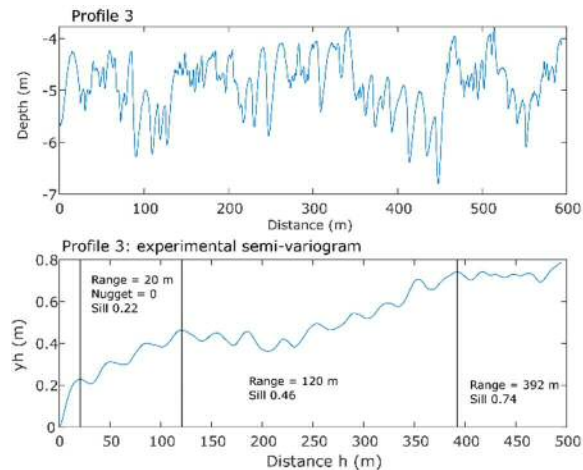


Figure 4. Displays the de-trended bed profile 3 (top) and its empirical semi-variogram (bottom).

Figure 4 displays multiple scales of bedforms superimposed on a varying mean depth. The empirical semi-variogram for this profile likewise produces several scales: 20 m, 120m and 394 m as defined by the range, and two fluctuating sill values. Hand measured group mean dune heights are 0.89 m, length 18.6m stoss slope = 9.68°, lee slope 21.9°.

Figure 5 displays the bed profile and semi-variogram across a section of barchanoid shaped dunes with considerable bedform superposition on both stoss and lee slopes. Here the semi-variogram produced two distinct sill values with elevations dissimilar to those of the host (length 78m, height 1.5m) and superimposed dunes (4.9 m long and 0.27 m high). The two distinct scales of undulating topography indicate a distinct lack of equilibrium in bedform shape but also indicate that the semi-variogram is less capable of measuring bedform scale which such a range of bedform scales.

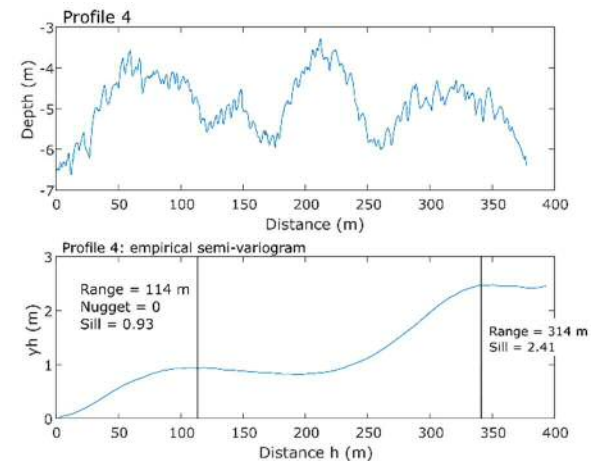


Figure 5. Displays the de-trended bed profile 4 (top) and its empirical semi-variogram (bottom).

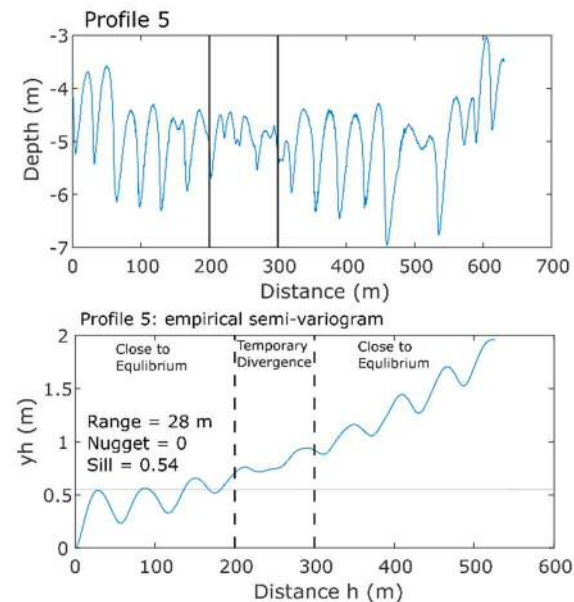


Figure 6. Displays the de-trended bed profile 5 (top) and its empirical semi-variogram (bottom).

Figure 6 displays the bed profile of a section of bed where bedforms are migrating off the tail of a mid-channel bar. There is a complete lack of superimposed bedforms in the section. The lateral extent of the uniform 2D dunes is ~170m wide at the northern extent and is gradually reduced to 70m in width at the southern extent of the survey area, as the 2D dunes merge with the secondary dunes near bed profile 4. A profile taken through the centre of this train of dunes using the MBES data gives a very consistent dune geometry (Figure 6), with group mean heights of ~ 1.6m, lengths of 34m, Stoss slope angle of 6.8° and Lee slopes of 22°. The consistency of dune shape and size is surprising considering the change in depth across the transect of 15 to 22m. Despite this change in boundary condition, the dune 2D and planform shape and size is remarkably regular and the empirical semi-variogram attests to this regularity, producing regular sine waves until ~200-300m where a sequence of smaller dunes produces a temporary sill in the semi-variogram.

To compare the empirical semi-variograms produced from the bedform profiles in Figures 3-6, Figure 7 plots them all normalised by the range of each semi-variogram alongside the idealised triangular dune profile semi-variogram of Figure 1.

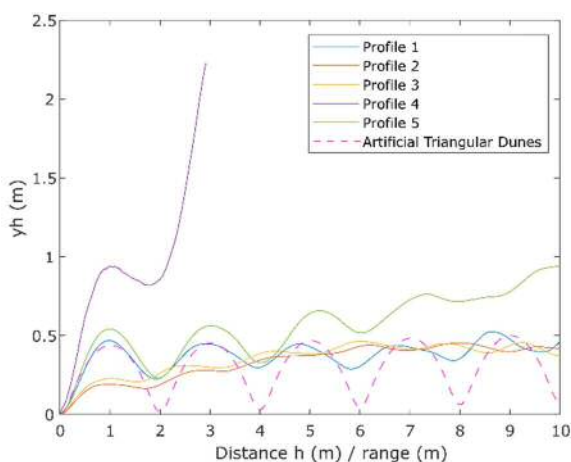


Figure 7. Empirical semi-variograms for all bedform profiles, as well as the idealised triangular dunes in Figure 1. The lag distance  $h$  has been normalised by the respective ranges.

Figure 7 Produces the observation that if you normalise the semi variogram by the range of the semi-variogram; the close-to equilibrium bedform profiles overlap. Here we see that the semi-variograms of profiles 1 and 5 most closely those of the idealised dune forms – with peaks and troughs of matching from 3-4 wavelengths. The semi-variograms of Profiles 2 and 3 are more like each other than the idealised bedform profile – suggesting a lateral connectivity to the amount of dis-equilibrium of the bed state measured in Profiles 2 and 3. Profile 4 displays the furthest match with the idealised dune semi-variogram. As seen in Figure 2 and 5, this bedform profile consists of two distinct scales of bedforms, larger barchan shapes but also smaller bedforms migrating over the barchan bedforms on both lee and stoss slopes as also seen in the Amazon (Almeida et al., 2016). The train of barchan dunes is present in this location during the dry season and with a difference in discharge of ~ 45,000 m<sup>3</sup>s<sup>-1</sup> between low and high flows in 2013 it is certainly not unreasonable that these barchan-like bedforms are being eroded at this stage.

## 5 CONCLUSIONS

By comparing the empirical semi-variogram produced from an idealised train of dunes with the empirical semi-variogram produced from a range of real bedform profiles we found that it is, at present, qualitatively possible to define the degree of (dis) equilibrium of a single bedform profile. This technique and observation opens up a new way of quantifying the state of equilibria in a train of bedforms that does not require a repeated set of measurements over time – as is uncommon in large scale MBES surveys.

## 6 ACKNOWLEDGEMENTS

This study was supported by awards NE/J021970/1, NE/J021571/1 and NE/J021881/1 from the UK Natural Environmental Research Council (NERC) and

the Academy of Finland funded project SCART (grant number 267463).

## 7 REFERENCES

- Almeida, R. P. de, Galeazzi, C. P., Freitas, B. T., Janikian, L., Ianniruberto, M., & Marconato, A. 2016. Large barchanoid dunes in the Amazon River and the rock record: Implications for interpreting large river systems. *Earth and Planetary Science Letters*, 454, 92–102.
- Baas, J. H. 1994. A Flume Study on the Development and Equilibrium Morphology of Current Ripples in Very Fine Sand. *Sedimentology*, 41(2), 185–209.
- Baas, J. H. 1999. An empirical model for the development and equilibrium morphology of current ripples in fine sand. *Sedimentology*, 46, 123–138.
- Bartholdy, J., Bartholomae, A., & Flemming, B. 2002. Grain-size control of large compound flow-transverse bedforms in a tidal inlet of the Danish Wadden Sea. *Marine Geology*, 188, 391–413.
- Blois, G., Barros, J. M., Christensen, K. T., & Best, J. L. 2012. An experimental investigation of 3D subaqueous barchan dunes and their morphodynamic processes. In *Marine and River Dune Dynamics 4* (pp. 35–38).
- Clifford, N. J., Robert, A., & Richards, K. S. 1992. Estimation of flow resistance in gravel-bedded rivers: A physical explanation of the multiplier of roughness length. *Earth Surface Processes and Landforms*, 17(2), 111–126.
- Dreano, J., Valance, A., Lague, D., & Cassar, C. 2010. Experimental study on transient and steady-state dynamics of bedforms in supply limited configuration. *Earth Surface Processes and Landforms*, 35(14), 1730–1743.
- Engel, P. 1981. Length of flow separation over dunes. *Journal of Hydraulic Division. American Society of Civil Engineers*, 107(HY10), 113–1143.
- Ewing, R. C., & Kocurek, G. A. 2010. Aeolian dune interactions and dune-field pattern formation: White Sands Dune Field, New Mexico. *Sedimentology*, 57, 1199–1219.
- Flemming, B. W. 2000. The role of grain size, water depth and flow velocity as scaling factors controlling the size of subaqueous dunes. In I. A. T. & T. G. (eds). (Ed.), *Proceedings of Marine Sandwave Dynamics* (pp. 55–61). Lille, France.
- Kadota, A., & Nezu, I. 1999. Three-dimensional structure of space-time correlation on coherent vortices generated behind dune crest. *Journal of Hydraulic Research*, 37(1), 59–80.
- Martin, R. L., & Jerolmack, D. J. (2013). Origin of hysteresis in bed form response to unsteady flows. *Water Resources Research*, 49(3), 1314–1333.
- Matheron, G. 1965. *Les Variables Regionalisees et Leur Estimation*. Paris: Masson.
- Myrow, P. M., Jerolmack, D. J., & Perron, J. T. 2018. Bedform Disequilibrium. *Journal of Sedimentary Research*, 88(9), 1096–1113.
- Naqshband, S., Ribberink, J. S., Hurther, D., & Hulscher, S. J. M. H. 2014. Bed load and suspended load contributions to migrating sand dunes in equilibrium. *Journal of Geophysical Research: Earth Surface*, 119(5), 1043–1063.
- Nelson, J. M., McLean, S. R., & Wolfe, S. R. 1993. Mean Flow and Turbulence Fields Over Two-Dimensional Bed Forms. *Water Resources Research*, 29(12), 3935–3953.
- Oliver, M. A., & Webster, R. 1986. Semi-Variogram for modelling the spatial pattern of landform and soil properties. *Earth Surface Processes and Landforms*, (11), 491–501.
- Perillo, M. M., Best, J. L., Yokokawa, M., & Sekiguchi, T. 2014. A unified model for bedform development and equilibrium under unidirectional, oscillatory and combined-flows. *Sedimentology*, 7(61), 2063–2085.
- Qin, J., Wu, T., & Zhong, D. 2015. Spectral behavior of gravel dunes. *Geomorphology*, 231, 331–342.
- Reesink, A. J. H., Parsons, D. R., Ashworth, P. J., Best, J. L., Hardy, R. J., Murphy, B. J., et al. 2018. The adaptation of dunes to changes in river flow. *Earth-Science Reviews*, 185, 1065–1087.
- Schindler, R. J., & Robert, A. 2005. Flow and turbulence structure across the ripple-dune transition: an experiment under mobile bed conditions. *Sedimentology*, 52(3), 627–649.
- Unsworth, C. A., Parsons, D. R., Hardy, R. J., Reesink, A. J. H., Best, J. L., Ashworth, P. J., & Keevil, G. M. 2018. The Impact of Nonequilibrium Flow on the Structure of Turbulence Over River Dunes. *Water Resources Research*, 54(9), 6566–6584.
- Wren, D. G., Kuhnle, R. A., & Wilson, C. G. 2007. Measurements of the relationship between turbulence and sediment in suspension over mobile sand dunes in a laboratory flume. *Journal of Geophysical Research*, 112(F3).

# Investigating idealized modelling of estuarine sand waves

Wessel M. van der Sande *University of Twente, Enschede, The Netherlands –*

*w.m.vandersande@student.utwente.nl*

Pieter C. Roos *University of Twente, Enschede, The Netherlands – p.c.roos@utwente.nl*

Suzanne J.M.H. Hulscher *University of Twente, Enschede, The Netherlands –*

*s.j.m.h.hulscher@utwente.nl*

**ABSTRACT:** Here we propose research to investigate the behavior of estuarine sand waves and how this is changed through human interventions in estuaries. To this end, we will develop idealized process-based models that describe the motion of water and sediment processes in estuaries. These models will account for processes that are known to play a role in similar bedforms in seas and rivers. A linear stability analysis of the flat bottom will reveal mechanisms of formation of sand waves; a nonlinear model will explain their equilibrium configuration. Scenarios will show how the bedforms behave under human interventions and climate change.

## 1 INTRODUCTION

Estuaries are hydrodynamically complex regions where a river meets saline water. In tidally influenced shallow (<100m depth) estuaries, sand waves can be found, which are large rhythmic bedforms. Their height and length are greatly site-dependent – with heights of about 2m in the Weser estuary, Germany (Nasner, 1974) versus 17m in the Long Island Sound (Fenster et al., 1990). Their height relative to the water depth shows more similarity amongst estuaries.

Estuarine sand waves are commonly asymmetric, with the steep slope facing the direction of migration (Bokuniewicz et al., 1977; Ludwick, 1972). In the Long Island Sound (U.S.), their migration rates are of the order of 50m per year (Bokuniewicz et al., 1977), and in the Bahía Blanca estuary (Argentina) they were measured to migrate 33m per year (Aliotta and Perillo, 1987).

Estuaries are the gateway to their hinterland, and therefore they are often used as harbor entrance (which is the case for e.g. the Rhine or Scheldt). To safely navigate in these estuaries, crests of sand waves are often dredged (Figure 1). Because sand waves migrate and regrow, costly surveillance missions need to be performed



Figure 1: Animation of a dredging ship (image from B3D Design)

regularly to ensure navigational safety. Moreover, dredging greatly alters the morphodynamical system and the estuarine ecology (Kennish, 2002). Estuaries function as spawning, feeding and nursery sites for a variety of species (Beck et al., 2001), and are being used as entry to riverine habitats for migratory fish, such as salmon. Therefore, optimizing the efficiency of dredging activities in estuaries is essential to preserve an ecosystem that is vital for the existence of several species.

Furthermore, sand waves are a major influencing factor of hydrodynamics (and vice versa). The water's movement is the leading factor in salt intrusion and flood risks, problems which humans are increasingly encountering (Ghosh Bobba, 2002; Townend and Pethick, 2002). How

sand waves influence these problems exactly is not yet known. Moreover, the sand wave-hydrodynamics interaction may be altered by changing hydrodynamical properties. Three ways that this might happen are anticipated: i) the effects of climate change: sea level rise and increased discharge variability (Booij, 2005; Church and White, 2006), ii) changes in the estuaries' planform geometry through land reclamation or widening of the seaway, and iii) changes in sediment input due to sediment trapping in reservoirs.

In summary, it is essential to know more about estuarine sand waves to:

1. Perform dredging more cost-efficiently and with minimal effect to the environment;
2. Foresee potential changes in the sand wave-hydrodynamics interaction due to:
  - i. Hydrodynamic effects of climate change;
  - ii. Land reclamation or broadening of the seaway;
  - iii. Sediment trapping upstream in man-made reservoirs

## 2 WHAT DO WE WANT TO UNCOVER?

The main aim of the proposed research is to provide universal explanations of estuarine sand wave formation and equilibrium configuration and to evaluate the long-term effect of human interventions on those. This

is subdivided into the following questions:

- Q1.What are the dominant hydrodynamic behavior and sediment transport processes in estuaries?
- Q2.What are the underlying physical mechanisms of formation of sand waves in estuaries?
- Q3.What are the underlying physical mechanisms of dynamic equilibrium configuration of sand waves in estuaries?
- Q4.What are the effects of anthropogenic influences on estuarine sand waves, such as dredging and climate change effects?

Figure 2 shows an overview of the objectives of the proposed research, and how the methodology (laid out below) relates to these.

## 3 OUR APPROACH

Central to the methodology will be the development of idealized process-based models. These models will be built on knowledge acquired in the first objective, and will then be applied to execute the other objectives (Figure 2).

The models will describe the motion of water in an estuary that affects the bed by mobilizing and depositing sediment. An idealized model is convenient to reveal physical mechanisms behind sand wave formation and equilibrium configuration. Also, idealized models are computationally relatively cheap to run. This makes it easily

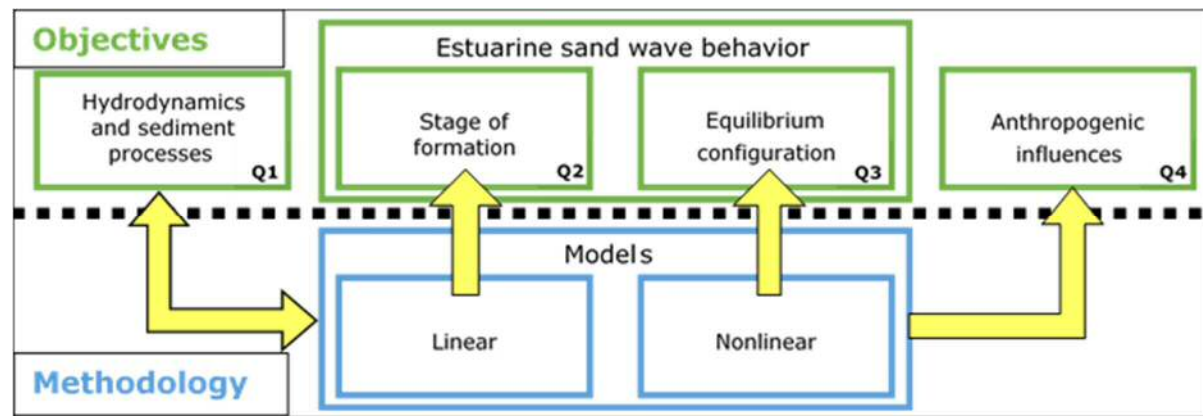


Figure 2. Visualization of the proposed research, linking the objectives to the methodologies. Hydrodynamic behaviour and sediment processes are required to develop the idealized process-based models, model tests will show whether these descriptions contain the right amount of detail. A linear stability analysis of the model will reveal mechanisms of formation; the nonlinear model will explain the equilibrium configuration of estuarine sand waves. The model parameters can then be tuned to mimic human interventions.

feasible to conduct sensitivity analyses with respect to parameters of interest (such as sediment size, river discharge statistics, and geometry) and to look at long-term morphological developments, either natural or after human interventions. Moreover, during the model formulation an appropriate turbulence model can be chosen, which will be important to correctly describe complex flow patterns such as flow separation at steep slopes. Complex process-based models are less suitable to reach the objectives of this research, because those are computationally expensive.

### 3.1 Hydrodynamic behavior and sediment transport processes

Knowledge of marine sand waves and river dunes will be combined and elaborated to choose descriptions of hydrodynamic behavior and sediment processes with which the following research steps can be executed (Figure 3). This requires finding descriptions which are accurate enough to later explain sand wave behavior, yet do not include processes that are irrelevant in this respect. It is expected that this investigation will be executed iteratively with the research activities lined out in the next two sections.

Central to this subproject will be finding a correct description of flow separation. Flow separation has proven to be highly relevant in river dune formation (Paarlberg et al., 2007). In tidal environments, this phenomenon is much more complex due to reversal of the flow when the tide changes. This can lead to time-varying flow separation (Lefebvre et al., 2013). This research will provide a proper formulation of flow separation either through a suitable turbu-

lence model or in a parametrized way. Also, water motions responsible for marine sand wave growth may need to be accounted for; these too require appropriate turbulence modeling (Borsje et al., 2013; Komarova and Hulscher, 2000).

### 3.2 Underlying mechanisms of formation

With the descriptions found previously, a coupled model will be developed. This will be employed to perform a linear stability analysis that explains formation of estuarine sand waves. The results will be analyzed to understand how the hydrodynamics interact with the bedforms. The wavelength and orientation of the modeled sand waves will be verified by comparing these with open source data from several U.S. estuaries with different characteristics (NOAA, 1998). This data has a horizontal resolution of 30m, which is high enough to determine the wavelength and orientation of real-world estuarine sand waves.

### 3.3 Underlying mechanisms of dynamic equilibrium configuration

To investigate the equilibrium configuration (i.e. height and shape) of estuarine sand waves, another idealized model will be developed that includes nonlinear interactions between flow and the bed. These occur when the height of the bedforms becomes significant compared to the water depth. This is also an important factor that determines the equilibrium configuration of marine sand waves and river dunes, and hence nonlinear models have previously been developed and employed to explain these bedforms (e.g. Ji and Mendoza, 1997; van den Berg et al., 2012; Campmans et al., 2018).

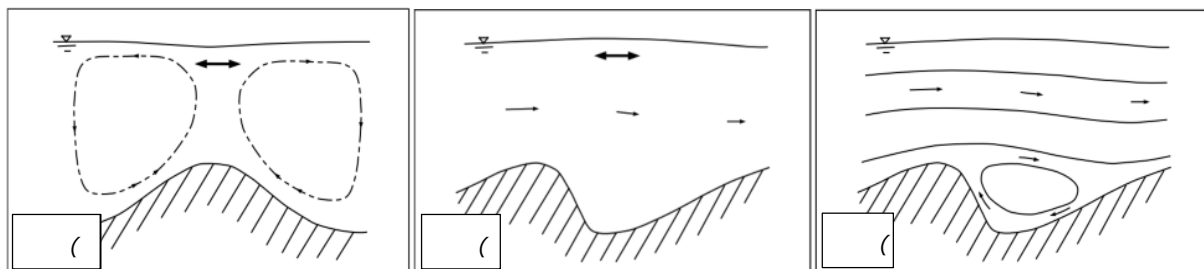


Figure 3: Schematized presentation of the shape and flow profiles (solid arrows) of a) marine sand waves, with dashed circulatory arrows showing residual flows that cause sand wave growth b) estuarine sand waves, with the question mark indicating that the underlying hydrodynamic mechanisms that govern the behavior of these bedforms are not yet understood and c) river dunes including flow separation in the trough (adapted from Hulscher and Dohmen-Janssen, 2005).

These models have the advantage that they can describe equilibrium configurations of bedforms, but at the cost of computation time.

The results of this model will be analyzed to understand how hydrodynamics interact with full-grown estuarine sand waves. The wavelength, orientation, height and shape of the modeled sand waves will be compared with the data on U.S. estuaries mentioned in previous section to establish a reasonable case for the model.

### 3.4 Effects of anthropogenic influences

The previously proposed models will be used by varying their parameters to describe the effects on the morphological timescale (decades) of the following human interventions: i) land reclamation and seaway widening (geometry changes), ii) reduction of riverine sediment supply (changing sediment size/input quantity), iii) dredging (changes to the bottom profile) and iv) climate change effects (sea level rise and increased discharge variability).

## 4 REFERENCES

- Aliotta, S., Perillo, G.M.E., 1987. A sand wave field in the entrance to Bahia Blanca Estuary, Argentina. *Marine Geology* 76, 1–14. [https://doi.org/10.1016/0025-3227\(87\)90013-2](https://doi.org/10.1016/0025-3227(87)90013-2)
- Beck, M.W., Heck, K.L., Able, K.W., Childers, D.L., Eggleston, D.B., Gillanders, B.M., Halpern, B., Hays, C.G., Hoshino, K., Minello, T.J., Orth, R.J., Sheridan, P.F., Weinstein, M.P., 2001. The Identification, Conservation, and Management of Estuarine and Marine Nurseries for Fish and Invertebrates. *Bioscience* 51, 633–641. [https://doi.org/10.1641/0006-3568\(2001\)051\[0633:TICAMO\]2.0.CO;2](https://doi.org/10.1641/0006-3568(2001)051[0633:TICAMO]2.0.CO;2)
- Bokuniewicz, H.J., Gordon, R.B., Kastens, K.A., 1977. Form and migration of sand waves in a large estuary, Long Island Sound. *Marine Geology* 24, 185–199. [https://doi.org/10.1016/0025-3227\(77\)90027-5](https://doi.org/10.1016/0025-3227(77)90027-5)
- Booij, M.J., 2005. Impact of climate change on river flooding assessed with different spatial model resolutions. *Journal of Hydrology* 303, 176–198. <https://doi.org/10.1016/j.jhydrol.2004.07.013>
- Borsje, B.W., Roos, P.C., Kranenburg, W.M., Hulscher, S.J.M.H., 2013. Modeling tidal sand wave formation in a numerical shallow water model: The role of turbulence formulation. *Continental Shelf Research* 60, 17–27. <https://doi.org/10.1016/j.csr.2013.04.023>
- Campmans, G.H.P., Roos, P.C., de Vriend, H.J., Hulscher, S.J.M.H., 2018. The Influence of Storms on Sand Wave Evolution: A Nonlinear Idealized Modeling Approach. *Journal of Geophysical Research: Earth Surface* 123, 2070–2086. <https://doi.org/10.1029/2018JF004616>
- Church, J.A., White, N.J., 2006. A 20th century acceleration in global sea-level rise. *Geophysical Research Letters* 33, 94–97. <https://doi.org/10.1029/2005GL024826>
- Fenster, M.S., Fitzgerald, D.M., Bohlen, W.F., Lewis, R.S., Baldwin, C.T., 1990. Stability of giant sand waves in eastern Long Island Sound, U.S.A. *Marine Geology* 91, 207–225. [https://doi.org/10.1016/0025-3227\(90\)90037-K](https://doi.org/10.1016/0025-3227(90)90037-K)
- Ghosh Bobba, A., 2002. Numerical modelling of salt-water intrusion due to human activities and sea-level change in the Godavari Delta, India. *Hydrological Sciences Journal* 47, S67–S80. <https://doi.org/10.1080/02626660209493023>
- Ji, Z.G., Mendoza, C., 1997. Weakly nonlinear stability analysis for dune formation. *Journal of Hydraulic Engineering* 123, 979–985.
- Kennish, M.J., 2002. Environmental threats and environmental future of estuaries. *Environmental Conservation* 29, 78–107. <https://doi.org/10.1017/S0376892902000061>
- Komarova, N.L., Hulscher, S.J.M.H., 2000. Linear instability mechanisms for sand wave formation. *Journal of Fluid Mechanics* 413, 219–246. <https://doi.org/10.1017/S0022112000008429>
- Lefebvre, A., Ernstsen, V.B., Winter, C., 2013. Estimation of roughness lengths and flow separation over compound bedforms in a natural-tidal inlet. *Continental Shelf Research* 61–62, 1–14. <https://doi.org/10.1016/j.csr.2013.04.030>
- Ludwick, J.C., 1972. Migration of Tidal Sand Waves in Chesapeake Bay Entrance, in Swift, D.J., Duane, D.B., Pilkey, O.H. (Eds.), *Shelf Sediment Transport*. Hutchinson and Ross, Stroudsburg, pp. 377–410.
- Nasner, H., 1974. Prediction of the Height of Tidal Dunes in Estuaries. *Coast. Engin.* 2, 1036–1050.
- NOAA, 1998. U.S. Estuarine Bathymetric Data [WWWDocument]. URL <https://www.ngdc.noaa.gov/mgg/bathymetry/estuarine/index.html> (accessed 4.25.18).
- Paarberg, A.J., Dohmen-Janssen, C.M., Hulscher, S.J.M.H., Terme, P., 2007. A parameterization of flow separation over subaqueous dunes. *Water Resources Research* 43, 1–10. <https://doi.org/10.1029/2006WR005425>
- Townend, I., Pethick, J., 2002. Estuarine flooding and managed retreat. *Philosophical Transactions of the Royal Society A: Mathematical, Physical and Engineering Sciences* 360, 1477–1495. <https://doi.org/10.1098/rsta.2002.1011>
- van den Berg, J., Sterlini, F., Hulscher, S.J.M.H., van Damme, R., 2012. Non-linear process based modelling of offshore sand waves. *Continental Shelf Research* 37, 26–35. <https://doi.org/10.1016/j.csr.2012.01.012>

# Environmental controls on the spatial variation in sand wave morphology and dynamics on the Netherlands Continental Shelf

Thaiënne van Dijk <sup>1</sup>Deltires, Utrecht, Netherlands – thaienne.vandijk@deltares.nl <sup>2</sup>University of Illinois in Urbana-Champaign, Champaign, IL, USA – vandijk@illinois.edu

John Damen University of Twente\*, Enschede, Netherlands (\*now VGZ, Arnhem) mail@johndamen.nl

Suzanne Hulscher Univeristy of Twente, Enschede, Netherlands – s.j.m.h.hulscher@utwente.nl

Tim Raaijmakers Deltires, Delft, Netherlands – tim.raaijmakers@deltares.nl

Tom Roetert Deltires, Delft, Netherlands – tom.roetert@deltares.nl

Jan-Joost Schouten Deltires, Delft, Netherlands – janjoost.schouten@deltares.nl

**ABSTRACT:** The morphology and dynamics of sand waves on continental shelves may interfere with navigation and offshore constructions. Understanding the controlling parameters of the spatial variation in sand wave morphology and dynamics will allow for better predictions of bed dynamics and thereby helps the optimisation of monitoring and maintenance strategies. Previous investigations are mostly local studies. However, for the explanation of spatial variation on continental shelves, large-scaled investigations are required. Quantified sand wave morphologies on the Netherlands Continental Shelf (NCS) and correlated environmental parameters reveal that sediment grain size and transport mode seem the controlling parameter/process. These also reveal that sand waves on the NCS are relatively high compared to the empirical relationship of Allen (1968). For sand wave dynamics, these relationships still have to be investigated. Preliminary results of migration rates on the Netherlands Continental Shelf are between 0 and 20 m/yr.

## 1 INTRODUCTION

Sand waves are a common feature on sandy continental shelves. The increase in sand wave heights may interfere with navigation. Certainly with increasing draughts of offshore vessels in shallow seas, such as the Southern Bight of the North Sea, calling on major harbours such as Rotterdam, water depths become increasingly critical. The migration of sand waves is important in the design and maintenance of offshore wind farms, cables and pipelines.

North Sea bathymetry shows that the occurrence and morphology of sand waves is spatially variable, and the analyses of time series show that also dynamics are spatially variable. A large-scaled study of vertical nodal seabed dynamics at the Netherlands Continental Shelf (NCS) revealed that sand waves are the most dynamic feature offshore, due to sand wave migration (Van Dijk

et al., 2012a). By understanding the processes that control these spatial variations, we can improve risk-based monitoring policies of continental shelves and the maintenance of fairways (Fig. 1).

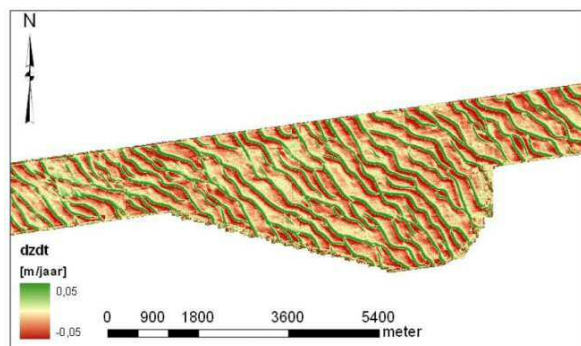


Figure 1. Vertical bed dynamics (m/yr) revealing sand wave migration in the Eurogeul, the approach channel to Rotterdam harbour (from Van Dijk et al., 2012b).

In this paper, quantified sand wave morphology of all sand waves on the NCS at 25-m resolution and correlations to the spatial

variation in environmental parameters and processes (Damen et al., 2018a) are presented. In addition, preliminary results of morphodynamics of sand waves may be investigated in a similar way.

## 2 METHODS AND RESULTS

### 2.1 Morphology

Using a scanning technique in the direction perpendicular to sand wave crests along transects 25 m apart, the quantification of all sand waves results in morphologic maps of sand wave lengths, heights and asymmetries (Damen et al., 2018a; heights are displayed in Fig. 2).

These maps show that the longest and lowest sand waves occur along the Holland coast, where also asymmetries are the largest. Distribution plots reveal the limits of sand wave morphologies for all sand waves on the NCS (Fig. 3).

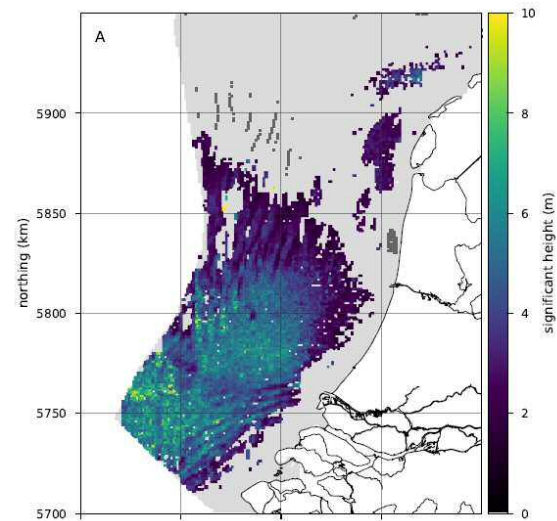


Figure 2. Quantified sand wave heights per  $\text{km}^2$  on the Netherlands Continental Shelf (after Damen et al., 2018a). Results of all individual sand waves are available in a repository (Damen et al., 2018b).

#### i. 2.1.1 Correlation to primary parameters

For the correlation of morphology to primary environmental parameters (depth,

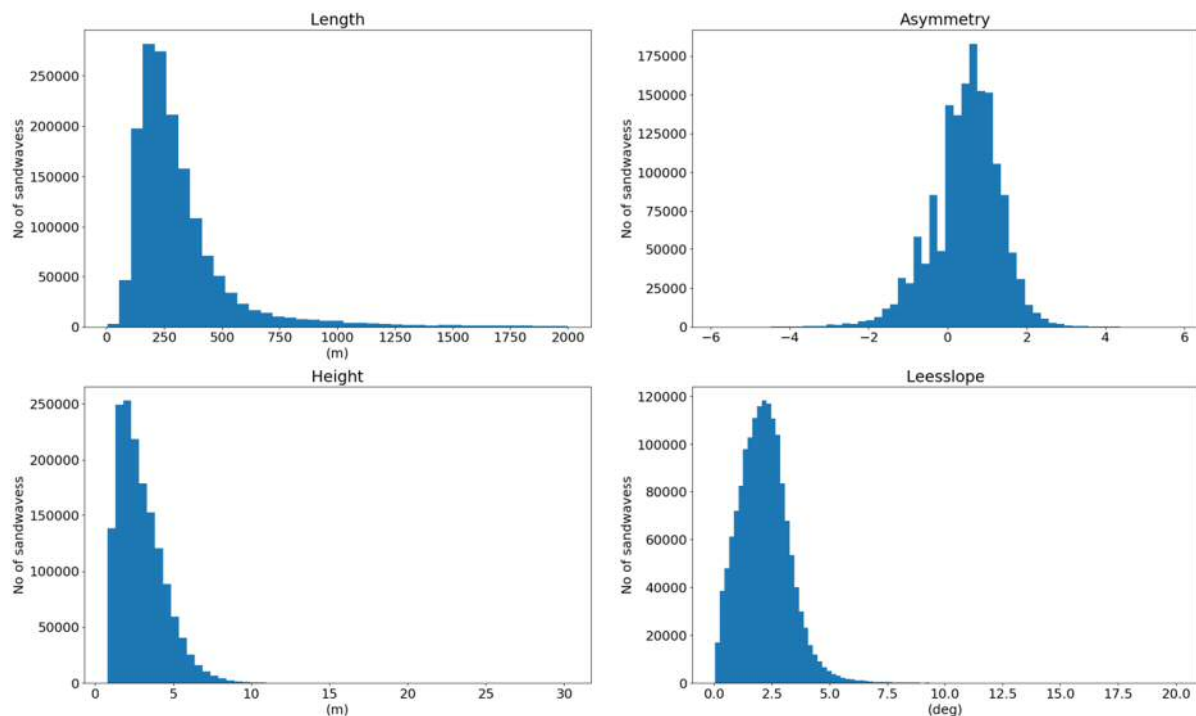


Figure 3. Distribution plots of lengths, asymmetries, heights and lee-slope angles of all sand waves on the NCS ( $n = 1.5$  million observations, after data repository Damen et al., 2018b). Most common lengths are 150-250 m, most common heights are 1-2 m, most sand waves are asymmetric, and lee-side slopes are mostly between 0.5 and 5 degrees, although slopes up to more than 11 degrees occur.

tidal current velocity, residual current, significant surface wave height and median grain size), sand waves were binned, in order to separate areas where four out of five parameters are more or less ‘constant’ and where merely one parameter varies. Most correlation results of the primary parameters with morphology were weak, thereby falsifying the hypotheses, except for median grain size and sand wave height (Fig. 4), and for the tidal (M2) current velocity and sand wave length.

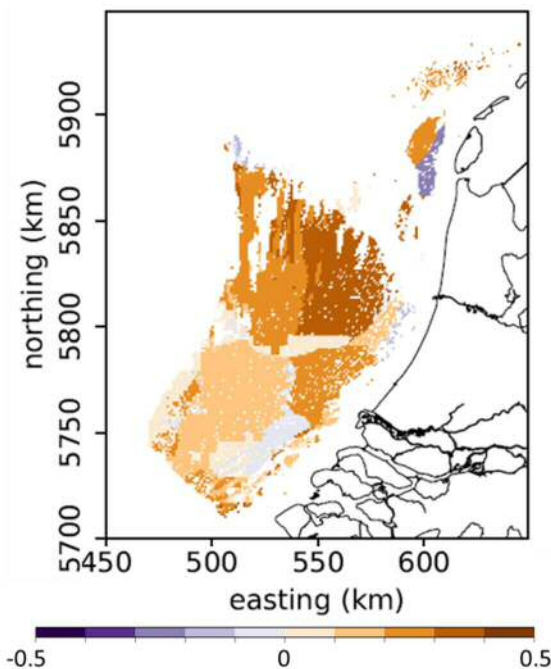


Figure 4. Correlation values (colour scale) of median grain size ( $D_{50}$ ) and sand wave height in bins of ‘constant’ water depth, tidal current and wave regimes (after Damen et al., 2018a).

Bi-variate plots were used to visualise the strengths of the correlations and to reveal limits of local conditions for sand wave occurrence and morphology.

The correlations, however, do not explain the variation in morphology in full. An inverse approach, of identifying areas of contrasting sand wave morphology and finding out the ranges and limits of local environmental parameters may provide additional insight.

## 2.1.2 Correlation to processes of sediment transport

Since the primary parameters were not conclusive, sand wave morphology was correlated to marine processes, such as the Rouse number of the mode of transport, Shields parameters of incipient motion for both the tide and waves, and the residual bed load transport (Damen et al., 2018a). Out of these, the Rouse number seems the dominant factor for sand wave lengths, and heights, as well as asymmetries.

## 2.2 Sand wave dynamics

Sand wave migration rates were determined from single- and/or multibeam time series at a number of sites distributed on the NCS and were found to be between 0 m/yr (stable) offshore Rotterdam and 20 m/yr near the Wadden island Texel. Migration directions were found to be to the south-west and to the north-east both on the larger shelf scale and more locally, the latter related to larger-scaled morphology, such as sand banks (e.g., Fig. 5). Although, to date not as quantitative as the morphologic results, the spatial variation in sand wave migration may be correlated to environmental parameters in a similar way as was done for morphology.

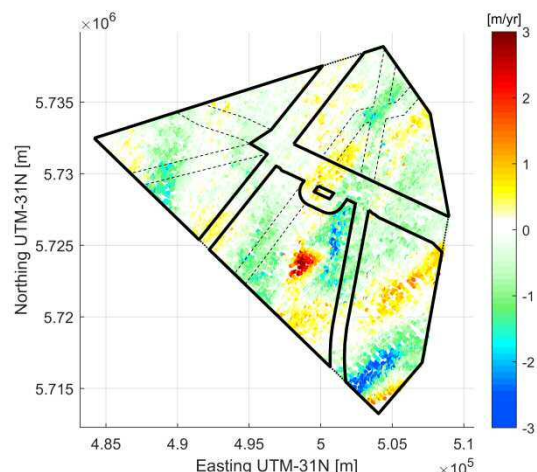


Figure 5. Example of opposite sand wave migration directions for the offshore wind farm site Borssele, over the period 2000 to 2015, based on 29522 transects (updated from Deltares, 2015). Colour scale is sand wave migration rates (m/year) with negative values (blue) indicating sand wave migration towards southwest and positive values (red) indicating sand wave migration towards northeast.

### 3 DISCUSSION

When the morphologies of sand waves on the NCS are compared to sand waves on other continental shelves, sand waves on the NCS are relatively high, exceeding the empirical relationship of Allen (1968) for heights as function of water depth,  $H = 0.086d^{1.19}$ . However, giant sand waves reported in the literature (e.g. Franzetti et al., 2013) exceed these heights even more. The new data reveal a new empirical relationship on steepness (Damen et al., 2018; see also Flemming, 2000).

### 4 CONCLUSIONS

The quantification of all sand waves on the Netherlands Continental Shelf reveals the distributions of sand wave lengths, heights, asymmetries and lee-slope angles. Correlating the primary parameters depth, tidal current velocity, residual current, significant surface wave height and median grain size to the morphology and dynamics of sand waves, most parameters were weak, except for median grain size (D50), which seems to control the occurrence and heights of sand waves, and the tidal current velocity seems to control the wavelength. Of the sedimentary processes, the Rouse number of sediment transport mode seems to control lengths, heights and asymmetries.

Sand wave migration rates vary between 0 m/yr near Rotterdam and 20 m/yr near Texel. Where the morphology seems to be controlled by D50, Shields parameter for tides, and the residual bed load transport, migration rates may be explained in a similar manner.

### 5 ACKNOWLEDGEMENTS

Data of the NCS were made available by the Netherlands Hydrographic Office (NLHO) of the Royal Netherlands Navy, Ministry of Defence, and Rijkswaterstaat (RWS), Ministry of Infrastructure and Water Management. The Borssele bathymetric

surveys were financed by the Dutch Ministry of Economic Affairs (RVO.nl). The work on the morphology of sand waves was part of John Damen's Ph.D. research at the University of Twente, within the project SMARTSEA (grant number 13275), which was in part funded by the Netherlands Organisation for Scientific Research (NWO), and co-financed by NLHO and RWS. The work on sand wave dynamics was done in applied projects at Deltares, with several project teams.

### 2. 6 REFERENCES

- Allen, J.R.L. (1968). Current Ripples. Amsterdam: North Holland Company, 433 pp.
- Damen, J.M., Van Dijk, T.A.G.P. & Hulscher, S.J.M.H. (2018a). Spatially varying environmental properties controlling observed sand wave morphology. *Journal of Geophysical Research: Earth Surface*, 123, 262–280. <https://doi.org/10.1002/2017JF004322>
- Damen, J.M., Van Dijk, T.A.G.P. and Hulscher, S.J.M.H. (2018b). Replication Data for: Spatially varying environmental properties controlling observed sand wave morphology. 4TU.Centre for Research Data (repository), <https://doi.org/10.4121/uuid:0d7e016d-2182-46ea-bc19-cdfda5c20308>.
- Flemming, B. W. (2000). The role of grain size, water depth and flow velocity as scaling factors controlling the size of subaqueous dunes. In A. Trentesaux, & T. Garlan (Eds.): Proc. 1st Intern. workshop on Marine Sandwave Dynamics, . France: University of Lille 1.
- Franzetti, M., Le Roy, P., Delacourt, C., Garlan, T., Cancouët, R., Sukhovich, A. and Deschamps, A. (2013). Giant dune morphologies and dynamics in a deep continental shelf environment: Example of the banc du four (Western Brittany, France). *Marine Geology*, 346, 17-30.
- Deltares (2015). Morphodynamics of Borssele Wind Farm Zone WFS-I and WFS-II – prediction of seabed level changes between 2015 and 2046, Deltares Report 1210520-000-HYE-0004, 62 pp. <http://offshorewind.rvo.nl/file/download/33453652>.
- Van Dijk, T.A.G.P., Kleuskens, M.H.P., Dorst, L.L., et al., (2012a). Quantified and applied sea-bed dynamics of the Netherlands Continental Shelf and the Wadden Sea. NCK-days 2012 conference proceedings, p. 223 – 227. <http://proceedings.utwente.nl/202/>
- Van Dijk, T.A.G.P., Van der Mark, C.F., Doornenbal, P.J., et al. (2012b). Onderzoek Meetstrategie en Bodemdynamiek. Deltares report 1203749-000-BGS-0006, 92 pp.

# On shapes and breaks: modelling the transient evolution of tidal sandbanks

Thomas J. van Veelen *Swansea University, Swansea, UK* – *thomas.vanveelen@swansea.ac.uk*

Pieter C. Roos *University of Twente, Enschede, Netherlands* – *p.c.roos@utwente.nl*

Suzanne J.M.H. Hulscher *University of Twente, Enschede, Netherlands* - *s.j.m.h.hulscher@utwente.nl*

**ABSTRACT:** Tidal sandbanks are large-scale dynamic bed forms observed in conjunction with sandwaves in shallow shelf seas such as the North Sea. Their evolution may display a single bank breaking into two or more banks, for which two mechanisms have been proposed in the literature and described in qualitative terms. However, there is no generic support from process-based models. Here we present a new idealised process-based model study into the transient evolution of tidal sandbanks. Key features are the inclusion of nonlinear dynamics for topographies that vary in both horizontal directions, and the focus on long-term evolution (centuries and longer). From our model results, we identify two paths of evolution, leading to either bank-breaking or a meandering crest. Which of these paths occurs is found to depend on initial topography, with bank orientation and bank length as major control parameters.

## 1 INTRODUCTION

Beds of shallow shelf seas typically show a wide variety of rhythmic bed forms, among which sandwaves and sandbanks are the largest (Reineck et al., 1971). In many places sandwaves and sandbanks exist together and interact. Understanding sandbank dynamics is therefore important for the study of sandwaves as it affects the environmental conditions (e.g. flow characteristics and water depth) in which sandwaves develop. In particular, the circulation around sandbanks has been found to adjust sandwaves (McCave & Langhorne, 1982). Furthermore, analysis of the Westhinder bank by Deleu et al. (2004) showed sandbanks affect the way sandwaves grow and migrate.

A key feature in the evolution of sandbanks is that they may break. This is a complex process that strongly impacts the topography of the seabed. Two mechanisms have been proposed to describe this behaviour. Caston (1972) examined the shapes of the

Norfolk Banks and suggested these represented different stages in the process of an isolated bank breaking into three separate banks. Alternatively, Smith (1988) proposed a mechanism of breaking into two separate banks after studying a kink in the North Hinder Bank. However, both hypotheses strongly rely on the interpretation of site-specific observations and have not been reproduced by process-based models.

Therefore, we developed a new idealised model, which includes tide-topography interactions, captures long-term nonlinear dynamics and allows for topographies that vary in both horizontal directions. Rather than focussing on equilibrium profiles, our interest lies in the transient evolution during which sandbanks display growth, expansion and change in shape. We focus on the qualitative behaviour, specifically whether bank-breaking occurs and how initial bank topography and hydrodynamic settings affect bank evolution.

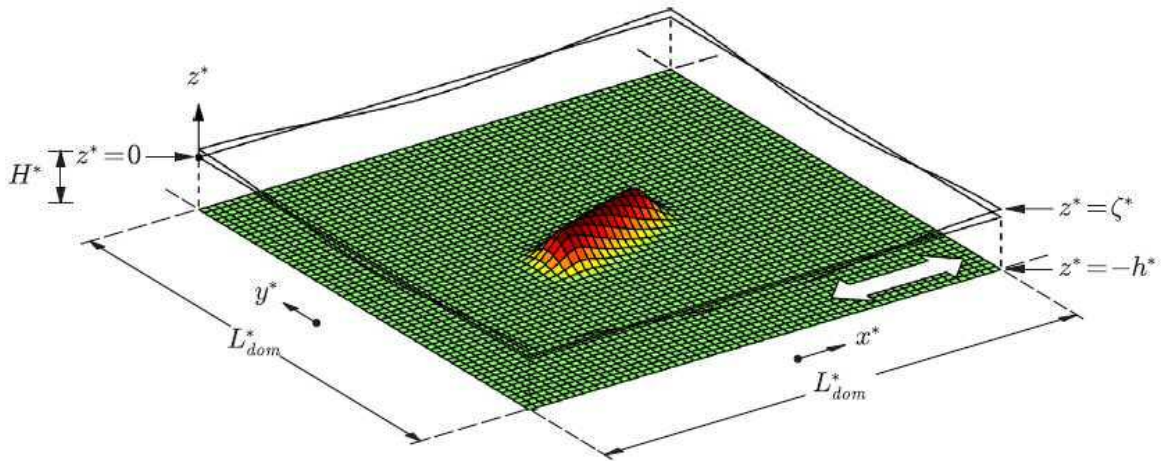


Figure 1. Definition sketch of the model geometry, showing a spatially periodic domain of dimension  $L_{dom}^*$ . The ambient water depth is  $H$ , the free surface is denoted by  $z^* = \zeta^*$  and the bed level by  $z^* = -h^*$ . A sandbank is imposed in the middle of the domain (see text). The basic flow (flow over a horizontal flat bed) is parallel to the  $x$ -axis, as denoted by the white double-headed arrow.

## 2 METHODS

The model geometry (Fig. 1) features a sandbank on an otherwise flat seabed. The hydrodynamics  $\mathbf{u} = (u, v)$  in the periodic domain are governed by the depth-averaged shallow water equations, including acceleration, advection, bed friction and Coriolis effect. The model is forced by a spatially uniform pressure gradient that, in case of a flat bed, would induce a symmetrical  $M_2$  tide.

Key variable is the spatiotemporally varying bed level  $h(x, y, t)$ . The initial topography is described by bank angle  $\theta_{bank}$  with respect to the principal tidal flow, bank length  $L_{bank}$ , bank height  $h_{bank}$  and bank width  $B_{bank}$ . The central part of the bank is uniform in along-crest direction and Gaussian in cross-bank direction. The bank ends are Gaussian in two dimensions.

The morphological loop structures our hydrodynamic and morphodynamic solution procedures. First, we split topography  $h$  into a uniform bed elevation  $h_0$  and a spatially varying component  $\epsilon h_1$ :

$$h = h_0 + \epsilon h_1 \quad (1)$$

Herein,  $\epsilon = \max h_{bank} / h_{mean}$  is the ratio between maximum bank amplitude and mean water depth  $h_{mean}$ .

Second, we introduce vorticity  $\eta = \partial v / \partial x - \partial u / \partial y$  and a solution vector  $\phi = (\eta, u, v, \zeta)$  to simplify the hydrodynamic equations. Now, as a novel solution method, we expand the solution vector in terms of  $\epsilon$ :

$$\phi = \sum_{j=0}^J \epsilon^j \phi_j = \phi_0 + \epsilon \phi_1 + \epsilon^2 \phi_2 + \dots + \epsilon^J \phi_J \quad (2)$$

We distinguish components  $\phi_0$ ,  $\phi_1$  and  $\phi_j$  for  $j \geq 2$ , which represent uniform flow over a flat bed (basic flow), first order flow (linear response) and higher order flow solutions (nonlinear response), respectively.

Third, the hydrodynamic solution is used to calculate bed load transport, which is commonly considered as the dominant mode for transporting grains around sandbanks (Besio et al., 2006). Furthermore, we account for bed slope effects and wind stirring.

Fourth, the bed level change is computed via the frequently used Exner's equation, which is numerically implemented via a fourth order Runge-Kutta scheme. For computational efficiency, it is updated on the time scale of morphological change rather than tidal cycle (Hulscher et al., 1993).

We refer to van Veelen et al. (2018) for further details on the solution procedure.

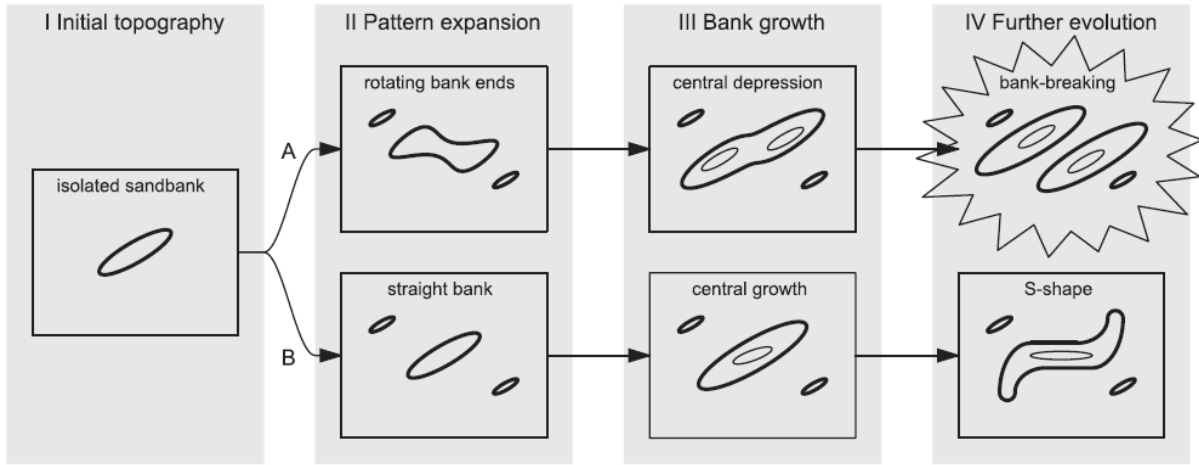


Figure 2. Classification scheme containing two paths of bank evolution (A and B), which, depending on initial orientation and bank length, result in either bank-breaking or a spatially meandering crest. The lines display general depth contours that outline the sandbank. The thin lines depict even shallower areas, i.e. a higher sandbank.

### 3 RESULTS

Based on our model runs, we distinguish two paths of sandbank evolution: banks that break and banks that attain meandering crests. Within each category, the behaviour is remarkably similar. Therefore, the two paths are featured in a classification scheme in Fig. 2.

Path A exhibits (I) an initially straight bank. Then, (II) the bank ends rotate in the direction of the fastest growing mode from linear stability analysis  $\theta_{fgm}$  (see e.g. Huthnance, 1982a). Furthermore, it expands its pattern in the form of parallel crests and troughs. What follows (III) is the formation of a central depression, while bank ends grow in amplitude, leading to (IV) bank-breaking.

Path B features (I) an initially straight bank that does not break. Instead, (II) the bank retains its shape as it expands its pattern. This is followed by (III) growth of the central part in amplitude. As the central part and the bank ends differ in amplitude, this may result in (IV) a spatially meandering crest, which resembles a weak S-shape.

A sensitivity analysis shows that the path depends on initial bank angle and length (Fig. 3). The bank angle controls to what

extent the bank ends can rotate. Bank-breaking will occur when the initial bank angle deviates sufficiently from the preferred angle from linear stability analysis. As it turns out, the required deviation depends on the initial bank length. Specifically, the deviation required reduces when bank length increases.

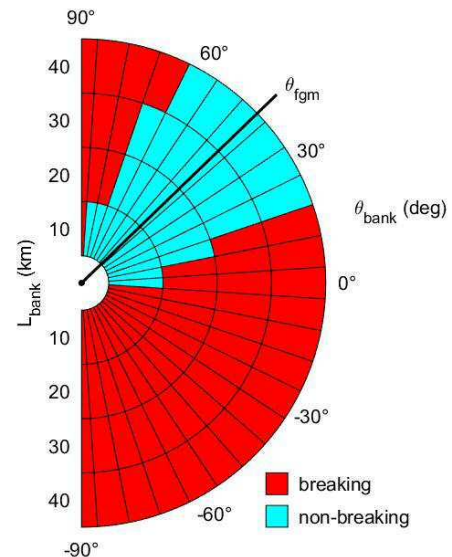


Figure 3. Regime diagram showing bank breaking as a function of bank orientation  $\theta_{bank}$  and length  $L_{bank}$ .

## 4 COMPARISON WITH EARLIER SANDBANK EVOLUTION STUDIES

Bank-breaking according to our regime diagram in Fig. 3 agrees with observational studies. For a bank parallel to the principal tidal flow, as described by Caston (1972), bank-breaking is reproduced. Furthermore, breaking of anticlockwise oriented banks with a kink, as described in Smith (1988), are a stage in our classification scheme of breaking banks (Fig 2, Path A: III).

Alternatively, the spatially meandering crests observed in non-breaking banks resemble model results by Huthnance (1982b), who used simplified flow conditions, and by Yuan et al. (2017), who found that meanders oscillate in time for banks with a fixed wave length. This oscillating behavior was not found in the present study.

## 5 CONCLUSIONS

Sandbank dynamics affect the environmental conditions (e.g. flow characteristics and water depth) in which sandwaves develop. Here, we developed an idealised process-based numerical model for the transient evolution of tidal sandbanks. As a novelty, it captures nonlinear hydrodynamics via an expansion in the ratio of bank amplitude and mean water depth.

The model results show that sandbanks follow a specific four-stage evolution, which results in either bank-breaking or a topography with meandering crests. Initial bank angle and length control which path occurs. Furthermore, it is found that sandbanks may break when the initial topography meets two criteria: (i) the bank orientation must differ sufficiently from the angle from linear stability analysis and (ii) a minimum bank length must be satisfied for separate growth of the bank ends. A so-called regime diagram visualizes the two criteria quantitatively (Fig. 3).

## 6 ACKNOWLEDGEMENTS

This work is part of the research programme SMARTSEA with project number 13275, which is (partly) financed by the Netherlands Organisation for Scientific Research (NWO). The first author is grateful for support by MARID and the British Society for Geomorphology (BSG; Wiley-Blackwell).

## 3. 7 REFERENCES

- Besio, G., Blondeaux, P., Vittori, G., 2006. On the formation of sand waves and sand banks. *J. Fluid Mech.* 557, 1–27.
- Caston, V.N.D., 1972. Linear sand banks in the Southern North Sea. *Sedimentology* 18, 63–78.
- Deleu, S., van Lancker, V.R.M., van den Eynde, D., Moerkerke, G., 2004. Morphodynamic evolution of the kink of an offshore tidal sandbank: the Westhinder Bank (Southern North Sea). *Cont. Shelf Res.* 24, 1587–1610.
- Hulscher, S.J.M.H., de Swart, H.E., de Vriend, H.J., 1993. The generation of offshore tidal sand banks and sand waves. *Cont. Shelf Res.* 13, 1183–1204.
- Huthnance, J.M., 1982a. On one mechanism forming linear sand banks. *Est. Coast. Shelf Sci.* 14, 79–99.
- Huthnance, J.M., 1982b. On the formation of sand banks of finite extent. *Est. Coast. Shelf Sci.* 15, 277–299.
- McCave, I.N., Langhorne, D.N., 1982. Sand waves and sediment transport around the end of a tidal sand bank. *Sedimentology* 29, 95–110.
- Reineck, H.E., Singh, I.B., Wunderlich, F., 1971. Einteilung der Rippeln und anderer mariner Sandkörper. *Senckenbergiana maritima* 3, 93–101.
- Smith, D.B., 1988. Stability of an offset kink in the North Hinder Bank. In: De Boer, P., Van Gelder, A., Nio, S.-D. (Eds.), *Tide-Influenced Sedimentary Environments and Facies*. D. Reidel Publishing Company, Dordrecht, 65–78.
- van Veelen, T.J., Roos, P.C., Hulscher, S.J.M.H., 2018. Process-based modelling of bank-breaking mechanisms of tidal sandbanks. *Cont. Shelf Res.* 167, 139–152.
- Yuan, B., de Swart, H.E., Panadès, C., 2017. Modeling the finite-height behavior of off-shore tidal sand ridges, a sensitivity study. *Cont. Shelf Res.* 137, 72–83.

# A combined method to calculate superimposed 2-D dune morphological parameters

**Li Wang** State Key Laboratory for Estuarine and Coastal Research, East China Normal University, Shanghai, China - twilight528400@hotmail.com

**Qian Yu** Ministry of Education Key Laboratory for Coast and Island Development, Nanjing University, Nanjing, China - qianyu.nju@gmail.com

**Shu Gao** State Key Laboratory for Estuarine and Coastal Research, East China Normal University, Shanghai, China - shugao@nju.edu.cn

**ABSTRACT:** Two-dimensional (2-D) subaqueous dunes often superimpose on giant dunes, sand bars or sand ridges. Mega-ripples may also be further superimposed on the 2-D dunes. A combined method was developed to analyse the geometry of the 2-D subaqueous dunes in this case, including 2-D Fourier analysis, wavelet transform, zero-crossing analysis, and various filtering. The regional dominant orientation and individual geometry parameters of 2-D submarine dunes can thus be obtained automatically with input of bathymetries. This method was successfully applied with both synthetic and observed bathymetries.

## 1 INTRODUCTION

Two-dimensional (2-D) dunes are common rhythmic bedform in submarine environments. They are often superimposed on large sand bodies, such as sand bars, sand ridges, and giant dunes. They are not only the results of sediment transport processes but also indicate sediment transport processes. Bedform wavelength and wave height are used to predict bed roughness (Yalin and Lai, 1985; Wang et al., 2016), and bedform asymmetry and orientation indicates the net sediment transport direction (McCave and Langhorne, 1982; Van Wesenbeck and Lanckneus, 2000). The understanding of modern submarine dune evolution is important for the restoration of paleo-sedimentary environments of sedimentary structures in boreholes and rocks (Baas et al., 2016). The formation and movement of submarine dunes may threaten the safety of submarine pipelines and navigation. (Németh et al., 2003). Thus, the bedform dynamics are one of the key issues of sedimentology.

Quantitative analysis of bedform morphology is the basis of the bedform study.

Bedform geometry can be quantitatively represented by a number of parameters, which are associated with two categories. The first category is related to the overall regional patterns. For bedforms in a region, there is a dominant orientation and the associated characterized wavelength. The second category contains individual geometry parameters, such as the position of dune ridge, depth of dune ridge, wavelength, wave height, symmetry, lee slope angle, etc of different 2-D submarine dunes.

The relationship between these parameters and the relationship between the parameters with environment factors (i.e., bed sediment grain size, water depth, current velocity) were highlighted and investigated widely (Yalin, 1964; Allen, 1968; van Rijn, 1984; Flemming, 1988). However, more data are still required for a comprehensive understanding of these relationships.

High-resolution multibeam bathymetry increases the volume and complexity of bathymetric data, and a number of methods has been proposed to automatically quantify the 2-D dunes morphology.

For the regional morphological patterns, two-dimensional Fourier analysis can con-

vert water depth matrix into a 2-D power spectrum. The main wavenumber can be extracted to calculate the regional dominant orientation and wavelength of submarine dunes (Van Dijk et al., 2008; Lefebvre et al., 2011; Cazenave et al., 2013). Anisotropic covariance analysis is also applied on the basis that the covariance in the direction of 2-D dune crests is the smallest, and the range value of the semi-variogram model in the direction perpendicular to the dune crests is the regional dominant wavelength of the submarine dunes (Dorst, 2004; Pluymakers et al., 2007; Van Dijk et al., 2008).

Zero-crossing analysis can be easily applied to calculate the individual geometry parameters of submarine dunes. However, it would be challenged by the superimposition of bedforms with different scales. Thus, separating bedforms of different scales is necessary. Based on the geostatistical analysis, bedforms at different scales can be obtained by Kriging interpolation in a variety of resolutions (Van Dijk et al., 2008). 2-D discrete Fourier analysis combined with Butterworth high-pass filtering can effectively eliminate the background topographic effects (Cazenave et al., 2013). However, the spectral leakage of this method tends to underestimate wave height (Van Dijk et al., 2017). Although wavelet transform is applied for one-dimensional profiles, it has an outstanding performance in separation of dunes at different scales (Gutierrez et al., 2013).

Different methods have good performance at different stages of 2-D dune morphology analysis. We create a combined method based on Matlab, including 2-D discrete Fourier transform, Wavelet transform, and zero-crossing analysis. With an input of coordinates and bathymetry data, the regional and individual geometry parameters of superimposed 2-D submarine dunes can be calculated automatically. The method was applied to a synthetic bathymetry, and two measured bathymetries. One is on a sand ridge off Jiangsu Coast, China, and the other is on a sandbank in the Dover Strait, UK.

## 2 METHODS AND MATERIALS

### 2.1 Methods

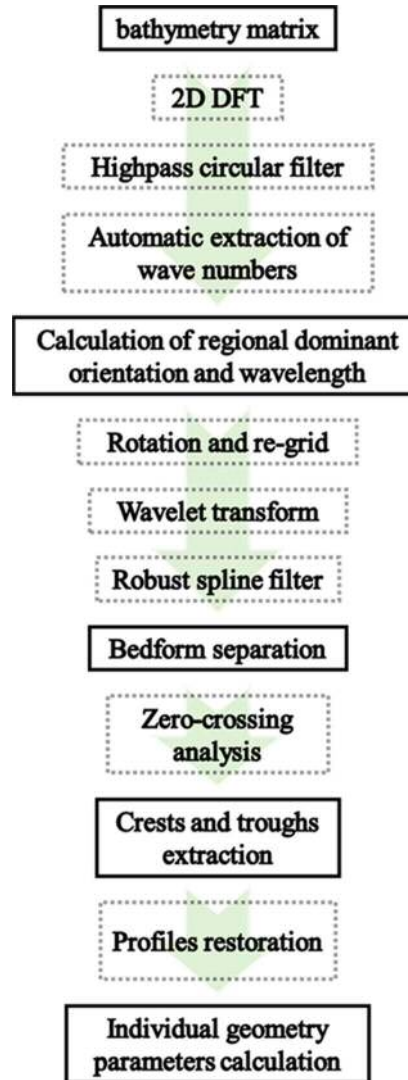


Figure 1. Flow chart of the combined method. Solid outlines indicate the products and functions of every steps. Dashed outlines indicate the processes and methods of every steps.

The method is divided into four steps. Firstly, it calculates regional dominant orientation and wavelength of the submarine dunes by 2-D discrete Fourier transform. Then, the matrix is rotated, re-gridded, and split into a number of 1-D profiles. Bedforms of different scales are separated by wavelet transform analysis. Thirdly, dune crests and troughs are extracted on the profiles by zero-crossing analysis. Finally, the individual geometry parameters are calculated on the profiles.

### 2.1.1 2-D Fourier analysis

Modified Cazenave et al (2013)'s 2-D Fourier analysis method is adopted to calculate the regional dominant orientation and the associated characterized wavelength. The power spectrum of the bathymetry matrix after the 2-D discrete Fourier transform is mirror symmetric and illustrate the spatial period of dunes. Circular filtering filters values near the coordinate origin in reciprocal coordinates. The line connecting two symmetrical wavenumbers passes through the coordinate origin. The regional dominant orientation of the 2-D dunes is the direction of the line. The distance from the selected wavenumber point to the origin of the coordinate is the reciprocal of the regional dominant wavelength of the dunes (Cazenave et al, 2013). The method provides an alternative parameter selection and ignores the influence of background topography. Here we detrend the bathymetry matrix in the x- and y-directions, in order to remove the influence of background terrain. We set the radius of the circular filter to 3 times the wavelength of interest and the power threshold of 90%.

### 2.1.2 Wavelet analysis

First, the bathymetry matrix is rotated according to the regional dominant orientation calculated by the 2-D Fourier analysis. Then the bathymetry matrix is re-grid and re-interpolate. Then it is split into 1-D water depth profiles which are perpendicular to the dune crestlines. The dune wavelengths of different scales can be extracted according to the wavelet transform power spectrum (Gutierrez et al, 2013). After the robust spline filter according to different wavelengths, three kinds of bedform profiles are separated.

### 2.1.3 Zero-crossing analysis

The zero-crossing analysis is performed to the bedform profiles of interest. The profiles separated by wavelet analysis are relatively smooth, but the effect of noise cannot be totally eliminated. A threshold for the distance of every other zero points is applied twice to eliminate the influence of noise.

The threshold is set to 0.3 times the regional dominant wavelength. Then, the extreme point between adjacent zero points is extracted as the trough or crest point of the dune.

### 2.1.4 Dune geometry parameters calculation

The background topography can influence the geometry parameter calculation (Figure 2). We propose a method to solve this problem. Wavelength and wave height are defined as the distance from adjacent troughs (AB in Figure 2), and the vertical distance from the crest to the wavelength line (CD in Figure 2), respectively. Symmetry is the ratio of (AD - DB) to AB in Figure 2, and the lee slope angle in Figure 2 is  $\angle CAD$ .

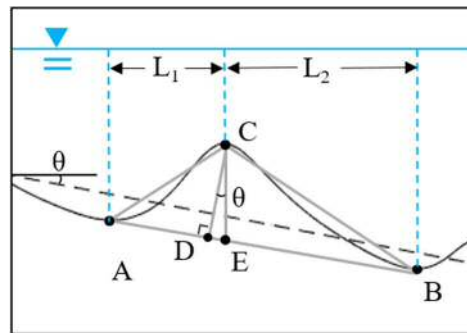


Figure 2. Schematic diagram of the definition of the dune geometry parameters. A and B are the troughs of the dune, and C is the crest. The blue line is the water line. The black dashed line represents the zero line of zero-crossing analysis.  $L_1$  and  $L_2$  are the horizontal distances of AC and BC.

## 2.2 Materials

### 2.2.1 Synthetic bathymetry

The synthetic bathymetry is constructed artificially, being the superimposition of bedforms with three different scales in the x-direction. The wavelength is 300 m, 16 m, and 1 m, respectively, and the corresponding wave height is 5 m, 1 m, and 0.1 m, respectively. The bathymetry in the y-direction is the same and repeated. Then, the matrix is rotated counter-clockwise by 45°, and a 200 m × 200 m rectangular bathymetry is selected. For the middle scale dunes, the large scale dunes is the background topography,

and the small scale dunes is noise. The present method is applied to extract the morphological parameters of the middle scale dunes. By the comparison between the calculation results and the original settings, the method performance can be evaluated.

### 2.2.2 Field observed bathymetries

Two observed bathymetries are used for morphological parameters calculation using the present method. One is located on a sand ridge off Jiangsu coast, China. The collection was on January 19, 2017, using an R2sonic 2024 multibeam echo-sounder. After correction and swath data cleaning with CARIS HIPS and SIPS, the data were gridded to 0.5 m resolution. We chose a 100 m × 400 m rectangular area on the northern slope of the sand ridge which dunes superimpose on. Thus, removing the background sand ridge influences is crucial to calculate the dune morphological parameters.

A 500 m × 1000 m rectangular area on a sandbank in the Dover Strait, about 25 km east of Kent Coast, London, UK, was selected from marine data sets held by the UK Hydrographic Office (<http://aws2.caris.com/ukho/mapViewer/map.action>). The bathymetry was gridded with horizontal resolution of 1 m. The present method is to identify and separate the dunes in two scales, and the morphological parameters are computed for each scale dunes.

## 3 RESULTS

In terms of artificial data, the present method yields that the dominant orientation, average wavelength, and wave height of the middle scale dunes are 45.00°, 16.10 m and 1.04 m, respectively. They are very close to the settings of 45°, 16 m and 1 m, respectively. Thus, the method is accurate and feasible.

The dune extraction (Figure 3a) of the observed bathymetry from China shows that almost all of the dune crests are accurately extracted. The spatial distributions of wave

length and wave height are shown in Figure 3.

Two scale dunes were extracted from the bathymetry in the Dover Strait (Figure 4). Red dots show the location of large scale dunes, with the dominant orientation, average wavelength, and average wave height of 135.37°, 187.50 m, and 1.99 m, respectively. However, for the small dunes, these values change to 95.50 °, 9.50 m, and 0.24 m.

## 4 DISCUSSION

### 4.1 Parameters selection of 2-D Fourier analysis

In the 2-D Fourier analysis, two parameters determine the accuracy of the extraction result, namely, being the radius of the circular filter and the threshold of wavenumber extraction. Cazenave et al. (2013) considered that the reciprocal of the radius of the circular filter is generally set to 10% of the long side of the bathymetry region. The length of the long side of the bathymetry area must be greater than 10 times the wavelength, suggesting that the reciprocal of the radius of the filter is greater than the wavelength of dunes. In this way, selecting more than 80% of the maximum peak power can meet the error requirement. However, the background topography of the observed bathymetry makes it difficult to select parameters. Combination of different parameter selections leads to different results, some of them being unreal. Thus, it is difficult to choose the correct wavenumber.

However, after detrending background topography, the results of different parameter combinations are consistent. In this way, we can set two fixed parameters. Thus, detrending does not only improve the selection of the wavenumbers, but also simplifies the selection process.

### 4.2 Correction of deviation of parameter calculation

Traditionally, bedform morphological parameters are determined based on the hori-

zontal coordinates, in Figure 2, the wavelength and the wave height being  $L_1 + L_2$  and CE, respectively. However, the background topography should be taken into account. The background topography is a flat slope with an anger of  $\theta$ , which is parallel to AB. The actual wavelength is  $(L_1 + L_2)/\cos\theta$ , which is equal to AB, and the wave height is  $CE*\cos\theta$ , which is equal to CD. The relative error of the wave steepness (the ratio of wave height to wavelength) is  $(\sin\theta/\cos\theta)^2$ , which increases with  $\theta$ . The relative error of the dune symmetry is  $2*St*\sin\theta/Sy$ , in which St and Sy are the wave steepness and symmetry, respectively. It increases as  $\theta$  and St increase and Sy decreases.

The effects of background topography can not be neglected for area with large value of  $\theta$  (i.e.,  $\sim 10^\circ$  or more), which is frequently associated with the lee slope of giant dunes. Assuming that St and Sy are 0.05 and 0.1, respectively, the relative error of the steepness and symmetry of the dunes with a slope of  $20^\circ$  would be 13% and 34%. To avoid errors caused by background terrain, we chose a revised method to calculate morphological parameters, as shown in 2.1.4. Thus, in this way, the geometry parameters of submarine dunes can be directly compared on different slopes of the background topography.

## 5 CONCLUSIONS

A combined method was developed to analyse the geometry of the 2-D subaqueous dunes, including 2-D Fourier analysis, wavelet transform, zero-crossing analysis, and various filtering. The regional dominant orientation and individual geometry parameters of 2-D superimposed dunes can thus be obtained automatically with input of bathymetries.

## 6 ACKNOWLEDGEMENT

This research was supported by the project NSFC 41676081, BK20171341 and

SKLEC-KF201803. We appreciate the captain and the crew of *Jiangsu Rudong 02315*.

## 7 REFERENCES

- Allen, J.R.L., 1968. On the character and classification of bed forms. *Geol. Mijnbouw*, 47(3), 173-185.
- Baas, J.H., Best, J.L., Peakall, J., 2016. Predicting bedforms and primary current stratification in cohesive mixtures of mud and sand. *Journal of the Geological Society*, 173(1), 12-45.
- Cazenave, P.W., Dix, J.K., Lambkin, D.O., et al., 2013. A method for semi-automated objective quantification of linear bedforms from multi-scale digital elevation models. *Earth Surface Processes and Landforms*, 38(3), 221-236.
- Dorst, L.L., 2004. Survey plan improvement by detecting sea floor dynamics in archived echo sounder surveys. *The International hydrographic review*, 5(2), 49–63.
- Flemming, B.W., 1988. Zur klassifikation subaquatischer, strömungstransversaler Transportkörper. *Bochumer geologische und geotechnische Arbeiten*, 29, 44-47.
- Gutierrez, R.R., Abad, J.D., Parsons, D.R., et al., 2013. Discrimination of bed form scales using robust spline filters and wavelet transforms: Methods and application to synthetic signals and bed forms of the Río Paraná, Argentina. *Journal of Geophysical Research: Earth Surface*, 118(3), 1400-1418.
- Lefebvre, A., Ernstsen, V.B., Winter, C., 2011. Bedform characterization through 2D spectral analysis. *Journal of Coastal Research*, 64, 781-785.
- McCave, I.N., Langhorne, N., 1982. Sand waves and sediment transport around the end of a tidal sandbank. *Sedimentology*, 29, 95–110.
- Nemeth, A., Hulscher, S.J.M.H., de Vriend, H.J., 2003. Offshore sand wave dynamics, engineering problems and future solutions. *Pipeline and gas journal*, 230(4), 67-69.
- Pluymakers, S., Lindenbergh, R., Simons, D., et al., 2007. A deformation analysis of a dynamic estuary using two-weekly MBES surveying. *OCEANS 2007-Europe*. IEEE, 2007.
- Van Dijk, T.A.G.P., Lindenbergh, R.C., Egberts, P.J.P., 2008. Separating bathymetric data representing multiscale rhythmic bed forms: A geostatistical and spectral method compared. *Journal of Geophysical Research: Earth Surface*, 113, F04017.
- Van Dijk, T.A.G.P., Lindenbergh, R.C., 2017. Methods for analysing bedform geometry and dynamics. In *Atlas of bedforms in the Western Mediterranean*. Springer International Publishing Switzerland, 7-13.
- Van Rijn, L.C., 1984. *Sediment Transport; Part II: Suspended Load Transport*. *Journal of Hydraulic Engineering*, 110(11), 1613-1641.

- Van Wesenbeek V., Lanckneus J., 2000. Residual sediment transport paths on a tidal sand bank: A comparison between the modified McLaren model and bedform analysis. *Journal of Sedimentary Research*, 70, 470–477.
- Wang, Y., Yu, Q., Jiao, J., Tonnon, P.K., Wang, Z.B., Gao., S., 2016. Coupling bedform roughness and sediment grain-size sorting in modelling of tidal inlet incision. *Marine Geology*, 381, 128–141.
- Yalin, M.S., 1964. Geometrical properties of sand wave. *Journal of the Hydraulics Division*, 90(5): 105-119.
- Yalin, M.S., Lai, G., 1985. On the form drag caused by sand waves. *Doboku Gakkai Ronbunshu*, 363, 245-248.

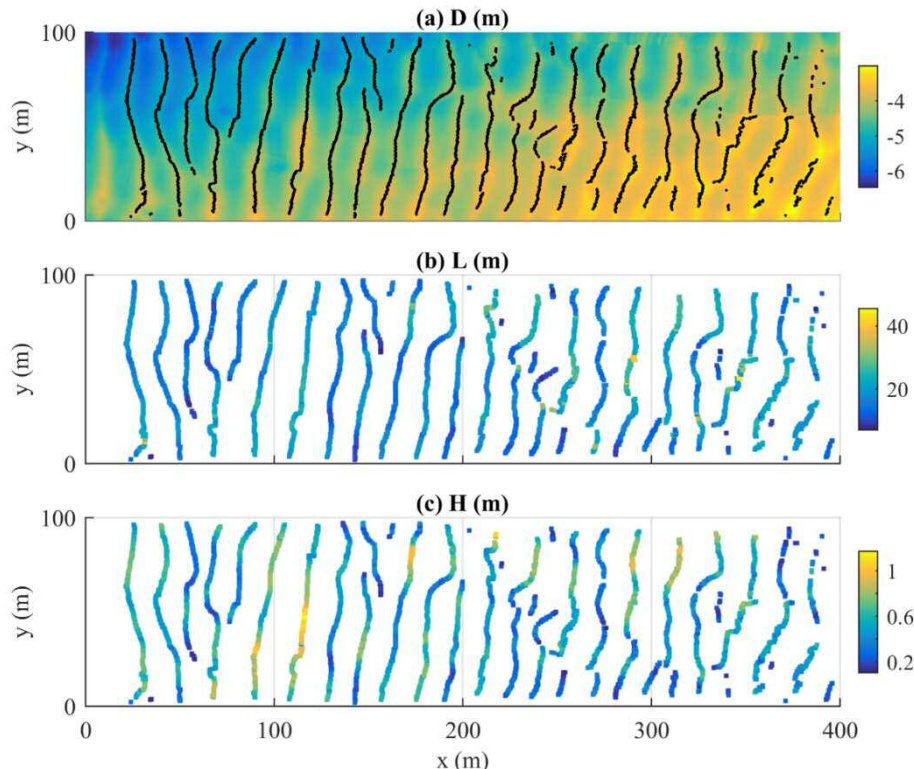


Figure 3. Dunes extraction of bathymetry from Jiangsu Coast, China and the Distribution of dune morphological parameters. (a) Dunes extraction (black dots mean the location of dune crest. The colour shows the water depth); (b) Distribution of wavelengths; (c) Distribution of wave heights.

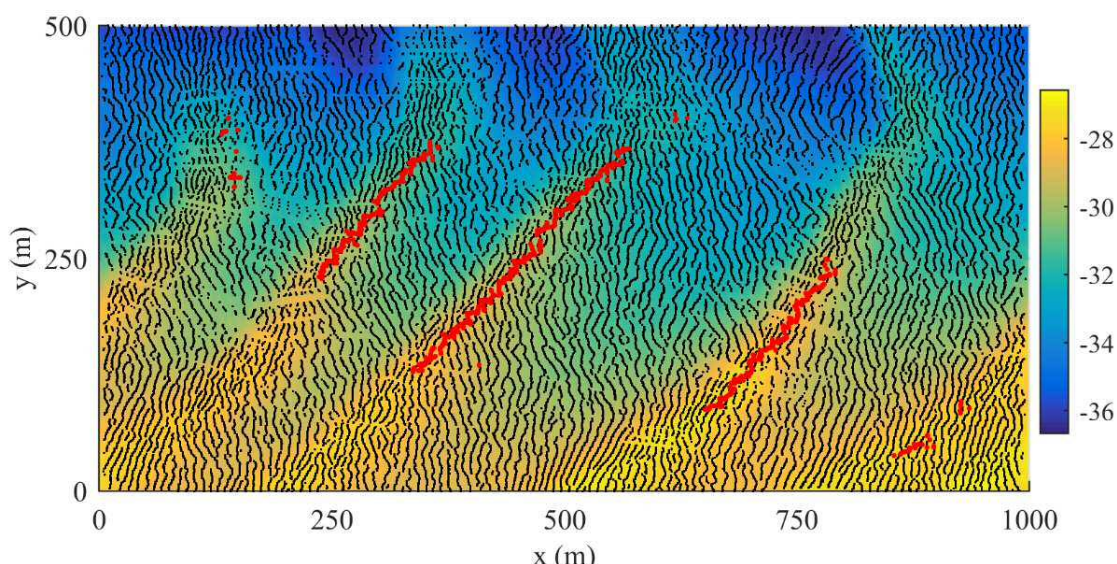


Figure 4. Dunes extraction of bathymetry from Dover Strait, UK. The colour shows the water depth. Black dots mean the location of small dune crests. Red dots mean the location of large dune crests.

# Deep-water sand dunes – case study from Upper Miocene outcrops in the southern Riffian Corridor, Morocco.

Wouter de Weger *Royal Holloway University of London (RHUL), London, UK –*

*wouter.deweger.2017@live.rhul.ac.uk*

F. Javier Hernandez-Molina *RHUL, London, UK – Javier.Hernandez-Molina@rhul.ac.uk*

Francisco J. Sierro Sánchez *University of Salamanca, Salamanca, Spain – Sierro@usal.es*

Domenico Chiarella *RHUL, London, UK – Domenico.Chiarella@rhul.ac.uk*

**ABSTRACT:** Bottom current controlled deposits have been recognized in both modern and ancient sedimentary records along continental margins and in abyssal plains. Despite the scientific and economic importance, bottom current deposits and their diagnostic criteria are still not properly understood. This study aims to improve our knowledge by investigating four Upper Miocene sandy contourite outcrops pertaining to the Southern Riffian Corridor (Morocco). Most common characteristics are the laterally migrating channelized sandbodies encased within hemipelagic background sedimentation. Bottom current controlled sedimentation, recognized by the stacking of sandy 2D and 3D “unidirectional” dunes, shows a direct relation with gravitational processes.

## 1 INTRODUCTION

In this sedimentological study, we investigate four upper Miocene sandy contourite outcrops from the Southern Riffian Corridor (SRC) (Morocco). Our aim is to increase understanding of the processes, products and characteristics of sandy contourite depositional features.

### 1.1 Geological setting

The Riffian Corridor (RC) (Fig. 1) was a marine gateway, connecting the Atlantic and Mediterranean, where water flowed over a submerged orogenic foreland. The corridor evolved during the latest collisional stage of the Betic-Rif Arc, up to around 8 Ma ago (Feinberg 1986; Wernli, 1988; Mutti et al. 2003). The gateway was limited northwards by the Rif orogenic wedge and southwards by the Atlas Mountains (Iribarren et al., 2009; Barbero et al., 2011).

### 1.2 Importance of the Riffian Corridor

The present-day Strait of Gibraltar allows the overflow of dense Mediterranean water (MOW) to feed the contourite channels along the Iberian and Portuguese margins. A

similar process is thought to have existed in the RC during Late Miocene.

This study focusses on the sandy, mixed carbonate-siliciclastic structures observed in deep marine settings of the SRC. These structures are interpreted as being the product of bottom currents, initiated by the overflow of dense MOW during the Late Tortonian.

Gradual closure of both the RC and the Betic corridors (in southern Spain) during the Late Tortonian to Early Miocene led to the onset of the Mediterranean Salinity Crisis (MSC) (e.g. Krijgsman et al., 1999; Garcia-Castellanos, 2011; Achalhi et al., 2016; Flecker et al., 2015; Capella et al., 2017b).

## 4. 2 FIELDWORK / METHODS

The fieldwork area (Fig.1) is located in the Saiss Basin (Northern Morocco). Two field-campaigns have been undertaken, focussing on 4 outcrops that are aligned along the northern margin of the former RC.

Detailed sedimentological logs and basin-scale sediment distribution studies have been undertaken to enable palaeogeographic, tectonic, palaeoceanographic, and, sedimentological reconstructions.

Palaeodepth reconstructions for the RC are critical for establishing the depositional

depth of sedimentation. In this study, values proposed by Capella et al., (2017a) and Capella (2017) based on microfossil assemblages; (1) P/B ratios, (2) depth-indicative benthic foraminifera, and (3) transfer functions are used.

### 3 RESULTS

The main data presented in this study are related to field observations and measurements regarding bedform distribution, size, geometries and composition.

All studied outcrops show different depositional features and styles and are characterized by a similar mixed bioclastic-

siliciclastic composition in the sand-dominated units.

(a) The easternmost outcrop, El Adergha, consists of extensive Blue Marl deposits which show a sudden increase in siliciclastic arenitic content towards the top. The arenitic interval, can be divided from the base to the top, into three main intervals consisting of a 3 m thick thin-bedded sandy marl dominated interval, a 14 m marl interval with sandy bi-gradational sequences and at the top, 17 m of medium to coarse-grained sandstone, with westward migrating cross-stratified bed-sets (Fig. 2a).

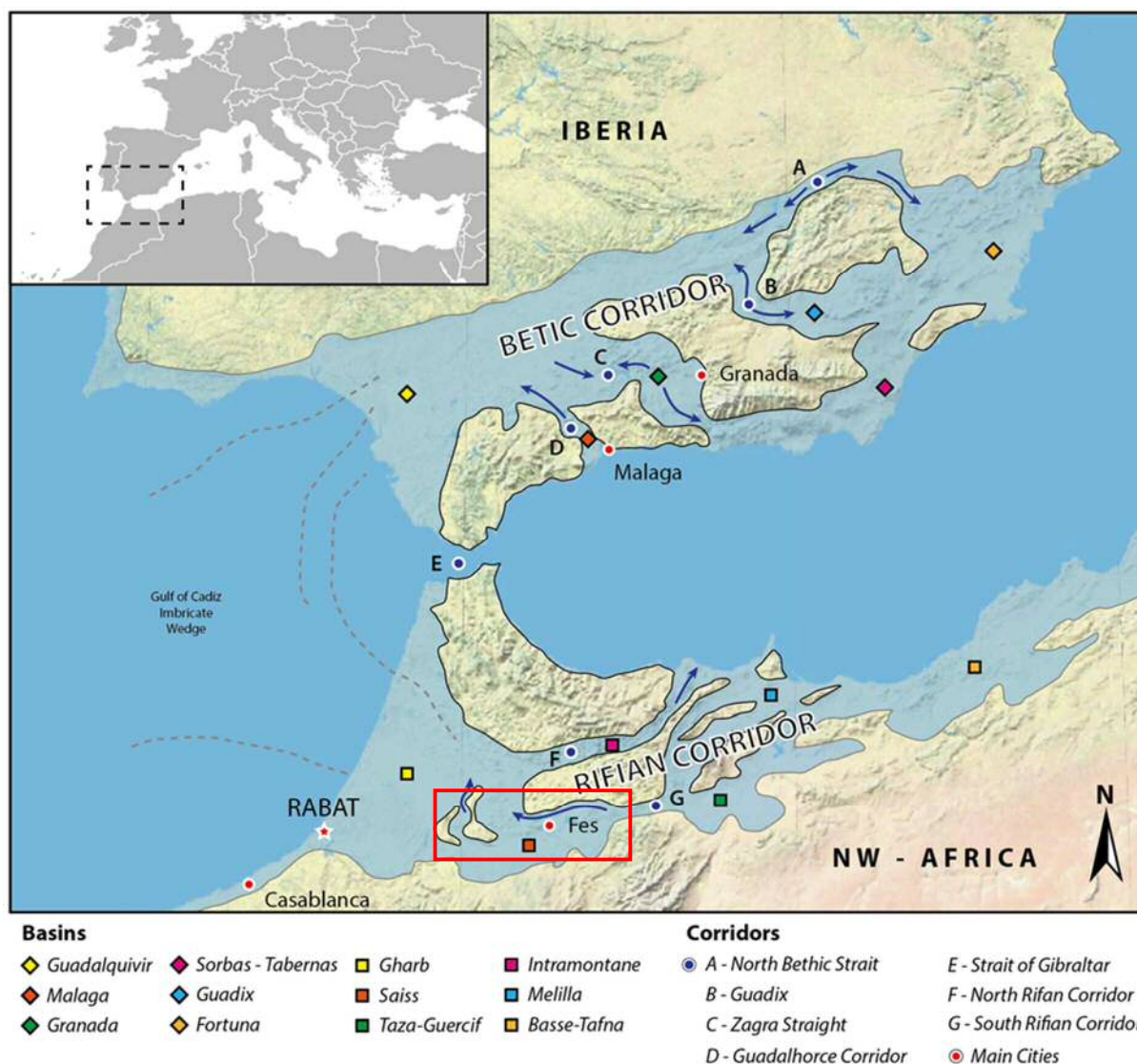


Figure 4. Palaeogeographic reconstruction of the Late Miocene Betic- and Riffian-Corridors in Southern Spain and Northern Morocco respectively. Bleu arrows indicate main palaeocurrent directions. The red box shows the main study area.

(b) The outcrop north of the city of Fes (Fes-north) shows both SSW- and W-directed palaeocurrent features (Fig. 2b). These commonly comprise cross-stratified bed-sets with mud caps and internal drapes. The SSW-directed component consists of breccia and slumped deposits.

(c) The Sidi Chahed outcrop is located west of the Moulay Yacoub city. The basal contact of the sand-dominated units in this section consists of the distinct sudden deposition of a medium-grained, scoured, monomictic, laterally extensive paraconglomerate, followed by a deeply incised channel that is filled with orthoconglomerates. These deposits are topped by SW-directed slumps. On top of this interval, the outcrop (Fig. 3) shows three sand intervals encased in blue marls with turbidite deposits. The sand intervals are upward fining and thinning sequences and consist of channel-shaped geometries filled by dominantly SW- to NW-directed, compound sandy 3D and 2D dunes (Fig. 2c).

(d) The Kirmta outcrop is located 10 km NE of the Sidi Chahed village. Similar to the other sections, the outcrop consists of three main sand units encased within the Blue Marl Formation. The sand units form extended, symmetric, shallow incised, channel shaped geometries. Between the sand units we find turbidite deposits, and there is no evidence of slumps, as encountered in the Sidi Chahed section. Sedimentary structures are scarcely preserved due to intense bioturbation. Locally, ripples and dunes indicate a dominant NNW flow direction (Fig. 2d).

### 3.1 Biostratigraphy

(a) The planktonic foraminiferal assemblage of the El Adergha section, characterized by the presence of *G. menardii* 5 with specimen of the *G. miotumida* group, implies an age between 7.35 and 7.25 Ma, which indicates a late Tortonian to early Messinian age. Benthic assemblages commonly reflect upper bathyal environments with species commonly found in upper slope / outer shelf environments. Estimated depo-

sitional depths range from 150 – 300 m water depth.

(b) The foraminiferal assemblages of the Fes-north outcrop indicate a latest Tortonian age between 7.51 and 7.28 Ma. Between the LCO of *G. menardii* 4 and the coiling change of the *G. scitula* group.

(c) The planktonic foraminiferal assemblage suggests a late Tortonian age between 8.35 and 7.51 Ma for the Sidi Chahed outcrop. The benthic foraminiferal assemblages suggest that the outcrop was deposited in upper bathyal environments, roughly equivalent to 250 – 400 m water depth. The upper part of the section contains less slope taxa, indicating a slightly shallower depth range (150 – 300 m water depth).

(d) Biostratigraphic work of the Kirmta outcrop is still in progress. First results, however, indicate an age between 8.37 and 7.31 Ma, i.e. between the first occurrence of *G. suterea* and the first common occurrence of *G. menardii* 5.

### 3.2 Palaeocurrents

Over 600 palaeocurrent data points have been

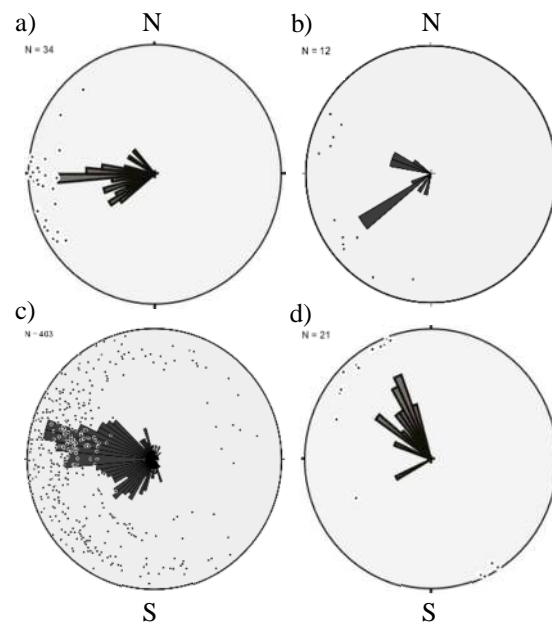


Figure 2. Palaeocurrent data for a) El Adergha, b) Fes-north, c) Sidi Chahed & d) Kirmta. These circular diagrams display palaeoflow directional data. In b and c we can easily differentiate between SW-directed gravitational and W-directed bottom cur-

measured over the four studied sections during the field campaigns. Measurements are primarily made on dunes and ripples and are plotted in rose diagrams (Fig. 2).

#### 4 DISCUSSION

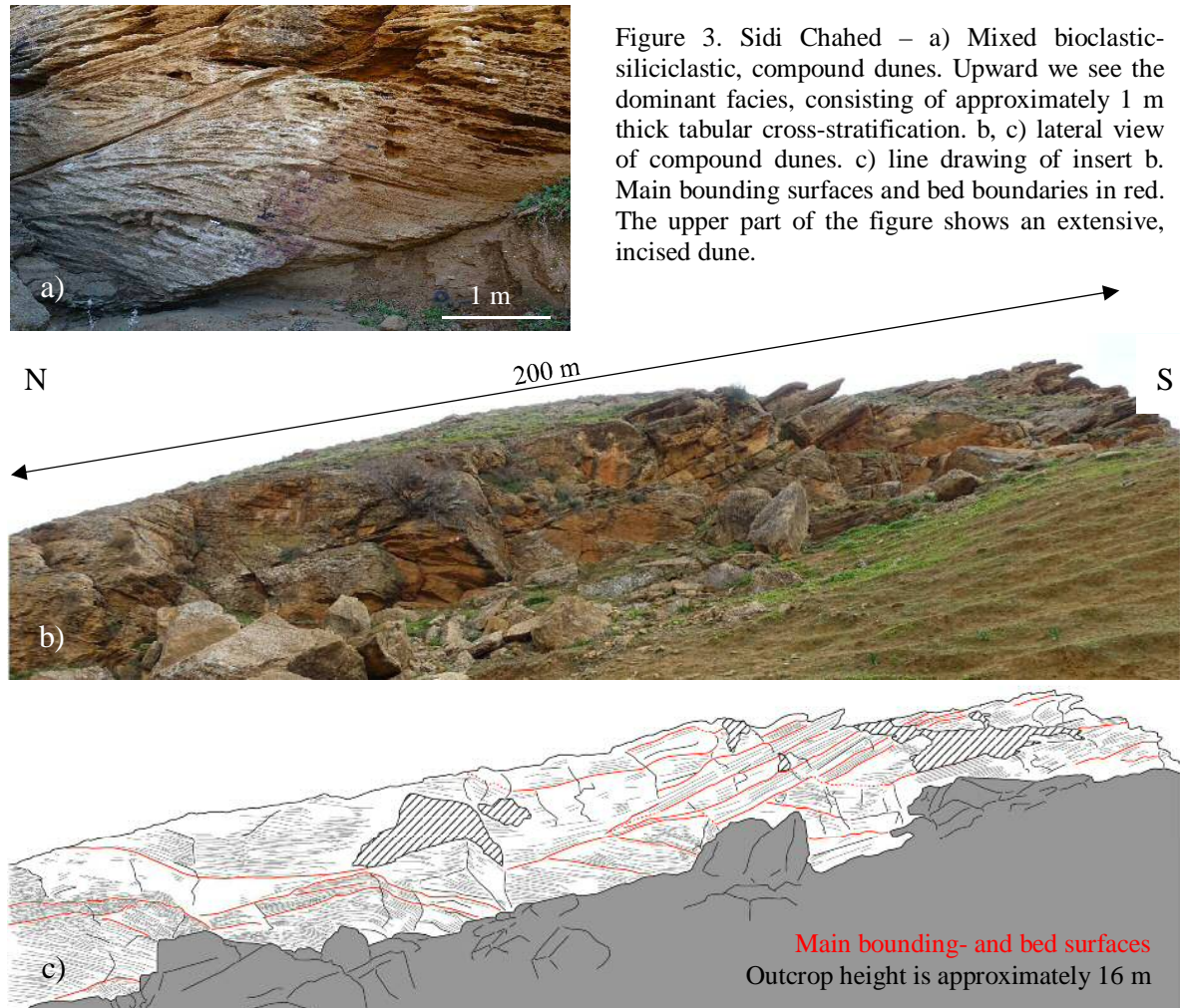
The SRC formed a gateway during the late Tortonian to early Messinian. This gateway allowed Atlantic – Mediterranean water exchange. The depositional features along the northern margin of this gateway indicate an interaction between dominantly southward-directed gravitational, and westward dominated contour parallel sedimentation in the slope of the submerged imbricated foreland. Tectonically induced gravita-

and 2D dunes migrating in channelized geometries at deep-water depths in slope environments.

Based on the bedform velocity diagrams for deep-water sedimentation proposed by Stow et al. (2009), along-slope bottom current velocities, induced by the overflow of dense Mediterranean water, might have well exceeded  $1 \text{ ms}^{-1}$ .

#### 5 CONCLUSION

The bottom current controlled deposits exposed in the remainder of the SRC form a unique example of sandy dunes in deep-water environments. These outcrops represent a good analogue for understanding both



tional processes dominantly precede the deposition of unidirectional compound 3D

conceptual and economic implications of

sandy dunes in modern and ancient deep-water systems.

## 6 ACKNOWLEDGMENTS

We are thankful to the JIP – contourite consortium funded by BP, ENI, Exxon Mobile, Spectrum and Total for enabling us to do the research. ONHYM is acknowledged for aiding in the field campaigns. And we are grateful to “The Drifters” Research Group collaborators for stimulating discussion and sharing their knowledge.

## 7 REFERENCES

- Achalhi, M., Münch, P., Cornée, J. J., Azdimousa, A., Melinte-Dobrinescu, M., Quillévéré, F., ... & Moussa, A. B., 2016. The late Miocene Mediterranean-Atlantic connections through the North Rifian Corridor: New insights from the Boudinar and Arbaa Taourirt basins (northeastern Rif, Morocco). *Palaeogeography, Palaeo-climatology, Palaeoecology*, 459, 131-152.
- Barbero, L., Jabaloy, A., Gómez-Ortiz, D., Pérez-Peña, J. V., Rodríguez-Peces, M. J., Tejero, R., ... & Asebriy, L., 2011. Evidence for surface uplift of the Atlas Mountains and the surrounding peripheral plateaux: Combining apatite fission-track results and geomorphic indicators in the Western Moroccan Meseta (coastal Variscan Paleozoic basement). *Tectonophysics*, 502(1-2), 90-104.
- Capella, W., 2017. Gateway to a vanishing ocean: the tectono-sedimentary evolution of the Rifian Corridor (Morocco) and the Late Miocene isolation of the Mediterranean, Doctoral dissertation, University Utrecht, 20 pp
- Capella, W., Hernández-Molina, F.J., Flecker, R., Hilgen, F.J., Hssain, M., Kouwenhoven, T.J., van Oorschot, M., Sierro, F.J., Stow, D.A.V., Trabucho-Alexandre, J., Tulbure, M.A., de Weger, W., Yousfi, M.Z., Krijgsman, W., 2017a. Sandy contourite drift in the late Miocene Rifian Corridor (Morocco): Reconstruction of depositional environments in a foreland-basin seaway. *Sedimentary Geology*, 355, 31-57.
- Capella, W., Matenco, L., Dmitrieva, E., Roest, W.M.J., Hessels, S., Hssain, M., Chakor-Alami, A., Sierro, F.J., Krijgsman, W., 2017b. Thick-skinned tectonics closing the Rifian Corridor. *Tectonophysics*, 710, 249-265.
- Feinberg, H., 1986. Les séries tertiaires des zones externes du Rif (Maroc): biostratigraphie, paléogéographie et aperçu tectonique. Éditions du Service géologique du Maroc. (No. 315).
- Flecker, R., Krijgsman, W., Capella, W., de Castro Martíns, C., Dmitrieva, E., Mayser, J.P., Marzocchi, A., Modestou, S., Ochoa, D., Simon, D., Tulbure, M., van den Berg, B., van der Schee, M., de Lange, G., Ellam, R., Govers, R., Gutjahr, M., Hilgen, F., Kouwenhoven, T., Lofi, J., Meijer, P., Sierro, F.J., Bachiri, N., Barhoun, N., Chakor Alami, A., Chacon, B., Flores, J.A., Gregory, J., Howard, J., Lunt, D., Ochoa, M., Pancost, R., Vincent, S., Yousfi, M.Z., 2015. Evolution of the Late Miocene Mediterranean-Atlantic gateways and their impact on regional and global environmental change. *Earth-Science Reviews*, Volume 150, 2015, Pages 365-392.
- Garcia-Castellanos, D., & Villaseñor, A., 2011. Messinian salinity crisis regulated by competing tectonics and erosion at the Gibraltar arc. *Nature*, 480(7377), 359.
- Iribarren, L., Vergés, J., & Fernàndez, M., 2009. Sediment supply from the Betic-Rif orogen to basins through Neogene. *Tectonophysics*, 475(1), 68-84.
- Krijgsman, W., Hilgen, F. J., Raffi, I., Sierro, F. J., & Wilson, D. S., 1999. Chronology, causes and progression of the Messinian salinity crisis. *Nature*, 400(6745), 652.
- Mutti, E., Tinterri, R., Benevelli, G., di Biase, D., & Cavanna, G., 2003. Deltaic, mixed and turbidite sedimentation of ancient foreland basins. *Marine and Petroleum Geology*, 20(6-8), 733-755.
- Stow, D. A., Hernández-Molina, F. J., Llave, E., Sayago-Gil, M., Díaz del Río, V., & Branson, A., 2009. Bedform-velocity matrix: the estimation of bottom current velocity from bedform observations. *Geology*, 37(4), 327-330.
- Wernli, R., 1988. *Micropaléontologie du Néogène post-nappes du Maroc septentrional et description systématique des foraminifères planctoniques*. Editions du Service géologique du Maroc.



# Near-bed turbulence dynamics and suspended sediment transport over mixed sand-clay substrates

Xuxu Wu *University of Hull, Hull, U.K.* – *x.wu@hull.ac.uk*

Daniel Parsons *University of Hull, Hull, U.K.* – *d.parsons@hull.ac.uk*

Jaco H. Baas *Bangor University, Bangor, U.K.* – *d.parsons@hull.ac.uk*

Dominique Mouazé *University of Caen, Caen, France* – *dominique.mouaze@unicaen.fr*

Stuart McLelland *University of Hull, Hull, U.K.* – *s.j.mclelland@hull.ac.uk*

Laurent Amoudry *National Oceanography Centre, Liverpool, U.K.* – *laou@noc.ac.uk*

Jorris Eggenhuisen *University of Utrecht, Utrecht, Netherlands.* – *j.t.eggenhuisen@uu.nl*

Matthieu Cartigny, *Durham University, Durham, U.K..* – *matthieu.j.cartigny@durham.ac.uk*

Gerben Ruessink *University of Utrecht, Utrecht, Netherlands.* – *b.g.ruessink@uu.nl*

**ABSTRACT:** This paper reports on a series of experiments that aim to provide a fuller understanding of ripple development within clay-sand mixture substrates under oscillatory flow conditions. The work was conducted in the Total Environment Simulator at the University of Hull and constituted 5 separate runs. The bed content was systematically varied in its composition ranging from a pure sand bed through to a bed comprising 7.4% clay. A series of state-of-the-art measurements were employed to quantify interactions of near-bed hydrodynamics, sediment transport, and turbulence over rippled beds formed by wave action, during and after, each run. The experimental results demonstrate the significant influence of the amount of cohesive clay materials in the substrate on sediment transport. Most importantly, the time averaged suspended sediment concentration (SSC) at height of 20 mm above bed significantly increased from the flat bed evolving to equilibrium wave ripples. Additionally, the clay remaining in the bed is able to stabilize the rippled bed by significantly decreasing ripple migration rate from 0.14 mm/s in Run 1 to 0.04 mm/s in Run 6.

## 1 INTRODUCTION

Sediment transport, which includes bedload and near-bed suspended load, is a dynamic process closely related to hydrodynamic forcing, turbulence, and bed substrate properties (Leeder, 2011). It directly contributes to bedform formation (e.g., ripples). In coastal environments, wave-induced turbulence over flat beds and the spatially and temporally generated vortex on the ripple lee side during oscillatory flow reversal (Ikeda et al., 1991) largely results in suspended sediments, dominating sediment transport (Nielsen, 1992). Although a number of flume and field investigations have previously studied sediment transport and morphodynamics under oscillatory flows (e.g., Green & Black, 1999), the co-evolution of the bed morphology and oscillatory flow

structures have only been examined for cases of cohesionless sand substrates (e.g., van der Werf et al., 2007; O’Hara Murray et al., 2011). There is thus a significant knowledge gap concerning the influence of substrate cohesiveness on sediment transport and bed-form generation.

The development rate of wave ripple dramatically decreases with initial bed clay fraction increase (Wu et al., 2018). The increasing bed resistance related to the initial bed clay fraction plays a vital role on slowing wave-induced ripple development. In the present paper, near-bed wave-generated turbulence and sediment transport dynamics are investigated over the evolving substrates. The objectives of this paper are i) to quantify sediment transport rates and processes across the different substrates; ii) to examine the evolution of near-bed turbulence from

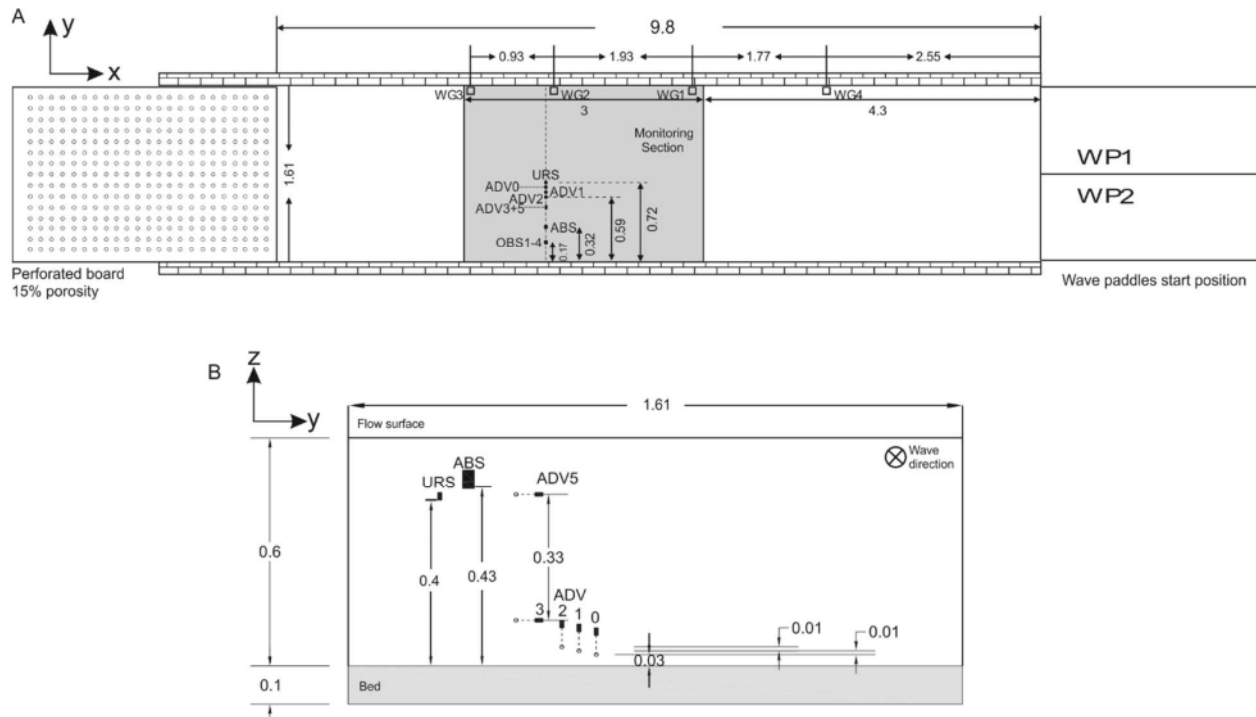


Figure 1. Plan view (A) and side view (B) of the experiment setup

the initial flat bed until ripple equilibrium morphologies are attained; iii) to find the relationship between initial bed clay fraction and rates of change in suspended sediment concentration through the experiments.

## 2 METHODOLOGY

Five large-scale flume experiments were conducted in the Total Environmental Simulator at the University of Hull, United Kingdom. The length and width of the tank are 9.8 m and 1.6 m, respectively, with a central monitoring section at a horizontal distance  $x=4.3$  m from the wave generating paddles (Figure 1A). In the monitoring section, an acoustic backscatter system (ABS) is mounted at a distance  $x=6.1$  m from wave generators and  $y=0.32$  m from the flume wall (Figure 1A), which is 0.43 m above the bed (Figure 1B). Additionally, five SonTek acoustic Doppler velocimeters (ADV), aligning with the ABS, are positioned at five different heights (from 0.03 m to 0.36 m above the bed) to form a vertical array of measurements (Figure 1). Three of the ADVs are downward looking probes and two are sideward looking probes (Figure 1B). In line with the ABS and ADVs, there is a fixed ultrasonic ranging system (URS)

for detecting ripple migration at distance  $y=0.72$  m from the side wall (Figure 1A). At the end of the flume, there is a perforated board with a porosity of 15%, mounted at an upstream dipping angle of 6° (Figure 1A). The perforated board is to disperse wave energy and thus minimize wave reflections. The sediment bed in the flume was 0.1 m thick at the start of the experiments. All experiments used a mean water depth of 0.6 m and the salinity of the water was held constant in all runs at ca. 19 psu, which is typical for estuarine conditions. Experimental Run 1 used a bed of well-sorted sand with a median diameter of 496  $\mu\text{m}$ . Wet kaolin clay, which is one of the most common clay types on Earth, was homogenously mixed with the same sand in Runs 3 to 6, with the initial clay fraction increasing from 4.2% to 7.4% (See Table 1 and Figure 2 in Wu et al., 2018). The experimental results of Run 02 that was conducted under irregular (polychromatic) wave are not discussed in this paper.

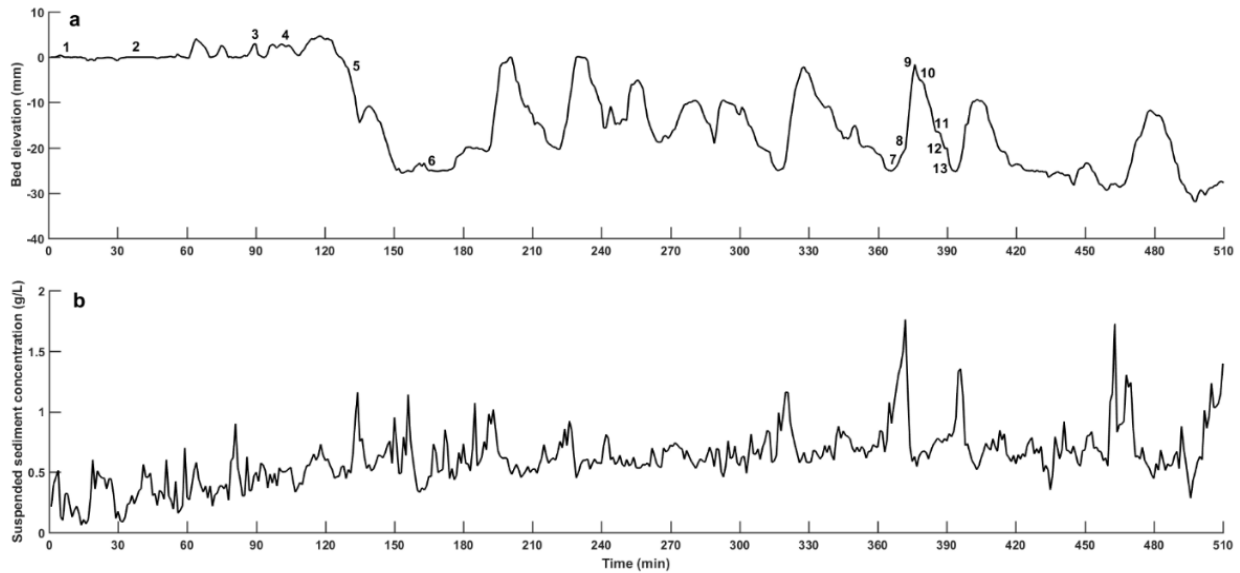


Figure 2. ABS detected bed elevation (a) and suspended sediment concentration (b) at 20 mm above the bed in Run 5 with 7.2% of initial bed clay fraction. The thirteen numbers of locations match numbered panels of phase averaged suspended sediment concentration field in Figure 3

### 3 RESULTS

#### 3.1 Near-bed suspended sediment concentration (SSC)

##### 3.1.1 Time averaged near-bed SSC

Representative example of suspended sediment concentration change over 20 mm above the bed with bedform development for Run 5 with the longest experimental duration of 510 mins is displayed in Figure 2. The bed was recorded to keep flat in the beginning 60 minutes. Over such a flat bed, the peak value of suspended sediment concentration (SSC) was about 0.7 g/L. However, the amount of suspended sediment was lower than 0.5 g/L at that time. With bed erosion, the SSC increased during the period between  $t = 60$  min and  $t = 120$  min. After that the bed elevation decreased significantly showing the formation of wave ripples. At the same time, there was an increase of the amount of suspended sediment, with maximum value of SSC exceeding 1 g/L. Then, ripple started to migrate beneath the ABS until the end of the experiment. Peak values

of the SSC repeatedly appeared on the ripples lee sides, in particular with extremely high values, superior to 1.5 g/L after  $t = 350$  min.

##### i. 3.1.2 Phase-averaged SSC

Figure 3 displays intrawave suspended sediment concentration field from 20 mm to 100 mm above bed, which equals to 4~5 ripple heights. The phase averaged velocity is also shown in the top left panel in Figure 3 to show the regular and asymmetrical wave. A wave period starts from peak value at phase angle as  $0^\circ$ . These contour plots reflect phase averaged intrawave SSC over 24 wave cycles. Over the flat bed in the beginning of experiment, the SSC field was characterized by laminar distribution gradually decreasing with height above 50 mm (Panel 1 to 3, Figure 3). At  $t = 105$  min, this type of suspended sediment profile was broken by a suspended sediment cloud at a phase angle of  $1.1\pi$  rad (Panel 4, Figure 3). A larger suspended sediment cloud was observed just before the flow reached its maximum negative velocity per wave cycle, sediments expanding up over 70 mm height at  $t$

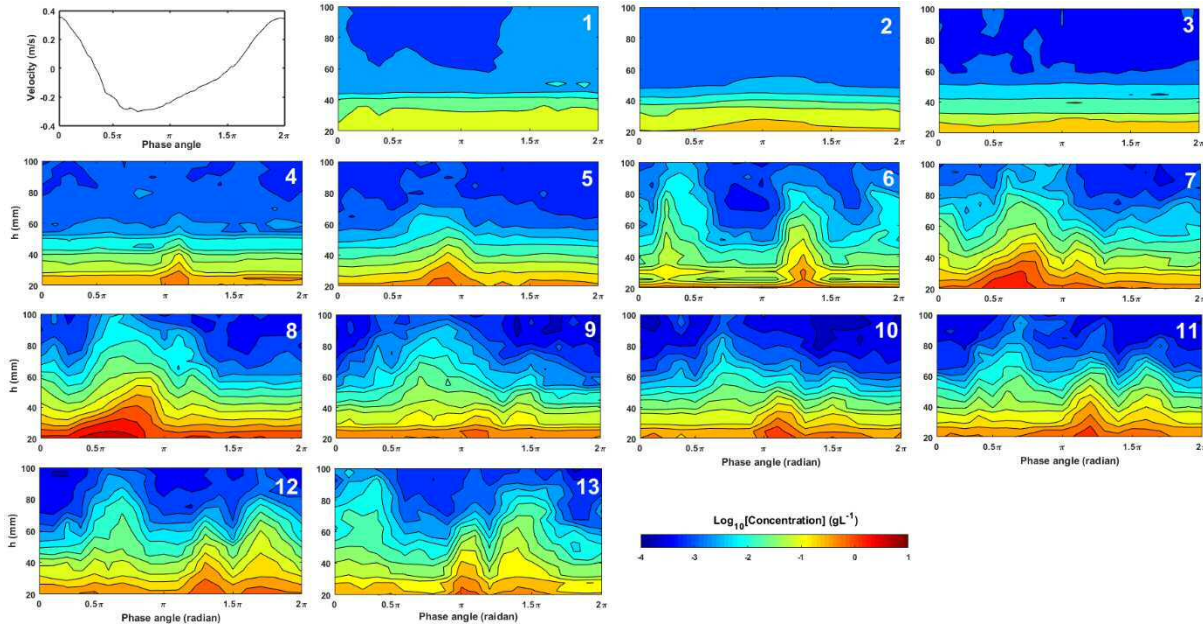


Figure 3. Wave velocity and phase averaged SSC profiles over the bed of Run 5 with 7.2% of initial bed clay fraction. The top left panel displays measured free stream velocity for over 24 successive wave periods. The thirteen numbered panels show phase-averaged suspended sediment concentration (SSC) for over 24 successive wave periods at respective time in Figure 2. The colours in the contour plots are defined in the colour bar as  $\log_{10}[\text{SSC}]$

= 130 min (Panel 5, Figure 3). It happened when the ripple was forming. The lamination of suspended sediment completely disappeared after  $t=160$  min, with concentration peak appearing in each half of the wave cycle and suspending sediments up to nearly 90 mm height (Panel 6, Figure 3).

During the time between  $t=360$  min and  $t=400$  min, an equilibrium wave ripple moved under the ABS probe. At the lee side of wave ripple (number 7 and 8), a high concentration cloud appeared after flow reversal from positive to negative in the first half wave cycle, matching the peak SSC value in Figure 2b. The concentration peaks of smaller magnitude in the second half of wave period above locations 7 and 8 (Panel 7 and 8, Figure 3), were probably associated with the passage of an advected suspension cloud forming at neighboring downstream ripples. There were no noteworthy SSC peaks at ripple crest (locations 9 and 10). At locations 11 to 13 on the stoss slope of ripple, the SSC peaks in the first half wave cycle were presumably caused by the pas-

sage of an advected suspension cloud from successive upstream ripples. In the succeeding half cycle, the formation of concentration peaks occurred at a phase angle of more than  $1.5\pi$  rad was similar to that above lee side due to vortex shedding during flow reversal. The ones generated between phase angle of  $1\pi$  and  $1.5\pi$  were assumed to relate with sediment trapped within new generated vortices (Figure 3).

### 3.3 Ripple migration

Bedform elevation profiles detected by the fixed URS is shown in Figure 4, which demonstrates different ripple migration rates with different initial bed clay fraction. At the beginning of the control experiment (Run 1, pure sand), a wave ripple slowly moved beneath the URS probe between  $t = 20$  min and  $t = 76$  min (Figure 4), with the rate of around 0.04 mm/s. After  $t = 75$  min, the mean migration rate increased to 0.14 mm/s with ripples reaching equilibrium.

In Run 3 with the lowest clay fraction of 4.2%, the bed was flat in the first 15

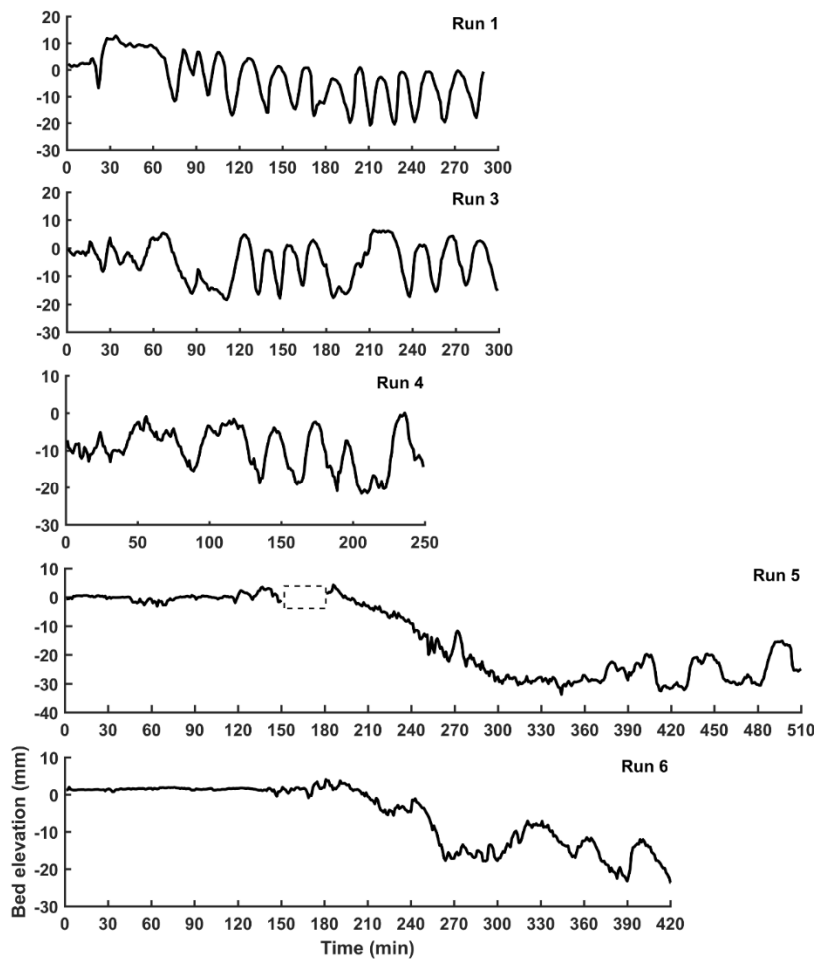


Figure 4. Bedform elevation profiles recorded by the fixed URS are used to determine wave ripple migration rate. The rectangle with dash line denotes data lost as technical problem of URS probe.

minutes, before ripple forming and starting to move. The fixed URS detected three migration of

small ripples with height smaller than 10 mm during period  $t = 15$  min and  $t = 50$  min (Figure 4). The mean migration rate after ripples developing to equilibrium ( $t > 60$  min; Wu et al., 2018) is 0.11 mm/s. In the beginning of Run 4 ( $t < 40$  min), there was only one small ripple movement detected. During time between  $t = 40$  min and  $t = 140$  min, the URS probe recorded two ripple movements (Figure 4). The ripple profiles had long flat crests, which indicates that ripple migration rate was relatively slow (Figure 4). However, the average migration rate increased notably from 0.04 mm/s to 0.1

mm/s in the following 2 hours, with four ripples migrating below the URS probe (Figure 4). Ripple migration rates for Run 5 and Run 6 with relatively higher initial clay fraction (7.4% and 7.6%, respectively) declined significantly. In Run 5, the bed elevation gradually decreased to around -30 mm during period between  $t = 180$  min and  $t = 300$  min. It possibly indicates a ripple trough forming beneath the URS probe during this time. Instead of larger ripple migration detected in the previous runs, there were three smaller ripples ( $\eta < 15$  mm) moving in the last 150 minutes of the experiments (Figure 4). Similarly to Run 5, the bed below the URS probe in Run 6 experienced a significant decrease in approximately 100 minutes.

Additionally, there were only small size ripple migration recorded (Figure 4).

#### 4 CONCLUSIONS

1. The suspended sediment concentration (SSC) field over the flat bed in each run was characterised by the lamination of suspended sediments, which immediately disappeared when the bed eroded. Several peak values of the SSC that related to vortices ejection and advection appeared in each wave cycle over both sides of wave ripples.

2. The time averaged SSC at height of 20 mm above the bed significantly increased from the flat bed evolving to equilibrium wave ripples.

3. The migration rate of wave ripples significantly decreased with an increase of the initial bed clay fraction.

#### 5 ACKNOWLEDGEMENT

This work was part of the COHWAV project, supported by Seventh Framework Programme of 508 the European Community through a grant from the Integrating Activity HYDRALAB IV within the Transnational Access Activities programme, under contract no. 261520. The authors highly appreciate the help and advice from Aaron Westlake, Nick Coulthard, Brendan Murphy, Kim Rosewell, Reinier Schrijvershof, and Leiping Ye during the setup and execution of the flume experiments.

#### 6 REFERENCES

- Green, M.O. & Black, K.P. 1999, Suspended-sediment reference concentration under waves: field observations and critical analysis of two predictive models, *Coastal Engineering*, vol. 38, no. 3, pp. 115-141.
- Leeder, M. 2011, *Sedimentology and sedimentary basins from turbulence to tectonics*, 2nd edn, Wiley-Blackwell, Noida.
- Ikeda, S., Horikawa, K., Nakamura, H. & Noguchi, K. 1991, "Oscillatory boundary layer over a sand ripple model", *Coastal Eng in Japan*, vol. 32, pp. 15-29.
- Nielsen, P. 1992, "Shear stress and sediment transport calculations for swash zone modelling", *Coastal Engineering*, vol. 45, no. 1, pp. 53-60.

O'Hara Murray, R., Thorne, P. & Hodgson, D. 2011, Intrawave observations of sediment entrainment processes above sand ripples under irregular waves, *Journal of Geophysical Research: Oceans*, vol. 116, no. C1.

Van der Werf, Jebbe J., Doucette, J., O'Donoghue, T. & Ribberink, J.S. 2007, Detailed measurements of velocities and suspended sand concentrations over full-scale ripples in regular oscillatory flow, *Journal of Geophysical Research: Earth Surface*, vol. 112, no. F2.

Wu, X., Baas, J. H., Parsons, D. R., Eggenhuisen, J., Amoudry, L., Cartigny, M., ... & Ruessink, G. 2018, Wave ripple development on mixed clay-sand substrates: Effects of clay winnowing and armoring. *Journal of Geophysical Research: Earth Surface*, vol. 123, pp. 2784-2801.

# Enigmatic Bedforms in the Deep Sea

Daniel R. Parsons *University of Hull, Hull, UK – d.parsons@hull.ac.uk*

& Monterey Coordinated Canyon Experiment Team & Bute Inlet Monitoring Team

**ABSTRACT:** Bedforms are ubiquitous features present in a full range of sedimentary environments. Recent work has identified the presence of large scale crescentic bedforms within submarine canyons and channel systems, related to gravity driven sediment laden turbidity currents that periodically flow through these systems. The formation and controls of these bedforms are not fully understood and their interpretation of the geological rock record is hampered by a lack of process-deposit knowledge for these systems and the bedform features they produce. This paper describes these enigmatic crescentic bedforms in the context of bedforms elsewhere, highlighting a range of novel and newly acquired datasets from Bute Inlet, Canada and Monterey Canyon, USA. The paper discusses the interactions between the possible controls on their formation and how this is captured in the depositional record.

## 1 INTRODUCTION

Submarine channels act as conduits for turbidity currents, which have been identified to be the most volumetrically important processes for the delivery of sediment and organic carbon to the deep sea (Bouma 2000; Peakall et al., 2007; Paull et al., 2010; Hage et al., 2018). Turbidity currents are of great importance not only to our general understanding of global sediment transport processes, but also because of the environmental hazards they pose to subsea infrastructure such as communication cables or pipelines (Piper et al., 1999, Carter et al., 2014) and tsunamis related to submarine slope failures (Prior et al., 1982).

Bathymetric mapping of submarine canyon-channel-fan systems has recently revealed that these zones can be dominated by upslope migrating crescentic bedforms (Symons et al., 2016; Hage, et al., 2018) and recent system-scale wide process studies in submarine systems have demonstrated links between seafloor morphology, upward migration of crescentic bedforms, sediment distribution and the evolving flow (Hughes Clarke, 2016).

Combinations of numerical and physical experiments over a number of years have explored the formation of cyclic steps in turbidity current settings, which have been shown to typically generate deposits characterised by back-stepping beds (e.g. Spinewine et al., 2009, Postma and Cartigny, 2014, Covault et al., 2017). In contrast, many outcrops that have been interpreted as cyclic step deposits do not show these regular back-stepping beds, and can be frequently characterized by asymmetric scours filled with massive sands (e.g. Duller et al., 2008, Dietrich et al., 2016). Modern analogues for these massive sands have been reported in sediment cores collected from crescentic bedforms in Monterey canyon (Paull et al., 2011); and similar bedforms have been associated with cyclic steps on the Squamish Delta, B.C., Canada (Hughes Clarke, 2016).

Very recent work has also identified that flows over these bedform features can be initially driven by a fast moving, dense basal layer (Paull et al., 2018). However, fundamental questions remain regarding the sediment concentration of the flows, and whether the basal layer persists, or if flows transition to a state in which turbulence alone supports sediment and what and how

this dense basal layer interacts with the bed morphology.

There is thus fundamental gap in understanding bedform dynamic in submarine canyon-channel-fan systems that is related to a need to obtain and integrate measurements from full scale supercritical turbidity currents, their associated bedforms and samples of their resultant deposits. Such integration, which has until very recently been out of reach, would allow the resolution of these discrepancies between model predictions of bedform dynamics and outcrop observations of bedform deposits from these settings.

Here we present the first combination of detailed (sub-minute resolution) 3D flow monitoring at multiple sites along a canyon-channel system, high-frequency seabed mapping, and sediment core data from two active turbidity current systems. The aims are to: 1) understand how crescentic bedforms are formed beneath supercritical flows; 2) use these observations to reconcile process mechanics and flow-form interactions and the elucidate discrepancies between existing experimental depositional models and outcrop observations; and 3) provide diagnostic criteria to confidently identify crescentic bedforms and thus supercritical flows in the geological rock record.

## 2 STUDY SITES AND DATASETS

Results will be presented from Monterey Canyon, USA and both Bute inlet and Squamish Inlet, Canada.

Bute and Squamish inlets are located on the western coastline of Canada. The fjords both have proximal deltas and have channels on the base of the fjords that extend, in the case of Bute, for over a length of 40 km. As such they represent modern examples of a submarine channel developing under the modification of turbidity currents (Prior & Bornhold, 1988; Conway, 2012).

Monterey canyon is located on the Pacific California mid coast extending from Moss Landing to over 2000 m.

### 2.1 Morphodynamics measurements

Modern bathymetric mapping and sampling techniques are increasingly being applied to submarine channel studies. Bathymetry was collected from a range of vessels across the study sites at different temporal resolutions, revealing unprecedented details of these types of bedform fields (Figure 1). This included daily surveys in Squamish and Bute Inlets to monthly repeat mapping using AUV in Monterey, targeted to map before and after distinct recorded events across a 12 month period. The data were analysed to understand the evolution of the bedform fields to compare bedform wavelength evolution with slope patterns formed by a range of supercritical flows.

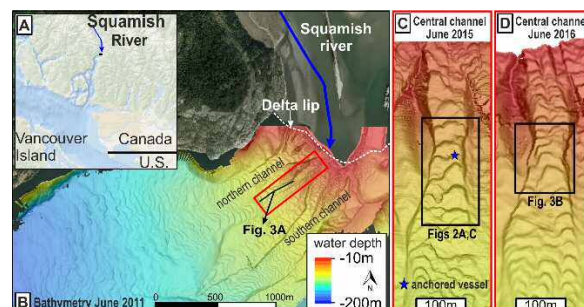


**Figure 1.** A. Squamish river location. B. Downstream of the delta lie three submarine channels covered by crescentic bedforms. C. Location of flow dynamics observations, June 2015. D. Location of coring expedition, June 2016 (from Hage et al. 2018).

### 2.2 Turbidity current monitoring

In both Bute and Monterey a suite of fixed moorings, were deployed (e.g. Figure 2). Each had a range of equipment installed, including Acoustic Doppler Current Profilers (ADCP). Moorings were placed within the submarine channel axis positioned from the proximal areas to the distal lobe of the system in the case of Bute and to over 1850 m in Monterey.

Flow and acoustic backscatter data were recorded for at least five months in each system. These captured the passage and evolution of episodic supercritical turbidity currents as they progressed through the channel systems.

In Bute, more than 20 turbidity currents were observed during this 5 month period. Most of the flows dissipated in the proximal part of the channel system with 11 events observed at 10 km downstream from the proximal delta. The supercritical turbidity currents drive an observed upstream migration of the knickpoints and reorganise some of the larger bedforms during each event.

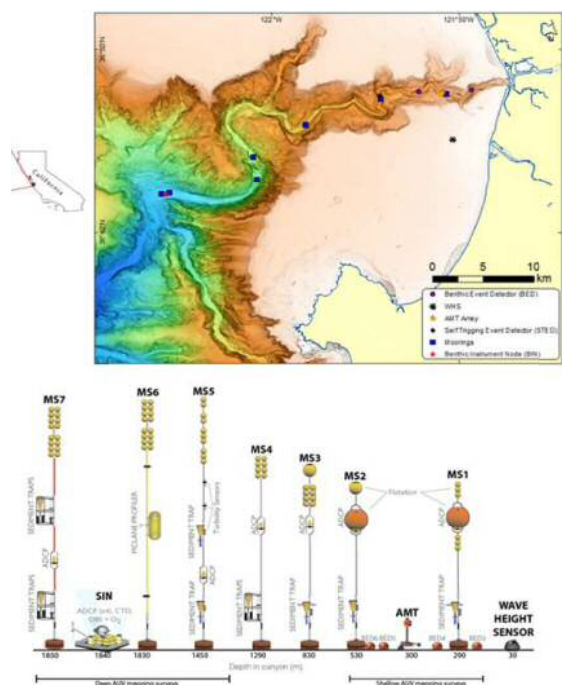


**Figure 2.** Map and schematic of the moorings in Monterey canyon experiment.

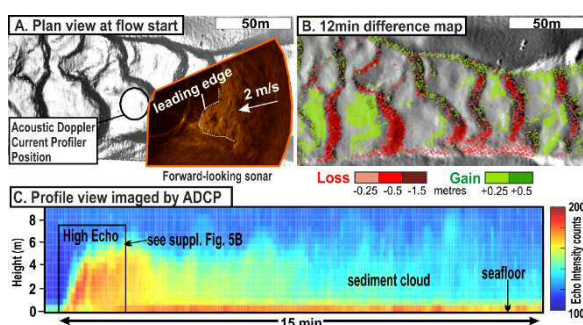


**Figure 3.** Observations of a turbidity current linked to crescentic bedforms A: Snapshot showing a plan view of the flow traveling over the bedforms; B: Seafloor change 12 min after the flow displayed in A & C; C: Time series view the turbidity current from Acoustic Doppler Current Profiler (location in A) (from Hage et al., 2019).

In Monterey a total of 15 flows were observed (Figure 4) by the instruments during the entire 18 month study period. Three of these flows ran out through the full array of instruments to past 1850 m water depth. The largest of these, on January 15th 2016, transported heavy objects several kilometres down the upper canyon. Our acoustic inversions demonstrate that, even for the largest of the flows, the suspended sediment concentration remains relatively dilute (<1%). But that the flows are driven by near-bed high-concentration basal layers.

### 2.3 Acoustic Inversion and Noise

As mentioned above, Acoustic Doppler Current Profilers have previously been deployed in submarine channels to measure density current flow structure and suspended sediment concentration at a single location. Within the Monterey Coordinated Canyon Experiment, the most detailed study of a submarine channel undertaken thus far, which demonstrates how flows evolve as they pass through an array of instruments (Figure 4). Paull et al. (2018) have demonstrated that the flows are initially driven by a fast moving, dense basal layer. However, fundamental questions remain regarding the sediment concentration of the flows, and whether the basal layer persists, or if flows transition to a state in which turbulence alone supports sediment.

Our acoustic inversions demonstrate that, even for the largest of the flows measured in the canyon, the suspended sediment concentration remains relatively dilute (<1%). However, periods of elevated acoustic noise were observed in the ADCP

data commencing with flow arrival at the moorings. This phenomenon was observed for all flows and was only occasionally absent in some of the distal observations of the flows. We infer that the noise is generated by particle collisions from a high concentration of sediment (> 9%) around the top of a dense basal layer that is mostly less than 1 m thick. We conclude that dense basal layers are present for the majority of the duration of the flows and that dilute suspensions run out for only a relatively short distance beyond the terminal location of the front of the dense layer.

We relate the magnitude of the particle collision noise to the velocity of the top of the basal layer and demonstrate that there is low shear between the dense layer and overlying dilute suspension in the body of the flows. This helps to explain the large density contrast (two to three orders magnitude) between the thin dense layer and the dilute suspension just a few meters above.

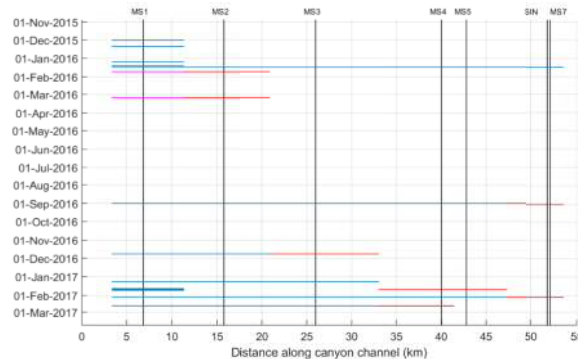


**Figure 4:** Timing and runout of monitored flows in Monterey Canyon. Vertical lines indicate the locations of the moorings and along the canyon channel. Horizontal lines represent the observed sediment density flow events. Blue lines indicate the presence of particle collision noise and red lines indicate where flow velocities and backscatter were observed without particle collision noise. Magenta lines indicate the likely occurrence of events at the MS1 location in the period after the instruments detached from the mooring anchor (Simmons et al., in prep.).

For the largest flow on January 15th, the longest observed duration of the particle collision 51 noise is ~ 1 hour 50 minutes at ~780 m water depth. In contrast, the shortest duration of ~ 52 30 minutes was observed at the distal end of the array (Figure 5). The basal layer stretched as it progressed down the canyon and was still flowing over a distance of greater than 26 km by the time the flow front reached the most distal mooring. The particle collision noise for this flow ceased nearly simultaneously at all moorings between ~780 m to ~1850 m water depth, indicating that the dense basal layer slowed so a similar speed at the same time over a vast distance along the canyon floor.

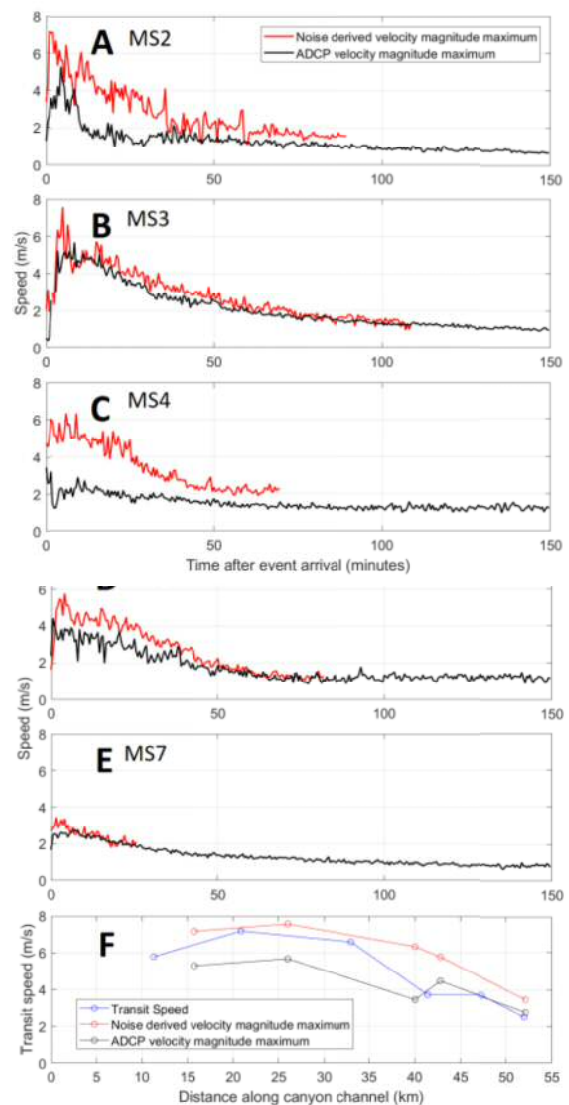


**Figure 5:** Velocity maximum from ADCP data and basal flow velocity derived from the particle collision noise for the five moorings that recorded data during the Jan 15 event, (F) flow speed derived from particle collision noise compared with the maximum ADCP velocity and transit speeds between the moorings (from Simmons et al., in prep).

#### 2.4 Deposits

Hage et al. analyse four months of near-daily bathymetrical surveys to study the stratigraphic evolution resulting from upstream migration of crescentic bedforms. The uppermost part of the stratigraphy (Fig. 3a) contains up to 3 m thick successions of individual beds that dip upstream. Individual back-stepping beds are 0.1 m to 0.5 m thick and result from the most recent turbidity current depositing sediment on the stoss-side of the bedform thus causing them to migrate upstream. They show that occasionally, large flows cause significant upstream migration of the bedforms, eroding the seafloor deeper and producing thicker, back-stepping beds. The lower portion of these thicker upstream migrating beds is preserved typically as 1 m to 2 m thick lens-shaped scour fills, as seen in the lower part of the final stratigraphy (Figure 6).

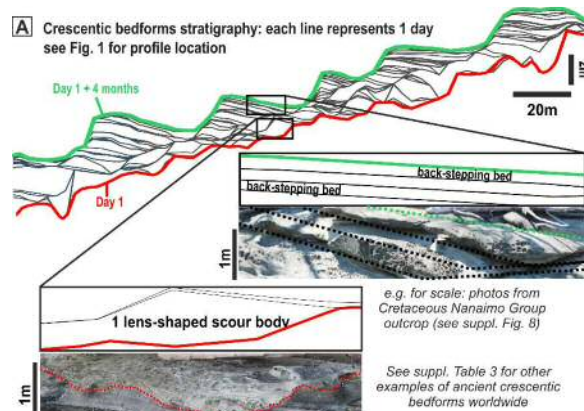


**Figure 6.** Along-strike stratigraphy computed from 106 bathymetrical surveys and comparison of the features with ancient crescentic bedforms deposits (from Hage et al., 2019).

Additional to the computed stratigraphy a set of cores to sample the facies characteristics were also acquired. The sediment cores all contain multiple units of massive sands, which are ungraded to poorly graded. Contacts between beds are sharp and erosive. Individual beds are therefore inferred to result from individual turbidity currents (Figure 7).

Envisaged deposit architectures can range between two end-members: 1) regular back-stepping beds that correspond to a full bedform preservation; 2) scours filled with massive sands that correspond to low bedform preservation (Figure 7). The preservation potential of these bedforms depends on both the magnitude of the formative turbidity currents and the net aggradation rates and the dynamics of any dense basal layers in the largest flows.

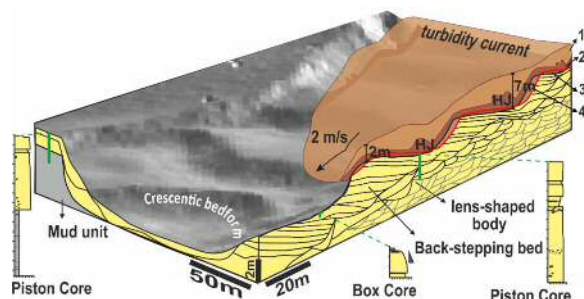


**Figure 7.** Summary schematic of crescentic bedforms formed by supercritical turbidity currents and their depositional architecture. 1: Low density upper part of the flow, 2: High density lower part of the flow with hydraulic jump formed on changing gradient over bedforms, 3: Deposition & 4: Erosion by active event. Red line corresponds to the resulting bathymetry after a single flow. Black lines are observations from Fig. 3A. Grey lines are predictions (from Hage et al., 2019).

### 3 SUMMARY

Crescentic bedforms in submarine canyon-channel-fan systems are enigmatic features. A suite of novel data has been collected from three systems where crescentic bedforms are ubiquitous. The results reveal a complex relationship between turbidity current flow characteristics, sediment transport dynamics, and the possible presence of a dense basal layer. The results are allowing insight into these processes and what these processes can produce in terms of signatures in the rock record.

### 4 ACKNOWLEDGEMENTS

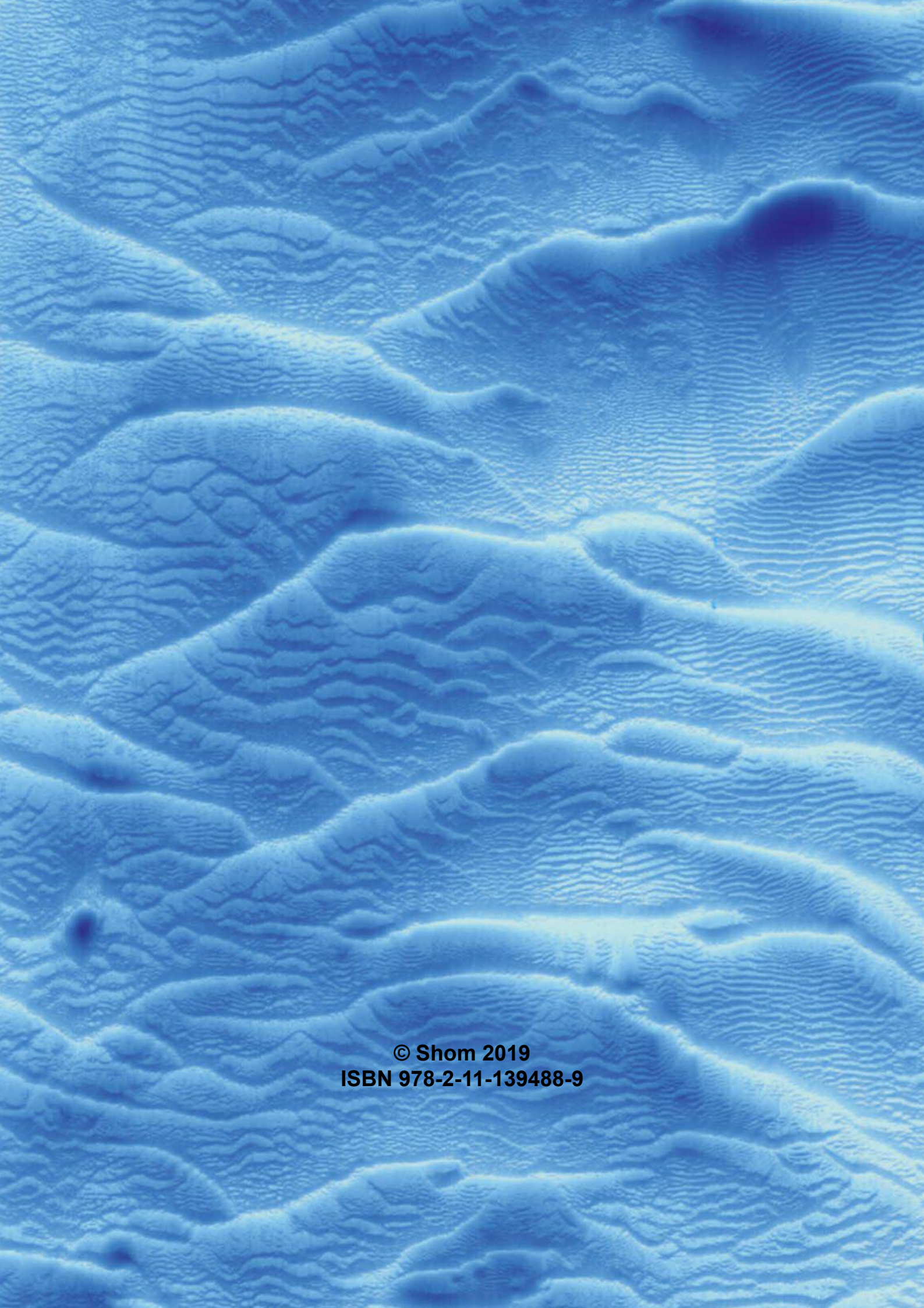
The projects described herein are based on a range of work conducted by large teams funded by a series of NERC grants, MBARI and the USGS, Chevron, ENI and the China Scholarship Council. We thank for all the crew members of CCGS Vector and RV John Strickland and the R/V Western Flyer.

### 5 REFERENCES

- Azpiroz-Zabala, M., et al., 2017. Newly recognized turbidity currents structure can explain prolonged flushing of submarine canyons. *Science Advances* 3(10), e1700200
- Bain, H. A., Hubbard, S.M. H. 2016. Stratigraphic evolution of a long-lived submarine channel system in the late Cretaceous Nanaimo Group, British Columbia, Canada. *Sedimentary Geology*, v. 337, p. 113-132.
- Bouma, A.H., 2000. Coarse-grained and ® ne-grained turbidite systems as end member models : applicability and dangers. 17, 137–143
- Carter L., Gavey R., Talling P., Liu J., 2014. Insights into submarine geohazards from breaks in subsea telecommunication cables. *Oceanography* 27, 58-67
- Cartigny, M.J.B. et al., 2014. Morphodynamics and sedimentary structures of bedforms under supercritical-flow conditions: New insights from flume experiments. *Sedimentology* 61(3), 712–748
- Cartigny, M.J.B., Postma, G., Van Den Berg, J.H. and Mastbergen, D.R. 2011. A comparative Study of sediment waves and cyclic steps based on geometries, internal structures and numerical modelling. *Marine Geology*, v. 280, p. 40–56.
- Clare, M.A., et al., 2016. Preconditioning and triggering of offshore slope failures and turbidity currents revealed by most detailed monitoring yet at a fjord-head delta. *Earth and Planetary Science Letters* 450, 208–220
- Conway, K.W., et al., 2012. Submarine channel evolution: Active channels in fjords, British Columbia, Canada. *Geo-Marine Letters* 32(4), 301–312
- Covault, J. A., Kostic, S., Paull, C. K., Ryan, H. F., and Fildani, A. 2014. Submarine channel initiation, filling and maintenance from sea-floor geomorphology and morphodynamic modelling of cyclic steps. *Sedimentology*, v. 61, p. 1031–1054.
- Dietrich, P., Ghienne, J.-F., Normandeau, A. and Lajeunesse, P. 2016. Upslope-migrating bedforms in a proglacial sandur delta: cyclic steps from river-derived underflows? *Journal of Sedimentary Research*, v. 86, p. 113–123.
- Dorrell, R.M., et al., 2016. Flow dynamics and mixing processes in hydraulic jump arrays: Implications for channel-lobe transition zones. *Marine Geology* 381, 181–193
- Duller, R. A., Mountney, N. P., Russell, A. J. and Cassidy, N. C. 2008. Architectural analysis of a volcaniclastic Jökulhlaup deposit, southern Iceland: sedimentary evidence for supercritical flow. *Sedimentology*, v. 55, p. 939–964.
- Fildani, A., Hubbard, S.M., Covault, J.A., Maier, K.L., Romans, B.W., Traer, M.T., Rowland, K.C. 2013. Erosion at inception of deep-sea channels. *Marine and Petroleum Geology*, v. 41, p. 48–61.
- Hage, S., et al., 2018. How to recognize crescentic bedforms formed by supercritical turbidity currents in the geological records: Insight from active submarine channels. *Geology* 46(6), 563–566
- Hayakawa, Y., Matsukura, Y., 2003. Recession rates of waterfalls in Boso Peninsula, Japan, and a predictive equation. *Earth Surface Processes and Landforms* 28 (6), 675–684
- Hughes Clarke, J. E., Marques, C. R.V., Pratomo, D. 2014. Imaging active mass-wasting and sediment flows on a fjord delta, Squamish, British Columbia. In: *Submarine mass movements and their consequences*, v. 37. Springer International Publishing, p. 249–260.
- Hughes Clarke, J.E., 2016. First wide-angle view of channelized turbidity currents links migrating cyclic steps to flow characteristics. *Nature Communications* 7, 11896
- Kostic, S. 2011. Modelling of submarine cyclic steps: controls on their formation, migration, and architecture. *Geosphere*, v. 7, p. 294–304.
- Kostic, S., Parker, G. 2006. The response of turbidity currents to a canyon-fan transition: internal hydraulic jumps and depositional signatures. *Journal of Hydraulic Research*, v. 44. (5), p. 631–653.
- Lang, J. and Winsemann, J. 2013. Lateral and vertical facies relationships of bedforms deposited by aggrading supercritical flows: from cyclic steps to humpback dunes. *Sedimentary Geology*, v. 296, p. 36–54.

- Lang, J., Brandes, C. and Winsemann, J. 2017. Erosion and deposition by supercritical density flows during channel avulsion and backfilling: Field examples from coarse-grained deepwater channel-levee complexes (Sandino Forearc Basin Southern Central America). *Sedimentary Geology*, v. 349, p. 79-102.
- Middleton, G.V., 1993. Sediment deposition from turbidity currents. *Annual review of earth and planetary sciences* 21, 80-114
- Migeon, S., Savoye, B., Zanella, E., Mulder, T., Faugeres, J.-C., Weber, O. 2001. Detailed seismic reflection and sedimentary study of turbidite sediment waves on the Var Sedimentary Ridge (SE France): significance for sediment transport and deposition and for the mechanisms of sediment-wave construction. *Marine and Petroleum Geology*, v. 18, p. 179-208.
- Ono, K., and Björklund, P.P. 2017. Froude supercritical flow bedforms in deepwater slope channels? Field examples in conglomerates, sandstones and fine-grained deposits. *Sedimentology*, doi:10.1111/sed.12396
- Paull, C.K., et al., 2010. Origins of large crescent-shaped bedforms within the axial channel of Monterey Canyon, offshore California. *Geosphere* 6(6), 755–774
- Paull, C.K., et al., 2018. Powerful turbidity currents driven by dense basal layers. *Nature Communication* 4114
- Peakall, J. et al., 2007. Flow processes and sedimentation in submarine channel bends. *Marine and Petroleum Geology* 24(6–9), 470–486
- Piper, D.J.W., Cochonat, P., and Morrison, M.L., 1999. The sequence of events around the epicentre of the 1929 Grand Banks earthquake: initiation of debris flows and turbidity currents inferred from sidescan sonar. *Sedimentology* 46, 79-97
- Ponce, J.J., and Carmona, A. N. 2011. Coarse-grained sediment waves in hyperpycnal clinoform systems, Miocene of the Austral foreland basin, Argentina. *Geology*, v. 39, p. 763-766.
- Postma, G. and Cartigny, M. J. B. 2014. Supercritical and subcritical turbidity currents and their deposits-a synthesis. *Geology*, v. 42, p. 987-990.
- Postma, G., Kleverlaan, K., Cartigny, M. J. B. and Mohrig, D. 2014. Recognition of cyclic steps in sandy and gravelly turbidite sequences, and consequences for the Bouma facies model. *Sedimentology*, v. 61, p. 2268-2290.
- Prior D.B., Coleman J.M., Bornhold B.D., 1982. Results of a known seafloor instability event. *Geo-Marine Letters* 2(3-4), 117-122
- Spinewine, B., Sequeiros, O., Garcia, M., Beaubouef, R., Sun, T., Savoye, B., and Parker, G. 2009. Experiments on wedge-shaped deep sea sedimentary deposits in minibasins and/or on channel levees emplaced by turbidity currents part II, morphodynamic evolution of the wedge and of the associated bedforms. *Journal of Sedimentary Research*, v. 79 (8), p. 608-628.
- Symons, W.O., Sumner, E. J., Cartigny, M. J. B. and Clare, M. A. 2016. Large-scale sediment waves and scours on the modern seafloor and their implications for the prevalence of supercritical flow. *Marine Geology*, v. 371, p. 130-148.
- Torrence, C. & Compo, G.P., 1998. A practical guide to wavelet analysis. *Bull Am Meteorol Soc* 79, 61-78
- Trites, A. 1995. The US repeat and VFR – visiting friends and relatives – visitor to Canada: come again, eh! *Journal of Tourism Studies* 6(1), 27-37
- Whipple K.X. & Tucker G.E., 1999. Dynamics of the stream-power river incision model: implications for height limits of mountain ranges, landscape response timescales, and research needs. *Journal of Geophysical Research, Solid Earth* 104 (B8), 17,661-17,674
- Xu, J.P., Sequeiros, O.E. & Noble, M.A., 2014. Sediment concentrations, flow conditions, and downstream evolution of two turbidity currents, Monterey Canyon, USA. *Deep-Sea Research Part I: Oceanographic Research Papers* 89, 11–34
- Yokokawa, M., Okuno, K., Nakamura, A., Muto, T., Miyata, Y. and Naruse, H. 2009. Aggradational cyclic steps: sedimentary structures found in flume experiments. *Proceedings 33rd IAHR Congress*, Vancouver, p. 5547-5554.

Shom  
Imprimé par nos soins  
CS 92803  
29228 Brest CEDEX 2  
Mars 2019  
Numéro d'éditeur : 2958



**© Shom 2019  
ISBN 978-2-11-139488-9**